THE UNIVERSITY *of* EDINBURGH

Chemical Records of Environmental Pollution in Ombrotrophic Peat Bogs

Joanna M. Cloy

PhD Thesis
The University of Edinburgh
2006

Acknowledgements

I would firstly like to thank my supervisor Professor John Farmer for his extensive guidance, encouragement and invaluable advice throughout this work. I couldn't have done it without him!

I would like to thank NERC for funding my PhD studentship, Dr. Margaret Graham for her assistance in the collection of peat cores, Dr. Lorna Eades for her assistance in elemental/isotopic analysis and ICP-MS and ICP-OES training, and Dr. Charun Yafa for his initial supervision and training in sample preparation and elemental analysis.

I would like to thank my co-supervisor Professor Angus MacKenzie at SUERC for his advice and assistance, particularly with respect to ^{210}Pb-dating. I would also like to thank my other co-supervisor Dr. Peter Anderson at CLARRC for his assistance in the determination of Hg.

I gratefully acknowledge Dr. Gordon Cook at SUERC for his advice and assistance with ^{14}C dating, along with Philip Naysmith and Carol Donnelly at SUERC for their assistance in making the ^{14}C AMS measurements and gamma spectrometric analysis, respectively.

I also gratefully acknowledge permission from Scottish Natural Heritage and Scottish Wildlife Trust to collect cores from Flanders Moss, The Red Moss of Balerno, Carsegowan Moss and Turclossie Moss.

A special thanks goes to my family and friends for their patience and encouragement and, last but not least, a huge thanks goes to my boyfriend Alastair for his continuous support, assistance and advice throughout my PhD, particularly during this last difficult year of thesis writing.

Abstract

Human activity has affected metal emissions to the atmosphere on a global scale for several thousand years, resulting in widespread contamination of the environment with toxic heavy metals such as Pb and Hg, thereby threatening both human and environmental health. In recent years ombrotrophic peat bogs have been used to study the changing rates and sources of atmospheric metal deposition, as they receive all their water and nutrients from the atmosphere by dry and wet deposition alone. Cores from such bogs have proved especially useful as archives of atmospheric Pb deposition as Pb is essentially immobile in ombrotrophic peat.

The work described in this thesis is primarily concerned with the use of ombrotrophic peat bogs to investigate environmental contamination in Scotland during pre-industrial, industrial and post-industrial (i.e. *ca.* post-1970 A.D.) times. Cores were collected from ombrotrophic peat bogs at four different geographical locations (Carsegowan Moss, SW; Flanders Moss, W Central; The Red Moss of Balerno, E Central; Turclossie Moss, NE) in Scotland. Air-dried peat samples were dry-ashed and dissolved using microwave-assisted HF/HNO_3 digestion. Elemental concentrations (e.g. Al, As, Ca, Cd, Co, Cr, Cu, Fe, Mg, Mn, Ni, P, Pb, S, Sb, Sc, Se, Ti, V, Y, Zn and Zr) and Pb isotope ratios (e.g. $^{206}Pb/^{207}Pb$) were determined using ICP-OES and ICP-MS as appropriate. For Hg determination, samples were digested with HNO_3/H_2SO_4 and then analysed by CVAAS. Certified reference materials (e.g. Ombrotrophic Peat (NIMT/UOE/FM001), Canadian Peat (1878 P), Bush Branches and Leaves (DC73349), Peach Leaves (GBW 08501) and Coal (BCR CRM No. 40 and NBS SRM 1635) were used for quality control purposes.

The distribution and behaviour of the potentially toxic trace elements (As, Cd, Co, Cr, Cu, Hg, Ni, Sb, Se, V and Zn) and of major elements (Ca, Fe, Mg, Mn, P and S) within the four ombrotrophic peat bogs was investigated and there was strong evidence that Ca, Fe, Mg, Mn, P, S, Se and Zn were mobile in ombrotrophic peat, while As, Cd, Co, Cr, Cu, Hg (at least during industrial and post-industrial periods), Ni, Sb and V, like Pb, were essentially immobile in ombrotrophic peat. Deposition records of conservative lithogenic elements (e.g. concentrations of Al, Sc, Ti, Y and Zr) that occur predominantly in soil dust were also investigated and the chosen conservative elements Sc, Ti and Zr were used in calculations to estimate anthropogenic enrichments of As, Cd, Co, Cr, Cu, Ni, Pb, Sb and V in peat bog profiles.

^{210}Pb- and ^{14}C- dated peat cores were used to reconstruct historical records of atmospheric anthropogenic As, Cd, Co, Cr, Cu, Ni, Pb, Sb and V deposition (since the pre-Roman (i.e. to *ca.* 380 B.C.)/Roman period) and atmospheric Hg deposition (since the onset of the industrial period) across Scotland. For Pb, on the basis of Pb isotopic composition (e.g. $^{206}Pb/^{207}Pb$), clear indications of contamination during the pre-Roman/Roman and Mediaeval periods were attributed to the mining and smelting of Pb ores (from Britain and elsewhere in Europe). During the industrial and post-industrial periods, variations in the relative importance of contributions of anthropogenic Pb from different sources were apparent. From *ca.* the early 17th century A.D. at three of the peat bog sites, the mining and smelting of indigenous Scottish Pb ores, until the early 20th century A.D., were found to be the most important sources of anthropogenic Pb deposition. In contrast, at the most southerly

site (Carsegowan Moss), influences from the use of both British Pb ores and imported Australian Pb ores (in more southern parts of Britain) since the late 19th century A.D. were evident. At each of the sites, the increasing importance of Australian-Pb-influenced car-exhaust emissions from the 1930s to late 1990s A.D., along with significant contributions from coal combustion (until the late 1960s A.D.) was evident. For Sb, in general, similarities between the major trends in the concentration profiles of anthropogenic Sb and Pb suggested common sources of these two elements. Perturbations in the anthropogenic Sb/Pb ratios since *ca.* 1800 A.D., however, were attributed to temporal variations in the relative importance of atmospheric emissions from different sources such as Pb ore mining/smelting, coal combustion and, in recent decades, automobile-related use of compounds of Pb (in leaded petrol) and of Sb (in brake linings). For Hg, in general, during the industrial and post-industrial periods, coal combustion and waste incineration, respectively, were likely to be the most important sources of Hg. For As, clear indications of contamination during the Mediaeval period were probably attributable to the mining and smelting of Pb and Cu ores, and for As, Cd, Co, Cr, Cu, Ni and V, during the industrial and post-industrial periods, a variety of sources (e.g. metallurgical activities, coal and oil combustion, use of phosphate fertilisers and waste incineration) were important to varying extents. Also, in recent years, atmospheric Cu emissions from automobile-related use of compounds of Cu (in motor oil, brake linings and tyres) may have been important.

Inter-site and inter-elemental comparison of records of atmospheric metal deposition across Scotland indicated that, in general, atmospheric As, Cr, Hg, Pb and Sb deposition was greatest during the industrial period (between the late 1880s and late 1960s A.D.) and atmospheric Cd, Co, Cu, Ni and V deposition was greatest during the industrial and post-industrial periods (between *ca.* 1900 and the early 2000s A.D.), although increases in As, Co, Cr, Hg, Pb and Sb deposition were earliest (during the late 19th and early 20th century A.D.) at the most southerly site (Carsegowan Moss). During the industrial and post-industrial periods, levels of As, Pb and Cd contamination were generally highest in the south of Scotland, Cu, Co and Sb in south and central Scotland, and Cr, Ni and V in central Scotland. Overall, the existence of a south to north As, Cd, Co, Cr, Cu, Ni, Pb, Sb and V pollution gradient in Scotland was evident.

1 INTRODUCTION

2 MATERIALS AND METHODS

4 THE RED MOSS OF BALERNO

6 CARSEGOWAN MOSS

1 INTRODUCTION

In setting out the aim and objectives of this research investigation, this chapter provides background information and a review of recent relevant literature.

1.1 INTRODUCTORY OVERVIEW AND AIM

Human activity has affected metal emissions to the atmosphere on a global scale for several thousand years, resulting in widespread contamination of the environment with toxic heavy metals such as Pb and Hg, and on a scale exceeding natural levels by several orders of magnitude, thereby threatening both human and environmental health. Extensive studies are required in order to understand and measure the extent of human impact on the global biogeochemical cycles of toxic elements. In recent years ombrotrophic peat bogs have been used to study the changing rates and sources of atmospheric metal deposition, as they receive all their water and nutrients from the atmosphere by dry and wet deposition alone. Cores from such bogs have proved especially useful as archives of atmospheric Pb deposition as Pb is essentially immobile in ombrotrophic peat. Ombrotrophic peat bogs and other environmental archives have been used to characterise historical trends and sources of environmental Pb contamination for many years but, more recently, elements such as Hg and Sb have received attention. The behaviour of many other potentially toxic trace metals in peat bogs, however, is still not yet fully understood. In order to distinguish between natural and anthropogenic sources of these metal contaminants in peat bog profiles, deposition records of conservative lithogenic elements that occur predominantly in soil dust have also been studied.

The primary aim of this investigation is to use ombrotrophic peat bogs to reconstruct chemical records of atmospheric metal deposition in Scotland. This work will build upon existing records of anthropogenic Pb deposition from the atmosphere, as well as improve understanding of the biogeochemical processes affecting other metals deposited in these bogs. Where possible, temporal records of their anthropogenic

deposition will also be reconstructed in order to understand more fully the environmental impact of human activities.

1.2 CLASSIFICATION OF METALS UNDER INVESTIGATION

In this thesis, the elements investigated are Al, As, Ca, Cd, Co, Cr, Cu, Fe, Hg, Mg, Mn, Ni, P, Pb, S, Sb, Sc, Se, Ti, V, Y, Zn and Zr, and these elements will be grouped according to the following terms, which are frequently used in the literature:

Trace metals (As, Cd, Co, Cr, Cu, Hg, Ni, Pb, Sb, Se, V and Zn)
Conservative elements (Al, Sc, Ti, Y and Zr)
Major elements (Ca, Fe, Mg, Mn, P and S)

Note that the term "trace metals" as used throughout this Chapter includes the metalloids As and Se, which have both metallic and non-metallic properties. Also, based on the general rule that heavy metals have a density exceeding a value of 4.5 g cm^{-3} (Witting, 1993), the trace metals listed above will also, on some occasions, be referred to as heavy metals (as this term is also frequently used in the literature).

1.3 ATMOSPHERIC METAL DEPOSITION

1.3.1 Mechanisms of atmospheric metal deposition

Metals occur in the atmosphere, principally in particulate form and emanate from natural and anthropogenic sources. The transfer of these airborne particles to land or water surfaces occurs through dry and wet deposition (Fig. 1.1), which is the first stage in the development of the atmospheric metal deposition record (Schroeder, 1987). The relative importance of dry and wet deposition of metals on surfaces depends primarily on geographical location (Livett, 1988). Altitude may also have an effect due to changes in the amount of precipitation, dust or biomass production with altitude (Zechmeister *et al.*, 2003). Also, the half-life of airborne particles is usually

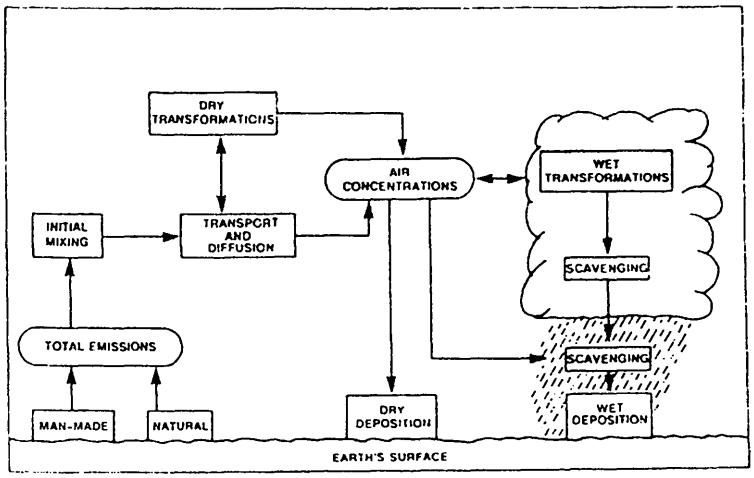

Figure 1.1: The major atmospheric pathways for metals (Schroeder, 1987).

on the order of days, depending on the size of the particles and atmospheric conditions. Large particles, for example, will promptly return to the surface and remain close to the emission source but smaller particles may be subjected to long range transport or even raised to higher altitudes, so that dispersal is more widespread. Particles reaching the stratosphere will eventually be distributed on a worldwide scale and those that remain in the troposphere will be transported in the zonal circulation before returning to the Earth's surface (Pierson *et al.*, 1973). Studies of regional and temporal trends in heavy metal atmospheric deposition in peat bog and lake sediments from Norway (Hvatum *et al.*, 1987), Sweden (Renberg *et al.*, 2002) and Scotland (Eades *et al.*, 2002) as well as ice cores in Greenland (Boutron *et al.*, 1991, 1994; Rosman *et al.*, 1997) found that some metal profiles were influenced by the long range transport of heavy metal pollution from continental Europe. The maintenance of a general south-north gradient therefore reflects the atmospheric circulation patterns associated with long range transport of pollutants (Martinez-Cortizas *et al.*, 2002a). Some anthropogenic sources of Pb are known to generate sub-micron size aerosols capable of travelling thousands of kilometres (Kempter *et al.*, 1997), but anthropogenic aerosols in general show a broad size distribution (Fig. 1.2) and the degree and extent to which these emissions (as well as natural emissions) spread will depend on the type and composition of the emission source (Nriagu, 1978).

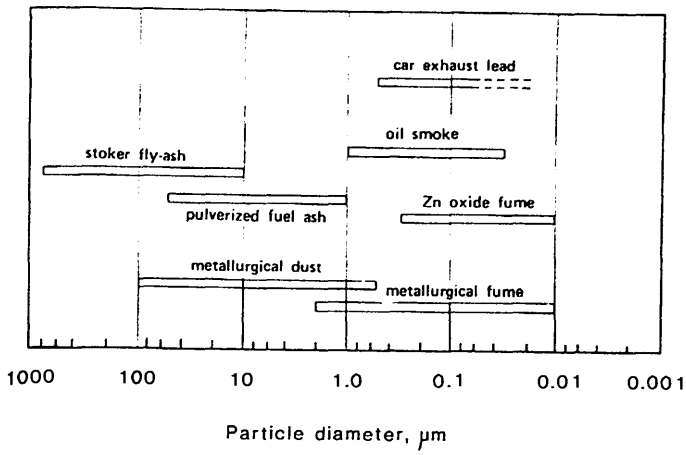

Figure 1.2: Particle sizes generated by some atmospheric pollution sources (Livett, 1988).

1.3.2 Overview of natural and anthropogenic sources of metal emissions to the atmosphere

1.3.2.1 Natural sources of metals

Soil dust is a major natural source of metals in the atmosphere and is produced from the weathering of rocks by processes such as wind erosion. Element concentrations in the Upper Continental Crust (UCC), as calculated by Wedepohl (1995), for the elements under investigation in this research project are shown in Table 1.1. Although levels of soil dust emissions for particular elements can vary widely depending on local geology, the concentrations in Table 1.1 provide a general indication of crustal abundance. They can also be used to calculate anthropogenic Enrichment Factors (EFs) for trace metals, relative to natural lithogenic elements such as Al, Ti, Sc, Zr and Y, which are thought to be present in the atmosphere primarily in the form of soil dust. The use of these conservative elements will be discussed in Section 1.8.

Oceans and volcanoes are also important geochemical sources of element release to the atmosphere, the former especially for Ca, Mg, P, S and Se, and the latter for S and Hg (Brimblecombe, 1996). Some other less important natural sources of metals include particles of smoke and ash supplied by forest fires, biogenic dusts (e.g. seeds,

Table 1.1: Element concentrations (mg kg^{-1}) in the Upper Continental Crust (UCC) (Wedepohl, 1995).

Element	Concentration in UCC (mg kg^{-1})
Al	77440
As	2.0
Ca	29450
Cd	0.102
Co	11.6
Cr	35
Cu	14.3
Fe	30890
Hg	0.056
Mg	13510
Mn	527
Ni	18.6
P	665
Pb	17
S	953
Sb	0.31
Sc	7
Se	0.083
Ti	3117
V	53
Y	20.7
Zn	52
Zr	237

pollen and other organic matter derived from plants and organic soils) and cosmogenic particles (e.g. from meteorites and cosmic dust). The biogenic component of atmospheric dust is often neglected, but Reimann and de Caritat (2000, 2005) suggested that it was quite a significant natural source of metals in the atmosphere. The contribution of natural sources to naturally occurring atmospheric Pb has been estimated as follows: windblown dust (85%), plant exudates (10%), forest fires, volcanic eruptions and meterorite impacts (3%) and radioactive decay and seasalt spray (2%) (Nriagu, 1978).

1.3.2.2 Anthropogenic sources of metals

Metals can also be introduced into the atmosphere by various anthropogenic activities and the domestication of fire may have marked the beginning of anthropogenic metal emissions (Nriagu, 1996). Table 1.2 contains emission factors

(i.e. μg or g of metal emissions per unit consumption or production) for the release of the trace metals under investigation (with the exception of Co as data for this metal were not available) to the atmosphere from various anthropogenic emission sources. These values were taken from a review by Nriagu and Pacyna (1988) of emission studies in Western Europe, the United States, Canada and Russia. The main anthropogenic sources of trace metals to the atmosphere are fossil fuel combustion, mining and metallurgical processes, waste incineration, agricultural application of fertilisers from agricultural activities, cement production and wood combustion.

Table 1.2: Emission factors for the release of trace metals to the atmosphere (Nriagu and Pacyna, 1988).

Source category	Unit	As	Cd	Cr	Cu	Hg	Ni
Coal combustion							
Electric utilities	μg MJ^{-1}	1.5-100	5-25	80-500	60-200	10-35	90-600
Industry and domestic	g t^{-1}	0.2-2.10	0.1-0.5	1.7-12	1.4-5.0	0.5-3.0	2.0-15.0
Oil combustion							
Electric utilities	μg MJ^{-1}	1.0-5.0	4-30	15-100	60-400		60-2500
Industry and domestic	g t^{-1}	0.02-0.2	0.05-0.2	1.0-5.0	0.5-3.0		20-80
Pyrometallurgical non-ferrous metal production							
Mining		5.0-10.0	0.1-0.5		20-100		~100
Pb production	g t^{-1} metal	200-400	10-50		60-80	2-4.0	85
Cu-Ni production	produced	1000-1500	200-400		1700-3600		900
Zn-Cd production		50-150	200-1000		50-150	8-45	
Secondary non-ferrous metal production	g t^{-1} waste		2.5-4.0		50-150		
Steel and iron manufacturing	g t^{-1} steel	0.5-3.5	0.04-0.4	4.0-40.0	0.2-4.0		0.05-10
Waste incineration							
Municipal	g t^{-1} waste	1.1-2.8	0.4-10	0.7-7.0	7.0-1.4	1.0-15	0.7-3.0
Sewage sludge		5.0-10	1.0-12	50-150	10-60	5-20	10-50
Phosphate fertilisers	g t^{-1} fertiliser		0.5-2.0		1.0-5.0		1.0-5.0
Cement production	g t^{-1} cement	0.2-1.0	0.01-0.60	1.0-2.0			0.1-1.0
Wood combustion	g t^{-1} wood	0.1-0.5	0.1-0.3		1.0-2.0	0.1-0.5	1.0-3.0

A blank space denotes an insignificant contribution from a particular source.

Table 1.2 (continued): Emission factors for the release of trace metals to the atmosphere (Nriagu and Pacyna, 1988).

Source category	Unit	Pb	Sb	Se	V	Zn
Coal combustion						
Electric utilities	$\mu g\ MJ^{-1}$	50-300	10-50	7-50	20-300	70-500
Industry and domestic	$g\ t^{-1}$	1.0-10.0	0.2-1.5	0.8-2.0	1.0-10.0	1.5-12.0
Oil combustion						
Electric utilities	$\mu g\ MJ^{-1}$	40-300		6-50	1200-9000	30-220
Industry and domestic	$g\ t^{-1}$	2.0-6.0		0.3-1.5	60-200	1.0-7.0
Pyrometallurgical non-ferrous metal production						
Mining		500-1000	1.0-10.0	1.0-2.5		50-100
Pb production	$g\ t^{-1}$ metal	3000-8000	50-100	10-50		50-120
Cu-Ni production	produced	1300-2600	50-200	50-150	5-10.0	500-1000
Zn-Cd production		1200-2500	10-20	20-50		100000-180000
Secondary non-ferrous metal production	$g\ t^{-1}$ waste	50-800	1-5	1-5		300-1600
Steel and iron manufacturing	$g\ t^{-1}$ steel	1.5-20.0	0.005-0.1	0.001-0.003	0.1-2.0	10-45
Waste incineration						
Municipal	$g\ t^{-1}$ waste	10-20	3.0-6.0	0.2-0.5		20-60
Sewage sludge		80-100	5-20	1.0-10	3.0-20	50-150
Phosphate fertilisers	$g\ t^{-1}$ fertiliser	0.4-2.0		0.003-0.009		10-50
Cement production	$g\ t^{-1}$ cement	0.02-16.0				2.0-20.0
Wood combustion	$g\ t^{-1}$ wood	2.0-5.0				2.0-10.0

Some of these anthropogenic activities employ high temperature processes (e.g. waste incineration) and emission factors for the volatile metals such as As, Cd, Cu, Hg, Pb, Sb, Se, and Zn, are particularly high for these activities (*cf.* Table 1.2) (Bowen, 1979). Hg and Se are special in that they can remain in the vapour phase at ambient temperatures, but the less volatile metals transfer to the surface of fine particles as they cool and have been discovered at enhanced concentrations on the surface of fly ashes, with enhancements being highest on the smaller particles, which remain in the atmosphere longer than larger particles (*cf.* Section 1.3). Although Ni and Cr are also found in enhanced concentrations on the surface of fly ashes, these

elements are not particularly volatile and it is possible that their enrichment arises from transfer to particle surfaces as volatile sulfides (Brimblecombe, 1996).

1.3.2.2.1 Metallurgical processes

Metals such as Cd, Cu, Hg, Pb and Zn occur in high concentrations in sulfide deposits and other ores, which often contain high concentrations of other metals such as As and Sb. Various non-ferrous pyrometallurgical processes are employed to extract and refine these metals and, during these processes, high concentrations of metals are emitted into the atmosphere, particularly during smelting operations, where high temperatures are employed (Drever, 1982; Brimblecombe, 1996). In contrast, Cr is derived primarily from the iron and steel industry, which involves the processing of Fe ores using high temperature electric arc and basic oxygen furnaces (Nriagu and Pacyna, 1988).

1.3.2.2.2 Fuel combustion

Metals are also found as impurities in fuels. Typical concentrations of both metallic and non-metallic trace elements in coal and crude oil as a function of their crustal abundance are shown in Fig. 1.3. The elements lying above the diagonal lines in Fig. 1.3 are those that are enriched in the fuels relative to the crust. With the exception of V and Ni, which are considerably enriched in oil, trace element abundances are generally much lower in oil than in coal (Brimblecombe, 1996). Element enrichments in coal are reflected in the emission factor values shown in Table 1.2, where combustion of coal in electric power plants and in industrial, commercial and residential burners is the major source of airborne Hg and Se and a very significant source of As, Cr, Pb and Sb. Combustion of oil for the same purpose is the most important source of V and Ni (Olmez and Gordon, 1985; Nriagu and Pacyna, 1988).

Not all trace metal components of fuels are of natural origin. Some may be the result of contamination during processing, while others are deliberately added. Tetra-alkyl Pb compounds were (and still are, in some developing countries) added to petrol as an anti-knock agent.

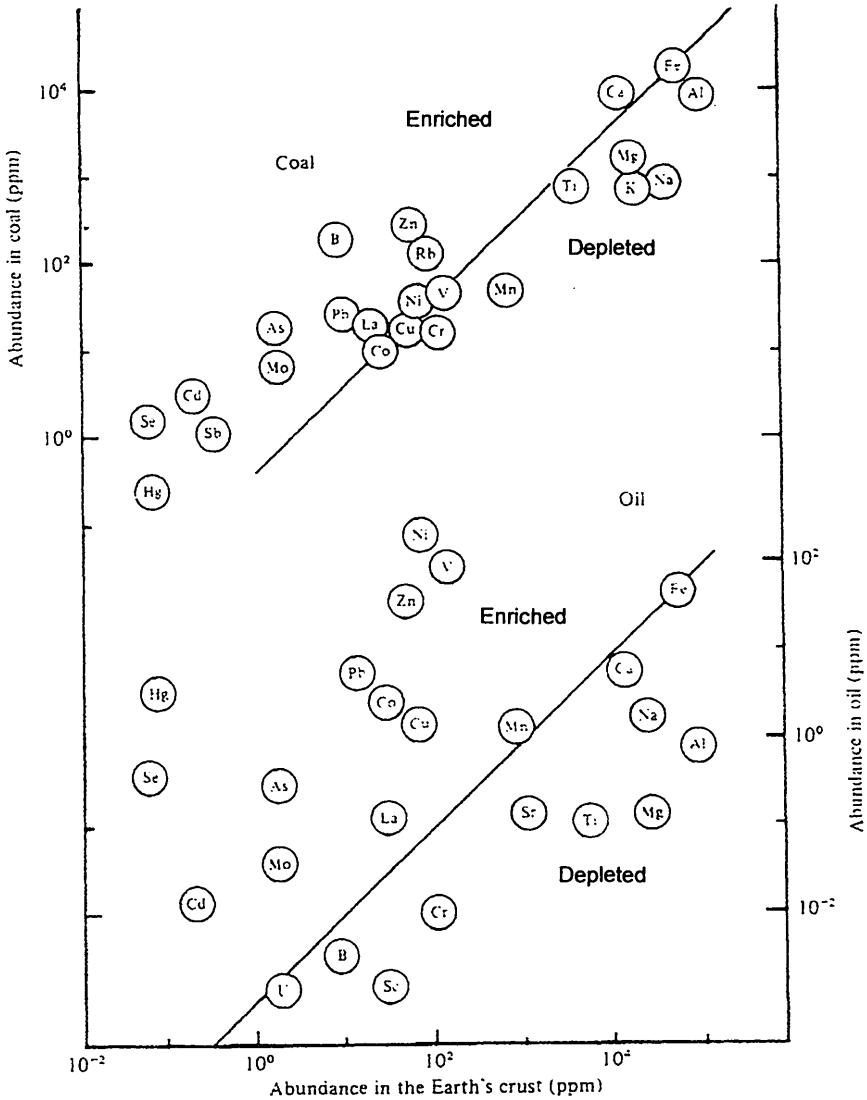

Figure 1.3: Elemental abundances in coal and oil compared with abundances in the Earth's crust. Diagonal lines indicate the position that would be occupied by elements showing no enrichment relative to Fe (Brimblecombe, 1996).

During its use, most airborne Pb, particularly in urban areas, originated from this exhaust emission source (Olmez and Gordon, 1985; Brimblecombe, 1996).

1.3.2.3 Other important sources

Applications of metals and their compounds in various industries can also lead to the emission of significant amounts of trace metals to the atmosphere, e.g. the use of Cd and Ni in the manufacture of Ni-Cd batteries, Cr in leather tanning and the various metals as catalysts in industrial processes and in paints and pigments (Oehme, 1979).

For Co (not shown in Table 1.2) elevated levels in the atmosphere may result from anthropogenic activities such as fossil fuel combustion, mining, smelting and refining of Co-bearing ores and also the use of phosphate fertilisers in agricultural processes (Oehme, 1979; Chemical Research Communications, 2003).

Finally, it must also be remembered that since prehistoric times natural sources of aerosols to the atmosphere have been supplemented with particles of a natural origin from anthropogenic activities such as forest clearance and soil cultivation for agriculture (Kempter *et al.*, 1997).

1.3.3 Environmental archives of atmospheric metal deposition

Many different environmental archives have been used to reconstruct historical records of atmospheric metal deposition. An ideal archive is one in which the record is perfectly preserved, e.g. where no significant post-depositional physical or chemical transformations are affecting concentration and speciation of the element of interest (Shotyk, 1996a). The most extensively studied environmental archives will be discussed below. Taken together these archives are proving to be very valuable for reconstructing, in detail, the chronology of environmental contamination across the globe (Monitoring and Assessment Research Centre, 1985; Shotyk *et al.*, 2000).

1.3.3.1 Ice deposits

Quantitative measurements of trace metals in ice cores from polar ice sheets (Greenland and Antarctica) and Alpine regions have been used by several research teams to reconstruct historical records of atmospheric metal deposition (Murozumi *et al.*, 1969; Boutron and Patterson, 1986; Boutron *et al.*, 1991, 1994; Rosman *et al.*, 1997; Matsumoto and Hinkley, 2001; Schwikowski *et al.*, 2004). Although virtually no chemical transformation occurs in ice cores after metal deposition has taken place, some problems are apparent. Heavy metal reactivity, for example, is governed primarily by temperature (Livett, 1988) and the extremely low metal concentrations, e.g. sub pg g^{-1}, may lead to problems in avoiding contamination as well as analytical difficulties (Shotyk, 1996a).

1.3.3.2 Lake sediments

Lake sediments have also been used as archives of atmospheric metal deposition (Renberg *et al.*, 1994, 2002; Farmer *et al.*, 1996, 1997a; Brannvall *et al.*, 1997; Eades *et al.*, 2002). Interpretation of the records, however, may be complicated by chemical diagenesis, bioturbation, resuspension and sediment focusing (Norton and Kahl, 1986, 1987; Norton *et al.*, 1990; Farmer, 1991).

1.3.3.3 Moss

Mosses and other bryophytes, such as lichen, serve as useful biomonitors for atmospheric metal deposition, as they receive their inorganic constituents only from atmospheric inputs and also, because of their high metal-binding capacity (Section 1.7.1), they have the ability to passively accumulate metals (Weiss *et al.*, 1999a). A major advantage of appropriately collected and stored moss samples over other environmental archives is that they have a known age and therefore problems that can arise from dating are avoided (Farmer *et al.*, 2002). They have especially been used in regional monitoring studies in Scandinavia (Rühling and Tyler, 1973, 1984; Steinnes, 1977, 1995). Unfortunately, however, as mosses eventually die and decompose in forest ecosystems, they usually leave behind no long-term historical records unless steps have been taken to collect and preserve samples (Shotyk, 1996a).

1.3.3.4 Tree rings and bark

Tree rings (Sheppard and Funk, 1975; Baes and McLaughlin, 1984) and tree bark (Satake *et al.*, 1996; Bellis *et al.*, 2001, 2002a) have also been investigated for use in regional studies of atmospheric pollution. It was found, however, that tree rings do not provide a record that is due exclusively to atmospheric inputs, as they may be affected by root uptake from soils, seasonal variations and radial translocation of metals (Shotyk, 1996a; Bindler *et al.*, 2004a; Patrick and Farmer, 2006). Tree bark records have been shown to more reliable, as they provide a direct measure of the level of pollution in the environment at the time of sample collection. Tree bark readily accumulates pollution on its surface but it does not, however, represent a

closed system and processes of dispersion and migration of deposited elements can occur. In contrast, tree bark pockets (outer layers of bark that have been enveloped by and grown in the tree trunk), have recently been shown to be more useful, as they represent an inert closed system (Bellis *et al.*, 2002b, 2004; Åberg *et al.*, 2004).

1.3.3.5 Peat deposits

The peat archive has always been valued and has increasingly become recognised as a sophisticated means of preserving records of atmospheric metal deposition since, unlike ice deposits which are restricted to the polar and alpine regions of the world, peatlands are widely distributed across the globe. They are also associated consistently with high precipitation and therefore atmospheric pollutant input would perhaps be expected to be higher compared with other environmental archives (Livett, 1988). Special types of peatlands called bogs, which generally receive their inorganic constituents from the atmosphere alone, are the most useful peatland archives of atmospheric metal deposition and will now be discussed in more detail.

1.4 OVERVIEW OF OMBROTROPHIC PEAT BOGS

1.4.1 Types and definition of peatlands

Peatlands are specialised waterlogged environments that support peat-forming vegetation. There are three main groups; bogs, fens and marshes, which develop as a result of complicated interactions between climate, vegetation, geology and topography and display their own characteristics (Lindsay, 1995; Bragg, 2002; Kellner, 2003). Marshes and fens are minerotrophic peatlands, which means that they receive their mineral nutrition not only from atmospheric rain and dust inputs, but also from percolating ground waters. They are therefore nutrient-rich environments that can be quite acidic or alkaline with pH values ranging from 4.0 – 9.0. Surface peat layers of bogs on the other hand are hydrologically isolated from the influence of local ground and surface waters and are fed exclusively by atmospheric deposition. This condition is characteristic of most bogs and is called ombrotrophic (Greek "ombros" meaning rain shower, "trophe" meaning nourishment). Bogs are

therefore nutrient-poor, acidic environments with pH values ranging from 3.5 – 4.5 (Damman, 1978; Clymo, 1987; Shotyk, 1988; Lindsay, 1995).

Marshes and fens are widely distributed across the globe but bogs are generally distributed in the northern, primarily boreal countries, such as Canada, United States, Russia, China, Sweden and Norway, that have high rainfall and low temperature climates. Bogs are also found in tropical countries, principally Indonesia and Malaysia, that have high rainfall and high temperature climates (Matthews and Fung, 1987; Brooks and Stoneman, 1997). Bogs will now be discussed in more detail since cores from Scottish bogs were used in this research investigation.

1.4.2 Peat bogs in Scotland

Peat bogs are specialised environments created by the steady growth of vegetation communities and the accumulation of their remains as peat over thousands of years. The three main types of bog that occur in Scotland, as classified by the National Peatlands Resource Inventory, are blanket bogs, intermediate bogs and raised bogs (Brooks and Stoneman, 1997).

1.4.2.1 Distribution of peat bogs in Scotland

Blanket bogs and intermediate bogs are widely distributed throughout Scotland, mainly in the upland areas (Fig. 1.4 a), while the less abundant raised bogs are more commonly found in the lowlands of Scotland (Fig. 1.4 b), distributed in three main areas: the north Solway coast, the Central Belt and the Grampian coast. Of the one million hectares of bogland in Scotland only thirty thousand hectares were originally raised bogs. After centuries of peat extraction, afforestation and drainage, that figure has been reduced dramatically and now only four thousand hectares of active raised bog remain. In spite of this, Scotland still has some of the best examples of this habitat in Europe (Scottish Wildlife Trust, 2005).

Figure 1.4: Distribution of a) blanket bogs and intermediate bogs and b) raised bogs in Scotland (Brooks and Stoneman, 1997).

1.4.2.2 Blanket bogs

Blanket bogs are vast unconfined areas of bogland that cover the ground like a blanket and they can develop in areas that are sufficiently cool and constantly wet to allow accumulation of peat on all but the more steeply sloping ground. They form on top of mineral soils that have become leached over time as a result of heavy rainfall. These bogs are generally ombrotrophic but, as they are relatively shallow, they can occasionally receive water and nutrients from mineral-rich sources and the occurrence of mineral soil islands and bedrock outcrops is common (Fraser, 1943; Lindsay, 1995; Brooks and Stoneman, 1997).

1.4.2.3 Intermediate bogs

Intermediate bogs occur under conditions of climate and topography that are marginal for the development of blanket bog but exceed those necessary for raised bog formation. Therefore they represent boglands where blanket bogs and raised bog coincide (Brooks and Stoneman, 1997).

1.4.2.4 Raised bogs

Raised bogs are domed areas of bogland that are found mainly on low plains or broad valley floors, although some raised bogs have been shown to form over a more varied terrain, including concave slopes on hillsides (Fraser, 1943; Daniels, 1978). Their surface peat layers are raised well above the elevation of surrounding mineral soils and above the influence of ground water flow. The underlying peat layers and margins of the bog, however, do consist of minerotrophic fen peat (Lindsay, 1995; Kellner, 2003). In this research project, peat cores from raised bogs were used to study atmospheric records of metal deposition as these bogs are often found to be truly ombrotrophic. This type of bog will now be discussed in more detail.

1.4.2.5 Formation of raised bogs

Many Scottish raised bogs began life as shallow water-filled basins of relatively impermeable glacial clays left after the most recent glacial period some ten thousand years ago. These water-filled basins became overgrown by fen vegetation, whose remains failed to decay completely and thus accumulated gradually, filling the basin with fen peat and trapped sediment (Fig. 1.5). Peat layers grew thicker until eventually the plants were no longer in contact with the mineral-rich ground water. Such conditions were intolerable to most plant species other than *Sphagnum* bog mosses (Fig. 1.6). These plants do not possess roots and can survive under conditions of very little nourishment. They absorb nutrients such as Ca and Mg from rainwater through hyaline cells in the surface of their leaves, which release hydrogen ions into the bog water, thus maintaining its acidity (Clymo, 1963; Richardson, 1981). They also have a very high water-holding capacity, which allows them to adapt to the highly stagnant waterlogged bog conditions. Decomposition of plant matter is inhibited in these bogs due to the low microbial activity (Lindsay, 1995; Brady and Weil, 1999) and, also, to some extent, because *Sphagnum* mosses are more resistant to decay compared with other plants (Richardson, 1981). The accumulation of bog plant remains over time resulted in the formation of a peat dome, thus producing a raised ombrotrophic peat bog system (Lindsay, 1995; Brooks and Stoneman, 1997).

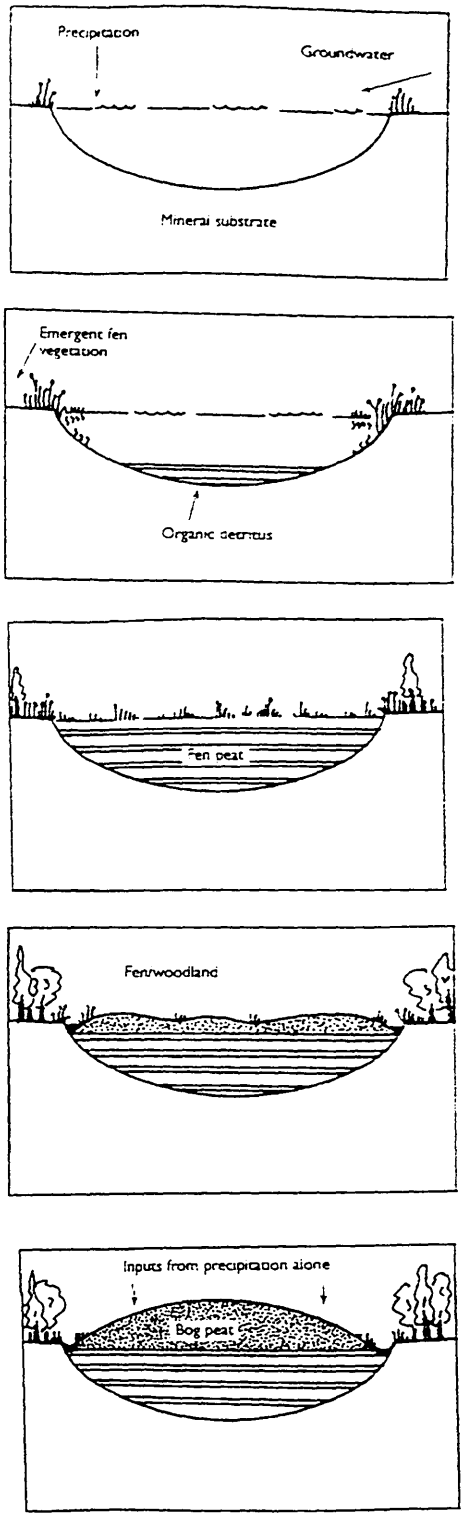

Figure 1.5: Stages in the formation of a raised peat bog (Brooks and Stoneman, 1997).

Figure 1.6: Photograph of *Sphagnum* moss stem.

1.4.2.6 Peat decomposition and accumulation

The decomposition of plant material occurs *via* aerobic decay processes in the aerated surface layers of the bog and slow anaerobic decay processes in the waterlogged deeper layers of the bog, as represented by the following simplified equations, where CH_2O represents the peat organic matter (Kellner, 2003):

$$\text{Aerobic decay: } CH_2O + O_2 \rightarrow CO_2 + H_2O$$

$$\text{Anaerobic decay: } 2CH_2O \rightarrow CH_4 + CO_2$$

Decomposition leads to the removal of organic matter in the form of gases such as carbon dioxide (CO_2) and methane (CH_4). During decomposition, the peat changes structure from the fresh plant material successively into amorphous humic matter and is accompanied by intense mass loss. As the overall decay is less than the accumulation of peat, however, the latter occurs at a rate of approximately two millimetres every year. After thousands of years of such accumulation, the central part of the bogs may rise more than ten metres above the fen deposits (Lindsay, 1995; Kellner, 2003).

1.4.2.7 Structure and hydrology of raised bogs

The great mass of plant accumulations that make up raised bogs provide their gross shape, structure and hydrological functions (Lindsay, 1995). The raised bog structure is made up of two layers, the upper thin layer (0.2 to 0.8 m deep), known as the acrotelm, and the lower much thicker layer (1 to 10 m deep), known as the catotelm

(Fig. 1.7). The acrotelm consists of largely vertical stems of *Sphagnum* mosses and vascular plants. Plant growth, death and aerobic and anaerobic decay processes all occur here along with water losses through evapotranspiration and lateral water flow, which is permitted in this layer due to its high hydraulic conductivity. The catotelm consists of a bulky amorphous mass of partly decayed plant material produced by the collapse of individual plant stems. Slow anaerobic decay occurs in this layer and, as it has a poor hydraulic conductivity, water movement is very slow with the result that the layer always remains completely saturated. Raised bogs develop and survive when water losses through seepage and surface evaporation are matched or exceeded by regular precipitation input, thus maintaining a stable water table within the bog that usually never drops down into the catotelm (Ingram, 1978; Damman, 1986; Lindsay, 1995; Bragg and Tallis, 2001).

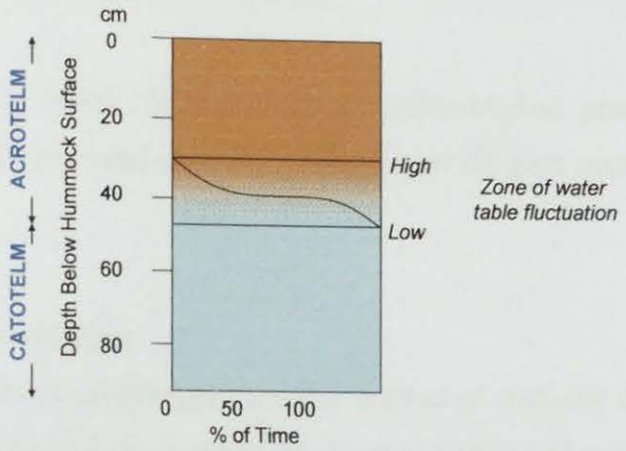

Figure 1.7: Raised bog structure (redrawn from Damman, 1986).

1.4.2.8 Raised bog surface microforms

The bog surface is characterised by zones of vegetation known as microforms (or micro-habitats) such as hummocks, hollows, pools, ridges and lawns, which each have their own assemblage of *Sphagnum* species. They evolve on the bog surface due to the intense competition between species for living space and are distributed on different parts of the bog surface in relation to the position of the water table (Lindsay, 1995). A photograph of the most common hummock-hollow topography observed on bog surfaces is shown in Fig. 1.8, hummocks being the more elevated mounds of peat and hollows the lower level water-filled peat depressions. The

processes and factors behind the development of these microforms are uncertain but their structures seem to be stable over time and are likely to be initiated and developed through the combined effect of hydrological and biological factors (Johnson and Damman, 1991; Kellner, 2003).

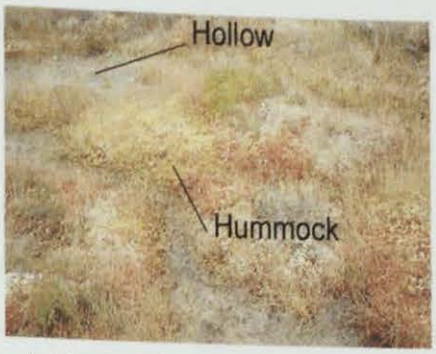

Figure 1.8: Photograph illustrating peat bog hummock-hollow topography.

1.5 PEAT MATRIX PROPERTIES

The interpretation of metal concentrations in ombrotrophic peat bog profiles is constrained by the physical and chemical properties of the peat matrix, which will be discussed below.

1.5.1 Peat composition

Peat is a brownish-black waterlogged organic deposit of partially decomposed plant remains and in its natural state is made up of water (90%) and solid material (10%) (Kellner, 2003). The chemical composition of peat can be understood in terms of the diagenetic processes that occur during death and decomposition of bog plants. The living plants contain mainly proteins, carbohydrates, lipids and polyphenols. When a plant dies and decomposes, its carbohydrates are rapidly released into the surroundings and nitrogen in plant proteins is lost, largely as ammonium salts going into solution, but some of the amino acids or their derivatives appear in the formation of peat humic substances. Traditionally, humic substances can be subdivided into humic acids, fulvic acids and humin (Stevenson, 1994) and the resulting peat has different proportions of these humic substances, with poorly humified peat containing more of the high molecular weight humic acids and well-humified peat

containing more of the low molecular weight fulvic acids. As the proportion of these substances is also different among different peat types and changes with peat depth, the diagenetic transformations that take place are very complex and still poorly understood (Blackford and Chambers, 1993; Kellner, 2003). The importance of these humic substances with respect to their use as a measure of decomposition and their role in metal-peat associations will be discussed in Section 1.7.1.

1.5.2 Ash content

Ash content is a measure of total peat inorganic content, which consists of both atmospheric mineral input and mineral components from plants present in the peat. It is quantified as mass of residual ash after peat combustion, which removes all organic matter present (Brooks and Stoneman, 1997). By definition, peat contains < 25% ash, with ombrotrophic bog peat typically containing < 15% ash (Hulme *et al.*, 1991; Shotyk, 1996a; Weiss *et al.*, 1998). Values in *Sphagnum* bog peat have been found as low as ≤ 2%, as inorganic material is predominantly supplied by airborne particles (Bindler, 2003). Ombrotrophic peat ash contents are variable from bog to bog and within bogs, both with regard to position in the bog and depth. Shotyk (1996a) stated that this difference may in part reflect the ash content of individual plant species, changing rates of peat accumulation and compaction and temporal differences in atmospheric dust inputs. Bindler (2003), for example, found higher ash contents in the surface and near surface peat samples from Swedish ombrotrophic peat bog profiles and suggested that these were attributed to nutrient retention and cycling and also possibly an increased influx of soil dust.

1.5.3 Bulk density

Peat bulk density is a measure of the dry weight per unit volume of fresh peat and is a function of changing rates of peat accumulation and compaction (Brooks and Stoneman, 1997). It is also thought to be a function of peat decomposition and Cocozza *et al.* (2003), using detailed spectroscopic characterisation of organic matter, provided evidence that peat bulk density did reflect the variation in peat decomposition in a core from Etang de la Gruère (EGR) in the Jura Mountains in

Switzerland. Shotyk *et al.* (2003) also studied the bulk density profile and concentration profile of the conservative element, Zr, in a peat core from Greenland and suggested that Zr concentrations should increase in concentration with increasing extent of peat decay. It was found that the differences in bulk density were comparable to those in Zr concentration, suggesting that bulk density is a reliable parameter that helps to take account of any changes in metal concentrations that result from the decomposition of organic matter. As different plant species are thought to decompose at different rates (Blackford and Chambers, 1993), however, bulk densities may be affected by the peat botanic composition.

1.5.4 Optical absorption of NaOH extracts of peat

Another direct method of determining peat decomposition (degree of peat humification) is by measuring the optical absorption of NaOH extracts of peat. This is based on the discovery by Overbeck (1947) that the colour of peat NaOH extracts is indicative of the degree of humification. Aaby (1986) later measured optical absorption of peat NaOH extracts by colorimetry as a more quantitative method of determining the degree of humification. This technique is possible as it utilises the luminescence properties of the polyphenolic groups present in humic and fulvic acid molecules, where luminescence intensity variations are proportional to the concentration of these dissolved acids. For this particular luminescence application, the absorption of light at a wavelength of 540 or 550 nm is examined, as these wavelengths represent a single point on the tail of an absorption curve of the organic acids, where the higher molecular weight humic acids, generally found in the poorly decomposed peat samples, exhibit lower percentage absorption values (Caseldine *et al.*, 2000). For the purpose of palaeoclimatic studies, Blackford and Chambers (1993) tested and improved this NaOH extraction procedure and concluded that it provided a robust and replicable record. Some workers have applied this procedure to determine the degree of humification in samples from peat cores for atmospheric deposition studies (Givelet *et al.*, 2003). The technique, however, has been criticised by Caseldine *et al.* (2000), who carried out a comparative study of optical properties of NaOH peat extracts and found that during boiling in NaOH any high molecular

weight aromatic organic acids are broken down to lower weight amino acids and sugars, therefore affecting the acid composition of the peat extracts. It was suggested, however, that, as long as a standard procedure is followed, the degree of extra breakdown caused should remain constant. Also, as with bulk density, optical NaOH peat extract measurements may be dependent on botanical composition, and, if differential decay between plant species is observed, the technique should be seen as unreliable (Caseldine *et al.*, 2000).

1.6 PEAT TROPHIC STATUS

Only truly ombrotrophic systems are usually considered for use in atmospheric metal deposition studies. Ombrotrophic peat bog layers, however, overlie minerotrophic fen peat layers and it is therefore important, when investigating atmospheric metal deposition in peat bog systems, to assess the trophic status of the peat. If possible, the depth at which the peat changes from being exclusively ombrotrophic (bog) to predominantly minerotrophic (fen) should be determined.

1.6.1 Identification of peat trophic status

Various properties can be used to independently evaluate the trophic status of peat bogs. For example, peat bog water pH and dissolved ion concentration measurements can indicate the ombrotrophic nature of peat bogs. The peat botanical composition can also give an indication of trophic status, since ombrotrophic peat is generally *Sphagnum*-dominated and minerotrophic peat is generally *Carex*-dominated (von Post and Granlund, 1925). The problem with this, however, is that plant species are often difficult to identify in more decomposed peat layers. Ash contents, however, can be used instead, as minerotrophic fen peats generally have higher ash contents than ombrotrophic bog peats (Shotyk, 1996a). Ca/Mg ratios have also been used by many workers (Shotyk, 1996a; Shotyk *et al.*, 1996 and 2002; Martinez-Cortizas *et al.*, 1997; Steinnes, 1997; Weiss *et al.*, 1997, 2002a). It can be assumed that peat with Ca/Mg ratios lower than or comparable to rainwater is ombrotrophic; otherwise, the peat has an additional non-atmospheric source of Ca and is therefore

minerotrophic (Shotyk, 1996a). The logic underlying this approach, as explained by Weiss *et al.* (2002a), is that, in seawater, the global average Ca/Mg ratio is very low (~ 0.32) (Berner and Berner, 1997) and in marine and coastal rainwaters, the global average Ca/Mg ratios are also low, ranging from ~ 0.5 to 1. Compared with the global average Ca/Mg ratio in the Earth's crust of ~ 1 (Wedepohl, 1995), terrestrial waters in which water-soil interactions have taken place generally have higher Ca/Mg ratios due to the preferential release of Ca over Mg during weathering. For example, the global average river water Ca/Mg ratio is 2.2 (Livingstone, 1963). Continental rainwater, however, is also enriched in Ca because of the increasing dissolution of mineral particles from soil-derived dust and global average Ca/Mg ratios from ~ 2 to 6 have been determined (Berner and Berner, 1997). When determining Ca/Mg ratios in peat bog profiles, those in local rainwater should also be measured, if possible, for comparison with those obtained for deeper peat layers and examination of influences from mineral dissolution.

1.7 BEHAVIOUR OF METALS DEPOSITED IN OMBROTROPHIC PEAT BOGS

The use of metal concentration profiles from ombrotrophic peat bogs for the reconstruction of atmospheric pollution histories relies upon the assumption that their vertical distribution in peat cores directly records temporal variations in input as a consequence of changing levels of atmospheric contamination. Metal concentration profiles, however, are potentially influenced by a whole range of interactions and processes occurring within the peat bog system, some of which have already been mentioned above (e.g. peat decomposition).

1.7.1 Interaction of metals with peat

The initial associations of metals in the peat bog system are determined by the nature of the surface on which they are deposited which, in the case of peat bogs, is dominated by moss species. The effective absence of a vascular system in mosses necessitates a relatively unrestricted exchange of solutes between the atmosphere and

the living plant tissue, and as mosses have evolved efficient uptake mechanisms for absorbing metals and other nutrients from their environment, they take up ions over their entire surface, accumulating metal ions extracellularly via ion-exchange and particulate trapping (Richardson, 1981). Zechmeister *et al.* (2003) found that the efficiency of uptake of the most common heavy metals by mosses followed the order Pb>Co,Cr>Cu,Cd,Ni,V>Zn>As. Clymo (1963) has shown that the high metal-binding ability of mosses is closely related to the high concentration of protonated anionic functional groups (ion exchange sites) in the form of unesterified polyuronic acids. The exceptional ability of *Sphagnum* species to accumulate metals is largely attributable to their high content (up to 30% by mass) of these acids.

It has been found that metal uptake increases sharply with death of the plant material and the onset of decay and that it continues to increase as decomposition proceeds, since the humic substances, formed on decomposition (*cf.* Section 1.5.1), have the greatest influence on the metal-binding properties of the peat (Livett, 1988). Humic substances contain many different functional groups and can be viewed as polyfunctional ligands (Fig. 1.9). These substances have a large specific area with aliphatic and aromatic components. It is the oxygen-containing carboxyl, phenolic and alcoholic hydroxyl functional groups that are in most abundance, providing sites for cation exchange and therefore metal binding, but the other functional groups, such as nitrogen-containing heterocycles, amines and nitriles and sulfur-containing sulfide and thiol groups, are also important (Sparks, 1995; Logan *et al.*, 1997; Kellner, 2003).

Humic-metal complexes can be grouped into two main types, outer-sphere and inner-sphere complexes, each of which has differing degrees of mobility and metal bioavailability. Outer-sphere complexes have a purely electrostatic nature and both the ligand(s) and the metal ion retain their hydration spheres. In this ionic type of interaction, the metals are held in an exchangeable form and are therefore easily displaced, becoming more mobile and available for plant uptake (Bonn and Fish, 1993).

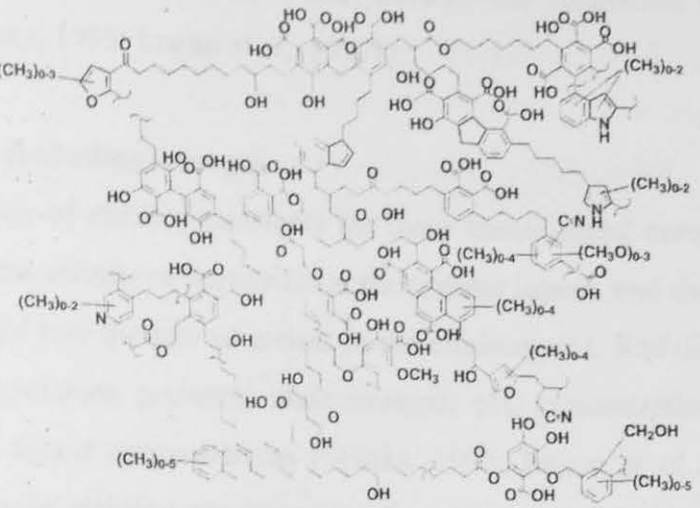

Figure 1.9: Schematic of humic acid structure (Sparks, 1995).

Inner-sphere complexes result in the formation of a covalent co-ordination bond between the ligand(s) and the metal ion, with partial or total breakdown of the hydration sphere of the metal. In this strong covalent type of interaction the metals are difficult to displace and are essentially immobile (Logan *et al.*, 1997). It should be noted, however, that in most cases complexes tend to have a component of both types of bonding and spectroscopic, conductimetric and kinetic evidence have been used to establish the degree to which a complex is of outer- or inner-sphere character. For example, the $CrSO_4^+$ complex was found to be about 27% outer and 73% inner sphere (Langmuir, 1997).

The ability of metal ions to react with specific ligand atoms determines which type of complex is formed and they can be classified using the concept of hard and soft acids and bases (Pearson, 1963). Metal cations that are small, compact and not very polarizable (e.g. Ca^{2+} and Mg^{2+}) prefer ligands that are less polarizable (e.g. O-containing ligands) and are known as hard acids and bases. The larger and more polarizable metal cations (e.g. Pb^{2+} and Cu^{2+}) prefer ligands that are more polarizable (e.g. S-, P- and N-containing ligands) and are known as soft acids and bases. In general, hard acids prefer to react with hard bases and soft acids prefer soft bases. The hard acid-hard base interactions tend to produce outer-sphere complexes, while

the soft acid-soft base interactions tend towards the formation of inner-sphere complexes (Sparks, 1995; Logan *et al.*, 1997).

1.7.2 Metal-binding strength

The determination of stability constants for these humic-metal complexes provides information on the affinity of the metal for the organic ligand, and therefore provides a valuable insight into the fate of metals in the environment. Stability constants are affected by temperature, pressure, ionic strength, pH, concentration of competing metal ions and ligand concentrations (Sparks, 1995; Logan *et al.*, 1997; Kellner, 2003). For example, stability constants were found to be slightly higher at pH 5 than pH 3.5, due to the higher dissociation of functional groups, particularly carboxyl groups, at the higher pH. Also, H^+ and the metal ions compete for binding sites on the ligand and less metal is bound at the lower pH (Schnitzer and Hansen, 1970). Krosshaven *et al.* (1992) examined the binding of Cd, Cu, Pb and Zn in organic matter and concluded that Pb and Cu are sorbed at all pH levels, whereas Cd and Zn appeared to be more influenced by pH. At the natural pH for peat bogs, the binding was found to be ~ 75-85%, which may suggest a slight mobility of Cd and Zn in ombrotrophic peat bogs.

Although the selectivity of organic matter for various cations does not conform to any absolute rules, some trends have been observed. For example, Irving and Williams (1948) found that humic complexes of bivalent ions followed the order of stability, $Pb^{2+}>Cu^{2+}>Cd^{2+}>Zn^{2+}>Ca^{2+}$. Gao *et al.* (1999) determined stability constants of complexes formed between humic acids extracted from peat and Pb^{2+}, Cu^{2+} and Zn^{2+} and found the same trend, with Pb^{2+} cations forming the most stable complexes. Livett *et al.* (1979) also indicated that peat had a greater affinity for Pb than for Zn or Cd. Also, Shotyk (1996b) reported that more than 99.9% of Cu^{2+}, Pb^{2+} and Zn^{2+} should be bound to an organic phase and that migration in the peat profile may be significantly retarded by organic complexation, especially for Pb. In the case of the major metals, Ca and Mg, Shotyk (1997) studied atmospheric deposition in oceanic peat bog profiles from Scotland and found that 91.5 to 99.9% of the highly

soluble, Ca^{2+} and Mg^{2+}cations, supplied to the bog were not retained by peat. As well as the solid phase organic matter (i.e. peat), the presence of dissolved organic matter is also important, especially with respect to the mobility of metals in peat bogs. Dissolved humic substances present in peat bog waters, for example, can form stable, soluble complexes with metals deposited in bogs and can lead to the migration of these metals within the peat bog profile (Sparks, 1995).

1.7.3 Other factors affecting the retention and mobility of metals in ombrotrophic peat bogs

The content and distribution of metals in ombrotrophic peat bogs is determined by their retention and mobility, which are influenced by metal-peat interactions, as well as by a variety of chemical and biochemical metal transformations which can take place. These transformations may facilitate the post-depositional migration of metals (and other elements) by liberation from the solid phase peat and removal by diffusive or advective flow in the peat bog waters (Görres and Frenzel, 1997; Shotyk *et al.*, 1997). Some of these complex metal/peat bog properties and processes which occur within the bog will now be discussed.

1.7.3.1 Metal speciation and peat bog pH-redox environment

The transport and partitioning of metals in peat bogs is controlled by the solubility of the specific chemical form present, which is firstly determined by the emission source of the deposited metals and in turn by the peat bog water pH and redox environment (expressed in terms of pE and E_h), which control the potential transformations of the deposited metals (Shotyk, 1988). It is generally impossible to say with certainty which forms of metals are released from natural and anthropogenic sources and what forms are deposited on the surface of ombrotrophic peat bogs, but, in general, metals released into the atmosphere are present as particulate matter in the form of oxides, sulfates or carbonates. Metals emitted from combustion processes, for example, are present as oxides, while metals emitted from smelters, which co-emit SO_x gases, might be expected to be released largely as sulfates and sulfides. It must be remembered, however, that the speciation of the emitted metals can

undergo complex reactions under the oxidising conditions of the atmosphere (Schroeder, 1987).

As mentioned previously in Section 1.4.1, peat bog waters are characteristically acidic with typical pH values in the range of ~ 3.5 – 4.5 but values can vary through the peat bog profile and pronounced seasonal differences have been observed (Shotyk, 1988). Atmospheric metal deposition in these acidic environments takes place at the usually high redox potential, aerobic acrotelm surface and, due to peat growth by accretion, deposited metals are progressively incorporated into the low redox potential, anaerobic catotelm. The redox boundary occurs at the zone of water table fluctuation (Damman, 1978) and Clymo (1983) suggested that one of the most important causes of metal remobilisation in peat bogs is the fluctuation in redox potential associated with water table movements in the acrotelm, which can exhibit inter-annual and seasonal variation.

The redox-sensitive elements Fe and Mn are considered to be subjected to post-depositional mobility. Under the aerobic acrotelm environment, Fe and Mn form insoluble $Fe(OH)_3$ and MnO_2 precipitates, but, under the reducing anaerobic catotelm environment, Fe and Mn are reduced to the soluble Fe^{2+} and Mn^{2+} cations (Shotyk, 1988, Steinmann and Shotyk, 1997). MacKenzie *et al.* (1998b), for example, studied Fe and Mn concentration profiles in an ombrotrophic peat core from west-central Scotland and found that the distribution of Fe and Mn did not correspond to temporal variations in deposition of either windborne minerals or inorganic material (i.e. ash content distribution). It was suggested that the distribution of these elements reflected reduction and dissolution under reducing conditions in the bog and the rapid decrease in Mn concentrations immediately below the surface, compared with the persistence of high Fe concentrations with depth, was attributable to Mn being more readily reduced and therefore being depleted closer to the surface than Fe. Other workers (Görres and Frenzel, 1997; Benoit *et al.*, 1998), however, suggested that the high surface concentrations of Mn found in peat bogs are most likely due to uptake and recycling by vegetation (i.e. plant bioaccumulation) (Section 1.7.3.3). If

the redox-driven Fe transport mechanism is accepted, the distribution profiles of Fe in peat bogs could provide an indication of the redox boundary (i.e. zone of water table fluctuation) (Damman, 1978; Shotyk, 1988; Benoit *et al.*, 1998) and also allow the examination of possible redox-related post-depositional migration processes occurring for the trace metals of interest in this investigation. For example, Clymo *et al.* (1990) found that the distinct Fe concentration peak, in an ombrotrophic peat core from south-west Scotland, occurred just between the high water table depth and where the pE becomes negative, i.e. the peat bog redox boundary.

S is another redox-sensitive element and wet deposition in the form of sulfate (SO_4^{2-}) is the main source of S to the surface layers of ombrotrophic peat bogs (Shotyk, 1988). Steinmann and Shotyk (1996) reported that inorganic S species in peat bog porewaters were present only in small amounts, in the form of sulfate in the aerobic acrotelm and sulfide (S^{2-}) in the anaerobic catotelm and that ~ 90-99% of the dissolved S species in peat bog pore waters were associated with humic matter. It is worth noting that anthropogenic processes, such as the burning of fossil fuels, increased atmospheric loadings of S greatly, mainly as sulfate provided by "acid rain", and cores from ombrotrophic peat bogs have been used to investigate atmospheric pollutant loading of S (Novák *et al.*, 2003; Bottrell *et al.*, 2004). P is another redox-sensitive element and its geochemistry in ombrotrophic peat bogs is probably affected by the concentration of dissolved organic matter, total dissolved Fe and pH (Shotyk, 1988). Others (Malmer, 1958; Damman, 1978) have suggested, however, that the high surface concentrations of P in peat bogs, as for Mn, are most likely due to plant bioaccumulation (Section 1.7.3.3).

The most common elements that regulate the redox potential in peat bogs are O, C, N, S and P, and the dissolution or precipitation of metals as oxides, carbonates, nitrates, sulphides and phosphates affects the abundance and distribution of metals in the bogs (Shotyk, 1988). These metal-containing compounds can themselves also affect the distribution of other metals in peat bogs, for example, Hg is thought to

have a high adsorptive affinity to Fe and Mn oxides and hydroxides (Roulet and Lucotte, 1995).

In the case of the heavy metals Cd, Cu, Pb and Zn, pE-pH diagrams (Fig. 1.10) suggest that these metals would perhaps be present in the form of dissolved metal cations (e.g. Cd^{2+}, Cu^{2+}, Pb^{2+} and Zn^{2+}) in acidic bog waters. These dissolved metal cations are potentially mobile, especially due to the high concentration of dissolved organic matter.

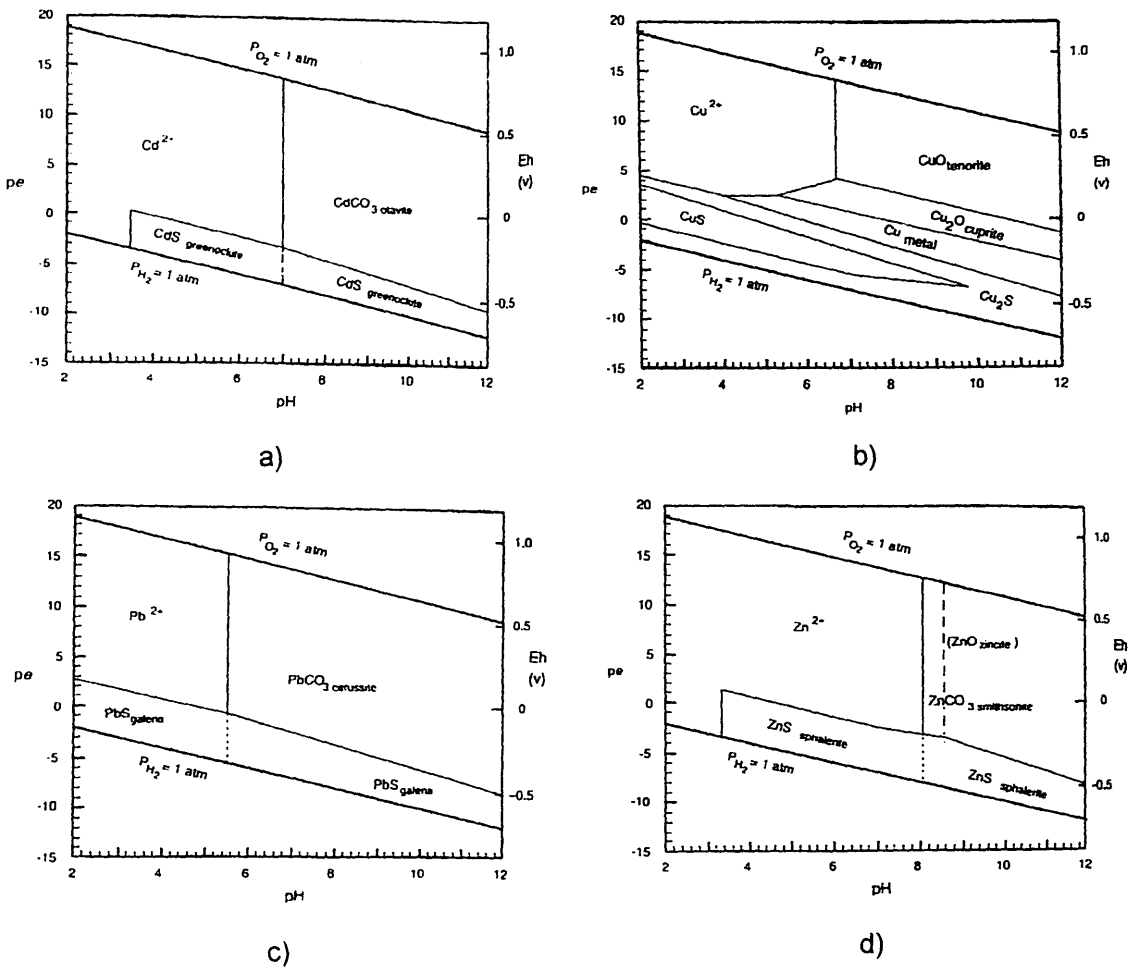

Figure 1.10: Simplified pE-pH diagram for the system a) Cd-CO_2-S-O-H_2O, b) Cu-S-O-H_2O, c) Pb-CO_2-S-O-H_2O and d) Zn-CO_2-S-O-H_2O at 25°C and 1 atm (Drever, 1982).

The abundance of solid organic matter in peat bogs, however, may hinder their mobility. For example, Shotyk (1988) reported that, under low pH conditions, Pb may be mobilised as Pb^{2+} regardless of the redox potential but, in view of the abundance of humic substances, much of the Pb may be complexed. The immobility

of Pb in ombrotrophic peat bogs is now well established and the most recent hypothesis by Shotyk (Sanderson, 2004) is that complexes formed between Pb and humic substances are so large that they are essentially immobile. The immobility of Pb will be discussed further in Section 1.7.4. It is worth noting that, as conditions become reducing in the catotelm and as sulfate reduction occurs, the Cd, Cu, Pb and Zn cations may precipitate as sulfides (CdS, CuS, HgS, PbS and ZnS) (Drever, 1982; Shotyk, 1988; Benoit *et al.*, 1998).

The behaviour of Hg is more complex as in its elemental form it has a high volatility, low chemical reactivity and low water solubility. The thermodynamically stable forms are shown in Fig. 1.11. Under aerobic, acidic peat bog conditions, its soluble forms are Hg^{2+} and Hg_2^{2+}, and under anaerobic acidic conditions, like Cd, Cu, Pb and Zn, it may be transformed to its sulfide in the presence of S (Drever, 1982).

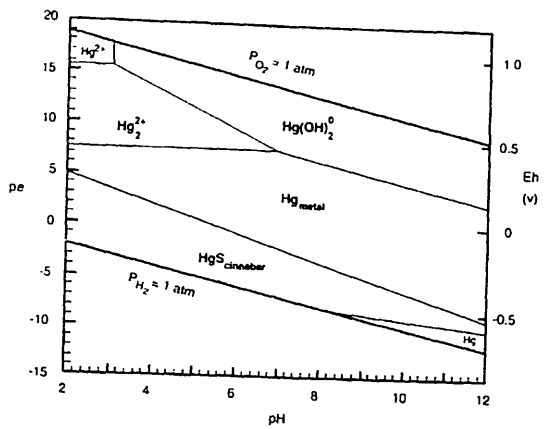

Figure 1.11: Simplified pE-pH diagram for the system Hg-S-O-H_2O at 25°C and 1 atm (Drever, 1982).

In contrast, the metalloids Se and As (Fig. 1.12) both occur in solution as anions or as neutral species rather than as cations. Under the acidic, oxidising conditions of the acrotelm, As (V) is the dominant form of As, which is present as arsenic acid (H_3AsO_4) and its arsenate anion ($H_2AsO_4^-$). The dominant forms of Se under these conditions are selenate (SeO_4^{2-}) and biselenite species ($HSeO_3^-$). When conditions become reducing in the catotelm, As (V) is reduced to As (III) and, as sulfate reduction occurs, As may also precipitate as a sulfide. In the case of Se, elemental Se and hydrogen selenide (H_2Se) species may form. Also, Farmer and Lovell (1986)

investigated As concentration profiles in sediments from Loch Lomond in Scotland and attributed the distribution of As to post-depositional diagenetic remobilisation processes in sediment reducing zones, followed by upward migration of As through interstitial waters and oxidation/adsorption/precipitation reactions in near-surface oxidising layers. Whether these processes are also important in the mobilisation of As in peat bogs needs to be investigated further. Nieminen *et al.* (2002) estimated Cu, Ni, Zn, Pb and As accumulation in the surface layers of an ombrotrophic peat bog near a Cu-Ni smelter in south-west Finland and reported that As, Ni and Zn were more mobile than Cu and Pb, but, since the amount of loss through migration remained unknown, the retention mechanisms of these elements required further investigation.

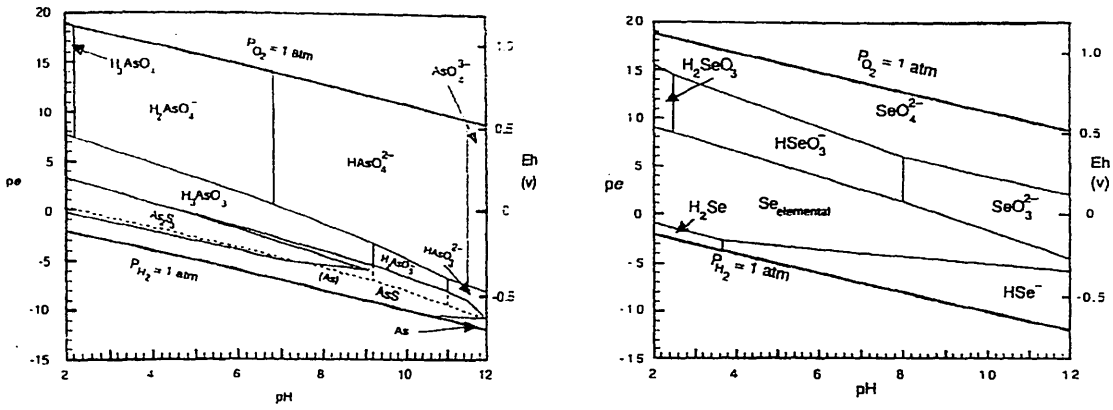

Figure 1.12: Simplified pE-pH diagram for the system a) As-O-H_2O and b) Se-O-H_2O at 25°C and 1 atm (Drever, 1982).

1.7.3.2 Peat bog hummock-hollow topography

As mentioned earlier in Section 1.4.2.8, ombrotrophic peat bog surfaces consist of a hummock-hollow topography. Hummocks and hollows are thought to have differential element mobility characteristics relating to differences in water table position and the hydrological processes taking place, with the result that there are conflicting views with regard to whether hummocks or hollows should be used to investigate atmospheric records of metal deposition. For example, Pakarinen and Tolonen (1976) and Pakarinen (1978) suggested that hummocks provide unfavourable conditions for pollution monitoring since metals are likely to be remobilised as a result of the more rapid water flow that can occur in these

microforms compared with hollows. Damman (1978) also suggested that elements were probably removed from these well-drained peat hummocks but accumulated in the waterlogged peat hollows. Norton *et al.* (1997) compared Pb and Hg fluxes to hummocks and hollows of an ombrotrophic peat bog in Maine, USA. Higher maximum atmospheric Pb and Hg fluxes, along with higher ^{210}Pb inventories, were recorded in hummocks and it was suggested that both microforms recorded trends in atmospheric deposition of Hg and Pb, but hollow cores were recording lower input values than hummock cores due to the enhanced interception of atmospheric particles and dry and occult deposition by hummocks. Hummock cores were also found to produce more reproducible data than hollow cores. Urban *et al.* (1990), however, suggested that diagenetic remobilisation of Pb in hollow cores accounted for the higher Pb concentrations and ^{210}Pb inventories found in hummock cores compared with hollow cores.

Benoit *et al.* (1998) recommended that sampling be carried out on hummocks rather than hollows because, in the former, a larger portion of peat lies above the high water table position and element retention is more efficient, compared with hollows, due to the deeper aerobic layer of hummocks. Livett (1988) also suggested that the higher accumulation rates of hummock peat might reflect small-scale changes in metal deposition more accurately than the slowly accumulating peat hollows. Biester *et al.* (2003) and Givelet *et al.* (2004), however, suggested that the above problems associated with hummocks and hollows should be avoided by using peat cores taken from "lawns", which are the microforms at the transition between hummock and hollow.

1.7.3.3 Vegetation uptake and nutrient cycling

Relocation of elements may also occur by advection, dispersion and diffusion by biological processes occurring in the living vegetation layer of the acrotelm (Kellner, 2003). There is evidence that relocation of some elements between different parts of *Sphagnum* mosses may occur (Clymo, 1983). For example, the essential element P has been found in high concentrations in the upper parts (capitula) of these moss

species due to nutrient cycling (Malmer, 1958; Damman, 1978). Often vascular plants, such as heather, grow on the surface of ombrotrophic peat bogs and they can absorb nutrients and other metals through their roots and subsequently relocate them both upwards into stems and leaves and downwards by root growth (Kellner, 2003).

For plants, the essential macronutrients are Ca, K, Mg, N, P and S, while essential micronutrients are B, Cu, Fe, Cl, Mn, Mo and Zn. Small concentrations of Se, Co, Si and V, however, also appear to be beneficial to plants (Faure, 1998). It would therefore be expected that these elements are subjected to nutrient recycling processes in peat bogs. For example, Weiss *et al.* (2002b) studied the geochemistry of a selection of major and trace elements in a forested tropical peat bog from Kalimantan in south-east Asia and reported that Ca, Mg, S and P were strongly enriched in the surface layers of the bog due to biological accumulation mechanisms. The relative importance of plant accumulation of the bioessential elements Cu and Zn is more difficult to determine, since these metals have a strong affinity for peat (Shotyk, 1988). Espi *et al.* (1997) measured changing concentrations of Cu, Zn, Cd and Pb in a high altitude peat bog from Bolivia and suggested that the living plant layer may be responsible for enrichments observed for Cu, Zn and Cd. They reported that, even though Cd has no biological function, it behaves in a similar way to Zn, as its coordination chemistry is similar.

Most metals that are not essential for plant growth (e.g. Pb) have been shown to be unaffected by plant bioaccumulation (Shotyk, 1988). For example, Krachler *et al.* (2003a) investigated V, Cr and Ni distribution profiles in a Swiss peat bog and found that these metals appeared to be associated with mineral particles that were well preserved in ombrotrophic peat layers and that there was no significant enrichment in the surface *Sphagnum* moss layer. They therefore concluded that these metals are effectively immobile (i.e. not available to the pore fluids for migration) and enrichments were suggested to be caused by the deposition of aerosols rather than by plant bioaccumulation.

Rausch *et al.* (2005a) compared the atmospheric deposition of Cu, Ni, Co, Zn and Cd recorded by three Finnish peat cores, one core representing a low-background site but the other two having known metal deposition histories from local point sources (a Cu-Ni mine and concentration plant, and Cu-Ni smelters, respectively). They found that Cu and Co accumulation rates reflected the general trends in deposition histories very well except for the site of greatest metal loading (the site situated next to the Cu and Ni smelters). Ni, Zn and Cd accumulation rates did not reflect the chronology of their atmospheric inputs and this was suggested to be due to plant uptake and cycling of these metals. In a more recent investigation of these sites, Rausch *et al* (2005b) found further evidence from peat pore waters for the post-depositional migration of these metals at the site situated next to the Cu and Ni smelters. They also reported that sites which are remote from point sources and receive metals exclusively by long-range transport are more conducive to preserving the chronology of deposition and that peat cores may or may not function as archives of atmospheric trace metals, depending on the concentration and chemical properties of the metal being considered, the mineralogical form at the time of deposition, and the pH of the bog waters.

Yafa (2004) studied the atmospheric deposition of a range of elements in a peat core from Flanders Moss ombrotrophic peat bog in west-central Scotland, a site which was also investigated in this research project. Elemental distributions of Mn, P, S and Zn were attributed to nutrient uptake and recycling, those of As, Cd, Cr, Cu, Pb, V and S to historical variations in anthropogenic emissions, those of Fe and P to post-depositional remobilisation and redistribution processes occurring in the bog, and that of Zn also possibly to the influence of sulfide formation.

In summary, so many diverse views have been expressed during the past 30 years concerning the possible mobility of elements in ombrotrophic peat bogs that it is difficult to arrive at a firm conclusion. In the case of Pb, however, it is now generally accepted that this element is essentially immobile in ombrotrophic peat bogs, as discussed in more detail below.

1.7.4 Immobility of Pb in ombrotrophic peat bogs

Ombrotrophic peat bogs were suggested many years ago to be useful archives of atmospheric deposition of Pb (Lee and Tallis, 1973). There has, however, been some speculation about the diagenetic mobility of Pb in peat bogs, including a suggestion by Urban *et al.* (1990) that Pb is mobile in peat hollows, especially around the water table (*cf.* Section 1.7.3.2). Damman (1978) also argued that Pb was subject to diagenetic mobility and re-deposition in the zone of water table fluctuation but Görres and Frenzel (1997) observed no preferential accumulation of Pb in this zone and chemical modelling, stratigraphical analysis and ^{210}Pb dating results reported by Bränvall *et al.* (1997) also illustrated that characteristic Pb profiles were not a result of hydrological or diagenetic causes. Vile *et al.* (1999) evaluated Pb mobility in peat profiles by adding either soluble or particulate Pb to intact peat cores that were maintained under different water level regimes. They found that Pb was retained in peat through physiochemical binding to organic matter even under conditions of fluctuating water table. Also, Weiss *et al.* (1999b) found that transformations involving pH, redox and dissolved organic matter in bog waters did not significantly affect the ability of peat to preserve the changing record of atmospheric Pb deposition while Espi *et al.* (1997) observed that bioaccumulation processes did not influence the distribution of Pb in peat bogs.

The isotopic composition of Pb (Section 1.10) in dated peat cores has also provided evidence that vertical downward migration of Pb in peat bogs does not occur, as consistency of peat core stable Pb isotope data with trends in historical inputs from various activities have been found by numerous workers (Shotyk *et al.* 1996a; Brännvall *et al.*, 1997; Farmer *et al.*, 1997b; Weiss *et al.*, 1997; MacKenzie *et al.*, 1998a, 1998b; Renberg *et al.*, 2001). Further evidence for the immobility of Pb in peat bogs has been provided by the comparable results obtained between different peat cores as well as with other environmental archives (*cf.* Section 1.3.3). It is now widely accepted that Pb is effectively immobilised by peat, and therefore that records of historical atmospheric Pb deposition are preserved in ombrotrophic peat bogs.

1.8 USE OF CONSERVATIVE ELEMENTS TO ESTIMATE ANTHROPOGENIC ENRICHMENTS OF METALS IN OMBROTROPHIC PEAT BOGS

Once the immobility of a metal in ombrotrophic peat is established, conservative elements can be used to estimate anthropogenic enrichments of this metal. Studies that rely exclusively upon analyses of metal *concentrations* in age-dated peat cores are inadequate when studying atmospheric metal deposition records in ombrotrophic peat bogs because accurate pollution histories cannot be obtained without including a detailed study of both the natural and anthropogenic sources of metals to the bogs (Shotyk, 1996a).

1.8.1 Conservative elements

Conservative elements are lithogenic elements that have no anthropogenic source and are therefore influenced by natural dust inputs alone and they may, in theory, serve as useful indicators of natural atmospheric aerosols deposited on bog surfaces (Görres and Frenzel, 1997). Elements that are emitted from anthropogenic activities are present in the atmosphere at concentrations that are considerably more than would be expected from the weathering of crustal materials (Brimblecombe, 1996) and, by normalising concentrations of these elements to a conservative element, the extent of anthropogenic enrichment can be readily quantified (Krachler *et al.*, 2003b). The effect of variations in peat matrix properties such as bulk density (*cf.* Section 1.5.3) and ash content (*cf.* Section 1.5.2) can also be easily eliminated by normalisation to a conservative element (Kempter *et al.*, 1997; Shotyk *et al.* 2003).

Although conservative elements have no significant anthropogenic sources, it must be remembered that there can, of course, be human-related impacts upon soil dust input (e.g. arising from clearance of land for agricultural purposes). Brännvall *et al.* (1997), for example, reported that transport of atmospheric soil dust was probably accelerated by the introduction and expansion of agriculture. Also, Kempter *et al.* (1997) studied Ti (and Pb) concentrations in ombrotrophic peat cores taken from

eight European regions and found that variations in concentrations of the conservative element, Ti, corresponded to changes in intensity of soil dust inputs from forest clearances and agricultural developments, as also indicated by pollen grain analyses.

Conservative elements are thought to behave conservatively during weathering as they are present in chemically resistant accessory minerals, which, unless intense weathering has taken place, generally remain preserved and unaltered after deposition in peat bog profiles, their distribution in peat profiles reflecting the abundance of mineral material originally released to the atmosphere. Conservative elements are also thought to be unaffected by redox reactions or plant uptake processes in peat bogs (Shotyk *et al.*, 2001). Uncertainty remains, however, as to which conservative element is the most suitable to use when correcting for natural metal contributions to total metal concentrations in peat bog profiles. The elements most commonly used are Al, Sc, Ti, Y and Zr, which will be discussed in Section 1.8.4.

1.8.2 Use of elemental ratios

Instead of just using the magnitude of metal concentrations in peat bogs, the magnitude of enrichments relative to an appropriate conservative element needs to be considered. Elemental ratios (M/X) in peat samples, where M is the concentration of the element of interest and X is the concentration of the conservative element, can be used to distinguish between soil dust and anthropogenic sources of the element of interest. Since the concentration of the conservative element in peat samples can be used as a quantitative indicator of the variation in natural, lithogenic inputs to the bog, any changes in the elemental ratio relates to changes in the relative amount of the element of interest supplied to the peat by an additional source (e.g. anthropogenic) or even an enrichment or depletion due to post-depositional redistribution of the element (Steinmann and Shotyk, 1997). Elemental ratios in crustal rock composition data, such as provided by Wedepohl (1995) (e.g. the UCC values shown in Table 1.1), or other chosen "reference" materials, such as

"background" peat samples, can be used for comparative purposes. Shotyk (1996a), for example, found that Pb/Sc ratios in a 2110 year-old peat core from EGR, Switzerland, were always at least seven times higher than the UCC Pb/Sc ratio (0.9) (calculated using data of Shaw *et al.* 1967, 1976, in Wedepohl (1995)), which was taken to represent pre-anthropogenic, soil-derived aerosols.

Reimann and de Caritat (2000, 2005), however, pointed out that elemental ratios differ substantially from rock type to rock type and do not reflect calculated or modelled crustal ratios, which assume that these rocks have fixed compositions. Also, local variations in soil mineralogy and natural elemental fractionation processes (e.g. physical and chemical fractionation) that occur during the transfer of elements from the crust to the atmosphere are not taken into account. Weiss *et al.* (1997) also argued that crustal values represent a global average which does not take into account local variations in rock chemistry, which leads to an overestimation or underestimation of enrichment. In an attempt to overcome this it was suggested that local "background" values, selected from an appropriate reference period in the peat bog profile, where metal inputs are at their lowest and can be attributed solely to natural atmospheric soil dust inputs, should be used instead. Shotyk *et al.* (1998), for example, established the average natural background Pb and Sc concentrations in a peat core from EGR, Switzerland (which represented 12,370 ^{14}C years before present (B.P) worth of deposition), as those dating from 8,030 to 5,320 ^{14}C years B.P. This was based on the assumption that natural background concentrations of Pb were those proportional to Sc concentrations and that anthropogenic Pb concentrations were those that increased out of proportion to Sc concentrations. The natural background Pb/Sc ratio, which was taken to represent that of pre-anthropogenic natural atmospheric soil dust, was then calculated and the respective lithogenic and anthropogenic Pb concentrations in the peat samples of interest were estimated as follows:

$$[Pb]_{lithogenic} = [Sc]_{peat} \times [Pb]/[Sc]_{background}$$

$$[Pb]_{anthropogenic} = [Pb]_{total} - [Pb]_{lithogenic}$$

This approach using peat background values, however, is also limited with regard to both the selection of the reference period for background values and also the assumption that there must be a homogeneous background M/X ratio or at least a negligible variation when compared with pollution periods (Martinez-Cortizas *et al.*, 2002a).

1.8.3 Enrichment Factors (EFs)

EFs normalise elemental ratios of individual samples to elemental ratios derived from a chosen "reference" material in order to indicate the degree to which an element is enriched in a sample, compared with the abundance of that element in the chosen "reference" material. For example, EFs using UCC values are calculated as follows:

$$EF_{UCC} = [M]/[X]_{peat} / [M]/[X]_{UCC}$$

The use of EFs calculated by normalising elemental ratios of individual samples to elemental ratios derived from crustal rock composition data (Wedepohl, 1995) has been successful in previous peat bog studies in characterising aerosols from anthropogenic and natural sources (Shotyk 1996a; Shotyk *et al.*, 1996, 1997; Kempter *et al.*, 1997). Pb has been the most widely studied element and high EFs observed close to the surface of bogs have been attributed to industrial and post-industrial pollution. Enrichments have also been found in deeper peat sections and these have been attributed to pre-industrial pollution, e.g. arising from ancient metallurgical activities (Martinez-Cortizas *et al.*, 2002a).

The use of EFs calculated using crustal values was first introduced in the 1970s (Duce *et al.*, 1975; Rahn, 1976) to discriminate between oceanic, terrestrial and potentially other sources of elements to the atmosphere in remote regions (e.g. off-shore, Antarctica and Arctic). Duce (1975) postulated that an element with an EF value near unity, in remote areas, has a probable natural crustal source and therefore elements with EFs > 1 are assumed to have originated from anthropogenic sources. It was suggested, however, that EFs must be used with caution when attempting to

ascertain atmospheric trace metal sources and Reimann and de Caritat (2000, 2005) have since questioned the extension in the application of EFs to a multitude of terrestrial media in much closer proximity to population and industrial countries and also the use of the arbitrary cut-off value of 1. Martinez-Cortizas *et al.* (2002b) also stated that EFs normalised to crustal proportions would be comparable only for remote areas where the atmospheric load is dominated by long-range transport, as EFs are meaningless when the bulk of the deposition in the area is strongly influenced by short- and medium-range transport. Weiss *et al.* (1997) evaluated the legitimacy of EFs calculated using crustal abundances by comparing the average background Pb/Sc ratio (4.1) in a Swiss EGR peat core (*cf.* Shotyk *et al.*, 1998), to the Pb/Sc ratio used to represent the Earth's crust (0.9) (Shaw *et al.*, 1967, 1976, in Wedepohl (1995)) and soil (5.0) (Bowen, 1979). The ~ 4-fold enhancement of the crustal ratio relative to the background ratio was thought attributable to the natural enrichment of Pb in fine fractions of soil, such as K-bearing rock-forming minerals, during intense weathering (Schütz and Rahn, 1982). They therefore suggested that, instead of average crustal composition data, soil composition data could be used, since the latter agreed better with the average background Pb/Sc ratio in the peat samples.

Reimann and de Caritat (2000, 2005), however, found that, even though there are local variations in geogenic element levels and different element "cocktails" emitted by different pollution sources, EFs always show the same elements as being highly enriched, regardless of where samples were taken. In further questioning the use of EFs, they demonstrated, using data from large-scale geochemical surveys, that assumptions fundamental to the EF concept were not met, reporting that each sample material reveals different aspects and reflects only part of a complicated system interacting at the Earth's surface. They suggested that processes influencing the regional distribution of chemical elements at the Earth's surface, as well as local substrate lithology, are related to factors like climate, landscape, vegetation, bioproductivity and distance to the coast. For example, they reported that the use of average crustal composition is irrelevant to the composition of natural dust since dust

contains a significant biogenic component which is also enriched in some metals due to the ability of plants to selectively uptake elements. They concluded that EFs do not provide a simple way of differentiating between anthropogenic and geogenic sources of elements. They recommended that, instead of using EFs, raw data from an area large enough to include background levels or allow meaningful comparisons should be collected and that multi-medium, multi-element regional geochemical mapping be used to differentiate reliably between anthropogenic and natural element sources.

In view of the controversy over the use of EFs, the research presented in this thesis will use elemental ratios to distinguish between anthropogenic and natural sources of the metals of interest. Although there can sometimes be specific-element-related problems with the approach, the use of elemental ratios in peat profiles can be of assistance. For example, the extent of contributions from sources that are unrelated to direct anthropogenic inputs can be estimated.

1.8.4 Selection of conservative element

1.8.4.1 Al

Many studies in the past have used Al as a conservative element to correct the changes in heavy metal concentrations for natural variations in the amount of mineral matter (Duce, 1975; Espi *et al.*, 1997; Martinez-Cortizas *et al.*, 1997; MacKenzie *et al.*, 1998b). Duce (1975), for example, used Al to compare the composition of atmospheric particulate material collected at remote northern and southern hemisphere sites to the composition of the Earth's crust. Although this element was chosen because of its abundance in crustal materials, lack of chemical reaction during atmospheric transport and ease of measurement, unfortunately the solubility of its oxides, hydroxides and silicates is enhanced under low pH conditions, such as those of peat bog waters (Faure, 1991). Helmer *et al.* (1990) found that, with peat bog acidity and the high concentrations of dissolved organic matter, as much as 80-90% of Al could be complexed with dissolved organic matter and subsequently

transported through the peat bog profile. This element was also found to be enriched in peat samples relative to Sc, suggesting that it tends to be slightly enriched in aerosols derived from soils (Shotyk *et al.*, 2001).

1.8.4.2 Y

Recently, Shotyk *et al.* (2001) suggested that Hf, Y and the rare earth elements (REE) can also be used as conservative elements to quantify atmospheric fluxes of soil dust. Of these elements, however, only Y was investigated in this research project. Y is well known for its stability against weathering and it was found to correlate significantly with Ti and Zr (Shotyk *et al.*, 2001). Nesbitt and Markovics (1997), however, studied weathering profiles of Y in siliciclastic sediments from Australia and found that it (along with the REE) was significantly enriched in the most highly weathered samples, thus indicating that it is perhaps not as stable as other conservative elements, such as Ti, Zr and Sc.

1.8.4.3 Ti and Zr

The dominant sources of Ti and Zr in the Earth's crust are rutile (TiO_2), ilmenite ($FeTiO_3$) and titanite ($CaTiSiO_5$), and zircon ($ZrSiO_4$), respectively, all being important accessory minerals in many rocks. In contrast to Al oxides, they are thermodynamically stable and exhibit extremely low solubility, even at low pH (Baes and Mesmer, 1976), and are thought to be highly resistant to chemical weathering. Ti and Zr, therefore, generally behave conservatively in acidic weathering environments (Nesbitt and Markovics, 1997) and both elements are widely used as conservative elements in geochemical studies, including peat bog studies of atmospheric metal deposition.

Ti is often preferred to other conservative elements due to its higher concentrations in peat samples (Shotyk *et al.*, 2001). Ti, however, is also found in aluminosilicates such as biotite, where it can become residually enriched during weathering (Milnes and Fitzpatrick, 1989), thereby casting doubt upon its use as a conservative element. Martinez-Cortizas *et al.* (2002b) carried out a study using two peat cores collected

from Spanish peat bogs at different altitudes and found that Ti was also physically fractionated during soil dust deposition processes. They calculated Pb EFs, normalising to the UCC and pre-anthropogenic background Pb/Ti ratios, and inconsistencies in both sets of Pb EFs were found between the cores. Ti accumulation appeared to be greater in the higher altitude peat core and this was attributed to both chemical and physical fractionation, i.e. the greater deposition of Ti-enriched finer particles at the higher elevation site but greater deposition of Ti-depleted, coarser soil dust particles at the lower elevation site. So, although geochemically conservative in most environments, Ti seems to fractionate physically during wind transport because it is already fractionated in the soils of the source area due to Ti enrichment in the finer fractions during chemical weathering. This was in agreement with the findings of Schütz (1989), where the size, mass and elemental concentrations of soil dusts drastically changed during transport, Ti being strongly enriched in the smaller soil fractions. Also, Ti appears to be quite abundant in coal (Fig. 1.3) and therefore it may be emitted as an anthropogenic contaminant in significant amounts during coal combustion.

Zr may also be fractionated during transport. For example, Shotyk *et al.* (2000) calculated Pb EFs, using Zr, in samples from a Swiss peat core and found that they were approximately 30% greater than those calculated using Sc. They suggested that, due to the higher density of zircon compared with Sc-containing ferromagnesian minerals, Zr may become depleted relative to Sc during long range transport of soil-derived aerosols.

1.8.4.4 Sc

Sc is a very insoluble element hosted in a variety of ferromagnesian minerals and is widely dispersed in crustal rocks. It is known to have only one oxidation state (III) and this dominates its geochemical properties, which are in some ways intermediate between that of Al and the REE (Shotyk *et al.*, 2003). Sc, however, like Ti and Zr, also forms oxides of very low solubility (Baes and Mesmer, 1976). Duce (1975) found that Sc concentrations in atmospheric particulates strongly correlated with

those of the crustal element, Al, and thereafter the use of Sc as a conservative element was investigated. For example, Schütz and Rahn (1982) studied soils from Texas and the Sahara and found that Sc was the least enriched of all the lithogenic elements studied (including Ti, Zr and REE), relative to Al in crustal rocks.

Sc is thought to be neither enriched nor depleted during chemical weathering (Shotyk *et al.*, 2002). For example, it is uniformly distributed in the UCC and the primitive mantle, showing no fractionation in any compartment (Krachler *et al.*, 2003b), and, in contrast to the other conservative elements, Sc is especially favoured as it exhibits no preference for specific mineral phases and thus tends to be uniformly distributed throughout the environment. However, like Ti, Sc is also present in coal, albeit at much lower concentrations, and, therefore, it may also be emitted as an anthropogenic contaminant in significant amounts during coal combustion.

1.9 OVERVIEW OF PEAT DATING TECHNIQUES

Each core collected from a peat bog will have its own unique age-depth relationship and therefore peat age dates must be determined in order to establish chronologies for interpreting historical records of atmospheric metal deposition. Peat core age-depth models can then be used to estimate peat accumulation rates, which are of value, since differences in these will affect the vertical concentration profiles of metals (Shotyk *et al.*, 2003). Various techniques are employed to date peat cores, such as radiometric dating, pollen and tephra analysis, which will now be discussed.

1.9.1 Radiometric dating techniques

The radiometric dating of peat makes use of radionuclides that have originated either from natural processes or anthropogenic activities.

1.9.1.1 Conventional ^{14}C dating

^{14}C dating was the first radiometric method developed and its practical and theoretical principles are well established. The main advantage of ^{14}C dating is that

its long half life (5,730 years, β-decay) means that it can be used to date back to ~50,000 years ago. As its accuracy for recent deposits less than 100 years old is low, however, it is used to date deeper peat layers (Livett, 1988). ^{14}C is produced naturally in the stratosphere by the reaction of cosmic-ray produced neutrons with ^{14}N to generate ^{14}C which is incorporated in CO_2. The radioactively labelled CO_2, in response to variations in solar activity and the geomagnetic field, is then actively taken up from the atmosphere by plants and ^{14}C gets fixed via photosynthetic activity along with the stable isotopes ^{12}C and ^{13}C. (Taylor, 1987; Livett, 1988; Goodsite *et al.*, 2001).

The atmospheric levels of naturally occurring ^{14}C have varied in response to variations in solar activity and the geomagnetic field through time with the result that raw ^{14}C ages need to be converted accurately into calendar years. This is usually done using wiggle matching, where the wiggles of tree-ring calibration curves, generated by the measurement of ^{14}C levels preserved in tree rings of known age, reflect the ^{14}C variations of the past (Stuiver and Braziunas, 1989; Turetsky *et al.*, 2004). Correction is also required for the natural isotopic fractionation of ^{14}C and ^{13}C from ^{12}C, resulting from photosynthetic uptake and conversion of $^{14}CO_2$ in plants. This is achieved by measuring $^{13}C/^{12}C$ ratios concentrations in samples, enabling determination of $\delta^{13}C$ values for use in correction of $^{14}C/^{12}C$ ratios for isotopic fractionation in the calculation of radiocarbon ages (McNichol *et al.*, 2001; Turetsky *et al.*, 2004).

1.9.1.2 ^{210}Pb

^{210}Pb is the most widely used natural radionuclide for dating recent peat deposits as it has a short half life (22.35 years, γ decay) and can be used to date peat up to 100-150 years old. ^{210}Pb is a decay product of the ^{238}U series (Section 1.10), and, as ^{238}U is widely dispersed in the Earth's crust, it is continually decaying to produce ^{210}Pb and other daughter isotopes. Within soils and sediments, ^{238}U decays to ^{226}Ra, which subsequently decays to inert ^{222}Rn gas, which itself decays to ^{210}Pb. In the environment, the ^{210}Pb pool has two components: a supported ^{210}Pb component

produced within the soil/sediment *via* radioactive decay of ^{222}Rn that didn't diffuse to the atmosphere and an un-supported ^{210}Pb component derived from ^{222}Rn that first diffused into the atmosphere where it subsequently decayed to ^{210}Pb. Unsupported ^{210}Pb has a residence time of ~ 5-30 days in the atmosphere from which it is removed via wet and dry deposition, for example onto the surface of peat bogs (Fig. 1.13).

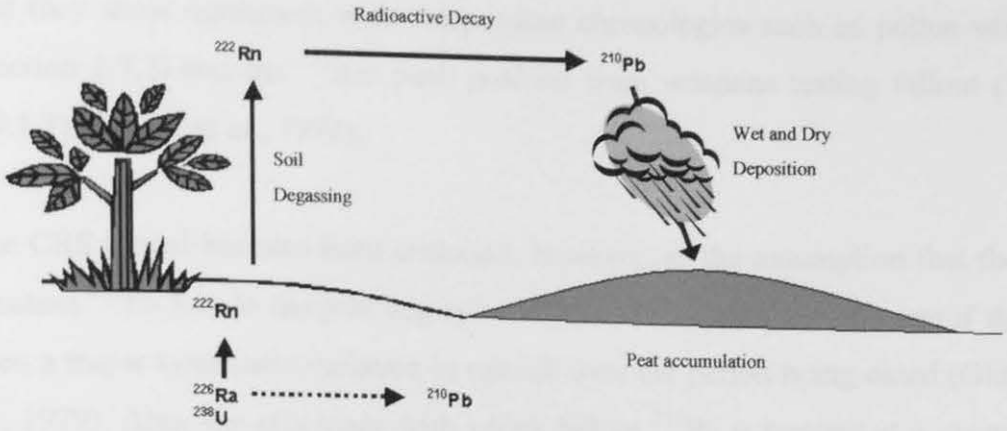

Figure 1.13: Environmental pathways of the radioactive ^{210}Pb isotope.

Supported ^{210}Pb is directly related to the amount of ^{226}Ra present in the sediment, whereas unsupported ^{210}Pb is not, and, since peat has a low mineral content, the supported ^{210}Pb component is usually negligible. It is the unsupported ^{210}Pb that is used for dating peat cores. This method, however, depends on the measurement of unsupported ^{210}Pb and the relationship of its rate of decay to the age of the peat deposit (Livett, 1988; Turetsky *et al.*, 2004). In general, activities of unsupported ^{210}Pb in peat cores are greatest in the youngest peat layers and decrease in older deeper peat layers as a result of radioactive decay (Appleby and Oldfield, 1978). There are two simple models used for calculating ^{210}Pb dates in peat cores, namely the constant initial concentration (CIC) model and the constant rate of supply (CRS) model. Both models assume a constant rate of ^{210}Pb supply, no mixing, and no post-depositional mobility of ^{210}Pb. The CIC model, however, assumes a constant initial ^{210}Pb concentration, generating a single accumulation rate and it is therefore limited for use on peat where the growth rate has been constant. It has generally been found to be inappropriate for dating peat, however, because peat undergoes organic decay, thereby affecting the concentration or specific activity of Pb. In contrast, the CRS

model takes the changing rates of bog plant growth and decay into account and therefore should be unaffected by resultant changes in mass and specific activity (Appleby and Oldfield, 1978; Oldfield *et al.*, 1979). This model is therefore preferred for ^{210}Pb dating of peat cores, and was used in this research investigation. ^{210}Pb dates derived using this model have been shown to be reliable as many workers have found that they show agreement with independent chronologies such as pollen variations (Section 1.9.2) and the ^{241}Am peak position from weapons testing fallout (Section 1.9.1.3) (Shotyk *et al.*, 1998).

The CRS model has also been criticised, however, as the assumption that there is a constant ^{210}Pb flux to the peat bog system makes it inappropriate for use if there has been a major systematic variation in rainfall over the period being dated (Oldfield *et al.*, 1979). Also, the efficiency with which fallout ^{210}Pb is trapped at a given site in the bog may vary through time because of small-scale irregularities over the surface of the bog with the potential to cause errors in the CRS model dates (Goodsite *et al.*, 2001).

1.9.1.3 ^{137}Cs and ^{241}Am

Another radiometric dating technique, which can provide a useful check on calculated ^{210}Pb chronologies, uses the distribution of fission-product radionuclides such as ^{137}Cs (half life 30 years, γ decay) and ^{241}Am (half life 433 years, γ decay) in recent peat. These products are known to have been emitted into the atmosphere during particular events in the history of radioactive fallout, notably the commencement of nuclear weapons testing from 1954, with peak fallout in 1963, and also fallout from the Chernobyl reactor accident in 1986 (Livett, 1988; Appleby *et al.*, 1997). At depths in peat corresponding to these times, peaks in the activity of these radionuclides should in principle be observed. A general disadvantage of the use of these radionuclides, however, for studies in the southern hemisphere is that their transport is subject to time-lag and their concentrations in these regions are often close to the detection limits (Oldfield *et al.*, 1979). It has been reported that ^{241}Am appears to be largely immobilised in peat but the main problem with its use is

the large amount of peat material required for counting in order to detect activity peaks (Oldfield *et al.*, 1979; Shotyk *et al.*, 2001). ^{137}Cs dating was first used for dating peat by Aaby and Jacobsen (1979) and Oldfield *et al.* (1979) but the remobilisation of ^{137}Cs, as a result of both uptake by living plants and downward diffusion in the organic-rich peat is a major drawback in the use of ^{137}Cs, greatly reducing its chronological value (MacKenzie *et al.*, 1997; Farmer *et al.*, 1997b), although the presence of mineral matter may help to restrict ^{137}Cs mobility.

1.9.1.4 Bomb ^{14}C

Thermonuclear weapon testing during the 1950s and 1960s A.D. also resulted in an "atmospheric bomb pulse" of man-made ^{14}C. ^{210}Pb radiometric dates are typically used to date the upper layers of peat cores but Goodsite *et al.* (2001) found that high resolution dating of peat deposits can be provided for the last fifty years using bomb ^{14}C. Shotyk *et al.* (2003) also used bomb ^{14}C to date macrofossils that had been extracted from peat samples more recent than 1950 A.D. by measuring ^{14}C concentrations in the samples and comparing them with the atmospheric concentration of ^{14}C recorded since the beginning of thermonuclear testing. A problem associated with using ^{14}C for dating recent deposits, however, is the "Suess effect", i.e. the dilution of natural ^{14}C in the atmosphere by fossil fuel combustion during the 19^{th} and 20^{th} centuries A.D., resulting in older dates than expected (Taylor, 1987; Livett, 1988).

1.9.2 Pollen dating techniques

Pollen is a biostratigraphical marker that is widely used for dating peat, the technique making use of the regional and local changes in pollen abundances or species composition (Turetsky *et al.*, 2004). Appleby *et al.* (1997), for example, made use of the fact that hemp was grown in the Swiss Jura Mountains until 1930 A.D., and results for this pollen marker were consistent with ^{210}Pb dating of peat cores in the region. Pollen abundance observed in peat profiles can also act as a marker for forest clearance associated with agriculture (Davies and Turner, 1979; Görres and Frenzel,

1997). The redistribution of pollen in peat, however, has been reported to be a source of error (Clymo and Mackay, 1987).

1.9.3 Tephra dating techniques

When the date of a volcanic event is known, peat stratigraphers can chemically characterise the tephra layers preserved within peat profiles and thus determine the source and date of a peat layer (Livett, 1988; Oldfield *et al.*, 1997). Volcanic ash is the smallest tephra fragment and can travel up to thousands of kilometres downwind from a volcano and even eruptions of relatively minor magnitude have the potential to leave ash horizons in distant peat bogs. For example, tephrachronologies have been developed in peatlands situated in Britain using Icelandic volcanic eruptions (Dugmore *et al.*, 1995, 1996). The dated peat horizons, however, might not be those of greatest interest and thus dates between them would necessarily have to be interpolated. Additionally, the tephra fallout from any given eruption is patchy and some peat bogs are too distant from any eruptive source and also, even within a single peat bog, tephra can be found in one core but not within others due to local variability in fallout (Pilcher *et al.*, 1996; Langdon and Barber, 2004).

1.9.4 Use of heavy metal deposition markers

Renberg *et al.* (2001) suggested that the historical atmospheric deposition of Pb itself could be used as a chronological marker in peat deposits in Europe, as its pollution history is well characterised (Section 1.11) and its isotopic composition (Section 1.10) can be related to patterns of Pb-based petrol additives and subsequent unleaded petrol use (Section 1.11). Turetsky *et al.* (2004) also suggested that deposition records of other heavy metals, such as Cu, Zn and V, could be used as their distribution in recent peats has also been linked to historical patterns of use. The immobility of these metals in peat bogs, however, has not been as well investigated or documented as that of Pb.

In conclusion, given the various problems associated with each of the peat dating techniques described above, it is recommended that two or more different dating techniques are used in building age chronologies for peat cores (Givelet *et al.*, 2004).

1.10 Pb ISOTOPIC COMPOSITION

Pb has four stable isotopes, ^{204}Pb, ^{206}Pb, ^{207}Pb and ^{208}Pb, the former being non-radiogenic and the latter three being formed continuously by radioactive decay in the ^{238}U, ^{235}U and ^{232}Th decay series, respectively (Fig. 1.14). The abundances of these isotopes in minerals and ores is determined by the original U:Th ratio and the age of formation of the material. The respective ratios of these four isotopes in Pb-bearing rocks and minerals are therefore specific to the type of rock (or ore deposits) from which the metal derives. Generally, Pb ores of a younger geological age contain a greater proportion of radiogenic to non-radiogenic Pb, and a higher concentration of ^{206}Pb relative to ^{207}Pb, than in older ores. Pb sources retain the characteristic isotopic signatures of the ore(s) from which they are derived and since anthropogenic and natural Pb in the environment often have different geological origins, it is therefore possible in principle to distinguish between Pb from such sources on the basis of isotope ratios (Chow *et al.*, 1975; Faure, 1986).

The principal Pb ore deposits in Britain are shown in Fig. 1.15. Radiogenic Pb isotope ratios ($^{206}Pb/^{207}Pb$, $^{208}Pb/^{206}Pb$ and $^{208}Pb/^{207}Pb$) have been used to "fingerprint" the predominant sources of atmospheric Pb pollutants and the $^{206}Pb/^{207}Pb$ ratio in particular has been used as it is the most sensitive to change. Characteristic $^{206}Pb/^{207}Pb$ ratios of some major anthropogenic atmospheric Pb source materials relevant to Scotland are shown in Table 1.3.

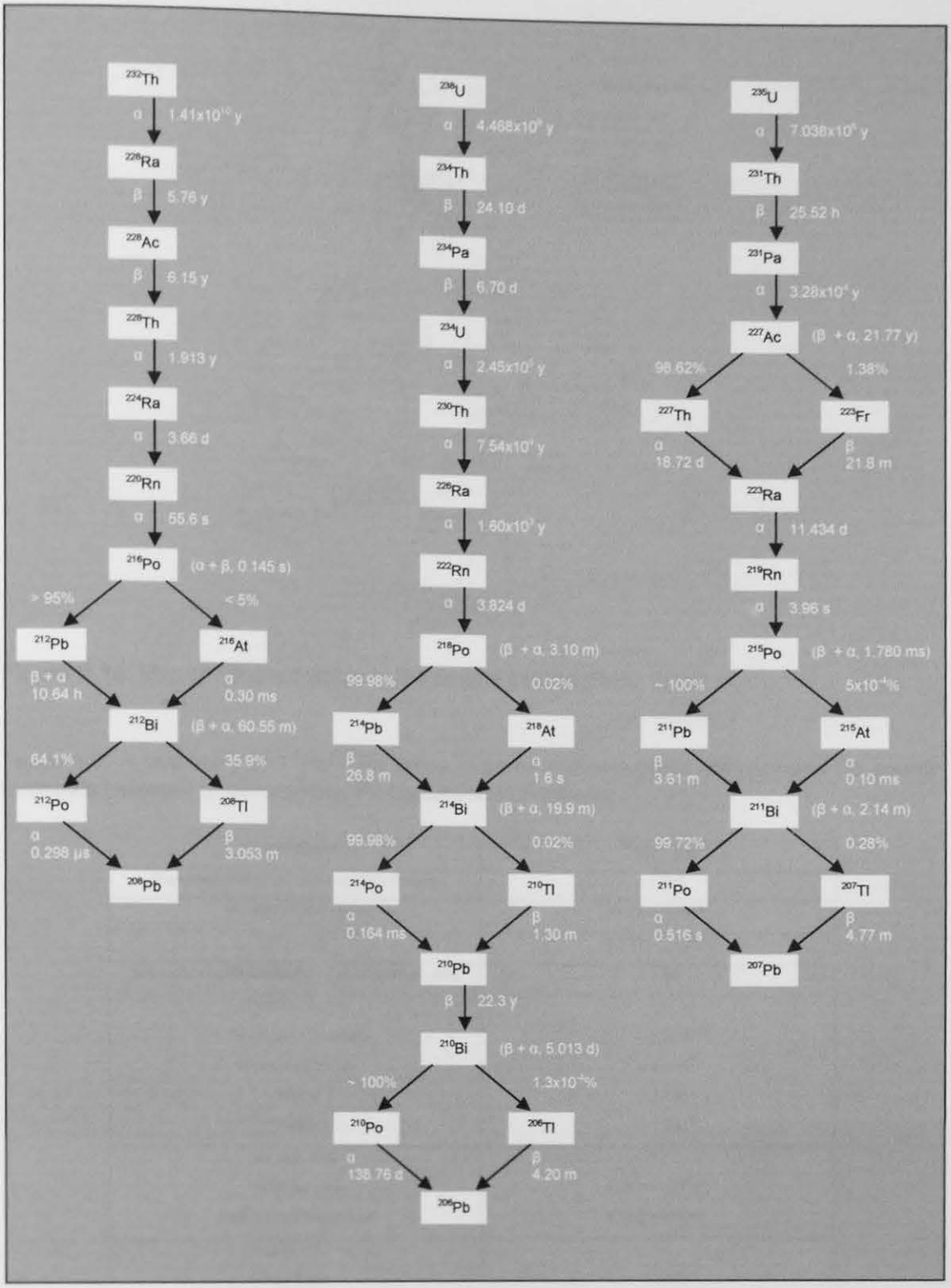

Figure 1.14: The radioactive decay series of ^{232}Th, ^{238}U and ^{235}U leading to formation of ^{208}Pb, ^{206}Pb and ^{207}Pb, respectively (Greenwood and Earnshaw, 1997).

Figure 1.15: Map of Pb ore districts in Britain and Ireland (Rohl, 1996).

Table 1.3: A summary of $^{206}Pb/^{207}Pb$ ratios in some anthropogenic atmospheric Pb source materials (relevant to atmospheric Pb deposition in Scotland).

Source material	$^{206}Pb/^{207}Pb$
Imported Australian (Broken Hill) Pb ores	~ 1.04[a]
Scottish leaded petrol	1.076 ± 0.011[b]
Fly Ash	1.143 – 1.155[c]
Imported Canadian (British Columbian) Pb ores	~ 1.16[a]
British Pb ores	
South-west Scotland	~ 1.170[a,d,e]
North-east Wales	~ 1.176[d]
Bristol	~ 1.183[d]
Cheshire	~ 1.181[d]
British coal	
Scottish coal	1.181 ± 0.011[f]
English and Welsh coal	1.184 ± 0.006[f]
Spanish Pb ores	
Rio Tinto	~ 1.164[g]
Murcia	~1.195[g]

[a]Sugden *et al.*, 1993, [b]Farmer *et al.*, 2000, [c]Monna et al., 1997, [d]Moorbath, 1962, [e]Rohl, 1996, [f]Farmer *et al.*, 1999, [g]Stos-gale *et al.*, 1995.

The isotopic ratios of different British Pb ores and coals are fairly close in value but the $^{206}Pb/^{207}Pb$ ratio for the Precambrian Pb ores imported from Broken Hill in

Australia is characteristically low (*cf.* Table 1.3). Pre-anthropogenic, natural sources of Pb, such as those derived from soils and minerals, have $^{206}Pb/^{207}Pb$ ratios (~ 1.20 – 1.23) greater than those found for atmospheric Pb derived from anthropogenic emissions, a feature which is useful in helping quantify the effects of human activities (Grousset *et al.*, 1994; Kylander *et al.*, 2005).

1.11 ATMOSPHERIC Pb POLLUTION HISTORY

The global history of estimated Pb production (Fig. 1.16) acts as the starting point for estimating the extent of historical Pb pollution of the atmosphere.

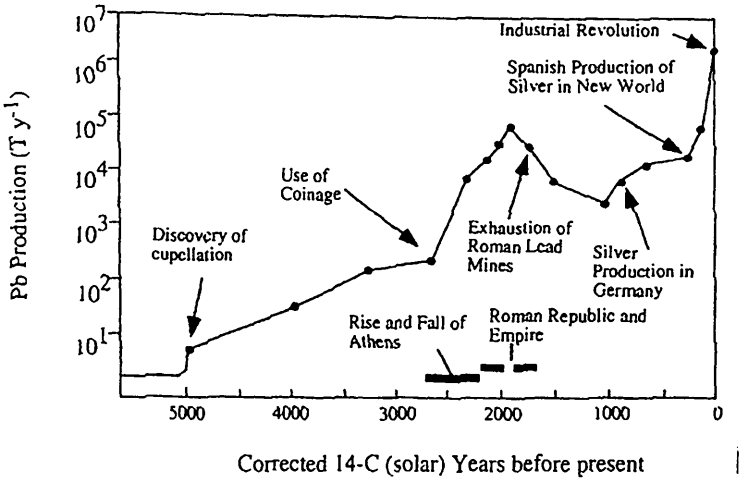

Figure 1.16: World Pb production during the past 5500 years (Weiss *et al.*, 1999c redrawn from Settle and Patterson, 1980).

Technologies for smelting Pb-Ag alloys from sulfide ores and cupelling Ag from the alloys were developed at least 5000 years ago. For example, the Greek mines at Laurium operated well before 3000 B.C. and the mines of the Iberian Peninsula operated from the late Bronze Age (*ca.* 2700 B.C.). Estimated world Pb production averaged 160 tonnes per year from *ca.* 4000 years ago until *ca.* 2700 years ago, when it rose to *ca.* 10,000 tonnes with the introduction of silver coinage, and thereafter to *ca.* 80,000 tonnes during the peak of the Roman Empire, *ca.* 2000 years ago, when almost every Pb/Ag deposit in the Mediterranean countries and western Europe had been discovered. Pb production declined during Mediaeval times, but the revival of mining in Europe started in the 11th century A.D. in Germany. In the New World, Pb was first mined in the early 15th century A.D. and large-scale mining of

Pb in Australia began in the mid-19th century A.D. With the onset of the industrial revolution (*ca.* 1750 A.D. in Britain), annual Pb production increased dramatically from 100,000 tonnes, *ca.* 300 years ago, to 1,000,000 tonnes *ca.* 70 years ago. This increase can be attributed to the advanced Pb mining and smelting technologies initiated by the huge demand for Pb (Settle and Patterson, 1980; Nriagu, 1998; Tylecote, 1976 and 1986; Martinez-Cortizas *et al.*, 1997). In Britain, Australian and Canadian Pb ores were imported to replace indigenous Pb ores during the early 19th century A.D. and used in the manufacture of tetra-alkyl Pb additives, for leaded petrol, which was introduced in Britain from the 1930s A.D. During the late 19th and early 20th centuries A.D., the exploitation of indigenous Pb ores declined as they became uneconomic. During the post-industrial era (*ca.* post-1970s A.D. in Britain) measures were also taken to reduce the maximum permitted Pb additive content in petrol. A decline in Pb emissions was observed during the most recent post-industrial years, due to the introduction of unleaded petrol since the mid-1980s and the outright ban on leaded petrol in Britain in 2000 (Farmer *et al.*, 1999, 2000 and 2005). In recent years, however, rates of atmospheric Pb deposition in Europe were still found to be ~ 700 times higher than the natural atmospheric Pb deposition of the past (Shotyk *et al.*, 1998).

1.12 ARCHIVES OF ATMOSPHERIC Pb DEPOSITION IN OMBROTROPHIC PEAT BOGS

Studies of Pb in ice cores from Greenland and Antarctica documented dramatic increases in atmospheric Pb deposition during the industrial period (Murozomi *et al.*, 1969) but, since *ca.* 1970 A.D., there has been an ~ 7-fold decrease (to *ca.* 1990 A.D.) in Pb concentrations in Greenland ice (Boutron *et al.*, 1991). Herbarium moss collections (Weiss *et al.*, 1999a; Farmer *et al.*, 2002), herbage and soils (Bacon *et al.*, 1996) have also been used successfully to reconstruct changing Pb concentrations in atmospheric deposition in various parts of Europe. The validity of the use of ombrotrophic peat bogs to characterise historical trends in atmospheric deposition of Pb is supported by the remarkable consistency of records with those

found in these other environmental archives. For example, synchronous changes in Pb concentration and isotopic ratio profiles in cores collected from lake and peat sediments from Sweden and Scotland have been found (Bränvall *et al.*, 1997; Farmer *et al.*, 1997b; MacKenzie *et al.*, 1998a).

Generally, in most European peat bog studies, the trends of atmospheric Pb deposition are similar to the history of global Pb production, at least until post-industrial times (*cf.* Fig. 1.16). For example, the trends were reflected in a dated EGR Swiss ombrotrophic peat core, representing a continuous record of atmospheric Pb deposition since 12,370 ^{14}C years B.P. (Fig. 1.17) (Shotyk *et al.*, 1998).

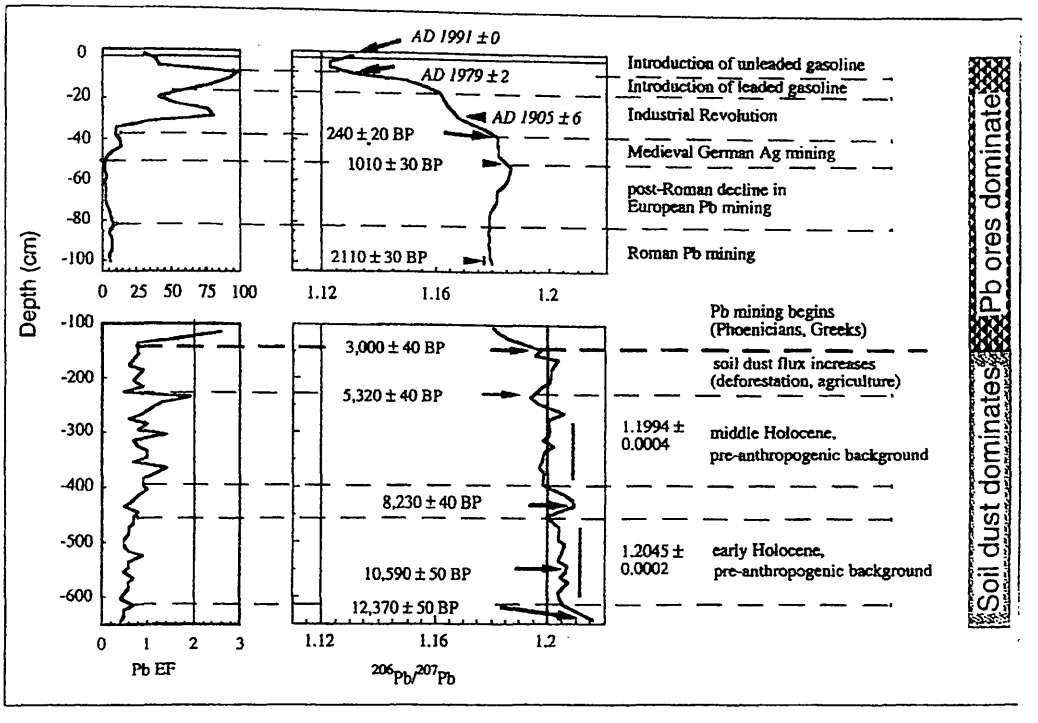

Figure 1.17: Pb EFs, $^{206}Pb/^{207}Pb$ isotopic ratio profiles and chronology of atmospheric Pb deposition in a Swiss peat bog since 12,370 ^{14}C years B.P. (Pb EFs were calculated as the ratio of Pb/Sc in peats, normalised to the background value) (Weiss *et al.* (1999c), redrawn from Shotyk *et al.* (1998)).

With respect to the $^{206}Pb/^{207}Pb$ ratio profile, one of the most important features in the top 100 cm of peat was firstly the shift from more radiogenic values (~ 1.18) to less radiogenic values (~ 1.17), accompanied by increasing Pb EFs (*cf.* Fig. 1.17). This shift is attributable to the mining and smelting of Pb ores indigenous to Europe and coal combustion during the industrial revolution. The ratio then continues to

decrease, reaching a minimum of ~ 1.12, with the introduction of leaded petrol and the use of imported Australian and Canadian Pb ores in the manufacture of alkyl lead additives, in which the Australian ores of lower $^{206}Pb/^{207}Pb$ ratio were predominantly used. In the surface peat samples, representing the most recent years, the Pb EFs decrease and $^{206}Pb/^{207}Pb$ ratios start to increase towards the surface. These trends are in line with the decrease in Pb emissions from leaded petrol due to the introduction of unleaded petrol. Similar $^{206}Pb/^{207}Pb$ trends during the industrial period have been found in Scottish, Swedish and Spanish peat cores. For example, Farmer *et al.* (1997) and MacKenzie *et al.* (1998a) observed a shift in $^{206}Pb/^{207}Pb$ ratios in Scottish peat bogs from a more or less constant value (1.16-1.18) for anthropogenic Pb emissions from coal burning and indigenous Pb mining and smelting emissions to ~ 1.12 - 1.15 during the 20th century from the use of leaded petrol.

Enrichments have also been found in the deeper pre-industrial sections of the Swiss EGR peat core (*cf.* Fig. 1.17), reflecting pre-industrial pollution and evidence of Pb deposition extending back to the Greek and Roman times. Also, even the low enrichments observed after the fall of the Roman Empire are still at least twice that in the pre-anthropogenic period (8030 – 5320 ^{14}C years B.P.). Similar historical records of ancient Pb mining and smelting have also been found in environmental archives throughout Europe (Bränvall *et al.*, 1997; Kempter *et al.*, 1997; Martinez-Cortizas *et al.*, 1997, 2002b; Kempter and Frenzel, 2000; Klaminder *et al.*, 2003; Le Roux *et al.*, 2004; Kylander *et al.*, 2005).With respect to the pre-anthropogenic, soil-dust-dominated sections of the $^{206}Pb/^{207}Pb$ ratio profile in the Swiss peat core, values are reasonably constant, ranging from 1.19-1.20, in good agreement with the $^{206}Pb/^{207}Pb$ ratio of ~ 1.20 found by Grousset *et al.* (1994), which was reported to represent that of natural soil dust from the UCC. Similar values have also been found in peat bogs in Sweden (~ 1.20 – 1.23) (Bränvall *et al.*, 1997; Kylander *et al.*, 2005). In most cases, however, Pb isotopic ratios in the pre-anthropogenic period in peat bogs show significant natural variations and these variations may result from climate-related changes in the mineralogical composition of the inputs and, therefore, the selection

of the reference period for background values is somewhat arbitrary (Shotyk *et al.*, 1998; Martinez-Cortizas *et al.*, 2002a).

In conclusion, the validity of the use of ombrotrophic peat deposits to characterise historical trends in atmospheric Pb deposition is supported by the compatibility of results from a wide range of peat deposits, agreement between temporal variations in atmospheric depositional fluxes of Pb inferred from ^{210}Pb-dated peat core data and known historical trends in industrial activity, and also the consistency of peat core stable Pb isotope data (MacKenzie *et al.*, 1998a).

1.13 ATMOSPHERIC DEPOSITION RECORDS OF OTHER TRACE METALS IN OMBROTROPHIC PEAT BOGS

With Pb immobility well established, it should be possible to assess the importance of post-depositional mobility of other metals of interest by extending investigations to other trace metals of environmental concern. Recent studies have indicated that Sb and Hg are also effectively immobile in peat, suggesting that historical records of atmospheric deposition can also be obtained for these (and perhaps other) metals using ombrotrophic peat bogs. In this thesis, however, anthropogenic fluxes of the naturally abundant and major/nutrient elements, Ca, Fe, Mg, Mn, P and S, were not investigated because it is generally accepted that these elements are mobile in ombrotrophic peat bogs.

1.13.1 Atmospheric deposition records of Sb in ombrotrophic peat bogs

Sb has a similar toxicity to Pb but its pollution history is not as well known, but, as Sb is found in practically all sulfide minerals (Boyle and Jonasson, 1984), and most Pb minerals and coals contain Sb, Shotyk *et al.* (2004) suggested that there should be a strong link between both the natural and anthropogenic geochemical cycles of Sb and Pb. These workers compared Sb and Pb profiles from peat bogs in Switzerland and Scotland. Using the lowest concentrations, atmospheric fluxes and enrichments of Sb found in peat core samples from EGR, Switzerland, dating from 8,020 to 5,320

^{14}C years B.P. as background values, they found that, in general, Sb enrichments were similar to those of Pb, suggesting that Sb, like Pb, is well preserved in ombrotrophic peat. These findings were also supported by those found in an earlier study where Shotyk *et al.* (1996b) found similar significant enrichments of Sb and Pb, dating back to the Roman times, for a peat bog profile from EGR, Switzerland, representing 2000 years of deposition.

1.13.2 Atmospheric deposition records of Hg in ombrotrophic peat bogs

Hg is a highly toxic metal and atmospheric Hg contamination occurs through long range vapour phase transport of Hg as more than 95% of atmospheric Hg is in the vapour phase, where it has a residence time of at least one year and can be transported thousands of kilometres (Mason *et al.*, 1994; Schroeder and Munthe, 1998). Hg is also believed to undergo cold condensation, whereby Hg substances within a certain range of volatility are repeatedly deposited and re-volatilised until finally being deposited and concentrated in colder high latitude regions (e.g. Greenland and Antarctic), and therefore its accumulation in these environments is of particular concern (Roos-Barraclough *et al.*, 2002a and b).

Rühling and Tyler (1973) reported that Hg was strongly retained by humic substances in peat and later studies by various workers assessed the utility of ombrotrophic peat bogs as archives of atmospheric Hg deposition, suggesting that Hg was essentially immobile in ombrotrophic peat (Madsen, 1981; Norton *et al.*, 1997; Benoit *et al.*, 1998). Madsen (1981) studied the atmospheric deposition of Hg in Danish peat cores and, although the general increase over the past 100-200 years was attributed to human activity, it was suggested that periodically elevated rates might have been caused by volcanic activity or associated climatic events. Similar trends were found by Roos-Barraclough *et al.* (2002a) and Roos-Barraclough and Shotyk (2003), who measured Hg concentrations in a peat core from EGR, Switzerland, extending back to natural pre-anthropogenic times. They found that pre-anthropogenic Hg deposition did not remain constant as concentrations were influenced by soil dust inputs, climate and increased volcanic and oceanic activity.

Also, Martinez-Cortizas *et al.* (1999) studied the Hg profile in a Spanish peat core representing 4000 ^{14}C years B.P. of deposition and found that anthropogenic emissions began ~ 2500 ^{14}C years B.P. with the onset of Hg mining in Spain.

Recently, Biester *et al.* (2003) investigated Hg concentration profiles in peat cores from three different bogs in Patagonia and suggested that peat Hg concentrations were strongly dependent on the extent of peat decomposition. Givelet *et al.* (2003), however, studied Hg deposition in peat cores from Ontario, Canada and measured optical absorption of NaOH peat extracts to investigate the effects of peat decomposition. Results revealed that changes in peat Hg concentrations were disproportional to the changes in peat decomposition. Also, Shotyk *et al.* (2003) studied Hg deposition in peat cores from Greenland and Denmark and found that differences in bulk density were not comparable to the differences in Hg concentration. Further research into the behaviour of Hg in peat is required before records of atmospheric Hg deposition can be established with the same degree of confidence as for atmospheric Pb deposition.

1.13.3 Atmospheric deposition records of As, Cd, Co, Cr, Cu, Ni, Se, V and Zn in ombrotrophic peat bogs

In comparison with Pb, Hg and Sb, few atmospheric deposition studies using ombrotrophic peat bogs have been carried out for the remaining trace metals under investigation in this thesis (As, Cd, Co, Cr, Cu, Ni, Se, V and Zn).

The toxic metal As, like Sb, is also present in coals and Pb minerals and therefore, its atmospheric deposition may too have been affected similarly to Pb by past metallurgical and coal burning activities. One of the few studies carried out was by Shotyk *et al.* (1996b), who found similar significant enrichments of As, Sb and Pb, dating back to the Roman times, for a peat bog profile from EGR, Switzerland, representing 2000 years of deposition.

Cu has been studied in peat from several locations, particularly in the context of examining the history of ancient mining regions (West *et al.*, 1997; Mighall *et al.*, 2002; Monna *et al.*, 2004). As, Cd and Zn, as well as Pb, have frequently been included in these studies.

Jones and Hao (1993) suggested that Cd, Cu, Pb and Zn concentration increases found in peat cores from northern England reflected the influence of industrial activities. Also, MacKenzie *et al.* (1998b) studied atmospheric deposition of contaminants in an ombrotrophic peat core from west-central Scotland. They found major increases in As, Co, Cu, Pb and Sb depositional fluxes from the mid-19th century A.D., with peak values occurring during the mid-20th century A.D., in agreement with the known history of industrial development in the area.

Krachler *et al.* (2003a) studied Cr, Ni and V deposition in a peat core from EGR, Switzerland, representing 12,370 ^{14}C years B.P worth of deposition. They found that measured Cr/Sc, Ni/Sc and V/Sc ratios were remarkably similar to their corresponding ratios in the Earths crust until the onset of the Industrial Revolution.

Stiennes (1997) studied Se deposition in Norwegian peat cores and suggested that natural marine sources of this metal were more important than anthropogenic sources.

It can be seen that further studies of atmospheric As, Cd, Co, Cr, Cu, Ni, Se, V and Zn deposition in ombrotrophic peat bogs is required.

1.14 OVERVIEW OF PEAT CORE COLLECTION TECHNIQUES

Collection techniques are important when using peat cores as archives of atmospheric metal deposition. Over the years, many kinds of peat samplers have been designed and constructed but the main types of corer used to collect undisturbed, uncompressed, intact peat cores have been the Wardenaar (Wardenaar,

1986, 1987) and Belarus (or Macaulay) (Jowsey, 1965) corers for topmost and deeper peat layers, respectively. Site selection is also important as, in the past, humans have disturbed peat bogs by drainage for land use, peat cutting for fuel, vegetation burning and reforestation (Brooks and Stoneman, 1997), all of which may affect the ombrotrophic properties of the bog or cause dating problems. For example, peat surfaces may have been lost during peat cutting. Cores should therefore be collected from relatively intact and undisturbed peat bogs where the peat is still in its natural growing state and, for reasons discussed earlier (*cf.* Section 1.7.3.2), they should be collected from peat hummocks or lawns from the most central raised parts of the bog. They should also, if possible, be collected from sites which have uniform composition of surface vegetation, as botanical composition may affect peat decomposition as well as metal retention (Section 1.16.3) (Damman, 1978; Givelet *et al.*, 2004).

1.15 OVERVIEW OF QUALITY ASSURANCE

With the growing interest in the use of ombrotrophic peat bogs as archives of atmospheric metal deposition, the need for accurate and precise analytical data is important, especially regarding ancient, pre-industrial and pre-anthropogenic peat samples where metal concentrations can be very low. Analytical precision can be determined from replicate measurements of individual samples but accuracy can only be determined through analyses of a comparable material for which elemental concentrations are known (Barbante *et al.*, 2000). In the past, workers have used international certified standard reference materials for plants and coals to judge recoveries and accuracy but these materials are not perfect. Peat, for example, has more mineral matter than living plants and is less resistant to decomposition in strong acids than coal, which also contains metallic sulfides. A candidate peat reference material (Canadian peat 1878P) consisting of *Carex* fen peat collected from Ontario, Canada was developed by the Ontario Geological Survey and an inter-laboratory comparison was carried out (Barbante *et al.*, 2000). "Information only" values for some elements in this reference material were obtained but, as this material

represented high ash content (~ 20%), minerotrophic fen peat, it was not the most suitable for ombrotrophic peat studies. Yafa *et al.* (2004) recently developed an ombrotrophic peat bog (low ash) certified reference material to provide an evaluation of the accuracy of chemical analyses of peat and ombrotrophic peat bog studies will benefit greatly from the use of this certified reference material.

1.16 PROBLEMS ASSOCIATED WITH THE USE OF OMBROTROPHIC PEAT BOGS AS ARCHIVES OF ATMOSPHERIC DEPOSITION

1.16.1 Post-depositional mobility

The possible post-depositional migration of elements (*cf.* Section 1.7) is a potential problem with respect to the use of ombrotrophic peat bogs as archives of atmospheric deposition, although Pb and possibly Sb and Hg do appear to be essentially immobile.

1.16.2 Peat dating

Variable peat accumulation rates due to changes in vegetation growth rates and peat decomposition occurring in peat bogs, as well as different hydrology and microtopography between sites, complicates the dating of peat cores (Damman, 1978; Oldfield *et al.*, 1979). For example, increasing peat compaction as a function of depth has been suggested to lead to inaccuracies in ^{210}Pb chronologies (MacKenzie *et al.*, 1997). Some workers have used the cumulative dry mass per unit area (g cm^{-2}) as the depth parameter in ^{210}Pb profiles in order to eliminate effects of compaction and overall trends of unsupported ^{210}Pb activities in all cores have been found to be similar (Damman, 1978; Appleby *et al.*, 1997). These problems also complicate peat core age-depth relationships and linear interpolations which assume that there is a constant age-depth relationship between dated points cannot be used when exponential age-depth profiles are obtained (Blackford, 2000). Also, accuracy in the determination of cut-off dates for certain trends in peat core profiles is affected

by the thickness of the peat core sampling interval (MacKenzie *et al.*, 1997; Givelet *et al.*, 2004).

1.16.3 Within-bog spatial variability

The surface of a bog is not a uniform feature and vegetation and micro-topography vary over small spatial scales, all of which can affect the interception and retention of atmospheric deposition over relatively short time-scales (Bindler *et al.*, 2004b). In addition, different positions on the bog surface appear to be differentially sensitive to recording changes in atmospheric deposition (*cf.* Section 1.7.3.2). Clymo (1963) also found marked differences in metal accumulative properties of different moss species, which may give rise to considerable vertical and horizontal heterogeneity in the distribution of metal ions in peat deposits. For example, Roos-Barraclough *et al.* (2002b) found that there appear to be differences in the efficiency of different species in scavenging Hg, suggesting that considerable variations in Hg concentration can occur within a peat slice from a peat core with different species composition. If these species-related metal retention effects are occurring, then their importance for other metals may need to be investigated. Weiss *et al.* (1999a) reported, however, that Pb isotope ratios show insignificant spatial variability and therefore their use is not affected by processes such as this. It has also been suggested that metal deposition is characterised by large spatial variability as a result of local and regional differences in the quantity and composition of bulk precipitation (Damman, 1986). In conclusion, various atmospheric, vegetation and micro-elemental factors can result in considerable spatial variations in the distribution of elements within peat bog profiles and, in order to assess spatial variability, more than one peat core should be collected from a peat bog site, as single peat cores may not be representative of the whole ecosystem (Bindler *et al.*, 2004b).

1.17 OBJECTIVES AND STRUCTURE OF THESIS

The specific objectives of this project were as follows:

1. To use cores collected from ombrotrophic peat bogs at four different geographical locations in Scotland to reconstruct records of atmospheric metal deposition across Scotland.
2. To develop and apply reliable analytical methods for high precision measurements of a range of elements (Al, As, Ca, Cd, Co, Cr, Cu, Fe, Hg, Mg, Mn, Ni, P, Pb, S, Sb, Sc, Ti, V, Y, Zn and Zr) in peat samples (Chapter 2).
3. To investigate the distribution and behaviour of a range of potentially toxic trace elements (As, Cd, Co, Cr, Cu, Hg, Ni, Sb, Se, V and Zn), major metals (Ca, Fe, Mg and Mn) and non-metals (P and S) within the four ombrotrophic peat bogs (Chapters 3, 4, 5 and 6).
4. To use ^{210}Pb and ^{14}C to date peat cores in order to characterise historical trends in sources and deposition of atmospheric Pb (and other potentially immobile metals, e.g. Hg, Sb) to the Scottish environment during the pre-industrial, industrial and post-industrial periods and, incorporating Pb isotope measurements, to extend recently established records of environmental Pb contamination across Scotland during these periods (Chapters 3, 4, 5 and 6).
5. To estimate variations in the extent of anthropogenic and natural sources of metals in peat bog profiles with time, by normalising metal (M) concentrations to conservative elements (X) (e.g. Al, Sc, Ti, Y and Zr), using M/X ratios (Chapters 3, 4, 5 and 6).
6. To carry out an inter-site and inter-elemental comparison of the historical records of anthropogenic metal deposition across Scotland (Chapter 7).
7. To summarise the main findings of this research and recommend further directions (Chapter 8).

2 MATERIALS AND METHODS

This chapter describes the peat bog sampling sites, peat core collection procedures, methods for the physical and chemical preparation of peat samples prior to analysis, analytical procedures for inductively coupled plasma optical emission spectrometry (ICP-OES), inductively coupled plasma mass spectrometry (ICP-MS), cold vapour atomic absorption spectrometry (CVAAS), flame atomic absorption spectrometry (FAAS), ^{210}Pb, ^{226}Ra and ^{137}Cs determination using gamma spectrometry, ^{14}C accelerator mass spectrometry (AMS) and UV-Vis spectrometry, quality assurance and additional work involving the determination of charcoal contents and the analysis of coal, herbarium moss and galena samples.

2.1 SAMPLING SITES

2.1.1 Geographical location of sampling sites

The four different sampling sites throughout Scotland chosen for this project are shown in Fig. 2.1. Flanders Moss and The Red Moss of Balerno in west-central and east-central Scotland, respectively, represent the sites influenced by industry (as the central belt of Scotland became heavily industrialised since the onset of the Industrial Revolution), whereas Turclossie Moss and Carsegowan Moss in the north-east and south-west of Scotland, respectively, represent the more remote rural sites.

2.1.2 Flanders Moss

2.1.2.1 Location and size

Flanders Moss lies 16 km to the west of Stirling in central Scotland (Fig. 2.2 a). Bound by the Campsie Fells, Fintry and Gargunnock Hills to the south and the Menteith Hills to the north, it is located on the north bank of the River Forth. Tributaries of Goodie Water run across the site (Fig 2.2 b). East Flanders Moss is the largest remaining lowland ombrotrophic peat bog in Britain with 548 ha of active

raised bog, equivalent to 13.7% of the total area of those left in Britain (Scottish Wildlife Trust, 2005).

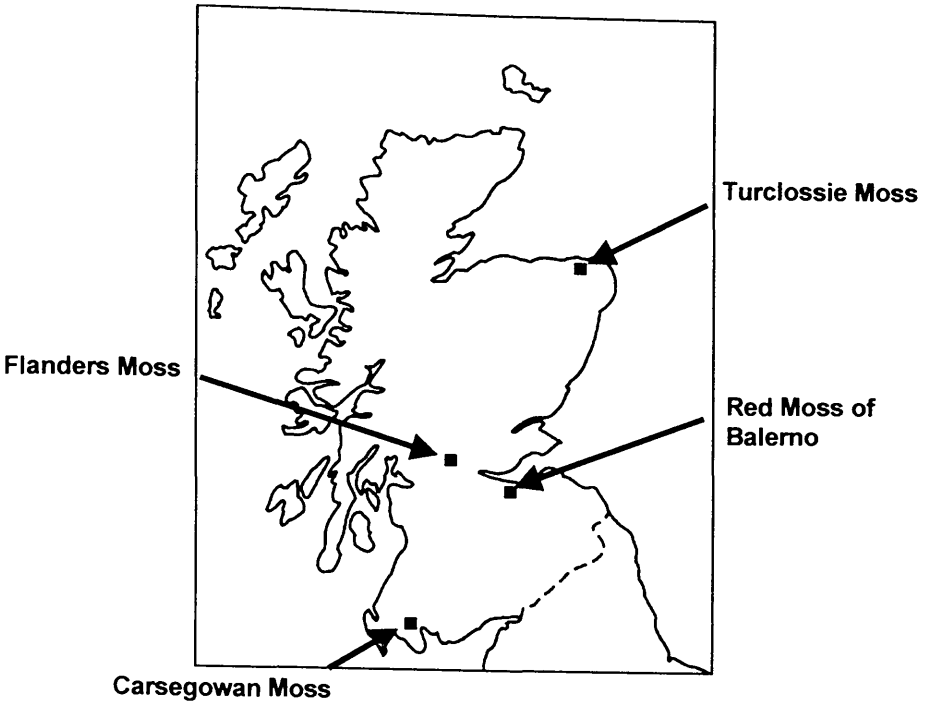

Figure 2.1: Sampling site locations in Scotland.

2.1.2.2 Geology

Flanders Moss represents a small part of a once extensive series of ombrotrophic peat bogs which were formed on top of Carse clay deposits left behind after the Menteith glacier melted more than 11,000 years ago (Hansom *et al.*, 2000).

2.1.2.3 Vegetation

Flanders Moss is still in a predominantly near natural state with vegetation dominated by *Sphagnum* species (including *S. papillosum*, *S. magellanicum* and less common species such as *S. molle and S. fuscum*), feather moss (*Pleurozium schreberi*), ribbed bog moss (*Aulacomnium palustre*), heather (*Calluna vulgaris*), cross-leaved heather (*Erica tetralix*), cotton grass (*Eriophorum vaginatum*), lichen (*Cladonia portentosa*) and fen communities with some scattered birch (Fig. 2.3). In terms of shape, the bog consists of convex domes with peat up to 4 m deep in the centre, the surface consisting of hummock/hollow microtopography (Scottish Natural Heritage, 2005).

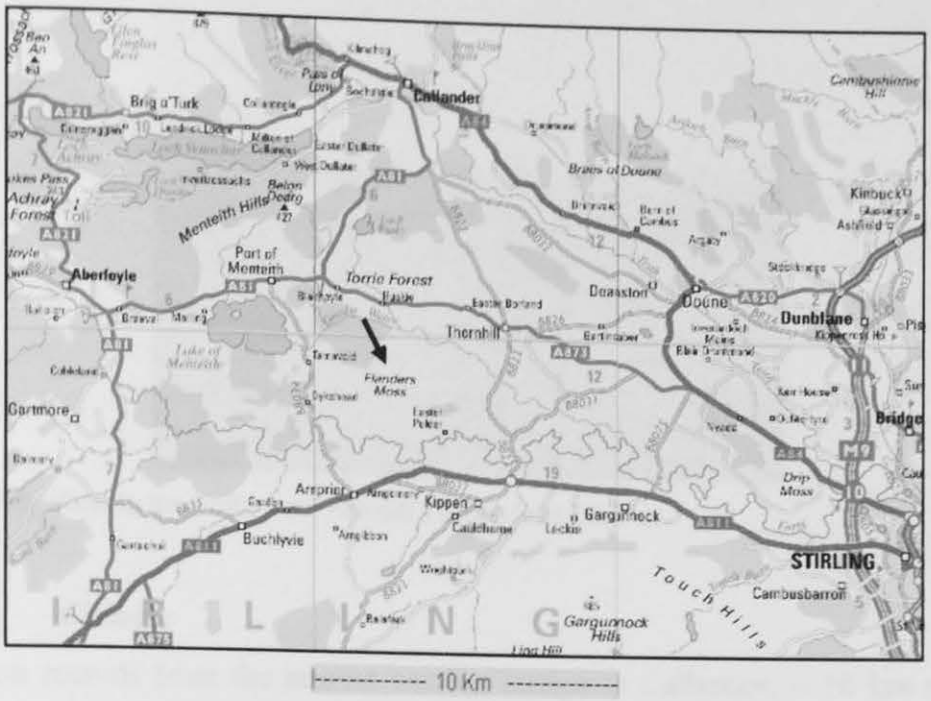

a)

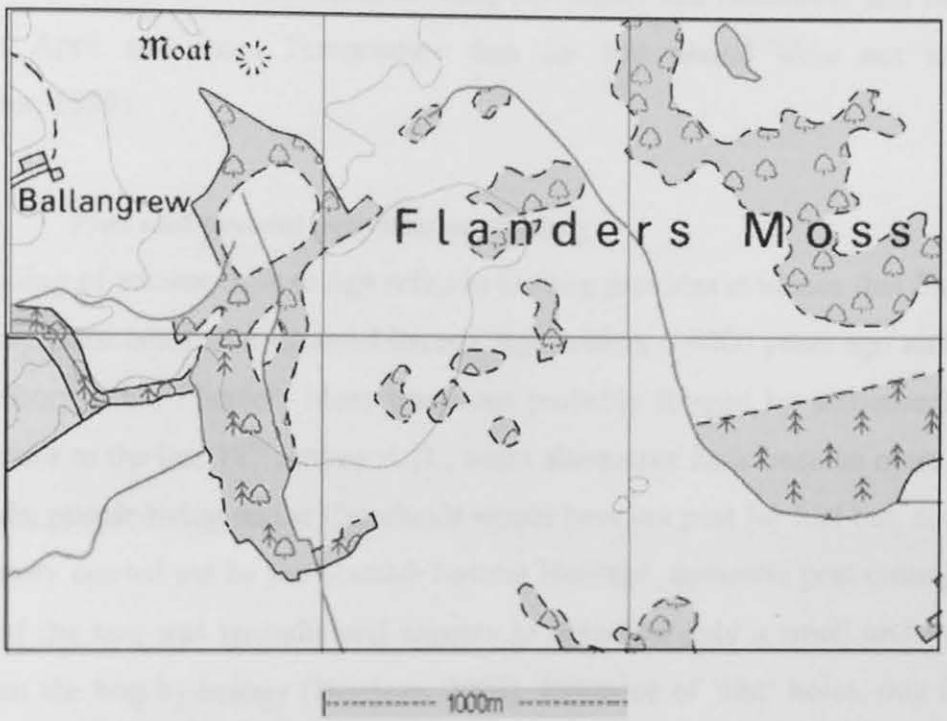

b)

Figure 2.2: Location of Flanders Moss peat bog a) scale 1:10 km and b) scale 1:1 km (Ordnance Survey, 2005).

Figure 2.3: View to the north from Flanders Moss peat bog.

2.1.2.4 Climate

Based on records from the nearest weather station at Callander, ~ 10 km north of Flanders Moss, from the period 1951 – 1980 A.D., the average annual rainfall was 152.2 cm y^{-1}, with the wettest months being November and December and the driest months April and June. Temperature data for this period were not available (Wheeler, 1999).

2.1.2.5 Past and present activities on the bog

The finding of ancient Bronze Age relics in the bog provides evidence that the newly emerging Carselands first attracted Bronze Age settlers ~ 4000 years ago and by the 15th century A.D., Flanders Moss was most probably fringed by settlement on all sides. Prior to the late 18th century A.D., when alternative fuels became more widely available, people living on the Carselands would have cut peat for fuel but, according to a survey carried out by the Scottish Natural Heritage, domestic peat cutting at the edges of the bog was sporadic and appears to have had only a small and localised effect on the bog hydrology (Harrison, 2002). Evidence of 'lint' holes, dug into the peat bog surface, indicates that it was used for flax-retting, a process where flax was soaked in soft peaty water to make it more pliable before spinning into linen. From 1767 A.D., however, many of the peat bogs that occupied the Carse of Stirling were reclaimed for agriculture by draining and digging out blocks of peat, which were

floated away down the River Forth. Past drainage effects resulted in a lowering of the water table on the bog that remains today but most damage came from the planting of trees by the Forestry Commission in the 1970s A.D. Since 1987 A.D., the remaining active areas of the bog have been preserved as a Scottish Wildlife Trust national nature reserve and the removal of invasive trees/scrub and blocking of drains in the southern sections of the bog have helped maintain a higher water level and preserve the bog plant communities (Brooks and Stoneman, 1997; Hansom *et al.*, 2000; Scottish Wildlife Trust, 2005; Scottish Natural Heritage, 2005). At present the site, which lies between two major roads, the A873 and A811, is surrounded mainly by agricultural land and some commercial forestry. There is a small aeroplane runway to the south-east of the bog.

2.1.3 The Red Moss of Balerno

2.1.3.1 Location and size

The Red Moss of Balerno lies ~ 8 km south of Edinburgh and 2 km south of the village of Balerno in east-central Scotland (Fig. 2.4 a). Situated on the north side of the Pentland Hills next to Threipmuir reservoir (Fig. 2.4 b), it is the largest remaining ombrotrophic peat bog (area 23 ha) in Midlothian (Scottish Wildlife Trust, 2005).

2.1.3.2 Geology

The Red Moss of Balerno began its existence as a shallow lake occupying a basin-like depression in the boulder clay sheet which extends over much of the Balerno area and is underlain by a series of mudstones, shales and cement stone bands (Scottish Wildlife Trust, 2001).

2.1.3.3 Vegetation

The Red Moss of Balerno site consists of two distinct sections, a low lying southern section of woodland and scrub with some underlying *Sphagnum* and a domed northern section mainly of *Sphagnum* species (including *S. capillifolium*, *S. magellanicum* and *S. papillosum*), feather moss (*Pleurozium schreberi*), heather

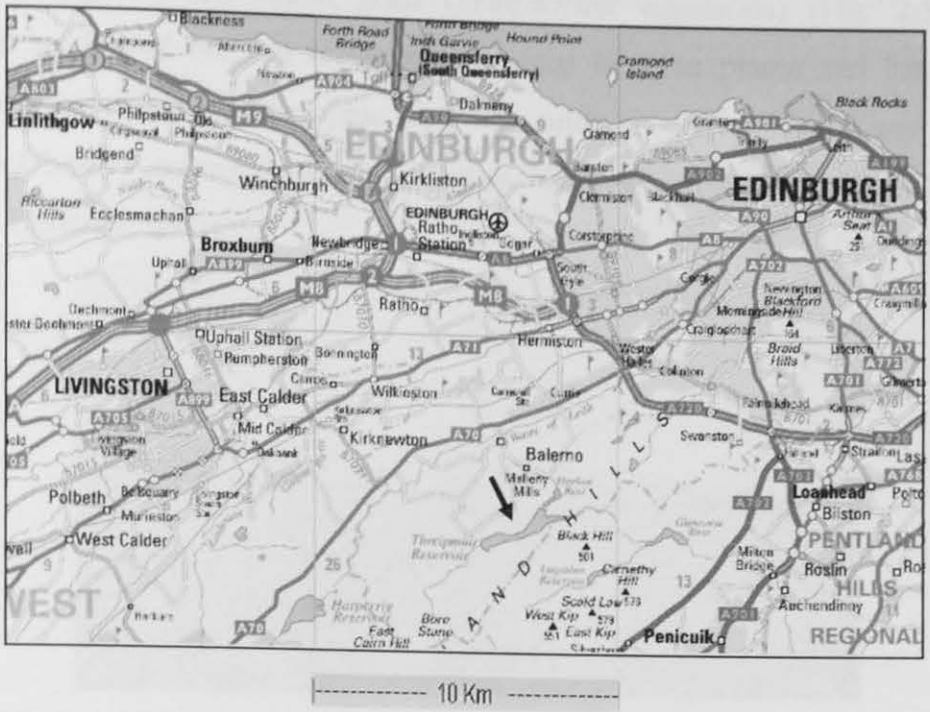

a)

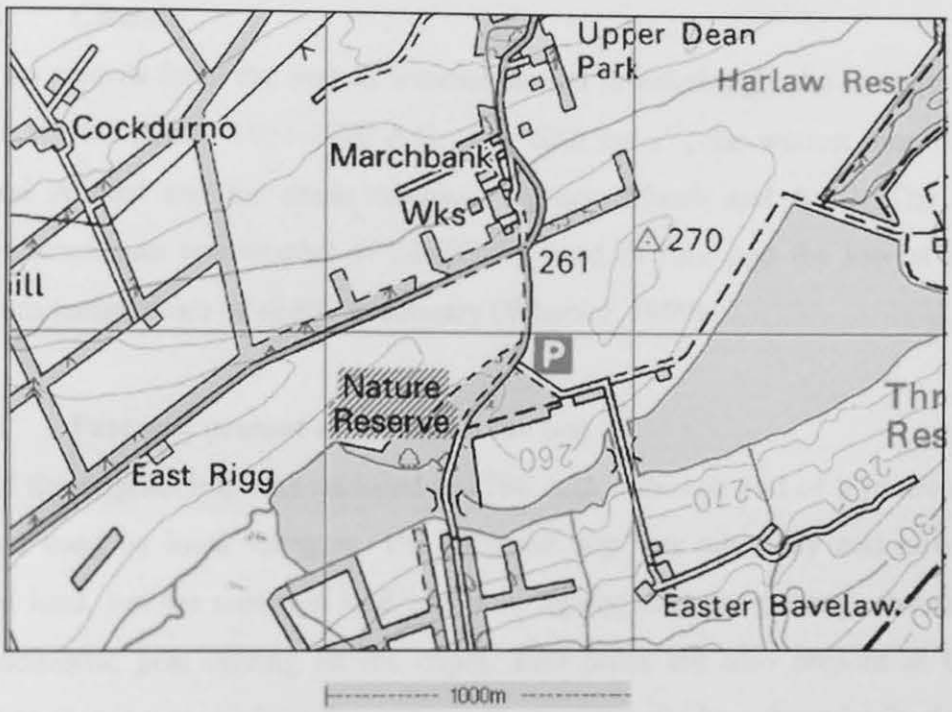

b)

Figure 2.4: Location of The Red Moss of Balerno peat bog a) scale 1:10 km and b) scale 1:1 km (Ordnance Survey, 2005).

(*Calluna vulgaris*) and cotton grass (*Eriophorum vaginatum*) (Fig. 2.5). This northern section of the bog is up to 6 m deep in some places and has all the characteristics of an ombrotrophic peat bog with its convex shape and surface hummock/hollow microtopography (Scottish Wildlife Trust 2001, 2005; Scottish Natural Heritage, 2005).

Figure 2.5: View to the north from The Red Moss of Balerno.

2.1.3.4 Climate

Based on records from the nearest weather station in Edinburgh, the average annual rainfall, for the period 1951-1980 A.D., was 62.6 cm y^{-1}, the wettest months being July and August and the driest months February, March and April. The highest average maximum temperature of 23.4°C occurred in June and the lowest average minimum temperature of -6.6°C in January (Wheeler, 1999).

2.1.3.5 Past and present activities on the bog

Most of the original bog was enclosed in 1768 A.D. although part of it remained as a common used by local villagers. The enclosed bog was cut away and now forms pastoral land, but the common land was only lightly used for grazing, shooting and some domestic peat cutting on the edges. Lint holes are also present at the site indicating that it was used for flax-retting. Parts of the site have been badly damaged by a drainage ditch running north-south and also a defunct aqueduct built on the south of the site in the late 19th century A.D. The aqueduct ran across the reserve from east to west and was used to carry water from the Harperrig reservoir in the

Pentlands to the Harelaw reservoir in order to supply the expanding city of Edinburgh with water. During the 1960s A.D. *Sphagnum* and *Polytrichum* moss was taken from the bog for horticultural purposes, but in 1986 A.D., The Red Moss of Balerno became part of the designated Pentlands Regional Park, protected as a Scottish Wildlife Trust wildlife reserve. The main drainage ditch was dammed and invading birch, pine and scrub were removed to preserve the natural state of the bog (Brooks and Stoneman, 1997; Scottish Wildlife Trust, 2001, 2005). At present the site is surrounded by areas of pastoral land and open forest or woodland, with a water treatment works situated to the north of the bog. The bog lies between two major roads, the A70 and A702 (*cf.* Fig. 2.4 a).

2.1.4 Turclossie Moss

2.1.4.1 Location and size

Turclossie Moss lies ~ 20 km east of Turriff and ~ 15 km south-west of Fraserburgh in north-east Scotland (Fig. 2.6 a). It lies in a flat basin to the south of the North Sea and is bounded by the hills of New Pitslago to the west, Craigculter to the south, Strichen to the east and Aberdour to the north. The Gonar burn, a tributary of North Ulgie Water, runs to the north of the bog (Fig. 2.6 b). Turclossie Moss represents the western end of a once much larger site of which only 63 ha of active raised bog remain (Scottish Wildlife Trust, 2005).

2.1.4.2 Geology

The Buchan area is underlain by metamorphic rocks (quartz mica schists) of Dalradian age which were covered with glacial deposits (clay and gravel). Turclossie Moss is not of lacustrine origin but is an ombrotrophic peat bog of the stream valley type, which formed on marshy ground along streams occupying a basin-like depression (Fraser, 1948).

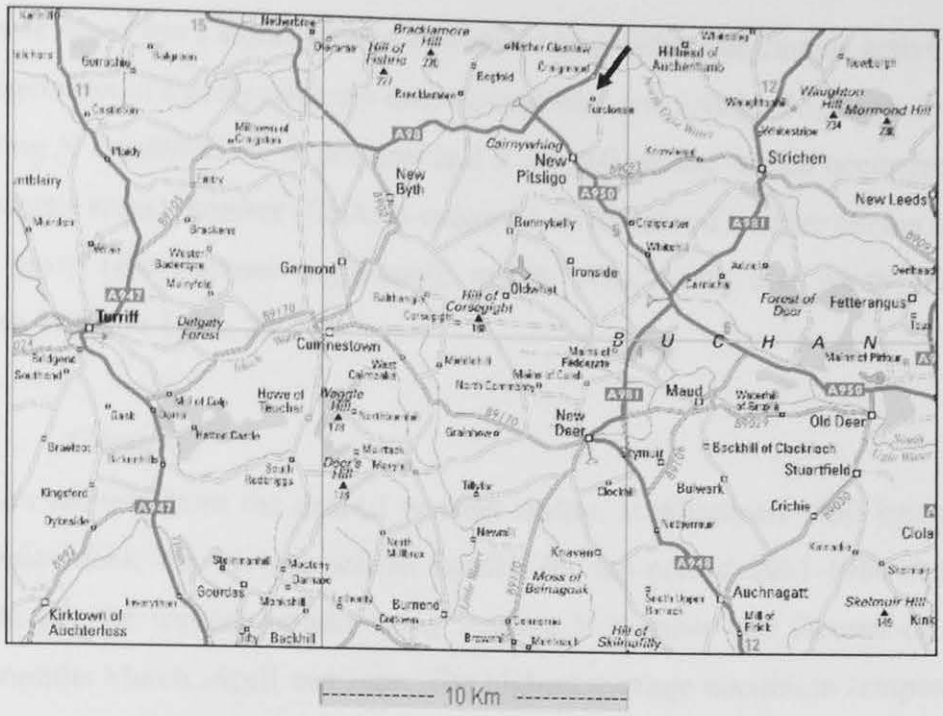

a)

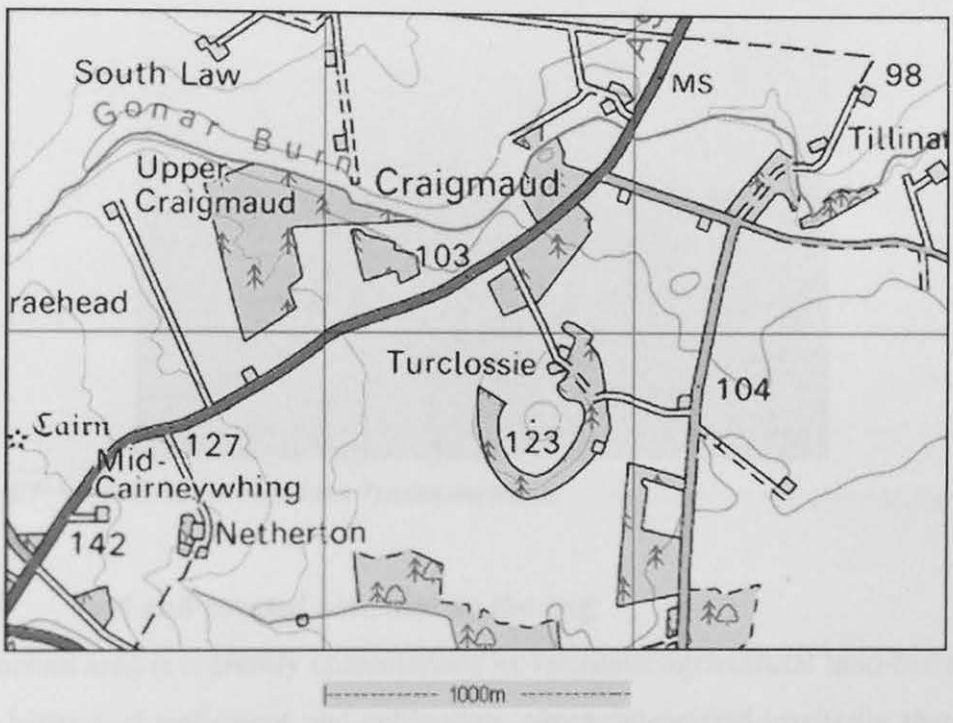

b)

Figure 2.6: Location of Turclossie Moss peat bog a) scale 1:10 km and b) scale 1:1 km (Ordnance Survey, 2005).

2.1.4.3 Vegetation

Turclossie Moss has a significant area of raised bog with a continuous active surface with vegetation in a predominantly near-natural state consisting of *Sphagnum species* (including *S. capillifolium, S. palustre* and *S. magellanicum,* which occur frequently in the wetter areas), heather (*Calluna vulgaris*), cross-leaved heather (*Erica tetralix*), cotton grass (*Eriophorum vaginatum*), marsh, fens, heath and scrub (Fig. 2.7) (Scottish Wildlife Trust, 2005).

2.1.4.4 Climate

Based on records from the nearest weather station at Aberdeen ~ 50 km south of Turclossie Moss, the average annual rainfall for the period 1951-1980 A.D., was 82.1 cm y^{-1}, the wettest months being August, November and December and the driest months March, April and June. The highest average maximum temperature of 22.9°C occurred in July and the lowest average minimum temperature of -5.8°C in January (Wheeler, 1999).

Figure 2.7: View to north-west from Turclossie Moss.

2.1.4.5 Past and present activities on the bog

The Buchan area is currently characterised by intensive agricultural land-use and has a long history of settlement and cultivation, which intensified gradually throughout the Mediaeval period, culminating in a rapid rural change which led to an increase in farm size and agricultural productivity during the late 18th century A.D. Turclossie Moss is a remnant of a much larger peatland and historical data indicates that

peatland losses in this part of north-east Scotland have been extensive and occurred rapidly during the 18th and 19th centuries A.D. when peatlands were regarded as fuel sources or wastelands which could be converted to agricultural use. This trend continued well into the 20th century A.D. with drainage, commercial peat cutting and afforestation becoming important. Coniferous afforestation of these peatlands during the 1960s and 1970s A.D. became a widespread form of damage to the bogs and, as a result of past peat cutting activities, Turclossie Moss is now surrounded by cut-over bogs on all sides which have resulted in a lowering of the water table. In 1996 A.D., however, the site was designated as a special area of conservation and, although privately owned, it is protected by Scottish Natural Heritage (Fraser, 1948; Johnston and Soulby, 2000; Scottish Wildlife Trust, 2005). At present the site is surrounded by agricultural land, deciduous woodland and commercial forest. The major roads which run to the north and south of the bog, are the A98 and A950, respectively.

2.1.5 Carsegowan Moss

2.1.5.1 Location and size

Carsegowan Moss in south-west Scotland lies ~ 6 km away from both Newton Stewart in the north and Wigtown in the south (Fig. 2.8 a). It is situated north of The Machars, the flat area of land between the Galloway hills in the north and the Solway Firth in the south. To the east of the bog runs Bishop Burn (Fig 2.8 b), a tributary of the River Cree which joins the Solway Firth at Wigtown Bay ~ 4 km east of the bog. With an area of 50 ha, Carsegowan Moss represents one of the largest surviving areas of relatively intact ombrotrophic peat bog in south-west Scotland (Scottish Wildlife Trust, 2005).

2.1.5.2 Geology

The close proximity of Carsegowan Moss to the Solway Firth and its very name, 'carse', the term used for the alluvial floodplain that occurs beside a river or estuary, indicate the estuarine origin of this bog, which formed on top of marine clay deposits that were left at the end of the last ice age when rising sea levels flooded the area.

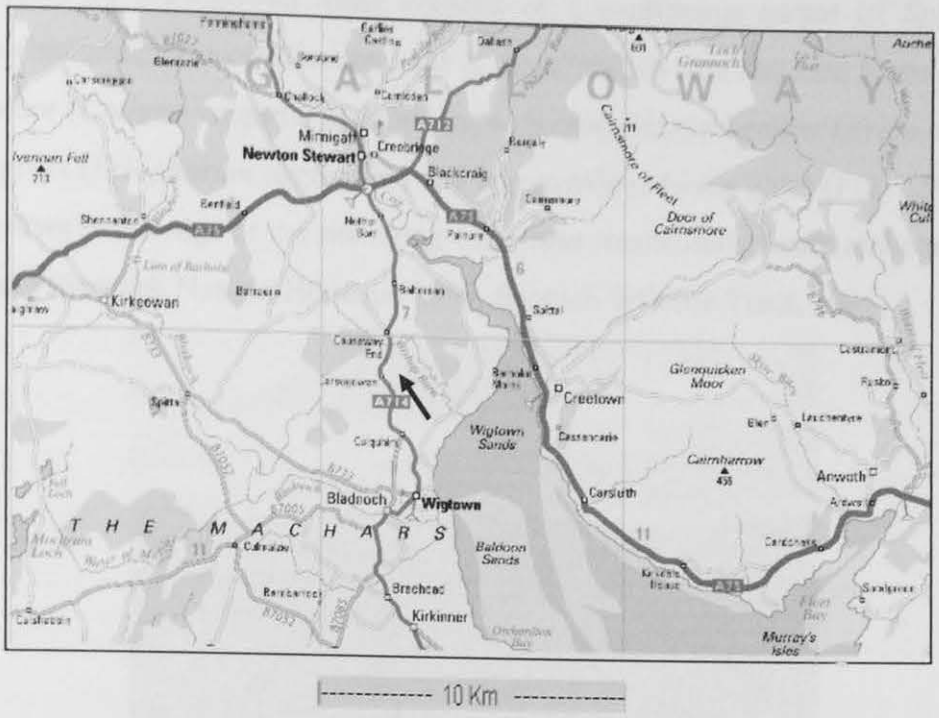

a)

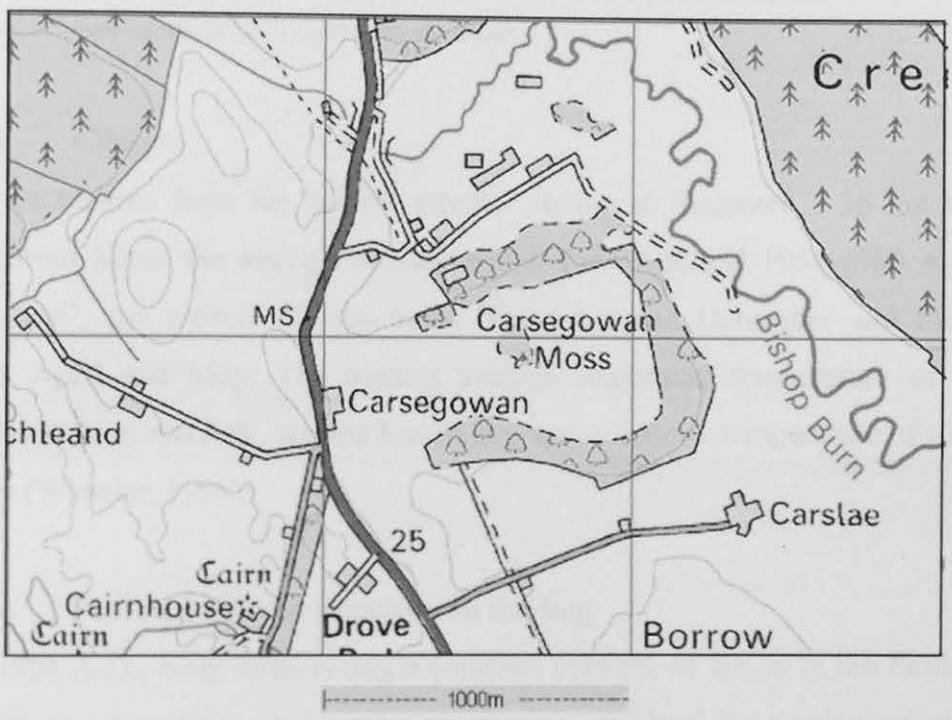

b)

Figure 2.8: Location of Carsegowan Moss peat bog a) scale 1:10 km and b) scale 1:1 km (Ordnance Survey, 2005).

2.1.5.3 Vegetation

The surface of Carsegowan Moss consists of a continuous carpet of *Sphagnum* species (including *S. magellanicum* and *S. capillifolium* and the rare *S. pulchrum*), but heather (*Calluna vulgaris*) is dominant with cross-leaved heather (*Erica tetralix*), cotton grass (*Eriophorum vaginatum*) and bog myrtle (*Myrica gale*) (Fig. 2.9). Birch scrub grows at the edge of the site along with some marsh, fens, heath and coniferous woodland (Scottish Natural Heritage, 2005; Scottish Wildlife Trust, 2005).

Figure 2.9: View to north from Carsegowan Moss.

2.1.5.4 Climate

Based on records from the nearest weather station at Stranraer ~ 36 km west of Carsegowan Moss, the average annual rainfall for the period 1951-1980 A.D. was 95.5 cm y^{-1}, the wettest months being November and December and the driest months April and May. The highest average maximum temperature of 23.9°C occurred in June and July, and the lowest average minimum temperature of -6.8°C in January (Wheeler, 1999).

2.1.5.5 Past and present activities on the bog

From 1908 A.D., early farmers dug a complex network of drains in the fields along the southern edge of the site in order to 'improve' the land for grazing animals and, at a later date, large east-west ditches were added. Coniferous planting in the north-west of the moss and peripheral peat cutting have also occurred in the last century.

These past activities on the bog have resulted in a lowering of the water table and drier conditions have encouraged the growth of birch scrub and some pine trees on the bog. One of the most interesting activities that took place in close proximity to the bog was the operation of "The Carsegowan Moss explosives factory" situated to the north of the present nature reserve (see Appendix A1 for site plan of the factory). This factory operated during WW2 from 1940 to 1945 A.D., manufacturing gun powder required for bomb detonators, aircraft flares and fuses in shells. A railway to the west of the bog was in operation from the 19th century A.D. and used to run between Newton Stewart and Wigtown. During WW2 a siding off the main railway line into the explosives factory was created for the transportation of materials to and from the site. This railway line was dismantled after the war and the major A714 road, situated to the west of the main railway line, is used as the major transport link today. The old site of the explosives factory is now privately owned and is used for agricultural purposes and as a plant nursery (Sawden, 2003). Carsegowan Moss was acquired by the Scottish Wildlife Trust as a nature reserve in 1993 A.D. and the damming of drainage ditches and removal of birch scrub and pine trees has resulted in a perceptible rise in the water table and noticeable increases in *Sphagnum* cover (Scottish Wildlife Trust, 2005). At present, the site is surrounded by agricultural land, woodland and some dense commercial forest.

2.2 PEAT CORE COLLECTION

2.2.1 Peat core collection procedure

Peat cores were taken from the centre of moss hummocks on domed parts of the bogs and sampling positions were recorded using a Global Positioning System (GPS). Long cores were collected using a Cuttle and Malcolm (1979) corer (Fig. 2.10) (110 cm x 5 cm x 5 cm) pushed vertically into the bog. Monoliths were collected using a monolith tin (50 cm x 15 cm x 7 cm), which was inserted into the vertical face of a freshly dug pit. Visual observations, including the position of the vegetation-peat interface, peat colour, wetness and amount of decomposition, were recorded for each collected peat core. The cores were sliced into sections on-site using a serrated

stainless steel knife and sections were packed into polyethylene bags and transported to the laboratory for processing. Moss samples collected from hummocks where cores were collected were identified using a *Sphagnum* field guide (Hill, 1992) and moss identification book (Jahns, 1980). Identification codes were allocated to peat cores according to the name of the site and year of core collection, the type of corer used (CM for Cuttle and Malcolm corer and M for monolith tin) and the number of the core, as often more than one core was collected from each site at a time (e.g. for use on different/future projects). Also, in the case of the Flanders Moss core collected in 2004, the identification code took account of the position on the bog from which the core was collected.

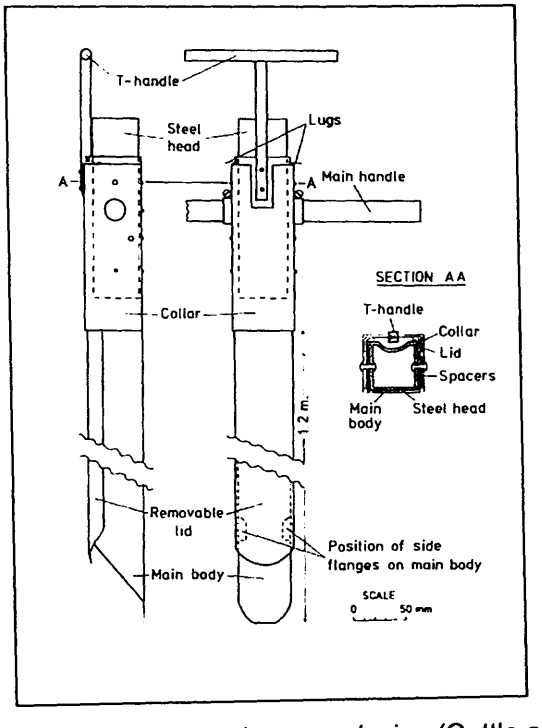

Figure 2.10: Details of the Cuttle and Malcolm corer design (Cuttle and Malcolm, 1979).

2.2.2 Details of peat cores collected at each site

2.2.2.1 Flanders Moss

Cores were collected in 2001 and 2004 from the south-west dome of the bog (56°09'N, 4°12'W) (Fig. 2.11). On 11th September 2001, a 106 cm in length peat core (FM01CM-1) with cross-sectional dimensions 5 cm x 5 cm was collected from a

S. palustre hummock, after ~ 7 cm of grassy vegetation was first cut with a knife to enable penetration of the corer. On 5th October 2004, a further 33 cm in length peat core (FM04-1-M) (Fig. 2.12) with cross-sectional dimensions 20 cm x 10 cm, was collected from a *S. papillosum and Aulacomnium palustre* hummock. The FM01CM-1 core was cut into 1-cm sections and the FM04-1-M core was cut into 3-cm sections in the field.

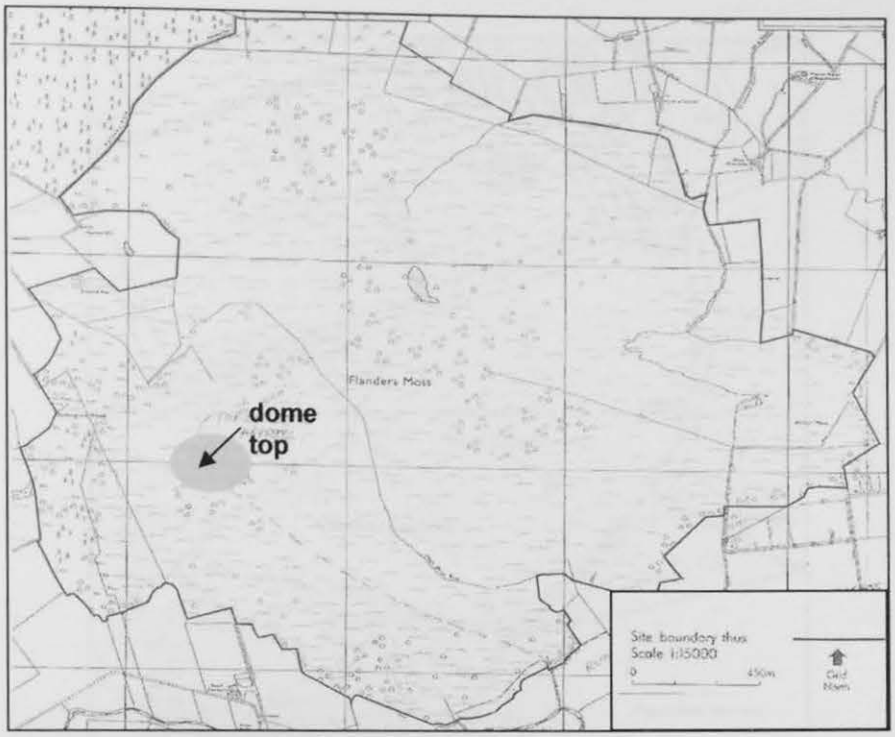

Figure 2.11: Location of the sampling site on Flanders Moss peat bog.

Figure 2.12: FM04-1-M peat core as collected in monolith tin.

2.2.2.2 The Red Moss of Balerno

Cores were collected from the eastern side of the northern section of the bog (55°51'N, 3°20'W) (Fig.2.13) on 3rd June 2003. An 83 cm in length core (RM03CM-1) and a 96 cm in length core (RM03CM-2) (Fig. 2.14), each with cross-sectional dimensions 5 cm x 5 cm, were collected from *Pleurozium schreberi* hummocks (~ 3 m apart) and cut into 2-cm sections in the field.

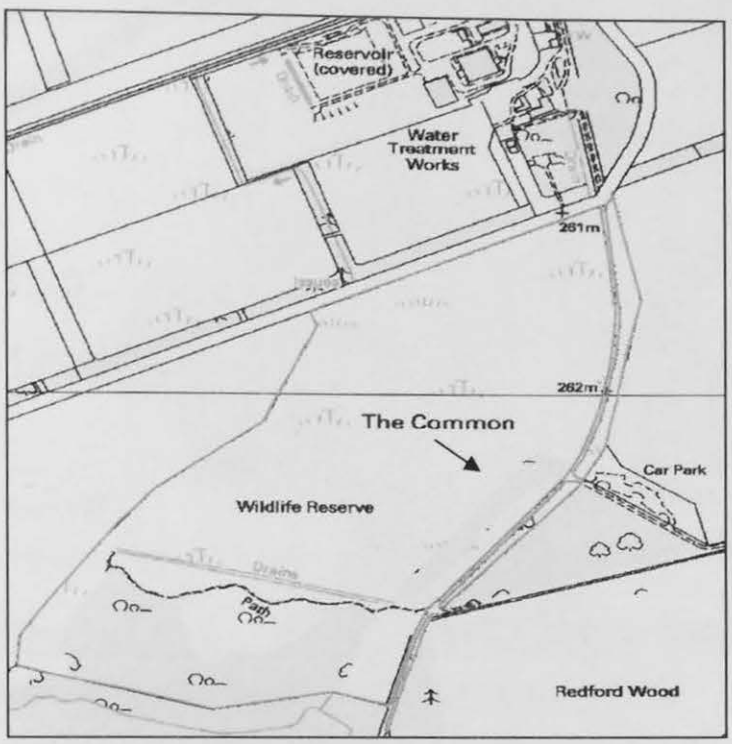

Figure 2.13: Location of the sampling site on The Red Moss of Balerno peat bog.

Figure 2.14: RM03CM-2 peat core as collected in corer casing.

2.2.2.3 Turclossie Moss

Cores were collected from the south-east of the bog (57°37'N, 2°11'W) (Fig.2.15) on 3rd August 2004. A 109 cm in length core (TM04CM-2) (Fig. 2.16) with cross-sectional dimensions 5 cm x 5 cm and a 47 cm in length core (TM04M-1) (Fig. 2.17) with cross-sectional dimensions 15 cm x 12 cm were collected from the

same *S. capillifolium* hummock. Also, a 112 cm in length core (TM04CM-4) (Fig. 2.18) with cross-sectional dimensions 5 cm x 5 cm, was collected from the bottom of the pit from which the TM04M-1 core had been previously taken, by inserting the Cuttle and Malcolm corer immediately into the peat below. All peat cores were cut into 2-cm sections in the field.

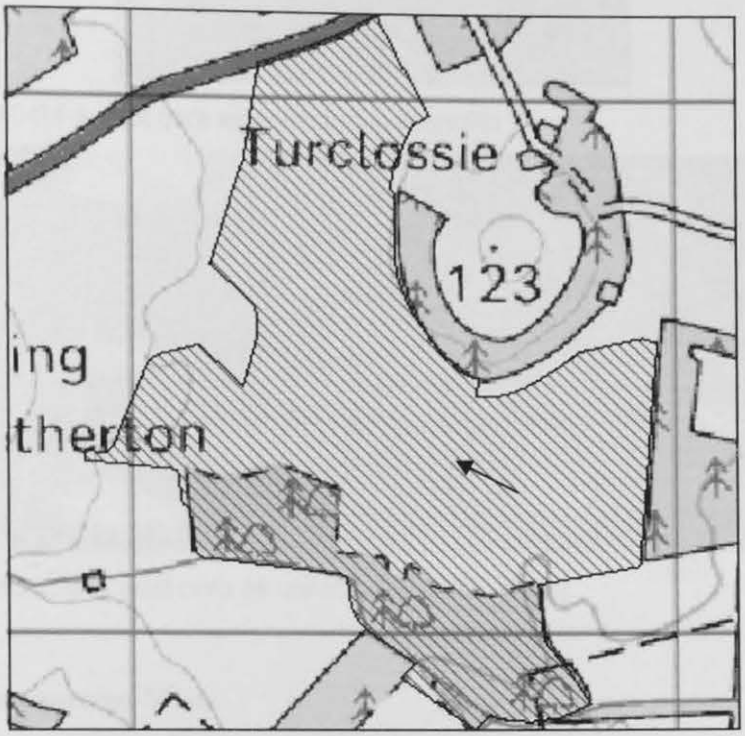

Figure 2.15: Location of the sampling site on Turclossie Moss peat bog.

Figure 2.16: TM04CM-2 peat core as collected in corer casing.

Figure 2.17: TM04M-1 peat core as collected in monolith tin.

Figure 2.18: TM04CM-4 peat core as collected in corer casing.

2.2.2.4 Carsegowan Moss

Cores were collected from the centre of the bog (55°12'N, 2°43'W) (Fig.2.19) on 4th May 2004. A 106 cm in length core (CM04CM-1) (Fig. 2.20) with cross-sectional dimensions 5 cm x 5 cm was collected from a *S. magellanicum* hummock and a 50 cm in length core (CM04M) with dimensions 15 cm x 9 cm was collected from a *S. capillifolium* hummock (~ 3 m away from the CM04CM-1 hummock), both cores being cut into 2-cm sections in the field.

Figure 2.19: Location of the sampling site on Carsegowan Moss peat bog.

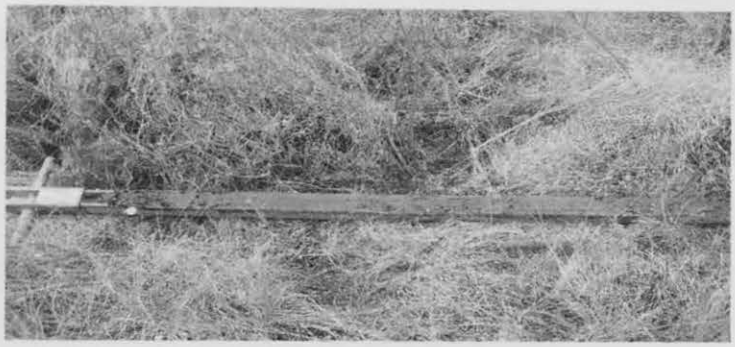

Figure 2.20: CM04CM-1 peat core as collected in corer casing.

2.3 PHYSICAL PREPARATION AND DETERMINATION OF PHYSICAL PROPERTIES OF PEAT SAMPLES

2.3.1 Physical preparation of peat samples

On return to the laboratory, wet peat sections were weighed and subsequently air-dried at 30°C for ~ 30 days on drying trays, before being re-weighed and ground using a ceramic mortar and pestle to < 2 mm and stored in labelled air-tight polyethylene bags.

2.3.2 Determination of physical properties of peat samples

2.3.2.1 Wet/dry weight ratios and water contents

Using the wet weights and air-dried weights of the peat sections, wet/dry weight ratios and water contents (weight per cent) were determined using the following equations:

$$\text{Wet/dry weight ratio} = \text{mass of wet peat (g)} / \text{mass of air-dried peat (g)}$$

$$\text{Water content (\%)} = [(\text{mass of wet peat (g)} - \text{mass of air-dried peat (g)}) \times 100] / \text{mass of wet peat (g)}$$

2.3.2.2 Moisture and ash contents

The moisture contents (weight per cent) of the air-dried peat sections were determined by accurately weighing out ~ 0.25 g sub-samples of air-dried peat into pre-weighed Pyrex beakers and heating them in an oven at 105°C for at least sixteen hours, before cooling to room temperature in a desiccator and re-weighing. The ash contents (weight per cent) of the peat sections were determined by placing these Pyrex beakers (containing 105°C dried peat sub-samples) in a Eurotherm Carbolite muffle furnace for four hours at 450°C, before cooling to room temperature in a desiccator and re-weighing. The moisture and ash contents (weight per cent) were determined using the following equations:

$$\text{Moisture content of air-dried peat (\%)} = [(\text{mass of air-dried peat (g)} - \text{mass of peat dried at 105°C (g)}) \times 100] / \text{mass of air-dried peat (g)}$$

$$\text{Ash content of 105°C dried peat (\%)} = \text{mass of ash (g)} \times 100 / \text{mass of peat dried at 105°C (g)}$$

Note that ash contents were expressed relative to the peat sub-sample dry weights at 105°C (i.e. corrected for air-dried peat moisture contents). Also, moisture contents of each certified reference material that was used (see Section 2.10) were determined for at least three sub-samples.

2.3.2.3 Bulk densities

Two different methods were used to determine peat bulk densities. The most common method, which uses the estimated volume of each peat section based on the cross-sectional area of the core and peat section thickness, was used for all cores except TM04CM-2, TM04CM-4 and CM04CM-1. For these three cores, bulk densities were determined using a more accurate method which involved the removal of plugs of known volume from each wet peat section using a stainless steel tube of diameter 16 mm (Roos-Barraclough *et al.*, 2002). Wet plugs were weighed, air-dried and re-weighed (*cf.* Section 2.3.1) before being ground along with the remaining peat from the corresponding sections from which the plugs were taken. Bulk densities (g cm^{-3}) were determined using the following equations as appropriate:

$$\text{Bulk density} = \text{mass of air-dried peat section (g)} / \text{volume of peat section } (cm^3)$$

$$\text{Bulk density} = \text{mass of air-dried peat plug (g)} / \text{volume of peat plug } (cm^3)$$

Note that bulk densities were expressed relative to the peat section or plug dry weights at 105°C (i.e. corrected for air-dried peat moisture contents). Reproducibility between the two methods of bulk density determination was checked (using the CM04CM-1 core) and was found to be good. The average of the ratios of the densities (section/plug) determined using the two methods was 0.74 ± 0.09.

2.4 CHEMICAL PREPARATION OF SAMPLES FOR ANALYSIS

Peat samples were digested using a modified USEPA Method 3052 Protocol microwave-assisted HF-HNO_3 digestion method (Yafa and Farmer, 2006). This total-total digestion method (i.e. complete dissolution of all mineral materials where elements are held within the peat) involved transferring the ashed peat sub-samples (*cf.* Section 2.3.2) into Teflon microwave digestion vessels with 9 ml HNO_3 (16 M) and 0.5 ml of concentrated HF. The vessels were then sealed and digested in a CEM MARS 5 microwave digestion system (CEM, Buckingham, UK) using the microwave programme shown in Table 2.1.

Table 2.1: CEM MARS 5 microwave digestion system settings.

Stage	Power (W)	%	Ramp (min)	Pressure (psi)	Temp (°C)	Hold (min)
1	1200	100	3.0	300	175	0.0
2	1200	100	2.5	300	180	9.5

Control vessel pressures and temperatures were monitored during the digestion procedure. A batch of 14 samples could be digested at a time and each batch included at least one sample blank and one sample of NIMT/UOE/FM001 peat reference material (Yafa *et al.*, 2004), for blank correction (see Section 2.5) and quality assurance (see Section 2.10), respectively. After cooling, the digests were transferred into Teflon beakers and evaporated down to approximately 1 ml on a hotplate, before being made up to 25 ml in polypropylene volumetric flasks with 2 % (v/v) HNO_3 and stored in Sterilin tubes prior to analysis. Duplicate samples were digested for the FM01CM-1, RM03CM-2, TM04CM-2, TM04CM-4 and CM04CM-1 peat sections, but only single samples for the FM04-1-M, RM03CM-1, TM04M-1 and CM04M peat core sections.

Note that all reagents used in sample preparation and analysis were of the highest analytical quality available, i.e. Aristar HNO_3 (69 %) and HF (48 %) (VWR, Poole, UK) and high purity water (18.2 MΩ cm) from a Milli-Ro water system (Millipore, Watford, UK). All glassware used was acid washed (heated in 5 M HNO_3 for four hours then heated in deionised water for four hours).

2.5 DETERMINATION OF ELEMENTAL CONCENTRATIONS USING ICP-OES

Elemental concentrations (Al, Ca, Cd, Co, Cr, Cu, Fe, Mg, Mn, Ni, P, Pb, S, Ti, V and Zn) were determined in digest solutions using ICP-OES. Two different instruments were used during this research project: the Thermo Jarrell Ash IRIS ICP-OES (Thermo Electron Cambridge, UK), equipped with a cross-flow nebuliser, glass concentric spray chamber and autosampler, was used for the analysis of FM01CM-1, RM03CM-1, RM03CM-2 and half of the CM04CM-2 core samples; a

Perkin Elmer Optima 5300 DV ICP-OES (Perkin Elmer, Beaconsfield, UK), equipped with a Gem-cone cross-flow nebuliser, Scott spray chamber and AS 93 plus autosampler was used for analysis of FM04-1-M, TM04CM-2, TM04CM-4, TM04M-1, CM04M, the second half of the CM04CM-1 core samples and also the additional coal and galena samples (see Section 2.15). Instrumental operating conditions for each instrument are shown in Table 2.2.

Table 2.2: ICP-OES instrumental operating conditions.

Parameter	Thermo Jarrell Ash IRIS ICP-OES	Perkin Elmer Optima 5300 DV ICP-OES
Power (kW)	1400	1400
Plasma gas flow (L min^{-1})	15	15
Auxillary gas flow (L min^{-1})	0.75	0.20
Nebuliser gas flow (L min^{-1})	0.75	0.80
Pump rate (ml min^{-1})	1.85	1.50
Sample delay (sec)	40	30
Rinse time (sec)	40	30
Replicates	3	3
Replicate time (sec)	30	60
Stabilisation time (sec)	10	15
Viewing position	Axial	Axial

Prior to sample analysis the response of the instruments was calibrated using a reagent blank (2 % v/v HNO_3) and a set of multi-element standards, with elemental concentration ranges indicated in Table 2.3. All standards used for sample analysis were prepared in 2 % v/v HNO_3 on a daily basis by adequate dilution of the relevant Fisher or VWR 1000 mg L^{-1} standard stock solutions.

Table 2.3: ICP-OES calibration standard concentrations.

Element (s)	Concentration (mg L^{-1}) standard 1 (very low level)	Concentration (mg L^{-1}) standard 2 (low level)	Concentration (mg L^{-1}) standard 3 (medium level)	Concentration (mg L^{-1}) standard 4 (high level)
Al	6.25	12.5	25	50
Ca	3.75	7.5	15	30
Fe, Mg, S	2.50	5.0	10	20
P	1.25	2.5	5	10
Ti	0.625	1.25	2.5	5
Pb, Zn	0.25	0.5	1	2
Cd, Co, Cr, Cu, Mn, Ni, V	0.125	0.25	0.5	1

The standards prepared covered the concentration range expected in the samples and were within the linear concentration range for each element. Calibration curves were generated for each chosen element emission line in the instrumental software and only those with correlation coefficients (R^2) of at least 0.999 or better were acceptable for use. Reagent blanks, sample blanks and reference material samples were included in each batch of sample analyses and, in order to check (and correct if necessary) for drift in the instrument response, an appropriate calibration standard was re-analysed after every ten samples (method of bracketing standards). Sample solution concentrations were blank corrected by subtracting the average concentrations in the sample blank solutions (if detectable) and elemental concentrations in peat/reference materials were determined using the following equation:

$$C = C_O \times V_L / M_{sample}$$

Where C = Concentration (mg kg^{-1})

C_O = blank corrected concentration of element in digest solution (mg L^{-1})

V_L = final volume of extract (L)

M_{sample} = Mass of air-dried peat sub-sample corrected for moisture content (kg)

Note that elemental concentrations were expressed on a 105°C dried weight basis (i.e. corrected for moisture contents in air-dried material).

Emission lines used for each element, chosen on the basis of sensitivity and absence of spectral interferences, are shown for each ICP-OES instrument in Table 2.4. Detection limits for each element were estimated as three times the standard deviation of the mean for the sample blank (after running a sample blank solution through the instrument ten times) (Miller and Miller, 2000) and are shown, expressed in terms of peat concentration (mg kg^{-1}), in Table 2.4. Where elemental concentrations were below or close to the detection limit, samples were re-analysed by ICP-MS (see Section 2.7).

Table 2.4: Element emission lines used and estimated detection limits determined by the Thermo Jarrell Ash IRIS ICP-OES and Perkin Elmer Optima 5300 DV ICP-OES.

Element	Thermo Jarrell Ash IRIS ICP-OES emission line (nm)	Perkin Elmer Optima 5300 DV ICP-OES emission line (nm)	Thermo Jarrell Ash IRIS ICP-OES detection limit (mg kg^{-1})[a]	Perkin Elmer Optima 5300 DV ICP-OES detection limit (mg kg^{-1})
Al	308.2	308.2	3	9
Ca	317.9	317.9	0.7	3
Cd	228.8	228.8	0.3	0.03
Co	228.6	228.6	0.5	0.06
Cr	283.5	283.6	0.5	2
Cu	224.7	224.7	0.4	0.3
Fe	239.5	239.6	0.4	4
Mg	279.5	279.1	2	0.6
Mn	260.5	260.6	0.1	0.02
Ni	231.6	231.6	1	0.07
P	178.2	178.2	5	1
Pb	220.3	220.3	3	0.2
S	180.7	180.7	5	8
Ti	334.9	334.9	0.5	0.2
V	292.4	292.4	0.5	0.07
Zn	202.5	202.6	0.2	1

[a]Yafa (2004).

Typical internal analytical precision (1 SD) on the measured element concentrations in peat digest solutions, based on the standard deviation of the mean value for three consecutive determinations, was $\leq \pm$ 8%. Mean external analytical precision (1 SD) on the measured element peat concentrations, as determined by repeated analysis (n = 67) of the certified peat reference material NIMT/UOE/FM001 over the three-year project, ranged from ± 6 - 30% (see Table 2.9). This range is large because concentrations of some elements (e.g. Cd, Co and Cr) in the reference material were closer to the detection limits than others (e.g. Al, Ca, Fe, Mg, P and S) (*cf.* Tables 2.4 and 2.9). Note that a significant number of outlying values were omitted for Cd (n = 28) and Cr (n = 53), and for this reason, as well as the lower detection limits and greater accuracy of concentration determinations using ICP-MS, Cd and Cr concentrations determined by ICP-MS were used preferentially.

2.6 DETERMINATION OF Pb CONCENTRATIONS AND STABLE Pb ISOTOPIC RATIOS USING ICP-MS

Concentrations of Pb and stable Pb isotopic ratios ($^{206}Pb/^{207}Pb$, $^{208}Pb/^{206}Pb$ and $^{208}Pb/^{207}Pb$) were determined in digest solutions using a quadrupole ICP-MS. Concentrations of Pb were determined only in samples with Pb concentrations close to or below the ICP-OES detection limit (~ 3 and 0.2 mg kg^{-1} solid sample (or ~ 0.03 and 0.002 mg L^{-1} in solution) for Thermo Jarell Ash and Perkin Elmer ICP-OES instruments, respectively (*cf.* Table 2.4)). Measurements were carried out once (or twice if necessary) on samples which had already been analysed by ICP-OES, using a PlasmaQuad (PQ) 3 instrument (Thermo Electron, Winsford, UK), equipped with a Meinhard concentric nebuliser, quartz Scott spray chamber, nickel sampler and skimmer cones, Gilson autosampler and a Gilson Minipuls 3 peristaltic pump (Anachem, Luton, UK). Instrumental operating conditions for Pb concentration and Pb isotopic analysis are shown in Table 2.5.

Table 2.5: Instrumental operating conditions for Thermo Electron PQ3 ICP-MS.

Parameter	Setting
Detector mode	Pulse counting
Acquisition mode	Peak jumping
Dwell time (ms)	2.0
Reflected power (W)	1-3
Mass range (amu)	203.6-209.4
Argon coolant gas flow (L min^{-1})	13.1
Argon auxilliary gas flow (L min^{-1})	0.76-0.79
Argon nebuliser gas flow (L min^{-1})	0.81-0.85
Uptake rate (ml min^{-1})	0.55
Replicates for isotopic ratio determination	5
Replicates for concentration determination	3
Rinse time (sec)	30
Settle time (sec)	30
Uptake time (sec)	150
Acquisition time (sec)	60
Multiplier dead time (ns)	44-48

The instrument detector plateau and dead time were checked every six months (or if a new detector was fitted) to ensure satisfactory instrument sensitivity and to correct for isotope ratio dead time effects, respectively. Prior to sample Pb concentration and

Pb isotopic ratio analysis the instrument was optimised by tuning at mass 208 amu. When carrying out analysis that involved the simultaneous analysis of Pb concentrations and Pb isotopic ratios, the response of the instrument was calibrated for Pb concentration using a set of Pb standards with concentrations of 1, 5, 10, 20 and 40 μg L^{-1} and a solution of the National Institute of Standards and Technology (NIST) common Pb isotopic reference standard SRM 981, with $^{206}Pb/^{207}Pb = 1.093$, $^{208}Pb/^{206}Pb = 2.168$ and $^{208}Pb/^{207}Pb = 2.370$, was used for Pb isotopic ratio calibration and mass bias correction. Pb isotopic standards with concentrations of 6, 30 and 60 μg L^{-1} were used as appropriate to the levels of Pb in the samples. For analysis runs which involved the determination of Pb isotopic ratios alone, the instrument was calibrated only for Pb isotopic composition using the appropriate Pb isotopic standards.

If sample solution Pb concentrations were greater than ~ 60 μg L^{-1}, samples were diluted by the appropriate dilution factor using 2 % v/v HNO_3 and a sample blank was also chosen and diluted by the same factor for blank correction purposes. All blank corrections were carried out using the PQVision software (TG solutions, Winsford, UK). Standards were blank corrected using the 2 % v/v HNO_3 reagent blank solution that was analysed at the beginning of the run and samples were blank corrected with the appropriate diluted or undiluted sample blanks. The PQVision software also calculated and corrected for mass bias factors using the SRM 981 Pb isotopic ratio standards. In order to check and correct for drift in the instrument response, appropriate calibration standards (Pb concentration and SRM 981 Pb isotopic ratio standards) were re-analysed after every six to eight samples. For quality assurance, reference material samples (diluted if necessary) were also included in each batch of sample analyses. Pb concentrations in peat/reference material samples (expressed in terms of mg kg^{-1}) were determined (*cf.* Section 2.5) using the counts from the ^{206}Pb isotope.

The estimated detection limit for Pb concentration determination was 0.07 mg kg^{-1} and the typical internal analytical precision (1 SD) for Pb concentration

determination, based on the standard deviation of the mean value for five consecutive determinations of Pb concentration of a sample solution, was $\leq \pm$ 6%. For Pb isotopic ratio determination, based on the standard deviation of the mean value for five consecutive determinations of the isotopic ratio of a sample solution, the corresponding value for each individual isotope ratio measured ($^{206}Pb/^{207}Pb$, $^{208}Pb/^{206}Pb$ and $^{208}Pb/^{207}Pb$) was $\leq \pm$ 0.3%. Mean external analytical precision (1 SD) of measured Pb concentrations, as determined by repeated analysis (n = 10) of the low level Pb concentration certified Peach Leaves reference material GBW 08501 over the three year project, was ± 10% and mean external analytical precision (1 SD) of measured isotopic ratios, $^{206}Pb/^{207}Pb$, $^{208}Pb/^{206}Pb$ and $^{208}Pb/^{207}Pb$, as determined by repeated analysis (n = 59) of the certified peat reference material NIMT/UOE/FM001 over the three year project, was ± 0.17%, ± 0.29% and ± 0.28%, respectively (see Table 2.9).

2.7 DETERMINATION OF ELEMENTAL CONCENTRATIONS USING ICP-MS

Elemental concentrations (As, Cd, Co, Cr, Cu, Mn, Ni, Sb, Sc, Se, V, Y and Zr) were determined in digest solutions using ICP-MS. Using the same PQ3 instrument described in Section 2.6, measurements were carried out once (or twice if necessary) on samples which had already been analysed by ICP-OES. Instrumental operating conditions were the same as those shown in Table 2.5 with the exception of the mass range, which was 45 - 123 amu. Also, prior to sample concentration analysis the instrument was optimised by tuning at mass 120 amu and an instrument mass calibration was performed using PlasmaLab software (TG solutions, Winsford, UK). The instrument response was calibrated using a reagent blank (2 % v/v HNO_3) and a set of multi-element standards, with elemental concentrations of 1, 2, 5, 10, 50 and 100 $\mu g\ L^{-1}$.

Reagent blanks, sample blanks and reference material samples were included in each batch of sample analyses. Sample solution concentrations were blank corrected (i.e.

by subtracting the average concentrations in the sample blank solutions (if detectable)) and elemental concentrations in peat/reference material samples (expressed in terms of mg kg^{-1}) were determined. The rare elements Ga (^{71}Ga) and In (^{115}In) and also, at a later stage in the project, Rh (^{103}Rh), were used as possible internal standards to correct for any matrix effects and instrumental drift when determining elemental concentrations using ICP-MS. These elements were chosen to cover the range of masses being monitored and all blank, standard and sample solutions were spiked with the internal standard element(s) to give a final concentration of 10 μg L^{-1}. Unfortunately, these elements turned out to be present in the peat and reference materials at small but significant concentrations (≤ 1 mg kg^{-1}) and therefore this approach was unsuccessful. The repeated use of appropriate bracketing standard solutions, analysed after every eight samples, was used to make corrections for instrumental drift. While the internal standard method would have provided continuous monitoring for drift and may therefore be considered to be a more robust method, the bracketing standards approach used in this project appeared to be sufficient and successful, as demonstrated by the data for certified reference materials in Table 2.9.

The isotopes used for each element, chosen on the basis of isotopic abundance, the absence of polyatomic ion interferences and the quality of generated calibration curves, are shown in Table 2.6. Note that the PlasmaLab software corrected for interferences, where applicable, using its default interference correction equations (Thermo Electron, 2004). Detection limits were estimated for each element and are also shown in Table 2.6.

Typical internal analytical precision (1 SD) on the measured element concentrations in peat digest solutions, based on the standard deviation of the mean value for three consecutive determinations, was ≤ ± 10%. Mean external analytical precision (1 SD) on the measured element peat concentrations, as determined by repeated analysis (n = 63) of the certified peat reference material NIMT/UOE/FM001 over the three year project ranged from ± 7 - 30% (see Table 2.9). This range is large because

concentrations of some elements (e.g. Se) in the reference material were closer to the detection limits than others (e.g. Mn, Sb and Zr) (*cf.* Tables 2.6 and 2.9).

Table 2.6: Element masses used and estimated detection limits determined by the Thermo Electron PQ 3 ICP-MS.

Element	Mass (amu)	Estimated detection limit ($\mu g\ kg^{-1}$)
As	75	6.9
Cd	111	1.6
Co	59	1.3
Cr	52	3.4
Cu	65	66
Mn	55	5.1
Ni	60	20
Sb	123	0.38
Sc	45	2.8
Se	82	29
V	51	4.2
Y	89	0.20
Zr	90	1.5

2.8 CHEMICAL PREPARATION AND DETERMINATION OF Hg CONCENTRATIONS USING CVAAS

2.8.1 Peat cores chosen for Hg concentration determination

Concentrations of Hg were determined for peat cores from only three of the four sampling sites. For Flanders Moss, the 2-cm sections of a 100-cm FM01CM-1 sister core, FM01CM-2, collected from the same hummock as the FM01CM-1 peat core after removal of ~ 10 cm of grassy vegetation from the surface (Farmer *et al.*, 2006), were analysed as part of an associated undergraduate research project (Shimwell, 2002). For The Red Moss of Balerno, all of the sections of the RM03CM-2 peat core were analysed as part of this research project and, for Carsegowan Moss, the upper 48 cm of the CM04CM-1 core were analysed as part of another undergraduate research project (MacDonald, 2005).

2.8.2 Chemical preparation of peat samples

Samples were prepared using a modified HNO_3/H_2SO_4 digestion and wet oxidation method, specially developed by Ure and Shand (1974) for samples containing

organic matter, such as peat. Approximately 0.5 g air-dried peat sub-samples were accurately weighed out into Kjeldahl flasks, 10 ml of HNO_3 (16 M) and 10 ml of H_2SO_4 (18 M) were added, and the samples heated under reflux at ~ 60°C for two hours using a Fisons Kjeldahl apparatus. A batch of six samples could be digested at a time and each batch included at least one sample blank and a sample of NIMT/UOE/FM001 peat reference material. After cooling, 10 ml of deionised water was added via the condensers. Samples were then removed from the apparatus and ~ 50-60 ml of 6% (w/v) $KMnO_4$ added gradually to each sample in 5 ml aliquots until the purple colour was retained for at least one hour. To ensure complete oxidation, the $KMnO_4$ was reacted with the samples overnight at room temperature. Excess $KMnO_4$ was then reduced by adding ~ 1 ml of 20% (w/v) $NH_2OH.HCl$ to each sample, leaving clear solutions with a residue of insoluble material. Samples were left for one hour to allow the liberation of evolved gases, before being filtered through Whatman No. 541 filter papers. To the filtrate was added 1 ml of 0.4% (w/v) Dow Corning DB 110A Antifoaming agent and 1 ml of 1% $K_2Cr_4O_7$ and the sample solutions were then made up to 100 ml with deionised water. Single sample digestions and analyses were carried out for all of the FM01CM-2 and RM03CM-2 peat sections (with repeat digestions and analyses for selected samples). Duplicate sample digestions and analyses were carried out for CM04CM-1 peat sections.

2.8.3 Determination of Hg concentrations using CVAAS

Acid extractable Hg concentrations were determined in digest solutions using CVAAS. The instrument used was a continuous flow cold-vapour atomic absorption system consisting of a Varian VGA-76 accessory attached to a Varian SpectrAA 400 spectrometer (Varian Ltd, Oxford, UK). The 0.3% $NaBH_4$ and 5 M HCl reagents were prepared daily and the instrument operating conditions used are shown in Table 2.7. Prior to sample analysis the instrument response was calibrated using a reagent blank (5% v/v HNO_3) and a set of Hg standards with concentrations of 0.5, 1, 2, 4 and 5 $\mu g\ L^{-1}$. Absorbance values obtained for the standards were used to prepare calibration curves and using a linear regression fit, calibration equations were used to convert sample absorbance values to concentration values.

Table 2.7: Instrumental operating conditions for the determination of Hg using Varian VGA 76 and SpectrAA 400 CVAAS.

Parameter	Setting
Hollow Cathode Lamp (HCL) current (mA)	6
Analytical wavelength (nm)	253.7
Slit width (nm)	0.5
Slit height	Normal
Atom cell type	Flow through cell
Argon gas supply pressure (psi)	46
Measurement mode	Integration
Uptake rate (ml min^{-1})	10
Replicates	3
Measurement time (sec)	5
Delay time (sec)	60
Sample introduction	Manual

Reagent blanks, sample blanks and NIMT/UOE/FM001 peat reference material samples were included in each batch of sample analyses and, in order to check and correct for instrumental drift, bracketing standards were used with an appropriate calibration standard being re-analysed after every four to six samples. Sample solution concentrations were blank corrected by subtracting the average concentration in the sample blank solutions (if detectable) and Hg concentrations in peat/reference material samples (expressed in terms of $\mu g\ kg^{-1}$) were determined. The detection limit, determined using the 0.5 $\mu g\ L^{-1}$ standard, was found to be 40 $\mu g\ kg^{-1}$ (expressed in terms of solid concentration) and 0.20 $\mu g\ L^{-1}$ (expressed in terms of solution concentration). In some cases the sample concentrations measured were extremely low and close to the detection limit. Based on results that were obtained as part of this project, typical internal analytical precision (1 SD) on the measured Hg concentrations in peat digest solutions, based on the standard deviation of the mean value for three consecutive determinations, was $\leq \pm$ 8%. Mean external analytical precision (1 SD) of measured Hg concentrations as determined by repeated analysis (n = 23) of the certified peat reference material NIMT/UOE/FM001 over the project period was $\pm$ 21% (see Table 2.9).

2.9 DETERMINATION OF Fe CONCENTRATIONS USING FAAS

Concentrations of Fe were determined in 75 RM03CM-2 HNO_3/HF digest solutions using FAAS, because of analytical problems encountered with Fe analysis using the Thermo Jarrell Ash IRIS ICP-OES. A Thermo Electron ATI Unicam Solaar 929 FAAS (Thermo Electron, Cambridge, UK) with D_2 background correction was used as per the instrument operating conditions shown in Table 2.8.

Table 2.8: Instrumental operating conditions for the determination of Fe using Thermo Electron ATI Unicam Solaar 929 FAAS.

Parameter	Setting
Air/C_2H_2 gas flow (L min^{-1})	1.2
Analytical wavelength (nm)	346.6
Lamp current (%)	75
Slit width (nm)	0.2
Burner rotation (°)	30
Burner type (mm)	100
Background	Yes
Sample introduction	Manual
Replicates	3

Prior to sample analysis the instrument response was calibrated using a reagent blank (2 % v/v HNO_3) and a set of Fe standards with concentrations of 2.5, 5, 10 and 20 mg L^{-1}. The standards prepared covered the concentration range expected in the samples and were within the linear concentration range for Fe. Reagent blanks, sample blanks and NIMT/UOE/FM001 peat reference material samples were included in the batch of sample analyses and, in order to check (and correct if necessary) for instrumental drift, the 10 mg L^{-1} calibration standard was re-analysed after every ten samples. Sample solution concentrations were blank corrected and Fe concentrations in the peat and reference material were determined. Typical internal analytical precision (1 SD) on the measured Fe concentrations in peat digest solutions, based on the standard deviation of the mean value for three consecutive determinations, was $\leq \pm$ 7%. Mean external analytical precision (1 SD) of measured Fe concentrations as determined by the repeated analysis (n = 6) of the certified peat reference material NIMT/UOE/FM001 was $\pm$ 7% (see Table 2.9).

2.10 QUALITY ASSURANCE

To ensure the quality of analytical procedures and data, six different certified reference materials were prepared, digested and analysed alongside the samples: Ombrotrophic Peat (NIMT/UOE/FM001) (Yafa *et al.*, 2004), Canadian Peat (1878 P) (Barbante *et al.*, 2000), Bush Branches and Leaves (DC73349), Peach Leaves (GBW 08501), Coal (BCR CRM No. 40) and Coal (NBS SRM 1635). Note that the Canadian Peat reference material was not actually certified (*cf.* Section 1.15). A summary table of average values (± 1 SD) measured for each element and isotopic ratio, using each of the different analytical techniques, and reference material certified/information only values are shown in Table 2.9. All measurements for these six reference materials, including the moisture contents, are in Appendix A2.1 Tables A1 to A4, A2.2 Tables A1 and A2, A2.3 Tables A1 and A2, A2.4 Tables A1 and A2, A2.5 Tables A1 and A2 and A2.6 Tables A1 to A3. In general, good agreement between measured and certified/information only values was obtained for each of the elements/isotopic ratios in each of the reference materials. It is worth noting, however, that slightly low values were obtained for Al (using ICP-OES) and Cr (using ICP-OES and ICP-MS) in NIMT/UOE/FM001, Cd (using ICP-MS), Co (using ICP-OES and ICP-MS) and Zn (using ICP-OES) in Canadian Peat (1878 P) and V (using ICP-MS) and the $^{208}Pb/^{206}Pb$ ratio (using ICP-MS) in NBS SRM 1635 coal. Also, slightly high values were obtained for Cd (using ICP-MS) in BCR CRM No. 40 coal, Mn (using ICP-MS) in Bush Branches and Leaves (DC73349) and V (using ICP-OES) in NBS SRM 1635 coal (*cf.* Table 2.9).

Table 2.9: Summary of average (± 1 SD) elemental concentration (mg kg^{-1}), weight (%) and stable Pb isotopic ratio measurements, certified values and information only values (brackets) in Ombrotrophic Peat (NIMT/UOE/FM/001), Canadian Peat (1878 P), Bush Branches and Leaves (DC73349), Peach Leaves (GBW 08501), Coal (BCR CRM No. 40) and Coal (NBS SRM 1635) reference materials.

Element/isotopic ratio	Method	Reference Material	Measured value	Certified or information only value
Al	ICP-OES	NIMT/UOE/FM/001	2874 ± 643 mg kg^{-1} n = 67	(3692 ± 347 mg kg^{-1})
Al	ICP-OES	Canadian Peat (1878 P)	7346 ± 624 mg kg^{-1} n = 10	
Al	ICP-OES	Bush Branches and Leaves (NCS DC 73349)	0.20 ± 0.04 weight (%) n = 14	0.20 ± 0.03 weight (%)
Al	ICP-OES	Peach Leaves (GBW 08501)	903 ± 209 mg kg^{-1} n = 12	
Al	ICP-OES	BCR CRM No. 40 coal	24700 ± 400 mg kg^{-1} n = 2	
Al	ICP-OES	NBS SRM 1635 coal	0.32 ± 0.01 weight (%) n = 3	(0.32 weight (%))
As	**ICP-MS**	NIMT/UOE/FM/001	2.27 ± 0.21 mg kg^{-1} n = 63	(2.44 ± 0.55 mg kg^{-1})
As	**ICP-MS**	Canadian Peat (1878 P)	7.3 ± 0.81 mg kg^{-1} n = 11	(8.9 ± 0.75 mg kg^{-1})
As	**ICP-MS**	Bush Branches and Leaves (NCS DC 73349)	1.20 ± 0.10 mg kg^{-1} n = 15	1.25 ± 0.15 mg kg^{-1}
As	**ICP-MS**	BCR CRM No. 40 coal	14.2 ± 0.6 mg kg^{-1} n = 5	13.2 ± 1.1 mg kg^{-1}
As	**ICP-MS**	NBS SRM 1635 coal	0.43 ± 0.01 mg kg^{-1} n = 4	0.42 ± 0.15 mg kg^{-1}
Ca	ICP-OES	NIMT/UOE/FM/001	798 ± 74 mg kg^{-1} n = 67	(683 ± 198 mg kg^{-1})
Ca	ICP-OES	Canadian Peat (1878 P)	3.8 ± 0.2 weight (%) n = 10	
Ca	ICP-OES	Bush Branches and Leaves (NCS DC 73349)	1.67 ± 0.08 weight (%) n = 14	1.68 ± 0.11 weight (%)
Ca	ICP-OES	Peach Leaves (GBW 08501)	1.58 ± 0.05 weight (%) n = 12	
Ca	ICP-OES	BCR CRM No. 40 coal	1600 ± 400 mg kg^{-1} n = 6	
Ca	ICP-OES	NBS SRM 1635 coal	5600 ± 100 mg kg^{-1} n = 5	
Cd	ICP-OES	NIMT/UOE/FM/001	0.34 ± 0.10 mg kg^{-1} n = 28	0.38 ± 0.08 mg kg^{-1}
Cd	**ICP-MS**	NIMT/UOE/FM/001	0.40 ± 0.04 mg kg^{-1} n = 62	0.38 ± 0.08 mg kg^{-1}
Cd	**ICP-MS**	Canadian Peat (1878 P)	0.39 ± 0.07 mg kg^{-1} n = 10	(0.53 ± 0.03 mg kg^{-1})
Cd	**ICP-MS**	Bush Branches and Leaves (NCS DC 73349)	0.41 ± 0.11 mg kg^{-1} n = 5	(0.38 mg kg^{-1})
Cd	**ICP-MS**	BCR CRM No. 40 coal	0.19 ± 0.05 mg kg^{-1} n = 4	0.11 ± 0.02 mg kg^{-1}
Cd	**ICP-MS**	NBS SRM 1635 coal	0.04 ± 0.01 mg kg-1 n = 4	0.03 ± 0.01 mg kg^{-1}
Co	ICP-OES	NIMT/UOE/FM/001	1.27 ± 0.39 mg kg^{-1} n = 63	0.88 ± 0.09 mg kg^{-1}
Co	**ICP-MS**	NIMT/UOE/FM/001	0.88 ± 0.07 mg kg^{-1} n = 49	0.88 ± 0.09 mg kg^{-1}
Co	ICP-OES	Canadian Peat (1878 P)	1.3 ± 0.1 mg kg^{-1} n = 10	(1.8 ± 0.2 mg kg^{-1})
Co	**ICP-MS**	Canadian Peat (1878 P)	1.4 ± 0.4 mg kg^{-1} n = 11	(1.8 ± 0.2 mg kg^{-1})
Co	**ICP-MS**	Bush Branches and Leaves (NCS DC 73349)	0.50 ± 0.10 mg kg^{-1} n = 15	0.41 ± 0.05 mg kg^{-1}
Co	**ICP-MS**	BCR CRM No. 40 coal	8.1 ± 0.5 mg kg^{-1} n = 5	7.8 ± 0.6 mg kg^{-1}
Co	**ICP-MS**	NBS SRM 1635 coal	0.71 ± 0.05 mg kg^{-1} n = 4	(0.65 mg kg^{-1})

Table 2.9 (continued): Summary of average (± 1 SD) elemental concentration (mg kg^{-1}), weight (%) and stable Pb isotopic ratio measurements, certified values and information only values (brackets) in Ombrotrophic Peat (NIMT/UOE/FM/001), Canadian Peat (1878 P), Bush Branches and Leaves (DC73349), Peach Leaves (GBW 08501), Coal (BCR CRM No. 40) and Coal (NBS SRM 1635) reference materials.

Element/isotopic ratio	Method	Reference Material	Measured value	Certified or information only value
Cr	ICP-OES	NIMT/UOE/FM/001	5.64 ± 0.67 mg kg^{-1} n = 53	6.36 ± 0.44 mg kg^{-1}
Cr	**ICP-MS**	NIMT/UOE/FM/001	5.28 ± 0.40 mg kg^{-1} n = 63	6.36 ± 0.44 mg kg^{-1}
Cr	ICP-OES	Canadian Peat (1878 P)	12.5 ± 0.5 mg kg^{-1} n = 8	(8.0 ± 1.0 mg kg^{-1})
Cr	**ICP-MS**	Canadian Peat (1878 P)	8.3 ± 1.0 mg kg^{-1} n = 11	(8.0 ± 1.0 mg kg^{-1})
Cr	**ICP-MS**	BCR CRM No. 40 coal	32.2 ± 4.5 mg kg^{-1} n = 5	31.3 ± 2.0 mg kg^{-1}
Cr	**ICP-MS**	NBS SRM 1635 coal	2.3 ± 0.2 mg kg^{-1} n = 4	2.5 ± 0.3mg kg^{-1}
Cu	ICP-OES	NIMT/UOE/FM/001	6.06 ± 0.86 mg kg^{-1} n = 67	5.28 ± 1.04 mg kg^{-1}
Cu	**ICP-MS**	NIMT/UOE/FM/001	5.12 ± 0.34 mg kg^{-1} n = 63	5.28 ± 1.04 mg kg^{-1}
Cu	ICP-OES	Canadian Peat (1878 P)	195 ± 5 mg kg^{-1} n = 10	(195 ± 16 mg kg^{-1})
Cu	**ICP-MS**	Canadian Peat (1878 P)	217 ± 55 mg kg^{-1} n = 11	(195 ± 16 mg kg^{-1})
Cu	ICP-OES	Bush Branches and Leaves (NCS DC 73349)	6.2 ± 0.5 mg kg^{-1} n = 14	6.6 ± 0.8 mg kg^{-1}
Cu	**ICP-MS**	Bush Branches and Leaves (NCS DC 73349)	5.7 ± 0.4 mg kg^{-1} n = 15	6.6 ± 0.8 mg kg^{-1}
Cu	ICP-OES	Peach Leaves (GBW 08501)	8.3 ± 0.9 mg kg^{-1} n = 12	10.4 ± 1.6 mg kg^{-1}
Cu	ICP-OES	BCR CRM No. 40 coal	43.3 ± 4.6 mg kg^{-1} n = 6	
Cu	**ICP-MS**	BCR CRM No. 40 coal	44.2 ± 1.6 mg kg^{-1} n = 5	
Cu	ICP-OES	NBS SRM 1635 coal	3.1 ± 0.1 mg kg^{-1} n = 5	3.6 ± 0.3 mg kg^{-1}
Cu	**ICP-MS**	NBS SRM 1635 coal	3.4 ± 0.3 mg kg^{-1} n = 4	3.6 ± 0.3 mg kg^{-1}
Fe	ICP-OES	NIMT/UOE/FM/001	938 ± 86 mg kg^{-1} n = 63	921 ± 84 mg kg^{-1}
Fe	FAAS	NIMT/UOE/FM/001	1062 ± 72 mg kg^{-1} n = 6	921 ± 84 mg kg^{-1}
Fe	ICP-OES	Canadian Peat (1878 P)	9000 ± 500 mg kg^{-1} n = 10	(8700 ± 600 mg kg^{-1})
Fe	ICP-OES	Bush Branches and Leaves (NCS DC 73349)	1068 ± 92 mg kg^{-1} n = 14	1070 ± 57 mg kg^{-1}
Fe	ICP-OES	Peach Leaves (GBW 08501)	459 ± 61 mg kg^{-1} n = 12	431 ± 29 mg kg^{-1}
Fe	ICP-OES	BCR CRM No. 40 coal	6900 ± 500 mg kg^{-1} n = 6	
Fe	ICP-OES	NBS SRM 1635 coal	0.217 ± 0.018 weight (%) n = 5	0.239 ± 0.005 weight (%)
Hg	CVAAS	NIMT/UOE/FM/001	169 ± 35 µg kg^{-1} n = 23	(163 ± 15 µg kg^{-1})

Table 2.9 (continued): Summary of average (± 1 SD) elemental concentration (mg kg^{-1}), weight (%) and stable Pb isotopic ratio measurements, certified values and information only values (brackets) in Ombrotrophic Peat (NIMT/UOE/FM/001), Canadian Peat (1878 P), Bush Branches and Leaves (DC73349), Peach Leaves (GBW 08501), Coal (BCR CRM No. 40) and Coal (NBS SRM 1635) reference materials.

Element/isotopic ratio	Method	Reference Material	Measured value	Certified or information only value
Mg	ICP-OES	NIMT/UOE/FM/001	671 ± 65 mg kg^{-1} n = 67	582 ± 168 mg kg^{-1}
Mg	ICP-OES	Canadian Peat (1878 P)	3900 ± 170 mg kg^{-1} n = 10	
Mg	ICP-OES	Bush Branches and Leaves (NCS DC 73349)	0.44 ± 0.04 weight (%) n = 14	0.48 ± 0.04 weight (%)
Mg	ICP-OES	Peach Leaves (GBW 08501)	0.43 ± 0.04 weight (%) n = 12	0.47 ± 0.03 weight (%)
Mg	ICP-OES	BCR CRM No. 40 coal	1400 ± 300 mg kg^{-1} n = 6	
Mg	ICP-OES	NBS SRM 1635 coal	970 ± 40 mg kg^{-1} n = 5	
Mn	ICP-OES	NIMT/UOE/FM/001	7.30 ± 0.42 mg kg^{-1} n = 67	7.52 ± 0.41 mg kg^{-1}
Mn	**ICP-MS**	NIMT/UOE/FM/001	7.50 ± 0.71 mg kg^{-1} n = 57	7.52 ± 0.41 mg kg^{-1}
Mn	ICP-OES	Canadian Peat (1878 P)	225 ± 6 mg kg^{-1} n = 10	(206 ± 30 mg kg^{-1})
Mn	**ICP-MS**	Canadian Peat (1878 P)	229 ± 10 mg kg^{-1} n = 8	(206 ± 30 mg kg^{-1})
Mn	ICP-OES	Bush Branches and Leaves (NCS DC 73349)	62 ± 1 mg kg^{-1} n = 14	61 ± 5 mg kg^{-1}
Mn	**ICP-MS**	Bush Branches and Leaves (NCS DC 73349)	71 ± 3 mg kg^{-1} n = 10	61 ± 5 mg kg^{-1}
Mn	ICP-OES	Peach Leaves (GBW 08501)	75.4 ± 2.3 mg kg^{-1} n = 12	75.4 ± 5.4 mg kg^{-1}
Mn	ICP-OES	BCR CRM No. 40 coal	126 ± 9 mg kg^{-1} n = 6	139 ± 5 mg kg^{-1}
Mn	**ICP-MS**	BCR CRM No. 40 coal	143 ± 5 mg kg^{-1} n = 3	139 ± 5 mg kg^{-1}
Mn	ICP-OES	NBS SRM 1635 coal	19.4 ± 0.6 mg kg^{-1} n = 5	21.4 ± 1.5 mg kg^{-1}
Mn	**ICP-MS**	NBS SRM 1635 coal	21.5 ± 1.8 mg kg^{-1} n = 4	21.4 ± 1.5 mg kg^{-1}
Ni	ICP-OES	NIMT/UOE/FM/001	3.79 ± 1.20 mg kg^{-1} n = 61	4.10 ± 0.37 mg kg^{-1}
Ni	**ICP-MS**	NIMT/UOE/FM/001	4.42 ± 0.60 mg kg^{-1} n = 57	4.10 ± 0.37 mg kg^{-1}
Ni	ICP-OES	Canadian Peat (1878 P)	5.9 ± 0.9 mg kg^{-1} n = 9	(6.1 ± 0.7 mg kg^{-1})
Ni	**ICP-MS**	Canadian Peat (1878 P)	6.1 ± 1.1 mg kg-1 n = 10	(6.1 ± 0.7 mg kg^{-1})
Ni	**ICP-MS**	Bush Branches and Leaves (NCS DC 73349)	1.4 ± 0.3 mg kg^{-1} n = 14	1.7 ± 0.3 mg kg^{-1}
Ni	ICP-OES	BCR CRM No. 40 coal	24.5 ± 2.4 mg kg^{-1} n = 6	25.4 ± 1.6 mg kg^{-1}
Ni	**ICP-MS**	BCR CRM No. 40 coal	23.9 ± 1.5 mg kg^{-1} n = 4	25.4 ± 1.6 mg kg^{-1}
Ni	ICP-OES	NBS SRM 1635 coal	1.71 ± 0.25 mg kg^{-1} n = 4	1.74 ± 0.10 mg kg^{-1}
Ni	**ICP-MS**	NBS SRM 1635 coal	2.21 ± 0.74 mg kg-1 n = 4	1.74 ± 0.10 mg kg-1

Table 2.9 (continued): Summary of average (± 1 SD) elemental concentration (mg kg^{-1}), weight (%) and stable Pb isotopic ratio measurements, certified values and information only values (brackets) in Ombrotrophic Peat (NIMT/UOE/FM/001), Canadian Peat (1878 P), Bush Branches and Leaves (DC73349), Peach Leaves (GBW 08501), Coal (BCR CRM No. 40) and Coal (NBS SRM 1635) reference materials.

Element/isotopic ratio	Method	Reference Material	Measured value	Certified or information only value
P	ICP-OES	NIMT/UOE/FM/001	277 ± 20 mg kg^{-1} n = 67	(265 ± 8 mg kg^{-1})
P	ICP-OES	Canadian Peat (1878 P)	1800 ± 50 mg kg^{-1} n = 10	
P	ICP-OES	Bush Branches and Leaves (NCS DC 73349)	951 ± 34 mg kg^{-1} n = 14	1000 ± 40 mg kg^{-1}
P	ICP-OES	Peach Leaves (GBW 08501)	2666 ± 58 mg kg^{-1} n = 12	
P	ICP-OES	BCR CRM No. 40 coal	52.1 ± 3.3 mg kg^{-1} n = 6	
P	ICP-OES	NBS SRM 1635 coal	55 ± 1 mg kg^{-1} n = 5	
Pb	ICP-OES	NIMT/UOE/FM/001	173 ± 11 mg kg^{-1} n = 67	174 ± 8 mg kg^{-1}
Pb	ICP-OES	Canadian Peat (1878 P)	70.9 ± 4.7 mg kg^{-1} n = 10	(78.8 ± 2.9 mg kg^{-1})
Pb	ICP-OES	Bush Branches and Leaves (NCS DC 73349)	44 ± 3 mg kg^{-1} n = 14	47 ± 3 mg kg^{-1}
Pb	ICP-OES	BCR CRM No. 40 coal	22.4 ± 2.3 mg kg^{-1} n = 6	24.2 ± 1.7 mg kg^{-1}
Pb	**ICP-MS**	Peach Leaves (GBW 08501)	0.99 ± 0.10 mg kg^{-1} n = 10	0.99 ± 0.08 mg kg^{-1}
Pb	**ICP-MS**	NBS SRM 1635 coal	2.0 ± 0.2 mg kg^{-1} n = 5	1.9 ± 0.2 mg kg^{-1}
S	ICP-OES	NIMT/UOE/FM/001	750 ± 75 mg kg^{-1} n = 65	
S	ICP-OES	Canadian Peat (1878 P)	5700 ± 300 mg kg^{-1} n = 10	
S	ICP-OES	Bush Branches and Leaves (NCS DC 73349)	0.72 ± 0.08 weight (%) n = 14	0.73 ± 0.06 weight (%)
S	ICP-OES	Peach Leaves (GBW 08501)	1868 ± 714 mg kg^{-1} n = 12	
S	ICP-OES	BCR CRM No. 40 coal	2200 ± 61 mg kg^{-1} n = 6	
S	ICP-OES	NBS SRM 1635 coal	0.34 ± 0.08 mg kg^{-1} n = 5	0.33 ± 0.03 mg kg^{-1}
Sb	**ICP-MS**	NIMT/UOE/FM/001	2.37 ± 0.34 mg kg^{-1} n = 63	
Sb	**ICP-MS**	Canadian Peat (1878 P)	0.33 ± 0.07 mg kg^{-1} n = 11	(0.34 ± 0.05 mg kg^{-1})
Sb	**ICP-MS**	Bush Branches and Leaves (NCS DC 73349)	0.097 ± 0.010 mg kg^{-1} n = 15	0.095 ± 0.014 mg kg^{-1}
Sb	**ICP-MS**	BCR CRM No. 40 coal	4.24 ± 0.19 mg kg^{-1} n = 5	
Sb	**ICP-MS**	NBS SRM 1635 coal	0.14 ± 0.01 mg kg^{-1} n = 4	(0.14 mg kg^{-1})
Sc	**ICP-MS**	NIMT/UOE/FM/001	0.82 ± 0.15 mg kg^{-1} n = 63	
Sc	**ICP-MS**	Canadian Peat (1878 P)	0.83 ± 0.04 mg kg^{-1} n = 11	(1.04 mg kg^{-1})
Sc	**ICP-MS**	Bush Branches and Leaves (NCS DC 73349)	0.31 ± 0.02 mg kg^{-1} n = 13	0.32 ±0.04 mg kg^{-1}
Sc	**ICP-MS**	BCR CRM No. 40 coal	1.26 ± 0.14 mg kg^{-1} n = 3	
Sc	**ICP-MS**	NBS SRM 1635 coal	0.65 ± 0.06 mg kg^{-1} n = 4	(0.63 mg kg^{-1})

Table 2.9 (continued): Summary of average (± 1 SD) elemental concentration (mg kg^{-1}), weight (%) and stable Pb isotopic ratio measurements, certified values and information only values (brackets) in Ombrotrophic Peat (NIMT/UOE/FM/001), Canadian Peat (1878 P), Bush Branches and Leaves (DC73349), Peach Leaves (GBW 08501), Coal (BCR CRM No. 40) and Coal (NBS SRM 1635) reference materials.

Element/isotopic ratio	Method	Reference Material	Measured value	Certified or information only value
Se	ICP-MS	NIMT/UOE/FM/001	0.70 ± 0.16 mg kg^{-1} n = 58	
Se	ICP-MS	Canadian Peat (1878 P)	0.84 ± 0.19 mg kg^{-1} n = 11	(0.73 ± 0.08 mg kg^{-1})
Se	ICP-MS	Bush Branches and Leaves (NCS DC 73349)	0.10 ± 0.03 mg kg^{-1} n = 8	0.12 ± 0.02 mg kg^{-1}
Se	ICP-MS	BCR CRM No. 40 coal	1.26 ± 0.14 mg kg^{-1} n = 3	
Se	ICP-MS	NBS SRM 1635 coal	0.8 ± 0.1 mg kg^{-1} n = 4	0.9 ± 0.3 mg kg^{-1}
Ti	ICP-OES	NIMT/UOE/FM/001	391 ± 25 mg kg^{-1} n = 66	(357 ± 18 mg kg^{-1})
Ti	ICP-OES	Canadian Peat (1878 P)	370 ± 23 mg kg^{-1} n = 10	
Ti	ICP-OES	Bush Branches and Leaves (NCS DC 73349)	90 ± 4 mg kg^{-1} n = 14	95 ± 20 mg kg^{-1}
Ti	ICP-OES	Peach Leaves (GBW 08501)	36.9 ± 3.0 mg kg^{-1} n = 12	
Ti	ICP-OES	BCR CRM No. 40 coal	764 ± 63 mg kg^{-1} n = 6	
V	ICP-OES	NIMT/UOE/FM/001	7.95 ± 0.69 mg kg^{-1} n = 67	7.82 ± 1.08 mg kg^{-1}
V	ICP-MS	NIMT/UOE/FM/001	8.00 ± 0.87 mg kg-1 n = 63	7.82 ± 1.08 mg kg-1
V	ICP-OES	Canadian Peat (1878 P)	11.0± 1.4 mg kg^{-1} n = 10	(9.7 ± 1.2 mg kg^{-1})
V	ICP-MS	Canadian Peat (1878 P)	9.8 ± 2.0 mg kg^{-1} n = 11	(9.7 ± 1.2 mg kg^{-1})
V	ICP-OES	Bush Branches and Leaves (NCS DC 73349)	2.1 ± 0.4 mg kg^{-1} n = 14	2.4 ± 0.4 mg kg^{-1}
V	ICP-MS	Bush Branches and Leaves (NCS DC 73349)	2.3 ± 0.2 mg kg^{-1} n = 8	2.4 ± 0.4 mg kg^{-1}
V	ICP-OES	BCR CRM No. 40 coal	70.2 ± 6.5 mg kg^{-1} n = 6	
V	ICP-MS	BCR CRM No. 40 coal	68.3 ± 2.3 mg kg^{-1} n = 3	
V	ICP-OES	NBS SRM 1635 coal	6.0 ± 0.1 mg kg^{-1} n = 5	5.2 ± 0.5 mg kg^{-1}
V	ICP-MS	NBS SRM 1635 coal	4.3 ± 0.3 mg kg^{-1} n = 4	5.2 ± 0.5 mg kg^{-1}
Y	ICP-MS	NIMT/UOE/FM/001	1.22 ± 0.33 mg kg^{-1} n = 52	
Y	ICP-MS	Canadian Peat (1878 P)	3.54 ± 0.14 mg kg^{-1} n = 11	
Y	ICP-MS	Bush Branches and Leaves (NCS DC 73349)	0.67 ± 0.08 mg kg^{-1} n = 15	0.68 ± 0.02 mg kg^{-1}
Y	ICP-MS	BCR CRM No. 40 coal	3.94 ± 1.14 mg kg^{-1} n = 4	
Y	ICP-MS	NBS SRM 1635 coal	1.49 ± 0.14 mg kg^{-1} n = 4	

Table 2.9 (continued): Summary of average (± 1 SD) elemental concentration (mg kg^{-1}), weight (%) and stable Pb isotopic ratio measurements, certified values and information only values (brackets) in Ombrotrophic Peat (NIMT/UOE/FM/001), Canadian Peat (1878 P), Bush Branches and Leaves (DC73349), Peach Leaves (GBW 08501), Coal (BCR CRM No. 40) and Coal (NBS SRM 1635) reference materials.

Element/isotopic ratio	Method	Reference Material	Measured value	Certified or information only value
Zn	ICP-OES	NIMT/UOE/FM/001	30.6 ± 1.8 mg kg^{-1} n = 67	28.6 ± 1.9 mg kg^{-1}
Zn	ICP-OES	Canadian Peat (1878 P)	37 ± 1 mg kg^{-1} n = 10	(43 ± 3 mg kg^{-1})
Zn	ICP-OES	Bush Branches and Leaves (NCS DC 73349)	54 ± 3 weight (%) n = 14	55 ± 4 mg kg^{-1}
Zn	ICP-OES	Peach Leaves (GBW 08501)	23.4 ± 2.4 mg kg^{-1} n = 12	22.8 ± 2.5 mg kg^{-1}
Zn	ICP-OES	BCR CRM No. 40 coal	27.6 ± 4.5 mg kg^{-1} n = 6	30.2 ± 1.9 mg kg^{-1}
Zn	ICP-OES	NBS SRM 1635 coal	4.0 ± 0.8 mg kg^{-1} n = 5	4.7 ± 0.5 mg kg^{-1}
Zr	**ICP-MS**	NIMT/UOE/FM/001	12.1 ± 1.8 mg kg^{-1} n = 51	(13 ± 1.4 mg kg^{-1})[a]
Zr	**ICP-MS**	Canadian Peat (1878 P)	25 ± 6 mg kg^{-1} n = 8	
Zr	**ICP-MS**	Bush Branches and Leaves (NCS DC 73349)	2.50 ± 0.38 mg kg^{-1} n = 15	
Zr	**ICP-MS**	BCR CRM No. 40 coal	44.1 ± 4.0 mg kg^{-1} n = 5	
Zr	**ICP-MS**	NBS SRM 1635 coal	8.47 ± 0.51 mg kg^{-1} n = 4	
$^{206}Pb/^{207}Pb$	**ICP-MS**	NIMT/UOE/FM/001	1.176 ± 0.002 n = 59	(1.176 ± 0.001)
$^{208}Pb/^{206}Pb$	**ICP-MS**	NIMT/UOE/FM/001	2.094 ± 0.006 n = 59	(2.092 ± 0.002)
$^{208}Pb/^{207}Pb$	**ICP-MS**	NIMT/UOE/FM/001	2.461 ± 0.007 n = 59	(2.461 ± 0.003)
$^{206}Pb/^{207}Pb$	**ICP-MS**	Peach Leaves (GBW 08501)	1.164 ± 0.003 n = 10	
$^{208}Pb/^{206}Pb$	**ICP-MS**	Peach Leaves (GBW 08501)	2.117 ± 0.006 n = 10	
$^{208}Pb/^{207}Pb$	**ICP-MS**	Peach Leaves (GBW 08501)	2.463 ± 0.009 n = 10	
$^{206}Pb/^{207}Pb$	**ICP-MS**	NBS SRM 1635 coal	1.218 ± 0.002 n = 5	(1.210 ± 0.008)[b]
$^{208}Pb/^{206}Pb$	**ICP-MS**	NBS SRM 1635 coal	2.038 ± 0.003 n =5	(2.059 ± 0.011)[b]
$^{208}Pb/^{207}Pb$	**ICP-MS**	NBS SRM 1635 coal	2.481 ± 0.003 n = 5	(2.492 ± 0.018)[b]

[a]This value taken from Yafa (2004) was not corrected for peat 105°C moisture content, [b]Farmer *et al.* (1999).

2.11 ANALYSIS OF PEAT SAMPLES BY GAMMA SPECTROMETRY

^{210}Pb, ^{226}Ra, ^{137}Cs and ^{241}Am were determined in the upper sections of FM01CM-2 (the FM01CM-1 sister core), FM04-1-M, RM03CM-1, TM04M-1 and CM04M using gamma spectrometry. Air-dried peat sub-samples of ~ 1 – 20 g, depending on the amount of material available at different depths in the core, were accurately weighed into polycarbonate containers, which were then sealed and stored for a minimum of three weeks before analysis in order to allow ^{222}Rn to come to

radioactive equilibrium with ^{226}Ra. For the FM04-1-M, TM04M-1 and CM04M cores, which had more material available, sample weights of 10, 15 or 20 g were compressed into discs, using a 12-tonne hydraulic press, to give uniform counting geometries. The discs were then sealed in polycarbonate containers, as above. The equilibrated sample containers were positioned in a holder, which ensured reproducible geometry, on the end face of the detector for analysis. Canberra and EG&G Ortec instruments with low background, planar High Purity Ge gamma photon detectors were used for the FM01CM-2 core and FM04-1-M, RM03CM-1, TM04M-1 and CM04M cores, respectively. Detection efficiencies were determined for each counting geometry using standards prepared by spiking appropriate weights of peat, which had non-detectable activities of the nuclides of interest, with known activities of ^{210}Pb, ^{226}Ra and ^{137}Cs using certified standard solutions (Amersham plc). The standards were then prepared in the same geometry as the samples. The average detection limit for ^{210}Pb, ^{226}Ra, ^{137}Cs and ^{241}Am was ~ 1 Bq kg^{-1}.

2.12 CHEMICAL PRETREATMENT AND ANALYSIS OF PEAT SAMPLES BY ^{14}C AMS

2.12.1 Chemical pre-treatment of peat samples

Humic fractions from selected deep peat sections from the FM01CM-1, RM03CM-2, CM04CM-1 and TM04CM-4 cores were extracted using a standard acid-base-acid pre-treatment procedure (Cook and Dugmore, 1998). An air-dried peat sub-sample of approximately 2 – 3 g was weighed out into a Pyrex beaker to which, ~ 50 ml of HCl (1M) was added and the mixture heated for two to three hours at ~ 80°C on a hotplate. After cooling, the solution was filtered through Whatman GF/A glass fibre filter paper and discarded. The first humic acid fraction was extracted by adding ~ 50 ml of 2% (w/v) NaOH to the acid-washed peat, which was then heated as above. After cooling, the solution was filtered (as above) and acidified with ~ 5 ml of HCl (5M) to precipitate out the humic acid. The humic acid mixture was then heated to coagulate the precipitate, cooled and filtered, whereupon the first humic acid fraction was washed with deionised water, dried in a 105°C oven and weighed. This humic

acid extraction was repeated on the remaining peat (left on the filter paper) by repeating the procedure from the addition of NaOH. The humin fraction was then extracted by adding ~ 50 ml of HCl (1M) to the original remaining peat sample, which was heated, cooled, filtered, washed, dried and weighed. The humic acid 1 (HA1), humic acid 2 (HA2) and humin fractions obtained were stored in glass vials prior to ^{14}C AMS analysis.

2.12.2 ^{14}C AMS analysis

HA1 or HA2 fractions were dated by means of ^{14}C AMS, selected humin fractions from each core also being dated. The samples were firstly combusted at 850°C in sealed quartz tubes containing CuO as the oxidant and a small quantity of silver foil to remove halides. The CO_2 was then purified by cryogenic pumping and a 2 ml sub-sample converted to graphite by Fe/Zn reduction and analysed for ^{14}C using the NEC 5 MV terminal voltage instrument, operated at 4.5 MV and with carbon in the 4+ charge state. A further sub-sample of the CO_2 was used for $\delta^{13}C$ analysis using a VG Sira 10 isotope ratio mass spectrometer. The values were used to correct the $^{14}C/^{12}C$ ratios for isotopic fractionation prior to radiocarbon age determinations. The radiocarbon ages were subsequently calibrated to calendar age ranges using the Oxford Radiocarbon Accelerator Unit calibration program (OxCal 3). An example of an obtained radiocarbon analysis certificate is shown in Appendix A3.

2.13 UV-VIS SPECTROMETRY ANALYSIS OF NaOH EXTRACTS OF PEAT

The degree of decomposition of peat was measured by colorimetry on NaOH extracts of each peat section of the FM01CM-1, RM03CM-2, CM04CM-1, TM04CM-2 and TM04CM-4 cores.

2.13.1 Preparation of NaOH extracts of peat

NaOH extracts of peat were prepared using the Blackford and Chambers (1995) method as modified by Givelet *et al.* (2003). Approximately 0.02 g sub-samples of

air-dried peat were weighed out into test tubes and 10 ml of 8% (w/v) NaOH was added. The samples were shaken and then heated at 95 ± 5°C for one hour, made up to 20 ml with deionised water, shaken and left to stand for one hour before being re-shaken and filtered through Whatman No. 1 filter papers. Samples were diluted with an equal quantity of deionised water directly before colorimetric analysis.

2.13.2 UV-Vis spectrometry analysis of NaOH extracts of peat

Percentage absorption values of light at 550 nm (*cf.* Section 1.5.4) were measured for NaOH extracts using a Perkin Elmer Lambda 900 UV/Vis/NIR spectrophotometer (Perkin Elmer, Beaconsfield, UK). The internal analytical precision (1 SD) on the measured absorption values, based on the standard deviation of the mean value for three consecutive determinations, was $\leq \pm 0.02\%$.

2.14 DETERMINATION OF CHARCOAL CONTENT IN CARSEGOWAN MOSS PEAT SAMPLES

Additional work involving the determination of the charcoal contents (weight per cent) of sections from the upper 38 cm of the CM04CM-1 core was carried out as an independent check on extrapolated ^{210}Pb age dates for this core. It was assumed that charcoal content data could be used for this purpose due to a major explosion that occurred at the explosives factory (situated next to the Carsegowan Moss peat bog site (*cf.* Section 2.1.4.3)) in 1945 A.D. (Sawden, 2003). As charcoal makes up ~ 15% of the composition of gunpowder (Sawden, 2003), a substantial amount of charcoal would have most probably been deposited on the peat bog surface during this explosion. Charcoal contents were determined using a simple digestion and ignition technique devised by Winkler (1985). Approximately 0.5 g air-dried sub-samples of peat sections were weighed out into centrifuge tubes and 10 ml of HNO_3 (16 M) added, before heating at ~ 80°C for one hour. The samples were then centrifuged at 6000 rpm for five minutes, decanted, washed with deionised water until the supernatant was clear, and then transferred to pre-weighed Pyrex beakers and dried overnight in a 105°C oven. The beakers and samples were then cooled in a

desiccator, weighed, placed in a muffle furnace at 450°C for three hours and then cooled and weighed again. The charcoal contents (%) were determined using the following equation:

$$\text{Charcoal content (\%)} = [(\text{mass of digested peat residue (g)} - \text{mass of ashed peat residue (g)}) \times 100] / \text{mass of air-dried peat sample (g)}]$$

Note that the determined charcoal contents were then corrected for air-dried peat moisture contents.

2.15 COAL, HERBARIUM MOSS AND GALENA SAMPLE ANALYSIS

Additional work involving the determination of total elemental concentrations and Pb isotopic composition, following microwave assisted HNO_3/HF digestion (*cf.* Section 2.4), by ICP-OES and ICP-MS, as appropriate, in a selection of British coal samples (n = 18) that had previously been analysed for Pb concentrations and Pb isotopic composition (Farmer *et al.*, 1999) was carried out. Scottish herbarium moss samples (n = 44), which had also previously been analysed for Pb concentrations and Pb isotopic composition (Farmer *et al.*, 2002) were also prepared and analysed for total elemental concentrations as part of an undergraduate research project (Halter, 2005). Elemental concentrations in coal and moss were expressed on a 105°C dry weight basis (i.e. corrected for the moisture contents of air-dried coal and moss as described in Section 2.3.2.2). A sample of galena, collected from a slag heap from Wanlockhead Pb mines, south-west Scotland in October 1993, was prepared by firstly washing the sample with deionised water, drying it at room temperature and then breaking off a small piece of powdered material using a hammer. Duplicate ~ 0.1 g sub-samples were weighed into Teflon beakers, for which 9 ml of HNO_3 (16 M) and 1 ml of concentrated HF were added, and the samples heated on a hot plate at ~ 90°C for three hours. The sample solutions were then evaporated down to approximately 1 ml on a hotplate and made up to 25 ml in polypropylene volumetric flasks with 2 % (v/v) HNO_3. These digests were also analysed for total elemental concentrations and Pb isotopic composition using ICP-OES and ICP-MS, as

appropriate. Elemental concentrations were not expressed on a 105°C weight basis since galena has negligible moisture content.

The results for each of the peat bogs under investigation will now be presented in the following order: Flanders Moss, The Red Moss of Balerno, Turclossie Moss and Carsegowan Moss.

3 FLANDERS MOSS

This chapter contains the results for the Flanders Moss peat cores.

3.1 PEAT MATRIX PROPERTIES AND EVALUATION OF TROPHIC STATUS

This section presents the results for the following peat matrix properties determined in the Flanders Moss cores: visual observations, wet/dry weight ratios, water contents, ash contents, Ca/Mg ratios, bulk densities and NaOH peat extract absorptions. These results will be used to assess the hydrological and peat decomposition properties, as well as the trophic status, of the peat cores.

3.1.1 Visual observations

Visual observation depth profiles for the Flanders Moss peat cores, FM01CM-1 and FM04-1-M, are shown in Fig. 3.1.

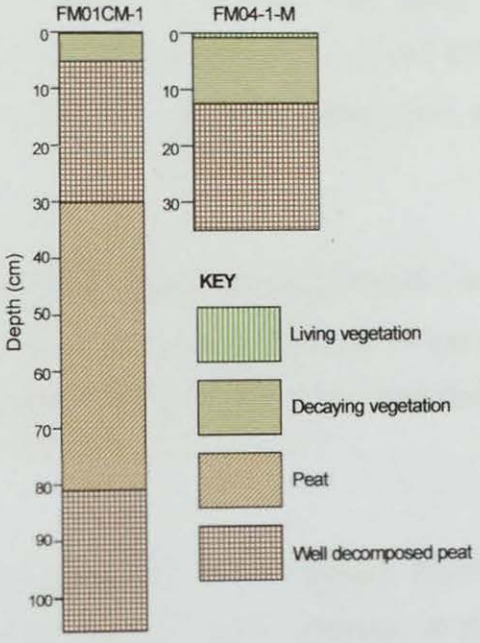

Figure 3.1: Visual observation depth profiles for FM01CM-1 and FM04-1-M.

As a result of the removal of some vegetation prior to the collection of the FM01CM-1 core (*cf.* Section 2.2.2.1), living vegetation is absent from the surface of

this core. The implications of this "missing" material, with respect to the dating of FM01CM-1, will be discussed later in Section 3.2.3 and 3.2.5. Also, since the position of the vegetation-peat interface was different in the two cores, its position will be indicated in the peat matrix property profiles.

3.1.2 Wet/dry weight ratios and water contents

Wet and dry weights, wet/dry weight ratios, water contents (determined after air-drying wet peat sections) and residual moisture contents (determined after oven-drying air-dried peat sections) for the FM01CM-1 and FM04-1-M peat cores are tabulated in Appendix A4.1 Table A1 and A4.2 Table A1, respectively. The wet/dry weight ratio and water content profiles for FM01CM-1 and FM04-1-M are shown in Figs. 3.2 and 3.3, respectively.

3.1.2.1 FM01CM-1

From the bottom of FM01CM-1 up to a depth of 30 cm, wet/dry weight ratios (10 – 16) and water contents (90 – 94%) were fairly constant (*cf.* Fig. 3.2). Thereafter, they declined and remained stable at ~ 6 and 83%, respectively, between 14 and 9 cm before increasing to 15 and 93%, respectively, at the top of the core.

3.1.2.2 FM04-1-M

The wet/dry weight ratios and water contents in FM04-1-M decreased from 11 and 91% at the bottom to 4.1 and 76%, respectively, at 24 cm (*cf.* Fig. 3.3). Thereafter, they increased to maximum values of 13 and 92%, respectively, at 12-6 cm.

3.1.2.3 Discussion

In terms of hydrological properties of the Flanders Moss peat bog, the high and constant wet/dry weight ratios and water contents at depth in FM01CM-1 are indicative of waterlogged catotelm peat layers, whereas variations in the uppermost FM01CM-1 sections and FM04-1-M are indicative of generally drier acrotelm peat

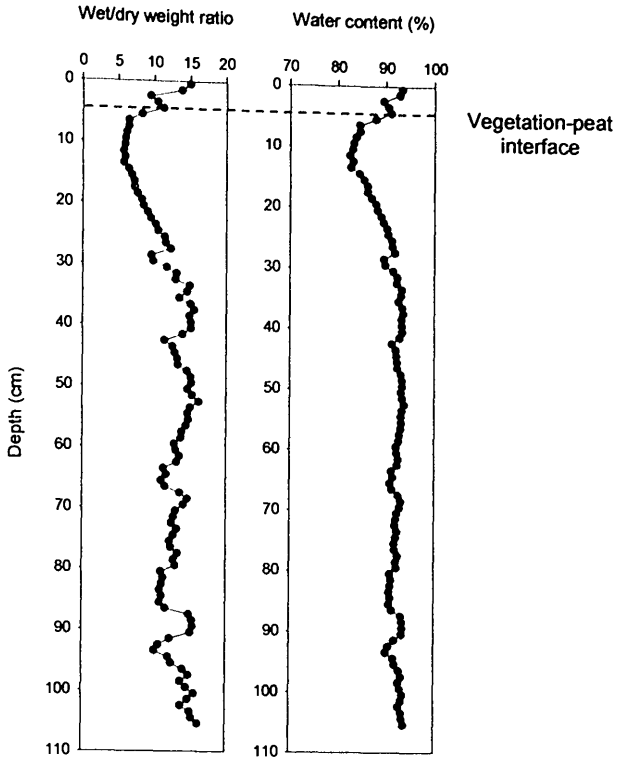

Figure 3.2: Depth profiles of wet/dry weight ratio and water content (% by weight) in the FM01CM-1 (0-106 cm) peat core.

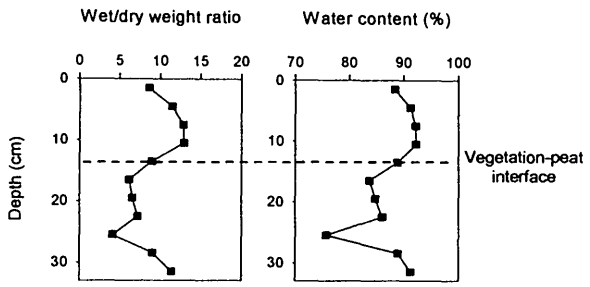

Figure 3.3: Depth profiles of wet/dry weight ratio and water content (% by weight) in the FM04-1-M (0-33 cm) peat core.

layers where water table fluctuations occur and dead/living water-absorbing *Sphagnum* moss is present. Based on these patterns, the acrotelm-catotelm boundary can be estimated to occur at a depth of ~ 30 cm in the FM01CM-1 core, as indicated on ensuing peat property profiles. The influence of peat bog water table fluctuations and associated redox boundaries on the redox-sensitive elements (Fe, Mn, P and S) (Damman, 1978; Clymo, 1983) will be investigated by comparing the water content and elemental concentration profiles in Section 3.7.

3.1.3 Ash contents and Ca/Mg ratios

Ash contents (expressed relative to sectional 105°C-dried peat weights) and Ca/Mg ratios (calculated using Ca and Mg concentration data from A4.1 Table A5 and A4.2 Table A5), for FM01CM-1 and FM04-1-M are tabulated in A4.1 Table A2 and A4.2 Table A2, respectively. The ash content and Ca/Mg ratio profiles for FM01CM-1 and FM04-1-M are shown in Figs. 3.4 and 3.5, respectively.

3.1.3.1 FM01CM-1

From the bottom of FM01CM-1 up to a depth of ~ 30 cm, the ash contents remained low and fairly constant (0.4 to 1.9%) before increasing to a prominent peak in the top 18 cm with a maximum of ~ 8% from 13 to 9 cm (*cf.* Fig. 3.4). Similarly from the bottom up to ~ 30 cm, the Ca/Mg ratio also remained low and constant (0.6 to 0.8), before increasing to a maximum of 1.5 near the top of the core.

3.1.3.2 FM04-1-M

There was a prominent peak in the ash content of FM04-1-M between 24 and 6 cm, with a maximum of 4.6% at 15 - 18 cm (*cf.* Fig. 3.5). The Ca/Mg ratio steadily increased from 0.81% at the bottom of the core to a peak of 1.6% at 12-15 cm, followed by an increase to 2.4% at the surface.

3.1.3.3 Discussion

The ash content values ($\leq$ 8%) in FM01CM-1 and FM04-1-M, are consistent with ombrotrophic conditions (< 15%) (Hulme *et al.*, 1991; Shotyk, 1996a; Weiss *et al.*, 1998), with the very low ash contents below ~ 30 cm in the former being consistent with those found in *Sphagnum* bog peat ($\leq$ 2%) (Bindler, 2003). Similarly, the Ca/Mg ratios in FM01CM-1 and FM04-1-M are within the range of those found in continental rain water (2 – 6) and marine and coastal rainwater (0.5 – 1) (Berner and Berner, 1997), again consistent with the ombrotrophic nature of these peat cores.

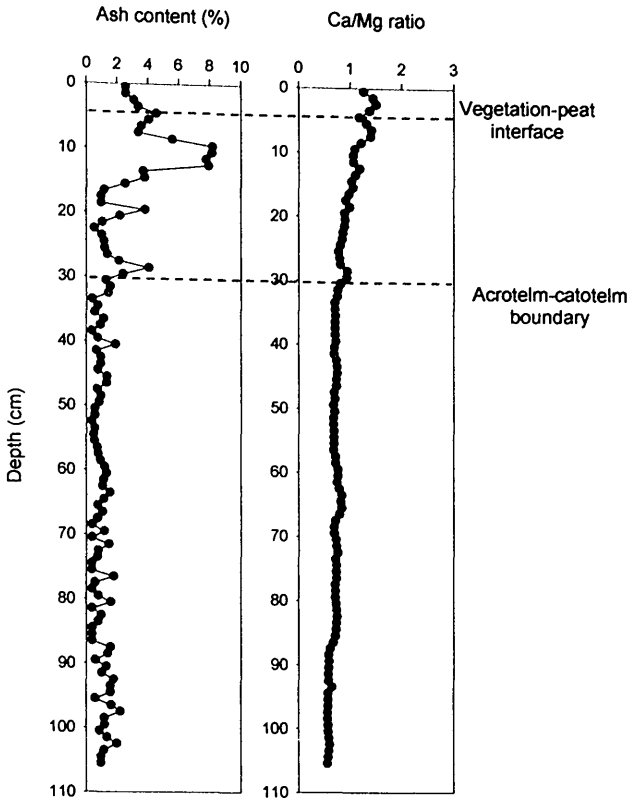

Figure 3.4: Depth profiles of ash content (% by weight) and Ca/Mg ratios in the FM01CM-1 (0-106 cm) peat core.

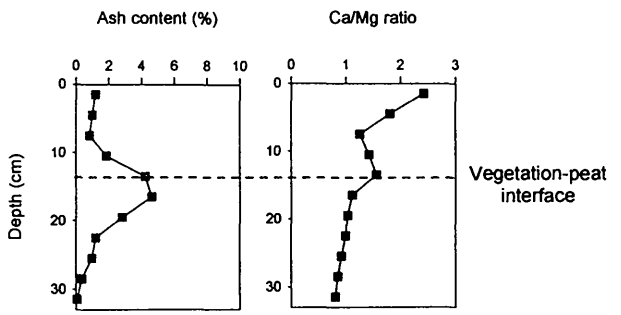

Figure 3.5: Depth profiles of ash content (% by weight) and Ca/Mg ratios in the FM04-1-M (0-33 cm) peat core.

The Ca/Mg ratio of rainwater in the Flanders Moss area was unknown and therefore unavailable for comparison. In view of their ombrotrophic nature, these Flanders Moss peat cores are suitable for use as archives of atmospheric metal deposition. The trends of increasing ash contents and Ca/Mg ratios in the near-surface acrotelm peat sections of FM01CM-1 and FM04-1-M (*cf.* Figs. 3.4 and 3.5) are attributable to

increased anthropogenic and natural dust inputs and to nutrient cycling, there being a preferential uptake of Ca over Mg by plants (Shotyk, 1996a; Weiss *et al.*, 1997). As mentioned in Section 1.5.2, however, the ash content of bog peats may also reflect the changing rates of peat accumulation and compaction (Shotyk, 1996a), which will be investigated in Section 3.1.4.3. Also, since ash contents are related to atmospheric dust inputs, FM01CM-1 and FM04-1-M ash content profiles will be compared with profiles of the conservative elements in Section 3.3.

3.1.4 Bulk density and NaOH peat extract absorption

The bulk density results for FM01CM-1 and FM04-1-M, which are relative to sectional 105°C-dried peat weights, are tabulated in A4.1 Table A2 and A4.2 Table A2, respectively, and the results for NaOH peat extract % absorptions at 550 nm for FM01CM-1 are tabulated in A4.1 Table A2. The bulk density and NaOH peat extract % absorption profiles for FM01CM-1 are shown in Fig. 3.6, and the bulk density profile for FM04-1-M is shown in Fig. 3.7.

3.1.4.1 FM01CM-1

From the bottom of FM01CM-1 up to a depth of 29.5 cm, bulk densities (range 0.031 – 0.13 g cm^{-3}) were fairly constant followed by a broad peak with a maximum of 0.22 g cm^{-3} at 11-12 cm. From the bottom of FM01CM-1 up to a depth of 46 cm, the mean NaOH peat extract absorption value was 20 ± 4%, above which there was a slight shift to higher values (18 - 41%) up to 9 cm, before decreasing towards the top of the core (*cf.* Fig. 3.6).

3.1.4.2 FM04-1-M

The bulk density profile for FM04-1-M exhibited a peak with a maximum (0.16 g cm^{-3}) at 16.5 cm, above which it decreased to a minimum (0.033 g cm^{-3}) near the surface of the core (*cf.* Fig. 3.7).

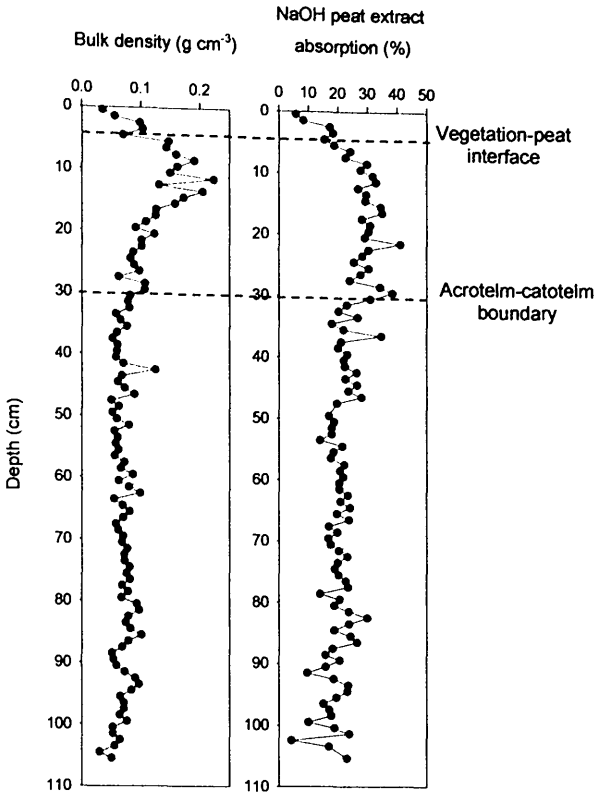

Figure 3.6: Depth profiles of bulk density (g cm^{-3}) and NaOH peat extract absorption (%) at 550 nm in the FM01CM-1 (0-106 cm) peat core.

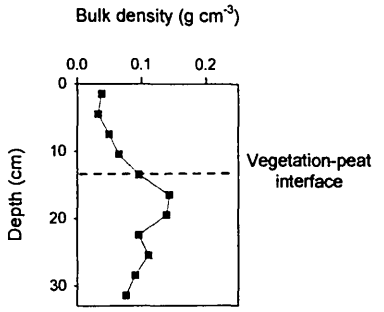

Figure 3.7: Depth profiles of bulk density (g cm^{-3}) in the FM04-1-M (0-33 cm) peat core.

3.1.4.3 Discussion

As mentioned in Sections 1.5.3 and 1.5.4, it is generally assumed that peat bulk densities and NaOH extract absorptions reflect the extent of peat decomposition. As mentioned in Section 1.4.2.6, during decomposition peat changes structure from the fresh plant material successively into amorphous humic matter and in the first stage, the degree of decomposition is governed by the nature of the environment in which the plant material was initially deposited and by the subsequent position of the water

table. In the second stage, when the peat is permanently waterlogged, the decomposition is very slow and the degree of decomposition depends mainly on the rate and duration of decomposition in aerobic conditions when the peat in question formed the upper layers of the bog (Kellner, 2003). Consequently, the extent of peat decomposition and accompanying mass loss in the acrotelm and catotelm differ and generally the rate of decomposition and mass loss is highest in the acrotelm and decreases exponentially with increasing depth of the peat profile (Biester *et al.*, 2003). The FM01CM-1 and FM04-1-M bulk density and NaOH peat extract absorption profiles (*cf.* Figs. 3.6 and 3.7) indicate a greater degree of decomposition and mass loss in the acrotelm peat layers i.e. greater bulk densities and NaOH absorptions in the acrotelm peat sections between ~ 30 and 4 cm in FM01CM-1 (*cf.* Fig. 3.6), and below 15 cm in FM04-1-M (*cf.* Fig. 3.7), relative to the lower, fairly constant bulk densities and NaOH absorptions in the catotelm peat sections beneath ~ 30 cm in FM01CM-1 (*cf.* Fig. 3.6).

The low bulk densities and absorption values at the surface of both cores are attributable to the presence of decomposing and living vegetation. It is apparent, however, that the FM01CM-1 absorption profile shows a less pronounced increase in the top ~ 30 cm sections (*cf.* Fig. 3.6) compared with those observed in the bulk density profile, which, like ash content, can reflect the contribution from inorganic content and the effects of peat compaction (Brooks and Stoneman, 1997). The FM01CM-1 bulk density and ash content profiles, plotted against air-dried mid-point cumulative weight rather than depth to eliminate the effects of peat compaction, are shown in Fig. 3.8. The FM01CM-1 and FM04-1-M mid-point cumulative weights, relative to sectional air-dried peat weights, are tabulated in A4.1 Table A1 and A4.2 Table A1, respectively. The near-surface increases in bulk density and ash content are coincident, providing evidence that the high inorganic contents present as a result of increased anthropogenic and natural atmospheric dust deposition and nutrient cycling, does indeed significantly influence bulk density values (*cf.* Fig. 3.8).

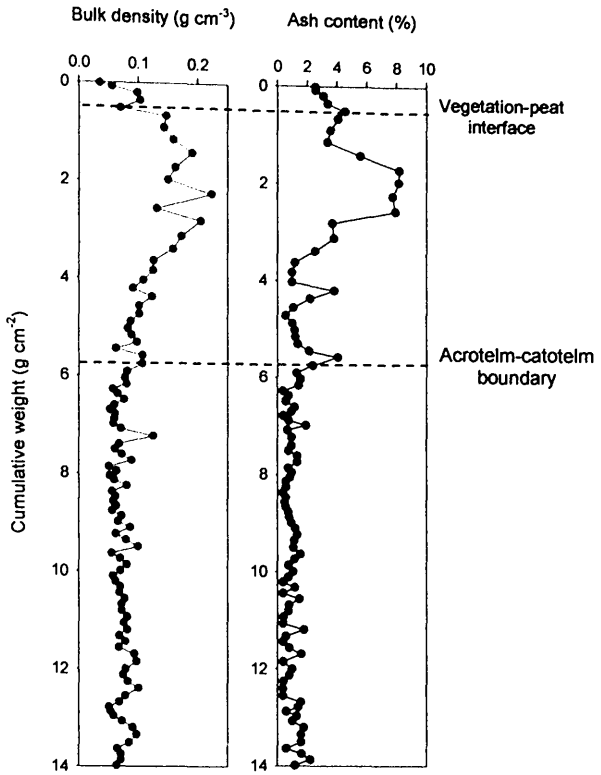

Figure 3.8: Comparison of bulk density (g cm^{-3}) and ash content (% by weight) *versus* cumulative weight (g cm^{-2}) in the FM01CM-1 peat core.

3.2 RADIONUCLIDES AND RADIOMETRIC DATING OF FLANDERS MOSS PEAT CORES

This section presents ^{210}Pb, ^{137}Cs and ^{14}C results for the Flanders Moss peat cores.

3.2.1 ^{210}Pb and ^{137}Cs

^{210}Pb and ^{137}Cs were determined in sections from the top 20 cm of FM01CM-2, the FM01CM-1 sister core from which FM01CM-1 ^{210}Pb dates were extrapolated, and in sections from the top 30 cm of FM04-1-M. ^{210}Pb and ^{137}Cs data for FM01CM-2 are presented elsewhere (Yafa, 2004) but the ^{210}Pb and ^{137}Cs data for FM04-1-M will be presented in this section.

^{226}Ra was not detected above background in any of the FM04-1-M peat sections, and therefore the total ^{210}Pb specific activities were taken to represent unsupported ^{210}Pb.

Also, ^{241}Am was not detected in any of the sections and therefore could not be used as an independent check on ^{210}Pb-derived dates. ^{210}Pb and ^{137}Cs specific activities and inventories for FM04-1-M are shown in Table 3.1.

Table 3.1: ^{210}Pb and ^{137}Cs specific activities (Bq kg^{-1}) and inventories (Bq m^{-2}) in the FM04-1-M peat core.

FM04-1-M section (cm)	Unsupported ^{210}Pb specific activity (Bq kg^{-1})	^{137}Cs specific activity (Bq kg^{-1})	Unsupported ^{210}Pb inventory (Bq m^{-2})	^{137}Cs inventory (Bq m^{-2})
0-3	396 ± 13	681 ± 10	517 ± 17	888 ± 18
3-6	330 ± 13	651 ± 10	376 ± 15	741 ± 12
6-9	216 ± 8	480 ± 7	370 ± 14	822 ± 12
9-12	200 ± 7	510 ± 7	448 ± 16	1142 ± 16
12-15	137 ± 5	276 ± 4	447 ± 17	900 ± 13
15-18	50 ± 5	114 ± 2	242 ± 24	550 ± 10
18-21	14 ± 6	95 ± 3	67 ± 29	450 ± 14
21-24	10 ± 2	42 ± 2	33 ± 7	138 ± 7
24-27	6 ± 2	32 ± 1	23 ± 8	122 ± 4
27-30	4 ± 2	30 ± 2	12 ± 6	92 ± 6

Specific activities (± 1 SD) are expressed relative to air-dried weight.

The inventories were calculated for each peat section using the following equation:

$$\text{Inventory (Bq m}^{-2}\text{)} = \text{specific activity (Bq kg}^{-1}\text{ air-dried) x mass of air-dried peat section (kg) / cross-sectional area (m}^{2}\text{)}$$

The ^{210}Pb specific activity decreased with depth (Fig. 3.9 a) in accordance with natural radioactive decay, but, in the case of ^{137}Cs, the profile is influenced by its diffusional movement in the organic-rich peat matrix after deposition from nuclear weapons testing (1963) and Chernobyl (1986) fallout. The activities were also plotted against air-dried mid-point cumulative weight (Fig. 3.9 b) to eliminate the effect of peat compaction on their profiles.

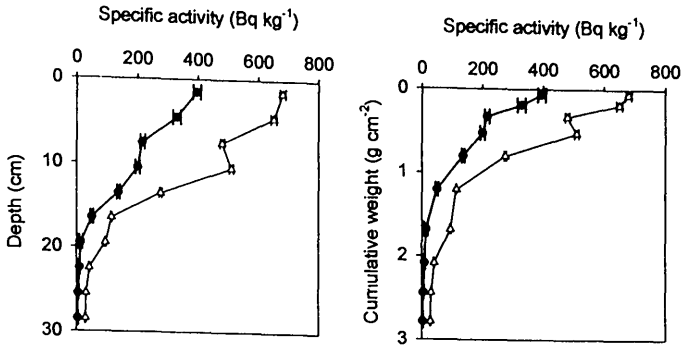

Figure 3.9: ^{210}Pb (closed circles) and ^{137}Cs (open triangles) specific activity (Bq kg^{-1}) *versus* a) depth (cm) and b) cumulative weight (g cm^{-2}) in the FM04-1-M peat core.

3.2.2 ^{210}Pb dating of FM04-1-M

The CRS model (Section 1.9.1.2) (Appleby and Oldfield, 1978, 1983; Oldfield and Appleby, 1985; Appleby *et al.*, 1997) was applied to the ^{210}Pb inventories (*cf.* Table 3.1) to generate an age for the bottom of each individual FM04-1-M section, using the following equation:

$$t_i = 1/\lambda \times \ln (I_{total}/I_i)$$

Where t_i = the age of depth i (y)

λ = the ^{210}Pb decay constant (ln $2/t_{1/2}$, where $t_{1/2}$ = 22.35 y)

I_{total} = the total unsupported ^{210}Pb inventory (Bq m^{-2})

I_i = the unsupported ^{210}Pb inventory below depth i (Bq m^{-2})

The total unsupported ^{210}Pb inventory of 2535 ± 53 Bq m^{-2} was calculated by summing the inventories of the individual sections. By interpolation, the mid-point date and associated error for each section was calculated (Table 3.2).

Table 3.2: Calculated ages and dates from the ^{210}Pb dating of the FM04-1-M peat core.

Depth (cm)	Age (y)	Date (AD)
0	0	2004 ± 0
1.5		2001 ± 1
3	7.3	1997 ± 2
4.5		1994 ± 2
6	14.0	1990 ± 2
7.5		1986 ± 2
9	22.2	1982 ± 1
10.5		1975 ± 2
12	36.2	1968 ± 2
13.5		1955 ± 3
15	61.4	1943 ± 3
16.5		1926 ± 6
18	94.4	1910 ± 8
19.5		1899 ± 7
21	116.3	1888 ± 6
22.5		1877 ± 8
24	137.5	1866 ± 10
25.5		1849 ± 15
27	172.1	1832 ± 17
28.5		
30		

Dates were rounded up to the nearest whole number.

3.2.3 FM04-1-M ^{210}Pb flux

The inventory-derived average ^{210}Pb flux (79 ± 2 Bq m^{-2} y^{-1}) was calculated using the following equation:

$$F = I_{total} \times \lambda$$

Where F = the unsupported ^{210}Pb flux (Bq m^{-2} y^{-1})

I_{total} = the total unsupported ^{210}Pb inventory (Bq m^{-2})

λ = the ^{210}Pb decay constant (ln $2/t_{1/2}$, where $t_{1/2}$ = 22.35 y)

This inventory-derived average ^{210}Pb flux is (i) higher than the value of 54 ± 4 Bq m^{-2} y^{-1} determined for the FM01CM-2 core (Farmer *et al.*, 2006; Yafa, 2004), (ii) higher than the value of 61 ± 4 Bq m^{-2} y^{-1} obtained for a peat core (99CM) collected from Flanders Moss in 1999 (Farmer *et al.*, 2006), (iii) lower than the value of 110 Bq m^{-2} y^{-1} previously obtained for a peat core collected from Flanders Moss in

1990 (Farmer *et al.*, 1997; MacKenzie *et al.*, 1997), (iv) much lower than the value of 144 ± 15 Bq m^{-2} y^{-1} obtained for a monolith peat core (96M) collected in 1996 (Farmer *et al.*, 2006). The theoretical rainfall-corrected ^{210}Pb flux of 102 ± 18 Bq m^{-2} y^{-1}, however, calculated for the Flanders Moss area using the average annual rainfall value of 132 cm y^{-1}, as quoted by MacKenzie *et al.* (1997), and the estimated average ^{210}Pb flux of 77 ± 14 Bq m^{-2} y^{-1} per metre of rainfall established for the UK by Smith *et al.* (1997), is in close agreement with the inventory-derived average ^{210}Pb flux for FM04-1-M.

Farmer *et al.* (2006) reported that the low inventory-derived average ^{210}Pb flux values for FM01CM-2 and 99CM provided evidence that there was at least 25 ± 10 years of material "missing" from the top of these cores. This evidence was strengthened when (i) the $^{206}Pb/^{207}Pb$ and elemental profiles of a monolith core collected in 1999 (99M), which was a sister core of 99CM, were compared with those for 96M, after plotting the former with a 3-cm upwards offset relative to 96M, and (ii) the 99M $^{206}Pb/^{207}Pb$ profile was compared with that of FM01CM-2, the best match occurring when the latter was plotted with a 21-cm downwards offset relative to 99M. It was deduced that the top of the FM01CM-2 core corresponded with *ca.* 1976 (Section 3.2.5). The removal of grassy vegetation prior to collection of the FM01CM-2 core accounted for at least part of the apparent 21-cm offset. Therefore its sister core, FM01CM-1, was believed to be similarly affected and was found to require a downwards off-set of 17.5 cm relative to 99M and an upwards offset of 3.5 cm relative to FM01CM-2.

3.2.4 FM04-1-M ^{137}Cs total inventory

The total ^{137}Cs inventory in FM04-1-M was 5.9 ± 0.4 kBq m^{-2}. This is generally in agreement with that deposited in west-central Scotland from the atmosphere following nuclear weapons testing (4-5 kBq m^{-2}, Peirson *et al.*, 1982) and the Chernobyl accident (1-5 kBq m^{-2}, Clark and Smith, 1988). It is, however, higher than the total ^{137}Cs inventory (2.6 kBq m^{-2}) previously obtained for a peat core collected from Flanders Moss in 1990 (Farmer *et al.*, 1997; MacKenzie *et al.*, 1997).

3.2.5 FM01CM-1 dates

Dates for the FM01-CM-1 core were obtained by extrapolation of corrected ^{210}Pb-derived dates for the FM01CM-2 sister core, aided by matching of the ^{206}Pb/^{207}Pb profiles of the two cores (Farmer *et al.*, 2006). Corrected ^{210}Pb dates and measured ^{206}Pb/^{207}Pb ratios for the top of FM01CM-2 and FM01CM-1 are shown in Table 3.3. Note that the FM01CM-1 ^{206}Pb/^{207}Pb ratio results will be discussed later in Section 3.4.1.

Table 3.3: Corrected ^{210}Pb dates and corresponding ^{206}Pb/^{207}Pb ratios for the FM01CM-2 and FM01CM-1 peat cores.

FM01CM-2			FM01CM-1		
Depth (cm)	Date (AD)[a]	^{206}Pb/^{207}Pb[a]	Mid-point depth (cm)	Extrapolated date (AD)	^{206}Pb/^{207}Pb
			0.5		1.133 ± 0.0012
			1.5		1.134 ± 0.0008
			2.5		1.135 ± 0.0022
0	1976 ± 7		3.5	1976 ± 7	1.134 ± 0.0016
1	1971 ± 8	1.139 ± 0.0012	4.5	1971 ± 8	1.140 ± 0.0013
2	1967 ± 9		5.5	1967 ± 9	1.145 ± 0.0013
3	1960 ± 9	1.150 ± 0.0012	6.5	1960 ± 9	1.151 ± 0.0022
4	1953 ± 9		7.5	1953 ± 9	1.156 ± 0.0014
5	1948 ± 10	1.162 ± 0.0013	8.5	1948 ± 10	1.160 ± 0.0021
6	1943 ± 10		9.5	1943 ± 10	1.163 ± 0.0016
7	1937 ± 11	1.170 ± 0.0010	10.5	1937 ± 11	1.169 ± 0.0005
8	1930 ± 11		11.5	1930 ± 11	1.168 ± 0.0015
9	1925 ± 12	1.171 ± 0.0011	12.5	1925 ± 12	1.170 ± 0.0012
10	1919 ± 12		13.5	1919 ± 12	1.173 ± 0.0018
11	1911 ± 13	1.171 ± 0.0004	14.5	1911 ± 13	1.172 ± 0.0008
12	1903 ± 14		15.5	1903 ± 14	1.171 ± 0.0020
13	1890 ± 16	1.169 ± 0.0010	16.5	1890 ± 16	1.174 ± 0.0013
14	1876 ± 19		17.5	1876 ± 19	1.174 ± 0.0017
15		1.172 ± 0.0011	18.5		1.174 ± 0.0022
16					

[a]Yafa (2004). Note that the shaded boxes indicate the 3.5 cm offset between FM01CM-2 and FM01CM-1.

3.2.6 Peat accumulation rates

3.2.6.1 CRS model

Using the CRS model, peat accumulation rates (in terms of mg cm^{-2} y^{-1} and cm y^{-1}) for each FM04-1-M section (Table 3.4) were calculated using the following equations:

Peat accumulation rate (mg cm^{-2} y^{-1}) = (mass of air-dried peat section (mg)/cross-sectional area (cm^2))/number of years in section

Peat accumulation rate (cm y^{-1}) = number of cm in section /number of years in section

The actual average accumulation rates over the depth interval 0-27 cm were 15 ± 1 mg cm^{-2} y^{-1} and 0.16 ± 0.02 cm y^{-1}.

Table 3.4: Sectional peat accumulation rates for the FM04-1-M peat core determined using the CRS model.

Section (cm)	Number of years	Accumulation rate (mg cm^{-2} y^{-1})	Accumulation rate (cm y^{-1})
0-3	7.3	18	0.41
3-6	6.6	17	0.45
6-9	8.2	21	0.37
9-12	14	16	0.21
12-15	25	13	0.12
15-18	33	15	0.091
18-21	22	22	0.14
21-24	21	16	0.14
24-27	35	11	0.086

Accumulation rates are expressed in terms of air-dried peat weight.

3.2.6.2 CIC model

Using the CIC model, which assumes that there is a constant initial ^{210}Pb concentration, accumulation rates of 17 mg cm^{-2} y^{-1} and 0.16 cm y^{-1} were calculated using the equation below (Faure, 1986), after plotting ln ^{210}Pb *versus* air-dried mid-point cumulative weight (Fig. 3.10 a) and depth (Fig. 3.10 b), respectively.

$$S = -\lambda/m$$

Where, S = the accumulation rate (g cm^{-2} y^{-1})

λ = the ^{210}Pb decay constant (ln $2/t_{1/2}$, where $t_{1/2} = 22.35$ y)

m = the gradient (cm^2 g^{-1})

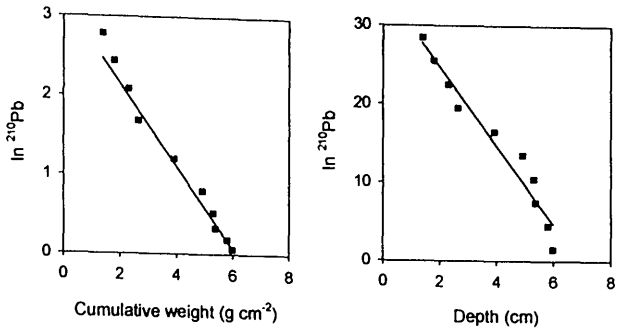

Figure 3.10: Profiles of ln [^{210}Pb (Bq kg^{-1})] *versus* a) cumulative weight and b) depth for the FM04-1-M peat core.

3.2.6.3 Discussion

The FM04-1-M peat accumulation rates derived using both of the ^{210}Pb models are in close agreement but are greater than those calculated for the 1990 Flanders Moss core (9.5 mg cm^{-2} y^{-1} and 0.07 cm y^{-1}) using the CIC model (Farmer *et al.*, 1997; MacKenzie *et al.*, 1997). This is perhaps indicative of varying peat growth rates at different positions (and possibly different time periods) within the bog. The calculated FM04-1-M accumulation rates (expressed in terms of cm y^{-1}) are in agreement, however, with the calculated average peat accumulation rate of 0.16 cm y^{-1} determined for the FM01CM-2 core using the CRS model.

3.2.7 ^{14}C

The ^{14}C AMS age dates determined for selected deep peat sections of the FM01CM-1 core are shown in Table 3.5. The calendar date ranges were derived from the ^{14}C dates as specified in Section 2.12.2. The age dates for the selected humin fractions are in close agreement with those obtained for the corresponding humic acid fractions, providing additional confidence in the accuracy of these results. The humic acid fraction dates were preferentially used since the humin fraction may contain many components unrelated to humification (Cook *et al.*, 1998). The age dates obtained for FM01CM-1 and FM04-1-M from ^{210}Pb and ^{14}C dating will be used in Section 3.3, 3.5, 3.6 and 3.8 to aid the interpretation of historical trends in atmospheric metal deposition.

Table 3.5: ^{14}C age dates of selected FM01CM-1 peat samples.

FM01CM-1 section (cm)	Fraction dated	$\delta^{13}C$ (‰)	Date (^{14}C years B.P.)	Date (calendar years A.D./B.C.)	Laboratory code
38-40*	Humic acid (HA2)	-27.0	1275 ± 35	A.D. 660 – 830	GU-12067
38-40*	Humin	-25.6	1300 ± 35	A.D. 650 - 780	GU-12070
48-50*	Humic acid (HA2)	-27.0	1380 ± 35	A.D. 600 – 720	GU-12066
56-57	Humic acid (HA2)	-27.3	1515 ± 40	A.D. 430 – 640	GU-12065
76-77	Humic acid (HA2)	-27.3	1830 ± 35	A.D. 120 – 260	GU-12063
85-86	Humic acid (HA2)	-27.9	1900 ± 35	A.D. 20 – 220	GU-12060
91-93*	Humic acid (HA2)	-27.7	2110 ± 35	210 – 40 B.C.	GU-12059
91-93*	Humin	-27.1	2080 ± 35	200 B.C. – A.D. 10	GU-12069
94-96*	Humic acid (HA2)	-27.2	2105 ± 35	210 – 40 B.C.	GU-12061

*Individual 1-cm sections were bulked together to provide sufficient material for dating.

3.3 CONSERVATIVE ELEMENTS

This section presents the Flanders Moss peat core results for the conservative elements (Al, Sc, Ti, Y and Zr), which are often used to represent atmospheric soil dust concentrations. The concentration profiles of these elements will be compared with the ash content profiles, which were presented in Section 3.1.3. Total Al, Sc, Ti, Y and Zr concentrations for FM01CM-1 and FM04-1-M, which are expressed relative to sectional 105°C-dried peat weights, are tabulated in A4.1 Table A3 and A4.2 Table A3, respectively. Al, Sc, Ti, Y and Zr concentration and ash content profiles for FM01CM-1 and FM04-1-M are shown in Figs. 3.11 and 3.12, respectively.

3.3.1 FM01CM-1

0-33 cm

All five elements (and ash content) exhibited prominent peaks in the uppermost ~ 20 cm of the core, with the following maximum values at the depths indicated:

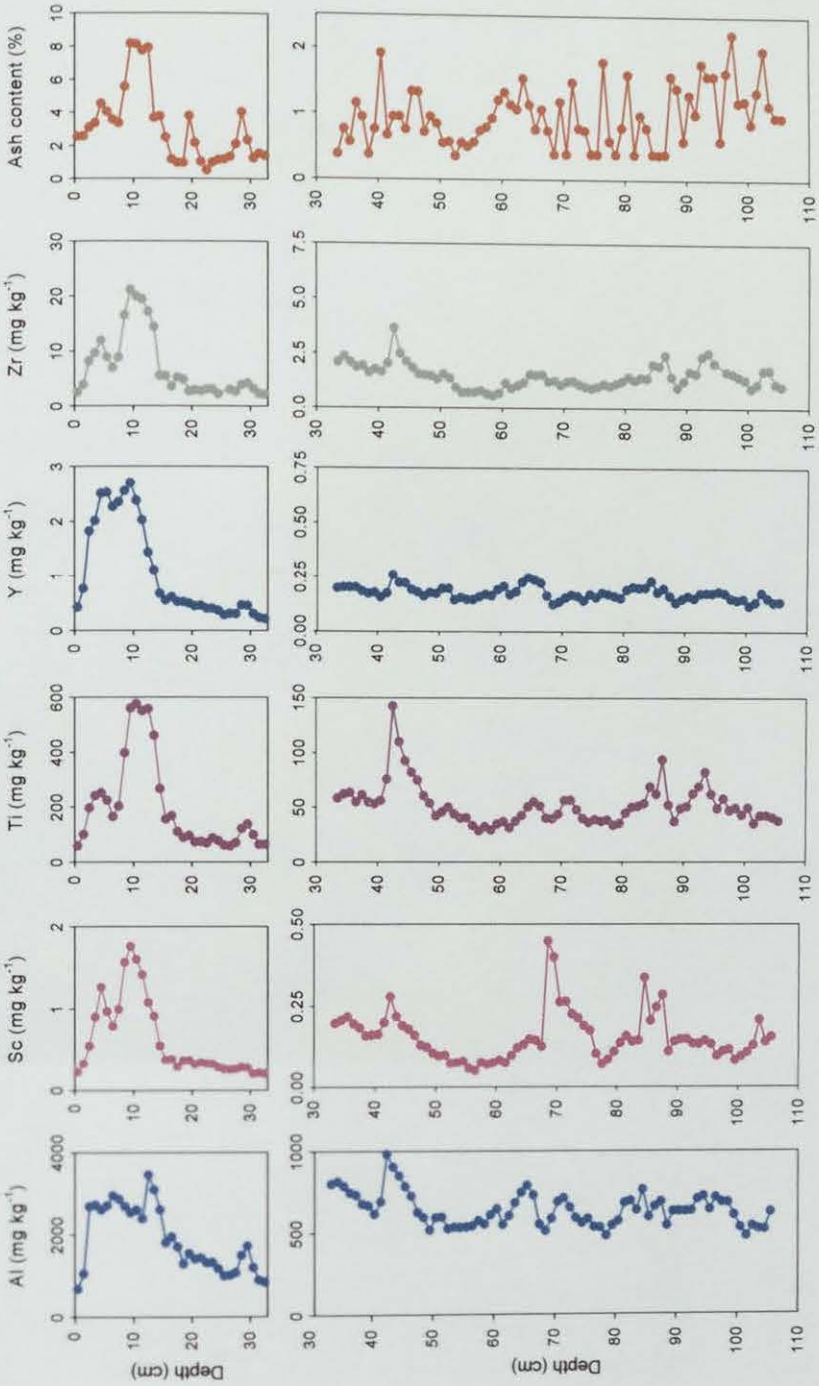

Figure 3.11: Depth profiles of Al, Sc, Ti, Y and Zr concentrations (mg kg^{-1}) and ash contents (% by weight) from 0-33 cm and 33-106 cm in the FM01CM-1 peat core.

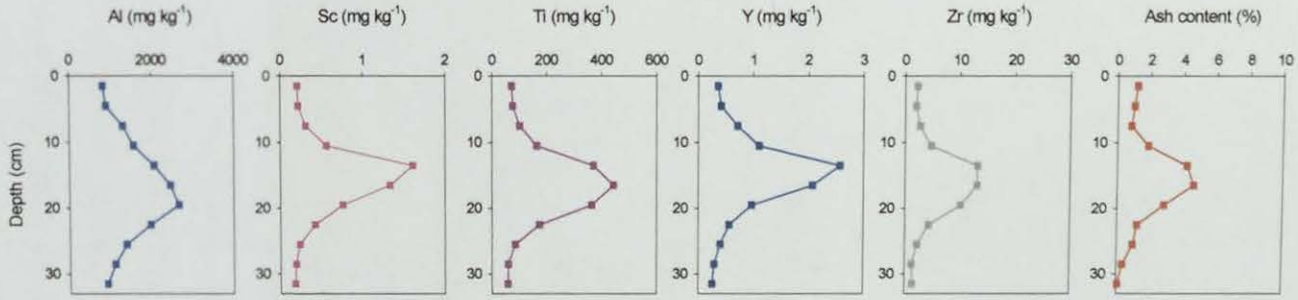

Figure 3.12: Depth profiles of Al, Sc, Ti, Y, Zr concentrations (mg kg^{-1}) and ash contents (% by weight) in the FM04-1-M (0-33 cm) peat core.

- Al – 3500 mg kg^{-1} at 12-13 cm
- Sc – 1.8 mg kg^{-1} at 9-10 cm
- Ti – ranging from 550 to 580 mg kg^{-1} between 9 and 13 cm
- Y – 2.7 mg kg^{-1} at 9-10 cm
- Zr – 20 mg kg^{-1} at 10-11 cm
- Ash content – ranging from 7.8 to 8.2% between 9 and 13 cm

Smaller near-surface peaks at a depth of 4.5 cm were apparent for all of the elements except Al, and also minor peaks at a depth of 29.5 cm for all of the elements except Sc. There was generally good correlation between the conservative element concentration profiles and the ash content profile (*cf.* Fig. 3.11).

33-106 cm

Note the change in scale on the concentration and ash content profiles (4-fold) on going from 0-33 cm to 33-106 cm (*cf.* Fig. 3.11). Mean concentrations in the core between depths of 33 and 106 cm were as follows: Al (640 ± 100 mg kg^{-1}), Sc (0.16 ± 0.08 mg kg^{-1}), Ti (53 ± 19 mg kg^{-1}), Y (0.18 ± 0.03 mg kg^{-1}) and Zr (1.5 ± 0.6 mg kg^{-1}). All elements exhibited peaks between 41 and 47 cm, which correlated well with the increase in ash content at these depths. Further peaks occurred at 64-67 cm, 71-73 cm and 82-89 cm for Al, 68-76 cm and 84-88 cm for Sc, 84-87 cm and 92-95 cm for Ti and Zr, and 63-67 cm and 80-87 cm for Y. Concentration minima for each of the elements occurred between depths of 52 and 59 cm with the following mean concentrations: Al (550 ± 16 mg kg^{-1}), Sc (0.070 ± 0.011 mg kg^{-1}), Ti (36 ± 6 mg kg^{-1}), Y (0.16 ± 0.01 mg kg^{-1}) and Zr (0.75 ± 0.12 mg kg^{-1}). The ash content profile was rather 'noisy', precluding precise correlation with the elemental profiles (*cf.* Fig. 3.11). Note that Sc, Ti and Zr concentrations were at a minimum in this zone (52-59 cm) but the minimum mean Al (530 ± 30 mg kg^{-1}) and Y (0.14 ± 0.01mg kg^{-1}) concentrations occurred at depths of 76-81 cm and 97-102 cm, respectively.

3.3.2 FM04-1-M

In FM04-1-M, all five elements (and ash content) exhibited prominent concentration peaks between ~ 24 and 6 cm in this core, above which they declined towards the surface (Fig. 3.12). The following maximum values occurred at the depths indicated:

- Al – 2700 mg kg^{-1} at 18-21 cm
- Sc – 1.6 mg kg^{-1} at 12-15 cm
- Ti – 440 mg kg^{-1} at 15-18 cm
- Y – 2.6 mg kg^{-1} at 12-15 cm
- Zr – 13 mg kg^{-1} at 12-18 cm
- Ash content – 4.6% at 15-18 cm

The profiles of the paired conservative elements Sc and Y, and Ti and Zr were most similar in appearance. That of Al looked different from the rest.

3.3.3 Discussion

Concentration increases in the near-surface peat sections of these cores, as found previously for ash content, are most likely caused by the increase in anthropogenic soil dust deposition, e.g. arising from the clearance of land for agricultural purposes or deforestation. The concentration profiles for the pairs of elements Sc and Y, and Ti and Zr, exhibited similar features (*cf.* Figs. 3.11 and 3.12) but, in each of the cores, the maximum Al concentrations occurred well below that of the other elements. These trends indicate that Al may well be mobile in ombrotrophic peat, (*cf.* Section 1.8.4.1), and for this reason Al will not be used to correct Pb concentrations for soil dust contributions in Section 3.5. The conservative element concentration minima in the 52-59 cm sections of FM01CM-1 (*cf.* Section 3.3.1) could be indicative of times when soil dust deposition was less important (e.g. greater land cover by vegetation) or possibly a climatic period characterised by wetter, less windy conditions. Note that on going from the mean concentrations in the 52-59 cm sections to the maximum concentrations in the 0-33 cm sections of FM01CM-1 (*cf.* Fig. 3.11), Sc and Y, and Ti and Zr, concentrations increased by 20-30-fold.

3.3.3.1 Intercomparison of Sc and Ti

As mentioned in Section 1.8.2, some workers use elemental ratios (M/X) in peat samples, where M is the concentration of the element of interest and X is the concentration of the conservative element, to quantify the extent of anthropogenic enrichment of elements by comparing these ratios to those for the Earth's crust. To investigate the conservative nature of Sc and Ti, where Sc and Ti, in general, can also be assumed to represent Y and Zr, respectively, Ti/Sc ratios in the peat core profiles were calculated and compared with the Ti/Sc ratio for the Earth's crust (445) (Wedepohl, 1995). Sc and Ti concentration and Ti/Sc ratio profiles for the FM01CM-1 and FM04-1-M cores are shown in Figs. 3.13 and 3.14, respectively. Ti/Sc values in FM01CM-1 and FM04-1-M are tabulated in A4.1 Table A3 and A4.2 Table A3, respectively.

Slight differences between the Sc and Ti concentration profiles, in terms of the peak positions and magnitude of increases are apparent in both cores, as indicated by the Ti/Sc ratio profiles (*cf.* Figs. 3.13 and 3.14). The mean Ti/Sc ratio (376 ± 117) in the 33-106 cm sections of the FM01CM-1 core is in relatively close agreement with the UCC Ti/Sc ratio (445), suggesting that natural soil dust contributions are perhaps the most important sources of these metals at these depths. In FM01CM-1 (0-33 cm) and FM04-1-M, a general decrease in Ti/Sc ratios occurs above and below the positions of maximum Ti/Sc ratios in the uppermost 33 cm, both of which could either be attributable to different soil dust sources or possibly direct non-soil-dust-related anthropogenic sources (e.g. coal combustion). Despite these slight variations in the Ti/Sc ratio profiles, the conservative elements Sc, Ti, Y and Zr will be used in Section 3.5 to normalise Pb concentrations in the Flanders Moss peat cores for soil dust contributions, using Pb/X concentration ratios (where X is the conservative element).

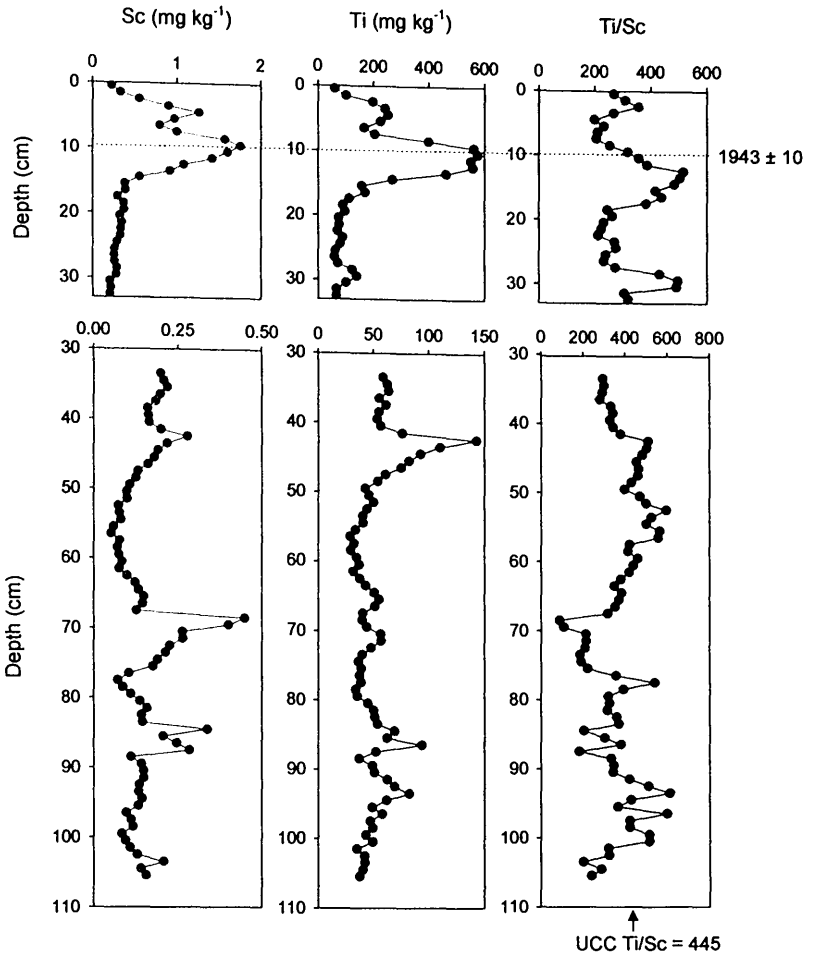

Figure 3.13: Depth profiles of Sc and Ti concentrations (mg kg^{-1}) and Ti/Sc ratios from 0-33 cm and 33-106 cm in the ^{210}Pb-dated FM01CM-1 peat core.

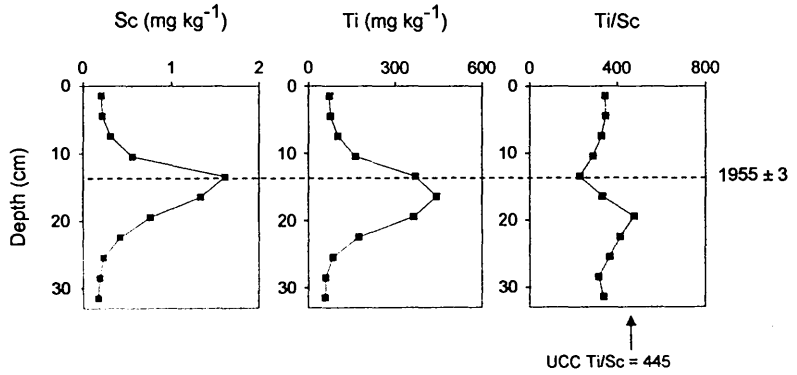

Figure 3.14: Depth profiles of Sc and Ti concentrations (mg kg^{-1}) and Ti/Sc ratios in the ^{210}Pb-dated FM04-1-M (0-33 cm) peat core.

3.4 Pb AND Pb ISOTOPIC RATIOS

This section presents the Pb concentration and Pb isotopic ratio results for the Flanders Moss peat cores. Total Pb concentrations and measured $^{206}Pb/^{207}Pb$, $^{208}Pb/^{206}Pb$ and $^{208}Pb/^{207}Pb$ isotopic ratios for FM01CM-1 and FM04-1-M are shown in Tables 3.6 and 3.7, respectively. Total Pb concentration and $^{206}Pb/^{207}Pb$ ratio profiles for FM01CM-1 and FM04-1-M are shown in Figs. 3.15 and 3.16, respectively.

3.4.1 FM01CM-1

0-33 cm

Pb concentrations increased from 4.4 mg kg^{-1} at 32-33 cm to a maximum value of 260 mg kg^{-1} at a depth of 8.5 cm, above which they decreased gradually towards the top of the core. The $^{206}Pb/^{207}Pb$ ratios remained constant at a mean value of 1.173 ± 0.002 from 33 cm to 12 cm, above which they declined steeply to a constant value of ~ 1.134 from 3.5 cm upwards.

33-106 cm

Note the change in scale on the Pb concentration (50-fold) on going from 0-33 cm to 33-106 cm (*cf.* Fig. 3.15). Pb concentrations were much lower than those in the uppermost 0-33 cm of the core but several distinct zones were apparent: a region of minimum concentrations (mean 1.1 ± 0.2 mg kg^{-1}) from 71 to 53 cm, above which Pb increased to 2.5 ± 0.3 mg kg^{-1} by 40 cm to 33 cm and below which from 71 to 102 cm there was a pronounced peak with a maximum concentration of 4.6 mg kg^{-1} at 90-91 cm. The $^{206}Pb/^{207}Pb$ ratio in the zone of minimum Pb concentration (53-71 cm) averaged 1.164 ± 0.006, with corresponding means of 1.168 ± 0.004 in the zone above (33-53 cm) and 1.176 ± 0.003 over the zone (71-102 cm) containing the Pb peak below (*cf.* Fig. 3.15).

Table 3.6: Total Pb concentrations (mg kg^{-1}) and Pb isotopic ratios in the FM01CM-1 peat core.

Section (cm)	Pb (mg kg^{-1})	$^{206}Pb/^{207}Pb$	$^{208}Pb/^{206}Pb$	$^{208}Pb/^{207}Pb$
0-1	68 ± 0*	1.133 ± 0.0012	2.130 ± 0.0044	2.414 ± 0.0066
1-2	85 ± 6*	1.134 ± 0.0008	2.133 ± 0.0025	2.418 ± 0.0038
2-3	140 ± 1*	1.135 ± 0.0022	2.128 ± 0.0052	2.415 ± 0.0062
3-4	145 ± 2*	1.134 ± 0.0016	2.113 ± 0.0042	2.397 ± 0.0021
4-5	158 ± 0*	1.140 ± 0.0013	2.124 ± 0.0021	2.421 ± 0.0026
5-6	195 ± 8*	1.145 ± 0.0013	2.114 ± 0.0018	2.419 ± 0.0018
6-7	230 ± 5*	1.151 ± 0.0022	2.109 ± 0.0020	2.425 ± 0.0044
7-8	241 ± 2*	1.156 ± 0.0014	2.103 ± 0.0026	2.432 ± 0.0026
8-9	264 ± 2*	1.160 ± 0.0021	2.103 ± 0.0037	2.437 ± 0.0026
9-10	224 ± 2*	1.163 ± 0.0016	2.099 ± 0.0019	2.440 ± 0.0022
10-11	200 ± 5*	1.169 ± 0.0005	2.098 ± 0.0026	2.455 ± 0.0030
11-12	142 ± 5*	1.168 ± 0.0015	2.092 ± 0.0020	2.444 ± 0.0029
12-13	96 ± 3*	1.170 ± 0.0012	2.097 ± 0.0035	2.454 ± 0.0062
13-14	76 ± 2*	1.173 ± 0.0018	2.097 ± 0.0033	2.459 ± 0.0071
14-15	55 ± 1*	1.172 ± 0.0008	2.098 ± 0.0054	2.458 ± 0.0071
15-16	45 ± 4*	1.171 ± 0.0020	2.093 ± 0.0043	2.451 ± 0.0024
16-17	45 ± 2*	1.174 ± 0.0013	2.096 ± 0.0020	2.461 ± 0.0043
17-18	35 ± 1*	1.174 ± 0.0017	2.093 ± 0.0055	2.457 ± 0.0050
18-19	35 ± 1*	1.174 ± 0.0022	2.093 ± 0.0055	2.458 ± 0.0055
19-20	29 ± 0*	1.174 ± 0.0011	2.096 ± 0.0029	2.461 ± 0.0043
20-21	28 ± 1*	1.176 ± 0.0012	2.092 ± 0.0027	2.461 ± 0.0048
21-22	26 ± 2*	1.174 ± 0.0011	2.094 ± 0.0039	2.460 ± 0.0052
22-23	23 ± 2*	1.173 ± 0.0018	2.091 ± 0.0026	2.454 ± 0.0036
23-24	18 ± 0*	1.174 ± 0.0012	2.092 ± 0.0035	2.456 ± 0.0043
24-25	15 ± 1*	1.174 ± 0.0022	2.092 ± 0.0044	2.457 ± 0.0070
25-26	11 ± 0*	1.172 ± 0.0005	2.091 ± 0.0036	2.451 ± 0.0051
26-27	12± 1*	1.172 ± 0.0031	2.091 ± 0.0038	2.446 ± 0.0088
27-28	10 ± 1*	1.171 ± 0.0011	2.094 ± 0.0061	2.450 ± 0.0057
28-29	16 ± 0*	1.176 ± 0.0013	2.093 ± 0.0046	2.460 ± 0.0043
29-30	14 ± 1*	1.174 ± 0.0018	2.093 ± 0.0050	2.457 ± 0.0074
30-31	7.5 ± 1.2*	1.174 ± 0.0019	2.093 ± 0.0066	2.452 ± 0.0074
31-32	5.5 ± 0.8*	1.169 ± 0.0014	2.098 ± 0.0054	2.445 ± 0.0035
32-33	4.4 ± 0.2*	1.171 ± 0.0018	2.096 ± 0.0037	2.446 ± 0.0019
33-34	2.37 ± 0.70*	1.167 ± 0.0014	2.096 ± 0.0026	2.445 ± 0.0019
34-35	2.57 ± 1.20*	1.165 ± 0.0018	2.099 ± 0.0013	2.443 ± 0.0049
35-36	2.90 ± 0.08	1.171 ± 0.0020	2.093 ± 0.0028	2.445 ± 0.0036
36-37	2.16 ± 1.10*	1.166 ± 0.0015	2.097 ± 0.0017	2.450 ± 0.0044
37-38	2.16 ± 0.01	1.166 ± 0.0023	2.106 ± 0.0027	2.442 ± 0.0058
38-39	2.82 ± 0.01	1.170 ± 0.0014	2.088 ± 0.0029	2.451 ± 0.0056
39-40	2.28 ± 0.04	1.167 ± 0.0021	2.104 ± 0.0045	2.447 ± 0.0043
40-41	2.31 ± 1.00*	1.165 ± 0.0008	2.100 ± 0.0029	2.440 ± 0.0044
41-42	1.25 ± 0.01	1.176 ± 0.0078	2.068 ± 0.0071	2.432 ± 0.0185
42-43	1.96 ± 0.10	1.166 ± 0.0025	2.132 ± 0.0118	2.446 ± 0.0114

Total Pb concentrations are relative to sectional 105°C-dried peat weights. *Total Pb concentrations determined by ICP-OES where standard deviations were calculated as the standard deviation of the mean value for two separate sample analyses. ICP-MS Pb concentration and Pb isotopic ratio standard deviations were calculated as the standard deviation from the mean value for five consecutive determinations of the concentration/ratio of a sample solution.

Table 3.6 (continued): Total Pb concentrations (mg kg^{-1}) and Pb isotopic ratios in the FM01CM-1 peat core.

Section (cm)	Pb (mg kg^{-1})	$^{206}Pb/^{207}Pb$	$^{208}Pb/^{206}Pb$	$^{208}Pb/^{207}Pb$
43-44	1.99 ± 0.01	1.167 ± 0.0012	2.096 ± 0.0019	2.444 ± 0.0041
44-45	1.86 ± 0.02	1.169 ± 0.0020	2.090 ± 0.0042	2.465 ± 0.0025
45-46	1.62 ± 0.05	1.164 ± 0.0015	2.122 ± 0.0067	2.465 ± 0.0095
46-47	1.49 ± 0.03	1.172 ± 0.0034	2.085 ± 0.0081	2.438 ± 0.0033
47-48	1.22 ± 0.01	1.159 ± 0.0024	2.108 ± 0.0043	2.445 ± 0.0089
48-49	0.74 ± 0.03	1.171 ± 0.0039	2.097 ± 0.0091	2.452 ± 0.0054
49-50	1.74 ± 0.02	1.173 ± 0.0087	2.073 ± 0.0127	2.431 ± 0.0185
50-51	1.41 ± 0.01	1.163 ± 0.0026	2.102 ± 0.0026	2.445 ± 0.0041
51-52	1.15 ± 0.01	1.169 ± 0.0030	2.091 ± 0.0066	2.445 ± 0.0066
52-53	1.24 ± 0.01	1.165 ± 0.0129	2.090 ± 0.0108	2.434 ± 0.0273
53-54	0.87 ± 0.01	1.160 ± 0.0032	2.093 ± 0.0064	2.430 ± 0.0034
54-55	0.91 ± 0.01	1.163 ± 0.0094	2.094 ± 0.0173	2.435 ± 0.0164
55-56	0.71 ± 0.01	1.163 ± 0.0034	2.095 ± 0.0029	2.438 ± 0.0051
56-57	1.39 ± 0.01	1.173 ± 0.0059	2.062 ± 0.0174	2.419 ± 0.0168
57-58	1.18 ± 0.01	1.164 ± 0.0052	2.097 ± 0.0042	2.441 ± 0.0070
58-59	1.11 ± 0.01	1.160 ± 0.0033	2.107 ± 0.0036	2.447 ± 0.0069
59-60	1.05 ± 0.01	1.156 ± 0.0014	2.108 ± 0.0048	2.436 ± 0.0034
60-61	1.03 ± 0.00	1.161 ± 0.0031	2.103 ± 0.0015	2.439 ± 0.0061
61-62	1.00 ± 0.01	1.158 ± 0.0030	2.104 ± 0.0035	2.43ɔ ± 0.0031
62-63	0.94 ± 0.00	1.160 ± 0.0009	2.103 ± 0.0055	2.437 ± 0.0048
63-64	1.05 ± 0.00	1.160 ± 0.0040	2.104 ± 0.0063	2.438 ± 0.0040
64-65	1.18 ± 0.01	1.173 ± 0.0040	2.097 ± 0.0064	2.458 ± 0.0087
65-66	1.14 ± 0.00	1.175 ± 0.0025	2.092 ± 0.0039	2.457 ± 0.0037
66-67	0.89 ± 0.04	1.155 ± 0.0041	2.112 ± 0.0129	2.434 ± 0.0082
67-68	1.13 ± 0.01	1.164 ± 0.0021	2.100 ± 0.0065	2.441 ± 0.0065
68-69	1.28 ± 0.04	1.172 ± 0.0024	2.097 ± 0.0066	2.452 ± 0.0073
69-70	0.94 ± 0.00	1.165 ± 0.0030	2.106 ± 0.0025	2.453 ± 0.0052
70-71	1.11 ± 0.01	1.169 ± 0.0030	2.096 ± 0.0090	2.453 ± 0.0062
71-72	1.40 ± 0.01	1.173 ± 0.0037	2.091 ± 0.0051	2.451 ± 0.0048
72-73	1.00 ± 0.02	1.180 ± 0.0025	2.074 ± 0.0074	2.445 ± 0.0070
73-74	1.38 ± 0.01	1.181 ± 0.0019	2.080 ± 0.0039	2.457 ± 0.0018
74-75	1.52 ± 0.03	1.178 ± 0.0016	2.077 ± 0.0043	2.442 ± 0.0043
75-76	1.67 ± 0.03	1.179 ± 0.0029	2.084 ± 0.0049	2.456 ± 0.0071
76-77	2.17 ± 0.01	1.174 ± 0.0024	2.088 ± 0.0037	2.451 ± 0.0042
77-78	1.81 ± 0.00	1.175 ± 0.0029	2.088 ± 0.0131	2.454 ± 0.0125
78-79	1.66 ± 0.07	1.168 ± 0.0025	2.097 ± 0.0159	2.443 ± 0.0189
79-80	2.39 ± 0.02	1.172 ± 0.0033	2.092 ± 0.0009	2.450 ± 0.0063
80-81	2.71 ± 0.05	1.176 ± 0.0019	2.082 ± 0.0045	2.449 ± 0.0046
81-82	2.49 ± 0.15	1.172 ± 0.0028	2.102 ± 0.0101	2.458 ± 0.0128
82-83	2.28 ± 0.09	1.176 ± 0.0052	2.095 ± 0.0072	2.459 ± 0.0061
83-84	2.51 ± 0.08	1.176 ± 0.0021	2.083 ± 0.0063	2.446 ± 0.0051
84-85	2.08 ± 0.08	1.179 ± 0.0015	2.102 ± 0.0057	2.471 ± 0.0075
85-86	2.68 ± 0.05	1.177 ± 0.0023	2.092 ± 0.0059	2.458 ± 0.0032
86-87	3.84 ± 0.03	1.177 ± 0.0016	2.088 ± 0.0029	2.457 ± 0.0018
87-88	2.56 ± 0.08	1.176 ± 0.0018	2.091 ± 0.0049	2.452 ± 0.0059
88-89	2.66 ± 0.03	1.177 ± 0.0010	2.082 ± 0.0026	2.448 ± 0.0032
89-90	2.74 ± 0.05	1.174 ± 0.0035	2.089 ± 0.0051	2.447 ± 0.0020
90-91	4.63 ± 0.05	1.174 ± 0.0022	2.084 ± 0.0070	2.446 ±0.0088
91-92	3.51 ± 0.07	1.176 ± 0.0033	2.090 ± 0.0045	2.458 ± 0.0033

Table 3.6 (continued): Total Pb concentrations (mg kg^{-1}) and Pb isotopic ratios in the FM01CM-1 peat core.

Section (cm)	Pb (mg kg^{-1})	$^{206}Pb/^{207}Pb$	$^{208}Pb/^{206}Pb$	$^{208}Pb/^{207}Pb$
92-93	3.01 ± 0.12	1.181 ± 0.0026	2.075 ± 0.0023	2.445 ± 0.0049
93-94	2.74 ± 0.05	1.177 ± 0.0026	2.094 ± 0.0064	2.463 ± 0.0072
94-95	2.51 ± 0.05	1.183 ± 0.0036	2.069 ± 0.0034	2.444 ± 0.0019
95-96	2.03 ± 0.06	1.174 ± 0.0037	2.092 ± 0.0094	2.450 ± 0.0043
96-97	2.67 ± 0.02	1.171 ± 0.0014	2.094 ± 0.0041	2.450 ± 0.0056
97-98	2.10 ± 0.01	1.171 ± 0.0013	2.095 ± 0.0026	2.456 ± 0.0041
98-99	1.95 ± 0.01	1.175 ± 0.0029	2.088 ± 0.0024	2.455 ± 0.0058
99-100	1.88 ± 0.02	1.174 ± 0.0027	2.098 ± 0.0030	2.462 ± 0.0062
100-101	1.99 ± 0.01	1.178 ± 0.0017	2.067 ± 0.0093	2.441 ± 0.0069
101-102	1.80 ± 0.01	1.169 ± 0.0015	2.103 ± 0.0046	2.457 ± 0.0060
102-103	1.60 ± 0.02	1.164 ± 0.0027	2.106 ± 0.0059	2.451 ± 0.0048
103-104	1.51 ± 0.01	1.168 ± 0.0017	2.102 ± 0.0037	2.454 ± 0.0032
104-105	1.25 ± 0.01	1.165 ± 0.0019	2.091 ± 0.0017	2.435 ± 0.0034
105-106	1.69 ± 0.01	1.165 ± 0.0008	2.099 ± 0.0040	2.445 ± 0.0037

Table 3.7: Total Pb concentrations (mg kg^{-1}) and Pb isotopic ratios in the FM04-1-M peat core.

Section (cm)	Pb (mg/kg)	$^{206}Pb/^{207}Pb$	$^{208}Pb/^{206}Pb$	$^{208}Pb/^{207}Pb$
0-3	15	1.139 ± 0.0023	2.114 ± 0.0062	2.409 ± 0.0040
3-6	20	1.135 ± 0.0034	2.116 ± 0.0059	2.402 ± 0.0039
6-9	57	1.130 ± 0.0017	2.121 ± 0.0029	2.398 ± 0.0016
9-12	100	1.134 ± 0.0008	2.154 ± 0.0036	2.443 ± 0.0031
12-15	190	1.158 ± 0.0004	2.125 ± 0.0013	2.461 ± 0.0017
15-18	160	1.170 ± 0.0010	2.110 ± 0.0019	2.470 ± 0.0006
18-21	77	1.174 ± 0.0011	2.086 ± 0.0031	2.448 ± 0.0020
21-24	40	1.172 ± 0.0018	2.085 ± 0.0023	2.443 ± 0.0021
24-27	20	1.177 ± 0.0010	2.081 ± 0.0023	2.448 ± 0.0038
27-30	12	1.175 ± 0.0030	2.080 ± 0.0056	2.443 ± 0.0060
30-33	18	1.207 ± 0.0021*	2.030 ± 0.0052*	2.450 ± 0.0065*

Total Pb concentrations are relative to sectional 105°C-dried peat weights. *Pb isotopic ratios considered to be outliers. Total Pb concentrations were determined by ICP-OES. Pb isotopic ratio standard deviations were calculated as the standard deviation from the mean value for five consecutive determinations of the ratio of a sample solution.

3.4.2 FM04-1-M

Concentrations of Pb increased from 18 mg kg^{-1} at 30-33 cm to a maximum value of 190 mg kg^{-1} at 12-15 cm, above which Pb concentration decreased towards the top of the core to a concentration of 15 mg kg^{-1} in the 0-3 cm section. The $^{206}Pb/^{207}Pb$ ratios remained constant at a mean value of 1.175 ± 0.002 from 30 to 18 cm then declined to 1.170 ± 0.001 at 15-18 cm, above which they declined to a minimum of 1.130 ± 0.002 at 6-9 cm before increasing to 1.139 ± 0.002 at 0-3 cm (*cf.* Fig. 3.16). Note that the reversal in the $^{206}Pb/^{207}Pb$ ratio trend was present at the top of this core but absent from the top of the FM01CM-1 core.

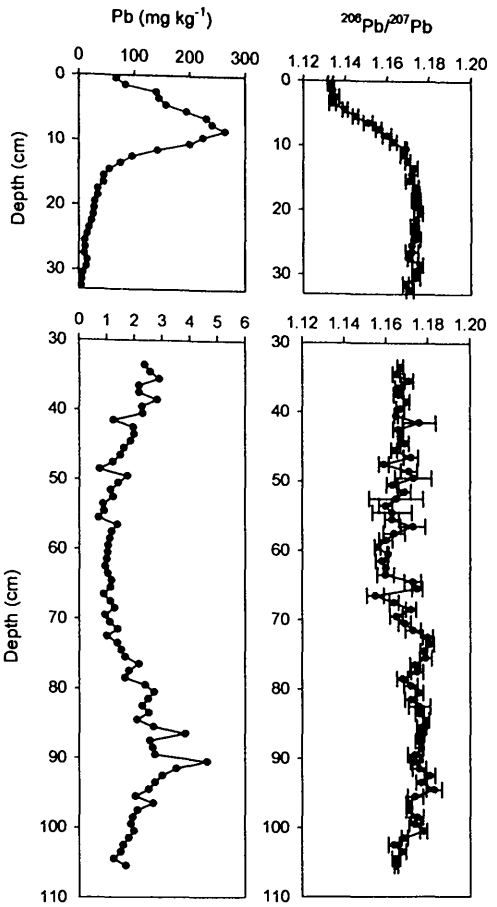

Figure 3.15: Depth profiles of Pb concentrations (mg kg^{-1}) and measured $^{206}Pb/^{207}Pb$ ratios from 0-33 cm and 33-106 cm in the FM01CM-1 peat core.

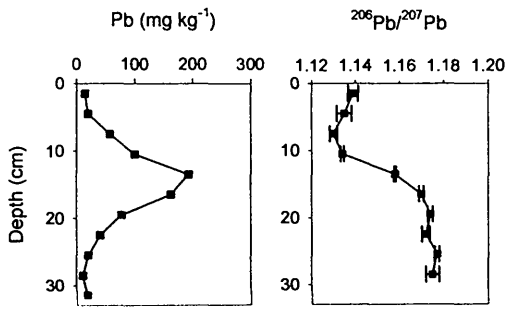

Figure 3.16: Depth profiles of Pb concentrations (mg kg^{-1}) and measured $^{206}Pb/^{207}Pb$ ratios in the FM04-1-M (0-33 cm) peat core.

3.4.3 Discussion

As Pb is essentially immobile in ombrotrophic peat, these Pb profiles represent historical records of atmospheric deposition of anthropogenic and natural Pb at Flanders Moss. Interpretations of historical trends in sources of atmospheric Pb

deposition in these peat cores will be discussed later in Section 3.6, after anthropogenic Pb enrichments have been estimated in Section 3.5.

3.5 USE OF CONSERVATIVE ELEMENTS TO ESTIMATE ANTHROPOGENIC ENRICHMENTS OF Pb

Pb/Sc, Pb/Ti, Pb/Y and Pb/Zr ratios for FM01CM-1 and FM04-1-M are tabulated in A4.1 Table A4 and A4.2 Table A4, respectively. Pb concentration, Pb/Sc, Pb/Ti, Pb/Y and Pb/Zr ratio profiles for FM01CM-1 and FM04-1-M are shown in Figs. 3.17 and 3.18, respectively.

3.5.1 FM01CM-1

0-33 cm

Pb/X ratios increased steadily from 33 cm upwards, exhibiting a slight decline between 15 and 12 cm, above which there were twin peaks with maximum Pb/Sc (300) and Pb/Y (160) ratios occurring at 0-1 cm, and maximum Pb/Ti (1.4) and Pb/Zr (27) ratios at 6-7 cm. In comparison the maximum Pb concentration was at 8-9 cm (*cf.* Fig. 3.17).

33-106 cm

Note the change in scale on the ratio profiles (10-fold for Pb/Sc, Pb/Ti and Pb/Zr, and 5-fold for Pb/Y) on going from 0-33 cm to 33-106 cm (*cf.* Fig. 3.17). Maximum Pb/Sc (31), Pb/Ti (0.091), Pb/Y (28) and Pb/Zr (2.7) ratios occurred at a depth of 90-91 cm. Pb/X ratio minima occurred between 41 and 72 cm with the following mean values: Pb/Sc (10 ± 5), Pb/Ti (0.025 ± 0.008), Pb/Y (6.7 ± 1.7) and Pb/Zr (1.0 ± 0.4).

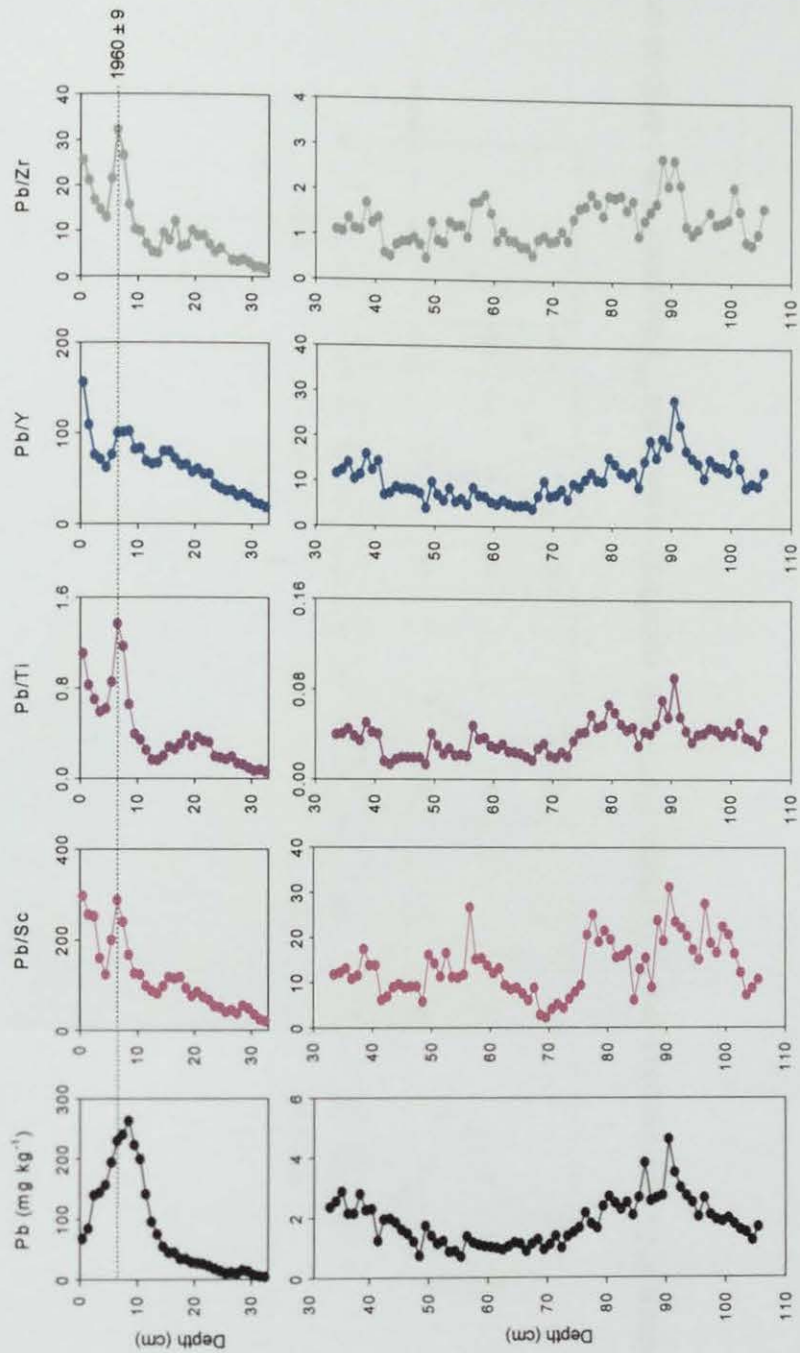

Figure 3.17: Depth profiles of Pb concentration (mg kg^{-1}), Pb/Sc, Pb/Ti, Pb/Y and Pb/Zr ratios from 0-33 cm and 33-106 cm in the ^{210}Pb-dated FM01CM-1 peat core.

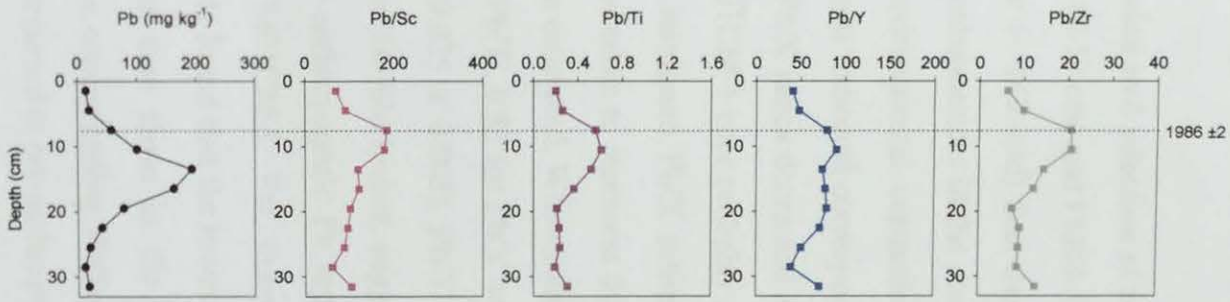

Figure 3.18: Depth profiles of Pb concentration (mg kg^{-1}), Pb/Sc, Pb/Ti, Pb/Y and Pb/Zr ratios in the ^{210}Pb-dated FM04-1-M (0-33 cm) peat core.

3.5.2 FM04-1-M

In the FM04-1-M core, Pb/X ratios decreased from 33 to 27 cm, above which they increased steadily, reaching maximum values between 12 and 6 cm before decreasing towards the surface of the core. The maximum value for Pb/Sc (190) occurred at 6-9 cm while those for Pb/Ti (0.61) and Pb/Y (91) were at 9-12 cm, and that for Pb/Zr (~ 21) was at 6-12 cm. In comparison, the maximum Pb concentration was at 12-15 cm (*cf.* Fig. 3.18).

3.5.3 Discussion and selection of conservative element

In the FM01CM-1 (0-33 cm) and FM04-1-M cores, Pb concentrations increased by a much greater factor (~ 140-fold) than those of the conservative elements, indicating the much smaller enhancement in the concentrations of these conservative elements relative to this environmental contaminant. Pb/X ratio profiles for each of the conservative elements indicated corresponding zones of maximum anthropogenic Pb enrichment. That Pb/X ratios decreased at the top of the FM04-1-M core but not at the top of the FM01CM-1 core probably reflects the loss of material from the top of FM01CM-1. The minimum Pb/X ratios between 41 and 72 cm in FM01CM-1 (33-106 cm) can be taken to represent the "background" Pb/X ratios from which Pb enrichments can be estimated. When compared with the UCC Pb/X ratios of 2.43 for Pb/Sc, 0.0055 for Pb/Ti, 0.82 for Pb/Y and 0.072 for Pb/Zr, the "background" Pb/Sc (10 ± 5), Pb/Ti (0.025 ± 0.008), Pb/Y (6.7 ± 1.7) and Pb/Zr (1.0 ± 0.4) ratios, however, were 4 to 14-fold higher, suggesting it is unlikely that Pb concentrations are unaffected by anthropogenic Pb inputs at any depth over the *ca.* 2500 years represented by FM01CM-1. For example, in a Swiss peat core from EGR, Shotyk *et al.* (2004) found that the lowest Pb concentrations (0.23 ± 0.04 mg kg^{-1}), a factor of 5 lower than those in the zone of minimum Pb concentrations in FM01CM-1, had a corresponding Pb/Sc ratios of 3.0, similar to that found in the UCC (2.43), and occurred in pre-anthropogenic peats dating from 5320 to 8020 ^{14}C y B.P.

As mentioned in Section 1.8.4.4, Sc is usually the favoured conservative element used for normalising metal concentrations for soil dust contributions, as it is believed to exhibit no preference for specific mineral phases and thus tends to be uniformly distributed throughout the environment. For this reason Sc and M/Sc concentration ratios (where M is the element of interest), will preferentially be used to assist in the estimation of the extent of Pb (and other essentially immobile metal) contributions from sources that are unrelated to direct anthropogenic inputs to the observed variations in the Pb (metal) concentration profiles in the rest of this Chapter.

3.6 HISTORICAL TRENDS IN SOURCES OF ATMOSPHERIC Pb DEPOSITION

Pb and Sc concentration, $^{206}Pb/^{207}Pb$ and Pb/Sc ratio profiles including age dates for FM01CM-1 and FM04-1-M are shown in Figs. 3.19 and 3.20, respectively. The most important historical periods of anthropogenic sources of atmospheric Pb deposition, based on trends in these profiles and corresponding age dates, can be summarised for FM01CM-1 and FM04-1-M, starting from the oldest to the most recent sources, as follows:

- FM01CM-1 (106 to 71 cm) - Pre-Roman and Roman period
- FM01CM-1 (71 to 33 cm) - Post-Roman and Mediaeval period
- FM01CM-1 (33 to 0 cm) and FM04-1-M – Industrial and post-industrial period

3.6.1 Pre-Roman and Roman atmospheric Pb sources and deposition

In FM01CM-1, it seems very likely that the elevated Pb/Sc ratios (mean 20 ± 6) associated with the elevated Pb concentrations from 96 to 86 cm, dated at 210-40 B.C. to 20-220 A.D., can be attributed to pre-Roman and Roman metallurgical activities (*cf.* Fig. 3.19). The Roman Pb mining industry is well documented (Tylecote, 1976, 1986; Shepherd, 1993) but, as the Romans didn't fully occupy Britain until after the Roman conquest in 43 A.D., these elevations in Pb

concentrations from 210 B.C. predate the Roman occupation by two centuries, consistent with the existence of a pre-Roman Pb extraction industry in the UK, as suggested by previous workers (Nriagu, 1983; Le Roux *et al.*, 2004).

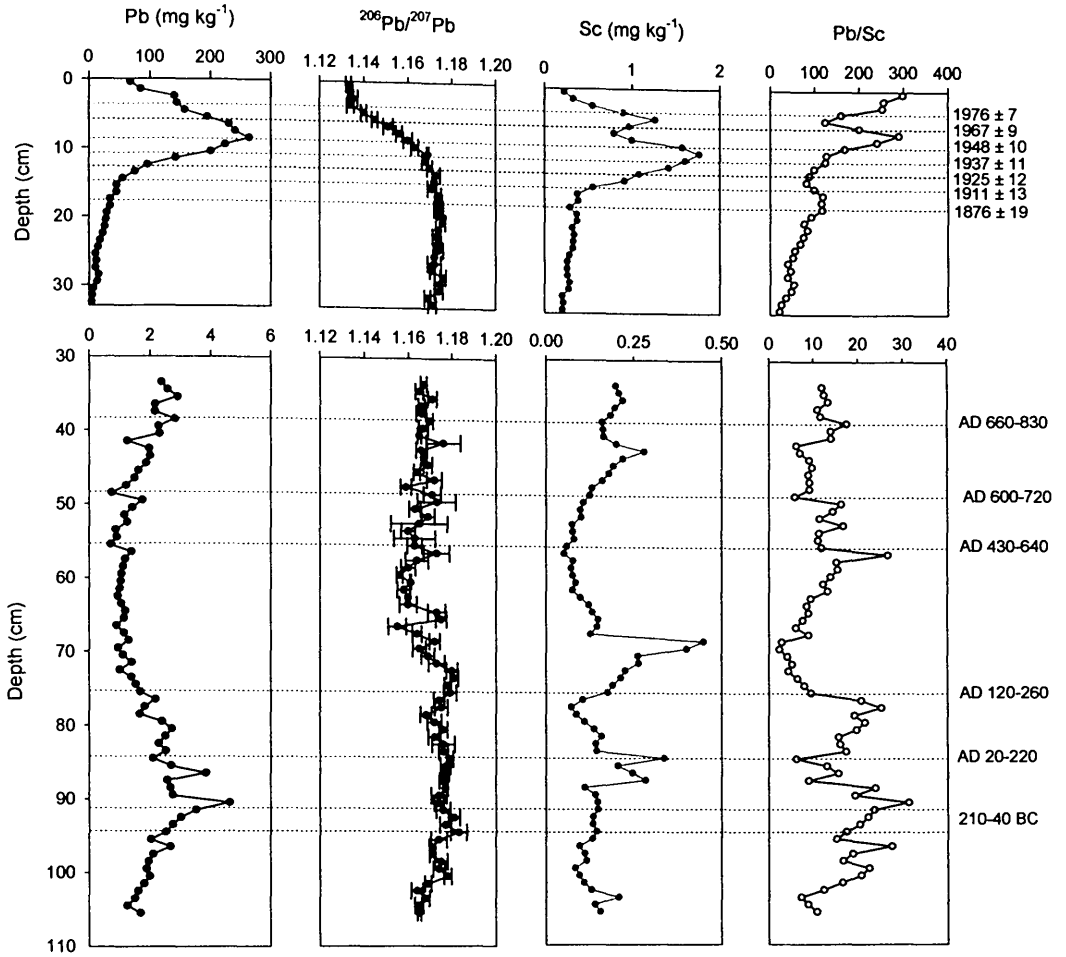

Figure 3.19: Depth profiles of Pb and Sc concentrations (mg kg^{-1}), measured $^{206}Pb/^{207}Pb$ and Pb/Sc ratios from 0-33 cm and 33-106 cm in the ^{210}Pb- and ^{14}C-dated FM01CM-1 peat core.

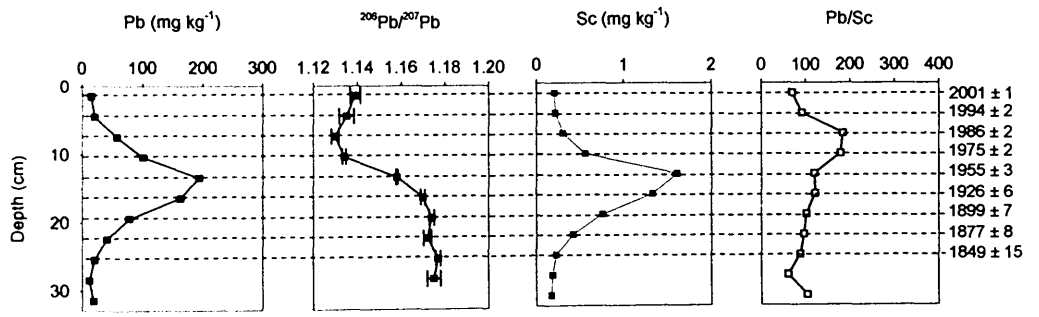

Figure 3.20: Depth profiles of Pb and Sc concentrations (mg kg^{-1}), measured $^{206}Pb/^{207}Pb$ and Pb/Sc ratios in the ^{210}Pb-dated FM04-1-M (0-33 cm) peat core.

Indeed, despite lower Pb concentrations over the earlier 96-102 cm depth interval, the corresponding Pb/Sc ratios were also enhanced at 21 ± 4. In the UK, the earliest pre-historic Cu mining is believed to have taken place from the early to mid Bronze Age (*ca.* 2396-1877 B.C.) (Mighall *et al.*, 2002) at Copa Hill in mid-Wales and from the vast amounts of bronze and Cu artefacts found on British prehistoric settlements and burial sites it is evident that Cu was available in quantity through the Bronze and Iron Ages, with the exploitation of the numerous Cu deposits located mainly in the north and west of the UK (Tylecote, 1986; Shepherd, 1993). Evidence has been found for the addition of Pb in varying amounts to mixtures of Cu and Sn during the late Bronze Age (*ca.* 900-500 B.C.) as a new technique to make bronze that flowed more freely during the casting process (Ritchie and Ritchie, 1991) and the mines of Alderley Edge in Cheshire, west-central England, are believed to have been worked mainly for Cu from the early Bronze Age (*ca.* 2000 B.C.) and possibly Pb by the late Bronze Age (*ca.* 500 B.C.) (Tylecote, 1976, 1986). Many bronze, Pb and stone implements have also been found in old surface workings at the Scottish Wanlockhead and Leadhills mines, suggesting that workings at these mines may date back to pre-Roman times (Shepherd, 1993). Iron working was also introduced *ca.* 500 B.C. and was well established before the arrival of the Romans and Fe workings in the Weald of Kent and Sussex (southern England) and Forest of Dean (central England) were extensively worked during the Roman occupation (Ritchie and Ritchie, 1991; Shepherd 1993). Cu and Fe metallurgy are also sources of Pb (and other metals such as As and Sb) to the environment (*cf.* Section 1.3.2.2.1), given the association of Pb (and these other metals) with sulfide minerals (Sparks, 1995). The main mining areas of Britain that were worked for Pb in Roman times and possibly, in some or all cases, before the conquest are: Somerset (Mendips), north-east Wales, Derbyshire, Yorkshire and Cheshire (Shepherd, 1993). The Mendip Pb mines in south-west England were worked by 49 A.D., only 6 years after the Roman conquest, further suggesting the prior existence of a local mining industry before the arrival of the Romans. The Pb deposits of north-east Wales were worked by the late 1st century A.D and those of Derbyshire, central England, by 117-138 A.D. (Tylecote, 1976, 1986; Shepherd, 1993).

In a Swiss peat core from EGR, Shotyk *et al.* (1998) attributed enrichments of Pb during the Roman period to ancient Pb mining and long-range transport of aerosols from the Iberian Peninsula during the period of greatest Roman mining, which occurred from 400 B.C. to 37 A.D. Rosman *et al.* (1997) also invoked this source to explain Pb enrichments at the same time in Greenland ice. Although production of metals in the Iberian Peninsula was still appreciable after 100 A.D., there was a general decline in activity as a result of the easier and cheaper production in the later acquired near-surface British ores (Shepherd, 1993). When Pb isotope ratios of the FM01CM-1 peat samples (96-86 cm) for the 210-40 B.C. to 20-220 A.D period are plotted along with those of various British Pb ores (Rohl, 1996) and Pb ores from southern Spain (Stos-Gale *et al.*, 1995) (Fig. 3.21), they are in much better agreement with those of British origin than those from the Spanish mines of Rio Tinto and Murcia (Carthagena), which were widely exploited during the Iron Age and Roman times (*ca.* 200 B.C. to 400 A.D.) (Tylecote, 1976; Shepherd, 1993). This supports the findings by Le Roux *et al.* (2004), based on research on Lindow Bog in north-west England, that environmental Pb contamination in Britain during this period resulted primarily from the mining and smelting of British ores.

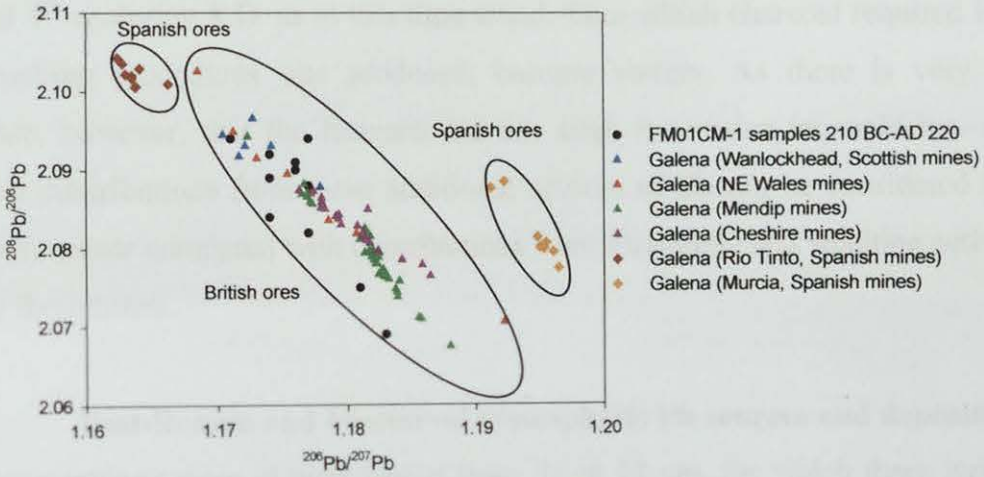

Figure 3.21: Plot of $^{208}Pb/^{206}Pb$ *versus* $^{206}Pb/^{207}Pb$ ratios for samples from 210 B.C.-220 A.D. in the FM01CM-1 peat core and for galena in various British and Spanish Pb ores (Stos-Gale *et al.*, 1995; Rohl, 1996).

From 86 to 76 cm, i.e. corresponding to 20-220 A.D. to 120-260 A.D., Pb concentrations and Pb/Sc ratios (mean 17 ± 5) were still elevated and the mean $^{206}Pb/^{207}Pb$ ratio (1.175 ± 0.003) was very similar to those for 96-86 cm (1.177 ± 0.003) and 96-102 cm (1.173 ± 0.003) and indeed 71-102 cm (1.176 ± 0.003) (*cf.* Fig. 3.19). Where it is possible to estimate the soil dust Pb contribution (mean 0.38 ± 0.15 mg kg^{-1} over 71-102 cm) and, by difference, the anthropogenic Pb contribution to the total Pb concentration via the use of the Pb/Sc ratios in peat and the UCC, it is not possible to do likewise for the $^{206}Pb/^{207}Pb$ ratio of the specifically anthropogenic Pb, as the Pb isotopic composition of the soil dust Pb, at least in the UK, is unknown. Kylander *et al.* (2005), however, characterised a Pb pre-pollution aerosol $^{206}Pb/^{207}Pb$ signature of 1.255 ± 0.026 in southern Europe which is more radiogenic than that found in western and northern Europe.

Interestingly, Le Roux *et al.* (2004) suggested that there was a correlation between atmospheric Pb deposition and increased soil dust created as a result of major woodland clearance which began, as indicated by peat core pollen diagrams, in the Iron Age and peaked during the Roman times (*ca.* 130-140 A.D.) (Dark, 1999). Also, Shepherd (1993) postulated the existence of British-Roman coal extraction in the late 2nd and 4th centuries A.D. as at this time wood, from which charcoal required in the ore smelting procedures was produced, became scarcer. As there is very little evidence, however, that the Romans did use coal, it remains inconclusive. Also, possible contributions from these additional sources of Pb can be considered to be relatively minor compared with contributions from Pb mining and smelting activities during these times.

3.6.2 Post-Roman and Mediaeval atmospheric Pb sources and deposition

Pb concentrations were at their lowest from 71 to 53 cm, for which there were no direct age-dates, with correspondingly low Pb/Sc ratios (11 ± 6), towards the end of (*ca.* 410 A.D.) and after the Roman occupation of Britain until *ca.* 650 A.D (*cf.* Fig. 3.19). This seems to be attributable to the decline in metallurgical activities during the 3rd century A.D. when exploitation of Pb ores became increasingly limited

by the engineering capabilities of the Romans (Patterson, 1972) and the general decline in Pb mining in western Europe after the fall of the Roman Empire (Shepherd, 1993). The mean $^{206}Pb/^{207}Pb$ ratio for this period was 1.164 ± 0.006, which is significantly less radiogenic than the mean value for the pre-Roman and Roman period peat samples (1.174 ± 0.005). It is interesting to speculate that these less radiogenic values could reflect contributions, albeit relatively minor, from long-range atmospheric deposition of Pb from metallurgical processing of Iberian Pb ores, by the Visigods, who founded an economically prosperous kingdom that lasted until the end of the 6th century A.D. (Puché and Bosch, 1996; Duarte, 1996). Martinez-Cortizas *et al.* (1997) attributed Pb enrichments in a peat core from north-west Spain to these same sources, although such low values of $^{206}Pb/^{207}Pb$ were not observed in Lindow Bog, north-west England. When Pb isotope ratios of the FM01CM-1 peat samples from 71 to 53 cm (estimated to correspond roughly to the period 400–600 A.D.) are plotted along with those of various British Pb ores (Rohl, 1996) and Pb ores from southern (Stos-Gale *et al.*, 1995) and north-west Spain (Kylander *et al.*, 2005) (Fig. 3.22), they are in much better agreement with the Pb ores from the Rio Tinto mines in southern Spain and possibly to some extent north-west Spain (Stos-Gale *et al.*, 1995). However, British mines also appear to contribute to the minor Pb sources at these peat core depths.

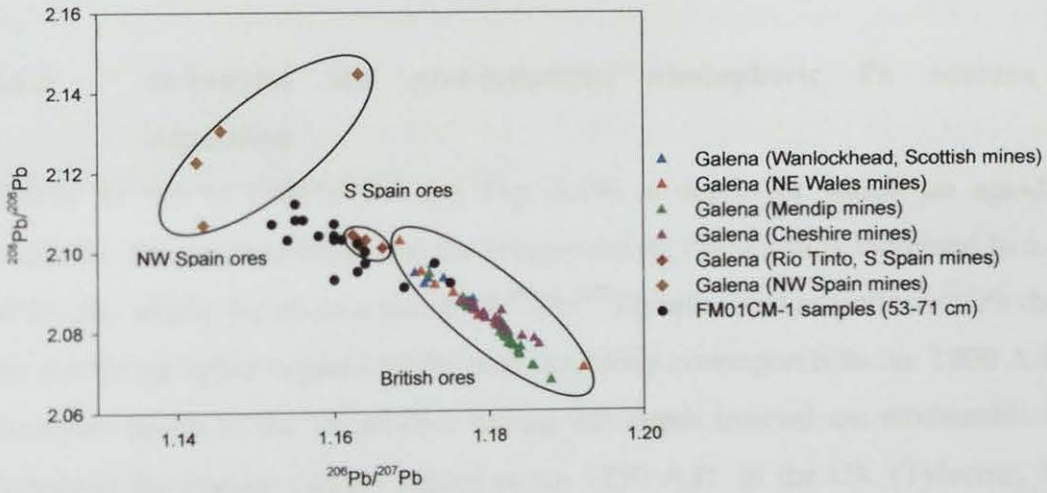

Figure 3.22: Plot of $^{208}Pb/^{206}Pb$ *versus* $^{206}Pb/^{207}Pb$ ratios for samples for the FM01CM-1 (53-71 cm) peat core and for galena in various British and Spanish Pb ores (Stos-Gale *et al.*, 1995; Rohl, 1996; Kylander *et al.*, 2005).

From 53 to 33 cm, for which there were no direct age-dates, Pb concentrations and Pb/Sc ratios (mean 12 ± 3) increased slightly but the mean $^{206}Pb/^{207}Pb$ ratio (1.168 ± 0.004) for this period was still less radiogenic, at least to the early Mediaeval period (*cf.* 840 A.D. in Monna *et al.* 2004, corresponding to ~38 cm in FM01CM-1). Due to the lack of archaeological knowledge during this pre-Mediaeval period, the origin of these Pb increases is rather uncertain (*cf.* Fig. 3.19). Above 38 cm (~ 840 A.D.), however, the Pb increases are most likely to be attributable to the influence of the growth in metal production during the Mediaeval period when Roman Pb mines were progressively being re-opened while new ones were being discovered, such as those in continental Europe, including the well known Mediaeval German Ag mining district in the Harz, which led to the development of the Ag mining industry and brought about the revival of mining in Europe by the 11th century (Bränvall *et al.*, 1999). Also, metallurgical processes were progressively being improved and a modified method of cupellation involving the melting of Cu ores with Pb to recover Ag was introduced in the mid-15th century and, by *ca.* 1500 A.D., both this and the Pb mining and smelting industry were prominent in Europe (Tylecote, 1976, 1986). It is interesting to note that Klaminder *et al.* (2003) found $^{206}Pb/^{207}Pb$ minima of ~ 1.155-1.17 in peat sections dated at *ca.* 1500 A.D. from Dumme Mosse and Traneröd Mosse in southern Sweden, close to the height of Mediaeval metal production in Europe (Bränvall *et al.*, 1999).

3.6.3 Industrial and post-industrial atmospheric Pb sources and deposition

Above 33 cm in FM01CM-1 (*cf.* Fig. 3.19), a depth for which no age-date is available, Pb concentrations and the corresponding Pb/Sc ratios increased to a depth of 23 cm, which, based on a match of $^{206}Pb/^{207}Pb$ ratios and associated ^{210}Pb dates in the overlying upper regions of the core, probably corresponds to *ca.* 1800 A.D and therefore trends in the Pb profiles during this depth interval are attributable to the Industrial Revolution, which started at *ca.* 1750 A.D. in the UK (Tylecote, 1976). This period was characterised by further improvements in metallurgical processes and the transition from charcoal to coke as the principal fuel. Since during this depth

interval (33-23 cm) the corresponding $^{206}Pb/^{207}Pb$ ratio remained fairly constant at 1.173 ± 0.002, it seems likely that emissions from the indigenous Scottish Pb mining industry, which developed during the 17th century A.D. (Wilson, 1921) at Wanlockhead and Leadhills, are responsible for the increasing Pb concentrations. Furthermore, the $^{206}Pb/^{207}Pb$ ratio of Pb ore from Wanlockhead and Leadhills is 1.170 ± 0.003 (*cf.* Table 1.4) (Moorbath, 1962; Sugden *et al.*, 1993; Rohl, 1996), similar to the value of 1.173 ± 0.002 observed from 33 to 23 cm in the FM01CM-1 core. Based on the agreement between ^{210}Pb dates in the FM01CM-1 and FM04-1-M cores at different depths (i.e. 1876 ± 19 A.D. for 17.5 cm in FM01CM-1 and 1877 ± 8 A.D. for 22.5 cm in FM04-1-M, for which the earliest ^{210}Pb date is 1832 ± 19 A.D. at 27 cm) (*cf.* Fig. 3.20), it seems likely that the depth of 33 cm in FM04-1-M corresponds to the late 1700s A.D.

From 23 cm (*ca.* 1800 A.D.) to 12 cm (1928 ± 11 A.D.) in FM01CM-1, Pb concentrations and the corresponding Pb/Sc ratios continued to increase but the mean $^{206}Pb/^{207}Pb$ ratio remained the same at 1.173 ± 0.002 (*cf.* Fig. 3.19). Similarly, from 33 cm (late 1700s A.D.) to 18 cm (1910 ± 8 A.D.) in FM04-1-M, Pb concentrations increased and the mean $^{206}Pb/^{207}Pb$ ratios (1.175 ± 0.002) (*cf.* Fig. 3.20) were similar to those of FM01CM-1. These trends again suggest contributions from indigenous Pb ore sources, which have lower $^{206}Pb/^{207}Pb$ ratios (1.170) than those of coal (1.181). The mining and smelting of indigenous Pb ores, however, was greatest in Scotland from 1850 to 1920 A.D. until closure in the 1930s A.D. (Wilson, 1921), and went into general decline in the UK after the 19th century A.D.

Over the time periods 1928 ± 11 A.D. to 1969 ± 8 A.D. in FM01CM-1 (12 to 5 cm) (Fig. 3.19) and 1910 ± 8 A.D. to 1968 ± 2 A.D. in FM04-1-M (18 to 12 cm) (*cf.* Fig. 3.20), the main features for the two cores were similar: maximum Pb concentrations (1948 ± 10 A.D; 1955 ± 3 A.D.), elevated Pb/Sc ratios (reaching 290; 122) and decreasing $^{206}Pb/^{207}Pb$ ratios (to 1.145 at 1967 ± 9 A.D.; 1.158 for 1943 ± 4 to 1968 ± 2 A.D.). The increasing influence of imported Australian Pb ($^{206}Pb/^{207}Pb$ = 1.04), used along with Pb from other sources in the manufacture of

alkylPb additives for petrol from the 1930s A.D. and then emitted to the atmosphere via vehicle exhaust emissions, can be seen in the decline in $^{206}Pb/^{207}Pb$ ratios. The intermediate values observed for $^{206}Pb/^{207}Pb$ ratios, however, indicate that there were significant contributions from other sources of Pb, such as coal combustion. Farmer *et al.* (1999, 2002), have previously demonstrated how varying emission contributions from coal combustion ($^{206}Pb/^{207}Pb$ = 1.181) and the mining, smelting and subsequent use of indigenous (1.170) and Australian (1.04) Pb could give rise to the observed trends in atmospheric $^{206}Pb/^{207}Pb$ during the 20th century A.D. Consumption of coal in the UK peaked in *ca.* 1950-1960 A.D. and was always greater than 150 Mt y^{-1} from *ca.* 1900 to 1970 A.D. (Farmer *et al.*, 1999). For 1930 A.D. in Scotland, the calculated estimated contributions to anthropogenic Pb in the atmosphere from Scottish coal (46%), Pb smelting in Scotland (35%) and sources in the rest of the UK (19%, with a directly measured $^{206}Pb/^{207}Pb$ ratio of 1.145 (Bacon *et al.*, 1996)) gave rise to a calculated $^{206}Pb/^{207}Pb$ ratio of 1.170 (Farmer *et al.*, 1999), the same as that observed in both Flanders Moss peat cores here.

From the late 1960s to the early 1980s A.D. (i.e. from 5 to 3 cm and 12 to 9 cm in FM01CM-1 and FM04-1-M, respectively) (Figs. 3.19 and 3.20), Pb concentrations and the corresponding Pb/Sc ratios, with the exception of Pb/Sc (180) for FM04-1-M, decreased. The corresponding $^{206}Pb/^{207}Pb$ ratios decreased dramatically (to 1.134), indicative of the decreasing influence of coal combustion and the increasing influence of vehicle exhaust emissions of Pb. From 1982 to 1990 A.D. (i.e. 9 to 6 cm) in FM04-1-M, Pb concentrations continued to fall while the Pb/Sc ratio, at 180, was the same as the previous value and the $^{206}Pb/^{207}Pb$ ratio attained its minimum value of 1.130. This suggests a period of maximum influence of petrol Pb on the $^{206}Pb/^{207}Pb$ ratio, although UK Pb emissions from car exhausts are known to have fallen, in response to reductions in the maximum permitted concentration of Pb in petrol, from *ca.* 8500 t y^{-1} in the early 1970s A.D. to *ca.* 7000 t y^{-1} by the early 1980s A.D., the final reduction to 0.15 g l^{-1} and the introduction of unleaded petrol in 1986 producing a sharp fall to *ca.* 2900 t in 1986 A.D. and *ca.* 2200 t by 1990 A.D. (Department for Environment, Food and Rural Affairs, 2002).

From 1990 to 2004 A.D. (i.e. 6 to 0 cm) in FM04-1-M (*cf.* Fig. 3.20), Pb concentrations and Pb/Sc ratios decline and $^{206}Pb/^{207}Pb$ ratios increase to 1.139 ± 0.002, indicating the steep fall in Pb emissions from car exhausts, for example to 800 t by 1997 A.D. (Department for Environment, Food and Rural Affairs, 2002), as the use of unleaded petrol became increasingly predominant and then complete with the ban on leaded petrol from 2000 A.D. The increase in $^{206}Pb/^{207}Pb$ ratios to the present also reflects the importance of other sources of Pb (e.g. waste incineration) relative to petrol at this time. The 3-isotope plot (Fig. 3.23) provides evidence of the contributions of these sources of Pb from Pb mining and smelting, coal burning and use of leaded petrol during the industrial and post-industrial era to the Pb deposited at Flanders Moss.

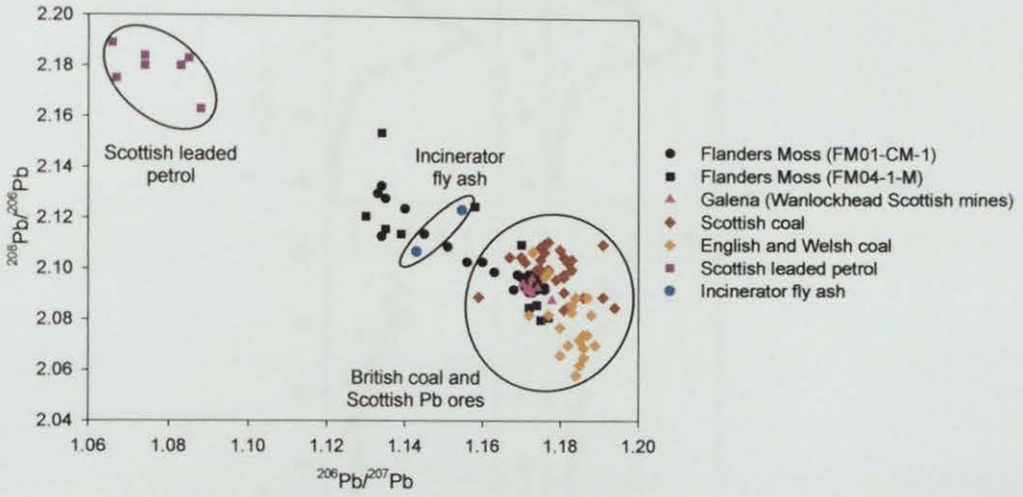

Figure 3.23: Plot of $^{208}Pb/^{206}Pb$ *versus* $^{206}Pb/^{207}Pb$ ratios for the FM01CM-1 (0-33 cm) and FM04-1-M (0-33 cm) peat samples, and for galena in Wanlockhead Scottish Pb ores (Rohl, 1996), British coal (Farmer *et al.*, 1999), leaded petrol (Farmer *et al.*, 2000) and incinerator fly ash (Monna *et al.*, 1997).

3.6.4 Historical trends in depositional fluxes and inventories of anthropogenic Pb

Taking Sc as an indicator of the concentration of lithogenic-derived aerosols supplied by rock weathering and soil formation, the contribution to the concentration of Pb supplied to the bog via atmospheric deposition of these aerosols was estimated as follows:

$$[Pb]_{lithogenic} = [Sc]_{sample} \times (Pb/Sc)_{UCC}$$

Anthropogenic Pb was then calculated as:

$$[Pb]_{anthropogenic} = [Pb]_{total} - [Pb]_{lithogenic}$$

FM01CM-1 and FM04-1-M anthropogenic Pb concentrations are tabulated in A4.1 Table A4 and A4.2 Table A4, respectively. Using FM01CM-1 as an example, note that there is very little difference between the "total" and calculated anthropogenic Pb concentrations in the top part of the core, i.e. the calculated lithogenic Pb concentrations in the top part of the core are very small in comparison (Fig. 3.24).

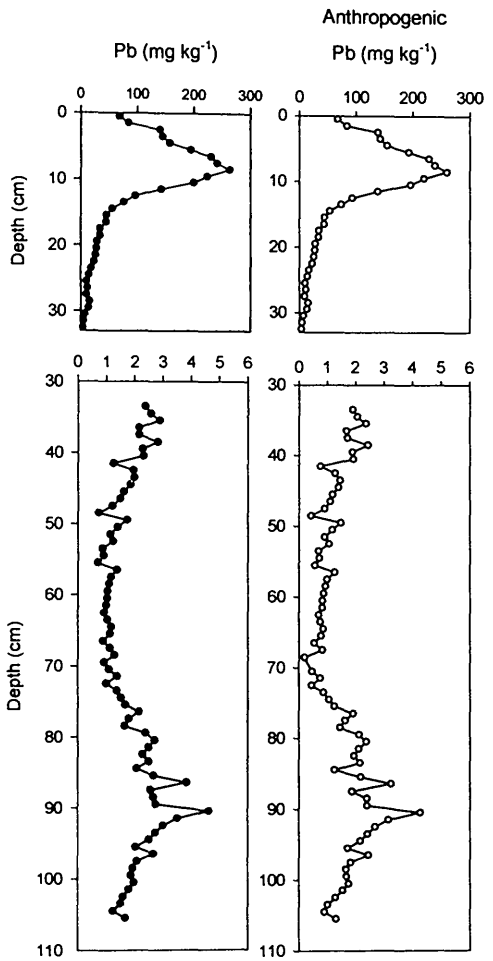

Figure 3.24: Depth profiles of Pb and calculated anthropogenic Pb concentrations (mg kg^{-1}) from 0-33 cm and 33-106 cm in the FM01CM-1 peat core.

The depositional flux of anthropogenic Pb over the period of each dated FM04-1-M peat section was estimated on the basis of the ^{210}Pb chronology and calculated using the following equation:

Anthropogenic Pb flux (mg m^{-2} y^{-1}) = anthropogenic Pb concentration in dated section (mg kg^{-1}) x mass of 105°C-dried peat section (kg)/cross-sectional area (m^2) x number of years in section (y)

Depositional fluxes of anthropogenic Pb since the mid-19th century A.D. (A4.2 Table A11) are plotted, along with the measured ^{206}Pb/^{207}Pb ratios, *versus* ^{210}Pb-derived calendar dates for FM04-1-M in Fig. 3.25.

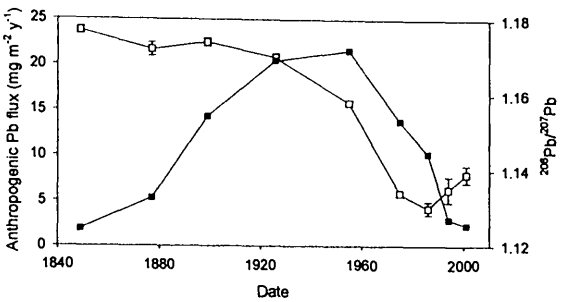

Figure 3.25: Calculated atmospheric depositional fluxes of anthropogenic Pb (mg m^{-2} y^{-1}) (closed squares) and measured ^{206}Pb/^{207}Pb ratios (open squares) for the FM04-1-M core *versus* ^{210}Pb-derived dates since 1840 A.D.

The maxima of ~ 21 mg m^{-2} y^{-1} for anthropogenic Pb fluxes from the mid-1920s to the mid-1950s A.D. are evident, with a corresponding decline in ^{206}Pb/^{207}Pb ratios, suggestive of the influence of contributions from emissions of both coal combustion and the use of Australian alkylPb additives in petrol. Maximum Pb depositional fluxes ranging from 20-60 mg m^{-2} y^{-1} have previously been observed for Flanders Moss (Farmer *et al.*, 1997; Farmer *et al.*, 2006), highlighting the significant variations in apparent depositional fluxes that can be found from the analysis of different cores from the same bog. It should also be borne in mind, however, that significant variations in apparent depositional fluxes can arise as a consequence of topographical and plant compositional features that affect the efficiency of particle trapping and retention (Norton *et al.*, 1997; Bindler *et al.*, 2004).

After 1960 A.D., the rapid decline in coal combustion emissions at the same time as the increase in vehicle exhaust emissions is reflected in the $^{206}Pb/^{207}Pb$ ratio, which reaches a minimum in the mid-1980s A.D. The Pb fluxes at the beginning of this period fell steadily, followed by a steeper decline during the mid-1990s A.D., due to the phasing out of leaded petrol at this time, evident by the increase in $^{206}Pb/^{207}Pb$ ratios. Evidence from other Flanders Moss peat cores, (including the sister core FM01CM-2 (see Section 3.8.2.2.3)), Scottish lake sediment cores and archival herbarium moss support these observed temporal trends in $^{206}Pb/^{207}Pb$ ratios (Farmer *et al.*, 1997, 2002, 2006; Eades *et al.*, 2002).

The anthropogenic Pb inventories were calculated for each section of the peat cores using the following equation:

Anthropogenic Pb inventory (g m^{-2}) = anthropogenic Pb concentration in section (mg kg^{-1}) x mass of 105°C-dried peat section (kg)/cross-sectional area (m^2)

The total anthropogenic Pb inventories for FM01CM-1 (i.e. from *ca.* 500 B.C. to mid-1980s A.D., given that the very top of the core was lost during collection) and FM04-1-M (i.e. from *ca.* late 1700s to 2004 A.D.) were 3.8 g m^{-2} and 2.1 g m^{-2}, respectively. In FM01CM-1, the anthropogenic Pb inventory was 0.045 g m^{-2} for the period embracing the Pb peak (71-102 cm) in the pre-Roman/Roman times, while, in comparison, the post-1800 A.D. Pb inventory (3.6 g m^{-2}) (corresponding to peat sections 0-23 cm), constituted 95% of the total anthropogenic Pb inventory for the core. Calculated cumulative post-1800 A.D. anthropogenic Pb inventories (% of total post-1800 A.D. inventory) for the Flanders Moss cores are plotted *versus* ^{210}Pb-derived calendar dates in Fig. 3.26.

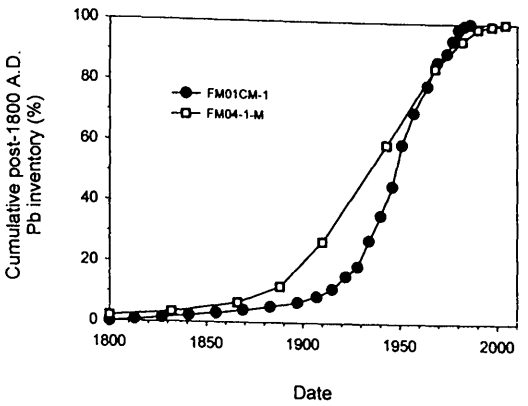

Figure 3.26: Calculated cumulative post-1800 A.D. anthropogenic Pb inventories (% of total post-1800 A.D. inventory) for the FM01CM-1 and FM04-1-M cores *versus* ^{210}Pb-derived dates. Note that dates in FM01CM-1 and FM04-1-M prior to *ca.* 1883 A.D. and *ca* 1832 A.D., respectively, were extrapolated. Also, dates in FM01CM-1 after *ca.* 1974 A.D. were extrapolated.

Maximum deposition occurred between the 1910s and 1960s A.D. Slight differences in trends between the two cores are at least partly attributable to differences in core sectioning. It should also be remembered, however, that the ^{210}Pb dating for FM01CM-1 is extrapolated from that of the FM01CM-2 sister core and this, with its associated uncertainty, may contribute to some differences in the vertical (temporal) distribution (%) of anthropogenic Pb inventories between the two cores here.

The geochemical behaviour of other elements (e.g. major and trace elements) within the Flanders Moss peat cores will now be investigated and, since Pb is essentially immobile in ombrotrophic peat bogs, the Pb profiles and characterised historical trends in sources of anthropogenic Pb will be used to aid the interpretation of trends observed in profiles of these other elements.

3.7 GEOCHEMICAL BEHAVIOUR OF MAJOR ELEMENTS

This section presents the results for the major elements (Ca, Fe, Mg, Mn, P and S) in the Flanders Moss peat cores. Since these elements are plant nutrients and/or redox-sensitive, the position of the vegetation-peat interface and, in the case of

FM01CM-1, the estimated acrotelm-catotelm boundary, will be indicated on their depth profiles. The water and ash content profiles, presented in Section 3.1, will also be plotted alongside their concentration profiles for comparison. Total Ca, Fe, Mg, Mn, P and S concentrations, expressed relative to sectional 105°C-dried peat weights, for FM01CM-1 and FM04-1-M are tabulated in A4.1 Table A5 and A4.2 Table A5, respectively. The Ca, Fe, Mg, Mn, P and S concentration and water and ash content profiles for FM01CM-1 and FM04-1-M are shown in Figs. 3.27 and 3.28, respectively.

3.7.1 FM01CM-1

All six elements exhibited concentration peaks or increases in the uppermost ~ 10 cm of the core, with the following maximum concentrations at the depths indicated:

- Ca – 1600 mg kg^{-1} at 2-3 cm
- Fe – 2300 mg kg^{-1} at 2-3 cm
- Mg – 1100 mg kg^{-1} at 2-3 cm but the maximum value (1800 mg kg^{-1}) in the core occurred at 79-80 cm
- Mn – 17 mg kg^{-1} at 2-3 cm but there was also a peak (11 mg kg^{-1}) at 9-10 cm
- P – 710 mg kg^{-1} at 4-5 cm
- S – 1500 mg kg^{-1} at 6-7 cm

Concentrations of Fe, Mn and P increased most dramatically from low constant values at depths beneath the acrotelm-catotelm boundary (~ 30 cm). Concentrations of Fe and Mn peaked 2 cm above the vegetation-peat interface (4-5 cm), while that of P peaked at the interface. Above these maxima, concentrations decreased towards the top of the core but still remained high. In comparison, concentrations of the other elements increased less markedly, with concentrations below ~ 15 cm remaining fairly high and constant throughout the core, with the exception of Mg, which increased gradually down to ~ 80 cm (*cf.* Fig. 3.27). Minima in Ca, Mg and S concentrations occurred at 11-14, 85-86 and 93-94 cm, coincident with water content

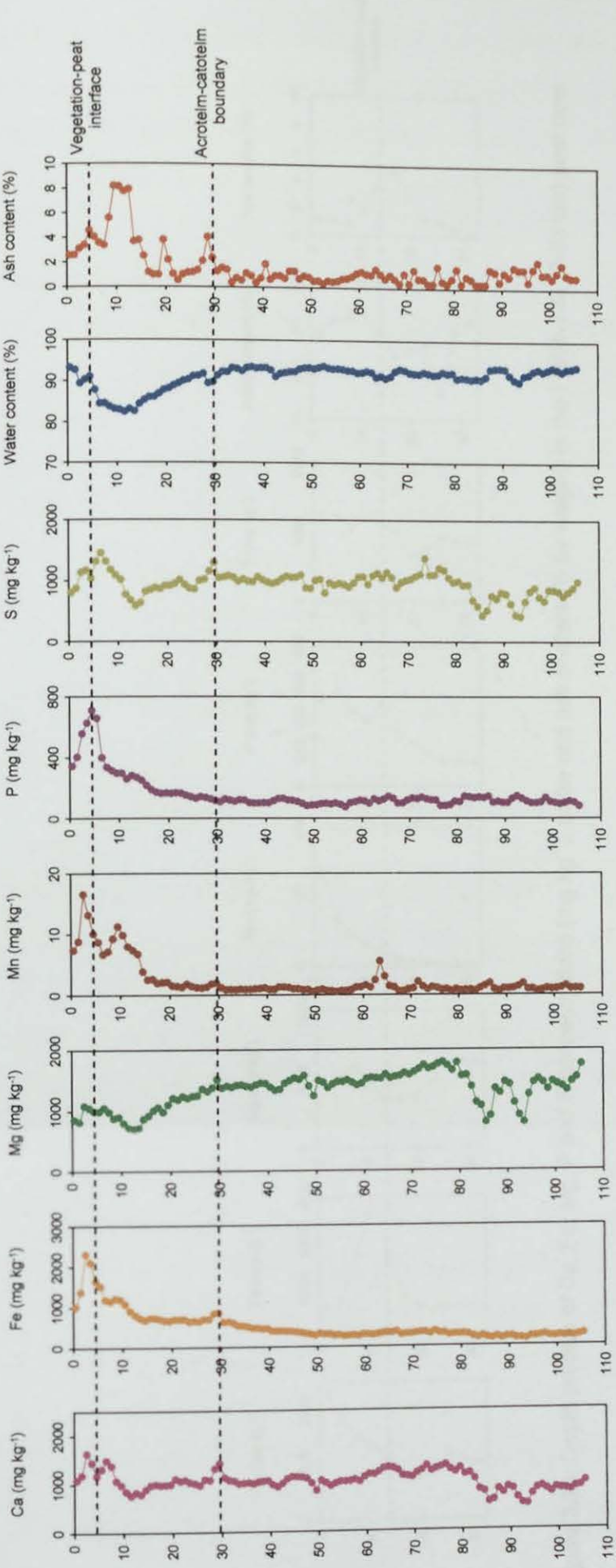

Figure 3.27: Depth profiles of Ca, Fe, Mg, Mn, P and S concentrations (mg kg^{-1}), water and ash content (% by weight) in the FM01CM-1 (0-106 cm) peat core.

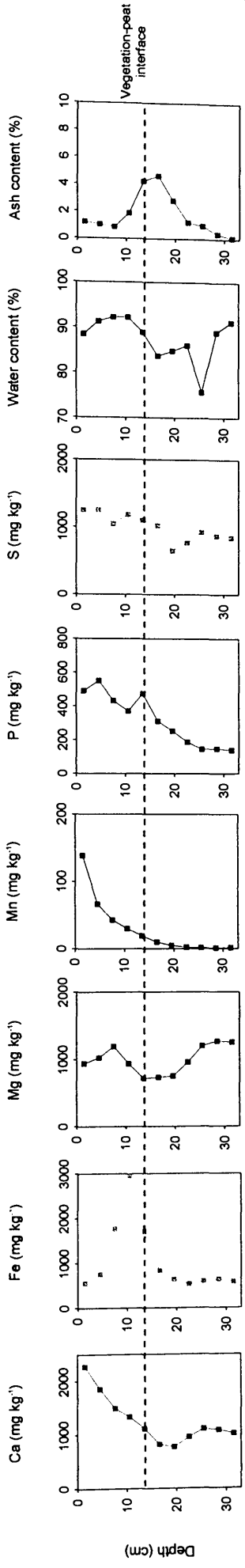

Figure 3.28: Depth profiles of Ca, Fe, Mg, P and S concentrations (mg kg^{-1}), water and ash content (% by weight) in the FM04-1-M (0-33 cm) peat core.

minima and ash content maxima. However, minor peaks in Ca, Fe, Mg, Mn and S concentrations and also ash content occurred between 28 and 30 cm, i.e. the same depth as the estimated acrotelm-catotelm boundary (~ 30 cm), where a corresponding minor decrease in the water content occurred.

3.7.2 FM04-1-M

All six elements exhibited concentration peaks or increases in the uppermost ~ 18 cm (*cf.* Fig. 3.28) and the following maximum concentrations occurred, at the depths indicated:

- Ca – 2300 mg kg^{-1} at 0-3 cm
- Fe – 3000 mg kg^{-1} at 9-12 cm
- Mg – 1200 mg kg^{-1} at 6-9 cm but the maximum value (1300 mg kg^{-1}) in the core occurred between 27 and 33 cm
- Mn – 140 mg kg^{-1} at 0-3 cm
- P – 550 mg kg^{-1} at 3-6 cm but there was also a peak (470 mg kg^{-1}) at 12-15 cm
- S – 1300 mg kg^{-1} between 6 and 0 cm

As observed in FM01CM-1, Fe and P concentrations increased markedly from the bottom of the core, with the former peaking 3 cm above, and the latter exhibiting a peak at the same position as the vegetation-peat interface (12-15 cm). The Fe concentrations then decreased towards the surface, whereas P concentrations continued to increase towards the surface (*cf.* Fig. 3.28). The Mn concentrations also increased markedly from the bottom of the core, reaching a maximum value at the surface but, in contrast to FM01CM-1, Mn concentrations in this core did not exhibit a sharp sub-surface concentration peak, due to its presence in the living vegetation. The Ca, Mg and S concentrations increased from minima between 12 and 21 cm to maximum values at the surface, with the exception of Mg, for which concentrations increased up to 6 cm followed by a small decrease towards the surface. Also, Ca, Mg and S concentration minima occurred in the same region as the water content minima, ignoring the value of 76% at 24-26 cm, and ash content maxima.

3.7.3 Discussion

3.7.3.1 Sources of major elements

The main sources of the major elements, Ca, Fe, Mg, Mn, P and S are soil-derived aerosols from the weathering of crustal rocks and sea salt spray, and also, in the case of Fe, Mn and S, anthropogenic activities such as ferrous metal production, steel and Fe manufacture, burning of fossil fuels and waste incineration. Weiss *et al.* (1997) accounted for the ash content in a Swiss peat core by summing the following element oxides (SiO_2, Al_2O_3, TiO_2, Fe_2O_3, CaO, MgO and SO_2), and therefore it would be expected that the concentration profiles of these elements correlate well with that of the ash content. However, this correlation was not found for the Fe, Ca, Mg and S profiles in the Flanders Moss cores (*cf.* Figs 3.27 and 3.28). Martinez-Cortizas *et al.* (1997) reported that an irregular distribution of Ca and Mg concentrations in peat profiles indicated the existence of a salt effect where atmospheric inputs of sea salt cations and hydrogen ions compete for exchange sites. However, since there was not an irregular distribution of Ca and Mg in these Flanders Moss cores, sources from sea salt inputs appear to be minor. Also, sources of S from anthropogenic activities (e.g. coal burning) are thought to be recorded in peat bog S concentration profiles (Novák *et al.*, 2003; Bottrell *et al.*, 2004; Yafa, 2004), but the S profiles in the modern peat sections of the Flanders Moss cores were dissimilar to the Pb concentration profiles (Figs. 3.29 and 3.30), which are known to record sources of Pb from coal combustion. This provides evidence against the use of S profiles as records of anthropogenic deposition, perhaps due to other processes which influence the distribution of S in peat bogs, as discussed below.

3.7.3.2 Nutrient uptake and recycling

Trends in the Ca, Fe, Mg, Mn, P and S concentration profiles in the Flanders Moss peat cores (*cf.* Figs 3.27 and 3.28) did not appear to reflect their supply from the sources mentioned above in any simple way because of biological transformations that occur in the surface vegetation of peat bogs. Increased Ca, Mg, Mn, P, S and, perhaps to some extent, Fe concentrations in the zones of biological cycling, i.e. the

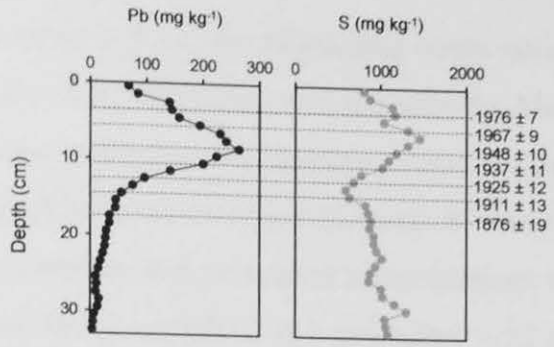

Figure 3.29: Depth profiles of Pb and S concentrations (mg kg^{-1}) from 0-33 cm in the ^{210}Pb-dated FM01CM-1 peat core.

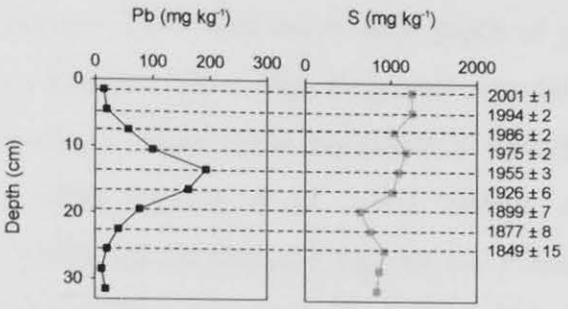

Figure 3.30: Depth profiles of Pb and S concentrations (mg kg^{-1}) in the ^{210}Pb-dated FM04-1-M (0-33 cm) peat core.

upper 5 cm of FM01CM-1 and upper 15 cm of FM04-1-M (remembering that the top of FM01CM-1 does not equate to the surface since some surface vegetation is 'missing'), were consistent with the rapid uptake and recycling of these essential macronutrients (Ca, Mg, P and S) and micronutrients (Fe and Mn) in the growing vegetation, as found by previous workers (Malmer, 1958; Damman 1978; Görres and Frenzel, 1997; Weiss *et al.*, 2002b; Yafa, 2004). It is worth noting that slight differences between the trends in concentrations of these elements in the biological zones of the two cores could reflect differential rates of nutrient cycling in the vegetation (Johnson and Damman, 1991), since the hummock-producing moss species in FM01CM-1 (*S. palustre*) and FM04-1-M (*S. papillosum and Aulacomnium palustre*) were different.

3.7.3.3 Redox cycling

As mentioned in Section 1.7.3.1, the fluctuating redox conditions in peat bogs can affect the distribution of the redox-sensitive elements Fe, Mn, P and S. Thus Fe, Mn, P and, perhaps to some extent S concentrations in the Flanders Moss cores did appear to have been subjected to redox cycling if the zone of water table fluctuation, where alternating redox conditions and associated accumulations of these elements occur, lies between ~ 3 and 30 cm in FM01CM-1 and below ~ 12 cm in FM04-1-M. These estimates are based on the position of the apparent diagenetic Fe peaks, at 2-3 cm and 9-12 cm in FM01CM-1 and FM04-1-M, respectively, and the acrotelm-catotelm boundary, and are in agreement with the measured acrotelm depth range of 30 ± 40 cm (Keleman and Ingram, 1999) and water table depth of ≤ 35 cm (Bragg, 2002) below the surface for Flanders Moss. The diagenetic remobilisation and enrichment of Fe and Mn in the zone of water table fluctuation is well documented (*cf.* Section 1.7.3.1) (Damman, 1978; Clymo *et al*, 1990; Shotyk and Steinmann, 1997; MacKenzie *et al.*, 1998) but documented less so for P and S. In the case of P, Damman (1978) proposed that mineralised P can be held in peat only as Fe and Al phosphates and that the low P content in anaerobic peat is associated with the reduction of Fe. The similarity between the Fe and P concentration profiles (*cf.* Figs. 3.27 and 3.28) in the Flanders Moss cores does indeed indicate the influence of Fe on the distribution of P, although the diagenetic P peaks occurred 2 and 3 cm beneath the Fe peaks in FM01CM-1 and FM04-1-M, respectively. The influence of Al on the distribution of P in the Flanders Moss cores was less apparent since the Al and P concentration profiles were dissimilar (*cf.* Figs. 3.11 and 3.12, Section 3.3), for example, the maximum Al concentrations occurred 8 and 6 cm below the diagenetic P peaks in FM01CM-1 and FM04-1-M, respectively. In the case of S, sulfate supplied to the bog is taken up by plants and incorporated into organic S compounds and Bayley *et al.* (1986) suggested that, during the summer when the water table in bogs is drawn down, some of this organic S may be oxidised to sulfate, which would then be available for dissimilatory reduction. Steinmann and Shotyk (1996), however, found that most (90-99%) of the dissolved S species in peat bog porewaters was associated with humic matter, which greatly reduces the availability of sulfate

for microbial reduction (*cf.* Section 1.7.3.1). Also, Damman (1978) proposed the precipitation of Al (III) as $Al_2(SO_4)_3$ in the presence of sulfate as the mechanism for Al accumulation in the zone of water table fluctuation in peat profiles; furthermore, Benoit *et al.* (1998) suggested that Al peaks occurred below the diagenetic Fe peaks, since the reduction of sulfate to sulfide occurs at lower pE than the ferric-ferrous conversion, and therefore that the Al peak marks the depth of sulfide oxidation. In the Flanders Moss cores, the position of the maximum Al concentrations in FM01CM-1 (12-13 cm) and FM04-1-M (18-21 cm) indeed occurred below those of Fe. However, corresponding S concentrations were at a minimum, which perhaps provides evidence against the precipitation of Al as Al sulfates in this peat bog.

Interestingly, Weiss *et al.* (2002) found that diagenetic effects on the Fe concentrations in a core from a forested peat bog in southeast Asia were negligible and that Fe profiles correlated with those of the lithogenic elements (Al, Ti, Y and Zr). They also found this to be the case for S, which again is not consistent with the findings in these Flanders Moss cores. The occurrence of corresponding minor peaks in Ca, Fe, Mg, Mn, S and ash content, however, at the acrotelm-catotelm boundary in FM01CM-1 is less clear (*cf.* Fig. 3.27). One explanation could be increased soil dust input, since increases in Al, Ti, Y and Zr also occur at this depth. Another explanation could be a decrease in hydraulic conductivity, and therefore water movement, experienced at this depth (Clymo *et al.*, 1990). Below this acrotelm-catotelm boundary, the interesting correlation in trends between Ca, Mg and S concentrations and the water content in the permanently reducing catotelm layers in FM01CM-1 could perhaps be attributable to ion exchange and/or dissolution processes (Shotyk, 1997).

In conclusion, the concentration profiles of Ca, Fe, Mg, Mn, P and S in the Flanders Moss peat cores were dissimilar to the ash content profiles and the main mechanisms for redistribution of these elements in ombrotrophic peat bogs applied, i.e. nutrient uptake and cycling (Ca, Fe, Mg, Mn, P and S) and redox cycling (Fe, Mn, P and S, where diagenetic Fe and Mn concentration peaks occurred above the corresponding

diagenetic P concentration peaks). In the next sections of this thesis, trends in these "mobile" elements will be used to aid the interpretation of the geochemical behaviour of trace elements (e.g. As, Hg and Sb) in ombrotrophic peat bogs.

3.8 GEOCHEMICAL BEHAVIOUR OF OTHER TRACE ELEMENTS

This section presents the results of the other trace elements (As, Cd, Co, Cr, Cu, Hg, Ni, Sb, Se, V and Zn) in addition to Pb, determined in the Flanders Moss peat cores. Some, like Pb, are environmental contaminants that are known to be toxic (e.g. Sb, Hg and As), but comparatively little is known about others.

3.8.1 Sb

Total Sb concentrations, expressed relative to sectional 105°C-dried peat weights, for FM01CM-1 and FM04-1-M are tabulated in A4.1 Table A6 and A4.2 Table A6, respectively. The Sb, Pb and Sc concentration profiles for FM01CM-1 and FM04-1-M are shown in Figs. 3.31 and 3.32, respectively.

3.8.1.1 FM01CM-1

0-33 cm

Sb concentrations increased from 0.10 mg kg^{-1} at 32-33 cm to a maximum value of 4.2 mg kg^{-1} at a depth of 8.5 cm, coincident with the Pb maximum, above which concentrations gradually decreased towards the top of the core (*cf.* Fig. 3.31).

33-106 cm

Note the changes in scale on the Sb and Pb (50-fold) and Sc (4-fold) concentrations on going from 0-33 cm to 33-106 cm. The same distinct zones as those observed earlier for Pb concentrations (Section 3.6) were apparent for Sb: a region of minimum concentrations (mean 0.016 ± 0.004 mg kg^{-1}) from 86 cm to 53 cm, above which Sb increased steadily to 0.10 mg kg^{-1} by 33 cm and below which from 86 cm to 96 cm there was a pronounced peak with a maximum concentration (0.072 mg kg^{-1}) at 92-93 cm (*cf.* Fig. 3.31).

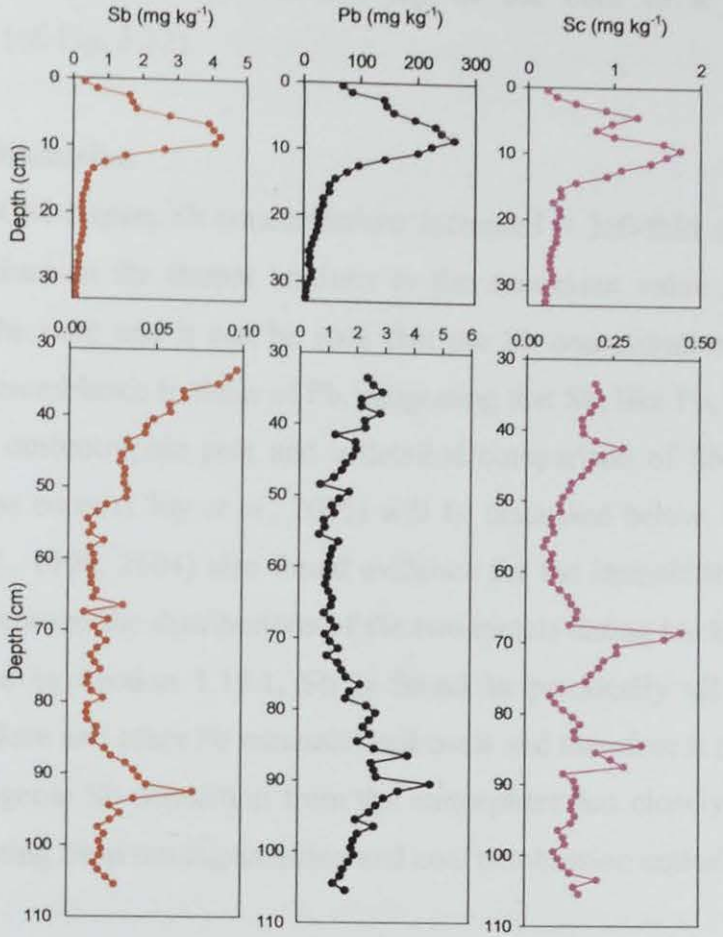

Figure 3.31: Depth profiles of Sb, Pb and Sc concentrations (mg kg^{-1}) from 0-33 cm and 33-106 cm in the FM01CM-1 (0-33 cm) peat core.

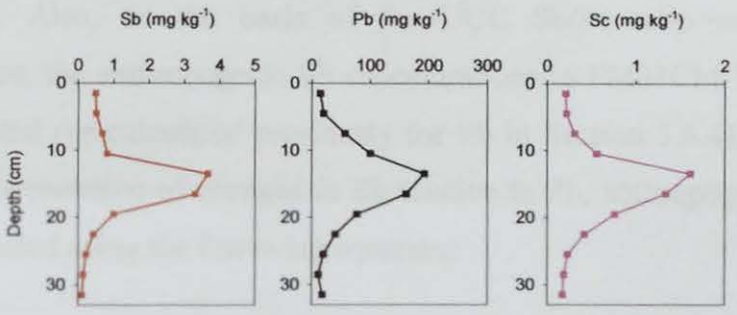

Figure 3.32: Depth profiles of Sb, Pb and Sc concentrations (mg kg^{-1}) in the FM04-1-M (0-33 cm) peat core.

3.8.1.2 FM04-1-M

Sb concentrations increased from 0.12 mg kg^{-1} at 30-33 cm to a maximum value of 3.7 mg kg^{-1} at 12-15 cm, again coincident with the Pb maximum, above which

concentrations decreased towards the top of the core to a concentration of 0.50 mg kg^{-1} (*cf.* Fig. 3.32).

3.8.1.3 Discussion

In the FM01CM-1 core, Sb concentrations increased ~ 260-fold on going from the minimum values in the deeper sections to the maximum value in the uppermost sections of the core and it can be seen that the Sb concentration profiles show a remarkable resemblance to those of Pb, suggesting that Sb, like Pb, is also essentially immobile in ombrotrophic peat and a detailed comparison of Sb and Pb in these Flanders Moss cores (Cloy *et al.*, 2005) will be discussed below. Previous workers (Shotyk *et al.*, 1996, 2004) also found evidence for the immobility of Sb based on similarities between the distributions of the two metals dating back to Roman times. As mentioned in Section 1.13.1, Sb is found in practically all sulfide minerals (including galena and other Pb minerals) and coals and therefore it might be expected that anthropogenic Sb deposition from the atmosphere has closely followed that of the Pb emanating from mining/smelting and coal combustion emissions in the past.

3.8.1.3.1 The use of Sc as an indicator of soil dust input of Sb

To compare the trends in sources of Sb that are unrelated to direct anthropogenic inputs, Sb/Sc ratios can be used in the same way that Pb/Sc ratios were used for Pb in Section 3.5. Also, on the basis of the UCC Sb/Sc ratio and measured Sc concentrations, the anthropogenic Sb concentrations in FM01CM-1 and FM04-1-M were calculated (as calculated previously for Pb in Section 3.6.4). Furthermore, to assist the interpretation of changes in Sb relative to Pb, anthropogenic Sb/Pb ratios can be calculated using the following equation:

$$Sb/Pb_{anthropogenic} = [Sb]_{anthropogenic} / [Pb]_{anthropogenic}$$

Anthropogenic Sb concentrations, Sb/Pb (anthropogenic) and Sb/Sc ratios in the FM01CM-1 and FM04-1-M cores are tabulated in A4.1 Table A6 and A4.2 Table A6, respectively. The Sb, Pb and Sc concentration and measured $^{206}Pb/^{207}Pb$, Sb/Sc,

Pb/Sc and anthropogenic Sb/Pb ratio profiles for FM01CM-1 and FM04-1-M, including age-dates, are shown in Figs. 3.33 and 3.34, respectively. The lowest Sb/Sc ratios occurred over the depth region 67-75 cm, with a mean value of 0.066 ± 0.016, close to the corresponding ratio of 0.044 for the UCC. In the Swiss EGR peat core, Shotyk *et al.* (2004) found the lowest Sb concentrations (0.008 ± 0.003 mg kg^{-1}), a factor of ~ 8 lower than those in the zones of minimum Sb concentrations in FM01CM-1, in peats dating from 5320 to 8020 ^{14}C y B.P., with corresponding Sb/Sc and Sb/Pb ratios of 0.105 and 0.035 ± 0.014, respectively. The corresponding UCC Sb/Sc and Sb/Pb ratios of 0.044 and 0.018 demonstrate the variability that can occur in such ratios of elemental concentrations.

3.8.1.3.2 Historical trends in sources of atmospheric Sb deposition

The same historical periods as those found and discussed for Pb (*cf.* Section 3.6) are also used here to discuss anthropogenic Sb deposition.

Pre-Roman and Roman atmospheric Sb sources and deposition

In FM01CM-1 (106-71 cm), as with the Pb concentration and corresponding Pb/Sc ratio data, it seems very likely that the elevated Sb/Sc ratios (mean 0.29 ± 0.05) associated with the elevated Sb concentrations from 96 to 86 cm, dated at 210-40 B.C. to 20-220 A.D., can be attributed to pre-Roman and Roman metallurgical activities. Despite the lower Sb concentrations over the earlier 96-102 cm depth interval (as observed for Pb), the corresponding Sb/Sc ratios were also enhanced at 0.19 ± 0.05. From 86 to 76 cm, i.e. corresponding to 20-220 A.D. to 120-260 A.D., Sb concentrations and Sb/Sc ratios (mean 0.11 ± 0.04) were much less elevated, while those of Pb and Pb/Sc were still elevated (*cf.* Fig. 3.33). Over the depth intervals from 71 to 102 cm the mean anthropogenic Sb/Pb ratios were 0.010 ± 0.004 (71-76 cm), 0.0040 ± 0.0020 (76-86 cm), 0.012 ± 0.006 (86-96 cm) and 0.0089 ± 0.0010 (96-102 cm), with an overall average of 0.0084 ± 0.0050 (71-102 cm) (*cf.* Fig. 3.33).

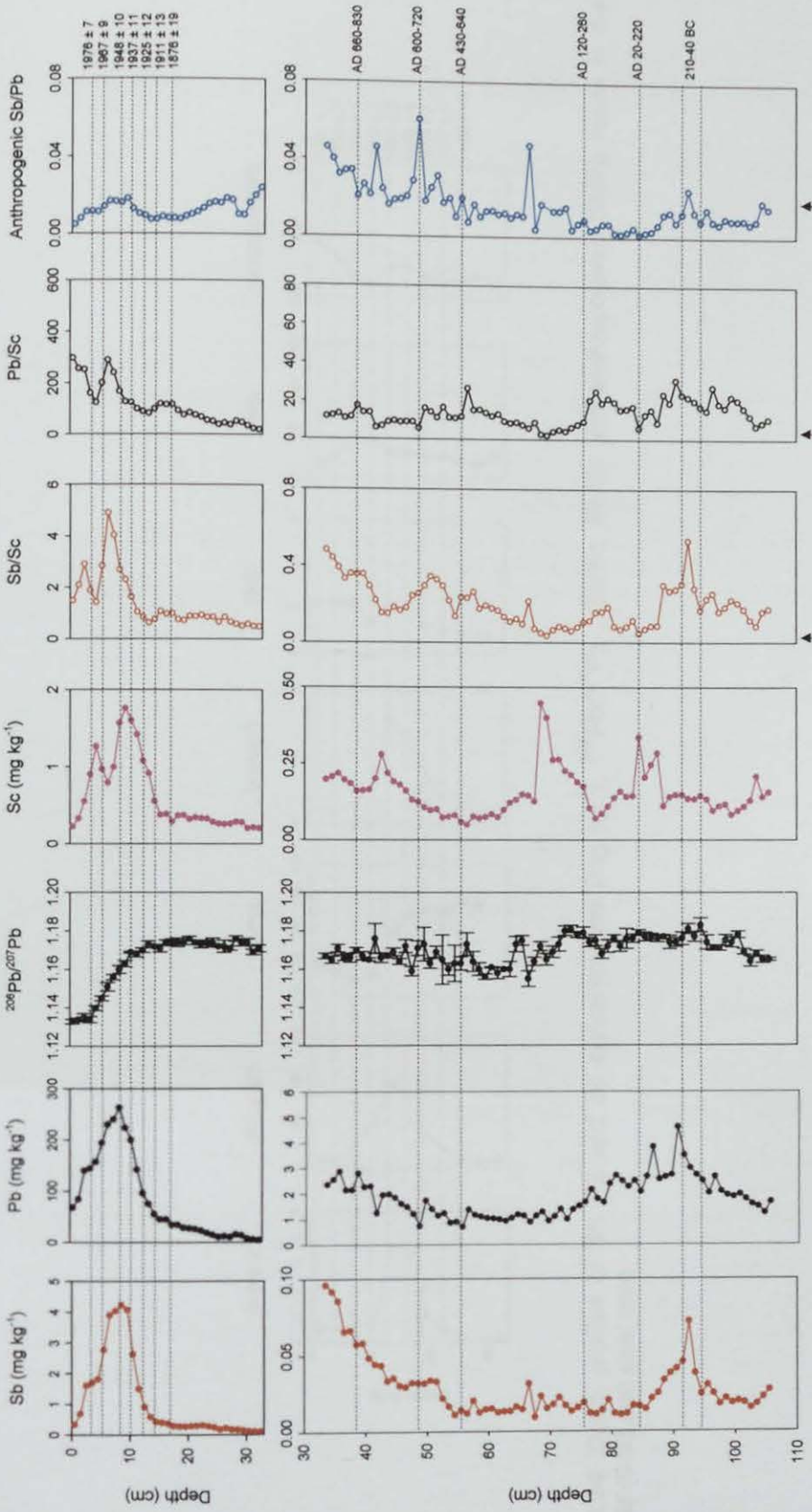

Figure 3.33: Depth profiles of Sb, Pb and Sc concentrations (mg kg^{-1}), $^{206}Pb/^{207}Pb$, Sb/Sc, Pb/Sc and anthropogenic Sb/Pb ratios from 0-33 cm and 33-106 cm in the ^{210}Pb- and ^{14}C-dated FM01CM-1 peat core.

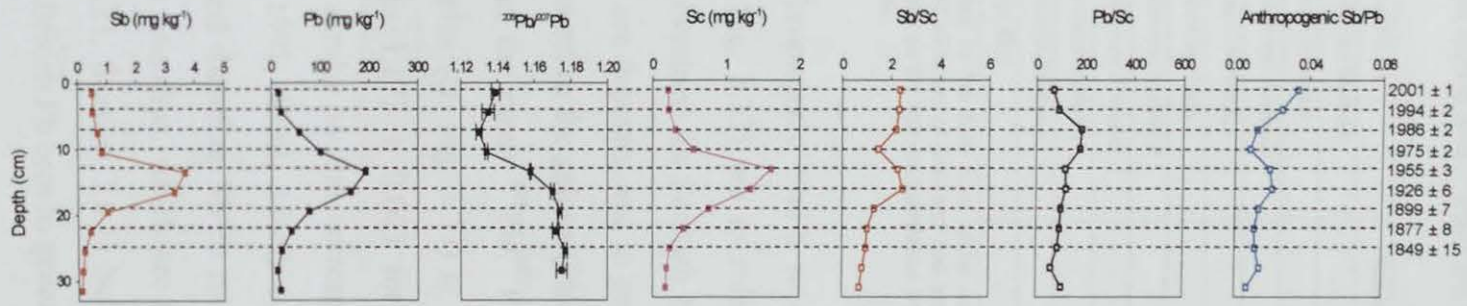

Figure 3.34: Depth profiles of Sb, Pb and Sc concentrations (mg kg^{-1}), $^{206}Pb/^{207}Pb$, Sb/Sc, Pb/Sc and anthropogenic Sb/Pb ratios in the ^{210}Pb-dated FM04-1-M (0-33 cm) peat core.

To assist the interpretation of changes in Sb/Pb ratios in peat core profiles, the Sb/Pb ratios (and $^{206}Pb/^{207}Pb$ ratios) measured in various Scottish Pb ore samples are shown in Table 3.8.

Table 3.8: Measured Sb/Pb and $^{206}Pb/^{207}Pb$ ratios in Scottish Pb ore samples.

Location of Pb ore	Measured Sb/Pb ratio (± SD)	Measured $^{206}Pb/^{207}Pb$ ratio (± SD)
Glensanda (west-central Scotland)	0.00020	1.147 ± 0.0010
Tyndrum (central Scotland)	0.00030	1.149 ± 0.0023
Doria Quarry (west-central Scotland)	0.00024	1.161 ± 0.0018
Blebo (east-central Scotland)	0.0029	1.169 ± 0.0010
Leadhills (central Scotland)	0.0033	1.170 ± 0.0019
Wanlockhead (south-west Scotland)*	0.0056 ± 0.0004	1.173 ± 0.0026
Wanlockhead (south-west Scotland)	0.0041	1.173 ± 0.0015
Strontian (west-central Scotland)	0.00090	1.176 ± 0.0028
Lossiemouth (northern Scotland)	0.00018	1.178 ± 0.0020
Mean (± SD)	**0.0020 ± 0.0021**	**1.166 ± 0.011**

*Pb ore sample collected in the field from which duplicate sub-samples were analysed. Other samples were provided by the National Museum of Scotland and single sub-samples were analysed. Pb isotopic ratio standard deviations were calculated as the standard deviation from the mean value for five consecutive determinations of the ratio of a sample solution.

The average anthropogenic Sb/Pb ratios over the 71-102 cm depth interval in FM01CM-1 (*cf.* Fig. 3.33) are in relatively good agreement with the values of 0.0033 – 0.0056 obtained for Scottish Pb ore samples from the main Wanlockhead and Leadhills Pb ore deposits, and in general, the mean Sb/Pb ratios are in line with the <0.8% Sb content in the galena (PbS) of Pb ores (Shotyk *et al.*, 2005). It should also be noted that the mean $^{206}Pb/^{207}Pb$ ratio (1.176 ± 0.003) for the 71-102 cm FM01CM-1 samples (*cf.* Fig. 3.33) is close to the measured $^{206}Pb/^{207}Pb$ ratios of 1.170 ± 0.002 to 1.173 ± 0.003 for the Wanlockhead and Leadhills Pb ores (*cf.* Table 3.8), similar to the corresponding literature values (Moorbath, 1962; Sugden *et al.*, 1993; Rohl, 1996) (*cf.* Table 1.4). Unfortunately, Sb and Pb concentrations, and therefore Sb/Pb ratios, were not available for other British Pb ores, such as the Mendips, which are known to have been exploited during these times (*cf.* Fig. 3.21, Section 3.6.1) but these Scottish Pb ores can be taken to be representative of British Pb ores in general.

Post-Roman and Mediaeval atmospheric Sb sources and deposition

Over the depth interval 71 to 53 cm, Sb concentrations and the corresponding Sb/Sc ratios (0.15 ± 0.07), as observed for the Pb and Pb/Sc ratios, were at their lowest towards the end of (*ca.* 410 A.D.) and after the Roman occupation of Britain until *ca.* 650 A.D (*cf.* Fig. 3.33). The corresponding mean anthropogenic Sb/Pb ratio was 0.013 ± 0.004 (excluding the single outlier peak of 0.048 at 66-67 cm). Thereafter, to 33 cm, Sb concentrations rose more rapidly than those of Pb, which is reflected by the increase in mean Sb/Sc and Pb/Sc ratios from 0.15 ± 0.07 and 11 ± 6, respectively, between 71 and 53 cm, to 0.29 ± 0.01 and 12 ± 3, respectively, between 53 and 33 cm. The corresponding mean anthropogenic Sb/Pb ratio was also higher, averaging 0.028 ± 0.009 (excluding the single outlier peak of 0.061 at 48-49 cm). The higher anthropogenic Sb/Pb ratios, which indeed averaged 0.032 ± 0.008 from 41 to 33 cm, could reflect influences from continental Europe during the growth of the Mediaeval Ag mining industry. It is well known that British Pb (and Cu) ores have a lower Ag content than those found on the continent and therefore British ores were not exploited as widely as those from continental Europe during this period (Tylecote, 1976, 1986; Shepherd, 1993). Thus, the higher anthropogenic Sb/Pb ratios observed during this depth interval, which roughly corresponds to the Mediaeval period, could perhaps reflect the correspondingly high Sb contents in Pb ores of high Ag content (Craddock, 1995; Mass *et al.*, 2002).

Industrial and post-industrial atmospheric Sb sources and deposition

For the depth interval 33 to 23 cm in FM01CM-1, Sb concentrations and Sb/Sc ratios (0.67 ± 0.15) increased but the corresponding anthropogenic Sb/Pb ratio (0.017 ± 0.004) was lower than from 53 to 33 cm (0.028 ± 0.009) (*cf.* Fig. 3.33). Again, as mentioned for Pb (Section 3.6.3), these trends are attributable to the indigenous Scottish Pb mining industry developed during the 17th century at Wanlockhead and Leadhills, as emissions from there would have had the effect of increasing atmospheric Sb (and Pb) concentrations, while lowering the anthropogenic Sb/Pb ratio from its former higher value in Mediaeval times. From 23 cm (*ca.* 1800 A.D.) to 12 cm (1928 ± 11 A.D.), Sb concentrations and mean Sb/Sc

ratios (0.87 ± 0.13) continued to increase. The mean anthropogenic Sb/Pb ratio of 0.0093 ± 0.0019, however, was lower than from 33 to 23 cm. Similarly, from 33 cm (late 1700s A.D.) to 18 cm (1910 ± 8 A.D.) in FM04-1-M (*cf.* Fig. 3.34), Sb concentrations increased while the mean Sb/Sc (0.98 ± 0.24) and anthropogenic Sb/Pb (0.011 ± 0.003) ratios were similar to those in FM01CM-1. The lower anthropogenic Sb/Pb ratio is indicative of relatively greater inputs of Pb, including, as further suggested by the specific value of the observed $^{206}Pb/^{207}Pb$ ratios (range 1.173 to 1.175 in both cores), contributions from indigenous Pb ore sources (e.g. at Wanlockhead and Leadhills).

Over the time periods 1928 ± 11 A.D. to 1969 ± 8 A.D. in FM01CM-1 (12-5 cm) (*cf.* Fig. 3.33) and 1910 ± 8 A.D. to 1968 ± 2 A.D. in FM04-1-M (18-12 cm) (*cf.* Fig. 3.34), the main features for the two cores were similar: maximum Sb/Sc ratios (4.9; 2.5), elevated Pb/Sc ratios, increased mean anthropogenic Sb/Pb ratios (0.014 ± 0.003; 0.020 ± 0.001), and decreasing $^{206}Pb/^{207}Pb$ ratios. As mentioned in Section 3.6.3, in the case of Pb, these trends are attributable to the decline in mining and smelting of indigenous Pb ores in the UK after the 19th century A.D. and the increasing influence of imported Australian Pb ores and coal combustion. To assist the interpretation of the apparent increase in Sb/Pb ratios at these depth intervals, the measured Sb/Pb ratios determined in a selection of British (and Irish) coal samples that had previously been analysed for Pb concentrations and Pb isotopic composition (Farmer *et al.*, 1999) are shown in Table 3.9. These measured Sb/Pb ratios in coal (mean 0.036 ± 0.032) are an order of magnitude higher than those of indigenous Pb ore sources (0.0020 ± 0.0021) strongly suggesting that the increase in anthropogenic Sb/Pb ratios, over the first 70 years of the 20th century A.D. (*cf.* Figs. 3.33 and 3.34) is attributable to inputs of Sb and Pb from coal combustion. Using the following calculated estimated percentage contributions to anthropogenic Pb in the atmosphere for 1930 in Scotland presented in Section 3.6.3: Scottish coal (46%), Pb smelting in Scotland (35%) and sources in the rest of the UK (19%) and the measured Sb/Pb ratio values for coal (0.036) and the indigenous Pb ores from Wanlockhead and Leadhills (0.0056), along with an estimated value for sources in the rest of the UK of

Table 3.9: Measured Sb/Pb ratios in British and Irish coal samples.

Location of coal	Measured Sb/Pb
Rigside (central Scotland)	0.0042
Connaught (Republic of Ireland)	0.0050
Allanton (central Scotland)	0.0076
Glenbuck (west-central Scotland)	0.010
Nr. Buckhaven (east-central Scotland)	0.014
Damside (central Scotland)	0.015
Hallside (central Scotland)	0.019
Seaham (north-east England)	0.022
House of Water (west-central Scotland)	0.023
Plains (Mussel) (central Scotland)	0.027
Blindwells (east-central Scotland)	0.034
Coalburn (central Scotland)	0.034
Point of Ayr (northern Wales)	0.044
Shotts (central Scotland)	0.049
Dalquhandy (central Scotland)	0.067
Slieveardagh (Northern Ireland)	0.079
Longannet (east-central Scotland)	0.080
Gedling (east-central England)	0.12
Mean (± SD)	**0.036 ± 0.032**

0.026 (based on a 2:1 ratio for coal:smelter Pb emissions (*cf.* Table 4 in Farmer *et al.*, 1999), yields an estimated anthropogenic Sb/Pb ratio of 0.023, which is close to the maximum values of 0.018 and 0.020 observed in FM01CM-1 and FM04-1-M, respectively. This is further confirmation of the influence of coal combustion on Sb emissions during the first 70 years of the 20th century A.D.

From the late 1960s A.D. to the early 1980s A.D. (i.e. from 5 to 3 cm and 12 to 9 cm in FM01CM-1 and FM04-1-M, respectively) (*cf.* Figs. 3.33 and 3.34), Sb concentrations and corresponding Sb/Sc ratios (1.7 ± 0.3; 1.2) decreased, as seen earlier for Pb concentrations (Section 3.6). The corresponding mean anthropogenic Sb/Pb ratios also decreased quite markedly (to 0.012 ± 0.001; 0.008) as did the $^{206}Pb/^{207}Pb$ (to 1.134), indicative of the decreasing influence of coal combustion and the increasing influence of vehicle exhaust emissions of Pb. From 1982 to 1990 A.D. (i.e. 9 to 6 cm) in FM04-1-M, Sb concentrations continued to fall while the Sb/Sc ratio increased to 2.2. The anthropogenic Sb/Pb ratio of 0.012, however, was higher

than 0.008, while the $^{206}Pb/^{207}Pb$ ratio attained its minimum value of 1.130. This evidence suggests a new source of Sb during the period of maximum influence of petrol Pb on the $^{206}Pb/^{207}Pb$ ratio. Results in the 0-3 cm sections of FM01CM-1 were in broad agreement with those in FM04-1-M (6-9 cm), *viz.* decreasing Sb concentrations, higher Sb/Sc ratios and an anthropogenic Sb/Pb ratio of 0.0082 ± 0.0033.

The suggestion of new recent sources of Sb, while inputs of Pb have been declining is strengthened by the data for the top 6 cm (1990-2004 A.D.) of FM04-1-M: (i) Sb concentrations and Sb/Sc ratios (2.4 ± 0.0) levelling out while Pb concentrations and Pb/Sc ratios (81 ± 14) decline, (ii) a significant increase in the corresponding mean anthropogenic Sb/Pb ratio to 0.030 ± 0.006, and (iii) an increase in the $^{206}Pb/^{207}Pb$ ratio to 1.139 ± 0.02. Thus, while Pb emissions from car-exhausts fell steeply as the use of unleaded petrol became increasingly predominant followed by the ban on leaded petrol from 2000 A.D., the input of Sb from comparatively new recent sources (i.e. not coal combustion, which has been declining) has probably contributed to the increase in the Sb/Pb ratio. Such recent sources could include the release of Sb from automotive brake linings, where it has been used instead of asbestos to improve heat resistance, and from the degradation or combustion of a variety of other products, including plastics, to which it is added (in the form of Sb_2O_3) as a flame retardant (Sternbeck *et al.*, 2002; Shotyk *et al.*, 2005).

3.8.1.3.3 Historical trends in depositional fluxes and inventories of anthropogenic Sb

Depositional fluxes of anthropogenic Sb (A4.2 Table A11) were calculated for the dated FM04-1-M peat sections as done previously for Pb (Section 3.6.4). Depositional fluxes of anthropogenic Sb and Pb since the mid-19th century A.D. are plotted, along with the anthropogenic Sb/Pb and measured $^{206}Pb/^{207}Pb$ ratios, *versus* ^{210}Pb-derived calendar dates for FM04-1-M in Fig. 3.35. The maximum anthropogenic Sb flux of ~ 0.42 mg m^{-2} y^{-1} occurs from the mid-1920s to the mid-1950s A.D., coincident with the maximum anthropogenic Pb flux.

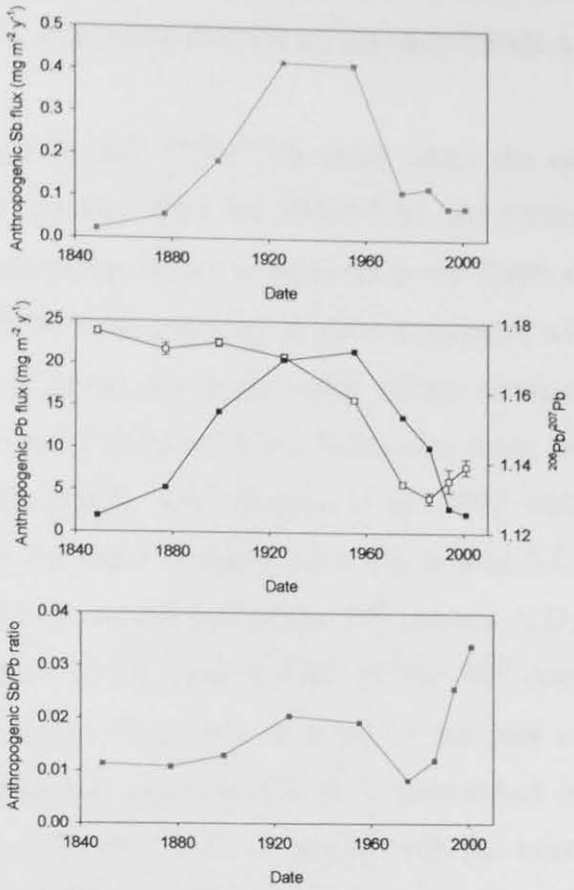

Figure 3.35: Calculated atmospheric depositional fluxes of anthropogenic Sb and Pb (mg m^{-2} y^{-1}) (closed squares), and the anthropogenic Sb/Pb and measured $^{206}Pb/^{207}Pb$ ratios (open squares) for the FM04-1-M core *versus* ^{210}Pb-derived dates since 1840 A.D.

The influence of contributions from coal combustion emissions explains both the enhancement in the associated anthropogenic Sb/Pb ratio over the late 19th century A.D. to ~ 0.020 at that time and, to a certain extent, the limitation of the post-19th century A.D. decline in $^{206}Pb/^{207}Pb$ that stemmed from the introduction and use of Australian Pb in alkylPb additives in petrol. After 1960 A.D., the rapid decline in coal combustion emissions at the same time as the increase in vehicle exhaust emissions was reflected not only in the fall in $^{206}Pb/^{207}Pb$ ratio but also in the steeper decline in anthropogenic Sb fluxes (to ~ 0.11 mg m^{-2} y^{-1}) relative to those of Pb, with a concomitant decline in the corresponding Sb/Pb ratio to its minimum value of 0.008 in the mid-1970s A.D. Thereafter, the Sb fluxes stayed relatively constant while those of Pb, due to the phasing out of leaded petrol, continued to fall. The

increase in the anthropogenic Sb/Pb ratio, however, probably began slightly earlier, in the mid-1970s A.D., increasing to 0.034 by the early 2000s A.D.

The anthropogenic Sb/Pb and $^{206}Pb/^{207}Pb$ ratios since the mid-19th century A.D. *versus* ^{210}Pb-derived calendar dates for FM04-1-M and FM01CM-1 are shown in Fig. 3.36. The corresponding values of anthropogenic Sb/Pb ratios and $^{206}Pb/^{207}Pb$ ratios for core FM01CM-1 are generally in good agreement with those for FM04-1-M. Likewise there is broad agreement with values obtained independently for preserved herbarium and freshly collected *Sphagnum* moss samples of known age collected across Scotland (Fig. 3.37) (Farmer *et al.*, 2002; Halter, 2005; Halter and Farmer, *in prep.*). In the moss samples there was a near 3-fold increase from the lower Sb/Pb values of the second half of the 19th century A.D., for most of the 20th century A.D. and then, in the final decade of the 20th century A.D., a 10-fold increase, somewhat greater than that observed in the peat cores. Interestingly, a freshly collected *Sphagnum* moss sample at Wanlockhead in 2000 A.D. had an anthropogenic Sb/Pb ratio of 0.0023, in accord with the much lower Sb/Pb ratios measured in former Pb mining/smelting areas.

The total anthropogenic Sb inventories for FM01CM-1 (i.e. from *ca.* 500 B.C. to mid-1980s A.D., given that the very top of the core was lost during collection) and FM04-1-M (i.e. from *ca.* late 1700s to 2004 A.D.) were 0.051 g m^{-2} and 0.035 g m^{-2}, respectively. In FM01CM-1, the anthropogenic Sb inventory was 0.00022 g m^{-2} for the period embracing the Sb peak (86-96 cm) in the pre-Roman/Roman times, while, in comparison, the post-1800 A.D. anthropogenic Sb inventory (0.049 g m^{-2}) (corresponding to peat sections 0-23 cm), constituted 95% of the total anthropogenic Sb inventory for the core, as for Pb (*cf.* Section 3.6.4).

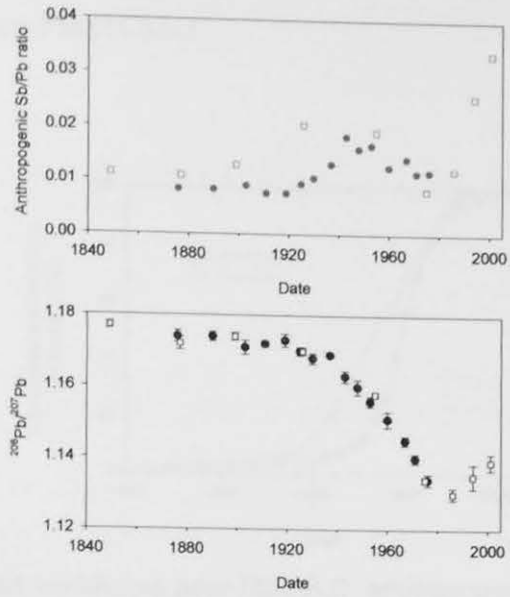

Figure 3.36: Anthropogenic Sb/Pb and measured $^{206}Pb/^{207}Pb$ ratios *versus* ^{210}Pb-derived dates, since 1840 A.D for the FM04-1-M (open symbols) and FM01CM-1 cores (shaded symbols).

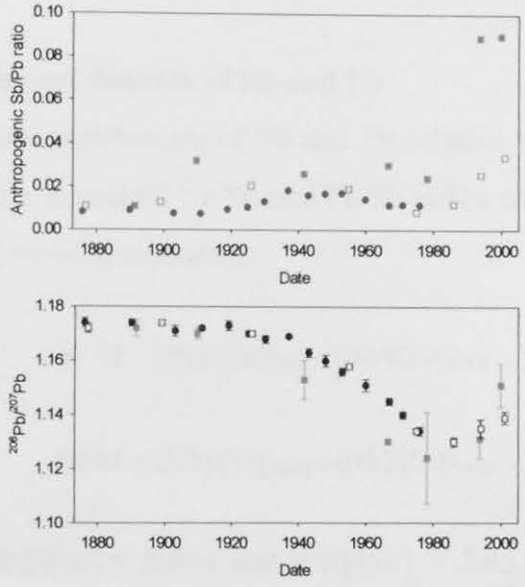

Figure 3.37: Anthropogenic Sb/Pb and measured $^{206}Pb/^{207}Pb$ ratios *versus* dates, since *ca.* 1870 A.D, for Scottish herbarium moss samples (green symbols) and the FM04-1-M (open symbols) and FM01CM-1 cores (shaded symbols).

Calculated cumulative post-1800 A.D. anthropogenic Sb inventories (% of total post-1800 A.D. inventory) for the Flanders Moss cores are plotted *versus* ^{210}Pb-derived calendar dates in Fig. 3.38. Maximum deposition occurred between the 1910s and 1960s A.D., as found for Pb (*cf.* Section 3.6.4), and again, slight differences in trends between the two cores are at least partly attributable to differences in core sectioning,

as well as uncertainties with respect to extrapolation of ^{210}Pb dates for the FM01CM-1 core from FM01CM-2.

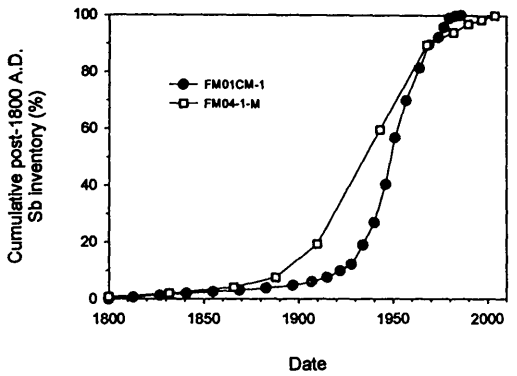

Figure 3.38: Calculated cumulative post-1800 A.D. anthropogenic Sb inventories (% of total post-1800 A.D. inventory) for the FM01CM-1 and FM04-1-M cores *versus* ^{210}Pb-derived dates. Note that dates in FM01CM-1 and FM04-1-M prior to *ca.* 1883 A.D. and *ca* 1832 A.D., respectively, were extrapolated. Also, dates in FM01CM-1 after *ca.* 1974 A.D. were extrapolated.

3.8.1.3.4 Maximum enrichments of Sb and Pb

The extent of maximum enrichments of Sb and Pb relative to "natural background" can be calculated, using measured Sb/Sc and Pb/Sc ratios and corresponding values for the UCC, *via* the following equations:

$$\text{Sb EF} = ([\text{Sb}]/[\text{Sc}])_{\text{MAX}} / ([\text{Sb}]/[\text{Sc}])_{\text{UCC}}$$

$$\text{Pb EF} = ([\text{Pb}]/[\text{Sc}])_{\text{MAX}} / ([\text{Pb}]/[\text{Sc}])_{\text{UCC}}$$

In which the UCC [Sb]/[Sc] = 0.044 and [Pb]/[Sc] = 2.43. Also, instead of using UCC Sb/Sc and Pb/Sc ratios, those of Shotyk *et al.* (2004) for Swiss natural background peat (SNBP), i.e. [Sb]/[Sc] = 0.11 and [Pb]/[Sc] = 3.0, can be used. The maximum enrichments of Sb and Pb for the Flanders Moss peat cores calculated using UCC and SNBP elemental concentration ratios are shown in Tables 3.10 and 3.11, respectively. Notwithstanding the uncertainties (*cf.* Section 1.8.3) inherent in calculating enrichments in this manner, it thus appears that Sb (24-110) and Pb (61-120) exhibit similar degrees of enrichment.

Table 3.10: Maximum enrichments of Sb for FM01CM-1 and FM04-1-M, calculated relative to upper continental crust (UCC) and Swiss natural background peat (SNBP) Sb/Sc concentration ratios.

	UCC	SPNB
Peat core	**Sb**	**Sb**
FM01CM-1 (*ca.* 1960 ± 9 A.D.)	110	47
FM04-1-M (*ca.* 1926 ± 6 A.D.)	58	24

Table 3.11: Maximum enrichments of Pb for FM01CM-1 and FM04-1-M, calculated relative to upper continental crust (UCC) and Swiss natural background peat (SNBP) Pb/Sc concentration ratios.

	UCC	SPNB
Peat core	**Pb**	**Pb**
FM01CM-1 (*ca.* 1980s A.D.)	120	99
FM04-1-M (*ca.* 1986 ± 2 A.D.)	76	61

3.8.2 Hg

3.8.2.1 Hg concentrations in FM01CM-2 peat core

Concentrations of Hg, expressed relative to sectional air-dried peat weights, were determined for only the FM01CM-1 sister core, FM01CM-2 and are tabulated in A4.3 Table A1 and plotted in Fig. 3.39 (Shimwell, 2002). There was a general increase in Hg concentrations from ~ 150 μg kg^{-1} at 15 cm, to the maximum concentration of 550 μg kg^{-1} at 4-6 cm, with a subsequent decline to 370 μg kg^{-1} in the 0-2 cm section. The lowest concentrations were 37-86 μg kg^{-1}, which occurred at a depth of 88-100 cm. There was also a broad peak in the Hg concentration from 42-64 cm, where values reached 160-200 μg kg^{-1}, a significant increase of 50-100 μg kg^{-1} over adjacent sections.

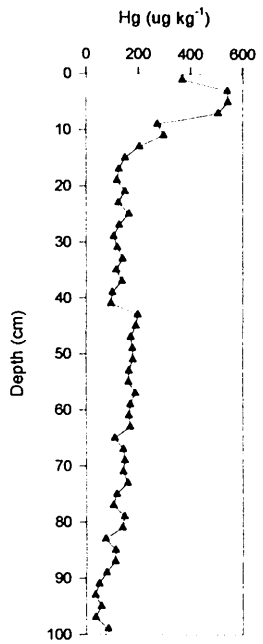

Figure 3.39: Depth profile of Hg concentrations (μg kg^{-1}) in the FM01CM-2 (0-100 cm) peat core.

3.8.2.2 Discussion

As mentioned in Section 1.13.2, previous workers have found evidence to suggest that Hg, like Pb, is essentially immobile in ombrotrophic peat (Benoit *et al.*, 1998; Bindler *et al.*, 2001; Roos-Barraclough *et al.*, 2002a; Givelet *et al.*, 2003; Shotyk *et al.*, 2003). However, other workers have suggested that redox-related transformations of Fe, Mn and S affect Hg concentration profiles in peat bogs (Roulet and Lucotte, 1995; Paquette and Helz, 1995). Also, Biester *et al.* (2003) suggested that humification processes and mass losses during the diagenesis of peat might have a strong influence on Hg concentrations. To investigate the geochemical behaviour of Hg in this Flanders Moss peat core, FM01CM-2 Hg concentrations are plotted alongside Pb, Fe, Mn, S and Se concentrations and NaOH peat extract absorptions in the FM01CM-1 core, in Fig. 3.40.

3.8.2.2.1 Assessment of the immobility of Hg in ombrotrophic peat

In the uppermost peat sections (0-33 cm), zones which contained elevated Hg concentrations were also elevated with respect to Pb.

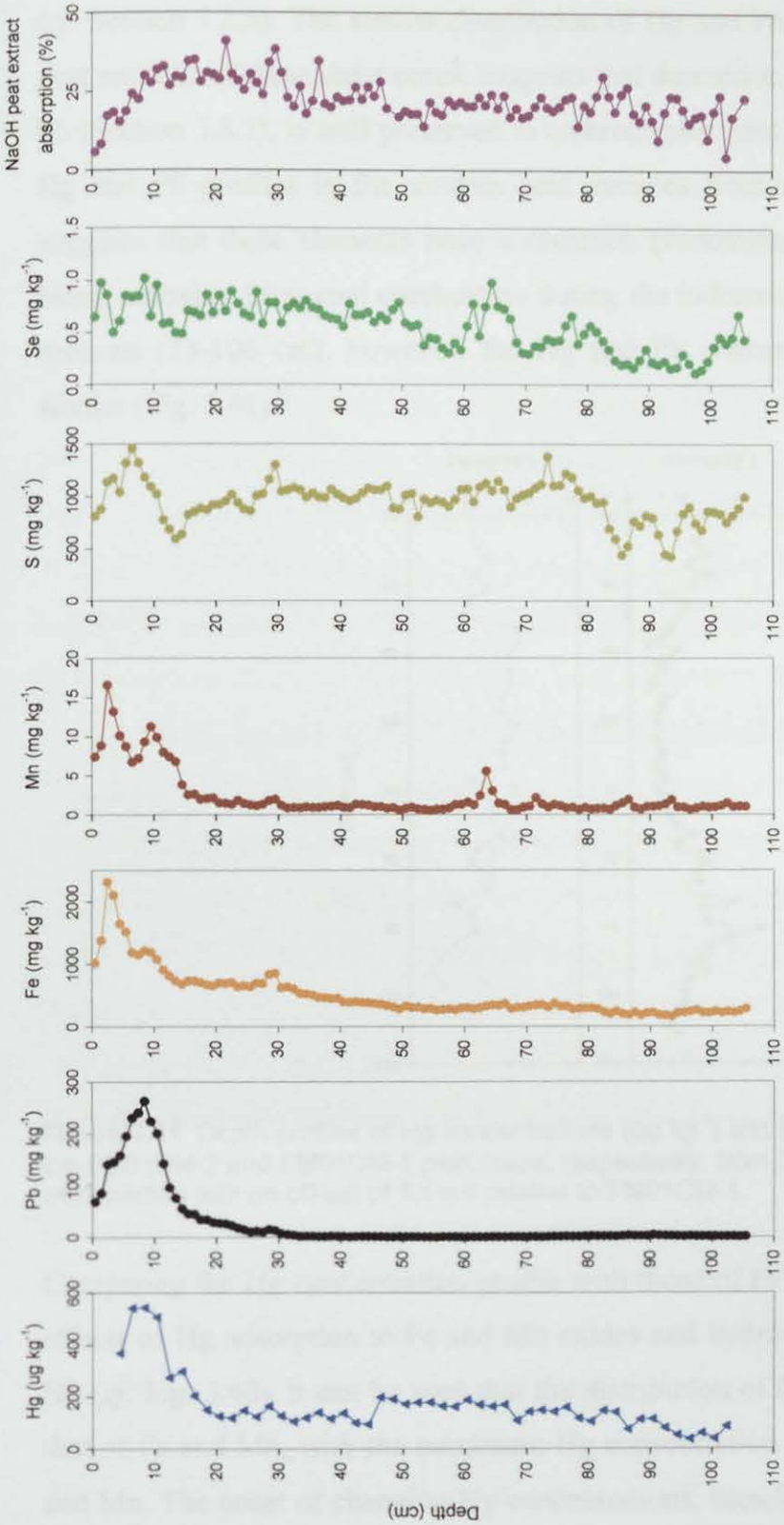

Figure 3.40: Depth profiles of Hg concentrations (µg kg^{-1}) in the FM01CM-2 (0-100 cm) peat core and Pb, Fe, Mn, S and Se concentrations (mg kg^{-1}) and NaOH peat extract absorption (%) in the FM01CM-1 (0-110 cm) peat core. Hg concentrations were plotted with an off-set of 3.5 cm relative to FM01CM-1.

The maximum Hg concentration in FM01CM-2 occurred at the same depth (8.5 cm) as the Pb concentration maximum in FM01CM-1, after taking into account the required 3.5 cm offset of the FM01CM-2 sections relative to the FM01CM-1 sections (*cf.* Section 3.2.5). The similar distribution of Hg and Pb, at least in the uppermost peat sections of these sister cores, suggests that deposition of Hg, as found earlier for Sb (Section 3.8.1), is well preserved in ombrotrophic peat bogs. The similarity of the Hg and Pb profiles in the modern peat samples from the uppermost peat layers suggests that these elements have a common predominant source, the most likely being emission from coal combustion during the industrial period. In the lower peat sections (33-106 cm), however, the Hg and Pb concentration profiles were less similar (Fig. 3.41).

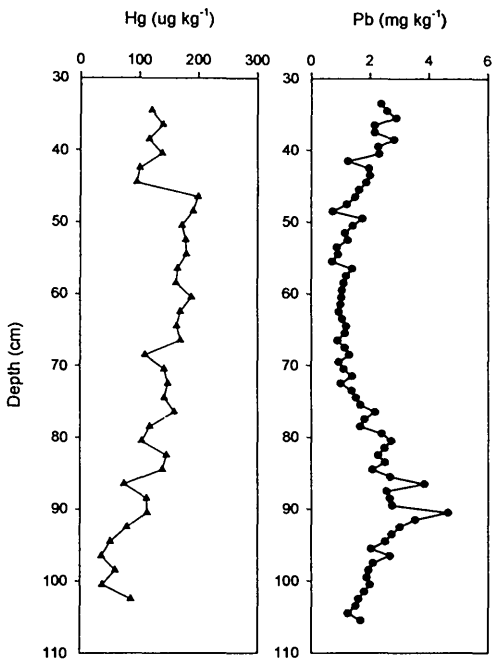

Figure 3.41: Depth profiles of Hg concentrations (μg kg^{-1}) and Pb concentrations (mg kg^{-1}) in the FM01CM-2 and FM01CM-1 peat cores, respectively, from 33-106 cm. Hg concentrations were plotted with an off-set of 3.5 cm relative to FM01CM-1.

Comparing the Hg concentration profile with those of Fe and Mn, in order to assess effects of Hg adsorption to Fe and Mn oxides and hydroxides on the distribution of Hg (*cf.* Fig. 3.40), it can be seen that the distribution of Hg is clearly different from that of Fe and Mn, with the maximum Hg concentration occurring below that of Fe and Mn. The onset of changing Hg concentrations, therefore, precedes and pre-dates

the changes in Mn and Fe profiles which are known to be diagenetically influenced, providing further evidence that Hg, like Pb, is essentially immobile in ombrotrophic peat. These findings are consistent with those found by Givelet *et al.* (2003) in peat cores from three different peat bogs in Ontario. Also, comparing the Hg concentration profile with that of S, in order to assess the possible formation of HgS precipitates, it is apparent that the Hg concentration increases in the anaerobic catotelm peat sections, particularly between ~ 45 and 67 cm, may be related to the corresponding S concentration increases, therefore indicating some control of Hg as HgS precipitates.

The conservative element, Sc, has been used to distinguish between natural and anthropogenic sources of Pb in the Flanders Moss peat cores. However, in the case of Hg, Givelet *et al.* (2003) suggested that natural inputs of Hg from soil dust were insignificant in pre-anthropogenic times and therefore that soil dust represents a negligible source of Hg. Along with other workers (Roos-Barraclough *et al.*, 2006), they proposed that Br and Se could be used as suitable "reference elements" for Hg to quantify the natural inputs of Hg to peat bogs, since their inputs are independent of soil dust. Although Br concentrations in the Flanders Moss peat cores were not available, Se concentrations were determined in the FM01CM-1 peat core. When the Hg and Se concentration profiles are compared they appear very different (*cf.* Fig. 3.40). Givelet *et al.* (2003) also found dissimilar Hg and Se concentration profiles in recent peats (0-50 cm) in the Canadian peat cores and suggested that this could be due to the differences between their chemical behaviour as well as the physical and chemical processes affecting the atmospheric transport and deposition of Hg and Se. Givelet *et al.* (2003), however, found that Hg/Se ratios in ombrotrophic peats dating from pre-anthropogenic times were remarkably constant for thousands of years, suggesting that their rates of accumulation in pre-anthropogenic peats were in constant proportions, despite the differences in natural atmospheric sources of these elements, e.g. Se primarily in the form of $(CH_3)_2Se$ from oceans and Hg in its volatile, unreactive, gaseous elemental form from volcanic emissions (Nriagu and Pacyna, 1988; Mason *et al.*, 1994; Schroeder and Munthe, 1998). Unfortunately,

FM01CM-2 Hg concentrations could not be normalised to Se concentrations since these concentration values were determined in its sister core FM01CM-1 (A4.1 Table A7). A potential problem when Se is used to normalise Hg concentrations, however, is the contribution of anthropogenic Se from coal combustion (Roos-Barraclough *et al.*, 2006), metallurgical activities and waste incineration, which are similar to those of Hg (*cf.* Table 1.2, Section 1.3.2.2). Also, since the Hg and Se concentrations in the modern sections of the Flanders Moss peat cores were dissimilar, it seems very likely that Se is mobile in ombrotrophic peat, suggesting that this element cannot be used as a reference element for atmospheric Hg deposition. Also, since trends in the Se concentration profile in FM01CM-1 appear to suggest the mobility of Se in ombrotrophic peat, this element will not be considered any further in this chapter.

Comparing the Hg concentration profile with the NaOH peat extract absorption profile to assess effects of organic matter decomposition processes on the distribution of Hg, the changes in Hg concentrations do not relate to the changes in peat humification. These findings are again consistent with those of Givelet *et al.* (2003), and therefore physical processes such as peat decomposition cannot explain the magnitude of the variation in Hg concentrations with depth in this peat bog profile. Unfortunately, FM01CM-2 Hg concentrations could not be normalised to NaOH peat extract absorption since these absorption values were determined in its sister core FM01CM-1.

3.8.2.2.2 Historical trends in sources of atmospheric Hg deposition

Since the origins of Hg in the lower peat sections of the FM01CM-2 core are uncertain, historical trends in sources of atmospheric Hg deposition during the industrial and post-industrial periods alone will be investigated. Hg concentration and $^{206}Pb/^{207}Pb$ ratio profiles in FM01CM-2 and Pb concentration and $^{206}Pb/^{207}Pb$ ratio profiles for FM01CM-1, including ^{210}Pb age-dates, are shown in Fig. 3.42.

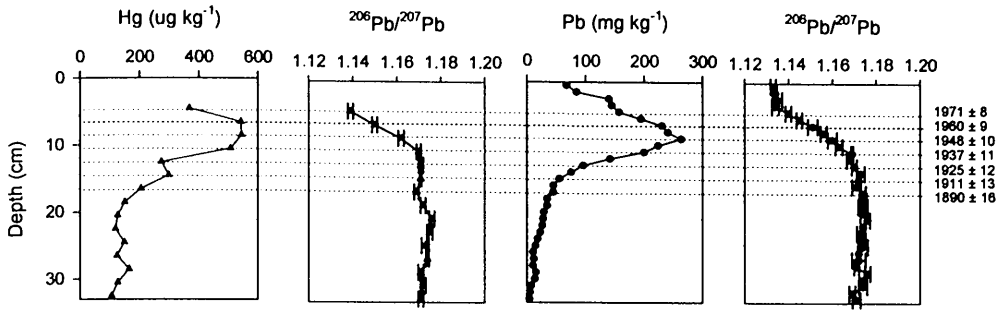

Figure 3.42: Depth profiles of Hg concentrations (μg kg^{-1}) and $^{206}Pb/^{207}Pb$ ratios (triangles) in the ^{210}Pb-dated FM01CM-2 peat core, and Pb concentrations (mg kg^{-1}) and $^{206}Pb/^{207}Pb$ ratios (circles) in the ^{210}Pb-dated FM01CM-1 peat core, from 0-33 cm. FM01CM-2 profiles were plotted with an off-set of 3.5 cm relative to FM01CM-1.

Note that FM01CM-2 $^{206}Pb/^{207}Pb$ data are presented elsewhere (Yafa, 2004; Farmer *et al.*, 2006). The Hg concentrations increased from a minimum (110 μg kg^{-1}) at a depth of 31-33 cm, for which no age-date was available, to 280 μg kg^{-1} at *ca.* 1925 ± 12 A.D. The corresponding $^{206}Pb/^{207}Pb$ ratios in both of the cores, remained fairly constant and in good agreement, averaging 1.172 ± 0.002 and 1.173 ± 0.002 in FM01CM-2 and FM01CM-1, respectively, and as mentioned in Section 3.6.3, Pb concentration increases until the early 20th century A.D. were strongly influenced by the indigenous Scottish Pb mining industry that developed during the 17th century A.D. It seems likely, however, that the increases in Hg concentration reflect emissions from coal combustion, as coal consumption in the UK increased dramatically from the 1700s to the 1920s A.D. (Farmer *et al.*, 1999). The absolute increase in Hg concentration from 280 to 550 μg kg^{-1} occurred between *ca.* 1925 and 1960 A.D., the depth of maximum Hg and Pb concentrations corresponding to *ca.* 1948 ± 10 A.D (*cf.* Fig. 3.42). During this period the corresponding $^{206}Pb/^{207}Pb$ ratios in both cores, decreased from ~ 1.170 to 1.150, these intermediate values reflecting significant emissions of Pb from both the use of less-radiogenic imported Australian Pb ores, used along with other sources in the manufacture of alkylPb additives in petrol from the 1930s A.D., as well as of coal combustion. It is worth noting that coal consumption in the UK increased from ~ 190 Mt y^{-1} in the 1920s A.D. to ~ 230 Mt y^{-1} in the 1950s A.D. (*cf.* Fig. 4, Farmer *et al.*, 1999). The significant increase in Hg concentrations therefore most likely resulted from coal combustion emissions, since leaded petrol emissions were not a source of

Hg. After 1960 A.D., the Hg (and Pb) concentrations decreased, the continuing decline from ~ 1.150 to 1.140 in the $^{206}Pb/^{207}Pb$ ratios up to 1976 A.D., being attributable to the fall in coal combustion emissions at the same time as the increase in vehicle exhaust emissions. During the post-industrial period (i.e. post-1970 A.D.), however, Hg emissions from other sources such as waste incinerators (*cf.* Table 1.2, Section 1.3.2.2) may have been important (Roos-Barraclough and Shotyk, 2003).

3.8.2.2.3 Historical trends in depositional fluxes and inventories of Hg

Depositional fluxes of Hg and Pb (A4.3 Table A1) since the late-19th century A.D. are plotted, along with the measured $^{206}Pb/^{207}Pb$ ratios, *versus* ^{210}Pb-derived calendar dates for FM01CM-2 in Fig. 3.43.

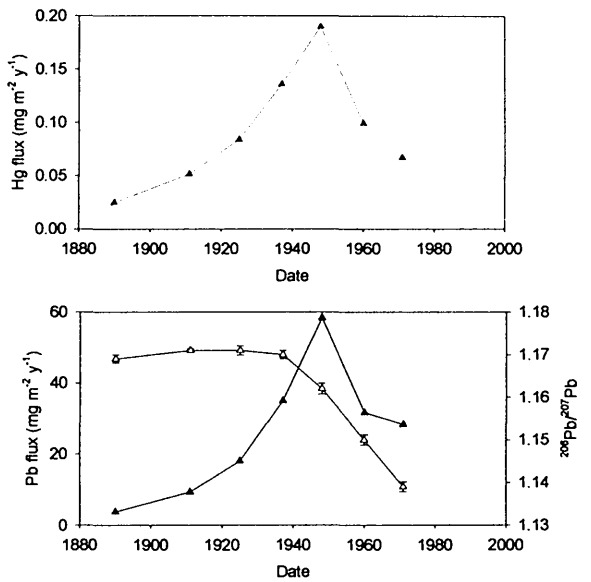

Figure 3.43: Atmospheric depositional fluxes of Hg and Pb (mg m^{-2} y^{-1}) (closed triangles) and measured $^{206}Pb/^{207}Pb$ ratios (open triangles) for the FM01CM-2 core *versus* ^{210}Pb-derived dates from 1880 to 1980 A.D.

Note that depositional fluxes of Pb are presented elsewhere (Yafa, 2004; Farmer *et al.*, 2006). There is a remarkable resemblance between the Pb and Hg depositional flux trends in FM01CM-2. The Hg and Pb fluxes increased ~ 10 and 20-fold, respectively, from values of ~ 0.024 and ~ 3.7 mg m^{-2} y^{-1} at *ca.* 1890 A.D. to maximum values of ~ 0.19 and ~ 58 mg m^{-2} y^{-1}, respectively at *ca.* 1950 A.D. Hg fluxes then declined more steeply than those of Pb, decreasing to 0.067 and

28 mg m^{-2} y^{-1}, respectively, in the early 1970s A.D, reflecting the decline in coal combustion but the continued input of Pb from the use of leaded petrol.

A modelled Hg wet deposition value of 0.013 mg m^{-2} y^{-1} was recorded in west-central Scotland during 1998 A.D. (Lee *et al.*, 2002). Unfortunately, since the most recent material was missing from the FM01CM-2 core, there is no Hg flux value for peat sections more recent than 1976 A.D. for comparison. Nevertheless, this wet deposition value does indicate that in recent years the rates of Hg deposition in Scotland have fallen. Also, comparing the Flanders Moss Hg fluxes during the industrial period to the average natural background accumulation rates measured in Canadian, Swiss and Swedish pre-anthropogenic peats, i.e. 1.4 ± 1 μg m^{-2} y^{-1} (Givelet *et al.*, 2003), 0.3-8 μg m^{-2} y^{-1} (Roos-Barraclough *et al.*, 2002a) and 0.5-1 μg m^{-2} y^{-1} (Bindler, 2003), respectively, the Flanders Moss Hg deposition rates at *ca.* 1950 A.D. were up to 600 times greater than natural background rates.

The total Hg inventory for the FM01CM-2 core (0-100 cm), given that the very top of the core was lost during collection, was 17 mg m^{-2}, and the Hg inventory (9.0 mg m^{-2}) from *ca.* 1800 to 1976 A.D. (corresponding to peat sections 0-20 cm in the case of FM01CM-2) constituted only 53% of the total Hg inventory, which is approximately half the proportion of the total found (95%) for the post-1800 A.D. anthropogenic Pb and Sb inventories in the FM01CM-1 (0-106 cm) core. Also, the pre-1800 A.D. inventory (i.e. 8.0 mg m^{-2}), which was deposited over a period of ~ 2000 years, can be estimated to represent a flux of ~ 4 μg m^{-2} y^{-1}, which is ~ 4 times greater than the natural background rates quoted above. It should also be noted that these Hg inventories determined in the FM01CM-2 core have not been corrected for natural Hg contributions. Calculated cumulative post-1800 A.D. Hg inventories (% of total post-1800 A.D. inventory) for FM01CM-2 are plotted *versus* ^{210}Pb-derived calendar dates in Fig. 3.44. Maximum deposition occurred between the 1910s and 1960s A.D., as found for Pb in FM01CM-1 (*cf.* Sections 3.6.4), bearing in mind that the time intervals were slightly different.

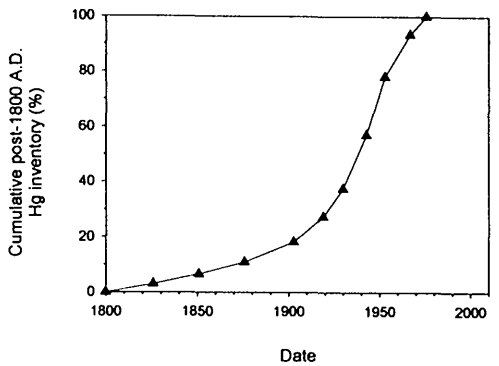

Figure 3.44: Calculated cumulative post-1800 A.D. Hg inventories (% of total post-1800 A.D. inventory) for the FM01CM-2 core *versus* ^{210}Pb-derived dates. Note that dates in FM01CM-2 prior to *ca.* 1876 A.D. and after *ca* 1976 A.D. were extrapolated.

3.8.3 As, Cd, Cu and Zn

Total As, Cd, Cu and Zn concentrations, expressed relative to sectional 105°C-dried peat weights, for FM01CM-1 and FM04-1-M are tabulated in A4.1 Table A7 and A4.2 Table A7, respectively. The Pb, S and ash content profiles, presented in Sections 3.4, 3.7 and 3.1, respectively, are plotted alongside their concentration profiles (Figs. 3.45 and 3.46) for comparison. Since uptake and recycling by plants and/or redox cycling processes may be important, the position of the vegetation-peat interface and, in the case of FM01CM-1, the estimated acrotelm-catotelm boundary, are indicated on their depth profiles.

3.8.3.1 FM01CM-1

All four elements exhibited concentration peaks in the uppermost ~ 15 cm of the core, with the following maximum concentrations at the depths indicated:

- As – 6.0 mg kg^{-1} at 9-10 cm
- Cd – 0.87 mg kg^{-1} at 7-8 cm
- Cu – 22 mg kg^{-1} at 9-10 cm
- Zn – 410 mg kg^{-1} at 1-2 cm but the maximum value (440 mg kg^{-1}) in the core occurred at 49-50 cm

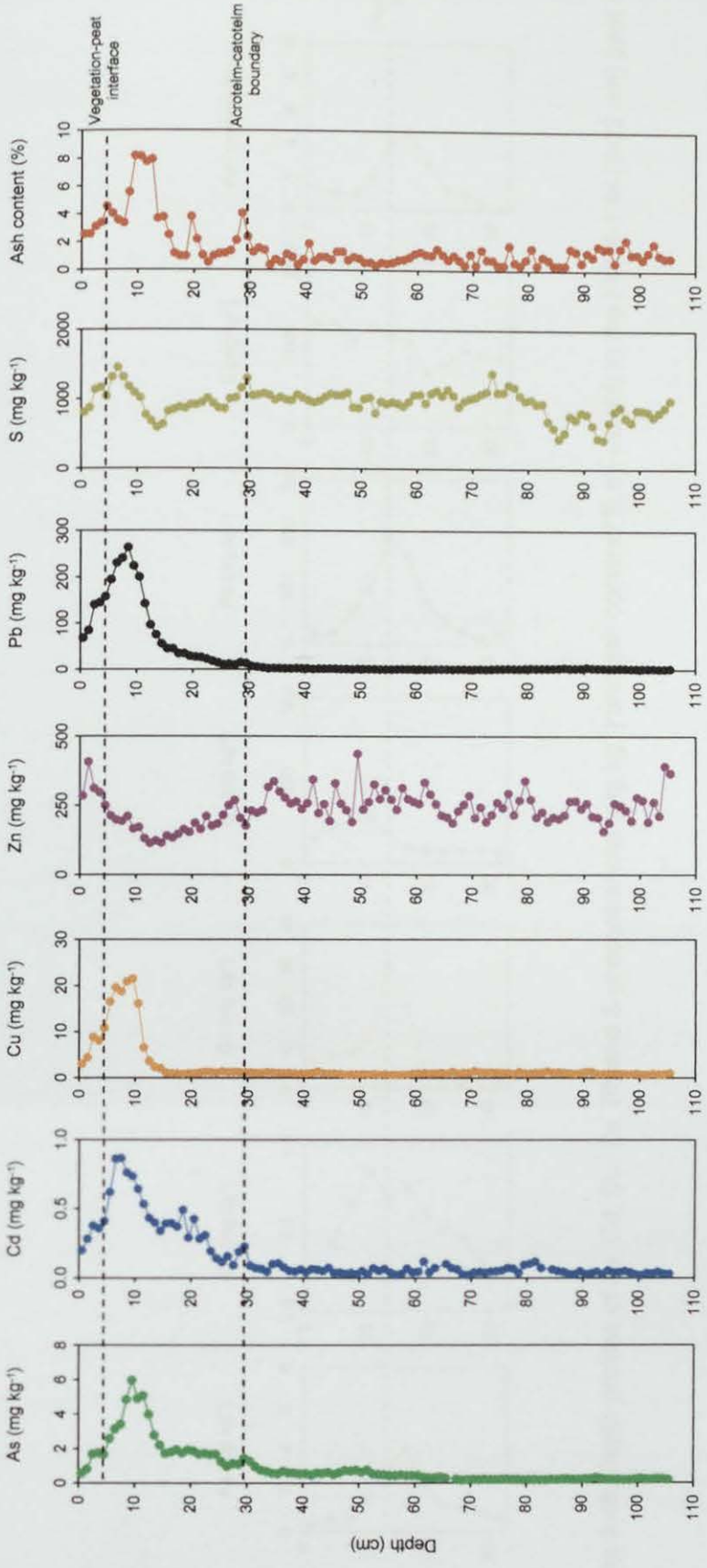

Figure 3.45: Depth profiles of As, Cd, Cu, Zn, Pb and S concentrations (mg kg^{-1}) and ash content (% by weight) in the FM01CM-1 (0-106 cm) peat core.

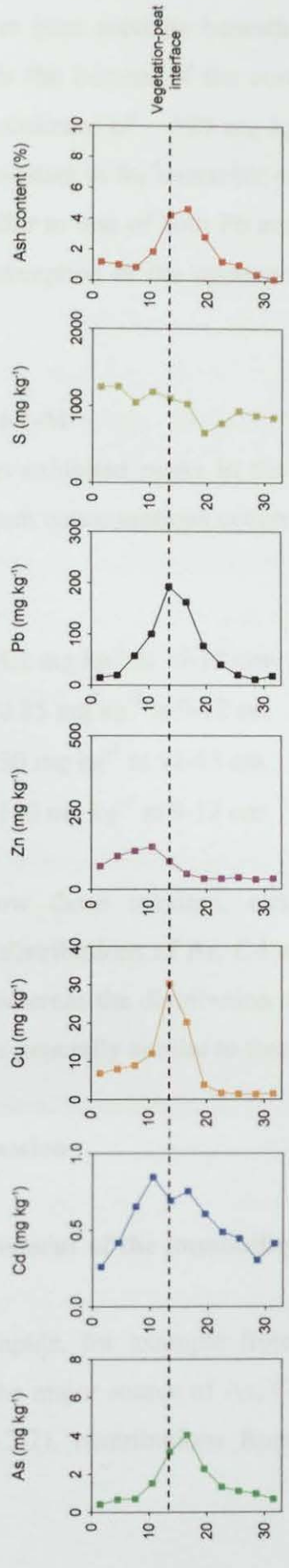

Figure 3.46: Depth profiles of As, Cd, Cu, Zn, Pb and S concentrations (mg kg^{-1}) and ash content (% by weight) in the FM04-1-M (0-33 cm) peat core.

Above these maxima, elemental concentrations decreased towards the top of the core. In the lower peat sections beneath the concentration peaks, concentrations decreased towards the bottom of the core, with the exception of Zn which, after decreasing to a minimum of ~ 120 mg kg^{-1} between 12 and 15 cm, increased and remained fairly constant in the anaerobic catotelm layers. The distributions of As, Cd and Cu were similar to that of both Pb and the ash content, whereas the distribution of Zn, with the exception of the uppermost peat sections, was similar to that of S (*cf.* Fig. 3.45).

3.8.3.2 FM04-1-M

All four elements exhibited peaks in the uppermost ~ 30 cm of the core and the following maximum concentrations occurred, at the depths indicated, for each of the elements:

- As – 4.1 mg kg^{-1} at 15-18 cm
- Cd – 0.85 mg kg^{-1} at 9-12 cm
- Cu – 30 mg kg^{-1} at 12-15 cm
- Zn – 140 mg kg^{-1} at 9-12 cm

Above and below these maxima, elemental concentrations decreased. As in FM01CM-1, the distributions of As, Cd and Cu were similar to that of both Pb and the ash content, whereas the distribution of Zn, with the exception of the uppermost peat sections, was generally similar to that of S (*cf.* Fig. 3.46).

3.8.3.3 Discussion

3.8.3.3.1 Assessment of the immobility of As, Cd, Cu and Zn in ombrotrophic peat

Anthropogenic inputs, for example from fuel combustion and non-ferrous metal production, are the major source of As, Cd, Cu and Zn to the atmosphere (*cf.* Table 1.2, Section 1.3.2.2), contributions from soil dust inputs being minor. Also, as

mentioned in Section 1.7.3.1, it is expected that Cd, Cu and Zn behave in a similar way to Pb in ombrotrophic peat since they are also strongly bound to organic matter (in the order Pb>Cu>Cd>Zn) and also, as for As, they could be susceptible to sulfide formation under reducing anaerobic conditions. In the case of the plant micronutrients, Cu and Zn, the distribution of these elements could also be influenced by uptake and cycling in the vegetation layer. Cd may also be affected by biological cycling as its chemical behaviour is similar to that of Zn (Espi *et al.*, 1997; Coggins *et al.*, 2006). In the case of As, influences from post-depositional diagenetic remobilisation have been found in lake sediments (Farmer and Lovell, 1986) and it has also been suggested that As (and Zn) are more mobile than Pb and Cu in ombrotrophic peats, with the amount lost through migration being unknown (Nieminen *et al.* (2002). Shotyk *et al.* (1996), however, found good agreement between the records of As atmospheric deposition and those of Pb and Sb in a Swiss EGR peat core. It has also been suggested that Cd and Zn are subjected to post-depositional mobility and that their concentrations and mineralogical forms at the time of deposition as well as the pH of the bog waters are important (Rausch *et al.*, 2005a and b).

The As, Cd and Cu concentration profiles in the Flanders Moss cores appear to have similar concentration profiles to those of Pb and the ash content, perhaps indicating that these elements are relatively immobile in ombrotrophic peat. Also, the As concentration peaks in the cores are distinctly different from those of Fe and P (Section 3.7), with As peaks occurring 7 cm and 5 cm beneath the diagenetic Fe and P peaks, respectively, in FM01CM-1, and 6 cm and 3 cm beneath the diagenetic Fe and P peaks, respectively, in FM04-1-M. This suggests that As has not been subjected to such diagenetic enrichment processes. The absence of surface enrichment in the Cd and Cu concentration profiles suggests that Cd and Cu have not been influenced by biological cycling. It is also worth noting that, in the FM01CM-1 core, there are minor increases in the As and Cd concentrations at the acrotelm-catotelm boundary (~ 30 cm), which are coincident with the increases in S concentration and ash content, as well as in some of the conservative elements (Al,

Ti, Y and Zr) and other major elements (Ca, Fe, Mg, Mn) (*cf.* Section 3.7). These minor As and Cd increases provides further evidence for the influence of soil dust inputs at this depth.

The Zn concentration profiles in the uppermost sections of the cores appear to indicate that Zn is affected by plant uptake and recycling, since the concentration maxima and increases occur within the zones of biological cycling, i.e. the upper 5-cm of FM01CM-1 and 15-cm of FM04-1-M (*cf.* Fig. 3.45 and 3.46). Also, as mentioned in Section 3.7, it is worth noting that slight differences between the trends and magnitudes of Zn concentrations in the biological zones of the two cores could be attributable to differential rates of nutrient cycling by the different hummock-producing moss species in FM01CM-1 and FM04-1-M. The coincident zones of Zn and S minima in the acrotelm peat and increases in the catotelm peat are possibly indicative of the influence of Zn sulfide formation and precipitation at depth. This relationship between Zn and S was also observed in the FM01CM-2 core (Yafa, 2004). Since Zn appears to be mobile within this ombrotrophic peat bog, this element will not be considered any further in this Chapter.

3.8.3.3.2 The use of Sc as an indicator of As, Cd and Cu soil dust input

As, Cd, Cu and Sc concentration profiles in FM01CM-1 and FM04-1-M, are shown in Figs. 3.47 and 3.48, respectively. Note the changes in scale on the As and Cd (5-fold), Cu (20-fold) and Sc (4-fold) concentrations on going from 0-33 cm to 33-106 cm in the FM01CM-1 core. To eliminate contributions to As, Cd and Cu from sources that are unrelated to direct anthropogenic inputs in the As, Cd and Cu profiles, As/Sc, Cd/Sc and Cu/Sc ratios can be used in the same way that Pb/Sc and Sb/Sc ratios were used for Pb and Sb in Sections 3.6 and 3.8.1. FM01CM-1 and FM04-1-M As/Sc, Cd/Sc and Cu/Sc ratios are tabulated in A4.1 Table A9 and A4.2 Table A9, respectively. The As/Sc, Cd/Sc, Cu/Sc and Pb/Sc ratio profiles in FM01CM-1 and FM04-1-M are shown in Figs. 3.49 and 3.50, respectively. In FM01CM-1, the region of minimum Pb/Sc ratios (ignoring the minimum values between 67 and 75 cm due to the large Sc concentration peak) was found to occur

between 41 and 72 cm (*cf.* Section 3.5). In contrast, the As/Sc, Cd/Sc and Cu/Sc ratios at these depths were quite high, and indeed, in the case of As/Sc, at a maximum, with mean values of 4.3 ± 2.4, 0.48 ± 0.32 and 7.9 ± 3.1, for As/Sc, Cd/Sc and Cu/Sc, respectively. Also, when comparing these As/Sc, Cd/Sc and Cu/Sc ratios with the UCC As/Sc, Cd/Sc and Cu/Sc ratios of 0.29, 0.015 and 2.04, respectively, they were 15, 30 and 4-fold higher, respectively. In comparison, the mean Pb/Sc ratio at these depths (10 ± 5) was 4-fold higher than the UCC Pb/Sc ratio of 2.43, which is the same as that found for the corresponding Cu/Sc ratios. The elevated M/Sc ratios relative to the corresponding UCC M/Sc ratios, as mentioned in Section 3.5 for Pb, are due to the concentrations of these metals (As, Cd and Cu) being affected by anthropogenic inputs at all depths over the *ca.* 2500 years represented by FM01CM-1, but it is worth noting that there are also specific-element-related problems associated with the approach of using UCC concentrations (*cf.* Section 1.8.2).

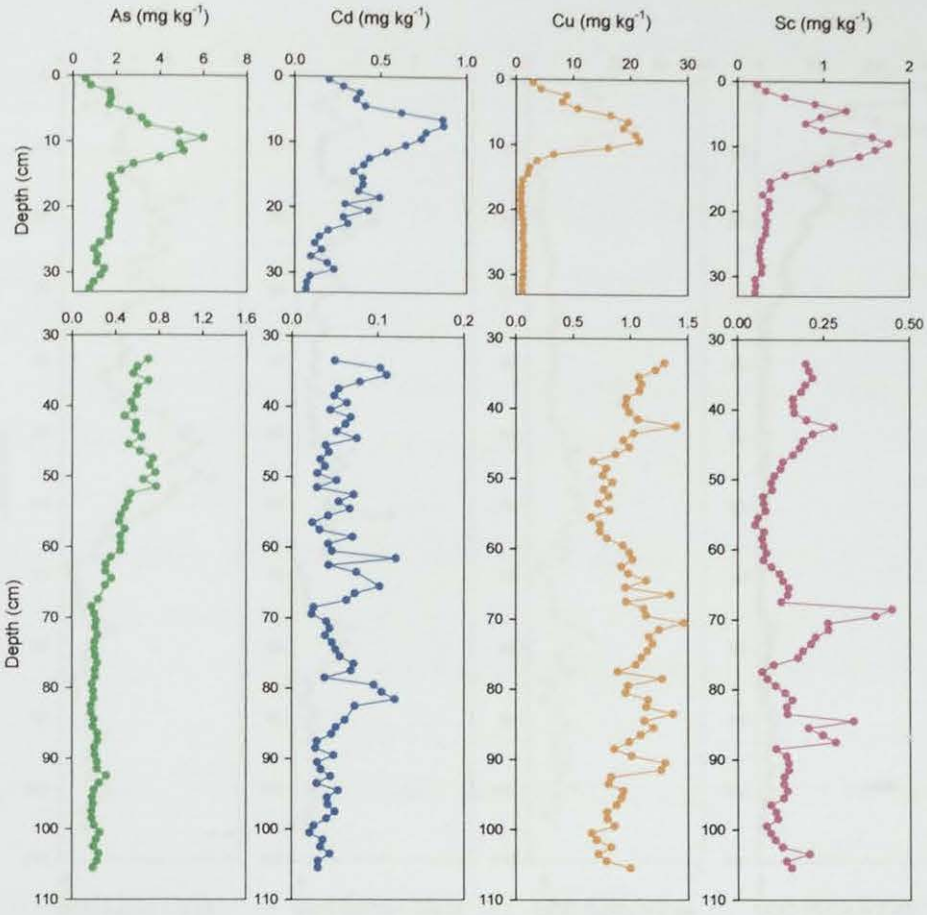

Figure 3.47: Depth profiles of As, Cd, Cu and Sc concentrations (mg kg^{-1}) from 0-33 cm and 33-106 cm in the FM01CM-1 peat core.

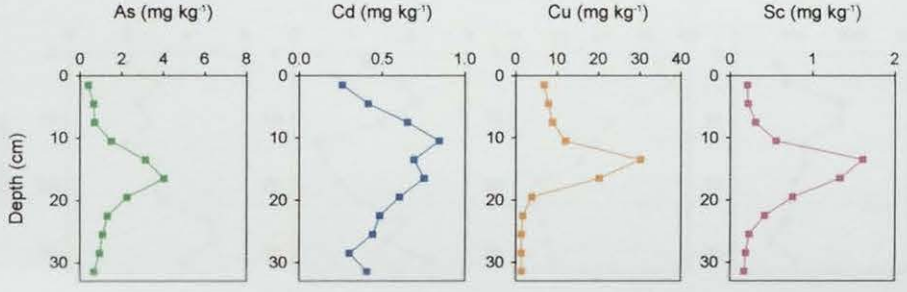

Figure 3.48: Depth profiles of As, Cd, Cu and Sc concentrations (mg kg^{-1}) in the FM04-1-M (0-33 cm) peat core.

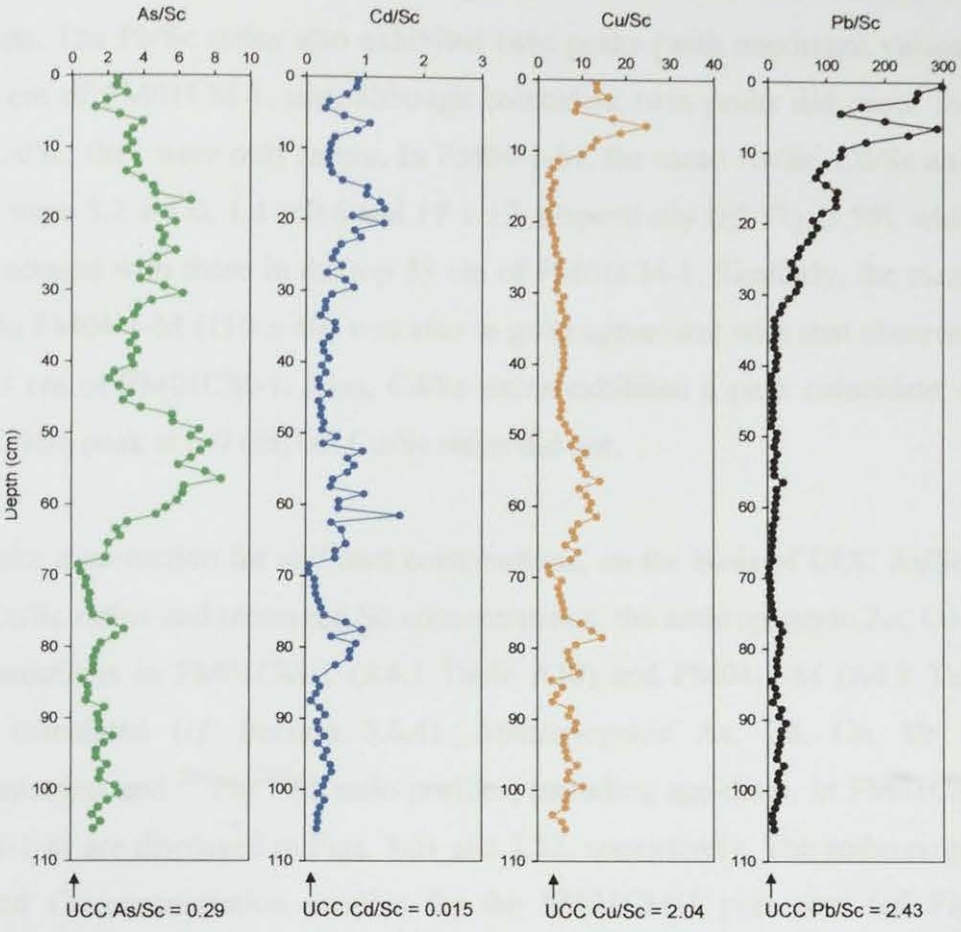

Figure 3.49: Depth profiles of As/Sc, Cd/Sc, Cu/Sc and Pb/Sc ratios in the FM01CM-1 (0-106 cm) peat core.

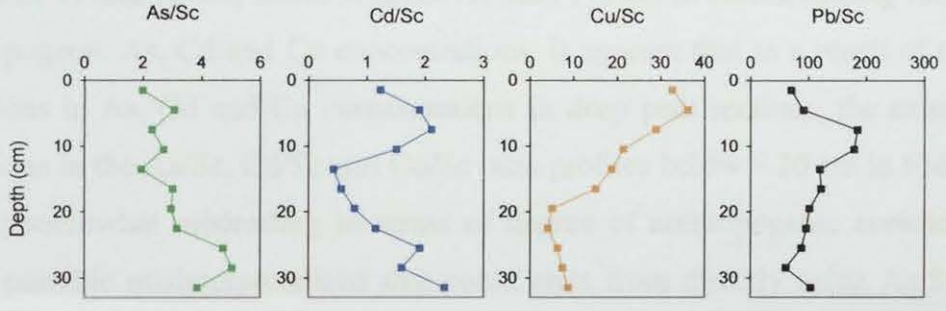

Figure 3.50: Depth profiles of As/Sc, Cd/Sc, Cu/Sc and Pb/Sc ratios in the FM04-1-M (0-33 cm) peat core.

In the upper 33 cm of FM01CM-1, the mean As/Sc, Cd/Sc and Cu/Sc ratios were 4.1 ± 1.2, 0.68 ± 0.30 and 7.4 ± 5.6, respectively, and were relatively close to the As/Sc, Cd/Sc and Cu/Sc ratios observed in the lower (41-72 cm) sections of FM01CM-1 (*cf.* Fig. 3.49). In comparison, the mean Pb/Sc ratio in the upper 33 cm

was 110 ± 80, which was ~ 10-fold greater than those in the lower (41-72 cm) sections. The Pb/Sc ratios also exhibited twin peaks (with maximum values) in the top 6-cm of FM01CM-1, and, although coincident twin peaks did occur for Cd/Sc and Cu/Sc, they were only minor. In FM04-1-M, the mean As/Sc, Cd/Sc and Cu/Sc ratios were 3.2 ± 1.0, 1.4 ± 0.6 and 17 ± 12, respectively (*cf.* Fig. 3.50), which were in agreement with those in the top 33 cm of FM01CM-1. Similarly, the mean Pb/Sc ratio in FM04-1-M (110 ± 40) was also in good agreement with that observed in the top 33 cm of FM01CM-1. Also, Cd/Sc ratios exhibited a peak coincident with the Pb/Sc ratio peak at 6-9 cm, but Cu/Sc ratios did not.

To make a correction for soil dust contributions, on the basis of UCC As/Sc, Cd/Sc and Cu/Sc ratios and measured Sc concentrations, the anthropogenic As, Cd and Cu concentrations in FM01CM-1 (A4.1 Table A10) and FM04-1-M (A4.2 Table A9) were calculated (*cf.* Section 3.6.4). Anthropogenic As, Cd, Cu, Pb and Sb concentration and $^{206}Pb/^{207}Pb$ ratio profiles, including age-dates, in FM01CM-1 and FM04-1-M are displayed in Figs. 3.51 and 3.52, respectively. The anthropogenic As, Cd and Cu concentration profiles for the FM01CM-1 peat core (*cf.* Fig. 3.51) indicate that the apparent increases in As/Sc, Cd/Sc and Cu/Sc ratios between the depths of 41 and 72 cm, mentioned above, didn't result in corresponding increases in anthropogenic As, Cd and Cu concentrations. It appears that as a result of the slight variations in As, Cd and Cu concentrations in deep peat sections, the extent of the variations in the As/Sc, Cd/Sc and Cu/Sc ratio profiles below ~ 20 cm in FM01CM-1 can be somewhat misleading in terms of degree of anthropogenic enrichment. To avoid possible misinterpretations that could arise from directly using As/Sc, Cd/Sc and Cu/Sc profiles to express anthropogenic enrichment in terms of estimated anthropogenic enrichment factors, the anthropogenic As, Cd and Cu concentration profiles alone (*cf.* Figs. 3.51 and 3.52) will be used in Section 3.8.3.3.3 in order to interpret historical trends in anthropogenic As, Cd and Cu.

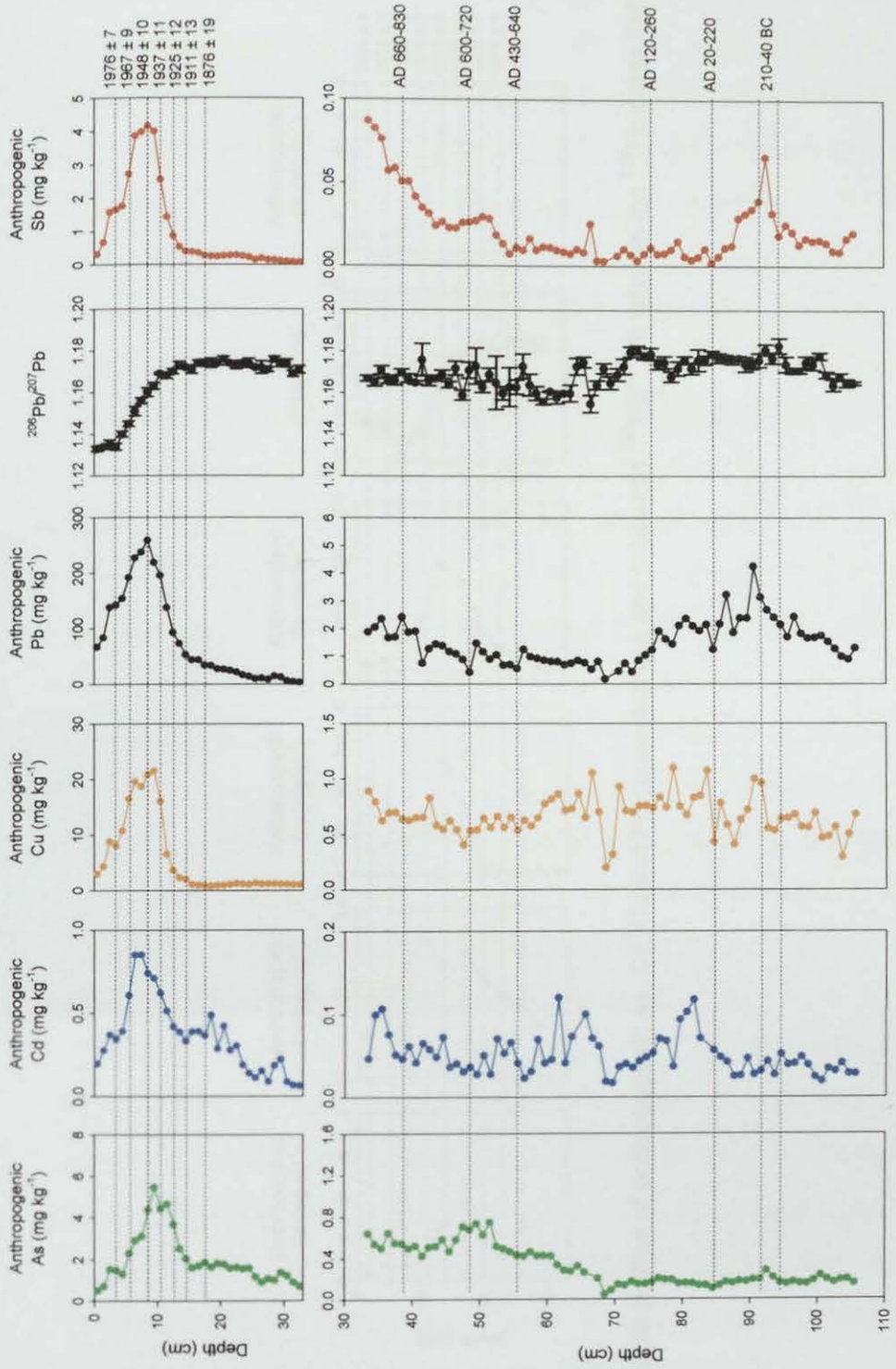

Figure 3.51. Depth profiles of anthropogenic As, Cd, Cu, Pb and Sb concentrations and measured $^{206}Pb/^{207}Pb$ ratios from 0-33 cm and 33-106 cm in the ^{210}Pb- and ^{14}C-dated FM01CM-1 peat core.

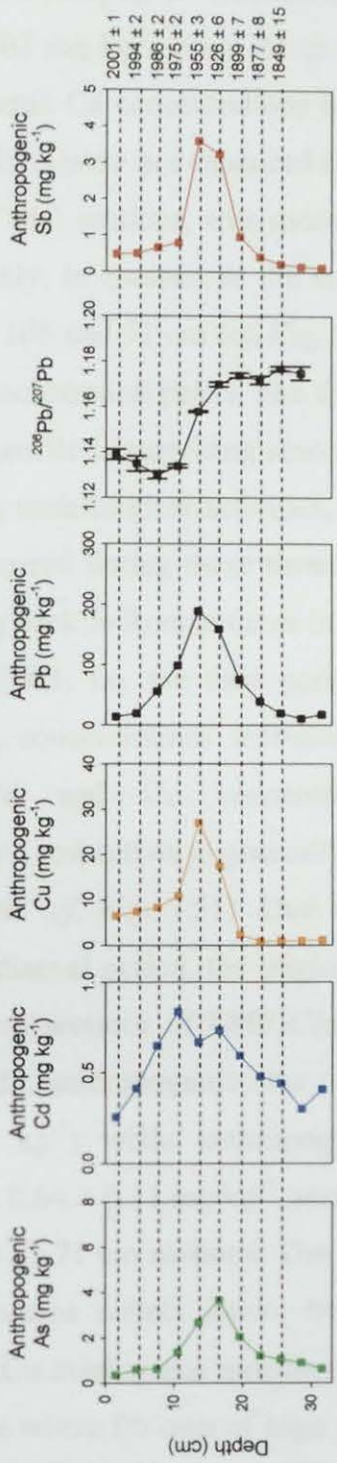

Figure 3.52: Depth profiles of anthropogenic As, Cd, Cu and Pb concentrations and measured $^{206}Pb/^{207}Pb$ ratios in the ^{210}Pb-dated FM04-1-M (0-33 cm) peat core.

3.8.3.3.3 Historical trends of anthropogenic As, Cd and Cu deposition

Pre-industrial atmospheric As, Cd and Cu sources and deposition

From 71 to 106 cm in FM01CM-1, i.e. the time period representing the pre-Roman and Roman period, anthropogenic As concentrations were at a minimum with a mean value of 0.17 ± 0.03 mg kg^{-1}. From 71 to 106 cm, with the exception of the slight peak in anthropogenic Cd concentrations between 83 and 80 cm, anthropogenic Cd and Cu concentrations were not enhanced relative to concentrations in the rest of the 33-106 cm FM01CM-1 sections, with mean values of 0.047 ± 0.023 and 0.68 ± 0.18 mg kg^{-1}, respectively, in contrast to the enhancement in Pb and Sb concentrations observed between 106 and 71 cm (*cf.* Fig. 3.51). The absence of pre-Roman/Roman As, Cd and Cu concentration peaks, like that observed in the anthropogenic Pb and Sb concentration profile is surprising since As, Cd and Cu are also emitted into the atmosphere during metallurgical activities, such as Pb and Cu mining and smelting processes that occurred during these times. Also, Shotyk *et al.* (1996) reported As enrichments dating back to Roman times in a peat core from Switzerland. From 53 to 71 cm in FM01CM-1, i.e. the time period representing the post-Roman period, anthropogenic As concentrations increased (mean 0.33 ± 0.14 mg kg^{-1}), while anthropogenic Cd and Cu concentrations (mean 0.065 ± 0.050 and 0.68 ± 0.21 mg kg^{-1}, respectively) generally remained the same as those in the lower 71-106 cm sections (*cf.* Fig. 3.51). Due to the lack of archaeological knowledge about this pre-Mediaeval period, the origin of these As increases is rather uncertain. In the 53 to 33 cm sections of FM01CM-1, i.e. the time period representing the Mediaeval period, anthropogenic As concentrations increased again (mean 0.58 ± 0.09 mg kg^{-1}) while anthropogenic Cd and Cu concentrations (mean 0.055 ± 0.022 and 0.64 ± 0.11 mg kg^{-1}, respectively) generally remained the same as those in the lower 53-71 cm sections. The increased As concentrations in these peat sections could perhaps reflect inputs from the developing metal industry (e.g. increased Pb and Cu mining and smelting) during Mediaeval times, particularly in continental Europe where Pb ores of high Ag content, and correspondingly high As contents, were exploited (Craddock, 1995; Mass *et al.*, 2002).

Industrial and post-industrial atmospheric As, Cd and Cu sources and deposition

As

Above 33 cm in FM01CM-1, anthropogenic As concentrations increased from 0.71 mg kg^{-1} at 33 cm (for which no age-date was available) to 1.6 mg kg^{-1} at 14 cm (*ca.* 1911 ± 13 A.D.) (*cf.* Fig. 3.51). Similarly, from the bottom of the FM04-1-M core (*ca.* late 1700s A.D.), anthropogenic As concentrations increased from 0.63 mg kg^{-1} to 2.0 mg kg^{-1} at 18 cm (*ca.* 1899 ± 7 A.D.) (*cf.* Fig. 3.52). These increases in As are most likely to be due to a combination of both metallurgical and coal combustion activities during this industrial period. After 1911 A.D. in FM01CM-1 and 1899 A.D. in FM04-1-M, anthropogenic As concentrations continued to increase, reaching a maximum of 5.5 mg kg^{-1} at *ca.* 1943 A.D. in FM01CM-1 (predating the maximum anthropogenic Pb (260 mg kg^{-1}) and Sb (4.2 mg kg^{-1}) concentrations by *ca.* 5 years), and reaching a maximum of 3.7 mg kg^{-1} at *ca.* 1926 A.D. in FM04-1-M (predating the maximum anthropogenic Pb (190 mg kg^{-1}) and Sb (3.6 mg kg^{-1}) concentrations by 29 years) (*cf.* Figs. 3.48 and 3.49). Note that the apparent "discrepancy" between 5 and 29 years in FM01CM-1 and FM04-1-M is a consequence of the greater resolution with the 1-cm thick sections in the former relative to the 3-cm thick sections in the latter. The dramatic increases in As concentrations have most likely resulted from coal combustion emissions at these times, when coal consumption in the UK continued to increase (Farmer *et al.*, 1999). Emissions from metallurgical activities, such as Pb and Cu-Ni production (*cf.* Table 1.2, Section 1.3.2.2), could have also contributed to an unknown extent. After 1943 A.D. in FM01CM-1 and 1926 A.D. in FM04-1-M, anthropogenic As concentrations decreased to 0.52 mg kg^{-1}, at the top of FM01CM-1 (*ca.* mid 1980s A.D.), and 0.72 mg kg^{-1} at *ca.* 1986 A.D. in FM04-1-M. The timings for the onset of these decreases seem somewhat premature since heavy industry and coal consumption did not go into decline in the UK until after the second half of the 20^{th} century A.D. (Farmer *et al.*, 1999). During the post-industrial period (i.e. post-1970 A.D.), however, it is worth noting that emissions from oil combustion and waste incineration (*cf.* Table

1.2, Section 1.3.2.2) perhaps became more important (Department of Trade and Industry, 1998; Matschullat, 2000; National Atmospheric Emissions Inventory, 2006). After 1986 A.D. in FM04-1-M, anthropogenic As concentrations continued to decrease slowly reaching a minimum of 0.42 mg kg^{-1} at *ca.* 2001 A.D (*cf.* Fig. 3.52), reflecting the decline in oil combustion, with the increasing use of natural gas (Department of Trade and Industry, 1998; National Atmospheric Emissions Inventory, 2006), as well as tighter emission controls following the introduction of legislation on air quality in the UK (MacKenzie *et al.*, 1998; Famer *et al.*, 1999).

Cd

Above 33 cm in FM01CM-1, anthropogenic Cd concentrations increased from 0.065 mg kg^{-1} at 33 cm (for which no age-date was available) to 0.39 mg kg^{-1} at 14 cm (*ca.* 1911 ± 13 A.D.) (*cf.* Fig. 3.51). Similarly, from the bottom of the FM04-1-M core (*ca.* late 1700s A.D.), anthropogenic Cd concentrations increased from 0.41 mg kg^{-1} to 0.59 mg kg^{-1} at 18 cm (*ca.* 1899 ± 7 A.D.) (*cf.* Fig. 3.52). Again, as found for As, these Cd increases are probably due to metallurgical activities and coal combustion during this industrial period. After 1911 A.D. in FM01CM-1 and 1899 A.D. in FM04-1-M, anthopogenic Cd concentrations continued to increase, reaching a maximum of 0.85 mg kg^{-1} between *ca.* 1953 and 1960 A.D. in FM01CM-1 (postdating the maximum anthropogenic Pb (260 mg kg^{-1}) and Sb (4.2 mg kg^{-1}) concentrations by *ca.* 5 years), and reaching a maximum of 0.84 mg kg^{-1} at *ca.* 1975 A.D. in FM04-1-M (postdating the maximum anthropogenic Pb (190 mg kg^{-1}) and Sb (3.6 mg kg^{-1}) concentration by 20 years) (*cf.* Figs. 3.51 and 3.52). These marked increases in Cd concentrations have most likely resulted from a combination of emission sources such as metallurgical activities and coal combustion (*cf.* Table 1.2, Section 1.3.2.2). After 1960 A.D. in FM01CM-1 and 1975 A.D. in FM04-1-M, anthropogenic Cd concentrations decreased to 0.20 mg kg^{-1} at the top of FM01CM-1 (*ca.* mid 1980 A.D.) and to 0.37 mg kg^{-1} at *ca.* 1986 A.D. in FM04-1-M. These decreases reflect the decline in heavy industry in the later part of the 20^{th} century A.D., when emissions from oil combustion and waste incineration (*cf.* Table 1.2, Section 1.3.2.2) became more important (Department of Trade and Industry,

1998; National Atmospheric Emissions Inventory, 2006). After 1986 A.D. in FM04-1-M, anthropogenic Cd concentrations decreased more rapidly, reaching a minimum of 0.20 mg kg^{-1} at *ca.* 2001 A.D (*cf.* Fig. 3.52), perhaps reflecting the decline in oil combustion (Department of Trade and Industry, 1998; National Atmospheric Emissions Inventory, 2006), as well as tighter emission tighter emission controls in the UK during this post-industrial period (MacKenzie *et al.*, 1998; Famer *et al.*, 1999).

Cu

Above 33 cm in FM01CM-1, anthropogenic Cu concentrations increased from 0.71 mg kg^{-1} at 33 cm (for which no age-date was available) to 1.5 mg kg^{-1} at 12 cm (*ca.* 1925 ± 12 A.D.) (*cf.* Fig. 3.51). From the bottom of the FM04-1-M core (*ca.* late 1700s A.D.), however, anthropogenic Cu concentrations increased more markedly from 1.2 mg kg^{-1} to 17 mg kg^{-1} at 15 cm (*ca.* 1926 ± 6 A.D.) (*cf.* Fig. 3.52). The onset of the greatest anthropogenic Cu concentration increases occurred at a later date (*ca.* 1925 A.D. compared with 1911 A.D.) than those of As and Cd, suggesting that emissions from metallurgical activities and fossil fuel combustion were less important for Cu in the earlier years of the industrial period. After 1925 A.D. in FM01CM-1 and 1926 A.D. in FM04-1-M, anthopogenic Cu concentrations increased, reaching a maximum of ~ 18 mg kg^{-1} between *ca.* 1943 and 1960 A.D. in FM01CM-1 (incorporating the maximum anthropogenic Pb (260 mg kg^{-1}) and Sb (4.2 mg kg^{-1}) concentrations), and reaching a maximum of 27 mg kg^{-1} at *ca.* 1955 A.D. in FM04-1-M (coincident with the maximum anthropogenic Pb (190 mg kg^{-1}) and Sb (3.6 mg kg^{-1}) concentrations) (*cf.* Figs. 3.51 and 3.52). These dramatic increases in Cu concentrations have most likely resulted from emissions from Cu-Ni, Zn-Cd and non-ferrous metal production and coal combustion (*cf.* Table 1.2, Section 1.3.2.2). After 1960 A.D. in FM01CM-1 and 1975 A.D. in FM04-1-M, anthropogenic Cu concentrations decreased to 2.6 mg kg^{-1} at the top of FM01CM-1 (*ca.* mid 1980 A.D.) and to 8.3 mg kg^{-1} at *ca.* 1986 A.D. in FM04-1-M. These decreases reflect the decline in heavy industry in the later part of the 20^{th} century A.D., when emissions from oil combustion and waste incineration (*cf.* Table 1.2,

Section 1.3.2.2) perhaps became important (Department of Trade and Industry, 1998; National Atmospheric Emissions Inventory, 2006). After 1986 A.D. in FM04-1-M, anthropogenic Cu concentrations decreased to a minimum of 6.5 mg kg^{-1} at *ca.* 2001 A.D (*cf.* Fig. 3.52), reflecting the decline in oil combustion (Department of Trade and Industry, 1998; National Atmospheric Emissions Inventory, 2006) and tighter emission controls in the UK during this post-industrial period (MacKenzie *et al.*, 1998; Famer *et al.*, 1999). It is worth noting that anthropogenic Cu concentrations at Flanders Moss remained relatively high, compared with As and Cd, after the late 1980s A.D. (*cf.* Fig. 3.52), declining less steeply relative to As, Cd and Pb, perhaps indicating emissions of Cu from comparatively new recent sources (i.e. not oil combustion or waste incineration). Such recent sources could include the release of Cu from automotive exhausts, as a result of its recent use as an antioxidant in motor oil, instead of traditional amine antioxidants (Cadle *et al.*, 1999; Chemical Research Communications, 2003), and new automotive brake linings and tyres (Sternbeck *et al.*, 2002; Boulter, 2004).

3.8.3.3.4 Historical trends in depositional fluxes and inventories of anthropogenic As, Cd and Cu

As performed earlier for Pb and Sb (Sections 3.6.4 and 3.8.1.3.3), the anthropogenic depositional fluxes of As, Cd and Cu were calculated for FM04-1-M (A4.2 Table A11). These fluxes, since the mid-19th century A.D., are plotted along with the anthropogenic Pb fluxes and measured $^{206}Pb/^{207}Pb$ ratios, *versus* ^{210}Pb-derived calendar dates for FM04-1-M in Fig. 3.53. Depositional fluxes of anthropogenic As were at a maximum of ~ 0.48 mg m^{-2} y^{-1} during the mid-1920s A.D. (*cf.* Fig. 3.53). For FM01CM-2, the FM01CM-1 sister core, Yafa (2004) and Farmer *et al.* (2006) found maximum As fluxes (~ 2.0 mg m^{-2} y^{-1}) during the 1930s and 1950s A.D. Despite the greater fluxes observed for that peat core, the trends are generally in agreement with those observed for the FM04-1-M core. Depositional fluxes of anthropogenic Cd were at a maximum (ranging from ~ 0.076 to 0.12 mg m^{-2} y^{-1}) between *ca.* 1900 and the mid-1980s A.D. (*cf.* Fig. 3.53), while those of

anthropogenic Cu were at a maximum (3.1 mg m^{-2} y^{-1}) during the mid-1950s A.D. (*cf.* Fig. 3.53).

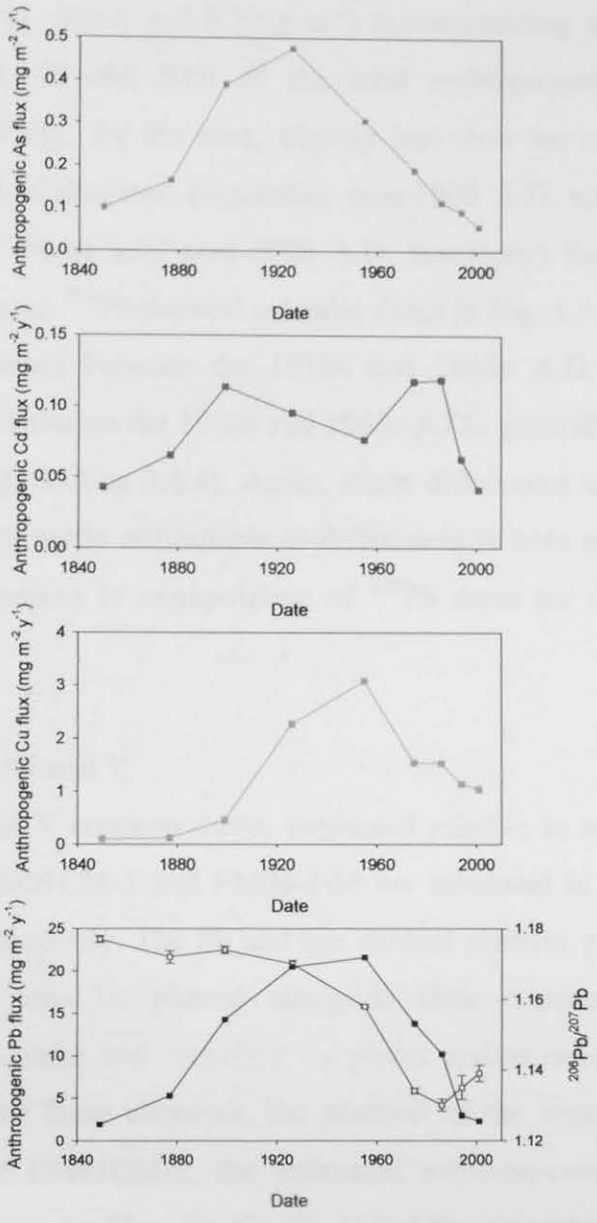

Figure 3.53: Calculated atmospheric depositional fluxes of anthropogenic As, Cd, Cu and Pb (mg m^{-2} y^{-1}) (closed squares) and the measured $^{206}Pb/^{207}Pb$ ratios (open squares) for the FM04-1-M core *versus* ^{210}Pb-derived dates since 1840 A.D.

Total anthropogenic As, Cd and Cu inventories in FM01CM-1 and FM04-1-M were calculated, as performed earlier for Pb and Sb (Section 3.6.4 and 3.8.1.3.3). The total anthropogenic As, Cd and Cu inventories for FM01CM-1 (i.e. from *ca.* 500 B.C. to mid-1980s A.D., given that the very top of the core was lost during collection) were

0.11 g m^{-2}, 0.019 g m^{-2} and 0.24 g m^{-2}, respectively. The total anthropogenic As, Cd and Cu inventories for FM04-1-M (i.e. from *ca.* late 1700s to 2004 A.D.) were 0.047, 0.016 and 0.22 g m^{-2}, respectively. For FM01CM-1, the post-1800 A.D. As, Cd and Cu inventories (0.081, 0.015 and 0.20 g m^{-2}) (corresponding to peat sections 0-23 cm) constituted 74, 79 and 83% of the total anthropogenic As, Cd and Cu inventories, respectively, for the core, slightly less than the corresponding values (95%) found for Pb. Calculated cumulative post-1800 A.D. anthropogenic As, Cd and Cu inventories (% of total post-1800 A.D. inventory) for the Flanders Moss cores are plotted *versus* ^{210}Pb-derived calendar dates in Fig. 3.54. Maximum As and Cu deposition occurred between the 1910s and 1960s A.D. and maximum Cd deposition occurred between the 1900s and 1960s A.D., generally in agreement with that found for Pb (*cf.* Section 3.6.4). Again, slight differences in trends between the two cores are at least partly attributable to differences in core sectioning, as well as uncertainties with respect to extrapolation of ^{210}Pb dates for the FM01CM-1 core from FM01CM-2.

3.8.4 Co, Cr, Ni and V

Total Co, Cr, Ni and V concentrations, expressed relative to sectional 105°C-dried peat weights, for FM01CM-1 and FM04-1-M are tabulated in A4.1 Table A8 and A4.2 Table A8, respectively. The Pb and ash content profiles, presented in Sections 3.1 and 3.4, will also be plotted alongside their concentration profiles for comparison. Since uptake and recycling by plants and/or redox cycling processes may be important for these elements, the position of the vegetation-peat interface and, in the case of FM01CM-1, the estimated acrotelm-catotelm boundary, are indicated on their depth profiles. Co, Cr, Ni, V and Pb concentration and ash content profiles for FM01CM-1 and FM04-1-M are shown in Figs. 3.55 and 3.56, respectively.

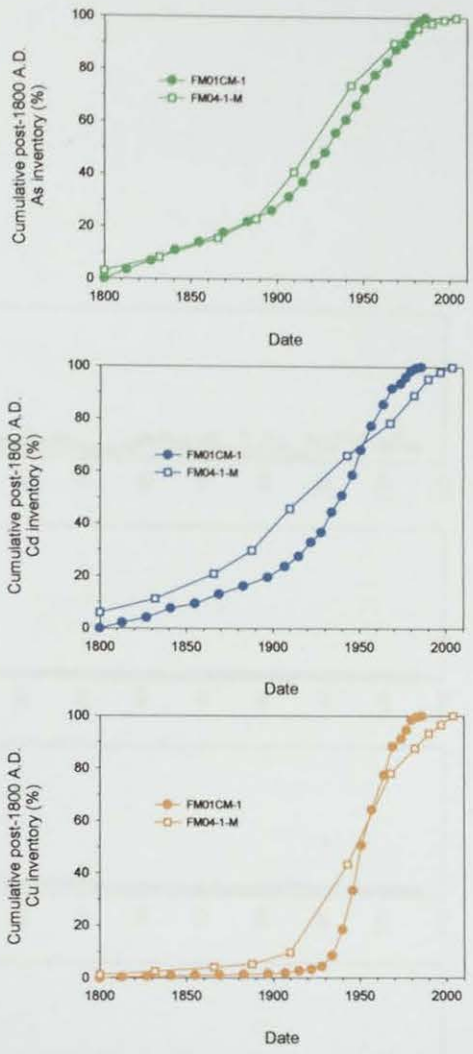

Figure 3.54: Calculated cumulative post-1800 A.D. anthropogenic As, Cd and Cu inventories (% of total post-1800 A.D. inventory) for the FM01CM-1 and FM04-1-M cores *versus* ^{210}Pb-derived dates. Note that dates in FM01CM-1 and FM04-1-M prior to *ca.* 1883 A.D. and *ca* 1832 A.D., respectively, were extrapolated. Also, dates in FM01CM-1 after *ca.* 1974 A.D. were extrapolated.

3.8.4.1 FM01CM-1

All four elements exhibited concentration peaks in the uppermost ~ 15 cm of the core, with the following maximum concentrations at the depths indicated, for each of the elements:

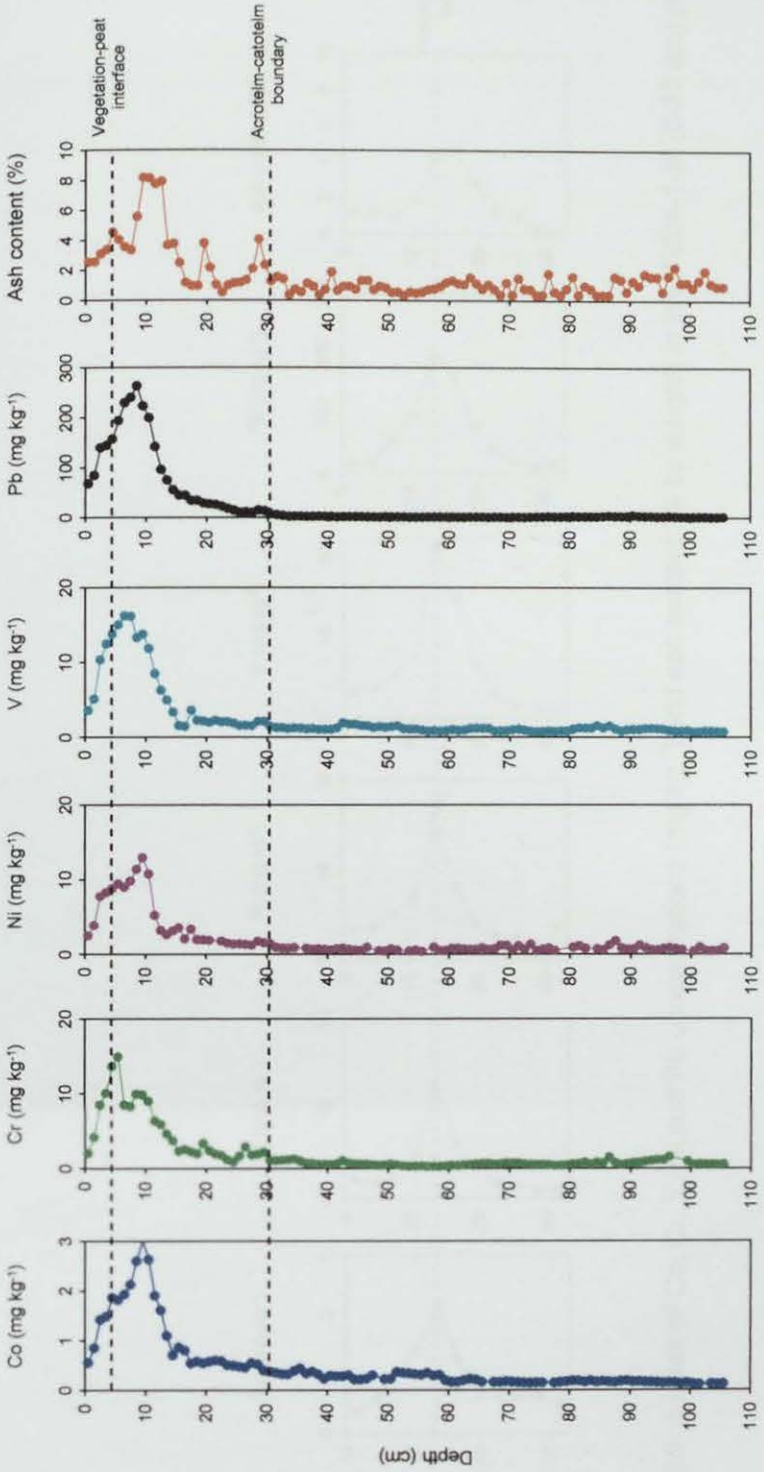

Figure 3.55: Depth profiles of Co, Cr, Ni, V and Pb concentrations (mg kg^{-1}) and ash content (% by weight) in the FM01CM-1 (0-106 cm) peat core.

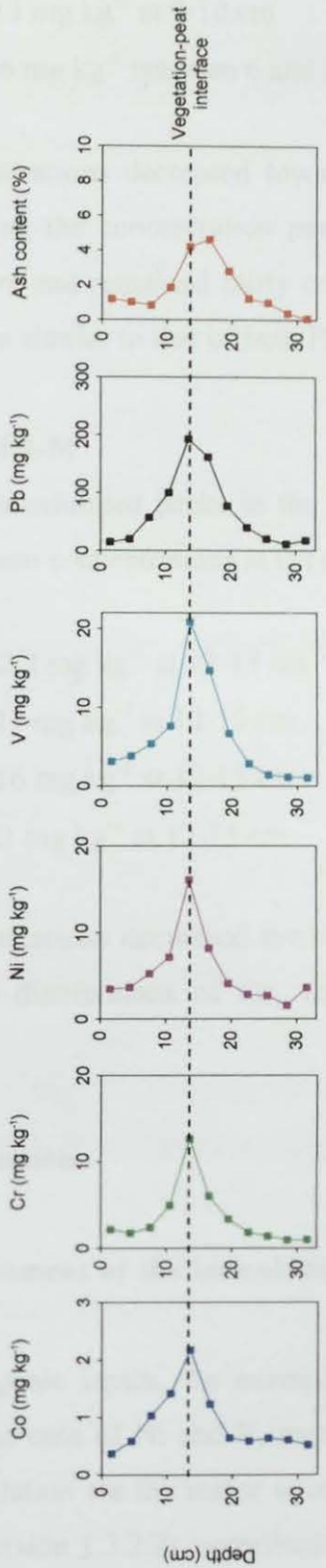

Figure 3.56: Depth profiles of Co, Cr, V, Ni and Pb concentrations (mg kg^{-1}) and ash content (% by weight) in the FM04-1-M (0-33 cm) peat core.

- Co – 3.0 mg kg^{-1} at 9-10 cm
- Cr – 15 mg kg^{-1} at 5-6 cm
- Ni – 13 mg kg^{-1} at 9-10 cm
- V – 16 mg kg^{-1} between 6 and 8 cm

Elemental concentrations decreased towards the top of the core and, in the peat sections underlying the concentration peaks, concentrations decreased towards the bottom of the core and remained fairly constant. In general the distributions of Co, Cr, Ni and V were similar to that of both Pb and the ash content (*cf.* Fig. 3.55).

3.8.4.2 FM04-1-M

All four elements exhibited peaks in the uppermost ~ 30 cm of the core, with the following maximum concentrations at the depths indicated:

- Co – 2.2 mg kg^{-1} at 12-15 cm
- Cr – 13 mg kg^{-1} at 12-15 cm
- Ni – 16 mg kg^{-1} at 12-15 cm
- V – 21 mg kg^{-1} at 12-15 cm

Elemental concentrations decreased towards the top and bottom of the core. As in FM01CM-1, the distributions of Co, Cr, Ni and V were similar to that of Pb (*cf.* Fig. 3.56).

3.8.4.3 Discussion

3.8.4.3.1 Assessment of the immobility of Co, Cr, Ni and V in ombrotrophic peat

Again, anthropogenic inputs, for example, from fuel combustion, particularly oil combustion in the case of Ni and V, metal production, steel and Fe manufacturing and waste incineration are the major source of Co, Cr, Ni and V to the atmosphere (*cf.* Table 1.2, Section 1.3.2.2), contributions from soil dust inputs being minor. The

behaviour of Co, Cr, Ni and V in peat bogs, however, is still not fully understood. It has been suggested that Ni and Co are subjected to post-depositional mobility and that their concentrations and mineralogical forms at the time of deposition as well as the pH of the bog waters are important (Rausch *et al.*, 2005a and b). It has also been suggested that Ni is more mobile than Pb and Cu in ombrotrophic peats and that the amount lost through migration is unknown (Nieminen *et al.* (2002). Krachler *et al.* (2003a), however, maintain that V, Cr and Ni are effectively immobile in ombrotrophic peats. The Co, Cr, Ni and V concentration profiles in the Flanders Moss cores (*cf.* Figs. 3.55 and 3.56) do appear to show anthropogenic increases like the Pb concentration profiles, indicating that these elements may also essentially be immobile in ombrotrophic peat. Also it is worth noting that the minor Co, Cr, Ni and V increases at the acrotelm-catotelm boundary (~ 30 cm) in the FM01CM-1 core, coincident with the slight increases in the ash content, other trace elements (As and Cd) and some major (Ca, Fe, Mg, Mn and S) and conservative elements (Al, Ti, Y and Zr), again provide further evidence (*cf.* Section 3.7) for the influence of soil dust inputs at this depth.

3.8.4.3.2 Use of Zr as a conservative "reference" element for Co, Cr, Ni and V

In Sections 3.5, 3.8.1.3.1 and 3.8.3.3.1, Sc was used as the conservative "reference" element from which M/Sc ratios and anthropogenic concentrations for Pb, Sb, As, Cd and Cu were calculated in order to eliminate contributions to concentrations of these elements from sources unrelated to direct anthropogenic inputs. In the case of the trace elements Co, Cd, Ni and V, however, Sc was unsuitable for use as a "reference element" as a result of the apparent inappropriateness of the UCC M/Sc ratios for these elements. When using V as an example, V, Sc and anthropogenic V (calculated using Sc) concentrations and V/Sc ratios in the FM01CM-1 core are plotted (Fig. 3.57), apparent "negative" concentrations of anthropogenic V are obtained over a significant part of the core. This further underlines the specific-element-related problems associated with the use of conservative elements and UCC M/X ratios to correct elemental concentrations for soil dust contributions (*cf.* Section 1.8.3). However, as it is necessary to eliminate contributions to Co, Cr, Ni and V from

sources unrelated to direct anthropogenic sources and since pre-anthropogenic M/Sc ratios from much greater peat depths were unavailable, Zr was chosen as the preferred conservative reference element for use with these elements. This was because the problem identified above, with the exception of a single "negative" anthropogenic V concentration obtained for the 94-95 cm section in FM01CM-1, did not occur when Zr was used instead of Sc.

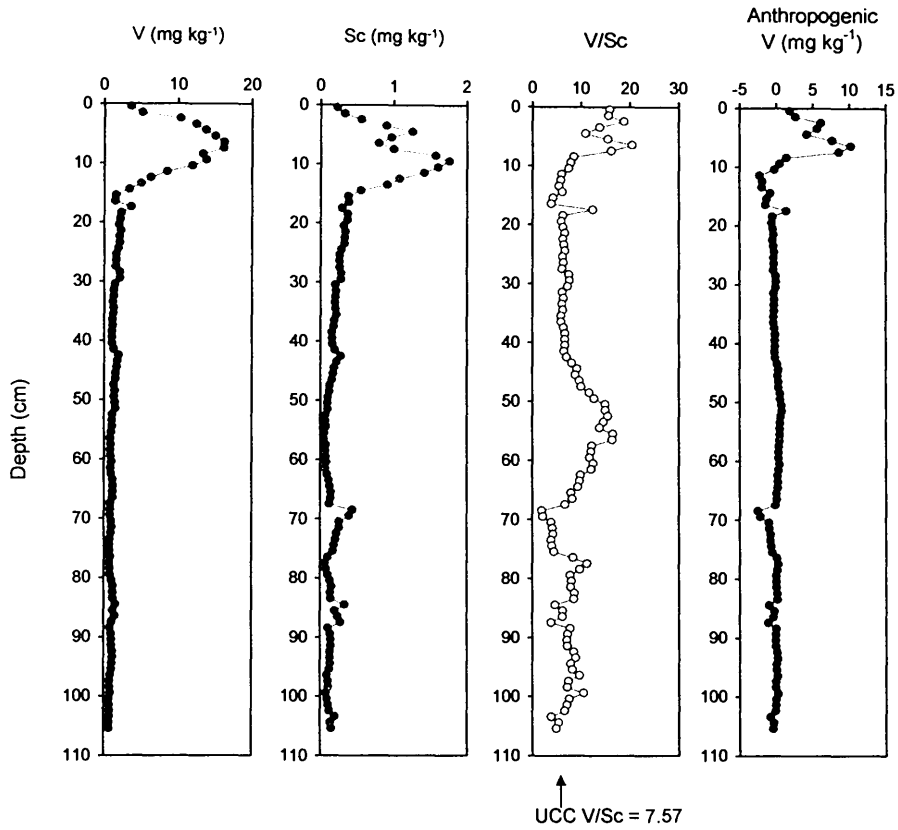

Figure 3.57: Depth profiles of V, Sc and anthropogenic V concentrations (mg kg^{-1}) in the FM01CM-1 (0-106 cm) peat core.

3.8.4.3.3 The use of Zr as an indicator of Co, Cr, Ni and V soil dust input

The Co, Cr, Ni, V and Zr concentration profiles in FM01CM-1 and FM04-1-M are shown in Figs. 3.58 and 3.59, respectively. Note the changes in scale on the Co (5-fold), Cr, Ni and V (10-fold) and Zr (4-fold) concentrations on going from 0-33 cm to 33-106 cm in the FM01CM-1 core. To eliminate contributions to Co, Cr, Ni and V from sources unrelated to direct anthropogenic inputs in the Co, Cr, Ni and V profiles, Co/Zr, Cr/Zr, Ni/Zr and V/Zr ratios can be used in the same way that M/Sc ratios were used for As, Cd, Cu, Pb and Sb in Sections 3.5, 3.6 and 3.8.3.3.2. The

Co/Zr, Cr/Zr, Ni/Zr and V/Zr ratios are tabulated in A4.1 Table A9 and A4.2 Table A9, respectively.

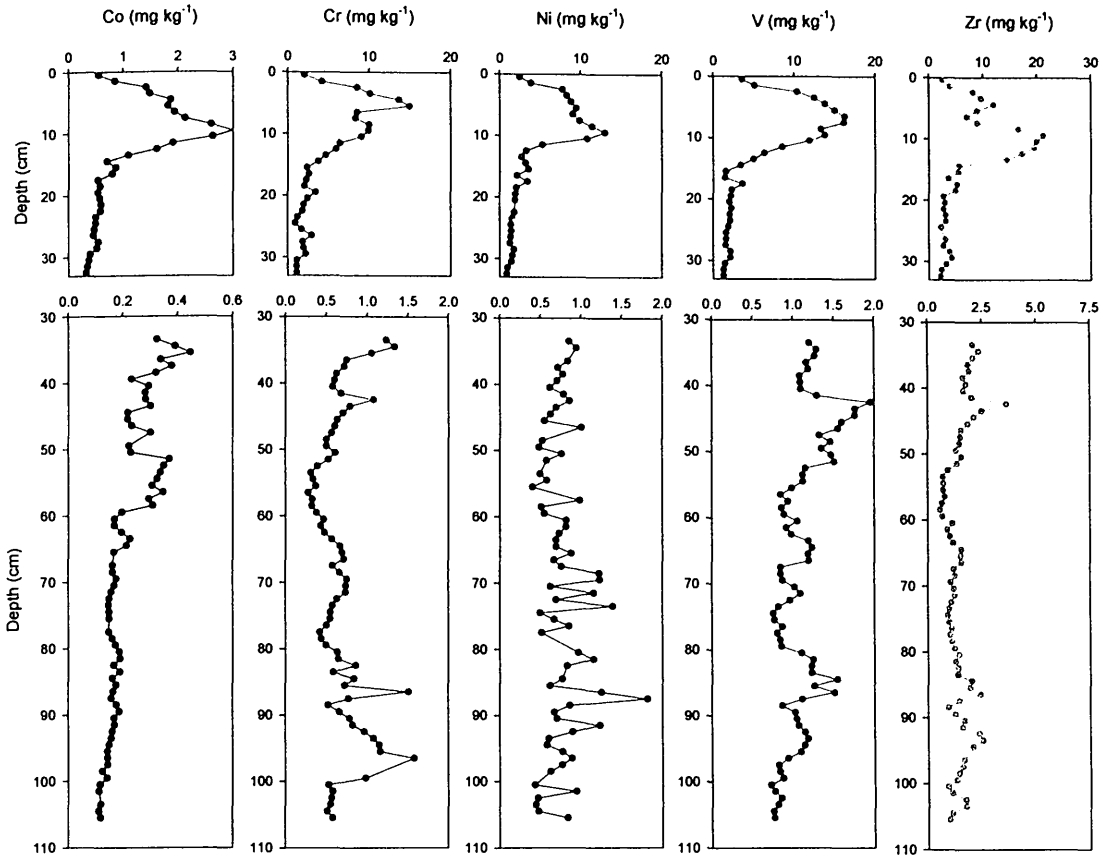

Figure 3.58: Depth profiles of Co, Cr, Ni, V and Zr concentrations (mg kg^{-1}) from 0-33 cm and 33-106 cm in the FM01CM-1 peat core.

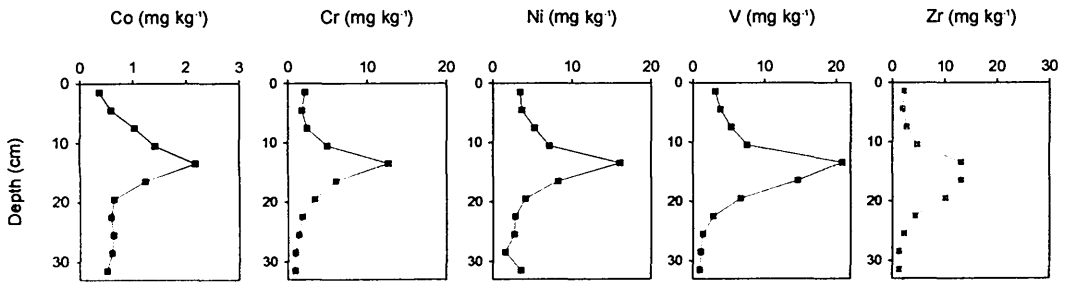

Figure 3.59: Depth profiles of Co, Cr, Ni, V and Zr concentrations (mg kg^{-1}) in the FM04-1-M (0-33 cm) peat core.

The Co/Zr, Cr/Zr, Ni/Zr, V/Zr and Pb/Zr ratio profiles in FM01CM-1 and FM04-1-M are shown in Figs. 3.60 and 3.61, respectively.

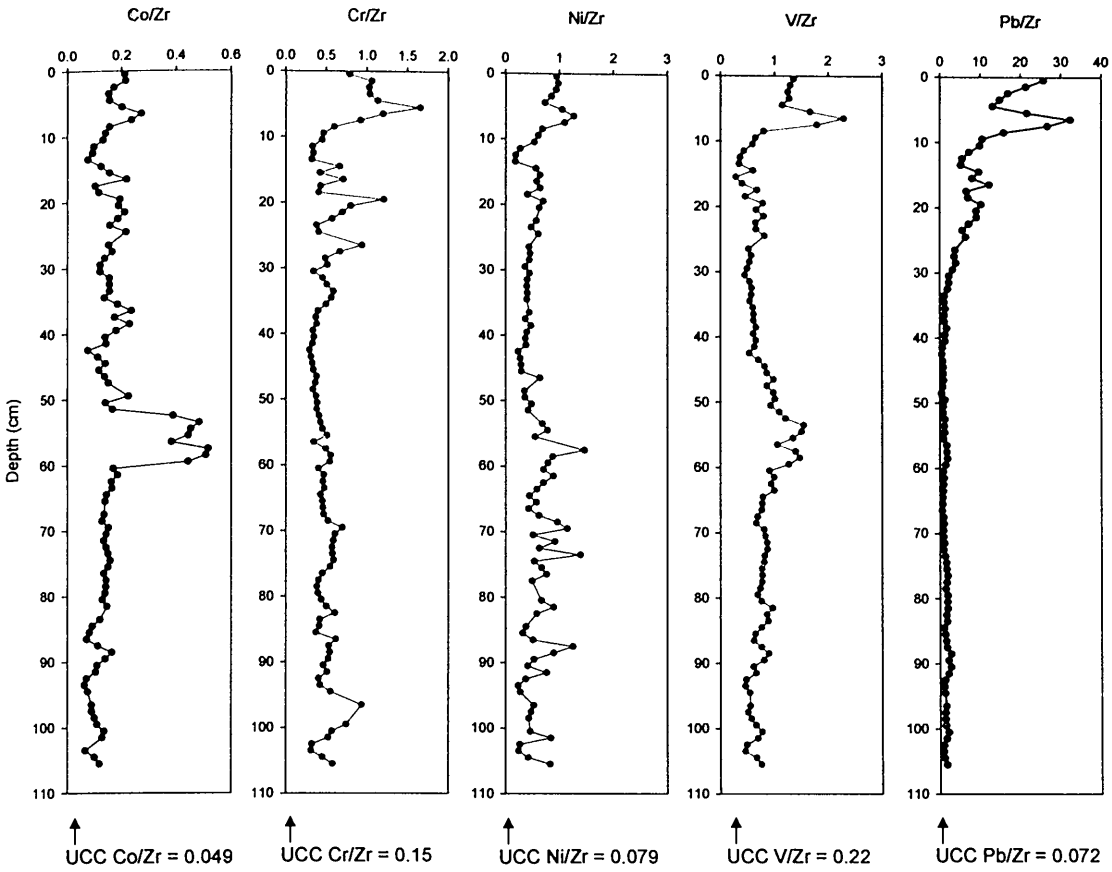

Figure 3.60: Depth profiles of Co/Zr, Cr/Zr, Ni/Zr, V/Zr and Pb/Zr ratios in the FM01CM-1 (0-106 cm) peat core.

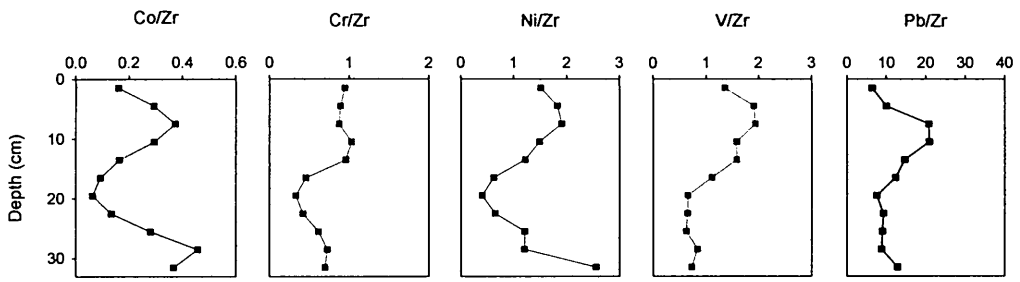

Figure 3.61: Depth profiles of Co/Zr, Cr/Zr, Ni/Zr, V/Zr and Pb/Zr ratios in the FM04-1-M (0-33 cm) peat core.

In FM01CM-1, the region of minimum Pb/Zr ratios occurred between 41 and 72 cm (*cf.* Section 3.5) and the mean Co/Zr, Cr/Zr, Ni/Zr and V/Zr ratios at these depths were 0.23 ± 0.14, 0.44 ± 0.09, 0.62 ± 0.29 and 0.98 ± 0.27, respectively. As found for the As/Sc, Cd/Sc and Cu/Sc ratios (*cf*, Fig. 3.49, Section 3.8.3.3.2), the Co/Zr, Ni/Zr and V/Zr ratios were high at these depths, and, indeed, in the case of Co/Sc, at a maximum. Also when comparing these Co/Zr, Cr/Zr, Ni/Zr and V/Zr ratios with

the UCC ratios of 0.049, 0.15, 0.079 and 0.22, respectively, they were 5-, 3-, 8- and 4-fold higher for Co/Zr, Cr/Zr, Ni/Zr and V/Zr, respectively. In comparison, the mean Pb/Zr ratio at these depths (1.0 ± 0.3) was 14-fold higher than the UCC Pb/Zr ratio of 0.072. The elevated M/Zr ratios relative to the corresponding UCC M/Zr ratios (*cf.* Section 3.5 for Pb) are probably due to the effects of anthropogenic inputs at all depths over the *ca.* 2500 years represented by FM01CM-1.

In the upper 33 cm of FM01CM-1, the mean Co/Zr, Cr/Zr, Ni/Zr and V/Zr ratios were 0.16 ± 0.05, 0.69 ± 0.33, 0.62 ± 0.27 and 0.81 ± 0.47, respectively, and as found in Section 3.8.3.2.2 for the As/Sc, Cd/Sc and Cu/Sc ratios, were relatively close to the Co/Zr, Cr/Zr, Ni/Zr and V/Zr ratios observed in the lower (41-72 cm) sections of FM01CM-1 (*cf.* Fig. 3.60). In comparison, the mean Pb/Zr ratio in the upper 33 cm was 11 ± 8, which, as found for the Pb/Sc ratios in Section 3.8.3.2.2, was ~ 10-fold greater than those in the lower (41-72 cm) sections. In FM04-1-M, the mean Co/Zr, Cr/Zr, Ni/Zr and V/Zr ratios were 0.24 ± 0.13, 0.72 ± 0.24, 1.3 ± 0.6 and 1.2 ± 0.5, respectively (*cf.* Fig. 3.61), which were in close agreement with those in the top 33 cm of FM01CM-1. In comparison, the mean Pb/Zr ratio in FM04-1-M (12 ± 5) was also in good agreement with that observed in the top 33 cm of FM01CM-1.

A correction for soil dust contributions, on the basis of UCC Co/Zr, Cr/Zr, Ni/Zr and V/Zr ratios and measured Zr concentrations, the anthropogenic Co, Cr, Ni and V concentrations in FM01CM-1 (A4.1 Table A11) and FM04-1-M (A4.2 Table A10) were calculated (*cf.* Section 3.6.4). For comparison, anthropogenic Pb concentrations were also calculated on the basis of measured and UCC Pb/Zr ratios and measured Zr concentrations (A4.1 Table A11 and A4.2 Table A10). Anthropogenic Co, Cr, Ni, V and Pb concentration and $^{206}Pb/^{207}Pb$ ratio profiles, including age-dates, in FM01CM-1 and FM04-1-M are displayed in Figs. 3.62 and 3.63, respectively.

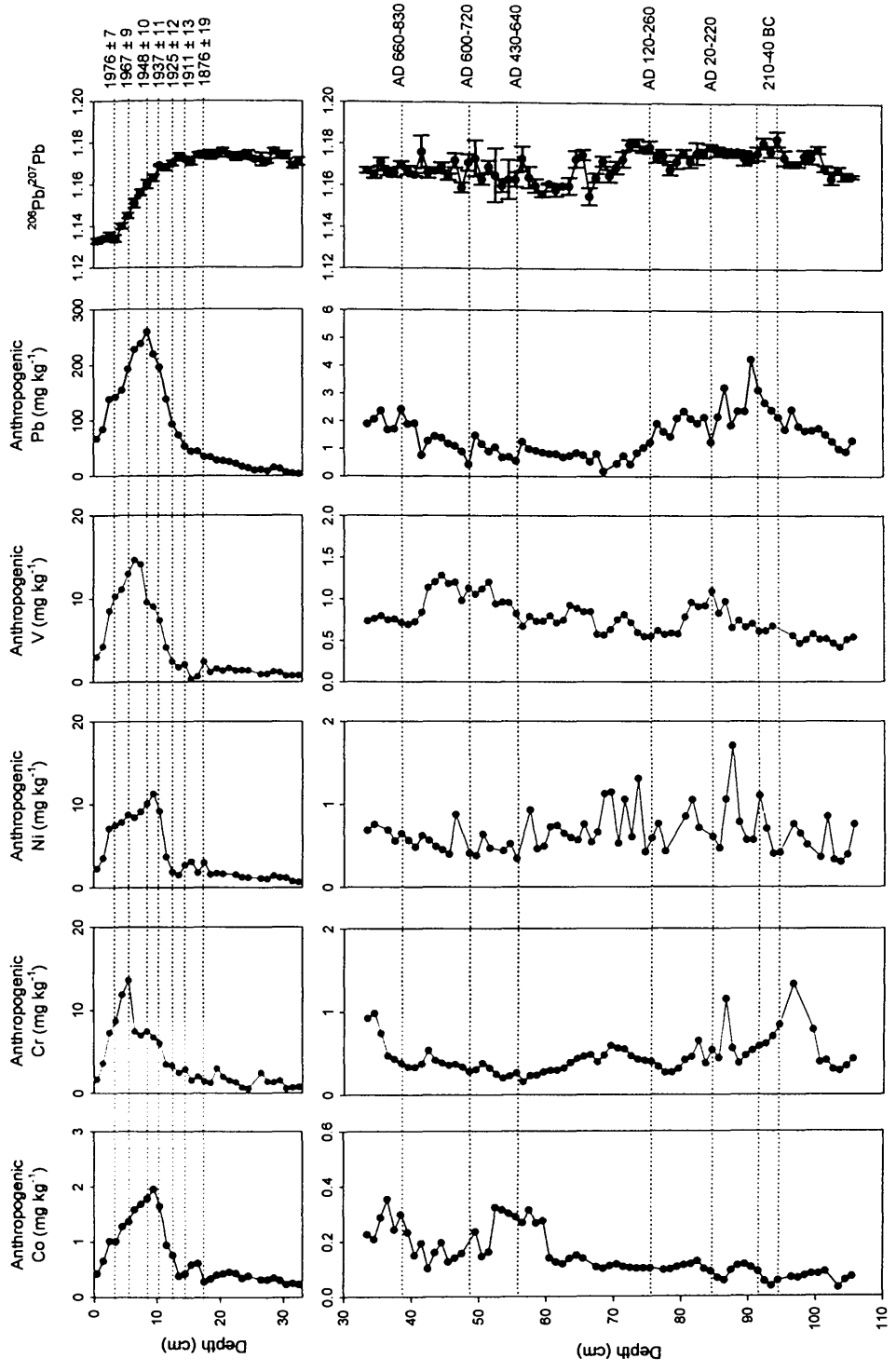

Figure 3.62: Depth profiles of anthropogenic Co, Cr, Ni, V and Pb concentrations (calculated using Zr as the conservative element) and measured $^{206}Pb/^{207}Pb$ ratios, from 0-33 cm and 33-106 cm in the ^{210}Pb- and ^{14}C-dated FM01CM-1 peat core.

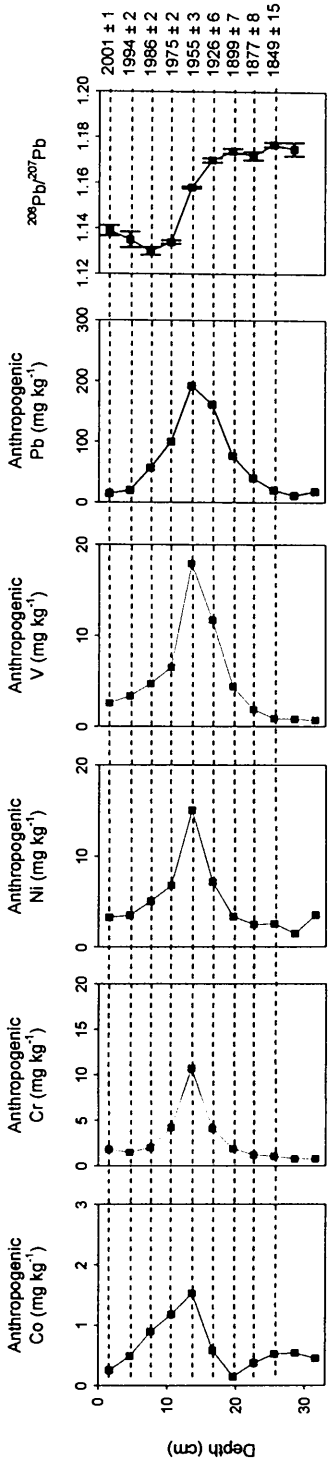

Figure 3.63: Depth profiles of anthropogenic Co, Cr, Ni, V and Pb concentrations (calculated using Zr as the conservative element) and measured $^{206}Pb/^{207}Pb$ ratios in the ^{210}Pb-dated FM04-1-M (0-33 cm) peat core.

As with the anthropogenic As, Cd and Cu concentration profiles (*cf.* Figs. 3.51 and 3.52, Section 3.8.3.3.2), the anthropogenic Co, Cr, Ni and V concentration profiles for the FM01CM-1 peat core (*cf.* Fig. 3.62) indicate that the apparent increases in Co/Zr, Ni/Zr and V/Zr ratios between the depths of 41 and 72 cm (*cf.* Fig. 3.60), didn't result in corresponding increases in anthropogenic Co, Ni and V concentrations. As found for the As/Sc, Cd/Sc and Cu/Sc ratios in the Flanders Moss cores (*cf.* Section 3.8.3.3.2), it appears that as a result of the slight variations in Co, Cr, Ni and V concentrations in deep peat sections, the Co/Zr, Cr/Zr, Ni/Zr and V/Zr ratio profiles can be somewhat misleading in terms of degree of anthropogenic enrichment. To avoid possible misinterpretations that could arise from directly using Co/Zr, Cr/Zr, Ni/Zr and V/Zr profiles to express anthropogenic enrichment in terms of estimated anthropogenic enrichment factors, the anthropogenic Co, Cr, Ni and V concentration profiles alone (*cf.* Figs. 3.62 and 3.63) will be used in Section 3.8.4.3.3 in order to interpret historical trends in anthropogenic Co, Cr, Ni and V.

3.8.4.3.4 Historical trends of anthropogenic Co, Cr, Ni and V deposition

Pre-industrial atmospheric Co, Cr, Ni and V sources and deposition

The anthropogenic Ni concentration profile in the 33-106 cm FM01CM-1 sections was rather 'noisy', precluding any historical interpretations of anthropogenic Ni deposition during the pre-industrial period (*cf.* Fig. 3.62). From 71 to 106 cm in FM01CM-1, i.e. the time period representing the pre-Roman and Roman period, anthropogenic Co concentrations were at a minimum (mean 0.087 ± 0.024 mg kg^{-1}), anthropogenic V concentrations (mean 0.66 ± 0.17 mg kg^{-1}) were not enhanced relative to concentrations in the rest of the 33-106 cm FM01CM-1 sections but anthropogenic Cr concentrations were slightly enhanced (mean 0.52 ± 0.24 mg kg^{-1}), although not to the same extent as the anthropogenic Pb concentrations at these depths (71-106 cm) (*cf.* Fig. 3.62). Enhanced Pb concentrations during this pre-Roman/Roman period, reflect emissions from Cu, Fe and Pb ore mining and smelting (*cf.* Section 3.6.1), but these activities are not considered to be a significant source of Cr (*cf.* Table 1.2, Section 1.3.2.2) (Nriagu and Pacyna, 1988) and, therefore, the

cause of these slightly enhanced anthropogenic Cr concentrations is unclear. From 53 to 71 cm in FM01CM-1, i.e. the time period representing the post-Roman period, anthropogenic Co and V concentrations increased (mean values of 0.19 ± 0.09 mg kg^{-1} and 0.77 ± 0.12 mg kg^{-1}, respectively) while anthropogenic Cr concentrations were at a minimum (mean 0.35 ± 0.15 mg kg^{-1}) (*cf.* Fig. 3.62).Due to the lack of archaeological knowledge about this pre-Mediaeval period, the origin of these Co and V increases is rather uncertain. In the 53 to 33 cm sections of FM01CM-1, i.e. the time period representing the Mediaeval period, anthropogenic Co concentrations (mean 0.21 ± 0.07 mg kg^{-1}) generally remained the same as those in the lower 53-71 cm sections (*cf.* Fig. 3.62) while anthropogenic Cr and V concentrations increased (mean 0.45 ± 0.20 and 0.96 ± 0.21 mg kg^{-1}, respectively). Enhanced Pb concentrations during this Mediaeval period, reflect emissions from Pb and Cu ore mining and smelting (*cf.* Sections 3.6.3.2), but these activities are not a significant source of Cr or V (*cf.* Table 1.2, Section 1.3.2.2) and again, therefore, the cause of their enhanced concentrations is unclear.

Industrial and post-industrial atmospheric Co, Cr, Ni and V sources and deposition

Co

Above 33 cm in FM01CM-1, anthropogenic Co concentrations increased from 0.24 mg kg^{-1} at 33 cm (for which no age-date was available) to a maximum of 2.0 mg kg^{-1} at 9 cm (*ca.* 1943 ± 10 A.D.) (predating the maximum anthropogenic Pb concentration (263 mg kg^{-1}) by *ca.* 5 years) (*cf.* Fig. 3.62). Similarly, from the bottom of the FM04-1-M core (*ca.* late 1700s A.D.), anthropogenic Co concentrations increased from 0.45 mg kg^{-1} to a maximum of 1.5 mg kg^{-1} at 12 cm (*ca.* 1955 ± 3 A.D.) (coincident with the maximum anthropogenic Pb concentration (190 mg kg^{-1})) (*cf.* Fig. 3.63). These increases in Co are most likely to be due to a combination of emission sources during the industrial period such as metallurgical activities, coal combustion and the use of phosphate fertilisers (Oehme, 1979; Chemical Research Communications, 2003). After 1943 A.D. in FM01CM-1 and

1955 A.D. in FM04-1-M, anthropogenic Co concentrations decreased to 0.43 mg kg^{-1} at the top of FM01CM-1 (*ca.* mid 1980 A.D.) and to 0.90 mg kg^{-1} at *ca.* 1986 A.D. in FM04-1-M. These decreases reflect the decline in heavy industry in the later part of the 20th century A.D., when emissions from oil combustion (*cf.* Fig. 1.3, Section 1.3.2.2.2) and waste incineration (Chemical Research Communications, 2003) perhaps became more important (Department of Trade and Industry, 1998; National Atmospheric Emissions Inventory, 2006). After 1986 A.D. in FM04-1-M, anthropogenic Co concentrations continued to decrease, reaching a minimum of 0.26 mg kg^{-1} at *ca.* 2001 A.D (*cf.* Fig. 3.63), reflecting the decline in oil combustion (Department of Trade and Industry, 1998; National Atmospheric Emissions Inventory, 2006), as well as tighter emission controls following the introduction of legislation on air quality in the UK during this post-industrial period (MacKenzie *et al.*, 1998; Famer *et al.*, 1999).

Cr

Above 33 cm in FM01CM-1, anthropogenic Cr concentrations increased from 0.81 mg kg^{-1} at 33 cm (for which no age-date was available) to a maximum of 14 mg kg^{-1} at 5 cm (*ca.* 1967 ± 9 A.D.) (post-dating the maximum anthropogenic Pb concentration (263 mg kg^{-1}) by *ca.* 19 years) (*cf.* Fig. 3.62). From the bottom of the FM04-1-M core (*ca.* late 1700s A.D.), anthropogenic Cr concentrations increased from 0.79 mg kg^{-1} to a maximum of 11 mg kg^{-1} at 12 cm (*ca.* 1955 ± 3 A.D.) (coincident with the maximum anthropogenic Pb concentration (190 mg kg^{-1})) (*cf.* Fig. 3.63). These increases in Cr are most likely to be due to coal combustion and steel and iron manufacturing (*cf.* Table 1.2, Section 1.3.2.2) during this industrial period. After 1967 A.D. in FM01CM-1 and 1955 A.D. in FM04-1-M, anthopogenic Cr concentrations decreased to 1.7 mg kg^{-1} at the top of FM01CM-1 (*ca.* mid 1980 A.D.) and to 2.0 mg kg^{-1} at *ca.* 1986 A.D. in FM04-1-M. These decreases reflect the decline in heavy industry in the later part of the 20th century A.D., when emissions from oil combustion and waste incineration (*cf.* Table 1.2, Section 1.3.2.2) became more important (Department of Trade and Industry 1998; National Atmospheric Emissions Inventory, 2006). It is worth noting that anthropogenic Cr concentrations

at Flanders Moss remained fairly constant after the late 1980s A.D. (*cf.* Fig. 3.63), rather than declining like Co, Ni, V and Pb, perhaps indicating emissions of Cr from comparatively new recent sources (i.e. not oil combustion or waste incineration). One such source could include the release of Cr from new automotive brake linings (Boulter, 2004).

Ni

Above 33 cm in FM01CM-1, anthropogenic Ni concentrations increased from 0.72 mg kg^{-1} at 33 cm (for which no age-date was available) to a maximum of 11 mg kg^{-1} at 9 cm (*ca.* 1943 ± 10 A.D.) (pre-dating the maximum anthropogenic Pb concentration (263 mg kg^{-1}) by *ca.* 5 years) (*cf.* Fig. 3.62). Similarly, from the bottom of the FM04-1-M core (*ca.* late 1700s A.D.), anthropogenic Ni concentrations increased from 3.5 mg kg^{-1} to a maximum of 15 mg kg^{-1} at 12 cm (*ca.* 1955 ± 3 A.D.) (coincident with the maximum anthropogenic Pb concentration (190 mg kg^{-1})) (*cf.* Fig. 3.63). These increases in Ni are most likely to be due to Cu-Ni production, coal combustion and possibly, from the 1930s, oil combustion (Shotyk *et al.*, 1996) during this industrial period (*cf.* Table 1.2, Section 1.3.2.2). After 1943 A.D. in FM01CM-1 and 1955 A.D. in FM04-1-M, anthropogenic Ni concentrations decreased to 2.3 mg kg^{-1} at the top of FM01CM-1 (*ca.* mid 1980 A.D.) and to 5.1 mg kg^{-1} at *ca.* 1986 A.D. in FM04-1-M. These decreases reflect the decline in heavy industry in the second half of the 20th century A.D., when emissions from oil combustion and waste incineration (*cf.* Table 1.2, Section 1.3.2.2) became more important (Department of Trade and Industry, 1998; National Atmospheric Emissions Inventory, 2006). After 1986 A.D. in FM04-1-M, anthropogenic Ni concentrations decreased slowly reaching a minimum of 3.3 mg kg^{-1} at *ca.* 2001 A.D (*cf.* Fig. 3.63), reflecting the decline in oil combustion (Department of Trade and Industry, 1998; National Atmospheric Emissions Inventory, 2006), as well as tighter emission controls in the UK during this post-industrial period (MacKenzie *et al.*, 1998; Farner *et al.*, 1999).

V

Above 33 cm in FM01CM-1, anthropogenic V concentrations increased from 0.80 mg kg^{-1} at 33 cm (for which no age-date was available) to a maximum of 14.7 mg kg^{-1} at 6 cm (*ca.* 1960 ± 9 A.D.) (post-dating the maximum anthropogenic Pb concentration (263 mg kg^{-1}) by *ca.* 12 years) (*cf.* Fig. 3.62). Similarly, from the bottom of the FM04-1-M core (*ca.* late 1700s A.D.), anthropogenic V concentrations increased from 0.72 mg kg^{-1} to a maximum of 18 mg kg^{-1} at 12 cm (*ca.* 1955 ± 3 A.D.) (coincident with the maximum anthropogenic Pb concentration (190 mg kg^{-1})) (*cf.* Fig. 3.63). These increases in V are most likely to be due to coal combustion and possibly, from the 1930s, oil combustion (Shotyk *et al.*, 1996) during this industrial period (*cf.* Table 1.2, Section 1.3.2.2). After 1960 A.D. in FM01CM-1 and 1955 A.D. in FM04-1-M, anthropogenic V concentrations decreased to 3.0 mg kg^{-1} at the top of FM01CM-1 (*ca.* mid 1980 A.D.) and to 8.5 mg kg^{-1} at *ca.* 1986 A.D. in FM04-1-M. These decreases perhaps reflect the decline in coal combustion in the second half of the 20th century A.D., when emissions from oil combustion (*cf.* Table 1.2, Section 1.3.2.2) became more important (Department of Trade and Industry, 1998; National Atmospheric Emissions Inventory, 2006). After 1986 A.D. in FM04-1-M, anthropogenic V concentrations continued to decrease, reaching a minimum of 2.6 mg kg^{-1} at *ca.* 2001 A.D (*cf.* Fig. 3.63), reflecting the decline in oil combustion (Department of Trade and Industry, 1998; National Atmospheric Emissions Inventory, 2006), as well as tighter emission controls in the UK during this post-industrial period (MacKenzie *et al.*, 1998; Famer *et al.*, 1999).

3.8.4.3.5 Historical trends in depositional fluxes and inventories of anthropogenic Co, Cr, Ni and V

The anthropogenic depositional fluxes of Co, Cr, Ni and V were calculated in FM04-1-M (A4.2 Table A11), but, Zr was used as the conservative element instead of Sc (*cf.* Section 3.6.4) to correct for soil dust contributions to total elemental concentrations. The anthropogenic depositional fluxes of Pb were also calculated on the basis of Zr (A4.2 Table A11). These fluxes, since the mid-19th century A.D., are

plotted along with the measured $^{206}Pb/^{207}Pb$ ratios, *versus* ^{210}Pb-derived calendar dates for FM04-1-M in Fig. 3.64.

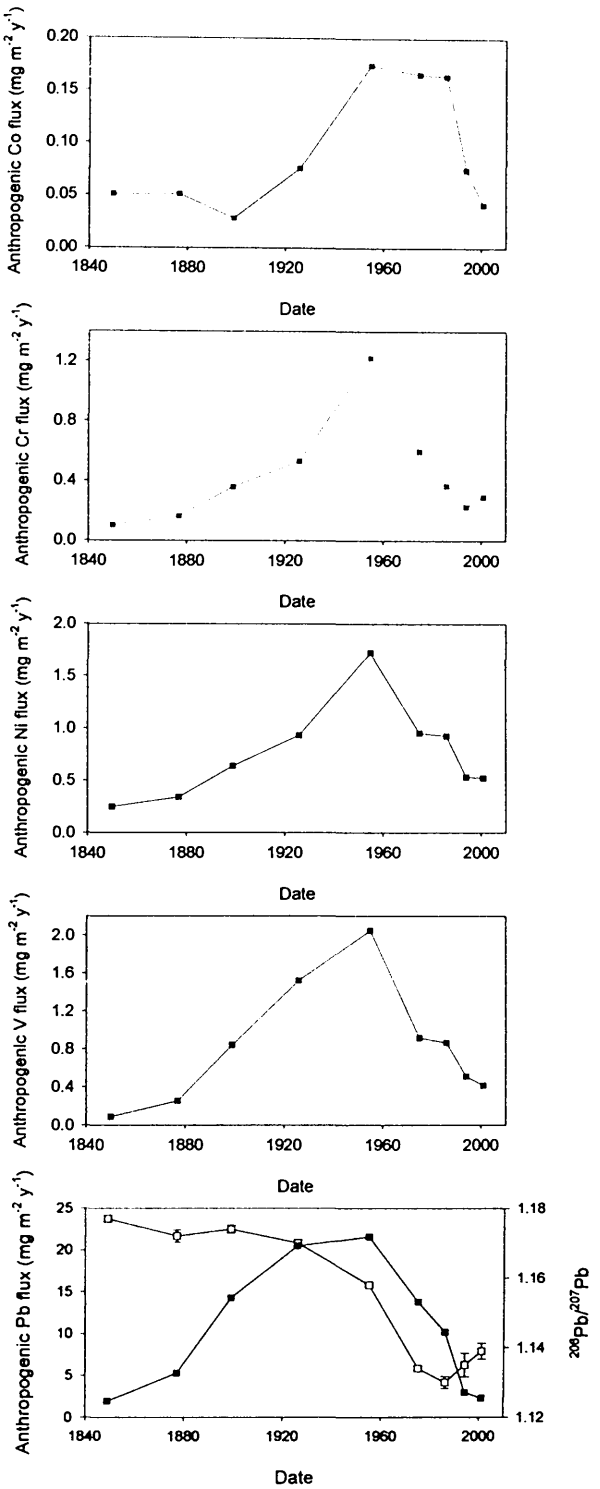

Figure 3.64: Calculated atmospheric depositional fluxes of anthropogenic Co, Cr, Ni, V and Pb (mg m^{-2} y^{-1}) (closed squares) and the measured $^{206}Pb/^{207}Pb$ ratios (open squares) for the FM04-1-M core *versus* ^{210}Pb-derived dates since 1840 A.D.

It is worth noting that when anthropogenic Pb fluxes calculated on the basis of Zr (*cf.* Fig. 3.64) are compared with those calculated on the basis of Sc (*cf.* Fig. 3.25), it is apparent that there is no change in either the magnitude or trends exhibited in the anthropogenic Pb fluxes, providing support for the use of either Sc or Zr as a conservative "reference" element to calculate elemental anthropogenic concentrations and fluxes of Pb. Depositional fluxes of Co were at a maximum (range ~ 0.16 to 0.17 mg m^{-2} y^{-1}) between the mid-1950s and mid-1980s A.D., while depositional fluxes of Cr, Ni and V exhibited maxima of 1.2, 1.7 and 2.0 mg m^{-2} y^{-1}, respectively, during the mid-1950s A.D. (*cf.* Fig. 3.64).

Total anthropogenic Co, Cr, Ni and V inventories in both Flanders Moss cores were calculated, as performed earlier for As, Cd, Cu, Pb and Sb (Sections 3.6.4, 3.8.1.3.3 and 3.8.3.3.3). The total anthropogenic Co, Cr, Ni and V inventories for FM01CM-1 (i.e. from *ca.* 500 B.C. to mid-1980s A.D., given that the very top of the core was lost during collection) were 0.038 g m^{-2}, 0.18 g m^{-2}, 0.19 g m^{-2} and 0.22 g m^{-2}, respectively. The total anthropogenic Co, Cr, Ni and V inventories for FM04-1-M (i.e. from *ca.* late 1700s to 2004 A.D.) were 0.017, 0.082, 0.14 and 0.16 g m^{-2}, respectively. For FM01CM-1, the post-1800 A.D. Co, Cr, Ni and V inventories (0.029, 0.14, 0.15 and 0.17 g m^{-2}) (corresponding to peat sections 0-23 cm) constituted 76, 82, 80 and 78% of the total anthropogenic Co, Cr, Ni and V inventories, respectively, for the core, slightly less than the corresponding value of 95% found for Pb, but similar to the 74, 79 and 83% found for As, Cd and Cu, respectively. Calculated cumulative post-1800 A.D. anthropogenic Co, Cr, Ni and V inventories (% of total post-1800 A.D. inventory) for the Flanders Moss cores are plotted *versus* ^{210}Pb-derived calendar dates in Fig. 3.65. Maximum Co and Cr deposition occurred between the 1930s and 1980s A.D. and 1910s and 1970s A.D., respectively, and maximum Ni and V deposition occurred between the 1910s and 1960s A.D. These trends, perhaps with the exception of Co, are generally in agreement with that found for Pb (*cf.* Section 3.6.4). Again, slight differences in trends between the two cores are at least partly attributable to differences in core

sectioning, as well as uncertainties with respect to extrapolation of ^{210}Pb dates for the FM01CM-1 core from FM01CM-2.

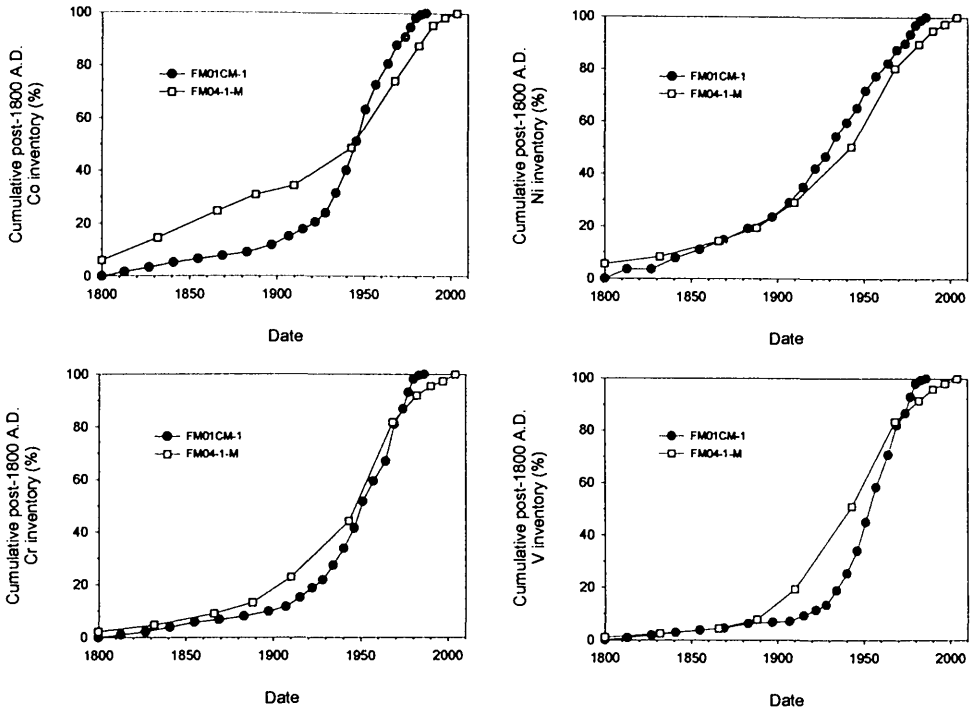

Figure 3.65: Calculated cumulative post-1800 A.D. anthropogenic Co, Cr, Ni and V inventories (% of total post-1800 A.D. inventory) for the FM01CM-1 and FM04-1-M cores *versus* ^{210}Pb-derived dates.

3.8.5 Comparison of As, Cd, Co, Cr, Cu, Hg, Ni, Pb, Sb and V depositional fluxes

To compare the depositional fluxes of the environmental contaminants known to be essentially immobile (Pb) and potentially immobile (As, Cd, Co, Cu, Cr, Hg, Ni, Sb and V) in ombrotrophic peat, the anthropogenic depositional fluxes of As, Cd, Co, Cu, Cr, Ni, Pb, Sb and V in FM04-1-M and depositional Hg fluxes in FM01CM-2, since the mid-19th century A.D., are plotted along with the measured ^{206}Pb/^{207}Pb ratios in FM04-1-M, *versus* ^{210}Pb-derived calendar dates in Fig. 3.66. Differences between the depositional fluxes of As, Cd, Co, Cr, Hg, Ni, Pb. Sb and V are due to differences in inputs from various sources which have changed with time.

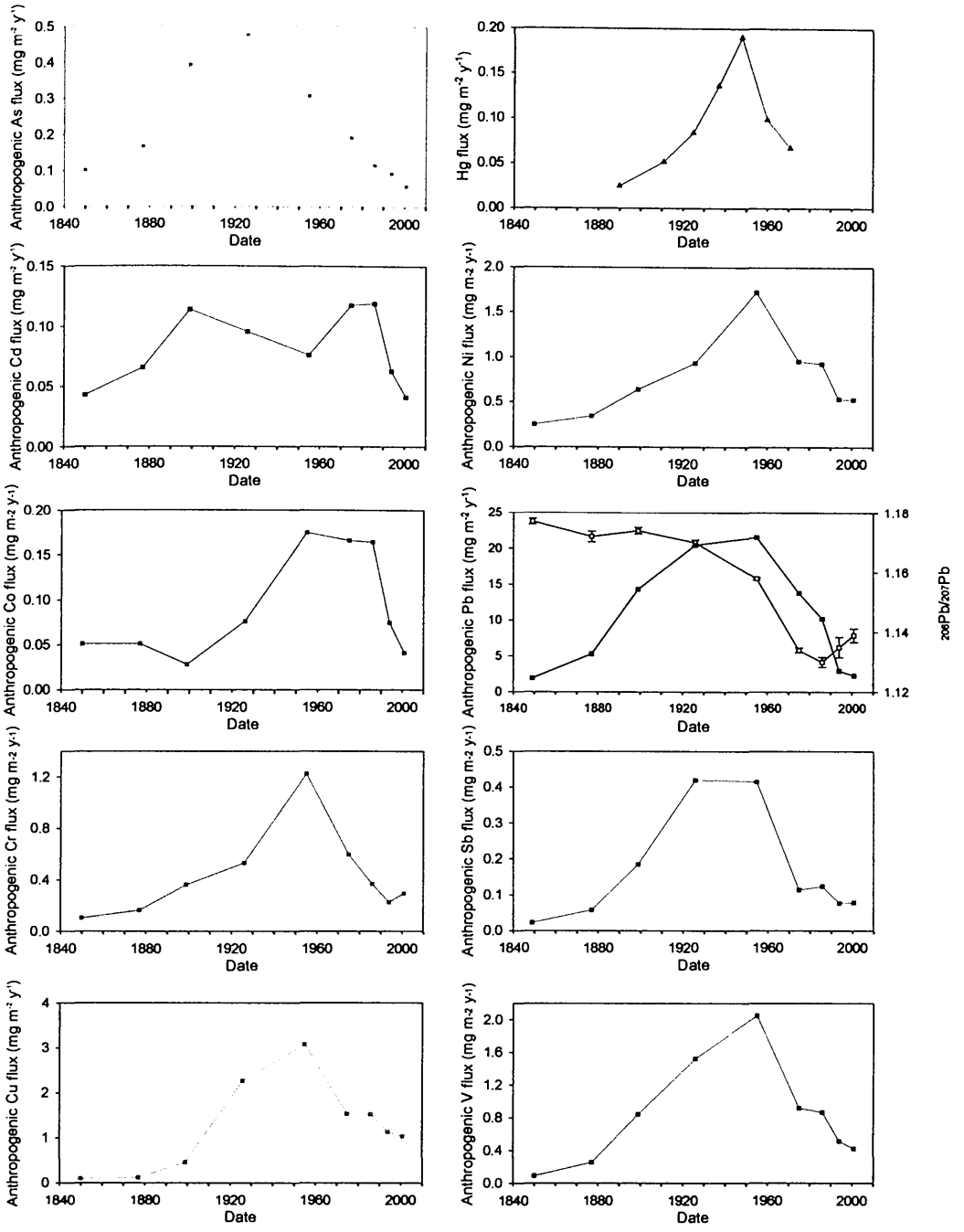

Figure 3.66: Calculated atmospheric depositional fluxes of anthropogenic As, Cd, Co, Cr, Cu, Ni, Pb, Sb and V (mg m^{-2} y^{-1}), along with the measured $^{206}Pb/^{207}Pb$ ratios for the FM04-1-M core and depositional Hg fluxes (mg m^{-2} y^{-1}) for the FM01CM-2 core, *versus* ^{210}Pb-derived dates since 1840 A.D.

3.9 CONCLUSIONS

The principal conclusions arising from the results for the Flanders Moss peat cores were as follows:

- Using Sc as a conservative element, anthropogenic enrichments of Pb at Flanders Moss were estimated and, on the basis of ^{210}Pb and ^{14}C dating and Pb isotopic composition (e.g. $^{206}Pb/^{207}Pb$), sources of atmospheric anthropogenic Pb deposition over the past 2500 years were investigated. In the pre-Roman/Roman period, the mining and smelting of British Pb ores appears to have been responsible for the small, but clearly discernible peak in anthropogenic Pb concentration in the Flanders Moss peat core. In the Mediaeval period, the mining and smelting of Pb ores from both continental Europe and Britain appear to have been responsible for the increase in anthropogenic Pb concentration. In the industrial and post-industrial periods, variations in the relative importance of contributions of anthropogenic Pb from different sources were apparent. Mining and smelting of indigenous Scottish Pb ores were found to be most important during the 17th century until the early 20th century A.D. and coal combustion and Australian-Pb-influenced car-exhaust emissions from the 1930s to late 1960s and late 1990s A.D., respectively. Derived atmospheric depositional fluxes of anthropogenic Pb were greatest in the industrial era, peaking between the mid-1920s and mid-1950s A.D.
- The major elements, Ca, Fe, Mg, Mn, P and S, and two trace elements, Se and Zn, were found to be subject to post-depositional mobility at Flanders Moss. Plant uptake and recycling affected Ca, Fe, Mg, Mn, P, S and Zn profiles while Fe, Mn, P and S were also influenced by redox cycling. Zn was also possibly influenced by sulfide formation in the catotelm peat layers of the bog.
- The general similarity between the Pb concentration profiles and those of the trace elements As, Cd, Co, Cr, Cu, Hg, Ni, Sb and V at Flanders Moss suggested that these latter elements were also essentially immobile in ombrotrophic peat.

- The Sb and Pb concentration profiles at Flanders Moss were remarkably similar. Using Sc as a conservative element, anthropogenic enrichments of Sb were estimated, and on the basis of anthropogenic Sb/Pb ratios and the characteristically low Sb/Pb ratios measured in British Pb ores and high Sb/Pb ratios measured in coals, sources of atmospheric anthropogenic Sb deposition were investigated. During the pre-Roman/Roman and Mediaeval periods, sources of anthropogenic Sb deposition were the same as those found for Pb, and this was also the case during the Industrial period, with the exception of leaded petrol. In the post-industrial period, the influence of anthropogenic inputs of Sb from comparatively new recent sources (e.g. automotive brake linings) was apparent. Derived atmospheric depositional fluxes of anthropogenic Sb, as for Pb, were greatest in the industrial era, peaking between the mid-1920s and mid-1950s A.D.
- The Hg concentration profile in the older catotelm peats of Flanders Moss was possibly influenced by sulfide formation. In the industrial and post-industrial periods, coal combustion and waste incineration, respectively, are likely to have been the most important sources of Hg. Derived atmospheric depositional fluxes of Hg were greatest in the industrial era, peaking at *ca.* 1950 A.D.
- Anthropogenic As, Cd and Cu concentrations were estimated using Sc as a conservative element. In the pre-Roman/Roman period there were no clear discernible peaks for any of these elements. In the Mediaeval period, the extensive mining and smelting of Pb and Cu ores is likely to have been responsible for the increase in anthropogenic As concentration. In the industrial and post-industrial periods, sources of As, Cd and Cu were attributable to a variety of sources (e.g. metallurgical activities, coal and oil combustion and waste incineration). Also, there may have been inputs of Cu from comparatively new recent anthropogenic sources (e.g. automobile exhaust and non-exhaust emissions, due to the use of Cu as an antioxidant in motor oil and its presence in new brake linings and tyres). Derived atmospheric depositional fluxes of anthropogenic As and Cu were greatest in the industrial era, peaking during the mid-1920s and mid-1950s A.D., respectively. Atmospheric

depositional fluxes of anthropogenic Cd were greatest in the industrial and post-industrial era, peaking between *ca.* 1900 and the mid-1980s A.D.

- Anthropogenic Co, Cr, Ni and V concentrations were estimated using Zr as a conservative element. In the pre-Roman/Roman period, only anthropogenic Cr concentrations were enhanced, and in the Mediaeval period, anthropogenic Cr and V concentrations increased but the sources of these increases were unclear. In the industrial and post-industrial periods, sources of Co, Cr, Ni and V were attributable to a variety of sources (e.g. metallurgical activities, coal and oil combustion, use of phosphate fertilisers and waste incineration). Also, there may have been inputs of Cr from comparatively new recent anthropogenic sources (e.g. automotive brake linings). Derived atmospheric depositional fluxes of anthropogenic Co were greatest in the industrial and post-industrial periods, peaking between the mid-1950s and mid-1980s A.D. Atmospheric depositional fluxes of anthropogenic Cr, Ni and V were greatest in the industrial era, peaking during the mid-1950s A.D.

4 THE RED MOSS OF BALERNO

This chapter contains the results for The Red Moss of Balerno peat cores, which will be treated in a similar way to the Flanders Moss peat core results (Chapter 3).

4.1 PEAT MATRIX PROPERTIES AND EVALUATION OF TROPHIC STATUS

4.1.1 Visual observations

Visual observation depth profiles for The Red Moss of Balerno peat cores, RM03CM-1 and RM03CM-2, are shown in Fig. 4.1. For RM03CM-1, only sectional material from the upper 31 cm was used in this research project.

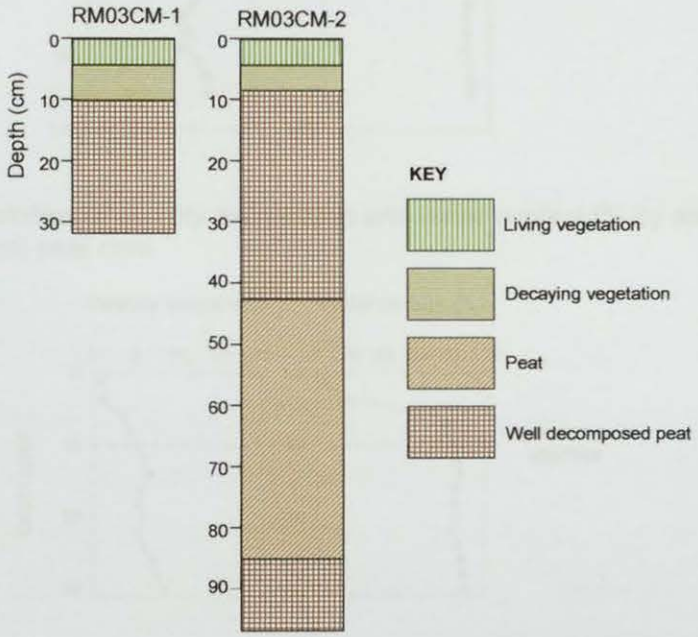

Figure 4.1: Visual observation depth profiles for RM03CM-1 and RM03CM-2.

4.1.2 Wet/dry weight ratios and water contents

Wet and dry weights, wet/dry weight ratios, water contents and residual moisture contents for RM03CM-2 and RM03CM-1 are tabulated in Appendix A5.1 Table A1 and A5.2 Table A1, respectively. The wet/dry weight ratio and water content profiles for RM03CM-2 and RM03CM-1 are shown in Figs. 4.2 and 4.3, respectively.

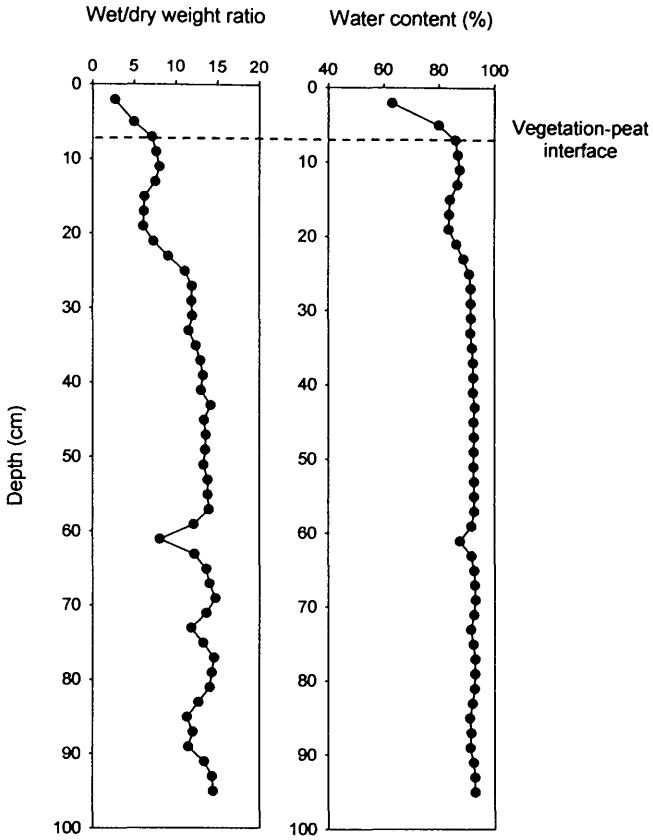

Figure 4.2: Depth profiles of wet/dry weight ratio and water content (% by weight) in the RM03CM-2 (0-96 cm) peat core.

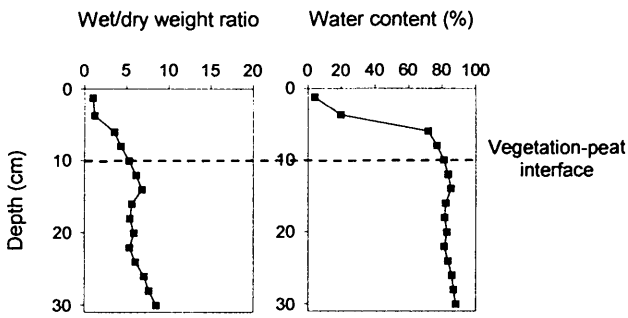

Figure 4.3: Depth profiles of wet/dry weight ratio and water content (% by weight) in the RM03CM-1 (0-31 cm) peat core.

4.1.2.1 RM03CM-2

From the bottom of RM03CM-2 up to 24 cm, wet/dry weight ratios (8.1 – 15) and water contents (88 – 93%) were fairly constant. Thereafter, they declined slightly and remained stable up to the vegetation-peat interface (6-8 cm) before decreasing to 2.7 and 63%, respectively, at the surface (*cf.* Fig. 4.2).

4.1.2.2 RM03CM-1

The wet/dry weight ratios and water contents in RM03CM-1 decreased from 8.5 and 88%, respectively, at the bottom of the core to 5.3 and 76% at the vegetation-peat interface (9-11 cm), above which they declined to 1.0 and 4% at the surface (*cf.* Fig. 4.3).

4.1.2.3 Discussion

In terms of hydrological properties of The Red Moss of Balerno peat bog, the relatively high and constant wet/dry weight ratios and water contents at depth in RM03CM-2 are indicative of waterlogged catotelm peat layers, whereas the lower values in the uppermost RM03CM-2 sections and RM03CM-1 are indicative of drier acrotelm peat layers. Based on these patterns, the acrotelm-catotelm boundary can be estimated to occur at a depth of ~ 25 cm in RM03CM-2 and ~ 22 cm in RM03CM-1.

4.1.3 Ash contents and Ca/Mg ratios

The profiles of ash contents and Ca/Mg ratios (A5.1 Table A2 and A5.2 Table A2), for RM03CM-2 and RM03CM-1 are shown in Figs. 4.4 and 4.5, respectively.

4.1.3.1 RM03CM-2

From the bottom of RM03CM-2 up to 24 cm, the ash contents remained low and fairly constant (0.36 – 1.1%) above which they increased, exhibiting a prominent peak between 24 and 0 cm with a maximum of 5.9% at 8-10 cm. The Ca/Mg ratios increased gradually from 0.40 at the bottom of the core to 1.8 at 20-22 cm, above which they were high (1.2 – 2.1) before increasing above the vegetation-peat interface to a maximum of 3.5 at the surface (*cf.* Fig. 4.4).

4.1.3.2 RM03CM-1

A prominent peak in the RM03CM-1 ash content occurred between 23 and 0 cm, with a maximum of 6.4% at 11-13 cm. The Ca/Mg ratios increased from 1.2 at the bottom of the core to 1.9 at the vegetation-peat interface (9-11 cm), above which

they increased to a maximum of 4.7 at 4 cm, followed by a decrease towards the surface (*cf.* Fig. 4.5).

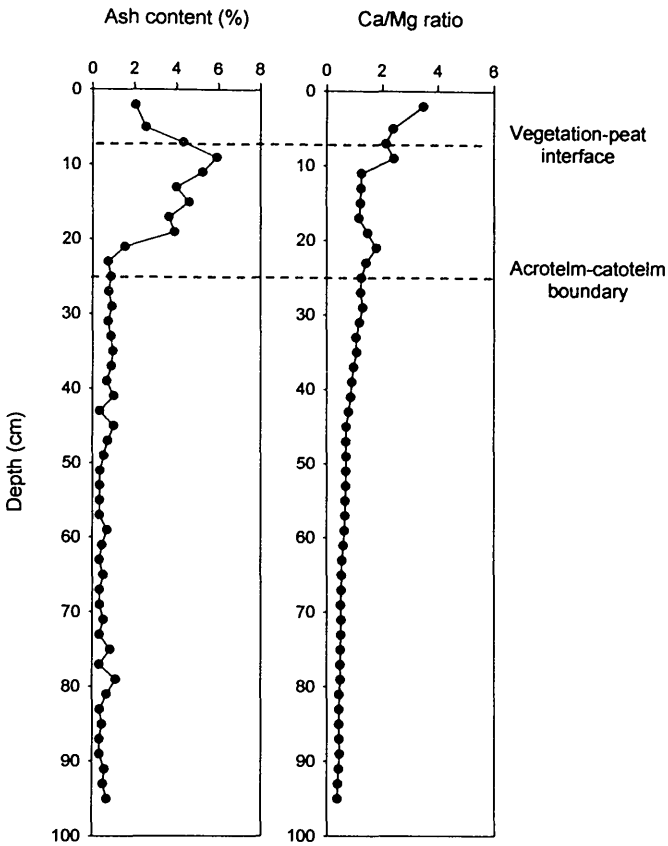

Figure 4.4: Depth profiles of ash content (% by weight) and Ca/Mg ratios in the RM03CM-2 (0-96 cm) peat core.

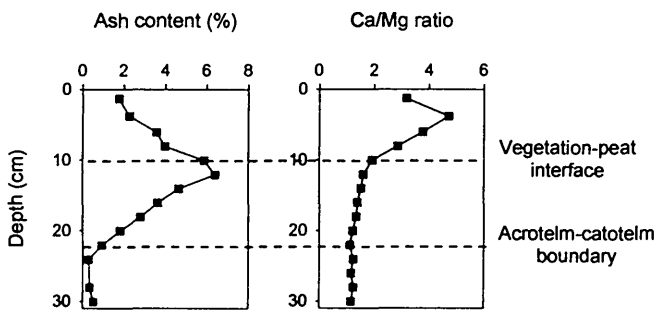

Figure 4.5: Depth profiles of ash content (% by weight) and Ca/Mg ratios in the RM03CM-1 (0-31 cm) peat core.

4.1.3.3 Discussion

The ash content values (< 8%) and Ca/Mg ratios (< 6) are consistent with ombrotrophic conditions in The Red Moss of Balerno cores. In 1982, pH

measurements of bog waters from the centre of the bog were ~ pH 3.6 (SWT, 2001), providing additional evidence for the ombrotrophic nature of this peat bog. These cores are therefore suitable for use as archives of atmospheric metal deposition.

4.1.4 Bulk density and NaOH peat extract absorption

The profiles of bulk density (A5.1 Table A2 and A5.2 Table A2), for RM03CM-2 and RM03CM-1 are shown in Figs. 4.6 and 4.7, respectively. The NaOH peat extract % absorptions at 550 nm for RM03CM-2 (A5.1 Table A2) are shown in Fig 4.6.

4.1.4.1 RM03CM-2

From the bottom of RM03CM-2 up to the acrotelm-catotelm boundary (24-26 cm), bulk densities (0.044 – 0.10 g cm^{-3}) were fairly constant (*cf.* Fig. 4.6) before exhibiting a broad peak up to the vegetation-peat interface, with a maximum of 0.17 g cm^{-3} at 19 cm. The NaOH peat extract absorptions in RM03CM-2 increased steadily from ~ 14% at the bottom of the core to a maximum of 45% at 27 cm, above which they slowly decreased to a minimum of 12% at the surface (*cf.* Fig. 4.6).

4.1.4.2 RM03CM-1

In RM03CM-1, bulk densities increased from 0.10 g cm^{-3} at the bottom of the core to a maximum (0.19 g cm^{-3}) at the acrotelm-catotelm boundary (21-23 cm), above which they remained high up to 17 cm, before decreasing to a minimum (0.014 g cm^{-3}) at the surface (*cf.* Fig. 4.7).

4.1.4.3 Discussion

As found for Flanders Moss (Section 3.1.4.3), the RM03CM-2 and RM03CM-1 bulk density and NaOH peat extract absorption profiles (*cf.* Figs. 4.6 and 4.7) indicate a greater degree of decomposition and mass loss in the acrotelm peat layers i.e. greater bulk densities and NaOH absorptions in the acrotelm peat sections between ~ 24 and 8 cm in RM03CM-2 (*cf.* Fig. 4.6), and between ~ 9 and 23 cm in RM03CM-1 (*cf.* Fig. 4.7), relative to the lower, fairly constant bulk densities and NaOH

absorptions in the catotelm peat sections beneath ~ 24 and 23 cm in RM03CM-2 and RM03CM-1, respectively (*cf.* Figs. 4.6 and 4.7).

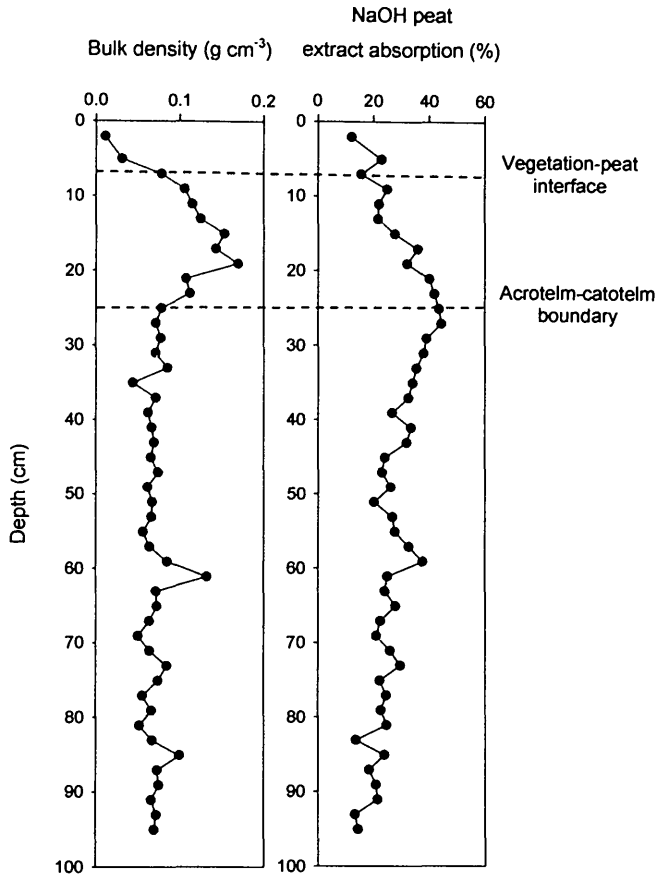

Figure 4.6: Depth profiles of bulk density (g cm^{-3}) and NaOH peat extract absorption (%) at 550 nm in the RM03CM-2 (0-96 cm) peat core.

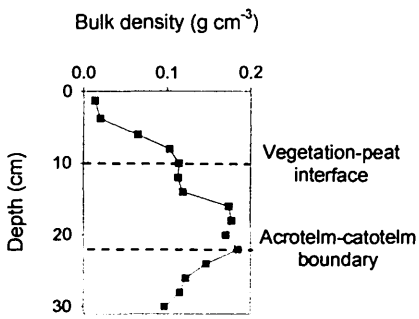

Figure 4.7: Depth profiles of bulk density (g cm^{-3}) in the RM03CM-1 (0-31 cm) peat core.

The low bulk densities and absorption values at the surface of both cores are attributable to the presence of decomposing and living vegetation. As found for Flanders Moss (Section 3.1.4.3), the less pronounced increases in absorption values

relative to bulk density values in the top ~ 24 cm sections of RM03CM-2 (*cf.* Fig. 4.6) are attributable to contributions from inorganic content to, and effects of peat compaction on, the bulk density profile. The RM03CM-2 bulk density and ash content profiles, plotted against air-dried mid-point cumulative weight (A5.1 Table A1) are shown in Fig. 4.8.

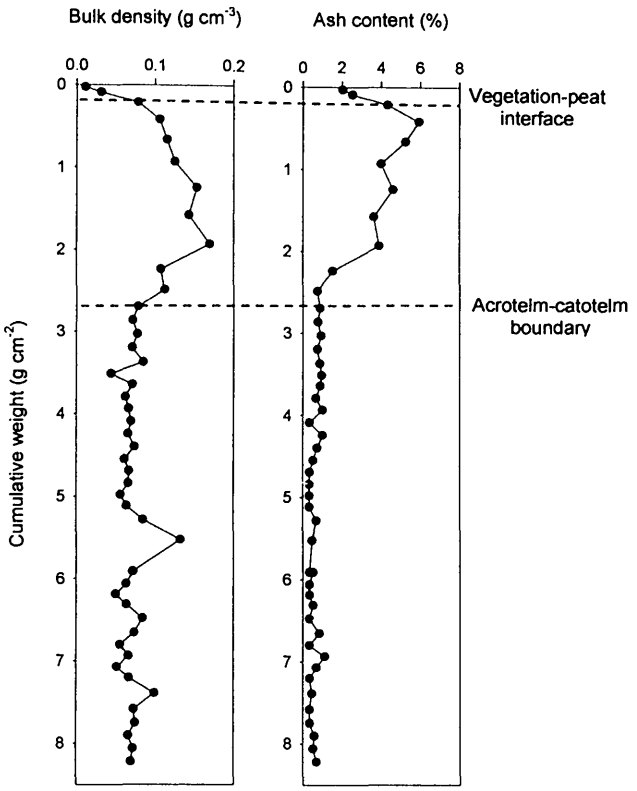

Figure 4.8: Comparison of bulk density (g cm^{-3}) and ash content (% by weight) *versus* cumulative weight (g cm^{-2}) in the RM03CM-2 peat core.

The near-surface increases in bulk density and ash content are similar (*cf.* Fig. 4.8), providing further evidence (*cf.* Section 3.1.4.3) that the high inorganic contents present as a result of increased anthropogenic and natural atmospheric dust deposition and nutrient cycling does indeed significantly influence bulk density values.

4.2 RADIONUCLIDES AND RADIOMETRIC DATING OF THE RED MOSS OF BALERNO PEAT CORES

4.2.1 ^{210}Pb and ^{137}Cs

^{210}Pb and ^{137}Cs were determined in sections from the top 21 cm of RM03CM-1. As ^{226}Ra was not detected above background in any of the RM03CM-1 sections, the total ^{210}Pb specific activities (Table 4.1) were taken to represent unsupported ^{210}Pb. The profiles of ^{210}Pb and ^{137}Cs specific activities are shown in Figs. 4.9 a (*vs.* depth in cm) and 4.9 b (*vs.* depth in g cm^{-2}).

Table 4.1: ^{210}Pb and ^{137}Cs specific activities (Bq kg^{-1}) and inventories (Bq m^{-2}) in the RM03CM-1 peat core.

RM03CM-1 section (cm)	Unsupported ^{210}Pb specific activity (Bq kg^{-1})	^{137}Cs specific activity (Bq kg^{-1})	Unsupported ^{210}Pb inventory (Bq m^{-2})	^{137}Cs inventory (Bq m^{-2})
0-2.5	325 ± 111	222 ± 27	127 ± 44	88 ± 12
2.5-5	470 ± 103	235 ± 26	269 ± 59	136 ± 16
5-7	452 ± 43	286 ± 13	658 ± 63	416 ± 20
7-9	250 ± 12	131 ± 4	584 ± 28	308 ± 8
9-11	222 ± 16	37 ± 4	568 ± 41	96 ± 12
11-13	145 ± 24	28 ± 6	372 ± 62	72 ± 16
13-15	62 ± 20	25 ± 6	166 ± 54	68 ± 16
15-17	20 ± 10	26 ± 7	78 ± 39	100 ± 32
17-19	13 ± 7	27 ± 6	52 ± 28	108 ± 24
19-21	20 ± 10	19 ± 9	78 ± 39	72 ± 36

Specific activities (± 1 SD) are expressed relative to air-dried weight.

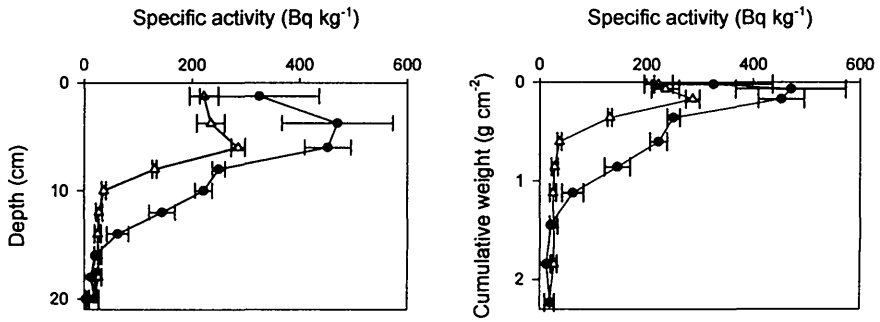

a) b)

Figure 4.9: ^{210}Pb (closed circles) and ^{137}Cs (open triangles) specific activity (Bq kg^{-1}) *versus* a) depth (cm) and b) cumulative weight (g cm^{-2}) in the RM03CM-1 peat core.

4.2.2 ^{210}Pb dating of RM03CM-1

The CRS model (Section 3.2.2) was applied to the ^{210}Pb inventories (*cf.* Table 4.1) to generate an age for the bottom of each individual RM03CM-1 section and, by interpolation, the mid-point date of each section was calculated (Table 4.2).

Table 4.2: Calculated ages and dates from the ^{210}Pb dating of the RM03CM-1 peat core.

Depth (cm)	Age (y)	Date (AD)
0	0	2003 ± 0
1.25		2003 ± 1
2.5	1.4	2002 ± 1
3.75		2000 ± 2
5	4.6	1998 ± 3
6		1994 ± 4
7	14.2	1989 ± 4
8		1983 ± 5
9	26.0	1977 ± 5
10		1968 ± 7
11	44.2	1959 ± 9
12		1948 ± 12
13	66.4	1937 ± 14
14		1928 ± 17
15	85.3	1918 ± 20
16		1911 ± 23
17	100.4	1903 ± 25
18		1895 ± 30
19	116.8	1886 ± 35
20		
21		

Dates were rounded up to the nearest whole number.

4.2.3 RM03CM-1 ^{210}Pb flux

The total unsupported ^{210}Pb inventory of RM03CM-1 was 2952 ± 136 Bq m^{-2}, with a corresponding inventory-derived average ^{210}Pb flux of 92 ± 4 Bq m^{-2} y^{-1}. This inventory-derived average ^{210}Pb flux is approximately double the theoretical rainfall-corrected ^{210}Pb flux of 48 ± 9 Bq m^{-2} y^{-1}, calculated for The Red Moss of Balerno area using the average annual rainfall value of 62.6 cm y^{-1} and the estimated average ^{210}Pb flux of 77 ± 14 Bq m^{-2} y^{-1} per metre of rainfall established for the UK by Smith *et al.* (1997). This high inventory-derived average ^{210}Pb flux value could reflect local differences in the composition and/or quantity of bulk precipitation. For example,

Farmer *et al.* (2005) determined a ^{210}Pb flux (198 ± 11 Bq m^{-2} y^{-1}) in an organic-rich soil core from Glensaugh, an upland catchment area in north-east Scotland, which was also double the anticipated theoretical value (96 ± 26 Bq m^{-2} y^{-1}) and suggested enhanced ^{210}Pb deposition under the conditions pertaining at the altitude of the Glensaugh catchment.

4.2.4 RM03CM-1 ^{137}Cs total inventory

The total ^{137}Cs inventory in RM03CM-1 was 1.5 ± 0.1 kBq m^{-2}. This is much less than that deposited in the east of Scotland from the atmosphere following nuclear weapons testing (2-3 kBq m^{-2}, Peirson *et al.*, 1982) and the Chernobyl accident (1-5 kBq m^{-2}, Clark and Smith, 1988), indicating loss of ^{137}Cs from the peat bog.

4.2.5 RM03CM-2 dates

Dates for RM03CM-2 were obtained by extrapolation of the ^{210}Pb-derived dates obtained for the RM03CM-1 sister core. The extrapolation of these dates was aided by matching the $^{206}Pb/^{207}Pb$ profiles of the two cores, which were plotted using a 2.25 cm offset between RM03CM-2 relative to RM03CM-1 (Fig. 4.10). Calculated and extrapolated ^{210}Pb dates and measured $^{206}Pb/^{207}Pb$ ratios for the top of RM03CM-1 and RM03CM-2 are shown in Table 4.3. Since no material was discarded from RM03CM-2, the offset of 2.25 cm is required due to the greater amount of vegetation present in RM03CM-1 (*cf.* Fig. 4.1). Note that the $^{206}Pb/^{207}Pb$ ratio results for these cores will be discussed in Section 4.4.1.

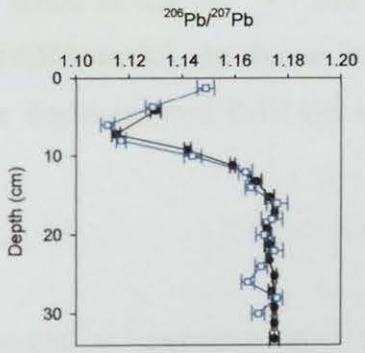

Figure 4.10: Depth profiles of $^{206}Pb/^{207}Pb$ ratio in the RM03CM-1 (0-31 cm) core (blue open squares) and from 0-31 cm in the RM03CM-2 core (black closed circles). The RM03CM-2 core was plotted with an offset of 2.25 cm relative to RM03CM-1.

Table 4.3: ^{210}Pb dates and corresponding $^{206}Pb/^{207}Pb$ ratios for the RM03CM-1 and RM03CM-2 peat cores.

RM03CM-1			RM03CM-2		
Depth (cm)	Calculated date (AD)	$^{206}Pb/^{207}Pb$[a]	Offset mid-point depth (cm)	Extrapolated date (AD)	$^{206}Pb/^{207}Pb$
0	2003 ± 0				
1.25	2003 ± 1	1.149 ± 0.0032			
2.5	2002 ± 1				
3.75	2000 ± 2	1.129 ± 0.0027	4.25	1999 ± 2	1.130 ± 0.0020
5	1998 ± 3				
6	1994 ± 4	1.112 ± 0.0026			
7	1989 ± 4		7.25	1988 ± 4	1.115 ± 0.0016
8	1983 ± 5	1.117 ± 0.0018			
9	1977 ± 5		9.25	1975 ± 6	1.142 ± 0.0013
10	1968 ± 7	1.144 ± 0.0033			
11	1959 ± 9		11.25	1956 ± 8	1.159 ± 0.0009
12	1948 ± 12	1.164 ± 0.0026			
13	1937 ± 14		13.25	1935 ± 15	1.168 ± 0.0020
14	1928 ± 17	1.166 ± 0.0020			
15	1918 ± 20		15.25	1916 ± 21	1.173 ± 0.0018
16	1911 ± 23	1.176 ± 0.0040			
17	1903 ± 25		17.25	1901 ± 26	1.175 ± 0.0010
18	1895 ± 30	1.174 ± 0.0040			
19	1886 ± 35		19.25		1.172 ± 0.0013
20		1.171 ± 0.0030			

Note that the shaded boxes indicate the 2.25 cm offset between RM03CM-1 and RM03CM-2.

4.2.6 Peat accumulation rates

4.2.6.1 CRS model

Peat accumulation rates (in terms of mg cm^{-2} y^{-1} and cm y^{-1}) for each RM03CM-1 section, calculated using the CRS model, are shown in Table 4.4. The actual average accumulation rates over the depth interval 0-19 cm were 17 ± 5 mg cm^{-2} y^{-1} and 0.16 ± 0.05 cm y^{-1}.

4.2.6.2 CIC model

Accumulation rates of 17 mg cm^{-2} y^{-1} and 0.13 cm y^{-1} were calculated using the CIC model and plotting ln ^{210}Pb *versus* air-dried mid-point cumulative weight (Fig. 4.11 a) and depth (Fig. 4.11 b), respectively.

Table 4.4: Sectional peat accumulation rates for the RM03CM-1 peat core determined using the CRS model.

Section (cm)	Number of years	Accumulation rate (mg cm^{-2} y^{-1})	Accumulation rate (cm y^{-1})
0-2.5	1.4	28	1.8
2.5-5	3.2	18	0.78
5-7	9.6	15	0.21
7-9	12	20	0.17
9-11	18	14	0.11
11-13	22	12	0.091
13-15	19	14	0.11
15-17	15	26	0.13
17-19	16	24	0.13

Accumulation rates are expressed in terms of air-dried peat weight.

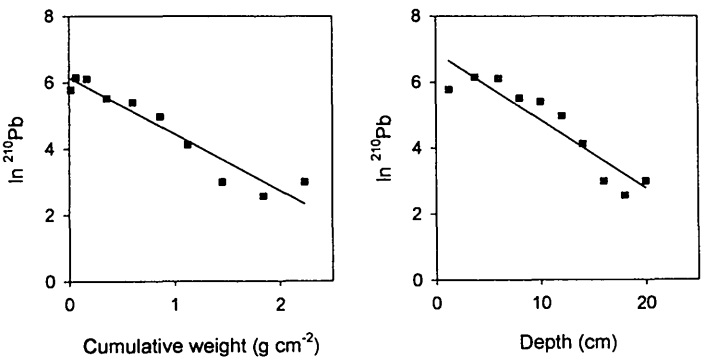

Figure 4.11: Profiles of ln [^{210}Pb (Bq kg^{-1})] *versus* a) cumulative weight and b) depth for the RM03CM-1 peat core.

4.2.6.3 Discussion

The RM03CM-1 peat accumulation rates derived using both of the ^{210}Pb models are in close agreement.

4.2.7 ^{14}C

The ^{14}C AMS age dates determined for selected deep peat sections of the RM03CM-2 core are shown in Table 4.5. As mentioned in Section 3.2.7, the age date for the selected humin fraction is in close agreement with that obtained for the corresponding humic acid fraction, providing additional confidence in the accuracy of these results.

Table 4.5: ^{14}C age dates of selected RM03CM-2 peat samples.

RM03CM-2 section (cm)	Fraction dated	$\delta^{13}C$ (‰)	Date (^{14}C years B.P.)	Date (calendar years A.D./B.C.)	Laboratory code
48-50	Humic acid (HA1)	-27.2	1000 ± 35	970 – 1070 A.D.	GU-12935
76-78	Humic acid (HA1)	-27.9	1195 ± 35	760 – 900 A.D.	GU-12936
76-78	Humin	-26.3	1265 ± 35	660 – 870 A.D.	GU-12937

4.3 CONSERVATIVE ELEMENTS

Profiles of total Al, Sc, Ti, Y and Zr concentrations for RM03CM-2 (A5.1 Table A3) and total Al and Ti concentrations for RM03CM-1 (A5.2 Table A3) are shown, along with ash contents, in Figs. 4.12 and 4.13, respectively.

4.3.1 RM03CM-2

0-40 cm

All five elements exhibited prominent peaks in the uppermost ~ 24 cm of the core, with the following maximum values at the depths indicated:

- Al – 2800 mg kg^{-1} at 10-12 cm
- Sc – 3.0 mg kg^{-1} at 10-12 cm
- Ti – 570 mg kg^{-1} at 14-16 cm
- Y – 4.4 mg kg^{-1} at 8-10 cm
- Zr – 17 mg kg^{-1} at 10-12 cm
- Ash content – 5.9% at 8-10 cm

There was generally good correlation between the conservative element concentration profiles and ash content profile (*cf.* Fig. 4.12).

40-96 cm

Note the change in scale on the concentration and ash content profiles (10-fold) on going from 0-40 cm to 40-96 cm (*cf.* Fig. 4.12).

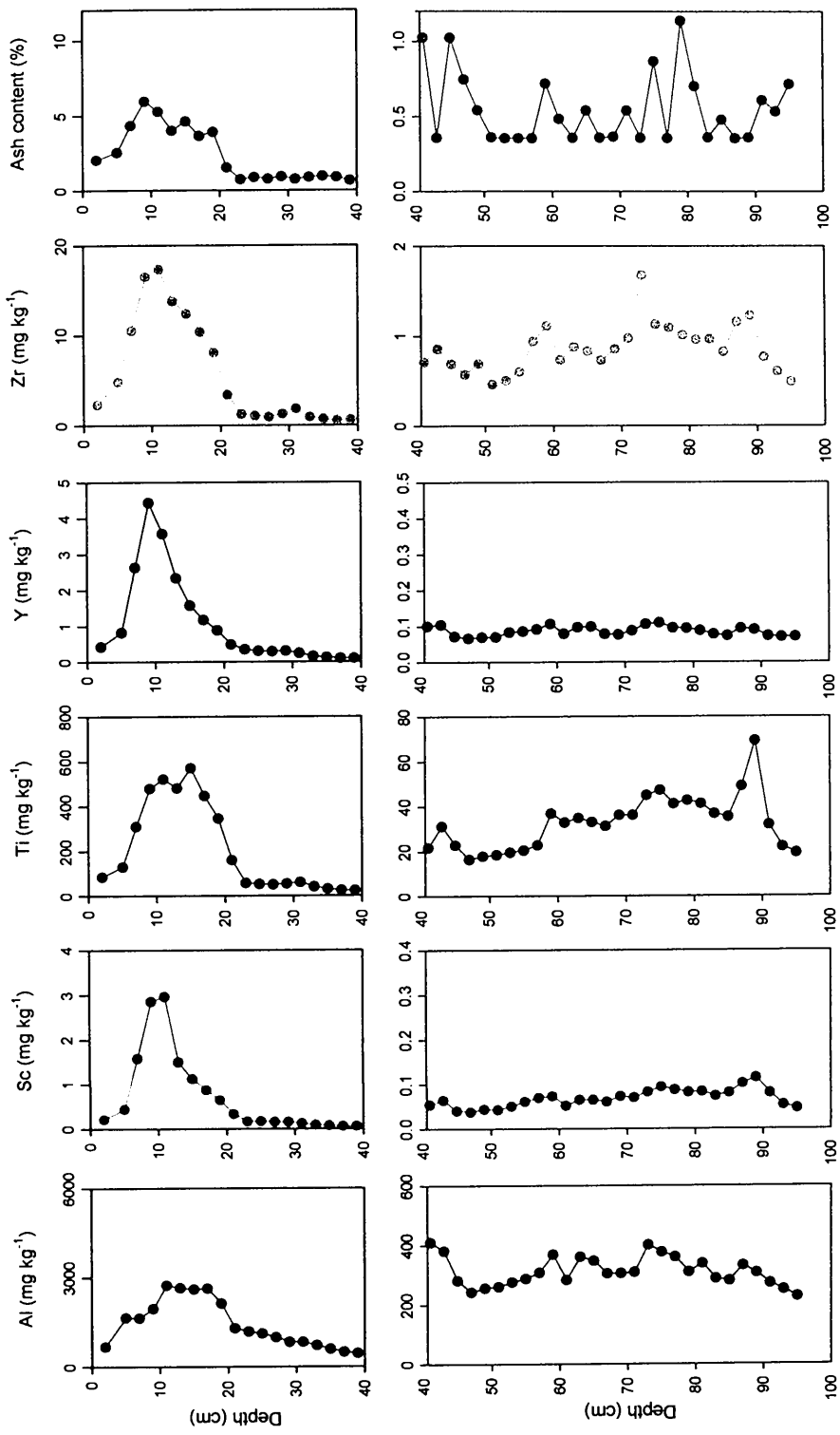

Figure 4.12: Depth profiles of Al, Sc, Ti, Y and Zr concentrations (mg kg^{-1}) and ash contents (% by weight) from 0-40 cm and 40-96 cm in the RM03CM-2 peat core.

Mean concentrations in the core between 40 and 96 cm were as follows: Al (310 ± 50 mg kg^{-1}), Sc (0.068 ± 0.019 mg kg^{-1}), Ti (33 ± 12 mg kg^{-1}), Y (0.086 ± 0.013 mg kg^{-1}) and Zr (0.86 ± 0.27 mg kg^{-1}). The following mean minimum concentrations occurred between 44 and 58 cm: Al (270 ± 20 mg kg^{-1}), Sc (0.050 ± 0.012 mg kg^{-1}), Ti (20 ± 2 mg kg^{-1}), Y (0.077 ± 0.010 mg kg^{-1}) and Zr (0.64 ± 0.16 mg kg^{-1}). Minor concentration peaks, which were coincident with the minor ash content peak, occurred at 59 cm for all of the conservative elements. Maximum concentrations occurred at 41 cm for Al, 89 cm for Sc and Ti, 75 cm for Y and 73 cm for Zr. The ash content profile below ~ 60 cm was rather 'noisy', precluding precise correlation with the elemental profiles (*cf.* Fig. 4.12).

4.3.2 RM03CM-1

Maximum Al (8500 mg kg^{-1}) and Ti (640 mg kg^{-1}) concentrations occurred at a depth of 11-13 cm, correlating well with the ash content maximum of 6.4% at the same depth (*cf.* Fig. 4.13). Note that the maximum Al concentration in RM03CM-1 was much higher than that in RM03CM-2 (*cf.* Fig. 4.12).

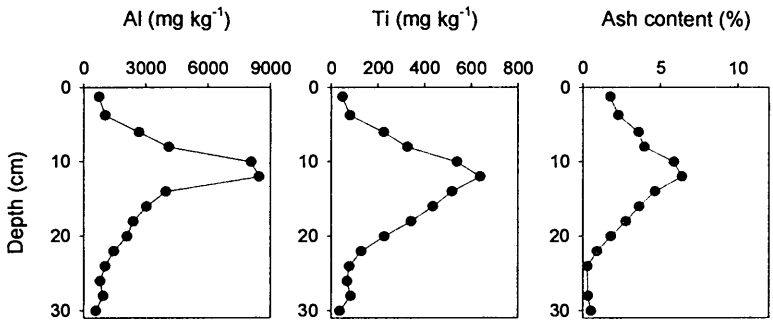

Figure 4.13: Depth profiles of Al and Ti concentrations (mg kg^{-1}) and ash contents (% by weight) in the RM03CM-1 (0-31 cm) peat core.

4.3.3 Discussion

As found at Flanders Moss (*cf.* Section 3.3.3), increases in Al, Sc, Ti, Y and Zr concentrations in the top ~ 24 cm peat sections of these cores are most likely caused by the increase in anthropogenic soil dust deposition. Also, the concentration profiles for pairs of elements Sc and Y, and Ti and Zr, at least in the uppermost ~ 40 cm of RM03CM-2, exhibited similar features (*cf.* Fig. 4.12). As discussed for Flanders

Moss cores (Section 3.5), Al will not be used in Section 4.5 to correct Pb concentrations for soil dust contributions at The Red Moss of Balerno.

4.3.3.1 Intercomparison of Sc and Ti

Profiles of Sc and Ti concentrations and Ti/Sc ratios (A5.1 Table A3) for RM03CM-2 are shown in Fig. 4.14. As for Flanders Moss (Section 3.3.3.1), slight differences between the Sc and Ti concentration profiles are apparent, as indicated by the Ti/Sc ratio profile. The UCC Ti/Sc ratio (445) is in good agreement with the mean Ti/Sc ratio (471 ± 74) in the 40-96 cm sections of the RM03CM-2 core, suggesting metal contributions from natural soil dust at these depths. Also, from 0-40 cm there was a general decrease in Ti/Sc ratios above the position of the maximum Ti/Sc ratios, which again (*cf.* Section 3.3.3.1) could be attributable to either different soil dust sources or direct non-soil-dust-related anthropogenic sources (e.g. coal combustion).

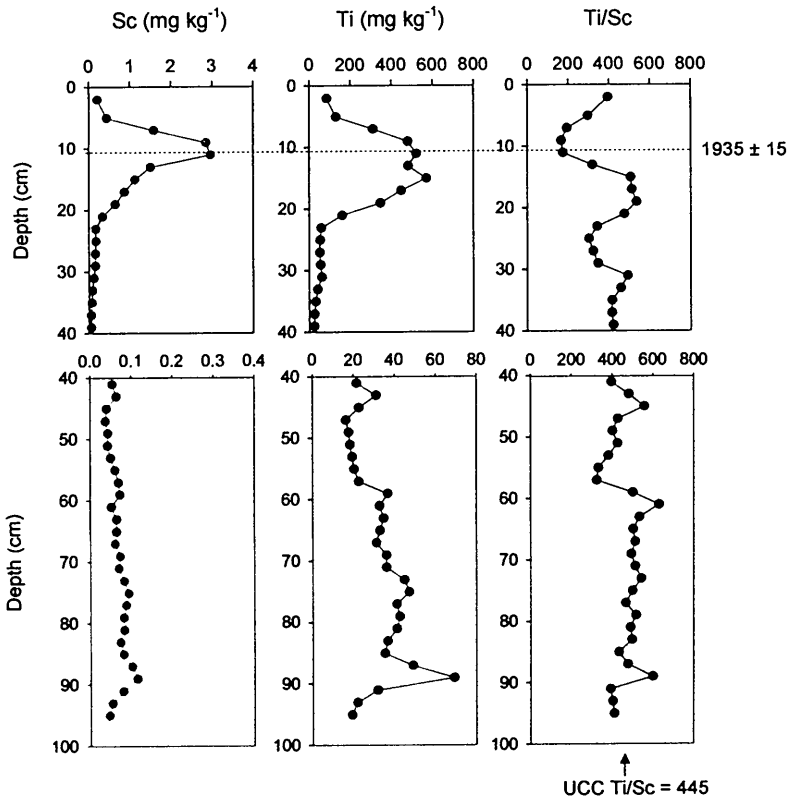

Figure 4.14: Depth profiles of Sc and Ti concentrations (mg kg^{-1}) and Ti/Sc ratios from 0-40 cm and 40-96 cm in the ^{210}Pb-dated RM03CM-2 peat core.

4.4 Pb AND Pb ISOTOPIC RATIOS

Profiles of Pb concentrations and measured $^{206}Pb/^{207}Pb$, $^{208}Pb/^{206}Pb$ and $^{208}Pb/^{207}Pb$ isotopic ratios for RM03CM-2 (Table 4.6) and RM03CM-1 (Table 4.7) are shown in Figs. 4.15 and 4.16, respectively.

4.4.1 RM03CM-2

0-40 cm

The Pb concentration increased from 9.2 mg kg^{-1} at 38-40 cm to a maximum value of 370 mg kg^{-1} at 8-10 cm, above which it decreased gradually towards the surface. The $^{206}Pb/^{207}Pb$ ratio remained constant (mean 1.175 ± 0.002) from 40 cm to 12 cm, above which it declined steeply to a minimum value of 1.115 before increasing to 1.130 at the surface (*cf.* Fig. 4.15).

40-96 cm

Note the change in scale on the Pb concentration (50-fold) on going from 0-40 cm to 40-96 cm. Several zones were apparent in the 40-96 cm sections: a region of minimum concentrations (mean 0.55 ± 0.18 mg kg^{-1}) from 94 to 70 cm, below which concentrations increased to 1.3 mg kg^{-1} at 95 cm and above which they increased to 6.9 mg kg^{-1} at 41 cm. The mean $^{206}Pb/^{207}Pb$ ratios between 94 and 70 cm and 70 and 40 cm were 1.156 ± 0.007 and 1.162 ± 0.006, respectively (*cf.* Fig. 4.15).

4.4.2 RM03CM-1

The Pb concentration increased from 4.4 mg kg^{-1} at 29-31 cm to a maximum of 260 mg kg^{-1} at 11-13 cm, above which it decreased to 2.0 mg kg^{-1} at the surface. The $^{206}Pb/^{207}Pb$ ratio remained fairly constant (mean 1.172 ± 0.004) from 31 to 15 cm followed by a decrease to 1.112 at 5-7 cm, and a subsequent increase to 1.149 at the surface (*cf.* Fig. 4.16).

Table 4.6: Total Pb concentrations (mg kg^{-1}) and Pb isotopic ratios in the RM03CM-2 peat core.

Section (cm)	Pb (mg kg^{-1})	$^{206}Pb/^{207}Pb$	$^{208}Pb/^{206}Pb$	$^{208}Pb/^{207}Pb$
0-4	15 ± 1	1.130 ± 0.0020	2.119 ± 0.0015	2.394 ± 0.0048
4-6	49 ± 2*	1.115 ± 0.0016	2.141 ± 0.0017	2.387 ± 0.0028
6-8	207 ± 23*	1.142 ± 0.0013	2.121 ± 0.0022	2.422 ± 0.0005
8-10	369 ± 13*	1.159 ± 0.0009	2.109 ± 0.0032	2.444 ± 0.0025
10-12	324 ± 3*	1.168 ± 0.0020	2.099 ± 0.0016	2.451 ± 0.0029
12-14	271 ± 10*	1.173 ± 0.0018	2.094 ± 0.0039	2.4560 ± 0.0013
14-16	225 ± 10*	1.175 ± 0.0010	2.091 ± 0.0021	2.458 ± 0.0014
16-18	126 ± 3*	1.172 ± 0.0013	2.081 ± 0.0026	2.438 ± 0.0029
18-20	85 ± 4*	1.173 ± 0.0019	2.081 ± 0.0028	2.442 ± 0.0022
20-22	64 ± 5*	1.173 ± 0.0007	2.082 ± 0.0016	2.441 ± 0.0021
22-24	56 ± 1*	1.175 ± 0.0008	2.084 ± 0.0012	2.448 ± 0.001
24-26	54 ± 3*	1.174 ± 0.0013	2.081 ± 0.0025	2.443 ± 0.0031
26-28	51 ± 7*	1.175 ± 0.0008	2.087 ± 0.0036	2.451 ± 0.0039
28-30	55 ± 6*	1.175 ± 0.0010	2.085 ± 0.0016	2.450 ± 0.0013
30-32	42 ± 6*	1.175 ± 0.0018	2.087 ± 0.0014	2.451 ± 0.0036
32-34	25 ± 1	1.178 ± 0.0010	2.081 ± 0.0019	2.451 ± 0 0028
34-36	18 ± 1	1.175 ± 0.0013	2.081 ± 0.0012	2.445 ± 0.0016
36-38	13 ± 0	1.176 ± 0.0009	2.080 ± 0.0032	2.446 ± 0.0034
38-40	9.20 ± 0.56	1.176 ± 0.0034	2.080 ± 0.0042	2.445 ± 0.0035
40-42	6.86 ± 0.66	1.176 ± 0.0007	2.080 ± 0.0017	2.447 ± 0.0023
42-44	4.63 ± 0.51	1.168 ± 0.0047	2.091 ± 0.0042	2.442 ± 0.0054
44-46	3.88 ± 0.05	1.170 ± 0.0016	2.085 ± 0.0023	2.439 ± 0.0031
46-48	2.21 ± 0.01	1.165 ± 0.0027	2.100 ± 0.0039	2.445 ± 0.0046
48-50	1.98 ± 0.02	1.163 ± 0.0007	2.085 ± 0.0021	2.425 ± 0.0026
50-52	2.52 ± 0.01	1.160 ± 0.0009	2.089 ± 0.0019	2.423 ± 0.0036
52-54	1.94 ± 0.00	1.163 ± 0.0014	2.083 ± 0.0031	2.422 ± 0.0027
54-56	1.63 ± 0.01	1.159 ± 0.0011	2.089 ± 0.0015	2.422 ± 0.0029
56-58	1.37 ± 0.01	1.161 ± 0.0029	2.090 ± 0.0074	2.428 ± 0.0041
58-60	1.39 ± 0.02	1.161 ± 0.0025	2.091 ± 0.0020	2.428 ± 0.0056
60-62	1.34 ± 0.01	1.160 ± 0.0027	2.088 ± 0.0050	2.422 ± 0.0018
62-64	1.38 ± 0.01	1.163 ± 0.0009	2.078 ± 0.0029	2.416 ± 0.0031
64-66	1.03 ± 0.01	1.150 ± 0.0017	2.101 ± 0.0024	2.417 ± 0.0042
66-68	0.80 ± 0.01	1.159 ± 0.0072	2.099 ± 0.0162	2.410 ± 0.0183
68-70	0.84 ± 0.00	1.159 ± 0.0034	2.098 ± 0.0110	2.431 ± 0.0084
70-72	0.61 ± 0.00	1.156 ± 0.0031	2.091 ± 0.0011	2.417 ± 0.0055

*Total Pb concentrations determined by ICP-OES where standard deviations were calculated as the standard deviation of the mean value for two separate sample analyses. ICP-MS Pb concentration and Pb isotopic ratio standard deviations were calculated as the standard deviation from the mean value for five consecutive determinations of the ratio/concentration of a sample solution.

Table 4.6 (continued): Total Pb concentrations (mg kg^{-1}) and Pb isotopic ratios in the RM03CM-2 peat core.

Section (cm)	Pb (mg kg^{-1})	$^{206}Pb/^{207}Pb$	$^{208}Pb/^{206}Pb$	$^{208}Pb/^{207}Pb$
72-74	0.56 ± 0.00	1.153 ± 0.0020	2.099 ± 0.0021	2.420 ± 0.0052
74-76	0.48 ± 0.00	1.158 ± 0.0052	2.098 ± 0.0168	2.430 ± 0.0246
76-78	0.92 ± 0.01	1.172 ± 0.0047	2.079 ± 0.0198	2.437 ± 0.0238
78-80	0.72 ± 0.01	1.149 ± 0.0019	2.101 ± 0.0038	2.415 ± 0.0032
80-82	0.73 ± 0.01	1.147 ± 0.0012	2.107 ± 0.0027	2.417 ± 0.0043
82-84	0.45 ± 0.00	1.150 ± 0.0026	2.100 ± 0.0063	2.414 ± 0.0095
84-86	0.28 ± 0.00	1.158 ± 0.0024	2.093 ± 0.0065	2.423 ± 0.0073
86-88	0.52 ± 0.01	1.161 ± 0.0016	2.090 ± 0.0040	2.426 ± 0.0025
88-90	0.45 ± 0.00	1.161 ± 0.0031	2.094 ± 0.0034	2.430 ± 0.0056
90-92	0.33 ± 0.01	1.162 ± 0.0023	2.087 ± 0.0022	2.425 ± 0.0052
92-94	0.54 ± 0.01	1.147 ± 0.0015	2.110 ± 0.0055	2.420 ± 0.0053
94-96	1.31 ± 0.01	1.159 ± 0.0028	2.094 ± 0.0041	2.426 ± 0.0033

Table 4.7: Total Pb concentrations (mg kg^{-1}) and Pb isotopic ratios in the RM03CM-1 peat core.

Section (cm)	Pb (mg/kg)	$^{206}Pb/^{207}Pb$	$^{208}Pb/^{206}Pb$	$^{208}Pb/^{207}Pb$
0-2.5	2.0	1.149 ± 0.003	2.102 ± 0.004	2.415 ± 0.007
2.5-5	8.8	1.129 ± 0.003	2.117 ± 0.006	2.389 ± 0.009
5-7	38	1.112 ± 0.003	2.142 ± 0.001	2.383 ± 0.006
7-9	104	1.117 ± 0.002	2.137 ± 0.003	2.387 ± 0.006
9-11	236	1.144 ± 0.003	2.111 ± 0.003	2.413 ± 0.010
11-13	255	1.164 ± 0.003	2.102 ± 0.002	2.447 ± 0.007
13-15	146	1.166 ± 0.002	2.094 ± 0.003	2.443 ± 0.007
15-17	98	1.176 ± 0.004	2.091 ± 0.003	2.460 ± 0.011
17-19	48	1.174 ± 0.004	2.092 ± 0.005	2.456 ± 0.014
19-21	37	1.171 ± 0.003	2.078 ± 0.005	2.434 ± 0.011
21-23	20	1.175 ± 0.003	2.094 ± 0.005	2.461 ± 0.012
23-25	10	1.170 ± 0.002	2.091 ± 0.002	2.447 ± 0.006
25-27	6.1	1.165 ± 0.003	2.095 ± 0.001	2.440 ± 0.005
27-29	5.3	1.176 ± 0.002	2.079 ± 0.005	2.445 ± 0.006
29-31	4.4	1.169 ± 0.002	2.097 ± 0.002	2.452 ± 0.004

Total Pb concentrations were determined by ICP-OES. Pb isotopic ratio standard deviations were calculated as the standard deviation from the mean value for five consecutive determinations of the ratio of a sample solution.

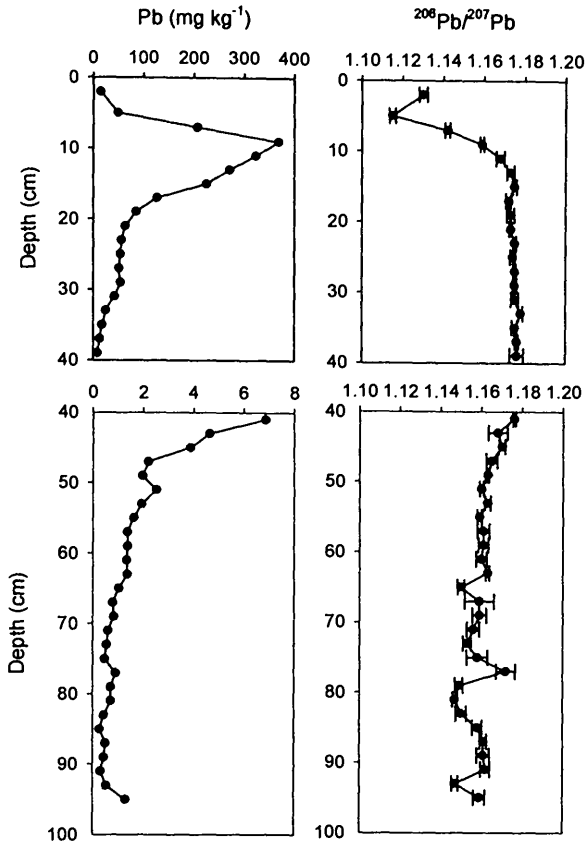

Figure 4.15: Depth profiles of Pb concentrations (mg kg^{-1}) and measured $^{206}Pb/^{207}Pb$ ratios from 0-40 cm and 40-96 cm in the RM03CM-2 peat core.

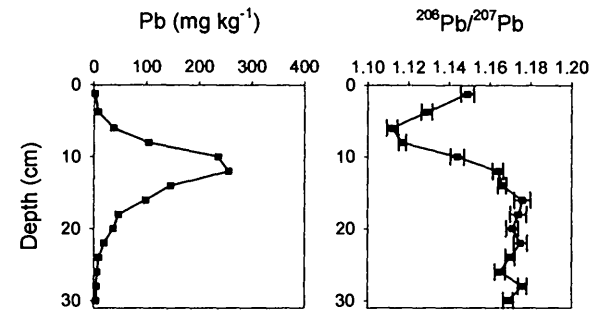

Figure 4.16: Depth profiles of Pb concentrations (mg kg^{-1}) and measured $^{206}Pb/^{207}Pb$ ratio in the RM03CM-1 (0-31 cm) peat core.

4.4.3 Discussion

As Pb is essentially immobile in ombrotrophic peat, these Pb profiles represent historical records of atmospheric deposition of anthropogenic and natural Pb at The Red Moss of Balerno. Interpretations of historical trends in sources of atmospheric

Pb deposition in these peat cores will be discussed in Section 4.6, after anthropogenic Pb enrichments have been estimated in Section 4.5.

4.5 USE OF CONSERVATIVE ELEMENTS TO ESTIMATE ANTHROPOGENIC ENRICHMENTS OF Pb

Profiles of Pb/Sc, Pb/Ti, Pb/Y and Pb/Zr ratios for RM03CM-2 (A5.1 Table A4) and Pb/Ti ratios for RM03CM-1 (A5.2 Table A3) along with Pb concentrations are shown in Figs. 4.17 and 4.18, respectively.

4.5.1 RM03CM-2

0-40 cm

The Pb/X ratios were at a maximum between 32 and 22 cm, averaging Pb/Sc (320 ± 20), Pb/Ti (0.90 ± 0.12), Pb/Y (170 ± 10) and Pb/Zr (42 ± 11). Above 22 cm, Pb/X ratios decreased before increasing again with minor Pb/Sc and Pb/Y ratio peaks at 15 cm and minor Pb/Ti and Pb/Zr ratio peaks between 16 and 4 cm. The Pb/X ratios decreased towards the surface (*cf.* Fig. 4.17). Note that the maximum Pb concentration (370 mg kg^{-1}) occurred at 8-10 cm.

40-96 cm

Note the change in scale on the ratio profiles (2-fold) on going from 0-40 cm to 40-96 cm (*cf.* Fig. 4.17). Maximum Pb/Sc (130), Pb/Ti (0.315), Pb/Y (68) and Pb/Zr (9.7) ratios occurred at a depth of 40-42 cm, below which Pb/X ratios decreased gradually towards the bottom of the core. Minimum mean Pb/Sc (6.7 ± 2.5), Pb/Ti (0.014 ± 0.006), Pb/Y (6.2 ± 1.8) and Pb/Zr (0.55 ± 0.20) ratios occurred between 70 and 94 cm, below which Pb/X ratios increased in the bottom section of the core.

4.5.2 RM03CM-1

In the RM03CM-1 core, Pb/Ti ratios increased steadily from the bottom of the core, exhibiting a broad peak between 17 and 5 cm with a maximum (0.44) at 10 cm,

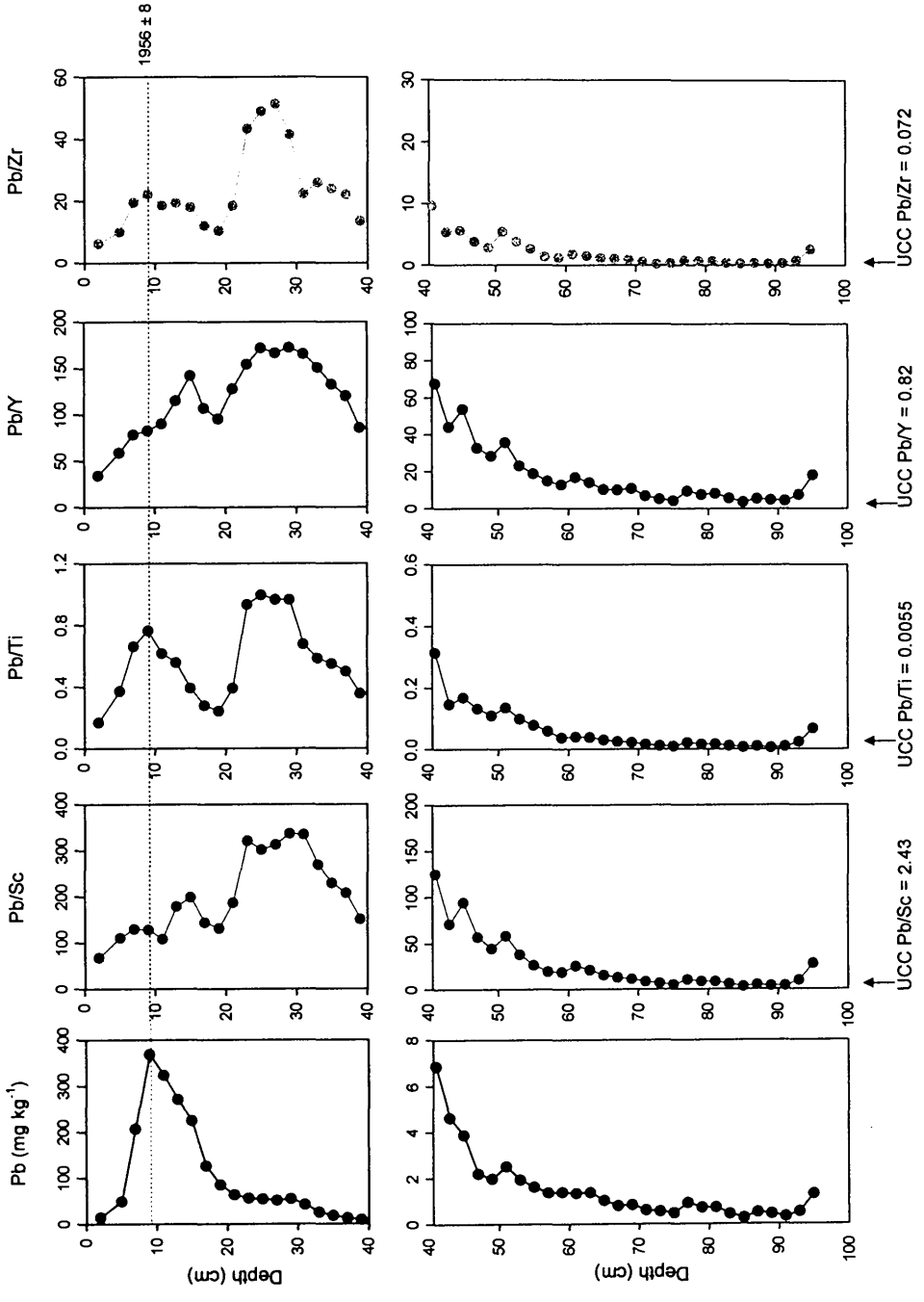

Figure 4.17: Depth profiles of Pb concentrations (mg kg^{-1}), Pb/Sc, Pb/Ti, Pb/Y and Pb/Zr ratios from 0-40 cm and 40-96 cm in the ^{210}Pb-dated RM03CM-2 peat core.

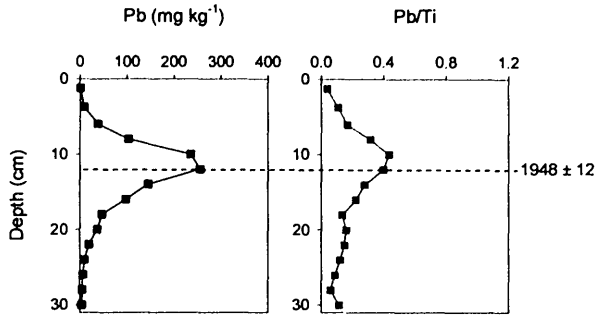

Figure 4.18: Depth profiles of Pb concentration (mg kg^{-1}) and Pb/Ti ratio in the ^{210}Pb-dated RM03CM-1 (0-31 cm) peat core.

above which Pb/Ti ratios decreased. Note that the maximum Pb concentration (260 mg kg^{-1}) occurred at 11-13 cm (*cf.* Fig. 4.18).

4.5.3 Discussion and selection of conservative element

The RM03CM-2 Pb/X ratio profiles for each of the conservative elements indicated corresponding zones of anthropogenic Pb enrichment (*cf.* Fig. 4.17). The minimum Pb/X ratios (Pb/Sc (6.7 ± 2.5), Pb/Ti (0.014 ± 0.006), Pb/Y (6.2 ± 1.8) and Pb/Zr (0.55 ± 0.20)) occurred between 70 and 94 cm in RM03CM-2 and, compared with the UCC Pb/X ratios of 2.43 for Pb/Sc, 0.0055 for Pb/Ti, 0.82 for Pb/Y and 0.072 for Pb/Zr, were 3 to 8-fold higher, as found for Flanders Moss (Section 3.5.3). It is therefore unlikely that Pb concentrations are unaffected by anthropogenic Pb inputs at any depth in RM03CM-2.

The maximum Pb/X ratios in RM03CM-2 occurred ~ 12 cm below the maximum Pb concentration peak, whereas the maximum Pb/Ti ratio in RM03CM-1 occurred ~ 2 cm above the Pb concentration peak, the latter being consistent with the findings for Flanders Moss (Section 3.5). The Pb/X ratios in RM03CM-2 above the Pb concentration peak (8-10 cm), however, were still elevated (*cf.* Fig. 4.17). Nevertheless, to avoid possible misinterpretations that could arise from directly using profiles of the Pb/X ratio in RM03CM-2 to express anthropogenic enrichment in terms of estimated anthropogenic enrichment factors for Pb, the anthropogenic Pb

concentrations (*cf.* Section 3.6.4) will instead be used to assist interpretation of historical trends in anthropogenic Pb deposition in Section 4.6.

As for Flanders Moss (*cf.* Section 3.5.3), Sc was used as the conservative element to enable calculation of anthropogenic Pb concentrations in RM03CM-2 (A5.1, Table A4), but, since Sc was not determined in RM03CM-1, Ti was used in the calculation of anthropogenic Pb concentrations (A5.2, Table A3) for that core. Note that, as illustrated for Flanders Moss (*cf.* Fig. 3.24, Section 3.6.4), there is very little difference between the "total" and calculated anthropogenic Pb concentrations in the top part of the RM03CM-2 core.

4.6 HISTORICAL TRENDS IN SOURCES OF ATMOSPHERIC Pb DEPOSITION

Anthropogenic Pb concentration and measured $^{206}Pb/^{207}Pb$ ratio profiles, including age dates, for RM03CM-2 and RM03CM-1 are shown in Figs. 4.19 and 4.20, respectively. The most important historical periods of anthropogenic sources of atmospheric Pb deposition can be summarised as follows:

- RM03CM-2 (96 to 40 cm) – Post-Roman and Mediaeval period
- RM03CM-2 (40-0 cm) and RM03CM-1 – Industrial and post-industrial period

4.6.1 Post-Roman and Mediaeval atmospheric Pb sources and deposition

At the bottom of the core (95 cm), for which no age-date was available, there was a significant increase in anthropogenic Pb concentration (1.20 mg kg^{-1}), possibly indicative of Pb deposition from indigenous Pb mining and smelting activities at the end of the Roman era (*ca.* 410 A.D.). Another explanation, however, is long-range atmospheric Pb deposition from post-Roman mining and smelting activities in Spain during the reign of the Visigods (after 410 A.D. to late 6^{th} century A.D.). Based on the age-dates of 760-900 A.D. and 970-1070 A.D. given for sections 76-78 and 48-50 cm, respectively, and, also, the corresponding $^{206}Pb/^{207}Pb$ ratio (1.159) in the 94-

96 cm section (*cf.* Fig. 4.19), which is significantly less radiogenic than values found in indigenous Pb ores but comparable to those found in Spanish Pb ores, the latter explanation is more likely.

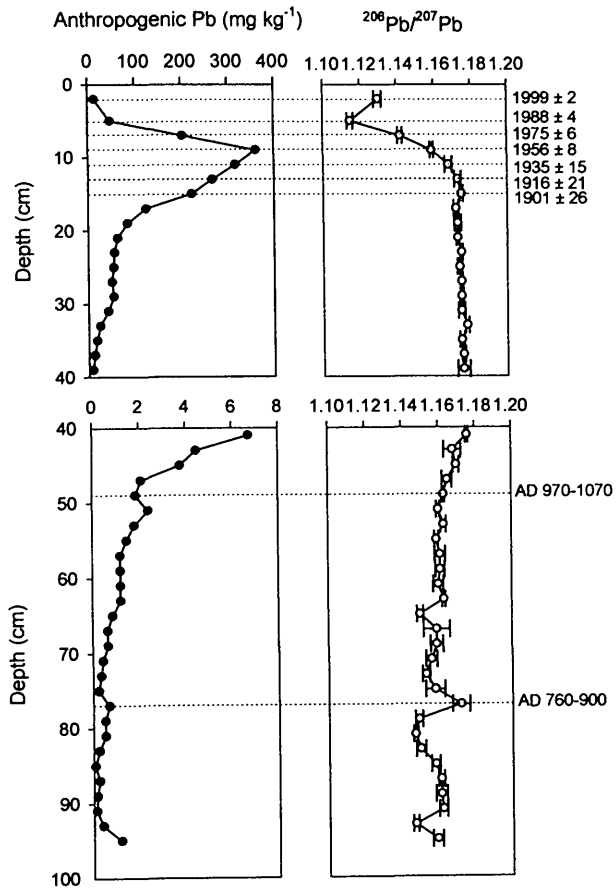

Figure 4.19: Depth profiles of anthropogenic Pb concentrations (mg kg^{-1}) and measured $^{206}Pb/^{207}Pb$ ratios from 0-40 cm and 40-96 cm in the ^{210}Pb- and ^{14}C-dated RM03CM-2 peat core.

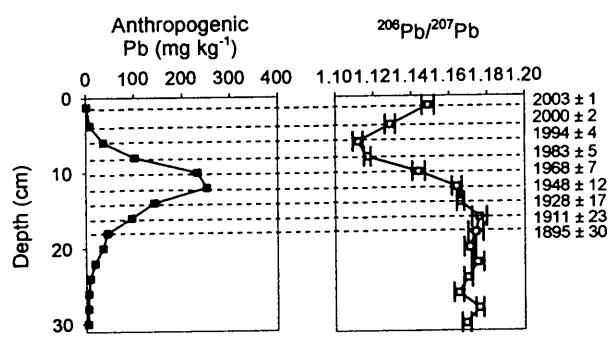

Figure 4.20: Depth profiles of anthropogenic Pb concentrations (mg kg^{-1}) (calculated using Ti as the conservative element) and measured $^{206}Pb/^{207}Pb$ ratio in the ^{210}Pb-dated RM03CM-1 (0-31 cm) peat core.

The minimum anthropogenic Pb concentrations (mean 0.35 ± 0.18 mg kg^{-1}) between 94 and 70 cm, for which there was a single age-date of 760-900 A.D. available for 76-78 cm, reflect a decline in metallurgical activities during the post-Roman and early Mediaeval era. The corresponding $^{206}Pb/^{207}Pb$ ratios for this period (mean 1.156 ± 0.007) were slightly less radiogenic than the underlying section. Above 70 cm up to a depth of 50 cm (970-1070 A.D.), anthropogenic Pb concentrations (mean 1.3 ± 0.5 mg kg^{-1}) and corresponding $^{206}Pb/^{207}Pb$ ratios (mean 1.160 ± 0.004) increased (*cf.* Fig. 4.19), possibly reflecting Pb emissions from Pb mining and smelting activities, especially in continental Europe, during the Mediaeval period.

Above 50 cm (970-1070 A.D.) to a depth of 40 cm, anthropogenic Pb concentrations increased markedly from 1.9 mg kg^{-1} to 6.7 mg kg^{-1} and $^{206}Pb/^{207}Pb$ ratios increased from 1.163 to 1.176. The latter value is comparable to those found in indigenous British Pb ores, indicating the increasing influence of Pb emissions from mining and smelting of indigenous Pb ores, as well as Pb ores from continental Europe, up to and including the late Mediaeval period (*ca.* 1500 A.D.). The latter brought about increases in metallurgical activity as well as improvements in procedures throughout Europe, particularly Britain (Tylecote, 1986).

4.6.2 Industrial and post-industrial atmospheric Pb sources and deposition

From 40 cm, a depth for which no age-date was available but, based on associated ^{210}Pb dates in the overlying upper regions, seems likely to correspond to the early 1700s A.D., to 12 cm (*ca.* 1926 A.D.) in RM03CM-2, anthropogenic Pb concentrations increased from 9.1 to 270 mg kg^{-1} and the corresponding $^{206}Pb/^{207}Pb$ ratios remained constant (mean 1.175 ± 0.002) (*cf.* Fig. 4.19). Similarly from 31 cm, which probably corresponds to the late 1700s A.D., to 15 cm (*ca.* 1918 A.D.) in RM03CM-1, anthropogenic Pb concentrations increased from 4.2 to 95 mg kg^{-1} while corresponding $^{206}Pb/^{207}Pb$ ratios remained constant (mean 1.172 ± 0.004) (*cf.* Fig. 4.20). These trends are consistent with Pb emissions from the mining and smelting of indigenous Scottish Pb ores, as found for Flanders Moss (*cf.* Section

3.6.3). Above 12 cm (*ca.* 1926 A.D.) in RM03CM-2, anthropogenic Pb concentrations continued to increase, reaching a maximum of 360 mg kg^{-1} at 8-10 cm (*ca.* 1956 A.D.) while corresponding $^{206}Pb/^{207}Pb$ ratios decreased to 1.159 (*cf.* Fig. 4.19). Similarly, above 15 cm (*ca.* 1918 A.D.) in RM03CM-1, Pb concentrations increased to a maximum of 250 mg kg^{-1} at 11-13 cm (*ca.* 1948 A.D.) and corresponding $^{206}Pb/^{207}Pb$ ratios decreased to 1.164 (*cf.* Fig. 4.20). As observed for Flanders Moss (Section 3.6.3), these trends are consistent with the general decline in the indigenous Scottish Pb mining industry and the increasing influence of the use of imported Australian Pb ore, predominantly via car exhaust emissions from the 1930s A.D. Also, the intermediate $^{206}Pb/^{207}Pb$ ratio values indicate that there were significant contributions from other sources of Pb, such as coal combustion.

From the late 1960s to the early/late-1990s A.D. (i.e. from 8 to 4 cm and 11 to 5 cm in RM03CM-2 and RM03CM-1, respectively), anthropogenic Pb concentrations decreased and corresponding $^{206}Pb/^{207}Pb$ ratios decreased dramatically to minimum values of 1.115 at 1988 A.D. in RM03CM-2 and 1.112 at 1994 A.D. in RM03CM-1 (*cf.* Figs. 4.19 and 4.20). As found for Flanders Moss (Section 3.6.3), these trends reflect the decreasing influence of coal combustion and the increasing influence of car exhaust emissions of Pb. From the early/late-1990s A.D. to 2003 A.D. (i.e. the top 4 cm of RM03CM-2 and top 5 cm of RM03CM-1, respectively), anthropogenic Pb concentrations continued to fall while the $^{206}Pb/^{207}Pb$ ratios increased to 1.130 at 1999 in RM03CM-2 and 1.149 at 2003 A.D. in RM03CM-1 (*cf.* Figs. 4.19 and 4.20), reflecting the steep fall in Pb emissions from car exhausts, consistent with findings at Flanders Moss (Section 3.6.3). The 3-isotope plot (Fig. 4.21) provides evidence for the multiple contributions to Pb deposition, during the industrial and post-industrial era, e.g. from the sources mentioned above and incinerator fly ash.

4.6.2.1 Historical trends in depositional fluxes and inventories of Pb

Depositional fluxes of anthropogenic Pb in RM03CM-2 (A5.1 Table A12) and RM03CM-1 (A5.2 Table A5) peat sections were estimated, on the basis of extrapolated and measured ^{210}Pb chronologies, and are plotted (since 1880 A.D.),

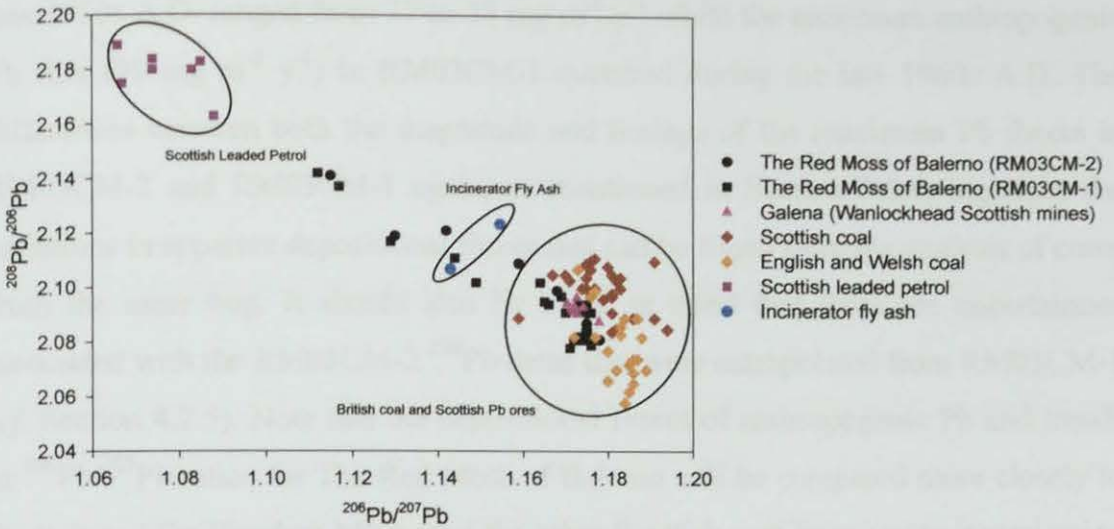

Figure 4.21: Plot of $^{208}Pb/^{206}Pb$ *versus* $^{206}Pb/^{207}Pb$ ratios for the RM03CM-2 (0-40 cm) and RM03CM-1 (0-31 cm) peat samples, and for galena in Wanlockhead Scottish Pb ores (Rohl, 1996), British coal (Farmer *et al.*, 1999), leaded petrol (Farmer *et al.*, 2000) and incinerator fly ash (Monna *et al.*, 1997).

along with the measured $^{206}Pb/^{207}Pb$ ratios, *versus* ^{210}Pb-derived calendar dates in Fig. 4.22.

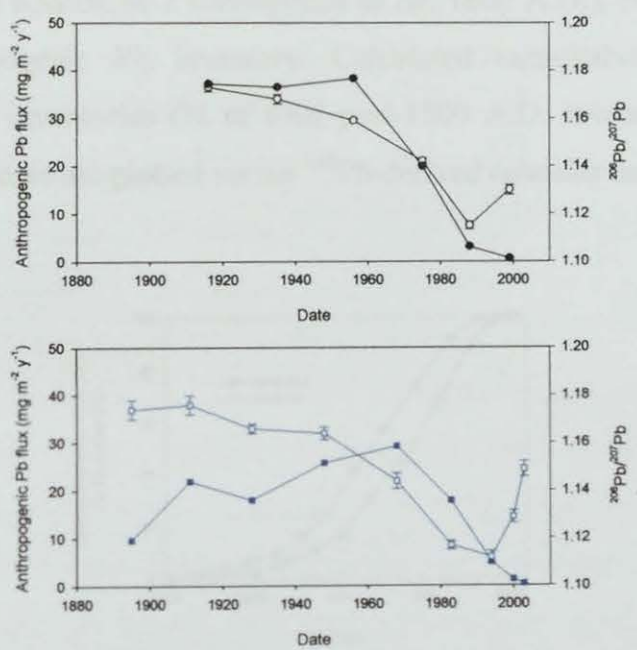

Figure 4.22: Calculated atmospheric depositional fluxes of anthropogenic Pb (mg m^{-2} y^{-1}) (closed symbols) and measured $^{206}Pb/^{207}Pb$ ratios (open symbols) for the RM03CM-2 (black) and RM03CM-1 (blue) cores *versus* ^{210}Pb-derived dates since 1880 A.D.

The maximum anthropogenic Pb fluxes in RM03CM-2 between the late 1910s and late 1950s A.D. ranged from 37 to 38 mg m^{-2} y^{-1} while the maximum anthropogenic Pb flux (29 mg m^{-2} y^{-1}) in RM03CM-1 occurred during the late 1960s A.D. The differences between both the magnitude and timings of the maximum Pb fluxes in RM03CM-2 and RM03CM-1 again, as mentioned in Section 3.6.4, highlight the variations in apparent depositional fluxes that can be found from the analysis of cores from the same bog. It should also be borne in mind that there are uncertainties associated with the RM03CM-2 ^{210}Pb dates that were extrapolated from RM03CM-1 (*cf.* Section 4.2.5). Note that the depositional fluxes of anthropogenic Pb and trends in ^{206}Pb/^{207}Pb ratios for The Red Moss of Balerno will be compared more closely to those found for Flanders Moss, and the other Scottish peat bogs under investigation in Section 7.5.3.

The total anthropogenic Pb inventories for RM03CM-2 (i.e. from *ca.* 600 to 2003 A.D.) and RM03CM-1 (i.e. from *ca.* late 1700s to 2003 A.D.) were 4.6 g m^{-2} and 2.5 g m^{-2}, respectively. The greatest contribution to anthropogenic Pb inventory in RM03CM-2 occurred during the post-1800 A.D. period (4.3 g m^{-2}) (assuming that a depth of 28 cm in RM03CM-2 corresponds to *ca.* 1800 A.D.), constituting 93% of the total anthropogenic Pb inventory. Calculated cumulative post-1800 A.D. anthropogenic Pb inventories (% of total post-1800 A.D. inventory) for The Red Moss of Balerno cores are plotted *versus* ^{210}Pb-derived calendar dates in Fig. 4.23.

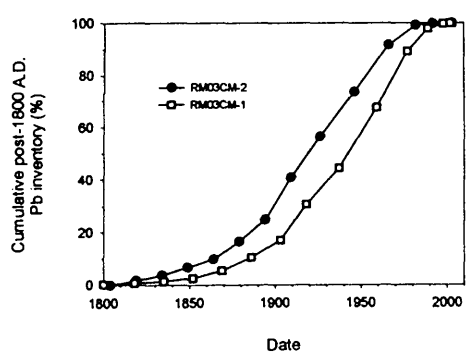

Figure 4.23: Calculated cumulative post-1800 A.D. anthropogenic Pb inventories (% of total post-1800 A.D. inventory) for the RM03CM-2 and RM03CM-1 cores *versus* ^{210}Pb-derived dates. Note that dates in RM03CM-2 and RM03CM-1 prior to *ca.* 1894 A.D. and *ca* 1886 A.D., respectively, were extrapolated.

Maximum deposition occurred between the 1900s and 1970s A.D. Differences in the vertical (temporal) distribution (%) of anthropogenic Pb inventories between the two cores, however, can perhaps be accounted for by the significant uncertainties associated with the ^{210}Pb dates extrapolated for RM03CM-2 from RM03CM-1 (*cf.* Table 4.3).

4.7 GEOCHEMICAL BEHAVIOUR OF MAJOR ELEMENTS

Profiles of total Ca, Fe, Mg, Mn, P and S concentrations, along with water and ash content, for RM03CM-2 (A5.1 Table A5) and RM03CM-1 (A5.2 Table A4) are shown in Figs. 4.24 and 4.25, respectively.

4.7.1 RM03CM-2

All six elements exhibited concentration peaks or increases in the uppermost ~ 12 cm of the core, with the following maximum concentrations at the depths indicated:

- Ca – 3600 mg kg^{-1} at 0-4 cm
- Fe – 4600 mg kg^{-1} at 8-10 cm
- Mg – 1100 mg kg^{-1} at 4-6 cm but the maximum value (1500 mg kg^{-1}) in the core occurred at 92-94 cm
- Mn – 260 mg kg^{-1} at 0-4 cm
- P – 880 mg kg^{-1} at 8-10 cm
- S – 1400 mg kg^{-1} at 8-10 cm

The Fe, Mn and P concentrations increased markedly from low constant values at depth. Both Fe and P concentrations exhibited peaks with maxima 2 cm below the vegetation-peat interface (6-8 cm), above which they decreased but still remained relatively high in the surface vegetation. The Mn concentrations also increased above 12 cm, but in contrast to Fe, exhibited a maximum at the surface. The S concentrations were at a maximum at the same depth as Fe and P. The Ca and Mg concentrations increased in the surface vegetation, but below ~ 24 cm, Ca, Mg and S

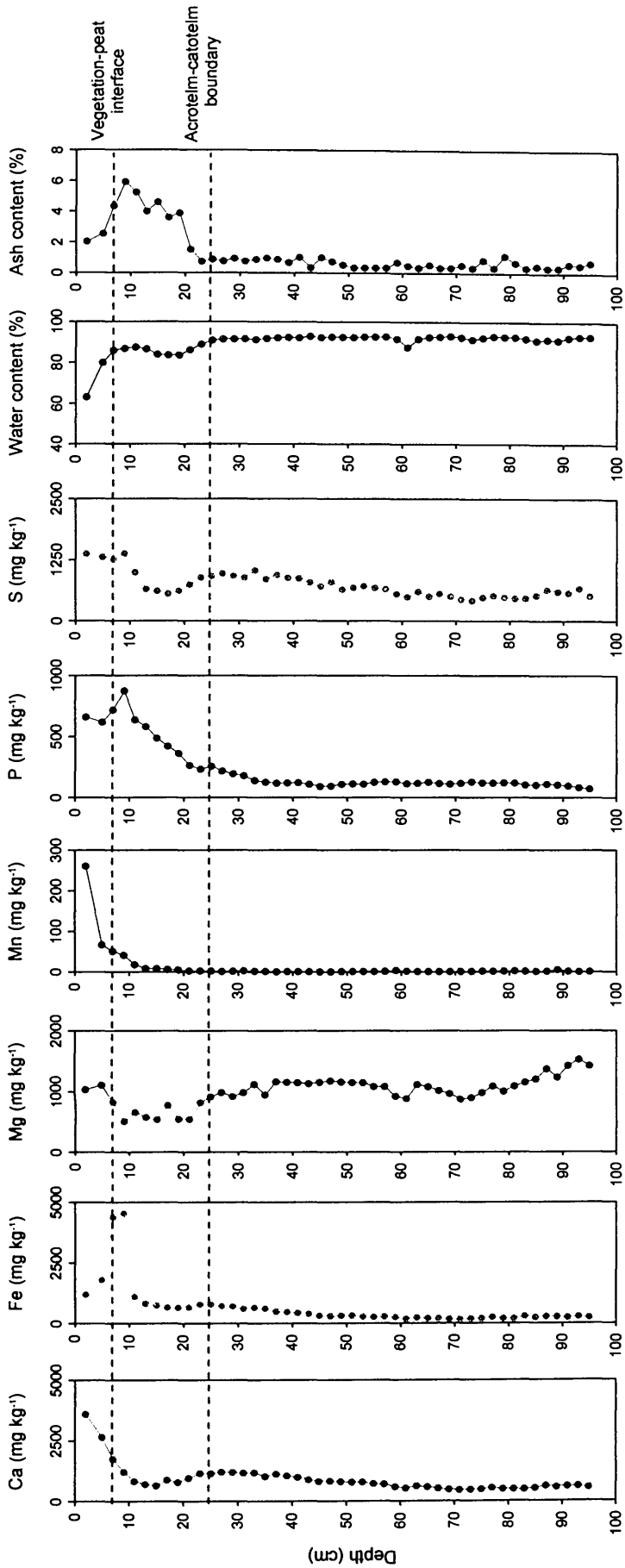

Figure 4.24: Depth profiles of Ca, Fe, Mg, Mn, Pand S concentrations (mg kg^{-1}), water and ash contents (% by weight) in the RM03CM-2 (0-96 cm) peat core.

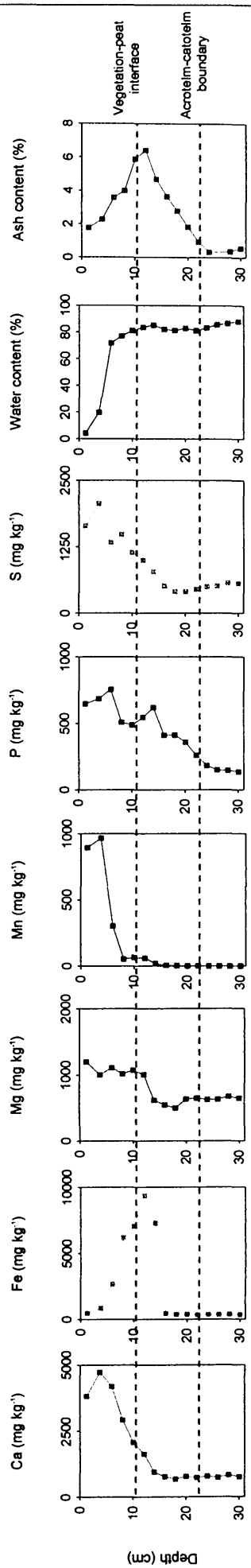

Figure 4.25: Depth profiles of Ca, Fe, Mg, Mn, P and S concentrations (mg kg^{-1}), water and ash contents (% by weight) in the RM03CM-1 (0-31 cm) peat core.

concentrations remained fairly high and constant, with the exception of the gradual increase in Mg concentrations towards the bottom of the core. Also, minima in Ca, Mg and S concentrations occurred between 12-22 cm (*cf.* Fig. 4.24), coincident with the below-surface minimum in the water content profile (*cf.* Section 3.7.1).

4.7.2 RM03CM-1

All six elements exhibited concentration peaks or increases in the uppermost ~ 15 cm of RM03CM-1 and the following maximum concentrations occurred, at the depths indicated:

- Ca – 4700 mg kg^{-1} at 2.5-5 cm
- Fe – 9400 mg kg^{-1} at 11-13 cm
- Mg – 1200 mg kg^{-1} at 0-2.5 cm
- Mn – 900 - 970 mg kg^{-1} between 0 and 5 cm
- P – 760 mg kg^{-1} at 5-7 cm but there was also a peak (620 mg kg^{-1}) at 13-15 cm
- S – 2100 mg kg^{-1} at 2.5-5 cm

Trends were consistent with those in RM03CM-2, i.e. Fe concentrations exhibited a peak with a maximum concentration 2 cm beneath the vegetation-peat interface (9-11 cm), Mn concentrations were at a maximum in the top 5 cm of the core and P concentrations exhibited peaks 4 cm below and 4 cm above the vegetation-peat interface. The Ca, Mg and S concentrations increased from minimum values between 13-21 cm to maximum values in the surface vegetation (0-5 cm) (*cf.* Fig. 4.25).

4.7.3 Discussion

The trends for The Red Moss of Balerno are consistent with those found for Flanders Moss (*cf.* Section 3.7.3). For example, there was no apparent correlation between the Ca, Fe, Mg, Mn, P and S concentration and ash content profiles (*cf.* Figs. 4.24 and 4.25) and the Ca and Mg concentration profiles indicated that contributions from sea salt inputs were minor. As found for Flanders Moss (Section 3.7.3), The Red Moss of

Balerno Ca, Fe, Mg, Mn, P and S concentration profiles are influenced by nutrient uptake and recycling, since their concentrations increased in the zones of biological cycling, i.e. the upper 8 cm of RM03CM-2 and 9 cm of RM03CM-1 (*cf.* Figs. 4.24 and 4.25). Also, as observed for Flanders Moss (Section 3.7.3), the influence of redox cycling on the Fe, Mn, P and perhaps to some extent S concentration profiles is apparent if the zones of water table fluctuation lie between ~ 6 and 26 cm in RM03CM-2 and between ~ 11 and 23 cm in RM03CM-1. These estimated acrotelm-catotelm boundary positions are supported by hydrological monitoring data obtained for The Red Moss of Balerno, which indicates that the water table fluctuates within a range of approximately 50 cm at this bog throughout the year (SWT, 2001). It is worth bearing in mind that the high surface Mn concentrations, attributable to nutrient uptake and recycling, in RM03CM-2 and RM03CM-1, mask the diagenetic Mn peaks that might well occur close to the depth of the diagenetic Fe peaks (8-10 cm and 11-13 cm in RM03CM-2 and RM03CM-1, respectively) (*cf.* Figs. 4.24 and 4.25). Also, as found for Flanders Moss, the similarity between the Fe and P concentration profiles for The Red Moss of Balerno indicates the influence of Fe on the distribution of P, although the maximum of the diagenetic P peak in RM03CM-1, as observed for Flanders Moss (*cf.* Section 3.7.3), occurred 2 cm below the diagenetic Fe peak (*cf.* Fig. 4.25).

4.8 GEOCHEMICAL BEHAVIOUR OF OTHER TRACE ELEMENTS

4.8.1 Sb

Concentrations of Sb (A5.1 Table A6) were determined only for RM03CM-2. The Sb profile, along with those of Pb and Sc, is shown in Fig. 4.26.

0-40 cm

The Sb concentrations increased from 0.064 mg kg^{-1} at 38-40 cm to a maximum value of 7.1 mg kg^{-1} at a depth of 11 cm, 2 cm below the Pb maximum, above which concentrations gradually decreased towards the top of the core (*cf.* Fig. 4.26).

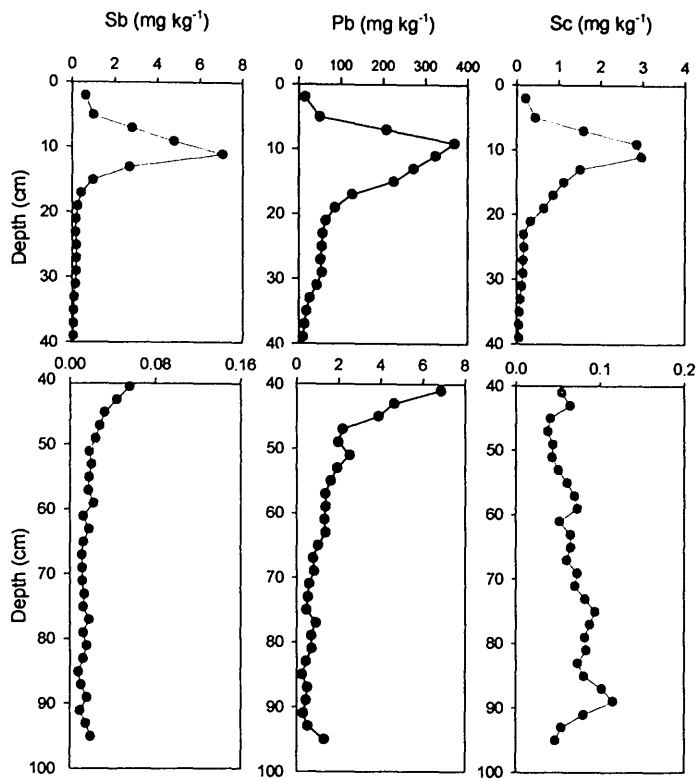

Figure 4.26: Depth profiles of Sb, Pb and Sc concentrations (mg kg^{-1}) from 0-40 cm and 40-96 cm in the RM03CM-2 peat core.

40-96 cm

Note the changes in scale on the Sb and Pb (50-fold) and Sc (20-fold) concentrations on going from 0-40 cm to 40-96 cm. The same zones as those observed earlier for Pb concentrations (Section 4.6) were apparent for Sb: a region of minimum concentrations (mean 0.013 ± 0.003 mg kg^{-1}) from 94 cm to 70 cm, above which concentrations increased steadily to 0.056 mg kg^{-1} by 40 cm and below which concentrations increased to a value of 0.020 mg kg^{-1} at the bottom of the core (*cf.* Fig. 4.26).

4.8.1.1 Discussion

As observed for Flanders Moss (*cf.* Section 3.8.1), the Sb and Pb profiles show a remarkable resemblance, providing further evidence that Sb, like Pb, is also essentially immobile in ombrotrophic peat.

4.8.1.1.1 The use of Sc as an indicator of soil dust input of Sb

The profile of Sb/Sc ratios (A5.1 Table A6), along with that of Pb/Sc ratios, in RM03CM-2 is shown in Fig. 4.27.

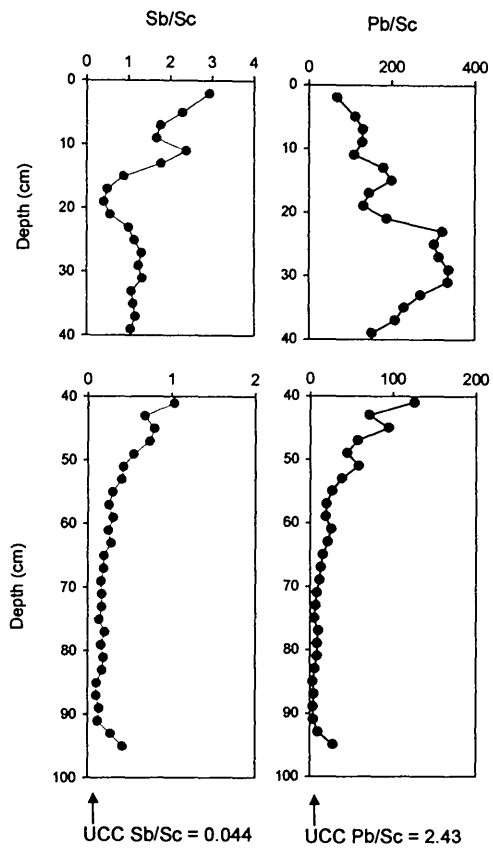

Figure 4.27: Depth profiles of Sb/Sc and Pb/Sc ratios from 0-40 cm and 40-96 cm in the RM03CM-2 peat core.

The maximum Sb/Sc ratio (2.9) occurred at 0-4 cm, which was 18 cm above the depths of the maximum mean Pb/Sc ratio (320 ± 20) (*cf.* Section 4.5.1). The Sb/Sc ratios exhibited a peak at 10-12 cm, below which they decreased down to 22 cm before increasing and remaining constant (mean 1.2 ± 0.1) down to 40 cm (*cf.* Fig. 4.27). As found for Pb/Sc ratios, the minimum mean Sb/Sc ratio (0.16 ± 0.05) occurred between 70 and 94 cm, which is ~ 4-fold greater than the corresponding UCC ratio (0.044), similar to the ~ 3-fold greater mean minimum Pb/Sc ratio (*cf.* Section 4.5.3). Due to the problems associated with directly using profiles of the Pb/Sc ratio in RM03CM-2 to indicate anthropogenic enrichments of Pb (*cf.* Section 4.5.3), anthropogenic Sb concentrations (A 8.1 Table A6), calculated on the basis of

the use of Sc as a conservative element (*cf.* Section 3.8.1.3.1), along with anthropogenic Sb/Pb ratios (*cf.* Section 3.8.1.3.1) will be used to interpret historical trends in anthropogenic Sb deposition.

4.8.1.1.2 Historical trends in sources of atmospheric Sb deposition

Anthropogenic Sb and Pb concentration, measured $^{206}Pb/^{207}Pb$ and anthropogenic Sb/Pb ratio profiles for RM03CM-2, including age-dates, are shown in Fig. 4.28.

Post-Roman and Mediaeval atmospheric Sb sources and deposition

At the bottom of the core (95 cm) there is an increase in anthropogenic Sb concentration (0.017 mg kg^{-1}), as observed for Pb (*cf.* Fig. 4.28), and the corresponding anthropogenic Sb/Pb ratio (0.015) is lower than that of the UCC Sb/Pb ratio (0.018) but greater than the range of values (0.0033 – 0.0056) obtained for the Wanlockhead and Leadhills Scottish Pb ore samples (*cf.* Table 3.10, Section 3.8.1.3.2). These trends perhaps provide evidence for the long-range atmospheric deposition of Sb, as well as Pb (*cf.* Section 4.6.1), from Spanish Pb ore mining and smelting activities during the reign of the Visigods (*cf.* Section 3.6.2). Over the depth interval 94 to 70 cm, for which there was a single age-date of 760-900 A.D. available for 76-78 cm, anthropogenic Sb concentrations (mean 0.0096 ± 0.0028 mg kg^{-1}) were at their lowest, as found for Pb (*cf.* Fig. 4.28), consistent with the decline in metallurgical activities during the post-Roman and early Mediaeval era (*cf.* Section 4.6.1). The corresponding mean anthropogenic Sb/Pb ratio was 0.034 ± 0.016 but given that the anthropogenic Sb and Pb concentrations were very small ($\leq$ 0.014, $\leq$ 0.71) at these depths the associated anthropogenic Sb/Pb ratios have quite a high uncertainty (typically ± 47%).

Above 70 cm up to a depth of 50 cm (970-1070 A.D.), anthropogenic Sb concentrations (mean 0.014 ± 0.004 mg kg^{-1}) increased, as found for Pb (*cf.* Fig. 4.28), while corresponding anthropogenic Sb/Pb ratios (mean 0.012 ± 0.003) decreased and remained fairly constant (*cf.* Fig. 4.28), consistent with increasing Sb and Pb emissions as a result of the gradual revival in Pb mining and smelting activities in continental Europe, during the Mediaeval period (*cf.* Section 4.6.1).

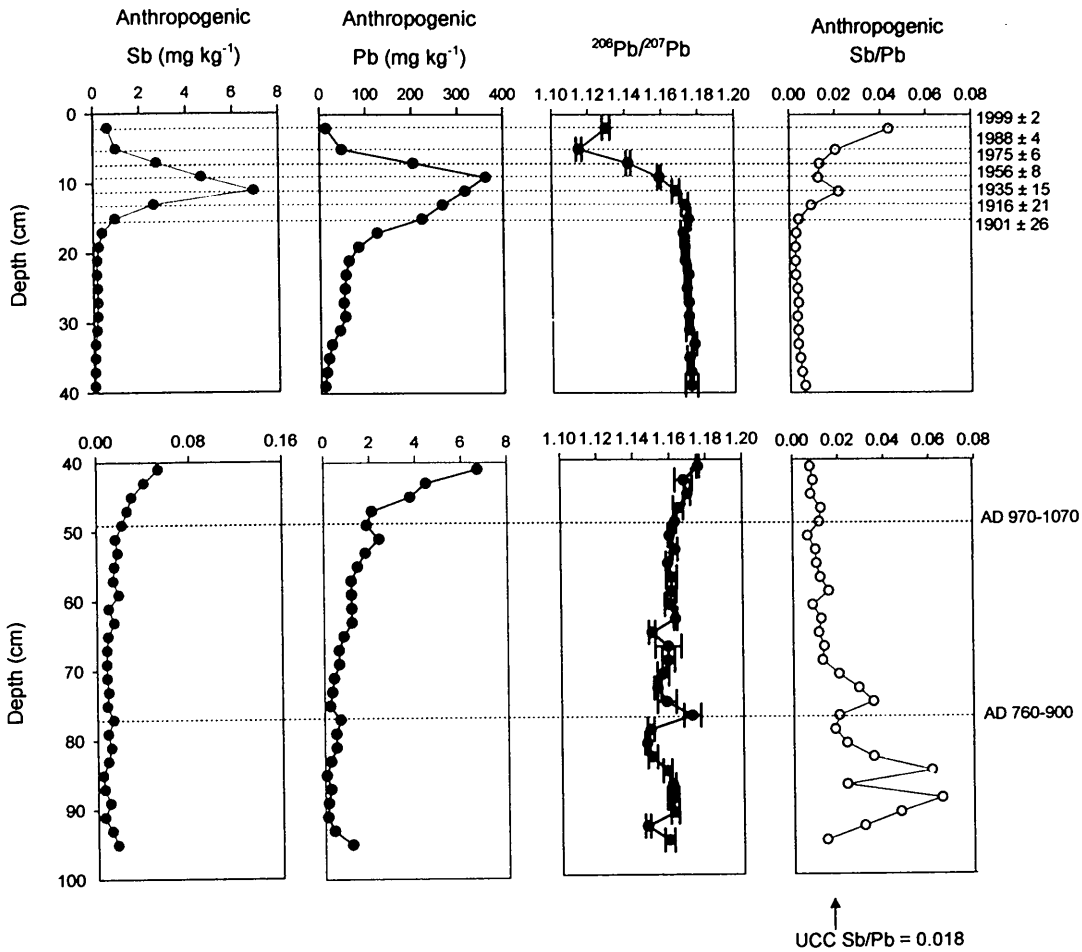

Figure 4.28: Depth profiles of anthropogenic Sb and Pb concentrations, measured $^{206}Pb/^{207}Pb$ and anthropogenic Sb/Pb ratios from 0-40 cm and 40-96 cm in the ^{210}Pb- and ^{14}C-dated RM03CM-2 peat core.

Above 50 cm (970-1070 A.D.) to a depth of 40 cm, anthropogenic Sb concentrations increased from 0.022 mg kg^{-1} to 0.054 mg kg^{-1}, but were less marked than those of Pb (*cf.* Fig. 4.28). The corresponding anthropogenic Sb/Pb ratios were unchanged (mean 0.010 ± 0.002) and, based on the corresponding increase in $^{206}Pb/^{207}Pb$ ratios (from 1.163 to 1.176) (*cf.* Section 4.6.1), these trends are consistent with Sb and Pb emissions from mining and smelting of indigenous Pb ores, as well as Pb ores from continental Europe, during the Mediaeval period (*cf.* Section 4.6.1).

Industrial and post-industrial atmospheric Sb sources and deposition

From 40 (*ca.* early 1700s A.D.) to 12 cm (*ca.* 1926 A.D.) in RM03CM-2 (*cf.* Fig. 4.28), anthropogenic Sb concentrations increased from 0.061 mg kg^{-1} to

2.6 mg kg^{-1}, exhibiting a steeper increase than the anthropogenic Pb concentrations (*cf.* Section 4.6.2) (*cf.* Fig. 4.28). The corresponding mean anthropogenic Sb/Pb ratio (mean 0.0044 ± 0.0019) was lower than that observed in the Mediaeval times (mean 0.010 ± 0.002) (40 to 50 cm section), consistent with trends of Sb and Pb emissions from the mining and smelting of indigenous Scottish Pb ores, as found for Flanders Moss (*cf.* Section 3.8.1.3.2). Anthropogenic Sb concentrations reached a maximum of 6.9 mg kg^{-1} at 10-12 cm (*ca.* 1935 A.D.), pre-dating the maximum anthropogenic Pb concentration (360 mg kg^{-1}) by *ca.* 21 years (*cf.* Fig. 4.28). The corresponding anthropogenic Sb/Pb ratio of 0.022, which is significantly higher than the mean value of 0.0044 ± 0.0019 between 40 and 12 cm, is attributable to the influence of Sb emissions from coal combustion (*cf.* Table 3.11, Section 3.8.1.3.2), as found for Flanders Moss (*cf.* Section 3.8.1.3.2).

After 1935 A.D. (10-12 cm) up to 1982 A.D. (6 cm) in RM03CM-2, both the anthropogenic Sb concentrations and the corresponding anthropogenic Sb/Pb ratios decreased, the latter to 0.013 (*cf.* Fig. 4.28), consistent with the decreasing influence of coal combustion and the increasing influence of vehicle exhaust emissions of Pb (*cf.* Section 4.6.2), as found for Flanders Moss (*cf.* Section 3.8.1.3.2). Between 1982 A.D. (6 cm) and 2003 A.D. (0 cm), the anthropogenic Sb concentrations continued to decrease (from 0.99 to 0.63 mg kg^{-1}), but not so markedly as Pb (*cf.* Fig. 4.28). The anthropogenic Sb/Pb ratios increased (from 0.021 to 0.044) and these trends, as observed for Flanders Moss (*cf.* Section 3.8.1.3.2), suggest a new recent source of Sb, (e.g. automotive brake linings, degradation or combustion of plastics).

4.8.1.1.3 Historical trends in depositional fluxes and inventories of anthropogenic Sb

Depositional fluxes of anthropogenic Sb (A5.1 Table A12) are plotted, along with those of anthropogenic Pb and the anthropogenic Sb/Pb and measured $^{206}Pb/^{207}Pb$ ratios, since 1900 A.D., *versus* ^{210}Pb-derived calendar dates for RM03CM-2 in Fig. 4.29.

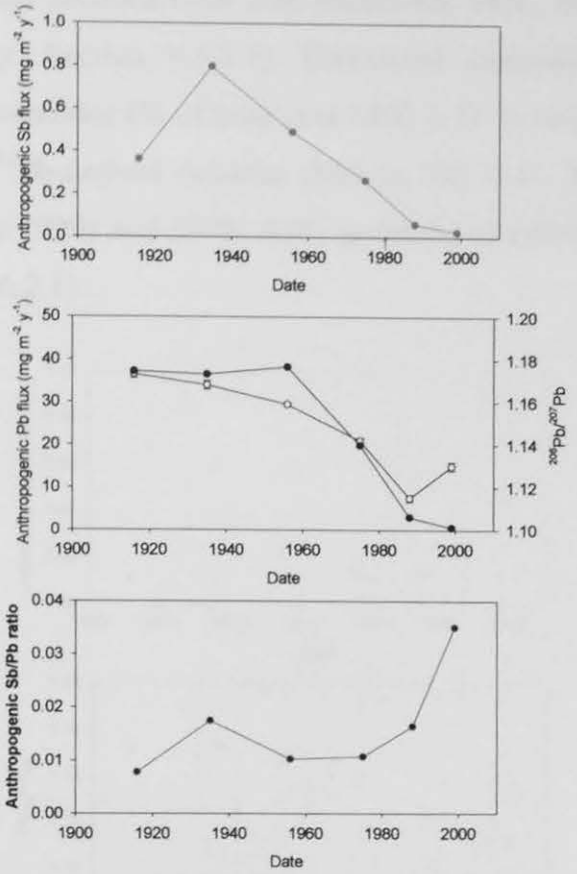

Figure 4.29: Calculated atmospheric depositional fluxes of anthropogenic Sb and Pb (mg m^{-2} y^{-1}) (closed circles), and the anthropogenic Sb/Pb and measured $^{206}Pb/^{207}Pb$ ratios (open circles) for the RM03CM-2 core *versus* ^{210}Pb-derived dates since 1900 A.D.

The maximum anthropogenic Sb flux (~ 0.80 mg m^{-2} y^{-1}) occurred during the mid-1930s A.D., during the anthropogenic Pb flux maxima (range 37 – 38 mg m^{-2} y^{-1}) from the 1920s to the late 1950s A.D. As observed at Flanders Moss (*cf.* Section 3.8.1.3.3), there is broad agreement between the anthropogenic Sb/Pb ratios in RM03CM-2 and Sb/Pb ratios obtained independently for preserved herbarium and freshly collected *Sphagnum* moss samples of known age collected across Scotland (Fig. 4.30) (Farmer *et al.*, 2002; Halter, 2005; Halter and Farmer, *in prep.*). Note that the depositional fluxes of anthropogenic Sb, and anthropogenic Sb/Pb ratios for The Red Moss of Balerno will be compared more closely to those found for Flanders Moss and the other Scottish peat bogs under investigation in Section 7.8.3.

The total anthropogenic Sb inventory for RM03CM-2 (i.e. from *ca.* 600 to 2003 A.D.), was 0.045 g m^{-2}, of which the post-1800 A.D. Sb inventory (0.044 g m^{-2})

(corresponding to peat sections 0-28 cm) constitutes 98%, in agreement with the findings for Pb (*cf.* Section 4.6.2.1). Calculated cumulative post-1800 A.D. anthropogenic Sb inventories (% of total post-1800 A.D. inventory) for RM03CM-2 are plotted *versus* ^{210}Pb-derived calendar dates in Fig. 4.31. Maximum deposition occurred between the 1910s and 1970s A.D., generally in agreement with that found for Pb (*cf.* Section 4.6.2.1).

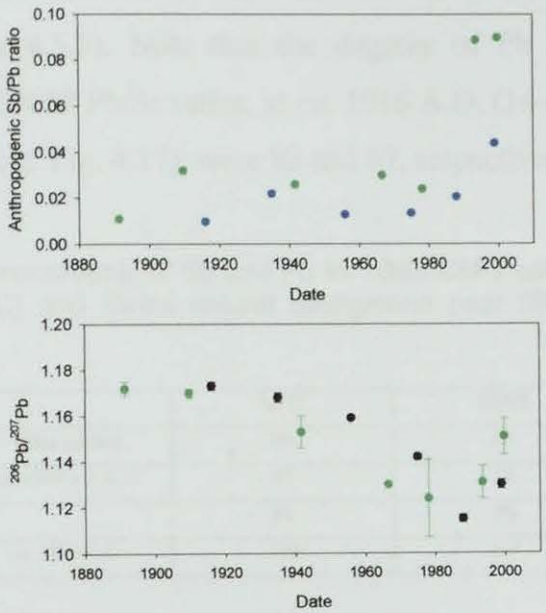

Figure 4.30: Anthropogenic Sb/Pb and measured ^{206}Pb/^{207}Pb ratios *versus* dates, since 1880 A.D, for herbarium moss samples (green symbols) and the RM03CM-2 core.

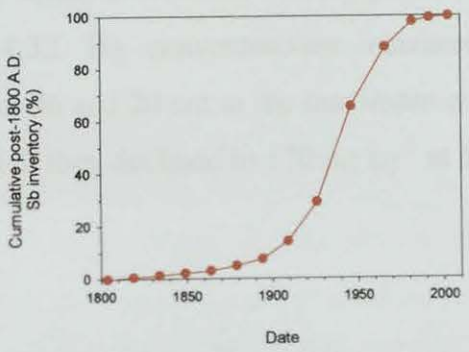

Figure 4.31: Calculated cumulative post-1800 A.D. anthropogenic Sb inventories (% of total post-1800 A.D. inventory) for the RM03CM-2 core *versus* ^{210}Pb-derived dates. Note that dates in RM03CM-2 prior to *ca.* 1894 A.D. were extrapolated.

4.8.1.1.4 Maximum enrichments of Sb and Pb

The maximum enrichments of Sb and Pb, for the RM03CM-2 peat core, calculated using UCC and SNBP elemental concentration ratios (*cf.* Section 3.8.1.3.4), are shown in Table 4.8. As found for Flanders Moss (Section 3.8.1.3.4), Sb and Pb exhibit similar degrees of enrichment in RM03CM-2. However, the maximum degree of Pb enrichment apparently occurred far earlier than that for Sb, but this reflects the problems associated with the use of maximum Pb/Sc ratios in RM03CM-2 (Section 4.5.3). Note that the degrees of Pb enrichment calculated relative to UCC and SNBP Pb/Sc ratios, at *ca.* 1916 A.D. (14-16 cm), where a minor Pb/Sc peak occurred (*cf.* Fig. 4.17), were 82 and 67, respectively.

Table 4.8: Maximum enrichments of Sb and Pb for RM03CM-2 calculated relative to upper continental crust (UCC) and Swiss natural background peat (SNBP) Sb/Sc and Pb/Sc concentration ratios.

	UCC	SPNB
Time period	**Sb**	**Sb**
ca. 1999 ± 2 A.D.	67	28
	Pb	**Pb**
ca. 1800 A.D.	139	112

4.8.2 Hg

The HNO_3/H_2SO_4 acid-extractable Hg concentrations (A5.1 Table A7) were determined for only the RM03CM-2 core. The Hg profile, along with Pb, Fe, Mn and S, is shown in Fig. 4.32. Hg concentrations increased from a mean value of 99 ± 23 μg kg^{-1} between 96 and 20 cm to the maximum concentration of 660 μg kg^{-1} at 10-12 cm, above which they declined to 170 μg kg^{-1} at the surface (*cf.* Fig. 4.32).

4.8.2.1 Discussion

4.8.2.1.1 Assessment of the immobility of Hg in ombrotrophic peat

The Hg concentrations, as for Pb, were elevated in the top ~ 28 cm sections of RM03CM-2, with the maximum Hg concentration (660 μg kg^{-1}) occurring 2 cm below the maximum Pb concentration (370 mg kg^{-1}) (*cf.* Fig. 4.32). The distribution of Hg and Pb, at least in the top ~ 28 cm sections, are similar, providing evidence for

the immobility of Hg in ombrotrophic peat, as found for Flanders Moss (Section 3.8.2.2).

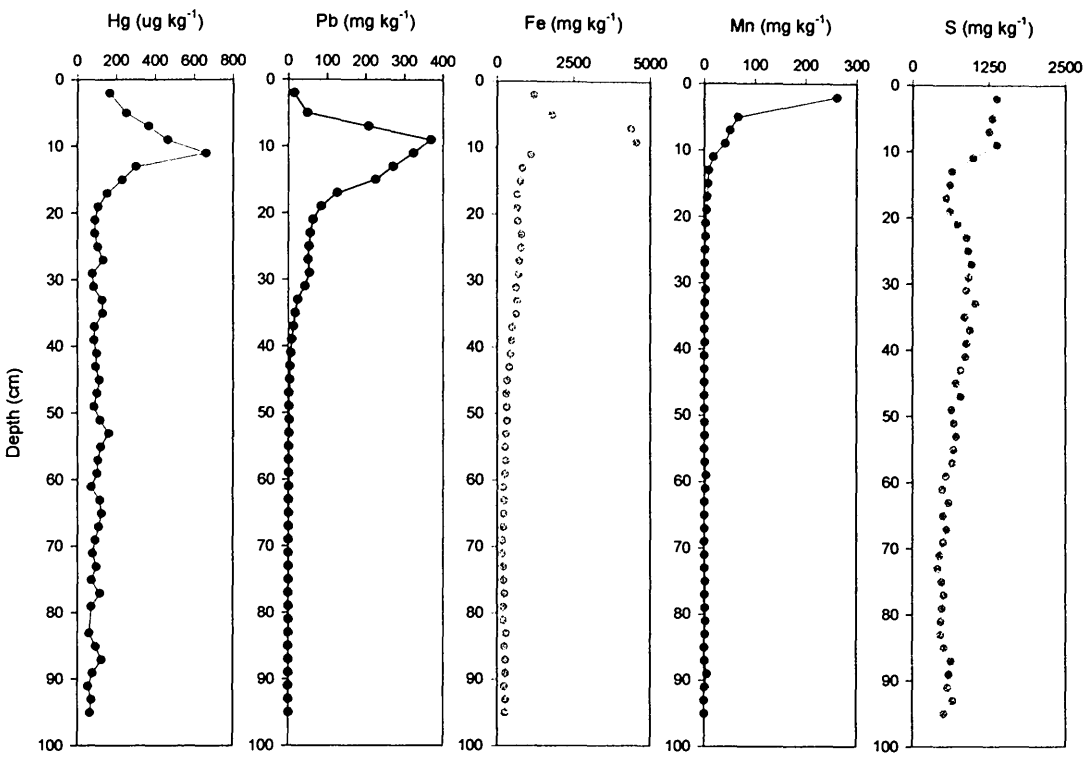

Figure 4.32: Depth profiles of Hg (μg kg^{-1}), Pb, Fe, Mn and S (mg kg^{-1}) concentrations in the RM03CM-2 (0-96 cm) peat core.

Comparing the Hg and Pb concentrations in the lower 30-96 cm sections of RM03CM-2 more closely (Fig. 4.33), however, the similarities between the Hg and Pb concentration profiles were less apparent, as also found in the lower peat sections of Flanders Moss (Section 3.8.2.2.1). Comparing the Hg concentration profile with those of Fe and Mn (*cf.* Fig. 4.32), as found for Flanders Moss (Section 3.8.2.2), the distribution of Hg is clearly different, with the maximum Hg concentration occurring below those of Fe and Mn, providing further evidence that the Hg profile is not affected by Hg adsorption to Fe and Mn oxides and hydroxides. Also, comparing the Hg concentration profile with that of S in the lower 30-96 cm sections (*cf.* Fig. 4.33), it is apparent that there are generally similar Hg and S concentration trends in these anaerobic catotelm peats, which may indicate some control of Hg as HgS precipitates, as found for Flanders Moss (Section 3.8.2.2.1).

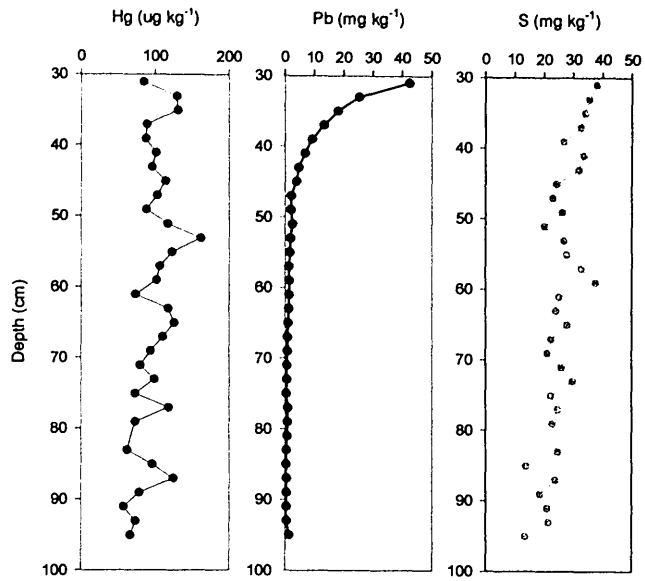

Figure 4.33: Depth profiles of Hg (μg kg^{-1}) and Pb and S (mg kg^{-1}) concentrations from 30 to 96 cm in the RM03CM-2 peat core.

4.8.2.1.2 Normalisation of Hg to Se and NaOH peat extract absorption (Abs)

The RM03CM-2 profiles for Hg and Se concentrations (A5.1 Table A7), NaOH peat extract absorptions, Hg/Se and Hg/Abs ratios (A5.1 Table A7) are shown in Fig. 4.34. Givelet *et al.* (2003) suggested that Se could be used as a "reference element" for Hg to quantify the natural inputs of Hg to peat bogs (*cf.* Section 3.8.2.2.1). When the RM03CM-2 Hg and Se concentration profiles are compared, it is apparent, in contrast to the differences observed at Flanders Moss (Section 3.8.2.2.1), that they show some similarities, particularly in the top ~ 16 cm. The Hg/Se ratio profile (*cf.* Fig. 4.34) exhibited a peak between 6 and 24 cm, with a maximum of 0.89 at 15 cm, beneath which ratios were at a minimum before they increased again below 32 cm, remaining high but fluctuating, towards the bottom of the core. Givelet *et al.* (2003) found that Hg/Se ratios in pre-anthropogenic peats were remarkably constant for thousands of years, suggesting that their rates of accumulation in pre-anthropogenic peats were in constant proportions. However, as mentioned in Section 3.8.2.2.1, the similarity in anthropogenic sources (e.g. coal combustion) of Hg and Se is a potential problem when Se is used to normalise Hg concentrations and may account for the similarities observed between the Hg and Se

profiles in the top ~ 16 cm of RM03CM-2 (*cf.* Fig. 4.34). Previous workers have investigated atmospheric deposition of Se in ombrotophic peat bogs (Steinnes, 1997; Frank *et al.*, 2003; Givelet *et al.*, 2003), but its behaviour is still relatively unknown and since the Se concentration profile for Flanders Moss strongly indicated that Se was mobile in ombrotrophic peat (Section 3.8.2.2.1), this element will not be considered any further in this chapter.

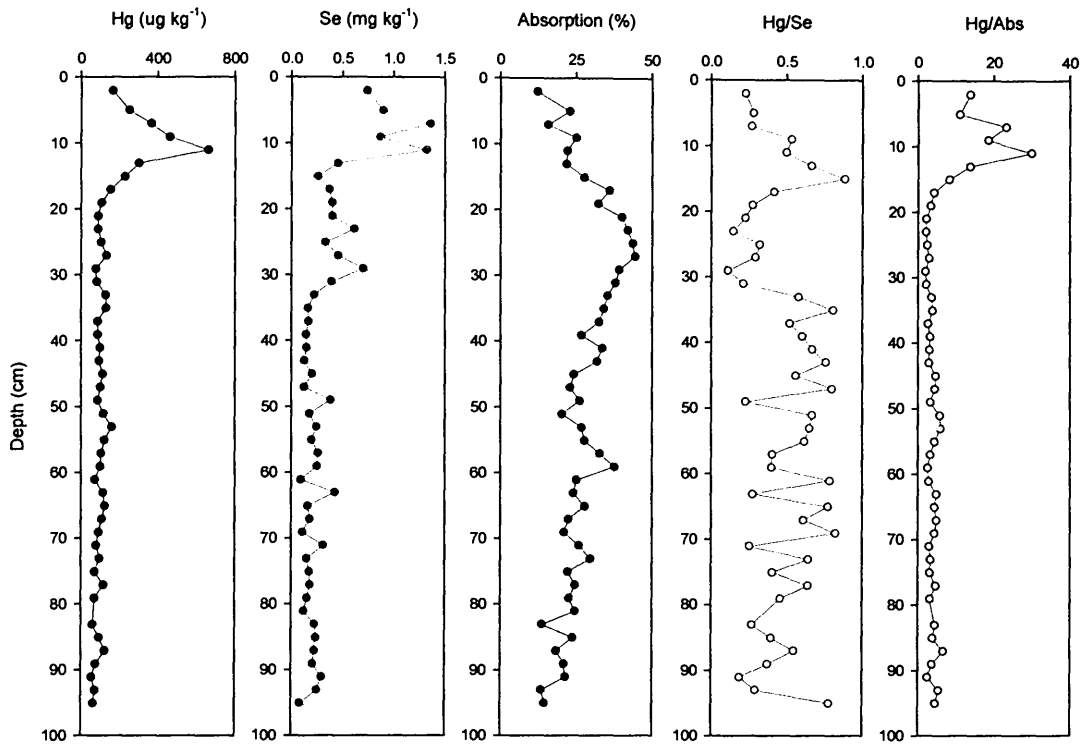

Figure 4.34: Depth profiles of Hg (µg kg^{-1}) and Se (mg kg^{-1}) concentrations, NaOH peat extract absorptions (%), Hg/Se and Hg/Abs ratios in the RM03CM-2 (0-96 cm) peat core.

Givelet *et al.* (2003) also suggested that Hg concentrations could be normalised to NaOH peat extract absorption in order to assess the effects of organic matter decomposition processes on the distribution of Hg (*cf.* Section 3.8.2.2.1). When the Hg concentration and NaOH peat extract absorption profiles in RM03CM-2 (*cf.* Fig. 4.34) are compared, changes in Hg concentrations do not relate to the changes in peat decomposition, as observed for Flanders Moss (*cf.* Section 3.8.2.2.1). Also, in contrast to the small changes in absorption within the peat profile, the changes in the Hg/Abs ratio profile (*cf.* Fig. 4.34) are far greater, indicating that organic matter

decomposition cannot explain the magnitude of the variation in Hg concentrations with depth in the profile, in agreement with findings by Givelet *et al.* (2003).

4.8.2.1.3 Historical trends in sources of atmospheric Hg deposition

Since the origins of Hg in the lower catotelm peat sections of the RM03CM-2 core are uncertain, historical trends in sources of atmospheric Hg deposition in the top 30 cm alone (i.e. during the industrial and post-industrial periods), will be investigated. The Hg and Pb concentration and $^{206}Pb/^{207}Pb$ ratio profiles for RM03CM-2, including ^{210}Pb age-dates, are shown in Fig. 4.35. From 30 cm (*ca.* late 1700 A.D.) to 12 cm (*ca.* 1926 A.D.) in RM03CM-2, Hg concentrations increased from 79 to 300 μg kg^{-1} at 10-12 cm. The Hg concentrations then reached a maximum (660 μg kg^{-1}) at 10-12 cm (*ca.* 1935 A.D.), pre-dating the maximum Pb concentration by *ca.* 21 years (*cf.* Fig. 4.35). These trends are consistent with Hg emissions from coal combustion, as found for Flanders Moss (*cf.* Section 3.8.2.2.2).

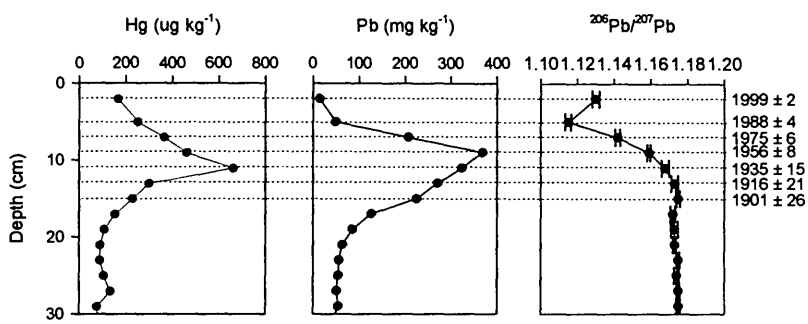

Figure 4.35: Depth profiles of Hg (μg kg^{-1}) and Pb (mg kg^{-1}) concentrations and measured $^{206}Pb/^{207}Pb$ ratios in the ^{210}Pb-dated RM03CM-2 peat core, from 0-30 cm.

After 1935 A.D., the Hg concentrations decreased (*cf.* Fig. 4.35), reflecting the decrease in coal combustion emissions. It is worth noting, however, that as for Pb, Hg emissions from other sources such as waste incinerators (*cf.* Table 1.3, Section 1.3.2.2) perhaps became important during the post-industrial period (i.e. post-1970 A.D.) (Roos-Barraclough and Shotyk, 2003).

4.8.2.1.4 Historical trends in depositional fluxes and inventories of Hg

Depositional fluxes of Hg (A5.1 Table A12) and anthropogenic Pb since 1900 A.D. are plotted, along with the measured $^{206}Pb/^{207}Pb$ ratios, *versus* ^{210}Pb-derived calendar

dates for RM03CM-2 in Fig. 4.36. Unfortunately, for reasons discussed in Section 3.8.2.2.1, anthropogenic Hg depositional fluxes could not be calculated. The maximum Hg flux (~ 0.085 mg m^{-2} y^{-1}) occurred during the mid-1930s A.D., coincident with the maxima (range 37 – 38 mg m^{-2} y^{-1}) in anthropogenic Pb fluxes, after which Hg fluxes declined to 0.0077 mg m^{-2} y^{-1} by 1999 A.D (*cf.* Fig. 4.36), in good agreement with the modelled Hg wet deposition value of ~ 0.006 mg m^{-2} y^{-1}, recorded in east-central Scotland during 1998 A.D. (Lee *et al.*, 2002).

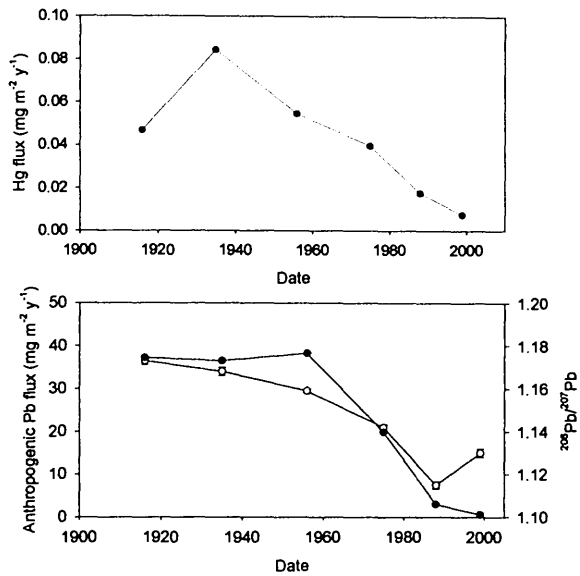

Figure 4.36: Calculated atmospheric depositional fluxes of Hg and anthropogenic Pb (mg m^{-2} y^{-1}) (closed circles) and measured $^{206}Pb/^{207}Pb$ ratios (open circles) for the RM03CM-2 core *versus* ^{210}Pb-derived dates since 1900 A.D.

The total Hg inventory for the RM03CM-2 core (0-96 cm) was 12 mg m^{-2}, and the post-1800 A.D. Hg inventory (7.1 mg m^{-2}) (corresponding to peat sections 0-28 cm) constituted only 59% of the total Hg inventory, which is approximately half the corresponding proportion (99%) found for Pb, as observed for Flanders Moss (Section 3.8.2.2.3). Calculated cumulative post-1800 A.D. Hg inventories (% of total post-1800 A.D. inventory) for RM03CM-2 are plotted *versus* ^{210}Pb-derived calendar dates in Fig. 4.37. Maximum deposition occurred between the 1890s and 1960s A.D., generally in agreement with that found for Pb (*cf.* Section 4.6.2.1).

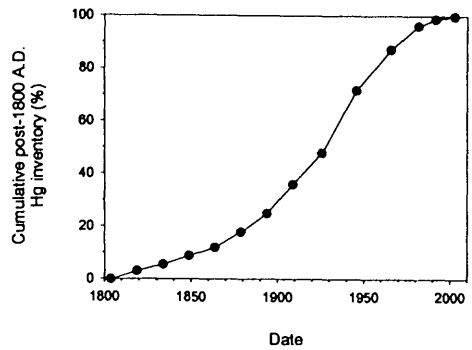

Figure 4.37: Calculated cumulative post-1800 A.D. Hg inventories (% of total post-1800 A.D. inventory) for the RM03CM-2 core *versus* ^{210}Pb-derived dates. Note that dates in RM03CM-2 prior to *ca.* 1894 A.D. were extrapolated.

4.8.3 As, Cd, Cu and Zn

Although concentrations of As and Cd were determined only for the RM03CM-2 core, concentrations of Cu and Zn were determined for both the RM03CM-2 and RM03CM-1 cores. Profiles for RM03CM-2 As, Cd, Cu and Zn concentrations (A5.1 Table A8), along with Pb and S concentrations and ash contents, are shown in Fig. 4.38. Profiles for RM03CM-1 Cu and Zn concentrations (A5.2 Table A3), along with Pb and S concentrations and ash contents, are shown in Fig. 4.39.

4.8.3.1 RM03CM-2

All four elements exhibited concentration peaks in the uppermost ~ 16 cm of the core, with the following maximum concentrations at the depths indicated:

- As – 5.8 mg kg^{-1} at 8-10 cm
- Cd – 3.0 mg kg^{-1} at 6-8 cm
- Cu – 40 mg kg^{-1} at 10-12 cm
- Zn – 210 mg kg^{-1} between 6 and 10 cm but the maximum value (410 mg kg^{-1}) in the core occurred at 34-36 cm

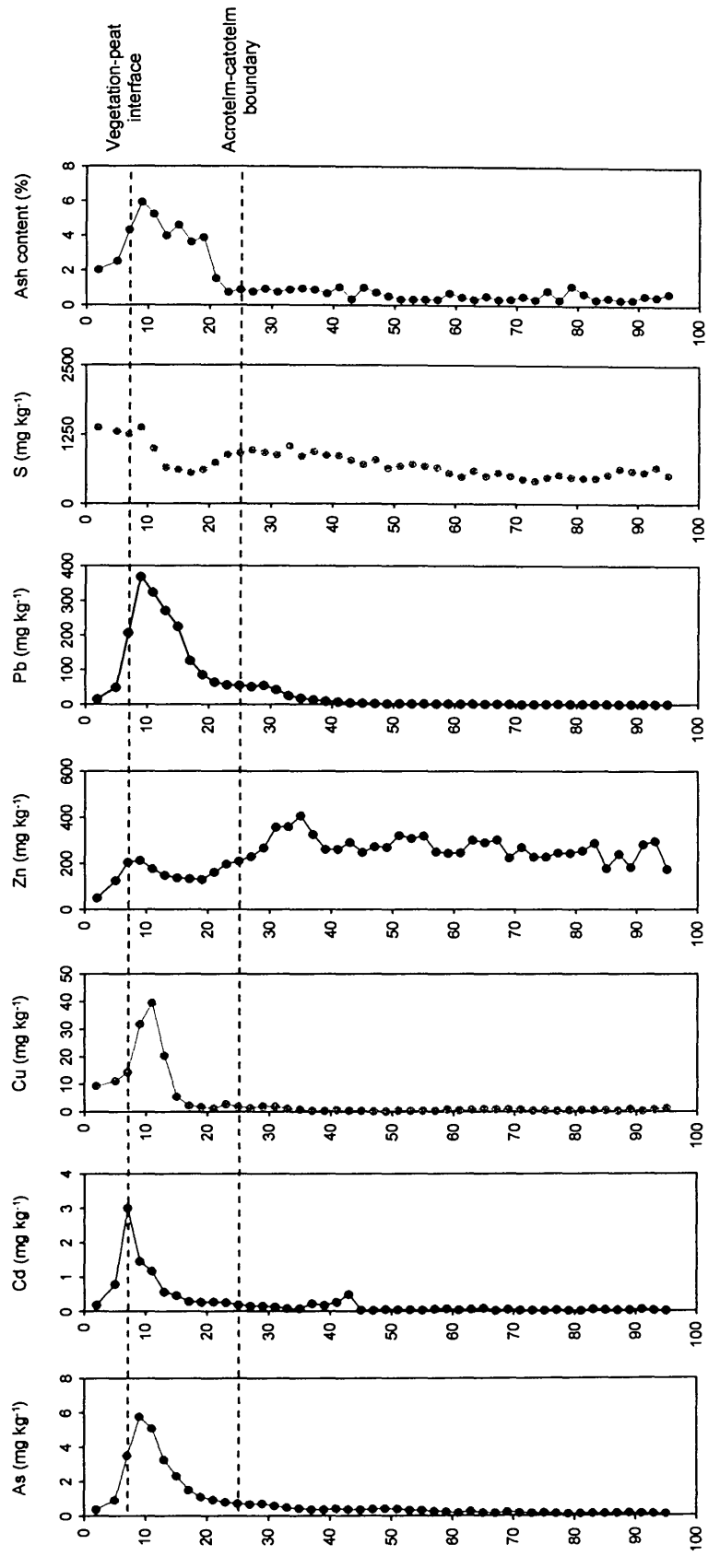

Figure 4.38: Depth profiles of As, Cd, Cu, Zn, Pb and S concentrations (mg kg^{-1}) and ash contents (% by weight) in the RM03CM-2 (0-96 cm) peat core.

Above these maxima, elemental concentrations decreased towards the surface, while below 16 cm, concentrations decreased towards the bottom of the core, with the exception of Zn. After decreasing to a minimum of ~ 130 mg kg^{-1} between 16 and 20 cm, Zn concentrations increased and remained fairly constant in the anaerobic catotelm layers. Also, Cd exhibited a minor peak (0.59 mg kg^{-1}) at 38-40 cm but, in general, the distributions of As, Cd and Cu were similar to those of Pb and the ash content. The distribution of Zn, with the exception of the uppermost peat sections, was similar to that of S (*cf.* Fig. 4.38).

4.8.3.2 RM03CM-1

Concentrations of Cu and Zn exhibited peaks in the uppermost ~ 17 cm of the core and the following maximum concentrations occurred, at the depths indicated (*cf.* Fig. 4.39):

- Cu – 38 to 41 mg kg^{-1} between 9 and 13 cm
- Zn – 270 mg kg^{-1} between 9 and 13 cm but the maximum value (300 mg kg^{-1}) in the core occurred at 29-31 cm

The Cu concentrations above and below the maxima decreased and the distribution of Cu was similar to that of both Pb and the ash content. The Zn concentrations above the maxima decreased but below the maxima remained high before increasing at the bottom of the core (*cf.* Fig. 4.39).

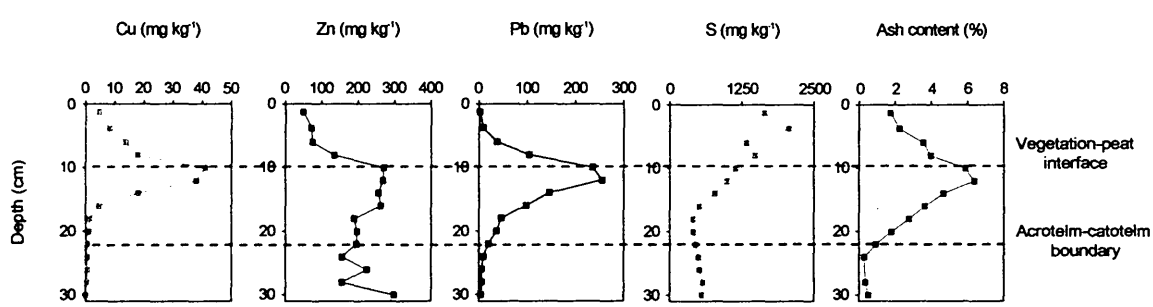

Figure 4.39: Depth profiles of Cu, Zn, Pb and S concentrations (mg kg^{-1}) and ash contents (% by weight) in the RM03CM-1 (0-31 cm) peat core.

4.8.3.3 Discussion

4.8.3.3.1 Assessment of the immobility of As, Cd, Cu and Zn in ombrotrophic peat

The As, Cd, Cu and Zn profile trends at The Red Moss of Balerno are generally consistent with those found for Flanders Moss (Section 3.8.3.3.1), i.e. indicative of As, Cd and Cu immobility in ombrotrophic peat and the influence of Zn sulfide formation and precipitation at depth. However, in contrast to the finding that the position of As concentration peaks were distinctly different from those of Fe and P for Flanders Moss (Section 3.8.3.3.1), the As concentration peak in RM03CM-2 (*cf.* Fig. 4.38), occurred at the same depth (8-10 cm) as those for Fe and P (*cf.* Fig. 4.24, Section 4.7.1). Given that the Pb concentration peak also occurred at this depth and since some anthropogenic sources of As and Pb are common (e.g. coal combustion), it is possible (but not certain) that As is unaffected by post-depositional mobility at The Red Moss of Balerno. Since Zn appears to be mobile in this bog it will not be considered any further in this Chapter.

4.8.3.3.2 The use of Sc and Ti as an indicator of As, Cd and Cu soil dust input

The As, Cd, Cu and Sc concentration profiles in RM03CM-2 are shown in Fig. 4.40, and, since Sc concentrations were not determined in RM03CM-1, Cu and Ti concentration profiles in RM03CM-1 are shown in Fig. 4.41. Note the changes in scale on the As and Cd (8-fold), Cu (25-fold) and Sc (20-fold) concentrations on going from 0-40 cm to 40-96 cm in RM03CM-2. The As/Sc, Cd/Sc and Cu/Sc ratios in RM03CM-2 (A5.1 Table A9) and Cu/Ti ratios in RM03CM-1 (A5.2 Table A3) were calculated and their profiles, along with Pb/Sc and Pb/Ti ratios, are shown in Figs. 4.42 and 4.43, respectively. As for Pb/Sc ratios (*cf.* Section 4.5.1), the As/Sc, Cd/Sc and Cu/Sc ratios were at a minimum between 70 and 94 cm, with mean values of 1.7 ± 0.4, 0.42 ± 0.18 and 7.8 ± 3.6, respectively (*cf.* Fig. 4.42). Also, when comparing these As/Sc, Cd/Sc and Cu/Sc ratios with the corresponding UCC As/Sc, Cd/Sc and Cu/Sc ratios, they were 6, 28 and 4-fold higher, respectively.

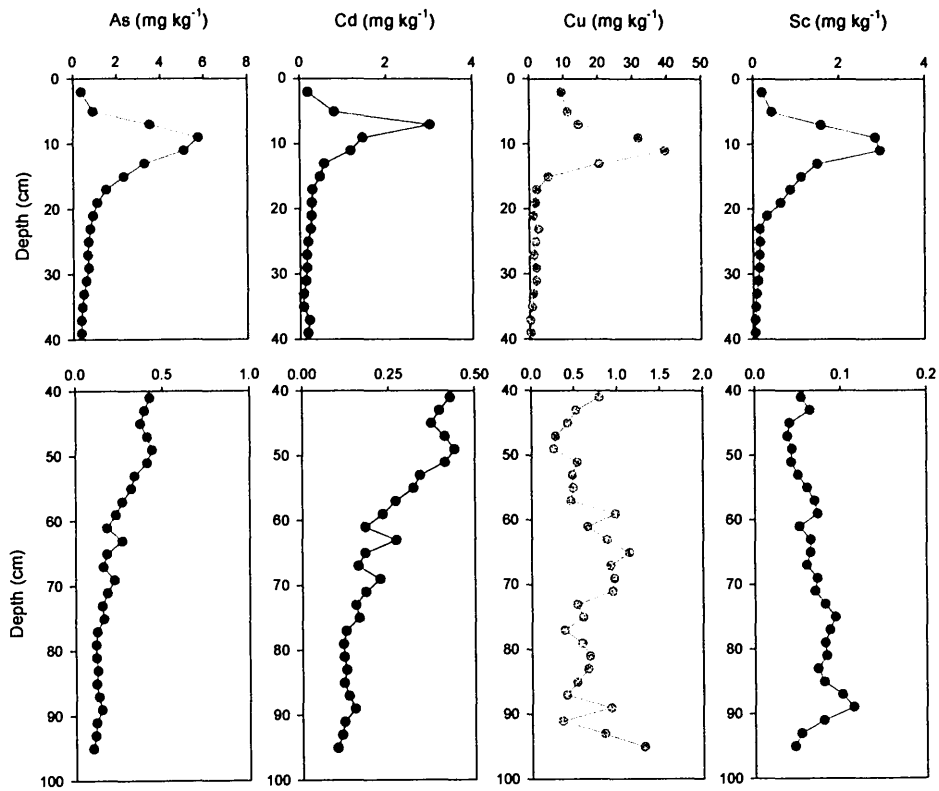

Figure 4.40: Depth profiles of As, Cd, Cu and Sc concentrations (mg kg^{-1}) from 0-40 cm and 40-96 cm in the RM03CM-2 peat core.

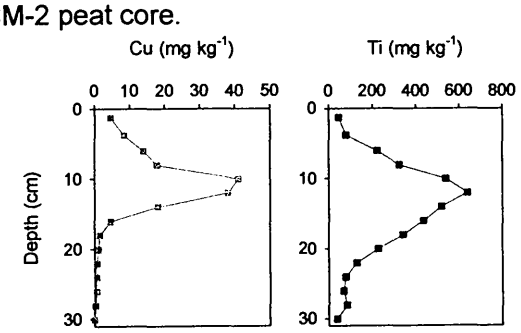

Figure 4.41: Depth profiles of Cu and Ti concentrations (mg kg^{-1}) in the RM03CM-1 (0-31 cm) peat core.

Maximum As/Sc, Cd/Sc and Cu/Sc ratios occurred between 44 and 52 cm, 36 and 44 cm and 0 and 6 cm, respectively (*cf.* Fig. 4.42), which were different from the region of maximum Pb/Sc ratios (between 32 and 22 cm) (*cf.* Section 4.5.1). The maximum Cu/Ti ratio in RM03CM-1 also occurred in the top 5 cm of the core, which was 6 cm above the maximum Pb/Ti ratio (*cf.* Fig. 4.43).

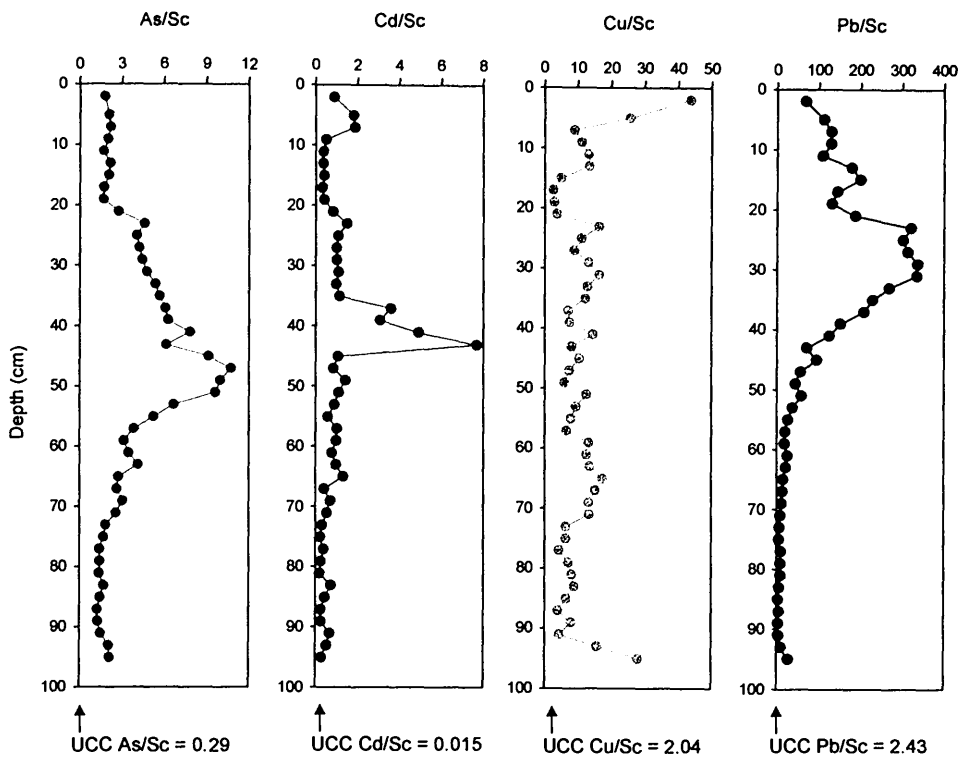

Figure 4.42: Depth profiles of As/Sc, Cd/Sc, Cu/Sc and Pb/Sc ratios in the RM03CM-1 (0-96 cm) peat core.

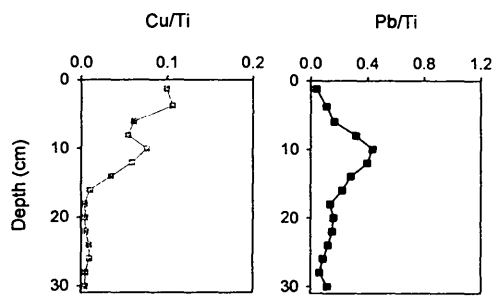

Figure 4.43: Depth profiles of Cu/Ti and Pb/Ti ratios in the RM03CM-1 (0-31 cm) peat core.

On the basis of the use of Sc as a conservative element, the anthropogenic As, Cd and Cu concentrations in RM03CM-2 were calculated (A5.1 Table A10) (*cf.* Section 3.8.3.3.2) and their profiles, along with anthropogenic Pb concentrations and measured $^{206}Pb/^{207}Pb$ ratios, including age-dates, are displayed in Fig. 4.44. Also, on the basis of the use Ti as a conservative element, anthropogenic Cu concentrations in RM03CM-1 were calculated (A5.2 Table A3) and plotted, along with anthropogenic Pb concentrations and measured $^{206}Pb/^{207}Pb$ ratios, including age-dates in Fig. 4.45.

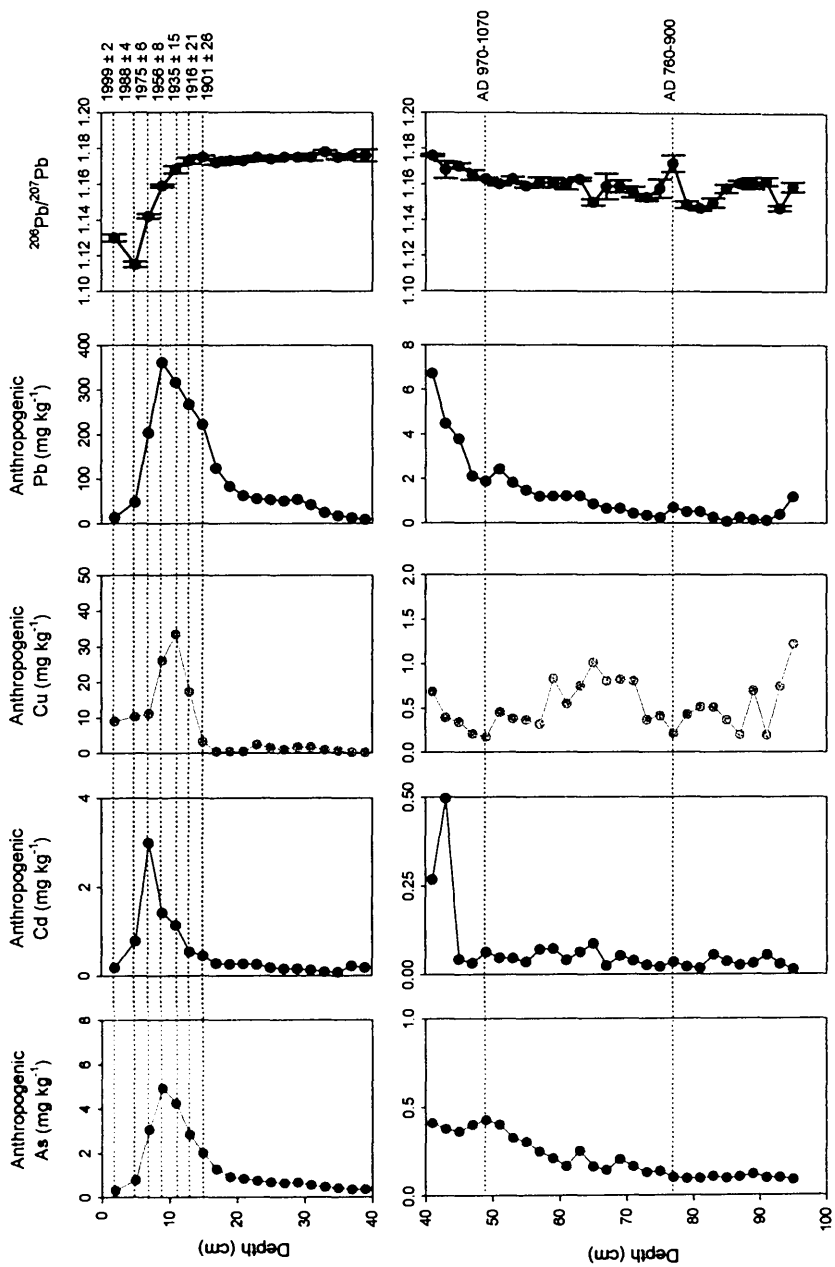

Figure 4.44: Depth profiles of anthropogenic As, Cd, Cu and Pb concentrations and measured $^{206}Pb/^{207}Pb$ ratios from 0-40 cm and 40-96 cm in the ^{210}Pb- and ^{14}C-dated RM03CM-2 peat core.

The anthropogenic As and Cd concentration profiles for the RM03CM-2 peat core indicate that the apparent increases in As/Sc and Cd/Sc ratios, between the depths of 44 and 52 cm and 36 and 44 cm (*cf.* Fig. 4.44), respectively, with the exception of the single outlier Cd/Sc ratio value at 42-44 cm, didn't result in corresponding increases in anthropogenic As and Cd concentrations. Therefore, as for Flanders Moss (Section 3.8.3.3.2), anthropogenic As, Cd and Cu concentration profiles alone (*cf.* Figs. 4.44 and 4.45) will be used in the next section to interpret historical trends in anthropogenic As, Cd and Cu.

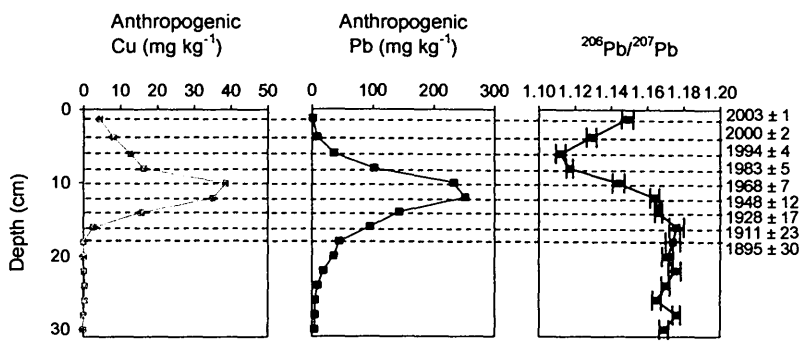

Figure 4.45: Depth profiles of anthropogenic Cu and Pb concentrations (calculated using Ti as the conservative element) and measured $^{206}Pb/^{207}Pb$ ratios in the ^{210}Pb-dated RM03CM-1 (0-31 cm) peat core.

4.8.3.3.3 Historical trends of anthropogenic As, Cd and Cu deposition

Pre-industrial atmospheric As, Cd and Cu sources and deposition

At the bottom of the core (95 cm), there was a marked increase in anthropogenic Cu concentration (1.20 mg kg^{-1}) (*cf.* Fig. 4.44), possibly indicative of long-range atmospheric Cu deposition from post-Roman mining and smelting activities during the reign of the Visigods, as found for Pb and Sb (Sections 4.6.1 and 4.8.1). The absence of corresponding anthropogenic As and Cd concentration increases is surprising since As and Cd are also emitted into the atmosphere during metallurgical activities. Between 94 and 70 cm anthropogenic As and Cd concentrations, as found for Pb (Section 4.6.1), were at their lowest with mean values of 0.11 ± 0.02 and 0.033 ± 0.012 mg kg^{-1}, respectively, whereas anthropogenic Cu concentrations remained fairly high (mean 0.45 ± 0.21 mg kg^{-1}) (*cf.* Fig. 4.44). Above 70 cm up to a

depth of 50 cm (970-1070 A.D.), anthropogenic As, Cd and Cu concentrations increased with mean values of 0.24 ± 0.08, 0.054 ± 0.019 and 0.63 ± 0.24 mg kg^{-1}, respectively. The anthropogenic As and Pb concentration profiles at these depths (70-50 cm) exhibited similar trends (*cf.* Fig. 4.44), and it seems likely that the increased As concentrations in these peat sections could perhaps reflect inputs from Pb and Cu mining and smelting during Mediaeval times. In contrast, the anthropogenic Cu and Pb concentration profiles at these depths were dissimilar, Cu exhibiting a broad peak between 70 and 58 cm. Above 50 cm (970-1070 A.D.) to a depth of 40 cm, anthropogenic As concentrations increased further (mean 0.40 ± 0.03 mg kg^{-1}) and anthropogenic Cd concentrations increased markedly from 0.063 mg kg^{-1} to 0.27 mg kg^{-1} (omitting the single high outlier value at 42-44 cm). Anthropogenic Cu concentrations also increased (from 0.17 mg kg^{-1} to 0.69 mg kg^{-1}), although these concentrations were generally lower than those observed in the 70 to 50 cm sections (*cf.* Fig. 4.44). As found for Pb (Section 4.6.1), these trends may indicate growing influences from Mediaeval mining and smelting activities.

Industrial and post-industrial atmospheric As, Cd and Cu sources and deposition

As

Above 40 cm (*ca.* early 1700s A.D.), anthropogenic As concentrations continued to increase, reaching a maximum of 4.9 mg kg^{-1} at *ca.* 1956 A.D. (coincident with the maximum anthropogenic Pb concentration), after which they decreased to 0.33 mg kg^{-1} at *ca.* 1999 A.D. (*cf.* Fig. 4.44). As found for Flanders Moss (*cf.* Section 3.8.3.3.3), these trends are consistent with As emissions from coal combustion and possibly metallurgical activities, such as Pb and Cu-Ni production (*cf.* Table 1.2, Section 1.3.2.2), until the decline in heavy industry in the later part of the 20^{th} century A.D., when emissions from oil combustion (up to the 1990s A.D.) and waste incineration (*cf.* Table 1.2, Section 1.3.2.2) perhaps became more important (Department of Trade and Industry, 1998; Matschullat, 2000; National Atmospheric Emissions Inventory, 2006).

Cd

Above 40 cm (*ca.* early 1700s A.D.), anthropogenic Cd concentrations continued to increase, reaching a maximum of 3.0 mg kg^{-1} at *ca.* 1975 A.D. (postdating the maximum anthropogenic Pb concentration by *ca.* 19 years), after which they decreased to 0.19 mg kg^{-1} at *ca.* 1999 A.D. (*cf.* Fig. 4.44). As found for Flanders Moss (*cf.* Section 3.8.3.3.3), these trends are likely to reflect Cd emissions from a combination of sources such as metallurgical activities and coal combustion (*cf.* Table 1.2, Section 1.3.2.2), until the decline in heavy industry in the later part of the 20th century A.D., when emissions from oil combustion (up to the 1990s A.D.) and waste incineration (*cf.* Table 1.2, Section 1.3.2.2) perhaps became more important (Department of Trade and Industry, 1998; National Atmospheric Emissions Inventory, 2006).

Cu

Above 40 cm (*ca.* early 1700s A.D.) in RM03CM-2, anthropogenic Cu concentrations increased to a maximum of 34 mg kg^{-1} at *ca.* 1935 A.D. (pre-dating the maximum anthropogenic Pb concentration by *ca.* 21 years), after which they decreased to 9.1 mg kg^{-1} at *ca.* 1999 A.D. (*cf.* Fig. 4.44). Although anthropogenic Cu concentrations in RM03CM-1 increased from 31 cm (*ca.* late 1700s A.D.), they reached a maximum (~ 40 mg kg^{-1}) between *ca.* 1937 and 1977 A.D. (coincident with the maximum anthropogenic Pb concentration), after which they decreased to 1.7 mg kg^{-1} at *ca.* 2003 A.D. (*cf.* Fig. 4.45). As found for Flanders Moss (*cf.* Section 3.8.3.3.3) these trends are likely to reflect Cu emissions from a combination of sources e.g. Cu-Ni, Zn-Cd and non-ferrous metal production and coal combustion (*cf.* Table 1.2, Section 1.3.2.2), until the decline in heavy industry in the later part of the 20th century A.D., when emissions from oil combustion (up to the 1990s A.D.) and waste incineration (*cf.* Table 1.2, Section 1.3.2.2) perhaps became more important (Department of Trade and Industry, 1998; National Atmospheric Emissions Inventory, 2006). Note that as found for Flanders Moss (*cf.* Section 3.8.3.3.3), anthropogenic Cu concentrations at The Red Moss of Balerno remained relatively high, compared with As and Cd, after the late 1980s A.D., declining less

steeply relative to As, Cd and Pb (*cf.* Figs. 4.44 and 4.45), perhaps providing further evidence for comparatively new recent sources of Cu e.g. automobile exhaust and non-exhaust emissions, due to the use of Cu as an antioxidant in motor oil and its presence in new brake linings and tyres (Cadle *et al.*, 1999; Sternbeck *et al.*, 2002; Chemical Research Communications, 2003; Boulter, 2004).

4.8.3.3.4 Historical trends in depositional fluxes and inventories of anthropogenic As, Cd and Cu

Anthropogenic depositional fluxes were calculated for As, Cd and Cu in RM03CM-2 (A5.1 Table A12) and for Cu in RM03CM-1 (A5.2 Table A5). Anthropogenic As, Cd and Cu fluxes, since 1900 A.D., are plotted along with the anthropogenic Pb fluxes and measured $^{206}Pb/^{207}Pb$ ratios, *versus* ^{210}Pb-derived calendar dates, for RM03CM-2 in Fig. 4.46. Anthropogenic Cu fluxes, since 1880 A.D., are plotted along with the anthropogenic Pb fluxes and measured $^{206}Pb/^{207}Pb$ ratios, *versus* ^{210}Pb-derived calendar dates, for RM03CM-1 in Fig. 4.47. Depositional fluxes of anthropogenic As were at a maximum (ranging from 0.40 to 0.52 mg m^{-2} y^{-1}) between the late 1910s and mid-1950s A.D. Depositional fluxes of anthropogenic Cd were at a maximum (0.29 mg m^{-2} y^{-1}) during the mid-1970s A.D., while those of anthropogenic Cu in RM03CM-2 (*cf.* Fig. 4.46) were at a maximum (3.9 mg m^{-2} y^{-1}) during the mid-1930s A.D. Depositional fluxes of anthropogenic Cu in RM03CM-1 (*cf.* Fig. 4.47) were at a maximum (4.9 mg m^{-2} y^{-1}) during the late-1960s A.D. The differences between Cu flux trends observed in RM03CM-2 and RM03CM-1 (*cf.* Figs. 4.46 and 4.47) could perhaps be attributable to depositional variability at the peat bog surface (Bindler *et al.*, 2004).

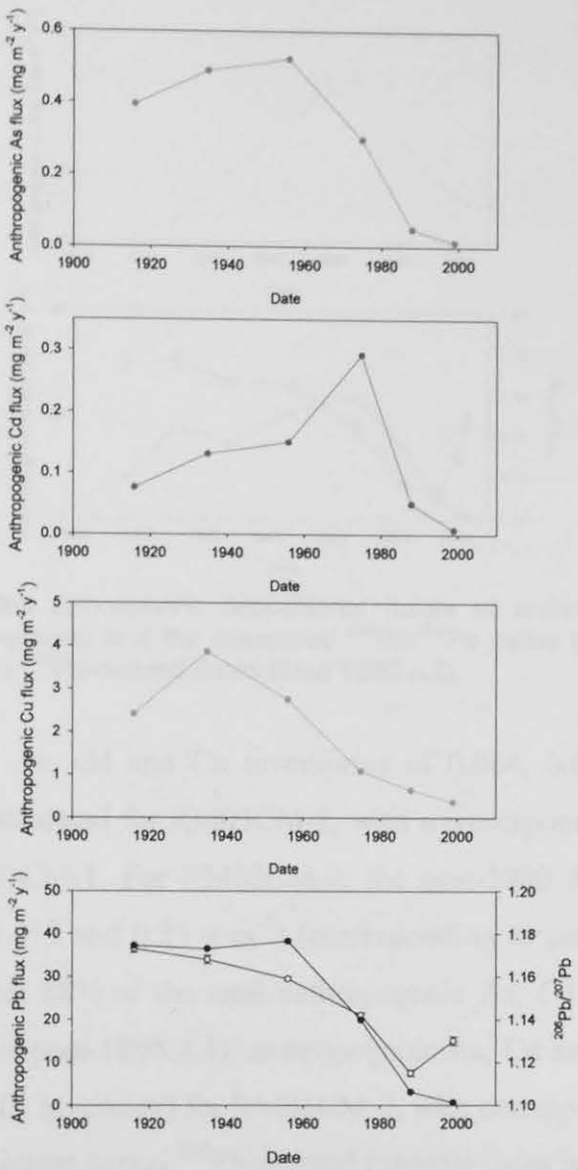

Figure 4.46: Calculated atmospheric depositional fluxes of anthropogenic As, Cd, Cu and Pb (mg m^{-2} y^{-1}) (closed circles) and the measured $^{206}Pb/^{207}Pb$ ratios (open circles) for the RM03CM-2 core *versus* ^{210}Pb-derived dates since 1900 A.D.

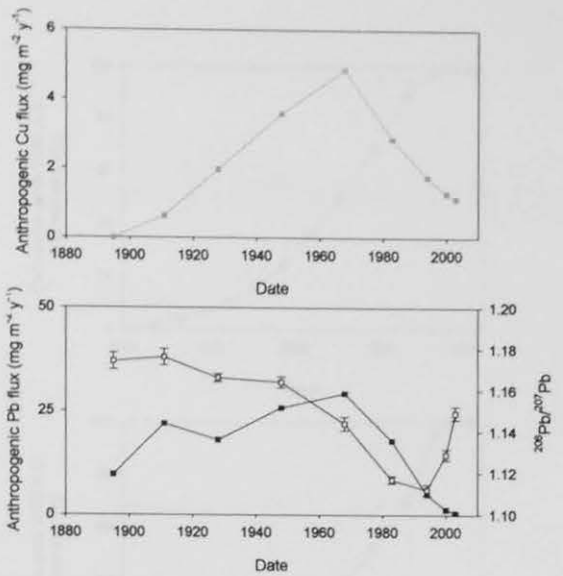

Figure 4.47: Calculated atmospheric depositional fluxes of anthropogenic Cu and Pb (mg m^{-2} y^{-1}) (closed squares) and the measured $^{206}Pb/^{207}Pb$ ratios (open squares) for the RM03CM-1 core *versus* ^{210}Pb-derived dates since 1880 A.D.

Total anthropogenic As, Cd and Cu inventories of 0.064, 0.021 and 0.26 g m^{-2}, respectively, were calculated for RM03CM-2, with a corresponding Cu inventory of 0.28 g m^{-2} for RM03CM-1. For RM03CM-2, the post-1800 A.D. As, Cd and Cu inventories (0.051, 0.017 and 0.23 g m^{-2}) (corresponding to peat sections 0-28 cm) constituted 80, 81 and 88% of the total anthropogenic As, Cd and Cu inventories. Calculated cumulative post-1800 A.D. anthropogenic As, Cd and Cu inventories (% of total post-1800 A.D. inventory) for RM03CM-2, with corresponding values for Cu in RM03CM-1, are plotted *versus* ^{210}Pb-derived calendar dates in Fig. 4.48.

Maximum As, Cd and Cu deposition occurred between the 1890s and 1960s A.D., 1890s and 1970s A.D. and 1910s and 1970s A.D., generally in agreement with that found for Pb (*cf.* Section 4.6.2.1). Again, as found for Pb, slight differences in trends of Cu deposition between the two cores can perhaps be accounted for by the significant uncertainties associated with the ^{210}Pb dates extrapolated for RM03CM-2 from RM03CM-1 (*cf.* Table 4.3).

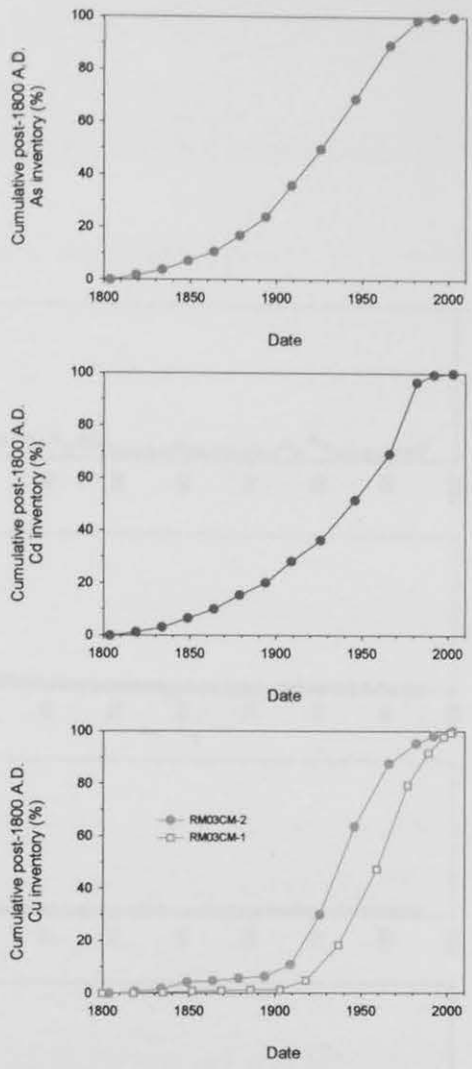

Figure 4.48: Calculated cumulative post-1800 A.D. anthropogenic As, Cd and Cu inventories (% of total post-1800 A.D. inventory) for the RM03CM-2 core and cumulative post-1800 A.D. anthropogenic Cu inventories (% of total post-1800 A.D. inventory) for the RM03CM-1 core *versus* ^{210}Pb-derived dates. Note that dates in RM03CM-2 and RM03CM-1 prior to *ca.* 1894 A.D. and *ca* 1886 A.D., respectively, were extrapolated.

4.8.4 Co, Cr, Ni and V

Concentrations of Co, Cr, Ni and V were determined only for the RM03CM-2 core. Profiles of Co, Cr, Ni and V concentrations (A5.1 Table A8), along with Pb concentrations and ash contents, are shown in Fig. 4.49. All four elements exhibited concentration peaks in the uppermost ~ 16 cm of the core, with the following maximum concentrations at the depths indicated:

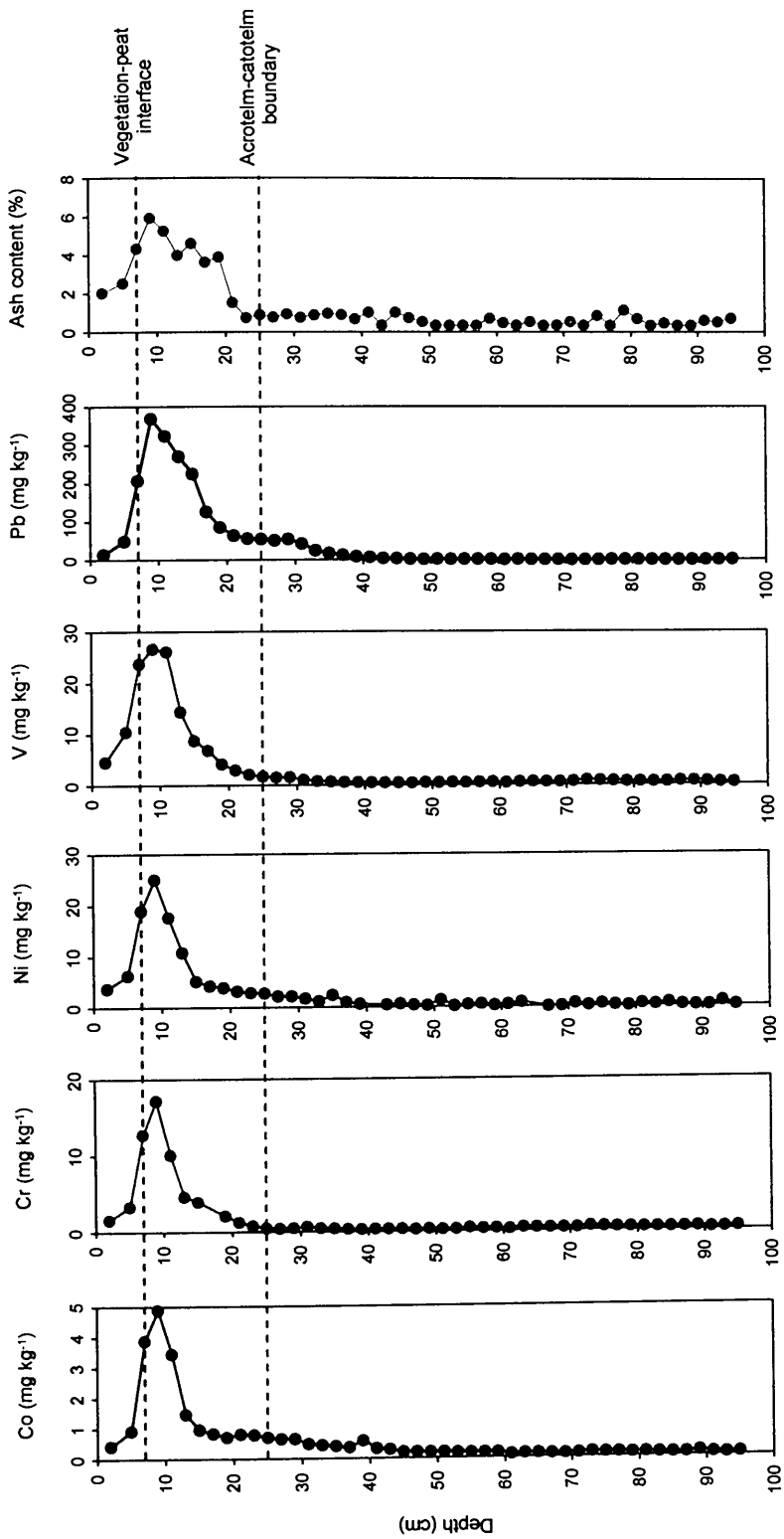

Figure 4.49: Depth profiles of Co, Cr, Ni, V and Pb concentrations (mg kg^{-1}) and ash contents (% by weight) in the RM03CM-2 (0-96 cm) peat core.

- Co – 4.9 mg kg^{-1} at 8-10 cm
- Cr – 17 mg kg^{-1} at 8-10 cm
- Ni – 25 mg kg^{-1} at 8-10 cm
- V – 26-27 mg kg^{-1} between 6 and 12 cm

Elemental concentrations decreased towards the top of the core and, in the peat sections underlying the concentration peaks, concentrations decreased towards the bottom of the core and remained fairly constant, with the exception of minor Co and Ni concentration peaks at 38-40 cm and 34-36 cm, respectively. In general the distributions of Co, Cr, Ni and V were similar to that of Pb (*cf.* Fig. 4.49).

4.8.4.1 Discussion

4.8.4.1.1 Assessment of the immobility of Co, Cr, Ni and V in ombrotrophic peat

The Co, Cr, Ni and V profile trends for The Red Moss of Balerno are generally consistent with those found at Flanders Moss (Section 3.8.4.3.1), again indicating that Co, Cr, Ni and V are relatively immobile in ombrotrophic peat.

4.8.4.1.2 The use of Zr as an indicator of Co, Cr, Ni and V soil dust input

As for Flanders Moss (*cf.* Section 3.8.4.1.2), Sc was unsuitable for use as a "reference element" for Co, Cd, Ni and V in RM03CM-2 and Zr was used instead. The Co, Cr, Ni, V and Zr concentration profiles in RM03CM-2 are shown in Fig. 4.50. Note the changes in scale on the Co (12-fold), Cr (20-fold), Ni (15-fold) and V (30-fold) and Zr (4-fold) concentrations on going from 0-40 cm to 40-96 cm in RM03CM-2. The Co/Zr, Cr/Zr, Ni/Zr and V/Zr ratios were calculated (A5.1 Table A9) and their profiles, including Pb/Zr ratios, in RM03CM-2 are shown in Fig. 4.51.

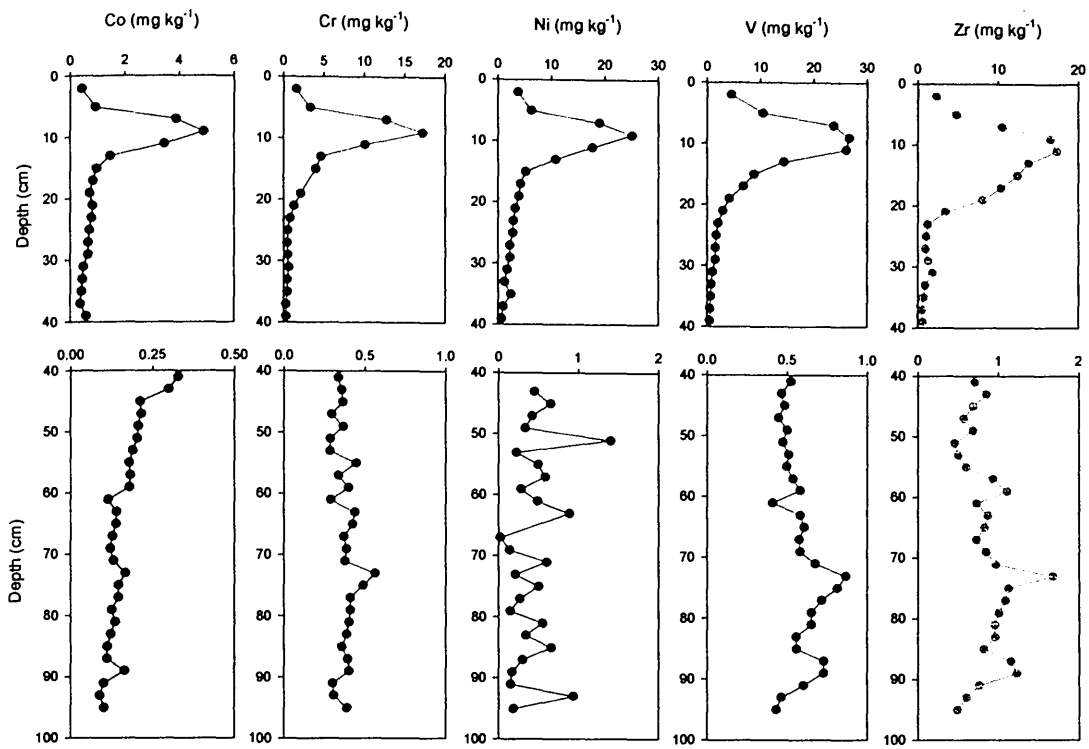

Figure 4.50: Depth profiles of Co, Cr, Ni, V and Zr concentrations (mg kg^{-1}) from 0-40 cm and 40-96 cm in the RM03CM-2 peat core.

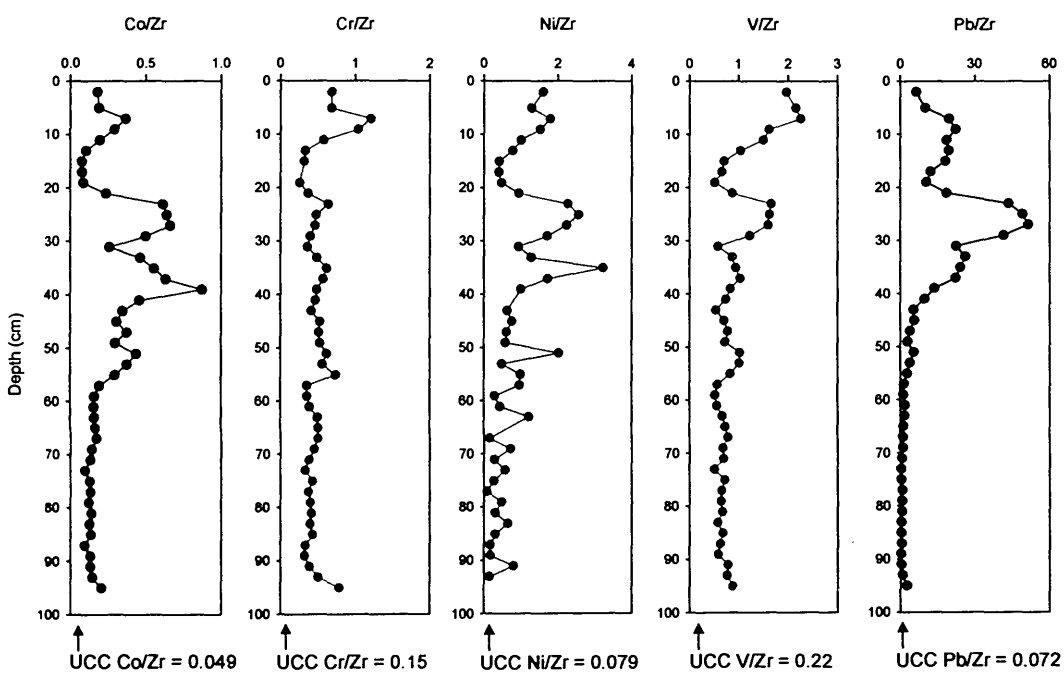

Figure 4.51: Depth profiles of Co/Zr, Cr/Zr, Ni/Zr, V/Zr and Pb/Zr ratios in the RM03CM-2 (0-96 cm) peat core.

As for Pb/Zr ratios (*cf.* Section 4.5.1), the Co/Zr, Cr/Zr, Ni/Zr and V/Zr ratios were at a minimum between 70 and 94 cm, with mean values of 0.13 ± 0.02, 0.40 ± 0.05, 0.41 ± 0.24 and 0.66 ± 0.08, respectively. These Co/Zr, Cr/Zr, Ni/Zr and V/Zr ratios, when compared with the UCC ratios of 0.049, 0.15, 0.079 and 0.22, respectively, were 3 to 5-fold higher. Maximum Co/Zr, Cr/Zr, Ni/Zr and V/Zr ratios occurred between 20 and 56 cm, 0 and 10 cm, 20 and 56 cm and 0 and 8 cm, respectively (*cf.* Fig. 4.51), which were different from the region of maximum Pb/Zr ratios (between 32 and 22 cm) (*cf.* Section 4.5.1).

On the basis of the use of Zr as a conservative element, the anthropogenic Co, Cr, Ni and V concentrations were calculated (A5.1 Table A11) (*cf.* Section 3.8.4.3.3) and their profiles, along with calculated anthropogenic Pb concentrations (A5.1 Table A11) and measured $^{206}Pb/^{207}Pb$ ratios, including age-dates, displayed in Fig. 4.52. The anthropogenic Co and Ni concentration profiles for RM03CM-2 indicate that the apparent increases in Co/Zr and Ni/Zr ratios between 20 and 56 cm (*cf.* Fig. 4.51), didn't result in corresponding increases in anthropogenic Co and Ni concentrations. Therefore, as for Flanders Moss (*cf.* Section 3.8.4.3.2), anthropogenic Co, Cr, Ni and V concentration profiles alone (*cf.* Fig. 4.52) will be used in Section 4.8.4.1.3 to interpret historical trends.

4.8.4.1.3 Historical trends of anthropogenic Co, Cr, Ni and V deposition

Pre-industrial atmospheric Co, Cr, Ni and V sources and deposition

The anthropogenic Ni concentration profile in the 40-96 cm RM03CM-2 sections was rather 'noisy', precluding any historical interpretations of anthropogenic Ni deposition during the pre-industrial period (*cf.* Fig. 4.52). At the bottom of the core (94-96 cm), there was an increase in anthropogenic Cr concentration (0.32 mg kg^{-1}) (*cf.* Fig. 4.52). Enhanced Pb and Sb concentrations during this post-Roman period were attributed to long-range atmospheric deposition from post-Roman metallurgical activities during the reign of the Visigods (*cf.* Sections 4.6.1 and 4.8.1), but these activities are not considered to be a significant source of Cr (*cf.* Table 1.2, Section

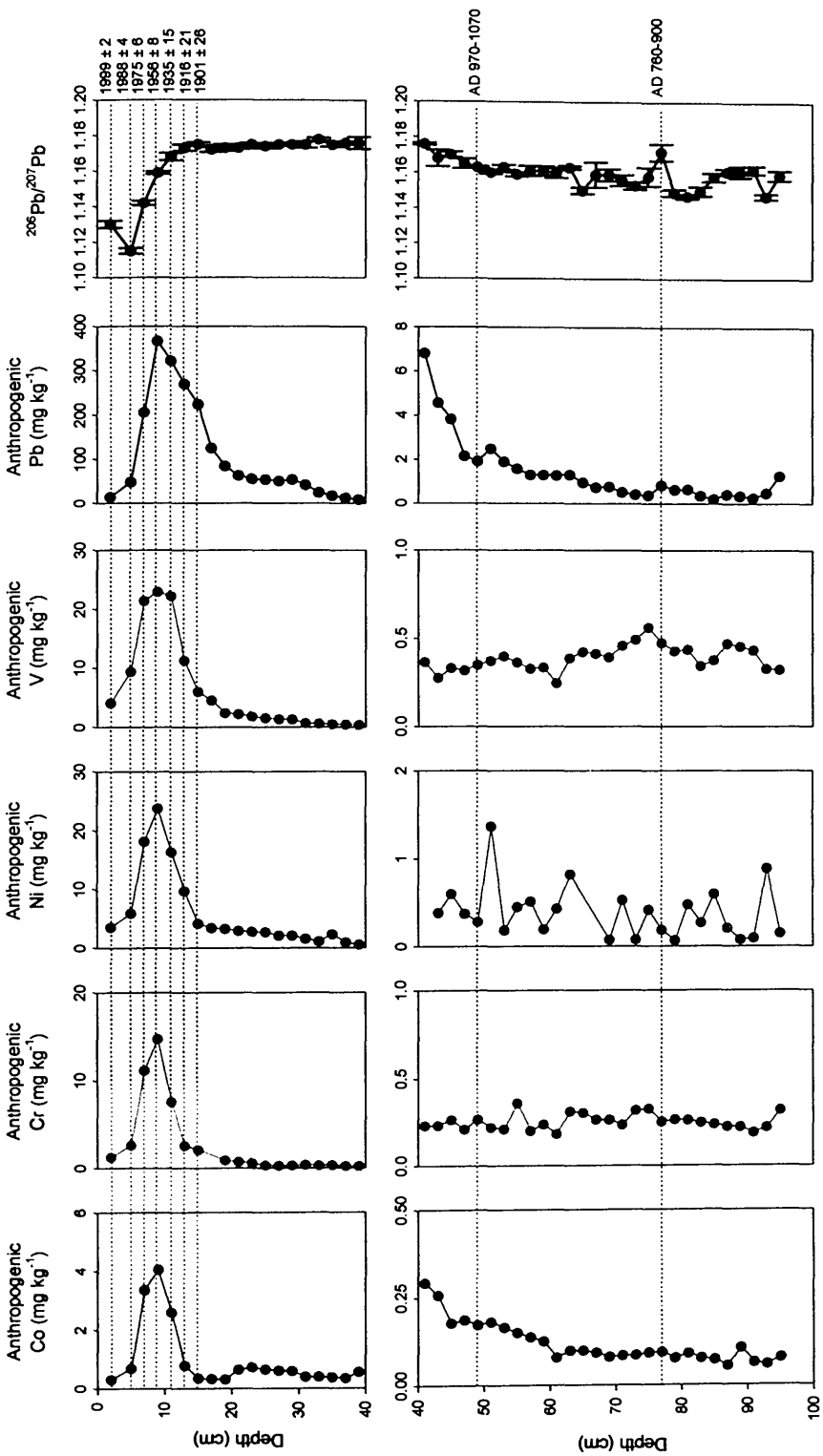

Figure 4.52: Depth profiles of anthropogenic Co, Cr, Ni, V and Pb concentrations (calculated using Zr as the conservative element) and measured $^{206}Pb/^{207}Pb$ ratios, from 0-40 cm and 40-96 cm in the ^{210}Pb- and ^{14}C-dated RM03CM-2 peat core.

1.3.2.2) (Nriagu and Pacyna, 1988), and, therefore, the cause of the slightly enhanced Cr concentration is unclear. Between 94 and 70 cm anthropogenic Co and Cr concentrations, as found for Pb (Section 4.6.1), were at their lowest, with mean values of 0.080 ± 0.015 and 0.25 ± 0.04 mg kg^{-1}, respectively. In contrast, anthropogenic V concentrations increased (mean 0.44 ± 0.06 mg kg^{-1}) (*cf.* Fig. 4.52). Above 70 cm up to a depth of 50 cm (970-1070 A.D.), anthropogenic Co and Cr concentrations increased, with mean values of 0.12 ± 0.04 and 0.25 ± 0.06 mg kg^{-1}, respectively. Corresponding anthropogenic V concentrations remained the same (mean 0.37 ± 0.05 mg kg^{-1}). Above 50 cm (970-1070 A.D.) to a depth of 40 cm, anthropogenic Co concentrations increased from 0.17 to 0.29 mg kg^{-1}, whereas anthropogenic Cr and V concentrations remained the same, with mean values of 0.24 ± 0.02 and 0.33 ± 0.03 mg kg^{-1}, respectively (*cf.* Fig. 4.52). Enhanced Pb concentrations during these periods reflect emissions from Mediaeval mining and smelting activities (*cf.* Sections 4.6.1), but these activities are not a significant source of Co or Cr (*cf.* Table 1.2, Section 1.3.2.2), and again, therefore, the cause of their enhanced concentrations is unclear.

Industrial and post-industrial atmospheric Co, Cr, Ni and V sources and deposition

Co

Above 40 cm (*ca.* early 1700s A.D.) anthropogenic Co concentrations continued to increase, reaching a maximum of 4.1 mg kg^{-1} at 1956 A.D. (coincident with the maximum anthropogenic Pb concentration (340 mg kg^{-1})), after which they decreased to 0.31 mg kg^{-1}, at *ca.* 1999 A.D. (*cf.* Fig. 4.52). As found for Flanders Moss (*cf.* Section 3.8.4.3.3), these trends are likely to reflect Co emissions from metallurgical activities, coal combustion and the use of phosphate fertilisers (Oehme, 1979; Chemical Research Communications, 2003), until the decline in heavy industry in the later part of the 20th century A.D., when emissions from oil combustion (*cf.* Fig. 1.3, Section 1.3.2.2.2) (up to the 1990s A.D.) and waste incineration (Chemical Research Communications, 2003) perhaps became more

important (Department of Trade and Industry, 1998; National Atmospheric Emissions Inventory, 2006).

Cr

Above 40 cm (*ca.* early 1700s A.D.) anthropogenic Cr concentrations increased to a maximum of 15 mg kg^{-1} at 1956 A.D. (coincident with the maximum anthropogenic Pb concentration), after which they decreased to 1.3 mg kg^{-1}, at *ca.* 1999 A.D. (*cf.* Fig. 4.52). As found for Flanders Moss (*cf.* Section 3.8.4.3.3), these trends are likely to reflect Cr emissions from coal combustion and steel and iron manufacturing (*cf.* Table 1.2, Section 1.3.2.2), until the decline in heavy industry in the later part of the 20^{th} century A.D., when emissions from oil combustion (up to the 1990s A.D.) and waste incineration (*cf.* Table 1.2, Section 1.3.2.2) perhaps became more important (Department of Trade and Industry, 1998; National Atmospheric Emissions Inventory, 2006). Note that in contrast to the anthropogenic Cr concentrations remaining constant after the late 1980s A.D. for Flanders Moss (*cf.* Section 3.8.4.3.3), for The Red Moss of Balerno they declined (*cf.* Fig. 4.50).

Ni

Above 40 cm (*ca.* early 1700s A.D.) anthropogenic Ni concentrations increased to a maximum of 24 mg kg^{-1} at 1956 A.D. (coincident with the maximum anthropogenic Pb concentration), after which they decreased to 3.6 mg kg^{-1}, at *ca.* 1999 A.D. (*cf.* Fig. 4.52). As found for Flanders Moss (*cf.* Section 3.8.4.3.3), these trends are likely to reflect Ni emissions from Cu-Ni production and coal combustion (*cf.* Table 1.2, Section 1.3.2.2), until the decline in heavy industry in the later part of the 20^{th} century A.D., when emissions from oil combustion (up to the 1990s A.D.) and waste incineration (*cf.* Table 1.2, Section 1.3.2.2) perhaps became more important (Department of Trade and Industry, 1998; National Atmospheric Emissions Inventory, 2006).

V

From 40 cm (*ca.* early 1700s A.D.) anthropogenic V concentrations increased to a maximum of ~ 20 mg kg^{-1} between 1926 and 1982 A.D. (coincident with the maximum anthropogenic Pb concentration), after which they decreased to 4.1 mg kg^{-1}, at *ca.* 1999 A.D. (*cf.* Fig. 4.52). As found for Flanders Moss (*cf.* Section 3.8.4.3.3), these trends are likely to reflect V emissions from coal combustion (*cf.* Table 1.2, Section 1.3.2.2), until the decline in heavy industry in the later part of the 20th century A.D., when emissions from oil combustion (up to the 1990s A.D.) became more important (Department of Trade and Industry, 1998; National Atmospheric Emissions Inventory, 2006).

4.8.4.1.4 Historical trends in depositional fluxes and inventories of anthropogenic Co, Cr, Ni and V

The anthropogenic depositional fluxes of Co, Cr, Ni and V in RM03CM-2 (A5.1 Table A12) were calculated, along with the anthropogenic depositional fluxes of Pb, using Zr (*cf.* Section 3.8.4.3.3). These fluxes, since 1900 A.D. are plotted along with the measured $^{206}Pb/^{207}Pb$ ratios, *versus* ^{210}Pb-derived calendar dates, for RM03CM-2 in Fig. 4.53. Maximum depositional fluxes of anthropogenic Co, Cr and Ni (0.43, 1.6 and 2.5 mg m^{-2} y^{-1}, respectively), occurred during the mid-1950s A.D., while that of V (2.1-2.6 mg m^{-2} y^{-1}) occurred between the mid-1930s and mid-1970s A.D (*cf.* Fig. 4.53).

Total anthropogenic Co, Cr, Ni and V inventories of 0.039, 0.10, 0.23 g m^{-2} and 0.24 g m^{-2}, respectively, were calculated for RM03CM-2. The post-1800 A.D. Co, Cr, Ni and V inventories (0.031, 0.089, 0.20 and 0.22 g m^{-2}) (corresponding to peat sections 0-28 cm) constituted 79, 89, 87 and 92% of the total anthropogenic Co, Cr, Ni and V inventories, respectively. Calculated cumulative post-1800 A.D. anthropogenic Co, Cr, Ni and V inventories (% of total post-1800 A.D. inventory) for RM03CM-2 are plotted *versus* ^{210}Pb-derived calendar dates in Fig. 4.54. Maximum Co deposition occurred between the 1910s and 1970s A.D. and maximum

Cr, Ni and V deposition occurred between the 1890s and 1970s A.D., generally in agreement with that found for Pb (*cf.* Section 4.6.2.1) (*cf.* Fig. 4.54).

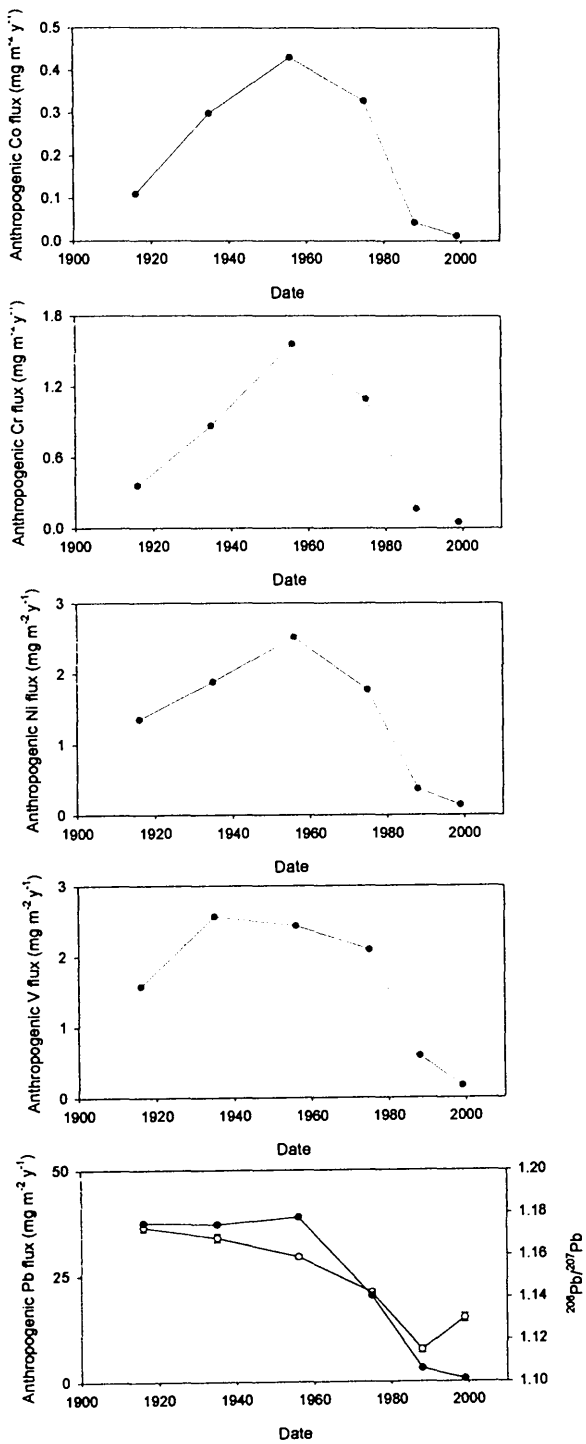

Figure 4.53: Calculated atmospheric depositional fluxes of anthropogenic Co, Cr, Ni, V and Pb (mg m^{-2} y^{-1}) (closed circles) and the measured $^{206}Pb/^{207}Pb$ ratios (open circles) for the RM03CM-1 core *versus* ^{210}Pb-derived dates since 1900 A.D.

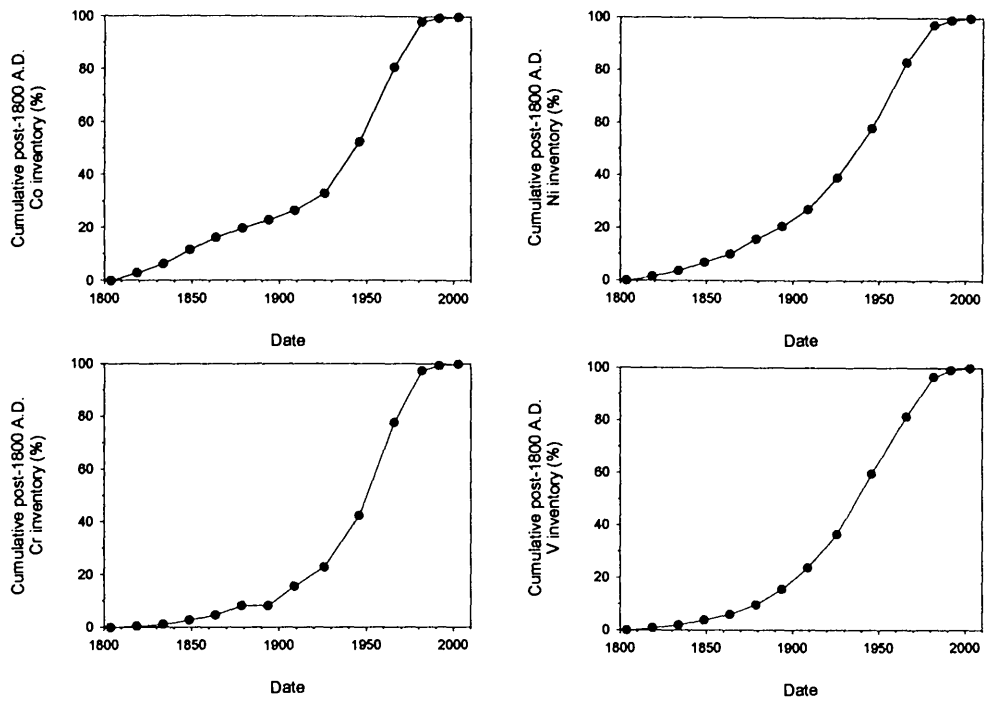

Figure 4.54: Calculated cumulative post-1800 A.D. anthropogenic Co, Cr, Ni and V inventories (% of total post-1800 A.D. inventory) for the RM03CM-2 core *versus* ^{210}Pb-derived dates. Note that dates in RM03CM-2 prior to *ca.* 1894 A.D. were extrapolated.

4.8.5 Comparison of As, Cd, Co, Cr, Cu, Hg, Ni, Pb, Sb and V depositional fluxes

The depositional fluxes of anthropogenic As, Cd, Co, Cu, Cr, Ni, Pb, Sb and V and depositional Hg fluxes in RM03CM-2 and RM03CM-1 since 1880 A.D. are plotted along with the measured ^{206}Pb/^{207}Pb ratios *versus* ^{210}Pb-derived calendar dates in Fig. 4.55. Differences between the depositional fluxes of As, Cd, Co, Cr, Hg, Ni, Pb. Sb and V are due to differences in inputs from various sources, which have changed with time.

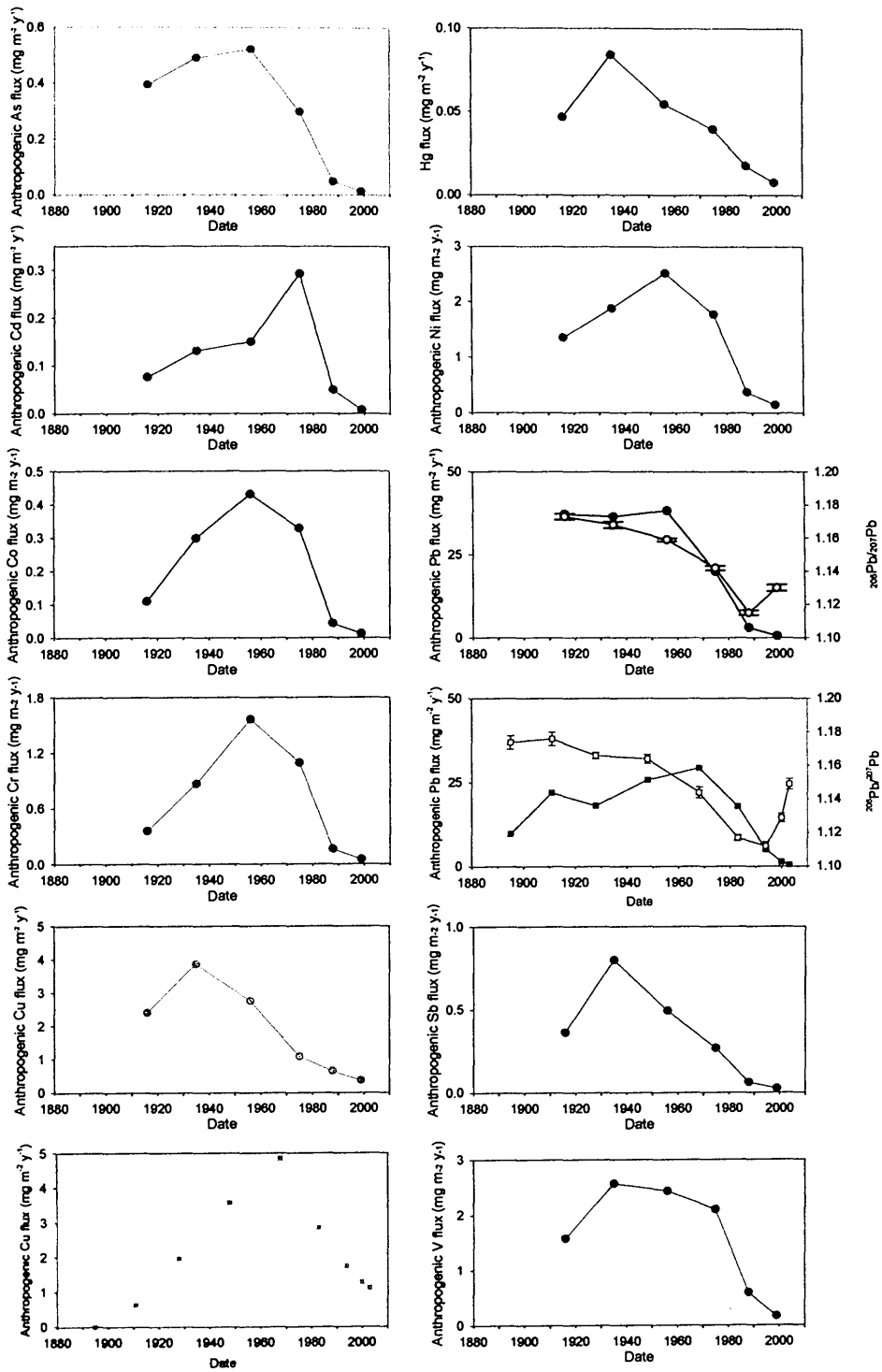

Figure 4.55: Calculated atmospheric depositional fluxes of anthropogenic As, Cd, Co, Cr, Cu, Ni, Pb, Sb and V (mg m^{-2} y^{-1}), depositional fluxes of Hg (mg m^{-2} y^{-1}) and measured $^{206}Pb/^{207}Pb$ ratios for the RM03CM-2 (circles) and RM03CM-1 (squares) cores *versus* ^{210}Pb-derived dates since 1880 A.D.

4.9 CONCLUSIONS

The principal conclusions arising from the results for The Red Moss of Balerno peat cores were largely consistent with those found for Flanders Moss (Section 3.9) and are summarised below:

- Using Sc as a conservative element, anthropogenic enrichments of Pb for The Red Moss of Balerno were estimated and, on the basis of ^{210}Pb and ^{14}C dating and Pb isotopic composition (e.g. $^{206}Pb/^{207}Pb$), sources of atmospheric anthropogenic Pb deposition were investigated. In the Mediaeval period, the mining and smelting of Pb ores was responsible for the increase in anthropogenic Pb concentration. In the industrial and post-industrial periods, variations in the relative importance of contributions of anthropogenic Pb from different sources (e.g. mining and smelting of indigenous Scottish Pb ores, coal combustion and Australian-Pb-influenced car-exhaust emissions) were apparent. Derived atmospheric depositional fluxes of anthropogenic Pb were greatest between the late 1910s and late 1960s A.D.
- The major elements, Ca, Fe, Mg, Mn, P and S, and two trace elements, Se and Zn, were found to be subject to post-depositional mobility at The Red Moss of Balerno. Plant uptake and recycling affected Ca, Fe, Mg, Mn, P, S and Zn profiles while Fe, Mn, P and S were also influenced by redox cycling. Zn was also possibly influenced by sulfide formation in the catotelm peat layers of the bog.
- The general similarity between the Pb concentration profiles and those of the trace elements As, Cd, Co, Cr, Cu, Hg, Ni, Sb and V at The Red Moss of Balerno suggested that these latter elements were also essentially immobile in ombrotrophic peat.
- The Sb and Pb concentration profiles at The Red Moss of Balerno were remarkably similar. Using Sc as a conservative element, anthropogenic enrichments of Sb were estimated and, on the basis of anthropogenic Sb/Pb ratios, sources of atmospheric anthropogenic Sb deposition were investigated. During the Mediaeval period, sources of anthropogenic Sb deposition were the

same as those found for Pb, and this was also the case during the Industrial period, with the exception of leaded petrol. In the post-industrial period, the influence of anthropogenic inputs of Sb from comparatively new recent sources (e.g. automotive brake linings) was apparent. Derived atmospheric depositional fluxes of anthropogenic Sb were greatest in the industrial period, peaking during the mid-1930s A.D.

- The Hg concentration profile in the older catotelm peats of The Red Moss of Balerno was possibly influenced by sulfide formation. In the industrial and post-industrial periods, coal combustion and waste incineration, respectively, are likely to have been the most important sources of Hg. Derived atmospheric depositional fluxes of Hg were greatest in the industrial period, peaking during the mid-1930s A.D.
- Anthropogenic As, Cd and Cu concentrations were estimated using Sc as a conservative element. In the Mediaeval period, the mining and smelting of Pb and Cu ores is likely to have been responsible for the increase in anthropogenic As concentration. In the industrial and post-industrial periods, sources of As, Cd and Cu were attributed to a variety of sources (e.g. metallurgical activities, coal and oil combustion and waste incineration). Also, there may have been inputs of Cu from comparatively new recent anthropogenic sources (e.g. automobile exhaust and non-exhaust emissions, due to the use of Cu as an antioxidant in motor oil and its presence in new brake linings and tyres). Derived atmospheric depositional fluxes of anthropogenic As, Cd and Cu were greatest between the late 1910s and mid-1950s A.D., during the mid-1970s A.D. and between the mid-1930s and late 1960s A.D., respectively.
- Anthropogenic Co, Cr, Ni and V concentrations were estimated using Zr as a conservative element. In the Mediaeval period, anthropogenic Co and Cr concentrations increased but the sources of these increases were unclear. In the industrial and post-industrial periods, sources of Co, Cr, Ni and V were attributable to a variety of sources (e.g. metallurgical activities, coal and oil combustion, use of phosphate fertilisers and waste incineration). Derived atmospheric depositional fluxes of anthropogenic Co, Cr and Ni were greatest

during the mid-1950s A.D and those of V were greatest between the mid-1930s and mid-1970s A.D.

- Differences between the timings of the maximum anthropogenic Cu fluxes, and to a lesser extent, anthropogenic Pb fluxes, were apparent for the two cores collected from The Red Moss of Balerno.

5 TURCLOSSIE MOSS

This chapter contains the results for the Turclossie Moss peat cores, which will be treated in a similar way to the results for the peat cores from the previous sites (Chapters 3 and 4).

5.1 PEAT MATRIX PROPERTIES AND EVALUATION OF TROPHIC STATUS

5.1.1 Visual observations

Visual observation depth profiles for the Turclossie Moss peat cores, TM04CM-2, TM04M-1 and TM04CM-4, are shown in Fig. 5.1.

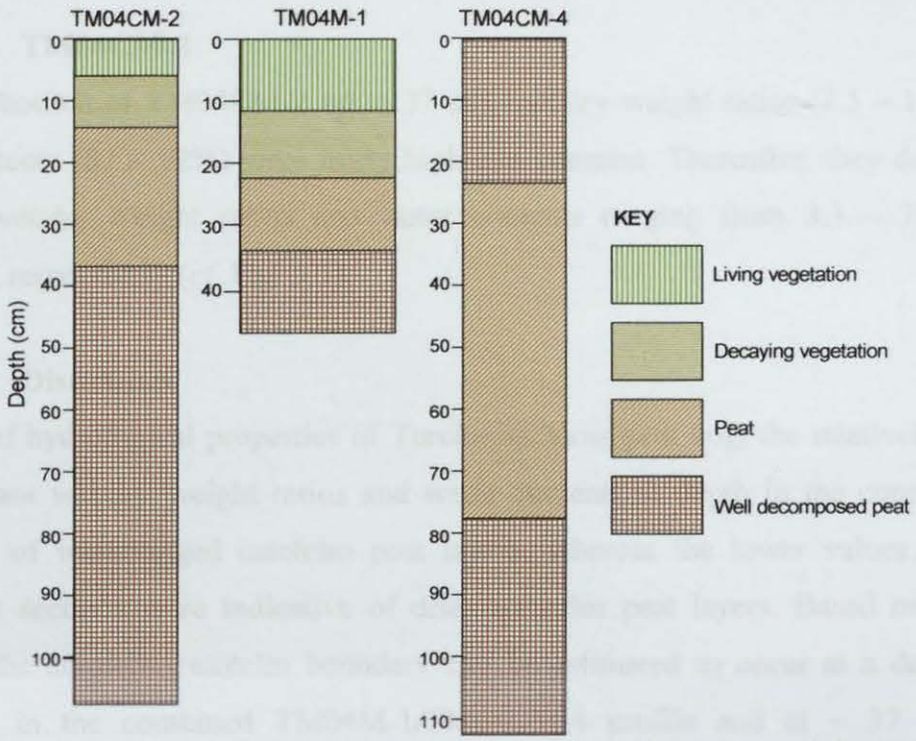

Figure 5.1: Visual observation depth profiles for TM04CM-2, TM04M-1 and TM04CM-4.

Note that the TM04CM-4 core represents the material collected directly below the TM04M-1 core and therefore results for these two cores will be presented and plotted as one profile (i.e. the surface of TM04CM-4 (0 cm) will be taken to be 47 cm).

5.1.2 Wet/dry weight ratios and water contents

Wet and dry weights, wet/dry weight ratios, water contents and residual moisture contents for TM04M-1 and TM04CM-4, and TM04CM-2 are tabulated in Appendix A6.1 Table A1 and A6.2 Table A1, respectively. The wet/dry weight ratio and water content profiles for TM04M-1 and TM04CM-4, and TM04CM-2 are shown in Figs. 5.2 and 5.3, respectively.

5.1.2.1 TM04M-1 and TM04CM-4

From the bottom of TM04CM-4 up to 54 cm, wet/dry weight ratios (7.6 – 12) and water contents (87 – 92%) were fairly high and constant. Thereafter, in the rest of TM04CM-4 and in TM04M-1 they declined slightly, wet/dry weight ratios and water contents ranging from 3.7 – 8.1 and 73 – 88%, respectively (*cf.* Fig. 5.2).

5.1.2.2 TM04CM-2

From the bottom of TM04CM-2 up to 37 cm, wet/dry weight ratios (7.5 – 13) and water contents (87 – 92%) were fairly high and constant. Thereafter, they declined slightly, wet/dry weight ratios and water contents ranging from 3.3 – 7.4 and 70 – 87%, respectively (*cf.* Fig. 5.3).

5.1.2.3 Discussion

In terms of hydrological properties of Turclossie Moss peat bog, the relatively high and constant wet/dry weight ratios and water contents at depth in the cores were indicative of waterlogged catotelm peat layers, whereas the lower values in the uppermost sections were indicative of drier acrotelm peat layers. Based on these patterns, the acrotelm-catotelm boundary can be estimated to occur at a depth of ~ 54 cm in the combined TM04M-1/TM04CM-4 profile and at ~ 37 cm in TM04CM-2.

5.1.3 Ash contents and Ca/Mg ratios

The profiles of ash contents and Ca/Mg ratios (A6.1 Table A2 and A6.2 Table A2), for TM04M-1 and TM04CM-4, and TM04CM-2 are shown in Figs. 5.4 and 5.5, respectively.

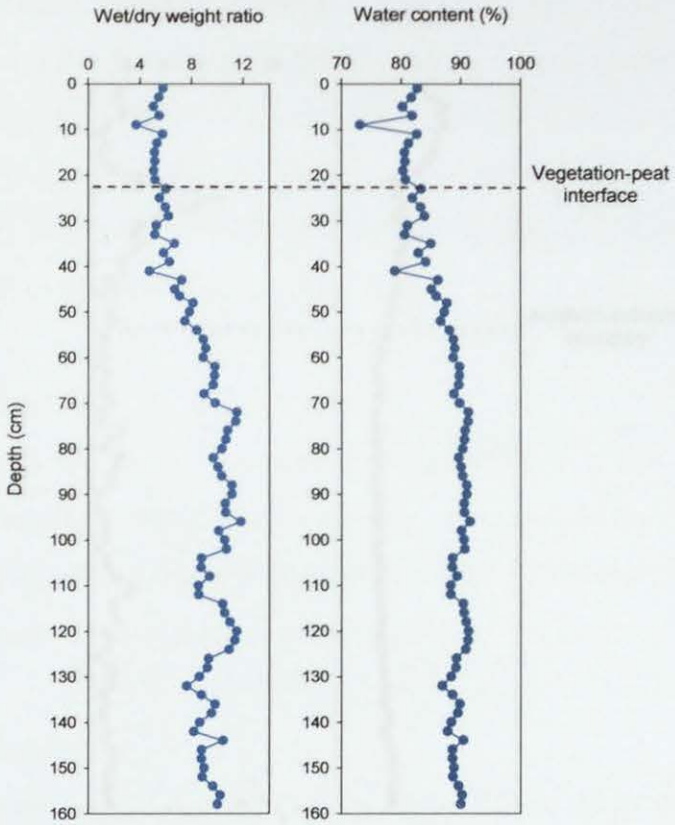

Figure 5.2: Depth profiles of wet/dry weight ratio and water content (% by weight) in the combined TM04M-1 (0-47 cm) and TM04CM-4 (47-159 cm) peat cores.

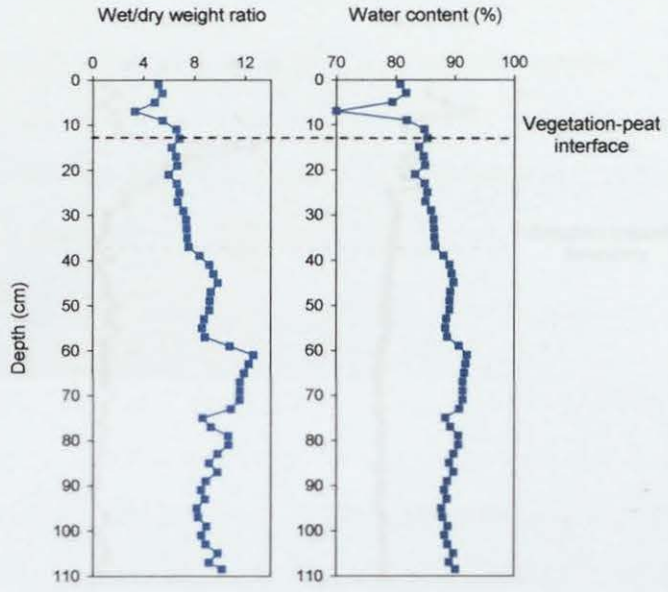

Figure 5.3: Depth profiles of wet/dry weight ratio and water content (% by weight) in the TM04CM-2 (0-109 cm) peat core.

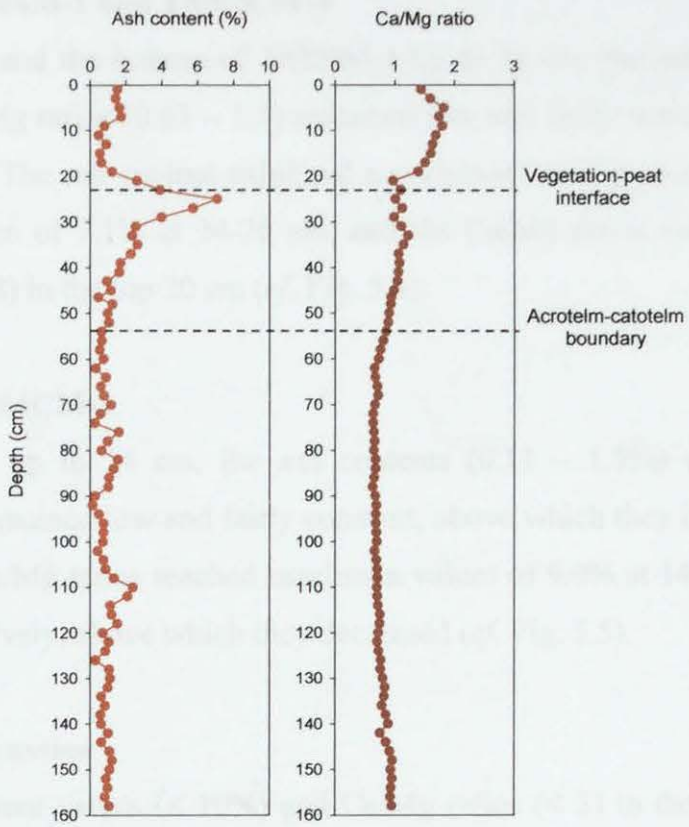

Figure 5.4: Depth profiles of ash content (% by weight) and Ca/Mg ratios in the combined TM04M-1 (0-47 cm) and TM04CM-4 (47-159 cm) peat cores.

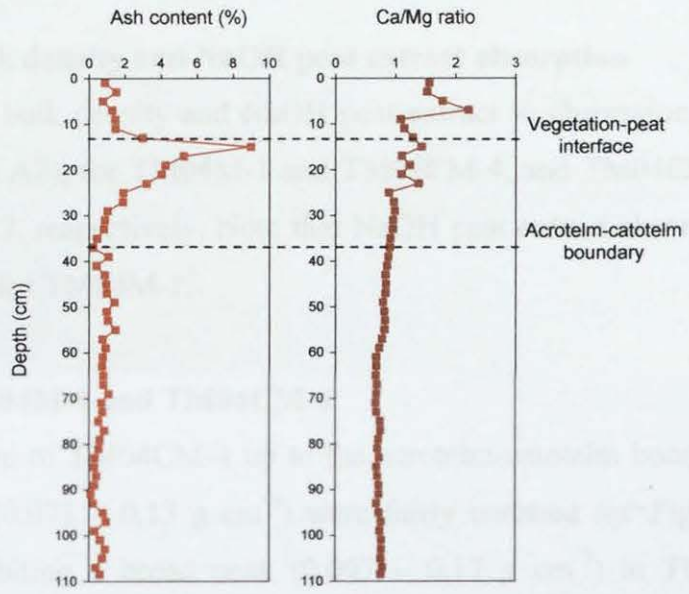

Figure 5.5: Depth profiles of ash content (% by weight) and Ca/Mg ratios in the TM04CM-2 (0-109 cm) peat core.

5.1.3.1 TM04M-1 and TM04CM-4

In TM04CM-4 and the bottom of TM04M-1 up to 36 cm, the ash contents (0.28 – 2.4%) and Ca/Mg ratios (0.63 – 1.1) remained low and fairly constant, above which they increased. The ash content exhibited a prominent peak between 38 and 20 cm, with a maximum of 7.1% at 24-26 cm, and the Ca/Mg ratios exhibited maximum values (1.4 – 1.8) in the top 20 cm (*cf.* Fig. 5.4).

5.1.3.2 TM04CM-2

In TM04CM-2 up to 24 cm, the ash contents (0.11 – 1.9%) and Ca/Mg ratios (0.68 – 0.99) remained low and fairly constant, above which they increased. The ash contents and Ca/Mg ratios reached maximum values of 9.0% at 14-16 cm and 2.2 at 6-8 cm, respectively, above which they decreased (*cf.* Fig. 5.5).

5.1.3.3 Discussion

As the ash content values (< 10%) and Ca/Mg ratios (< 3) in the Turclossie Moss cores are consistent with ombrotrophic conditions, these cores are suitable for use as archives of atmospheric metal deposition.

5.1.4 Bulk density and NaOH peat extract absorption

The profiles of bulk density and NaOH peat extract % absorptions (A6.1 Table A2 and A6.2 Table A2), for TM04M-1 and TM04CM-4, and TM04CM-2 are shown in Figs. 5.6 and 5.7, respectively. Note that NaOH peat extract absorption values were not determined for TM04M-1.

5.1.4.1 TM04M-1 and TM04CM-4

From the bottom of TM04CM-4 up to the acrotelm-catotelm boundary (53-55 cm), bulk densities (0.071 – 0.13 g cm^{-3}) were fairly constant (*cf.* Fig. 5.6). They then increased, exhibiting a broad peak (0.097 – 0.17 g cm^{-3}) in TM04M-1 between 42 and 24 cm, before decreasing at and above the vegetation-peat interface (22-24 cm). The NaOH peat extract absorption values in TM04CM-4 fluctuated greatly, ranging from 29 to 79%, exhibiting prominent peaks at 152, 138 and 66 cm.

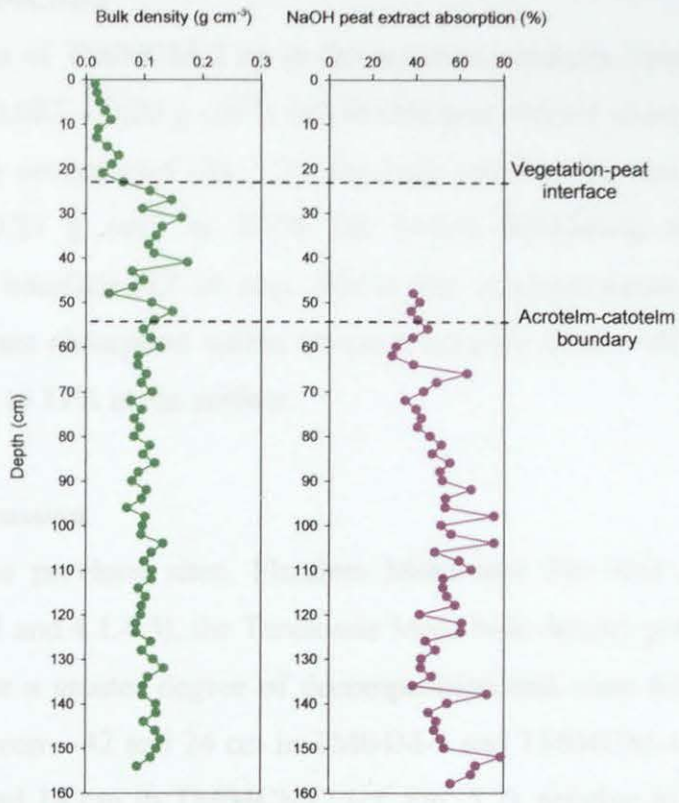

Figure 5.6: Depth profiles of bulk density (g cm^{-3}) and NaOH peat extract absorption (%) at 550 nm in the combined TM04M-1 (0-47 cm) and TM04CM-4 (47-159 cm) peat cores.

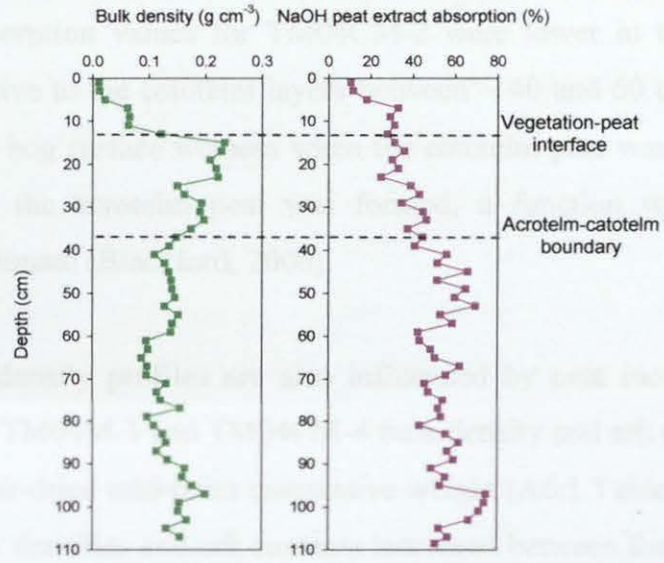

Figure 5.7: Depth profiles of bulk density (g cm^{-3}) and NaOH peat extract absorption (%) at 550 nm in TM04CM-2 (0-109 cm) peat core.

5.1.4.2 TM04CM-2

From the bottom of TM04CM-2 up to the acrotelm-catotelm boundary (36-38 cm), bulk densities (0.087 – 0.20 g cm^{-3}) and NaOH peat extract absorption values (41 - 75%) were fairly constant (*cf.* Fig. 5.7). The bulk densities then increased, reaching a maximum of 0.23 g cm^{-3} at 14-16 cm before decreasing at and above the vegetation-peat interface (12-14 cm). Above the acrotelm-catotelm boundary, the NaOH peat extract absorption values declined steadily from ~ 40 to ~30% at 6 cm and then steeply to 11% at the surface.

5.1.4.3 Discussion

As found at the previous sites, Flanders Moss and The Red Moss of Balerno (Sections 3.1.4.3 and 4.1.4.3), the Turclossie Moss bulk density profiles (*cf.* Figs. 5.6 and 5.7) indicate a greater degree of decomposition and mass loss in the acrotelm peat layers between ~ 42 and 24 cm in TM04M-1 and TM04CM-4 (*cf.* Fig. 5.6), and between ~ 36 and 14 cm in TM04CM-2 (*cf.* Fig. 5.7), relative to the catotelm peat sections beneath ~ 53 and 36 cm in TM04CM-4 and TM04CM-2, respectively (*cf.* Figs. 5.6 and 5.7). In contrast to findings at the other sites, however, the NaOH peat extract absorption values for TM04CM-2 were lower in the acrotelm layers (14-36 cm) relative to the catotelm layers between ~ 40 and 60 cm. This trend may indicate that the bog surface wetness when the catotelm peat was formed was lower than that when the acrotelm peat was formed, a function which is essentially determined by climate (Blackford, 2000).

Since the bulk density profiles are also influenced by peat inorganic content and compaction, the TM04M-1 and TM04CM-4 bulk density and ash content profiles are plotted against air-dried mid-point cumulative weight (A6.1 Table A1) in Fig. 5.8. In general, the bulk densities and ash contents increased between the acrotelm-catotelm boundary and vegetation-peat interface, perhaps providing further evidence (*cf.* Sections 3.1.4.3 and 4.1.4.3) that the peat inorganic content does influence bulk density values.

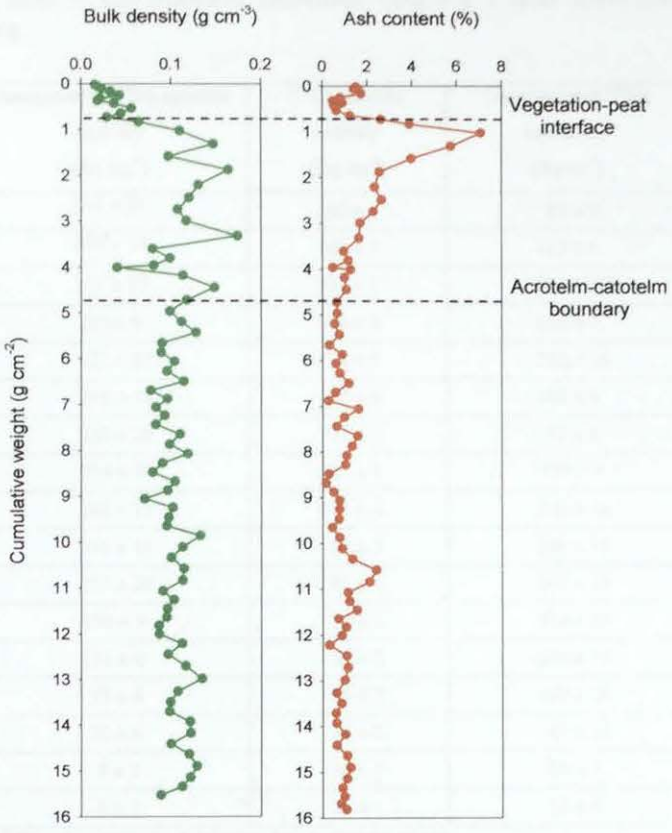

Figure 5.8: Comparison of bulk density (g cm^{-3}) and ash content (% by weight) *versus* cumulative weight (g cm^{-2}) in the combined TM04M-1 and TM04CM-4 peat cores.

5.2 RADIONUCLIDES AND RADIOMETRIC DATING OF TURCLOSSIE MOSS PEAT CORES

5.2.1 ^{210}Pb and ^{137}Cs

^{210}Pb and ^{137}Cs were determined in sections from the top 34 cm of TM04M-1. As ^{226}Ra was not detected above background in any of the TM04M-1 sections, the total ^{210}Pb specific activities (Table 5.1) were taken to represent unsupported ^{210}Pb. The profiles of ^{210}Pb and ^{137}Cs specific activities are shown in Figs. 5.9 a (*vs.* depth in cm) and 5.9 b (*vs.* depth in g cm^{-2}).

Table 5.1: ^{210}Pb and ^{137}Cs specific activities (Bq kg^{-1}) and inventories (Bq m^{-2}) in the TM04M-1 peat core.

TM04M-1 section (cm)	Unsupported ^{210}Pb specific activity (Bq kg^{-1})	^{137}Cs specific activity (Bq kg^{-1})	Unsupported ^{210}Pb inventory (Bq m^{-2})	^{137}Cs inventory (Bq m^{-2})
0-2	246 ± 21	190 ± 5	88 ± 8	67 ± 2
2-4	269 ± 15	162 ± 5	112 ± 6	68 ± 2
4-6	257 ± 19	131 ± 7	134 ± 10	68 ± 4
6-8	222 ± 9	134 ± 3	163 ± 7	98 ± 2
8-10	231 ± 17	133 ± 5	222 ± 16	128 ± 5
10-12	214 ± 18	87 ± 4	102 ± 9	41 ± 2
12-14	236 ± 20	121 ± 5	98 ± 8	50 ± 2
14-16	218 ± 9	121 ± 4	179 ± 7	99 ± 3
16-18	240 ± 13	114 ± 4	302 ± 16	143 ± 5
18-20	236 ± 11	85 ± 3	234 ± 11	84 ± 3
20-22	257 ± 20	91 ± 5	167 ± 13	59 ± 3
22-24	190 ± 9	70 ± 3	274 ± 13	101 ± 4
24-26	113 ± 6	56 ± 2	276 ± 15	137 ± 5
26-28	55 ± 8	46 ± 2	180 ± 26	151 ± 7
28-30	20 ± 6	35 ± 2	43 ± 13	76 ± 4
30-32	8 ± 2	26 ± 1	29 ± 7	96 ± 4
32-34	6 ± 2	25 ± 1	18 ± 6	73 ± 3

Specific activities (± 1 SD) are expressed relative to air-dried weight.

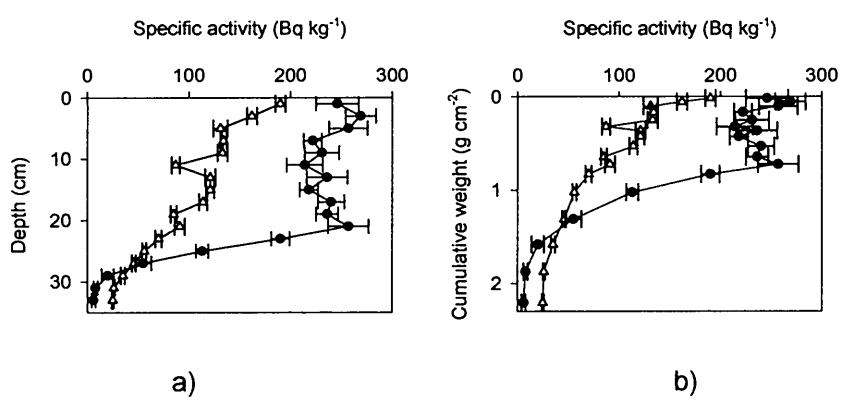

Figure 5.9: ^{210}Pb (closed circles) and ^{137}Cs (open triangles) specific activity (Bq kg^{-1}) *versus* a) depth (cm) and b) cumulative weight (g cm^{-2}) in the TM04M-1 peat core.

5.2.2 ^{210}Pb dating of TM04M-1

The CRS model (Section 3.2.2) was applied to the ^{210}Pb inventories (*cf.* Table 5.1) to generate an age for the bottom of each individual TM04M-1 section and, by interpolation, the mid-point date of each section was calculated (Table 5.2).

Table 5.2: Calculated ages and dates from the ^{210}Pb dating of the TM04M-1 peat core.

Depth (cm)	Age (y)	Date (AD)
0	0	2004 ± 0
1		2004 ± 1
2	1.1	2003 ± 1
3		2002 ± 1
4	2.6	2001 ± 1
5		2001 ± 1
6	4.4	2000 ± 1
7		1999 ± 2
8	6.8	1997 ± 2
9		1996 ± 2
10	10.3	1994 ± 2
11		1993 ± 2
12	12.1	1992 ± 2
13		1991 ± 2
14	13.9	1990 ± 2
15		1989 ± 2
16	17.4	1987 ± 2
17		1983 ± 2
18	24.5	1979 ± 2
19		1976 ± 3
20	31.4	1973 ± 3
21		1970 ± 3
22	37.3	1967 ± 3
23		1961 ± 4
24	50.4	1953 ± 4
25		1943 ± 6
26	72.9	1931 ± 7
27		1914 ± 10
28	108.2	1896 ± 12
29		1886 ± 12
30	129.0	1875 ± 12
31		1860 ± 17
32	160.1	1844 ± 22

Dates were rounded up to the nearest whole number.

5.2.3 TM04M-1 ^{210}Pb flux

The total unsupported ^{210}Pb inventory of TM04M-1 was 2620 ± 51 Bq m^{-2}, with a corresponding inventory-derived average ^{210}Pb flux of 81 ± 2 Bq m^{-2} y^{-1}. This inventory-derived average ^{210}Pb flux is slightly higher than the theoretical rainfall-corrected ^{210}Pb flux of 63 ± 11 Bq m^{-2} y^{-1}, calculated for the Turclossie Moss area using the average annual rainfall value of 82.1 cm y^{-1} and the estimated average

^{210}Pb flux of 77 ± 14 Bq m^{-2} y^{-1} per metre of rainfall established for the UK by Smith *et al.* (1997). As found for The Red Moss of Balerno (Section 4.2.3), this high inventory-derived average ^{210}Pb flux value could reflect local differences in the composition and/or quantity of bulk precipitation.

5.2.4 TM04M-1 ^{137}Cs total inventory

The total ^{137}Cs inventory in TM04M-1 was 1.5 ± 0.0 kBq m^{-2}. This is much lower than that deposited in the north-east of Scotland from the atmosphere following nuclear weapons testing (~ 2 kBq m^{-2}, Peirson *et al.*, 1982) and the Chernobyl accident (1-5 kBq m^{-2}, Clark and Smith, 1988), indicating loss of ^{137}Cs from the peat bog.

5.2.5 TM04CM-2 dates

An attempt was made to obtain dates for TM04CM-2 by extrapolation of the ^{210}Pb-derived dates obtained for the TM04M-1 sister core. The attempted extrapolation of these dates was aided by matching the ^{206}Pb/^{207}Pb profiles of the two cores, plotted against cumulative weight (Fig. 5.10) rather than linear depth in order to eliminate any effects from differential compaction arising from the collection of TM04M-1 and TM04CM-2 using different techniques, i.e. Cuttle and Malcolm corer and monolith tin, respectively.

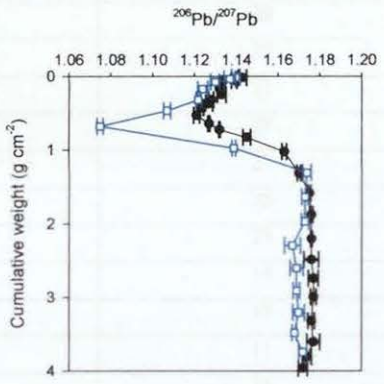

Figure 5.10: Profiles of measured ^{206}Pb/^{207}Pb ratios in the TM04M-1 (0-47 cm) core (black closed circles) and from 0-34 cm in the TM04CM-2 core (blue open squares) *versus* cumulative weight.

Unfortunately, partly as a result of the low $^{206}Pb/^{207}Pb$ ratios at 10-12 cm (1.107) and 12-14 cm (1.075) in TM04CM-2, extrapolation of dates was not readily achievable (*cf.* Fig. 5.10). Note that $^{206}Pb/^{207}Pb$ ratio results will be discussed in Section 5.4.1.

5.2.6 Peat accumulation rates

5.2.6.1 CRS model

Peat accumulation rates (in terms of mg cm^{-2} y^{-1} and cm y^{-1}) for each TM04M-1 section, calculated using the CRS model, are shown in Table 5.3. The actual average accumulation rates over the depth interval 0-32 cm were 13 ± 2 mg cm^{-2} y^{-1} and 0.20 ± 0.03 cm y^{-1}.

5.2.6.2 CIC model

The CIC model could not be used to calculate peat accumulation rates for TM04M-1, since plotting ln ^{210}Pb *versus* cumulative weight (Fig. 5.11 a) and depth (Fig. 5.11 b), respectively, resulted in a non-linear distribution of points, a consequence of the large amount of living and decaying vegetation at the top of the core (*cf.* Fig. 5.1).

Table 5.3: Sectional peat accumulation rates for the TM04M-1 peat core determined using the CRS model.

Section (cm)	Number of years	Accumulation rate (mg cm^{-2} y^{-1})	Accumulation rate (cm y^{-1})
0-2	1.1	33	1.8
2-4	1.5	29	1.3
4-6	1.8	28	1.1
6-8	2.4	31	0.83
8-10	3.5	27	0.57
10-12	1.8	27	1.1
12-14	1.8	23	1.1
14-16	3.6	23	0.56
16-18	7.1	18	0.28
18-20	6.8	15	0.29
20-22	5.9	11	0.34
22-24	13	11	0.15
24-26	23	11	0.087
26-28	35	9.3	0.057
28-30	21	10	0.095
30-32	31	12	0.065

Accumulation rates are expressed in terms of air-dried peat weight.

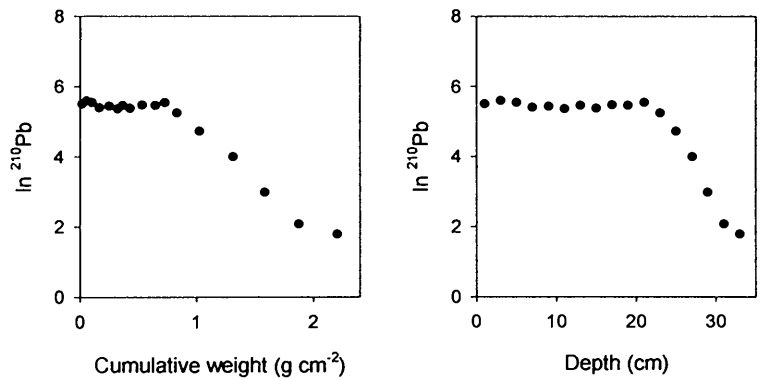

Figure 5.11: Profiles of ln [^{210}Pb (Bq kg^{-1})] *versus* a) cumulative weight and b) depth for the TM04M-1 peat core.

5.2.6.3 Discussion

The TM04M-1 peat accumulation rates could be derived using the CRS but not the CIC ^{210}Pb model, demonstrating why the CRS model is preferred (*cf.* Section 1.9.1.2).

5.2.7 ^{14}C

The ^{14}C AMS age dates determined for selected peat sections of the TM04CM-4 core are shown in Table 5.4.

Table 5.4: ^{14}C age dates of selected TM04CM-4 peat samples.

TM04CM-4 section (cm)	Fraction dated	δ^{13}C (‰)	Date (^{14}C years B.P.)	Date (calendar years A.D./B.C.)	Laboratory code
101-103	Humic acid (HA1)	-28.2	1385 ± 35	590 – 690 A.D.	GU-13608
129-131	Humic acid (HA1)	-27.7	1895 ± 35	50 – 220 A.D.	GU-13609
153-155	Humic acid (HA1)	-27.8	2190 ± 35	380 – 160 B.C.	GU-13610

5.3 CONSERVATIVE ELEMENTS

Profiles of total Al, Sc, Ti, Y and Zr concentrations for TM04M-1 and TM04CM-4 (A6.1 Table A3) and TM04CM-2 (A6.2 Table A3) are shown, along with ash contents, in Figs. 5.12 and 5.13, respectively.

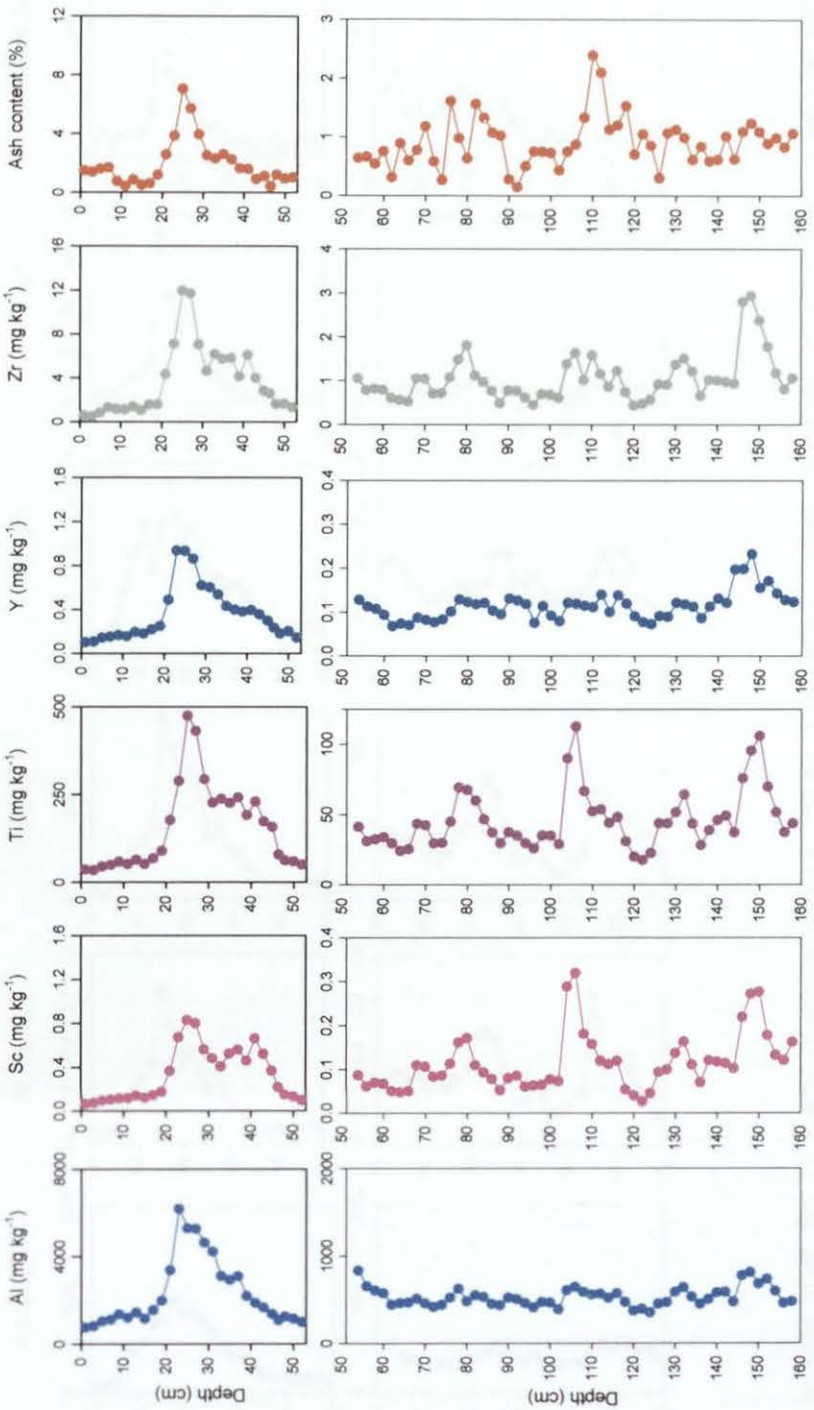

Figure 5.12: Depth profiles of Al, Sc, Ti, Y and Zr concentrations (mg kg^{-1}) and ash contents (% by weight) from 0-53 cm and 53-159 cm in the combined TM04M-1 and TM04CM-4 peat cores.

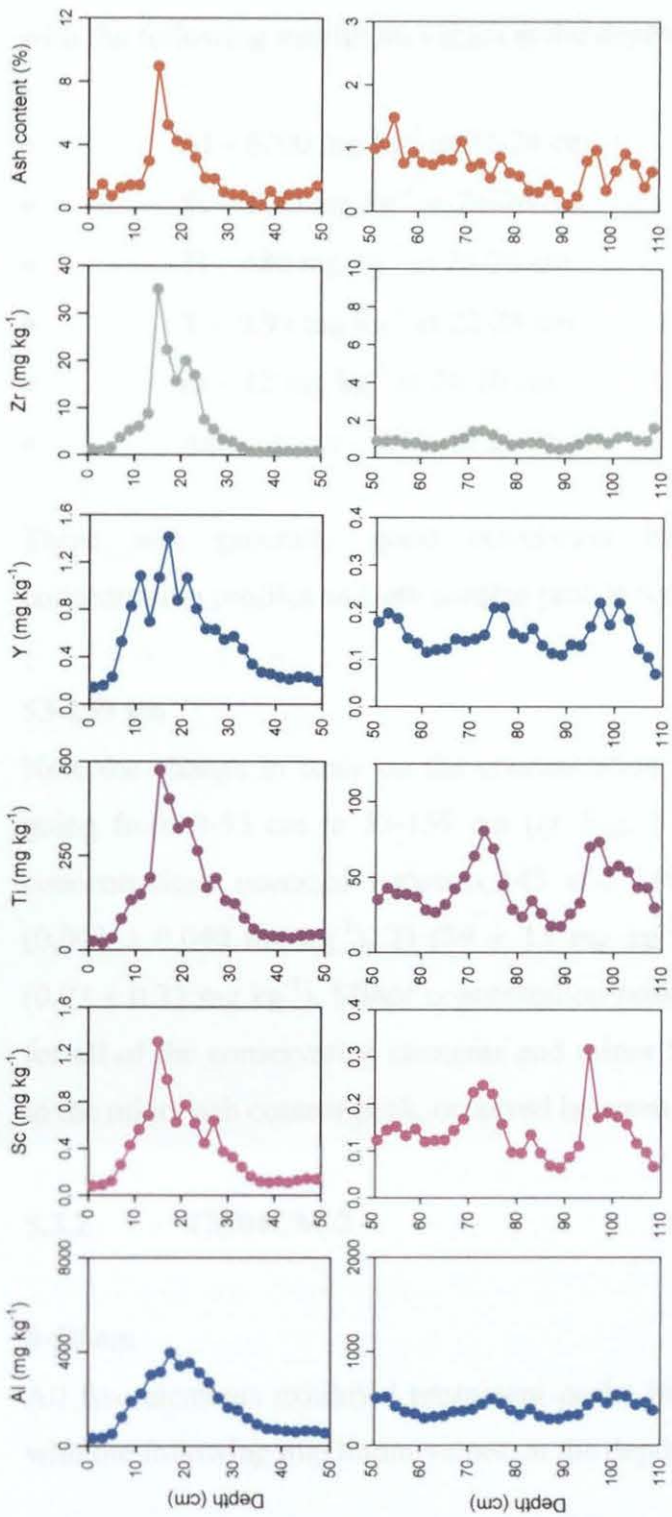

Figure 5.13: Depth profiles of Al, Sc, Ti, Y and Zr concentrations (mg kg^{-1}) and ash contents (% by weight) from 0-50 cm and 50-109 cm in the TM04CM-2 peat core.

5.3.1 TM04M-1 and TM04CM-4

0-53 cm

All five elements exhibited prominent peaks between 18 and 47 cm in TM04M-1, with the following maximum values at the depths indicated:

- Al – 6200 mg kg^{-1} at 22-24 cm
- Sc – 0.83 mg kg^{-1} at 24-26 cm
- Ti – 480 mg kg^{-1} at 24-26 cm
- Y – 0.94 mg kg^{-1} at 22-24 cm
- Zr – 12 mg kg^{-1} at 24-26 cm
- Ash content – 7.1% at 24-26 cm

There was generally good correlation between the conservative element concentration profiles and ash content profile (*cf.* Fig. 5.12).

53-159 cm

Note the change in scale on the concentration and ash content profiles (4-fold) on going from 0-53 cm to 53-159 cm (*cf.* Fig. 5.12). The following mean minimum concentrations occurred between 145 and 119 cm: Al (490 ± 90 mg kg^{-1}), Sc (0.093 ± 0.040 mg kg^{-1}), Ti (39 ± 13 mg kg^{-1}), Y (0.11 ± 0.03 mg kg^{-1}) and Zr (0.93 ± 0.33 mg kg^{-1}). Minor concentration peaks occurred between 151 and 145 cm for all of the conservative elements and minor Sc and Ti concentration peaks, close to the minor ash content peak, occurred between 107 and 103 cm (*cf.* Fig. 5.12).

5.3.2 TM04CM-2

0-50 cm

All five elements exhibited prominent peaks in the uppermost ~ 36 cm of the core with the following maximum values, at the depths indicated:

- Al – 4000 mg kg^{-1} at 16-18 cm
- Sc – 1.3 mg kg^{-1} at 14-16 cm
- Ti – 480 mg kg^{-1} at 14-16 cm
- Y – 1.4 mg kg^{-1} at 16-18 cm
- Zr – 35 mg kg^{-1} at 14-16 cm
- Ash content – 9.0% at 14-16 cm

Again there was generally good correlation between the conservative element concentration profiles and ash content profile (*cf.* Fig. 5.13).

50-109 cm

Note the change in scale on the concentration and ash content profiles (4-fold) on going from 0-50 cm to 50-109 cm (*cf.* Fig. 5.13). The following mean minimum concentrations occurred between 94 and 78 cm: Al (326 ± 38 mg kg^{-1}), Sc (0.10 ± 0.03 mg kg^{-1}), Ti (26 ± 6 mg kg^{-1}), Y (0.14 ± 0.03 mg kg^{-1}) and Zr (0.71 ± 0.16 mg kg^{-1}). Minor concentration peaks occurred between 78 and 70 cm and 104 and 94 cm for all of the conservative elements, the latter peaks being coincident with the minor ash content peak (*cf.* Fig. 5.13).

5.3.3 Discussion

As found at the previous sites (Sections 3.3.3 and 4.3.3), increases in Al, Sc, Ti, Y and Zr concentrations between 18 and 47 cm in TM04M-1 and the top ~ 36 cm of TM04CM-2 are most likely caused by the increase in anthropogenic soil dust deposition. In contrast to similarities observed between the profiles of the pairs of elements Sc and Y, and Ti and Zr at the previous sites, however, the pair (Al and Y) and group of elements (Sc, Ti and Zr), respectively, exhibited similar features in these Turclossie Moss cores (*cf.* Fig. 5.12 and 5.13). As for the previous sites (Sections 3.5 and 4.5), Al will not be used to correct Pb concentrations for soil dust contributions at Turclossie Moss in Section 5.5.

5.3.3.1 Intercomparison of Sc and Ti

Profiles of Sc and Ti concentrations and Ti/Sc ratios (A8.1 Table A3) for TM04M-1 and TM04CM-4 are shown in Fig. 5.14. As for the previous sites (Sections 3.3.3.1 and 4.3.3.1), slight differences between the Sc and Ti concentration profiles are apparent but the average Ti/Sc ratio (432 ± 78) throughout the combined profile (0-159 cm) (*cf.* Fig. 5.14), is in good agreement with the UCC Ti/Sc ratio (445), suggesting contributions of these metals solely from natural soil dust. There was no evidence for inputs of Ti and Sc from different soil dust sources or direct non-soil-dust-related anthropogenic sources (e.g. coal combustion) as suggested at the previous sites (*cf.* Sections 3.3.3.1 and 4.3.3.1).

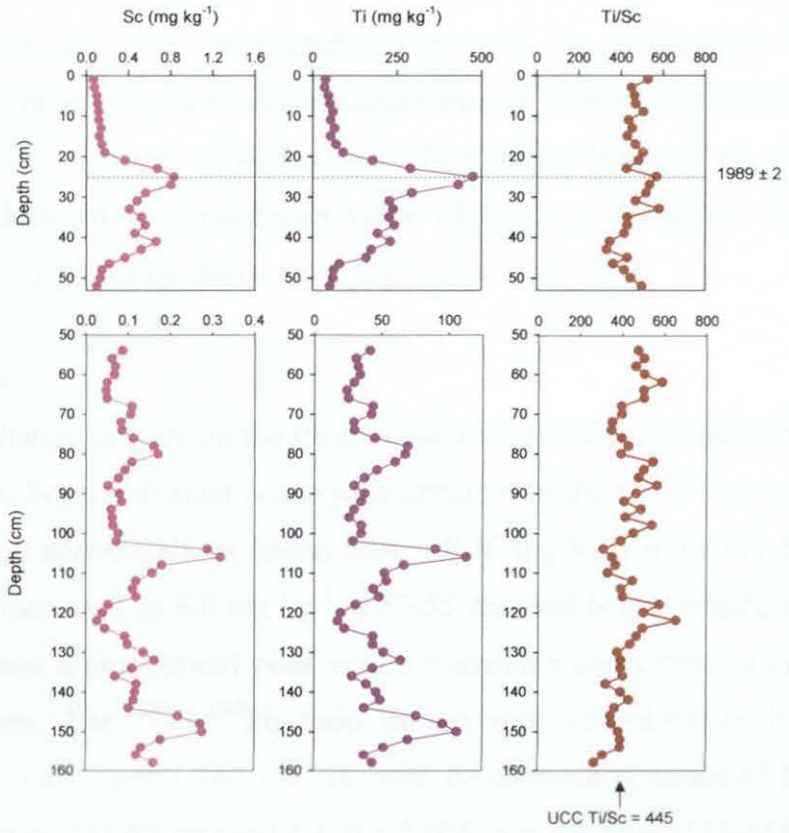

Figure 5.14: Depth profiles of Sc and Ti concentrations (mg kg^{-1}) and Ti/Sc ratios from 0-53 cm and 53-159 cm in the combined ^{210}Pb-dated TM04M-1 and TM04CM-4 peat cores.

5.4 Pb AND Pb ISOTOPIC RATIOS

Profiles of Pb concentrations and measured $^{206}Pb/^{207}Pb$, $^{208}Pb/^{206}Pb$ and $^{208}Pb/^{207}Pb$ isotopic ratios for TM04M-1 and TM04CM-4 (Table 5.5) and TM04CM-2 (Table 5.6) are shown in Figs. 5.15 and 5.16, respectively.

5.4.1 TM04M-1 and TM04CM-4

0-53 cm

The Pb concentration increased from 7.4 mg kg^{-1} at 51-53 cm to a maximum of 120 mg kg^{-1} between 28 and 22 cm, above which it decreased steeply to 13 mg kg^{-1} at 14-16 cm and then more gradually towards the surface (*cf.* Fig. 5.15). The $^{206}Pb/^{207}Pb$ ratio increased from a mean value of 1.165 ± 0.002 between 53 and 47 cm, to a fairly constant value (mean 1.176 ± 0.002) between 47 and 28 cm, above which it declined to a minimum value of 1.121 at 16-18 cm before increasing gradually to 1.143 at the surface (*cf.* Fig. 5.15).

53-159 cm

Note the change in scale on the Pb concentration (25-fold) on going from 0-53 cm to 53-159 cm. Several distinct zones were apparent in the 53-159 cm sections: a region of minimum concentrations (mean 0.64 ± 0.30 mg kg^{-1}) from 113 to 69 cm, above which Pb increased to 6.0 mg kg^{-1} at 53-55 cm, and below which, from 113 to 145 cm there was a pronounced peak with a maximum concentration of 3.0 mg kg^{-1} at 129-131 cm. The $^{206}Pb/^{207}Pb$ ratio in the zone of minimum Pb concentration (69-113 cm) averaged 1.148 ± 0.010, with corresponding means of 1.157 ± 0.005 in the zone above (53-69 cm) and 1.170 ± 0.005 over the zone (113-145 cm) containing the Pb peak below (*cf.* Fig. 5.15).

Table 5.5: Total Pb concentrations (mg kg^{-1}) and Pb isotopic ratios in the combined TM04M-1 (0-47 cm) and TM04CM-4 (47-159 cm) peat cores.

Section (cm)	Pb (mg kg^{-1})	$^{206}Pb/^{207}Pb$	$^{208}Pb/^{206}Pb$	$^{208}Pb/^{207}Pb$
0-2	2.9*	1.143 ± 0.0020	2.102 ± 0.0018	2.403 ± 0.0033
2-4	4.5*	1.139 ± 0.0014	2.105 ± 0.0027	2.398 ± 0.0034
4-6	5.7*	1.133 ± 0.0006	2.116 ± 0.0029	2.398 ± 0.0026
6-8	7.0*	1.132 ± 0.0008	2.120 ± 0.0026	2.399 ± 0.0027
8-10	9.4*	1.133 ± 0.0021	2.118 ± 0.0017	2.399 ± 0.0029
10-12	8.8*	1.128 ± 0.0012	2.122 ± 0.0020	2.395 ± 0.0031
12-14	11*	1.127 ± 0.0017	2.125 ± 0.0029	2.396 ± 0.0014
14-16	13*	1.123 ± 0.0014	2.125 ± 0.0025	2.386 ± 0.0012
16-18	21*	1.121 ± 0.0015	2.128 ± 0.0031	2.387 ± 0.0014
18-20	39*	1.127 ± 0.0005	2.129 ± 0.0010	2.398 ± 0.0016
20-22	63*	1.132 ± 0.0003	2.123 ± 0.0018	2.403 ± 0.0020
22-24	120*	1.145 ± 0.0018	2.117 ± 0.0011	2.424 ± 0.0026
24-26	118*	1.163 ± 0.0011	2.102 ± 0.0021	2.444 ± 0.0041
26-28	119*	1.170 ± 0.0009	2.095 ± 0.0009	2.451 ± 0.0018
28-30	56*	1.175 ± 0.0007	2.086 ± 0.0027	2.452 ± 0.0036
30-32	36*	1.176 ± 0.0008	2.085 ± 0.0022	2.451 ± 0.0027
32-34	31*	1.176 ± 0.0004	2.085 ± 0.0009	2.452 ± 0.0008
34-36	17*	1.176 ± 0.0036	2.079 ± 0.0044	2.460 ± 0.0186
36-38	15*	1.177 ± 0.0024	2.077 ± 0.0060	2.446 ± 0.0075
38-40	15*	1.177 ± 0.0014	2.089 ± 0.0040	2.457 ± 0.0052
40-42	8.4*	1.176 ± 0.0016	2.089 ± 0.0021	2.456 ± 0.0053
42-44	18*	1.177 ± 0.0031	2.091 ± 0.0046	2.462 ± 0.0014
44-46	10*	1.174 ± 0.0022	2.093 ± 0.0038	2.457 ± 0.0048
46-47	9.8*	1.172 ± 0.0022	2.094 ± 0.0044	2.454 ± 0.0053
47-49	8.1 ± 0.5*	1.167 ± 0.0026	2.111 ± 0.0020	2.458 ± 0.0074
49-51	8.3 ± 0.3*	1.163 ± 0.0023	2.115 ± 0.0032	2.456 ± 0.0042
51-53	7.4 ± 0.1*	1.164 ± 0.0023	2.110 ± 0.0045	2.454 ± 0.0100
53-55	6.0 ± 0.5*	1.164 ± 0.0030	2.102 ± 0.0049	2.444 ± 0.0064
55-57	5.0 ± 0.2	1.152 ± 0.0030	2.118 ± 0.0049	2.440 ± 0.0064
57-59	3.5 ± 0.0	1.161 ± 0.0024	2.112 ± 0.0031	2.452 ± 0.0026
59-61	3.8 ± 0.1	1.159 ± 0.0040	2.113 ± 0.0041	2.448 ± 0.0043
61-63	1.97 ± 0.03	1.158 ± 0.0027	2.117 ± 0.0030	2.450 ± 0.0051
63-65	1.74 ± 0.02	1.157 ± 0.0011	2.119 ± 0.0015	2.452 ± 0.0035
65-67	1.78 ± 0.02	1.154 ± 0.0033	2.107 ± 0.0024	2.429 ± 0.0077
67-69	2.01 ± 0.04	1.150 ± 0.0037	2.115 ± 0.0020	2.430 ± 0.0085
69-71	0.97 ± 0.03	1.151 ± 0.0018	2.114 ± 0.0029	2.430 ± 0.0046
71-73	0.72 ± 0.01	1.145 ± 0.0056	2.113 ± 0.0064	2.418 ± 0.0099
73-75	0.75 ± 0.01	1.134 ± 0.0044	2.125 ± 0.0038	2.410 ± 0.0059
75-77	1.68 ± 0.02	1.147 ± 0.0022	2.119 ± 0.0048	2.429 ± 0.0027
77-79	0.56 ± 0.01	1.142 ± 0.0060	2.114 ± 0.0064	2.436 ± 0.0084
79-81	0.62 ± 0.01	1.143 ± 0.0042	2.118 ± 0.0092	2.442 ± 0.0104
81-83	0.74 ± 0.01	1.151 ± 0.0015	2.108 ± 0.0033	2.447 ± 0.0050

*Total Pb concentrations determined by ICP-OES where standard deviations (where given) were calculated as the standard deviation of the mean value for two separate sample analyses. ICP-MS Pb concentration and Pb isotopic ratio standard deviations were calculated as the standard deviation from the mean value for five consecutive determinations of the ratio/concentration of a sample solution.

Table 5.5 (continued): Total Pb concentrations (mg kg^{-1}) and Pb isotopic ratios in the combined TM04M-1 (0-47 cm) and TM04CM-4 (47-159 cm) peat cores.

Section (cm)	Pb (mg kg^{-1})	$^{206}Pb/^{207}Pb$	$^{208}Pb/^{206}Pb$	$^{208}Pb/^{207}Pb$
83-85	0.38 ± 0.00	1.146 ± 0.0064	2.113 ± 0.0119	2.443 ± 0.0047
85-87	0.66 ± 0.01	1.142 ± 0.0043	2.119 ± 0.0083	2.442 ± 0.0060
87-89	0.32 ± 0.00	1.132 ± 0.0033	2.135 ± 0.0124	2.416 ± 0.0119
89-91	0.51 ± 0.00	1.139 ± 0.0046	2.118 ± 0.0030	2.411 ± 0.0067
91-93	0.42 ± 0.01	1.152 ± 0.0075	2.108 ± 0.0044	2.427 ± 0.0131
93-95	0.25 ± 0.00	1.147 ± 0.0040	2.119 ± 0.0069	2.429 ± 0.0065
95-97	0.69 ± 0.01	1.132 ± 0.0026	2.133 ± 0.0068	2.430 ± 0.0052
97-99	0.39 ± 0.00	1.146 ± 0.0025	2.120 ± 0.0108	2.430 ± 0.0103
99-101	0.47 ± 0.01	1.154 ± 0.0044	2.110 ± 0.0062	2.432 ± 0.0046
101-103	0.34 ± 0.01	1.144 ± 0.0064	2.120 ± 0.0074	2.452 ± 0.0113
103-105	0.59 ± 0.01	1.166 ± 0.0019	2.101 ± 0.0061	2.450 ± 0.0056
105-107	0.71 ± 0.01	1.148 ± 0.0052	2.121 ± 0.0059	2.435 ± 0.0070
107-109	0.64 ± 0.00	1.161 ± 0.0057	2.110 ± 0.0050	2.451 ± 0.135
109-111	0.75 ± 0.01	1.159 ± 0.0054	2.107 ± 0.0082	2.442 ± 0.0038
111-113	0.86 ± 0.01	1.172 ± 0.0035	2.099 ± 0.0061	2.459 ± 0.0057
113-115	1.41 ± 0.02	1.172 ± 0.0015	2.097 ± 0.0048	2.457 ± 0.0061
115-117	1.29 ± 0.02	1.169 ± 0.0029	2.096 ± 0.0057	2.448 ± 0.0028
117-119	1.46 ± 0.01	1.167 ± 0.0029	2.103 ± 0.0058	2.454 ± 0.0102
119-121	1.40 ± 0.01	1.165 ± 0.0017	2.101 ± 0.0025	2.446 ± 0.0023
121-123	1.47 ± 0.02	1.163 ± 0.0030	2.105 ± 0.0021	2.448 ± 0.0073
123-125	1.96 ± 0.01	1.159 ± 0.0026	2.111 ± 0.0044	2.445 ± 0.0023
125-127	2.02 ± 0.02	1.174 ± 0.0023	2.096 ± 0.0025	2.458 ± 0.0034
127-129	2.20 ± 0.01	1.174 ± 0.0024	2.097 ± 0.0033	2.459 ± 0.0032
129-131	2.96 ± 0.02	1.174 ± 0.0020	2.097 ± 0.0009	2.454 ± 0.0040
131-133	2.89 ± 0.05	1.171 ± 0.0017	2.098 ± 0.0014	2.463 ± 0.0026
133-135	2.72 ± 0.03	1.175 ± 0.0021	2.096 ± 0.0043	2.464 ± 0.0039
135-137	2.12 ± 0.02	1.177 ± 0.0019	2.100 ± 0.0013	2.458 ± 0.0049
137-139	2.10 ± 0.01	1.172 ± 0.0014	2.099 ± 0.0042	2.457 ± 0.0028
139-141	2.36 ± 0.02	1.173 ± 0.0021	2.103 ± 0.0017	2.464 ± 0.0043
141-143	1.95 ± 0.04	1.172 ± 0.0027	2.107 ± 0.0033	2.467 ± 0.0046
143-145	1.32 ± 0.01	1.162 ± 0.0023	2.112 ± 0.0018	2.451 ± 0.0048
145-147	0.87 ± 0.01	1.169 ± 0.0028	2.104 ± 0.0024	2.458 ± 0.0049
147-149	1.05 ± 0.02	1.173 ± 0.0031	2.100 ± 0.0036	2.462 ± 0.0076
149-151	0.62 ± 0.01	1.169 ± 0.0039	2.098 ± 0.0095	2.449 ± 0.0047
151-153	0.79 ± 0.01	1.162 ± 0.0044	2.098 ± 0.0056	2.436 ± 0.0036
153-155	1.18 ± 0.03	1.163 ± 0.0058	2.095 ± 0.0081	2.437 ± 0.0075
155-157	0.33 ± 0.01	1.147 ± 0.0041	2.111 ± 0.0032	2.420 ± 0.0082
157-159	0.57 ± 0.01	1.142 ± 0.0035	2.117 ± 0.0053	2.415 ± 0.0076

Table 5.6: Total Pb concentrations (mg kg^{-1}) and Pb isotopic ratios in the TM04CM-2 peat core.

Section (cm)	Pb (mg/kg)	$^{206}Pb/^{207}Pb$	$^{208}Pb/^{206}Pb$	$^{208}Pb/^{207}Pb$
0-2	0.42 ± 0*	1.140 ± 0.0020	2.121 ± 0.0045	2.417 ± 0.0054
2-4	0.68*	1.137 ± 0.0027	2.128 ± 0.0034	2.419 ± 0.0041
4-6	5.1*	1.130 ± 0.0021	2.127 ± 0.0031	2.403 ± 0.0067
6-8	24 ± 1*	1.124 ± 0.0024	2.132 ± 0.0023	2.397 ± 0.0053
8-10	50 ± 1*	1.122 ± 0.0011	2.122 ± 0.0010	2.380 ± 0.0032
10-12	95 ± 0*	1.107 ± 0.0017	2.149 ± 0.0013	2.38 ± 0.0045
12-14	840 ± 19*	1.075 ± 0.0014	2.182 ± 0.0006	2.345 ± 0.0025
14-16	181 ± 22*	1.139 ± 0.0009	2.128 ± 0.0017	2.424 ± 0.0025
16-18	120 ± 10*	1.174 ± 0.0020	2.105 ± 0.0031	2.471 ± 0.0039
18-20	61 ± 3*	1.173 ± 0.0016	2.089 ± 0.0016	2.451 ± 0.0030
20-22	38 ± 2*	1.173 ± 0.0019	2.088 ± 0.0024	2.450 ± 0.0033
22-24	28 ± 1*	1.167 ± 0.0038	2.094 ± 0.0030	2.445 ± 0.0051
24-26	18 ± 1*	1.169 ± 0.0031	2.095 ± 0.0017	2.449 ± 0.0061
26-28	11 ± 1*	1.169 ± 0.0016	2.090 ± 0.0022	2.444 ± 0.0037
28-30	10 ± 0*	1.170 ± 0.0028	2.091 ± 0.0019	2.446 ± 0.0057
30-32	8.5 ± 0.8*	1.168 ± 0.0011	2.093 ± 0.0029	2.444 ± 0.0042
32-34	8.4 ± 0.3*	1.172 ± 0.0019	2.090 ± 0.0016	2.450 ± 0.0023
34-36	7.5 ± 0.8*	1.172 ± 0.0011	2.086 ± 0.0028	2.445 ± 0.0042
36-38	5.9 ± 0.6*	1.171 ± 0.0020	2.087 ± 0.0025	2.445 ± 0.0041
38-40	6.2 ± 0.7*	1.166 ± 0.0026	2.088 ± 0.0013	2.436 ± 0.0054
40-42	5.4 ± 0.1*	1.167 ± 0.0003	2.093 ± 0.0021	2.443 ± 0.0030
42-44	5.6 ± 0.3	1.166 ± 0.0018	2.100 ± 0.0026	2.450 ± 0.0064
44-46	6.4 ± 0.3	1.169 ± 0.0013	2.100 ± 0.0026	2.454 ± 0.0049
46-48	6.1 ± 0.3	1.170 ± 0.0027	2.097 ± 0.0021	2.454 ± 0.0044
48-50	4.8 ± 0.2	1.166 ± 0.0026	2.098 ± 0.0015	2.447 ± 0.0065
50-52	3.6 ± 0.2	1.160 ± 0.0025	2.104 ± 0.0028	2.441 ± 0.0048
52-54	3.2 ± 0.2	1.163 ± 0.0034	2.101 ± 0.0016	2.444 ± 0.0068
54-56	2.5 ± 0.1	1.158 ± 0.0022	2.105 ± 0.0020	2.437 ± 0.0033
56-58	1.55 ± 0.06	1.158 ± 0.0033	2.097 ± 0.0034	2.428 ± 0.0060
58-60	1.59 ± 0.07	1.149 ± 0.0049	2.100 ± 0.0067	2.413 ± 0.0081
60-62	1.24 ± 0.06	1.144 ± 0.0028	2.107 ± 0.0059	2.411 ± 0.0114
62-64	1.33 ± 0.04	1.136 ± 0.0052	2.101 ± 0.0140	2.387 ± 0.0190
64-66	1.13 ± 0.06	1.136 ± 0.0020	2.111 ± 0.0010	2.397 ± 0.0045
66-68	1.12 ± 0.06	1.145 ± 0.0066	2.097 ± 0.0068	2.401 ± 0.0108
68-70	0.89 ± 0.03	1.131 ± 0.0048	2.112 ± 0.0185	2.389 ± 0.0166
70-72	0.72 ± 0.03	1.148 ± 0.0052	2.108 ± 0.0106	2.420 ± 0.0177
72-74	0.74 ± 0.04	1.131 ± 0.0005	2.117 ± 0.0016	2.395 ± 0.0015
74-76	0.77 ± 0.03	1.139 ± 0.0035	2.126 ± 0.0058	2.421 ± 0.0135
76-78	0.68 ± 0.02	1.143 ± 0.0037	2.120 ± 0.0075	2.422 ± 0.0089
78-80	0.59 ± 0.02	1.114 ± 0.0014	2.133 ± 0.0028	2.376 ± 0.0036
80-82	0.55 ± 0.02	1.114 ± 0.0028	2.134 ± 0.0039	2.378 ± 0.0018
82-84	0.53 ± 0.02	1.126 ± 0.0025	2.128 ± 0.0055	2.395 ± 0.0042
84-86	0.82 ± 0.04	1.138 ± 0.0091	2.107 ± 0.0139	2.397 ± 0.0073
86-88	0.40 ± 0.01	1.136 ± 0.0045	2.095 ± 0.0136	2.381 ± 0.0089

*Total Pb concentrations determined by ICP-OES where standard deviations were calculated as the standard deviation of the mean value for two separate sample analyses. ICP-MS Pb concentration and Pb isotopic ratio standard deviations were calculated as the standard deviation from the mean value for five consecutive determinations of the ratio/concentration of a sample solution.

Table 5.6 (continued): Total Pb concentrations (mg kg^{-1}) and Pb isotopic ratios in the TM04CM-2 peat core.

Section (cm)	Pb (mg kg^{-1})	$^{206}Pb/^{207}Pb$	$^{208}Pb/^{206}Pb$	$^{208}Pb/^{207}Pb$
88-90	0.53 ± 0.01	1.137 ± 0.0068	2.102 ± 0.0093	2.391 ± 0.0113
90-92	0.93 ± 0.02	1.143 ± 0.0023	2.108 ± 0.0054	2.409 ± 0.0025
92-94	0.98 ± 0.02	1.143 ± 0.0036	2.102 ± 0.0090	2.403 ± 0.0141
94-96	0.82 ± 0.03	1.149 ± 0.0033	2.092 ± 0.0121	2.404 ± 0.0087
96-98	1.15 ± 0.05	1.156 ± 0.0031	2.105 ± 0.0035	2.434 ± 0.0068
98-100	0.93 ± 0.06	1.168 ± 0.0039	2.077 ± 0.0108	2.426 ± 0.0089
100-102	1.00 ± 0.04	1.163 ± 0.0013	2.101 ± 0.0037	2.444 ± 0.0023
102-104	1.32 ± 0.01	1.175 ± 0.0045	2.080 ± 0.0043	2.444 ± 0.0091
104-106	1.12 ± 0.01	1.162 ± 0.0036	2.100 ± 0.0023	2.440 ± 0.0065
106-108	1.32 ± 0.02	1.163 ± 0.0033	2.101 ± 0.0023	2.443 ± 0.0065
108-109	1.34 ± 0.07	1.161 ± 0.0020	2.094 ± 0.0045	2.432 ± 0.0029

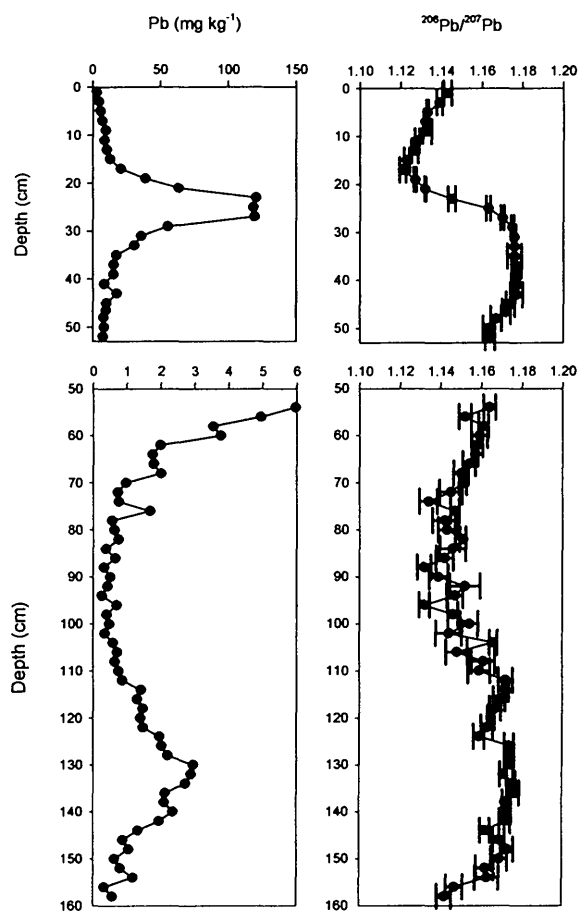

Figure 5.15: Depth profiles of Pb concentrations (mg kg^{-1}) and measured $^{206}Pb/^{207}Pb$ ratios from 0-53 cm and 53-159 cm in the combined TM04M-1 and TM04CM-4 peat cores.

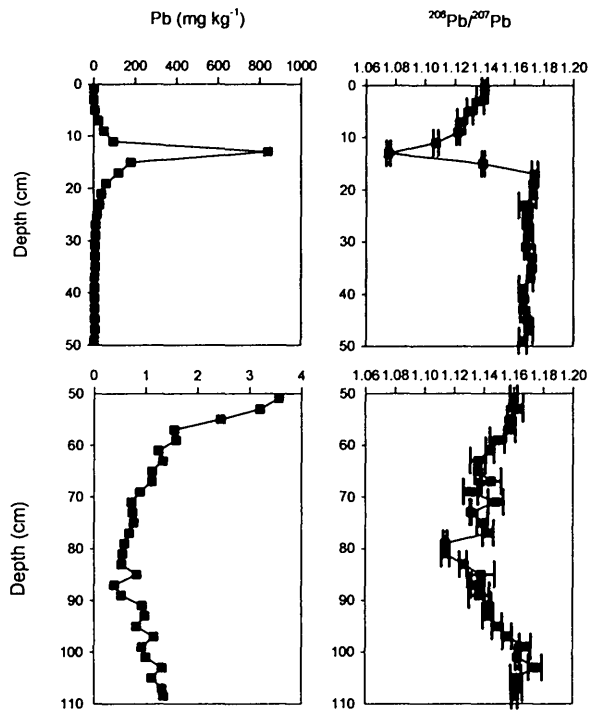

Figure 5.16: Depth profiles of Pb concentrations (mg kg^{-1}) and measured $^{206}Pb/^{207}Pb$ ratios from 0-50 cm and 50-109 cm in the TM04CM-2 peat core.

5.4.2 TM04CM-2

0-50 cm

The Pb concentration increased from 4.8 mg kg^{-1} at 48-50 cm to a maximum of 840 mg kg^{-1} at 12-14 cm, above which it decreased towards the surface (*cf.* Fig. 5.16). Above 50 cm the $^{206}Pb/^{207}Pb$ ratio was constant (mean 1.170 ± 0.003) up to 16 cm, above which it declined steeply to a minimum value of 1.075 at 12-14 cm before increasing gradually to 1.140 at the surface.

50-109 cm

Note the change in scale on the Pb concentration (250-fold) on going from 0-50 cm to 50-109 cm. Several zones were apparent in the 50-109 cm sections: a region of minimum concentrations (mean 0.66 ± 0.15 mg kg^{-1}) from 90 to 68 cm, below which concentrations increased to 1.3 mg kg^{-1} at 108-109 cm, and above which they

increased to 3.6 mg kg^{-1} at 50-52 cm. The mean $^{206}Pb/^{207}Pb$ ratios from 90 to 68 cm, 90 to 109 cm and 68 to 50 cm were 1.132 ± 0.011, 1.158 ± 0.011 and 1.150 ± 0.010, respectively (*cf.* Fig. 5.16).

5.4.3 Discussion

As Pb is essentially immobile in ombrotrophic peat, these Pb profiles represent historical records of anthropogenic and natural atmospheric Pb deposition at Turclossie Moss. The unusually high Pb concentration and very low $^{206}Pb/^{207}Pb$ ratio value, the latter comparable to that of leaded petrol itself (*cf.* Table 1.3, Section 1.10) in the 12-14 cm TM04CM-2 section (*cf.* Fig. 5.16) suggests that this section in the core has somehow been contaminated. Accordingly the TM04M-1 and TM04CM-4 cores have been chosen for use in the interpretation of historical trends in sources of atmospheric Pb deposition (Section 5.6). It is worth noting that there is good agreement between the Pb concentration and $^{206}Pb/^{207}Pb$ ratio profile trends in the TM04CM-2 sections below 14 cm with those in TM04M-1 and TM04CM-4 (Fig. 5.17).

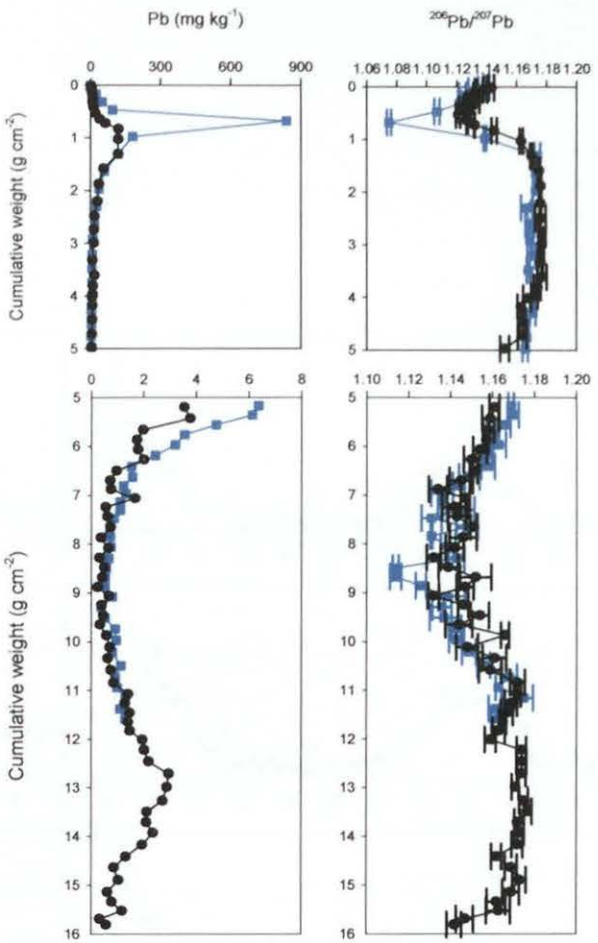

Figure 5.17: Profiles of Pb concentrations (mg kg^{-1}) and measured $^{206}Pb/^{207}Pb$ ratios from 0-57 cm and 57-159 cm in the combined TM04M-1 and TM04CM-4 cores (black closed circles) and from 0-44 cm and 44-107 cm in the TM04CM-2 core (blue closed squares) *versus* cumulative weight.

5.5 USE OF CONSERVATIVE ELEMENTS TO ESTIMATE ANTHROPOGENIC ENRICHMENTS OF Pb

Profiles of Pb/Sc, Pb/Ti, Pb/Y and Pb/Zr ratios for TM04M-1 and TM04CM-4 (A6.1 Table A4) along with Pb concentrations are shown in Fig. 5.18.

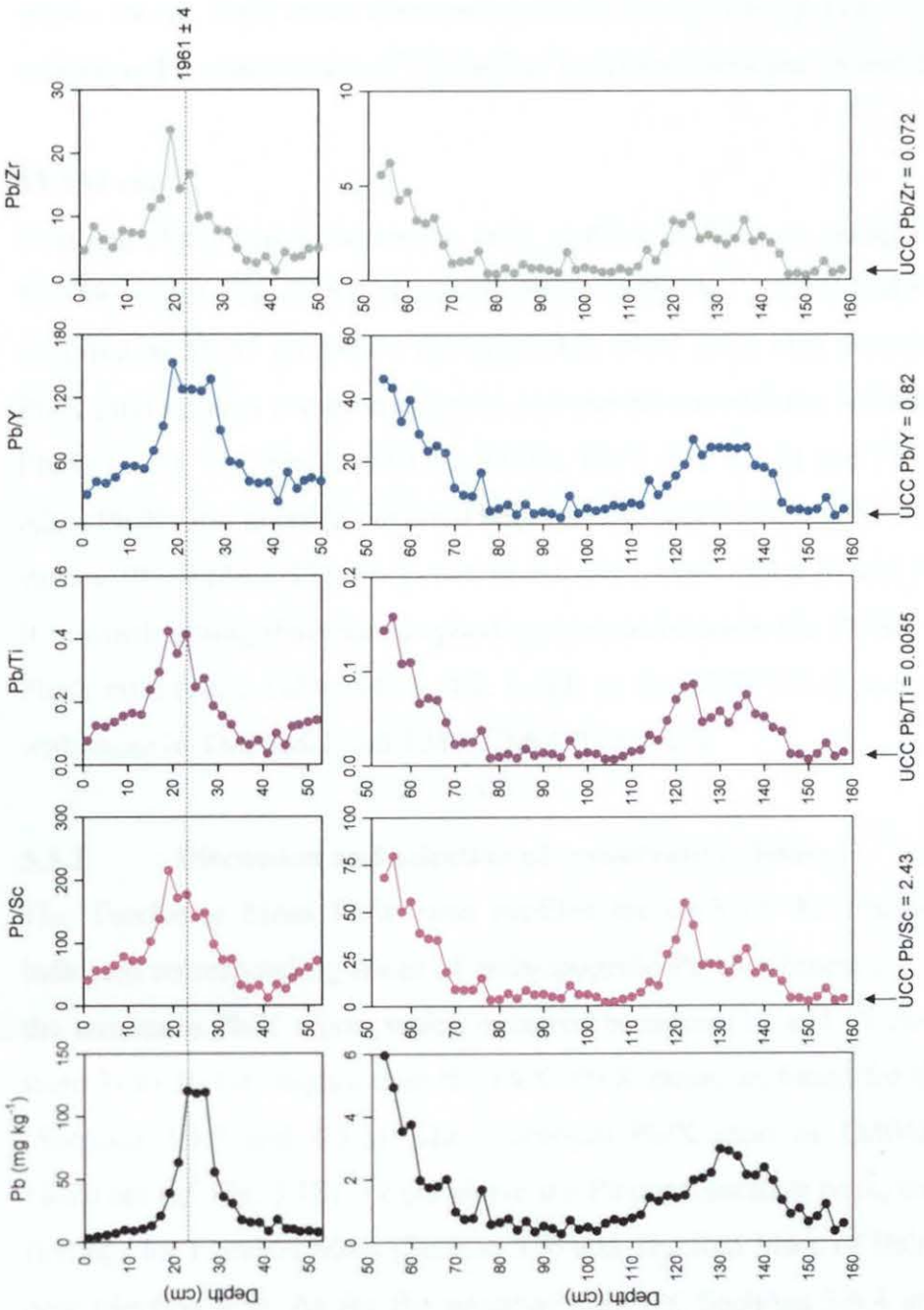

Figure 5.18: Depth profiles of Pb concentration (mg kg^{-1}), Pb/Sc, Pb/Ti, Pb/Y and Pb/Zr ratios from 0-53 cm and 53-159 cm in the combined ^{210}Pb-dated TM04M-1 and TM04CM-4 peat cores.

5.5.1 TM04M-1 and TM04CM-4

0-53 cm

The Pb/X ratios were at a maximum between 30 and 14 cm, with the following mean values: Pb/Sc (150 ± 40), Pb/Ti (0.31 ± 0.09), Pb/Y (120 ± 30) and Pb/Zr (13 ± 5). Above 14 cm, Pb/X ratios decreased towards the surface (*cf.* Fig. 5.18). Note that the maximum Pb concentration (120 mg kg^{-1}) occurred between 28 and 22 cm.

53-159 cm

Note the change in scale on the ratio profiles (3-fold) on going from 0-53 cm to 53-159 cm (*cf.* Fig. 5.18). Maximum Pb/Sc (80), Pb/Ti (0.16) and Pb/Zr (6.2) ratios occurred at 55-57 cm while the maximum Pb/Y ratio (46) occurred at 53-55 cm. Pb/X ratio minima occurred between 113 and 69 cm with the following mean values: Pb/Sc (6.2 ± 3.0), Pb/Ti (0.015 ± 0.008), Pb/Y (6.1 ± 3.3) and Pb/Zr (0.69 ± 0.33). Also, Pb/X ratio maxima occurred between 145 and 113 cm with the following mean values: Pb/Sc (24 ± 12), Pb/Ti (0.054 ± 0.018), Pb/Y (19 ± 6) and Pb/Zr (2.2 ± 0.7). It is worth noting that there is good agreement between the Pb/Sc, Pb/Ti, Pb/Y and Pb/Zr ratio (A6.2 Table A4) profile trends in the TM04CM-2 sections below 14 cm with those in TM04M-1 and TM04CM-4 (Fig. 5.19).

5.5.2 Discussion and selection of conservative element

The Turclossie Moss Pb/X ratio profiles for each of the conservative elements indicated corresponding zones of anthropogenic Pb enrichment (*cf.* Fig. 5.18). Also, the minimum Pb/X ratios, which occurred between 113 and 69 cm in TM04CM-4, were 3- to 10-fold higher than the UCC Pb/X ratios, as found for the previous sites (Sections 3.5.3 and 4.5.3). The maximum Pb/X ratio in TM04M-1 occurred at 18-20 cm (*cf.* Fig. 5.18) ~ 2 cm above the Pb concentration peak, consistent with the findings for Flanders Moss (Section 3.5) and The Red Moss of Balerno RM03CM-1 core (Section 4.5). As for the previous sites (*cf.* Sections 3.6.4 and 4.5.3), on the basis of the use of Sc as a conservative element, the anthropogenic Pb concentrations in the TM04M-1 and TM04CM-4 cores were calculated (A6.1, Table A4) and these

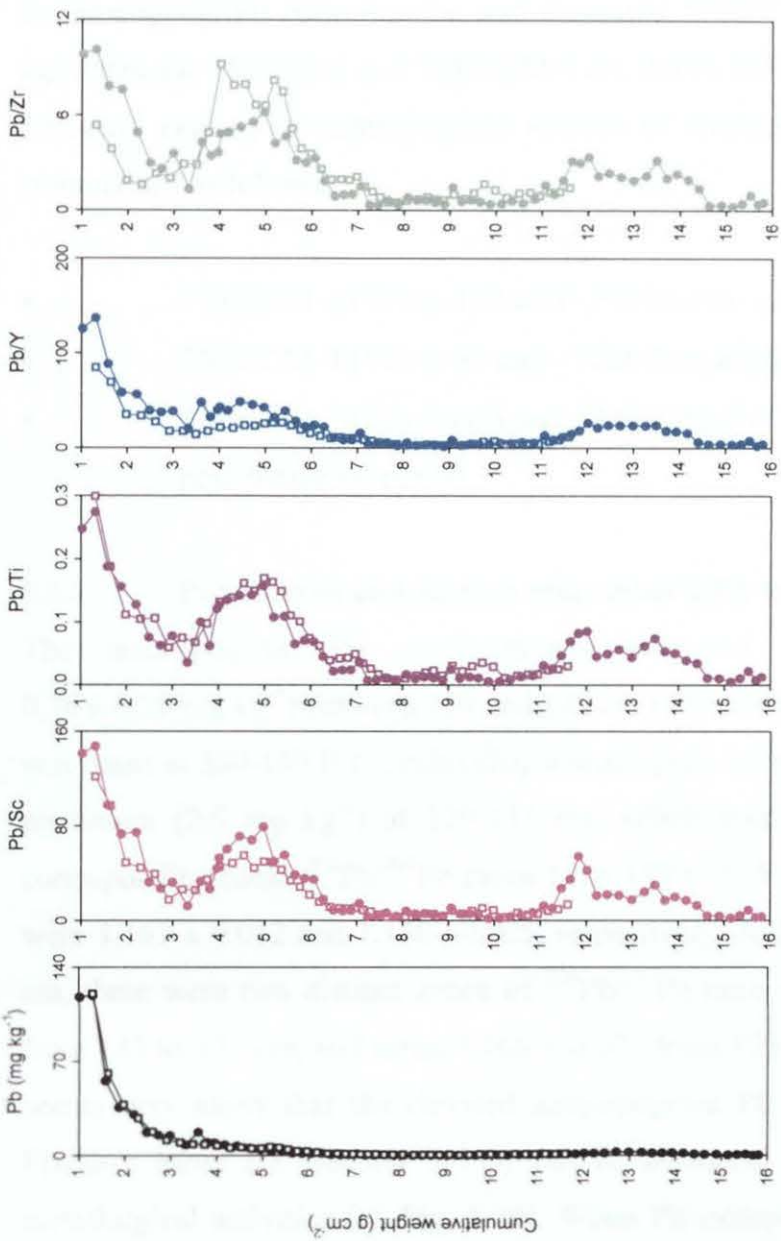

Figure 5.19: Profiles of Pb concentration (mg kg^{-1}), Pb/Sc, Pb/Ti, Pb/Y and Pb/Zr ratios from 24-159 cm in the combined TM04M-1 and TM04CM-4 cores (closed circles) and from 16-107 cm in the TM04CM-2 core (open squares) *versus* cumulative weight.

will be used in Section 5.6 in order to interpret historical trends in anthropogenic Pb deposition.

5.6 HISTORICAL TRENDS IN SOURCES OF ATMOSPHERIC Pb DEPOSITION

Anthropogenic Pb concentration and measured $^{206}Pb/^{207}Pb$ ratio profiles, including age dates, for TM04M-1 and TM04CM-4 are shown in Fig. 5.20. The most important historical periods of anthropogenic sources of atmospheric Pb deposition can be summarised as follows:

- TM04CM-4 (159 to 113 cm) - Pre-Roman and Roman period
- TM04CM-4 (113 to 53 cm) - Post-Roman and Mediaeval period
- TM04M-1 (47 to 0 cm) and TM04CM-4 (47 to 53 cm) – Industrial and post-industrial period

5.6.1 Pre-Roman and Roman atmospheric Pb sources and deposition

The anthropogenic Pb concentrations increased from low values (mean 0.36 ± 0.28 mg kg^{-1}) between 159 and 145 cm in TM04CM-4, for which 155-157 cm was dated at 380-160 B.C., exhibiting a broad peak between 145 and 113 cm, with a maximum (2.6 mg kg^{-1}) at 129-131 cm, which was dated at 50-220 A.D. The corresponding mean $^{206}Pb/^{207}Pb$ ratios from 159 to 145 cm and from 145 to 113 cm were 1.161 ± 0.012 and 1.170 ± 0.005, respectively. Although between 145 and 113 cm, there were two distinct zones of $^{206}Pb/^{207}Pb$ ratio values: mean 1.174 ± 0.002 from 143 to 125 cm, and mean 1.166 ± 0.005 from 125 to 113 cm (*cf.* Fig. 5.20). It seems very likely that the elevated anthropogenic Pb concentrations, as found at Flanders Moss (*cf.* Section 3.6.1), can be attributed to pre-Roman and Roman metallurgical activities (*cf.* Fig. 5.20). When Pb isotope ratios of the peat samples (113-145 cm) embracing the Pb peak in TM04CM-4 are plotted along with those of various British Pb ores and Pb ores from southern Spain (Fig. 5.21), as performed for Flanders Moss (*cf.* Fig. 3.21), they are in agreement with those of both British and

Spanish origin. Also, when the Pb isotope ratios measured in the bottom sections (104-109 cm) of TM04CM-2, which most likely represent the end of the pre-Roman/Roman Pb peak (*cf.* Fig. 5.17), are plotted (*cf.* Fig. 5.21), they also suggest long range anthropogenic Pb deposition at Turclossie Moss from Pb mining and smelting activities in the Spanish Rio Tinto mining district. In contrast, the Flanders Moss Pb peak samples were found to be in better agreement with British Pb ores (*cf.* Section 3.6.1).

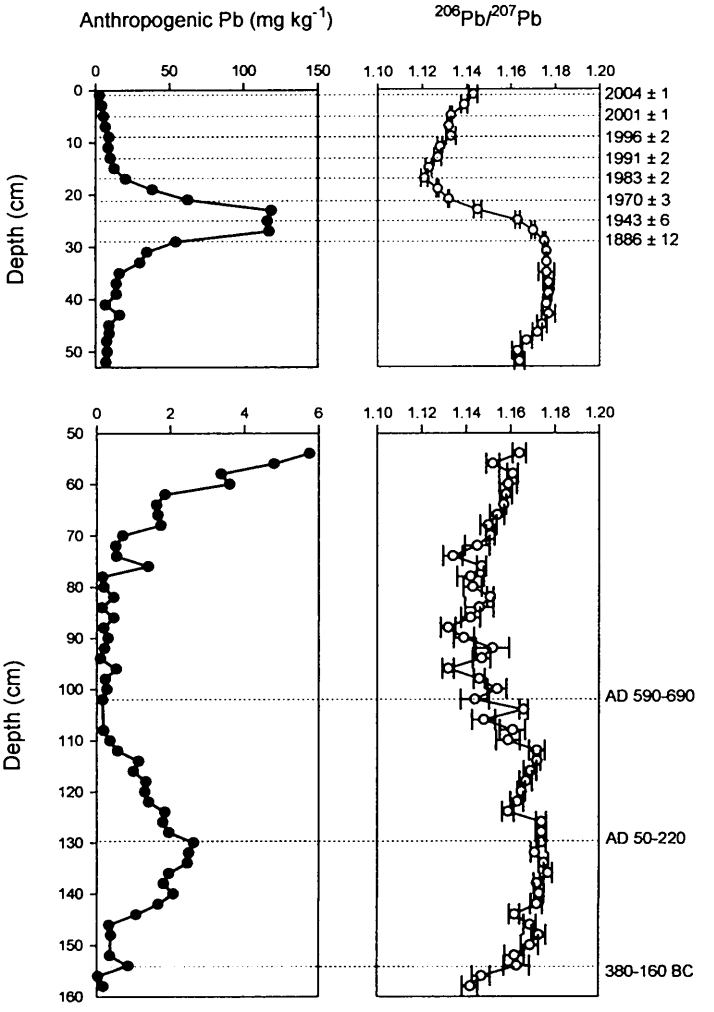

Figure 5.20: Depth profiles of anthropogenic Pb concentrations (mg kg^{-1}) and measured $^{206}Pb/^{207}Pb$ ratio from 0-53 cm and 53-159 cm in the combined ^{210}Pb- and ^{14}C-dated TM04M-1 and TM04CM-4 peat cores.

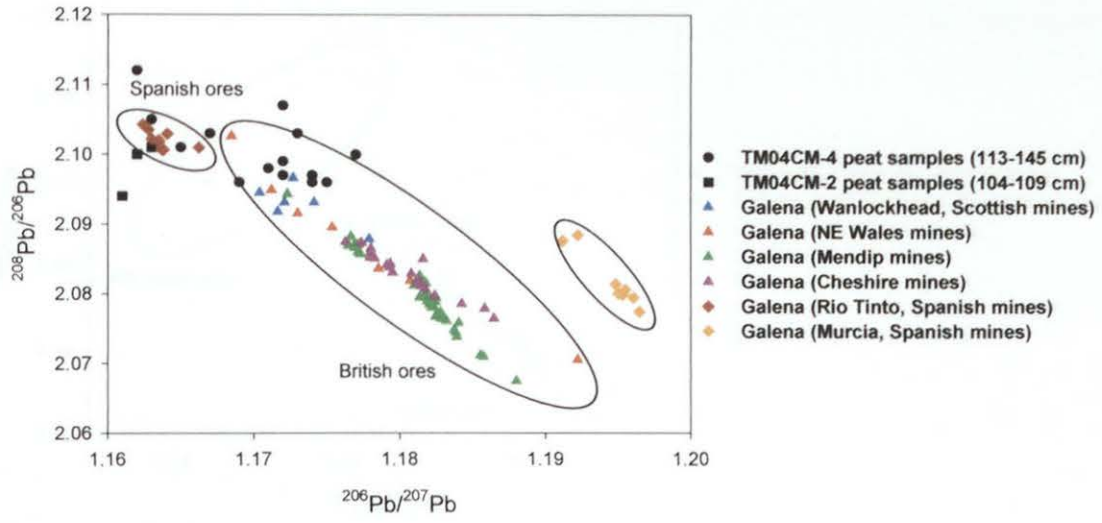

Figure 5.21: Plot of $^{208}Pb/^{206}Pb$ *versus* $^{206}Pb/^{207}Pb$ ratios for samples from 113-145 cm in TM04CM-4, 104-109 cm in TM04CM-2 and for galena in various British and Spanish Pb ores (Stos-Gale *et al.*, 1995; Rohl, 1996).

5.6.2 Post-Roman and Mediaeval atmospheric Pb sources and deposition

The minimum anthropogenic Pb concentrations (mean 0.35 ± 0.18 mg kg^{-1}) between 113 and 69 cm, for which there was a single age-date of 590-690 A.D. available for 101-103 cm, reflect a decline in metallurgical activities during the post-Roman and early Mediaeval era. The corresponding $^{206}Pb/^{207}Pb$ ratios for this period (mean 1.148 ± 0.010) were significantly less radiogenic than those in the pre-Roman and Roman period below. As suggested for Flanders Moss (*cf.* Section 3.6.2), these less radiogenic values could reflect contributions, albeit relatively minor, from long-range atmospheric deposition of Pb from metallurgical processing of Iberian Pb ores, by the Visigods. When Pb isotope ratios of the TM04CM-4 peat samples from 113 to 101 cm, where 101-103 cm corresponds to the late 6th century A.D. when the reign of the Visigods ended, are plotted along with those of various British and Spanish (southern and north-west) Pb ores (Fig. 5.22), they are in agreement with the Pb ores from these locations, consistent with the findings for Flanders Moss (*cf.* Section 3.6.2).

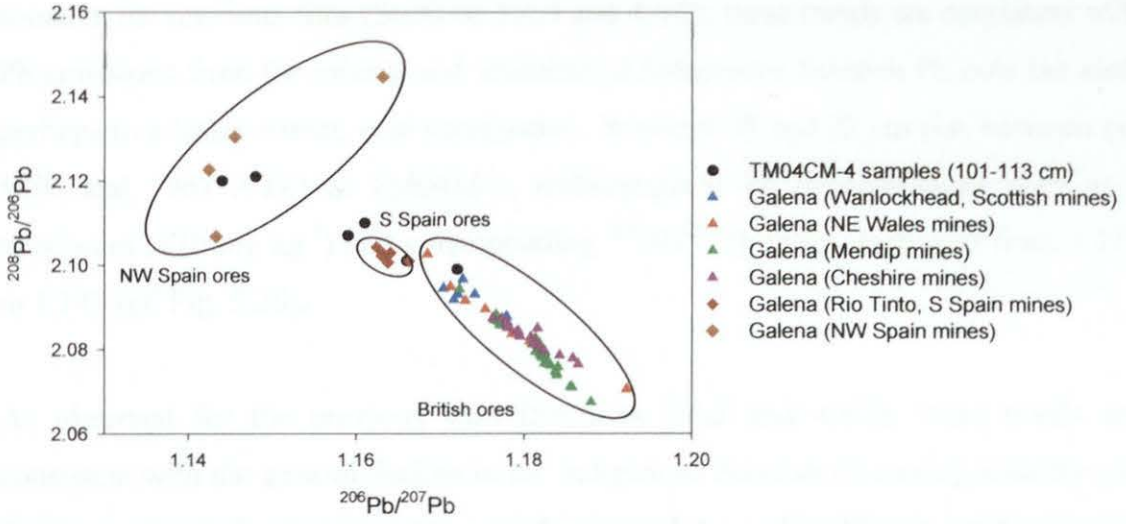

Figure 5.22: Plot of $^{208}Pb/^{206}Pb$ *versus* $^{206}Pb/^{207}Pb$ ratios for samples for the TM04CM-4 (101-113 cm) peat core and for galena in various British and Spanish Pb ores (Stos-Gale *et al.*, 1995; Rohl, 1996; Kylander *et al.*, 2005).

Above 69 cm up to a depth of 53 cm, anthropogenic Pb concentrations (mean 3.1 ± 1.6 mg kg^{-1}) and corresponding $^{206}Pb/^{207}Pb$ ratios (mean 1.157 ± 0.005) increased (*cf.* Fig. 5.20), reflecting the influence of Pb mining and smelting activities, especially in continental Europe, during the Mediaeval period.

5.6.3 Industrial and post-industrial atmospheric Pb sources and deposition

Between 53 and 47 cm in TM04CM-4, depths for which no age-dates were available but based on associated ^{210}Pb dates in the overlying upper regions seem likely to correspond to the mid-1500s and mid-1600s A.D., respectively, the mean anthropogenic Pb concentration and corresponding $^{206}Pb/^{207}Pb$ ratio were 7.6 ± 0.4 mg kg^{-1} and 1.165 ± 0.002, respectively (*cf.* Fig. 5.20). These increases in anthropogenic Pb concentrations and $^{206}Pb/^{207}Pb$ ratios, relative to those between 69 and 59 cm, are likely to reflect the increase in Pb mining and smelting activities in Britain, along with improvements in procedures, approaching the start of the Industrial Revolution (*ca.* 1750 A.D.) (Tylecote, 1986). Above 47 cm (*ca.* mid-1600s A.D.) up to 28 cm (*ca.* 1896 A.D.) in TM04M-1, the anthropogenic Pb concentrations increased from 9.2 to 54 mg kg^{-1} and the corresponding $^{206}Pb/^{207}Pb$

ratios increased and remained fairly constant (mean 1.176 ± 0.002) (*cf.* Fig. 5.20). As found at the previous sites (Sections 3.6.3 and 4.6.2), these trends are consistent with Pb emissions from the mining and smelting of indigenous Scottish Pb ores but also, perhaps to a lesser extent, coal combustion. Between 28 and 22 cm (i.e. between *ca.* 1896 and 1967 A.D.) in TM04M-1, anthropogenic Pb concentrations were at a maximum (120 mg kg^{-1}) and corresponding $^{206}Pb/^{207}Pb$ ratios decreased from 1.170 to 1.145 (*cf.* Fig. 5.20).

As observed for the previous sites (Sections 3.6.3 and 4.6.2), these trends are consistent with the general decline in the indigenous Scottish Pb mining industry and the increasing influence from the use of imported Australian Pb ore, predominantly via car exhaust emissions from the 1930s A.D. Also, the intermediate $^{206}Pb/^{207}Pb$ ratio values again indicate that there were significant contributions from other sources of Pb, such as coal combustion. After the late 1960s A.D. (i.e. above 22 cm in TM04M-1), anthropogenic Pb concentrations decreased at the same time as the corresponding $^{206}Pb/^{207}Pb$ ratios decreased to a minimum of 1.121 at 1983 A.D. (16-18 cm in TM04M-1) (*cf.* Fig. 5.20), reflecting, as at the previous sites (Sections 3.6.3 and 4.6.2), the decreasing influence of coal combustion and the increasing influence of car exhaust emissions of Pb. After 1983 A.D. (i.e. above 16 cm in TM04M-1), anthropogenic Pb concentrations continued to fall while the $^{206}Pb/^{207}Pb$ ratios increased to 1.143 at 2004 A.D. (*cf.* Fig. 5.20), reflecting the steep fall in Pb emissions from car exhausts, as well as the growing importance of other sources of Pb (e.g. waste incineration), consistent with findings at the previous sites (Sections 3.6.3 and 4.6.2). The 3-isotope plot (Fig. 5.23) provides evidence for the contributions to Pb deposition, during the industrial and post-industrial era, from the sources mentioned above.

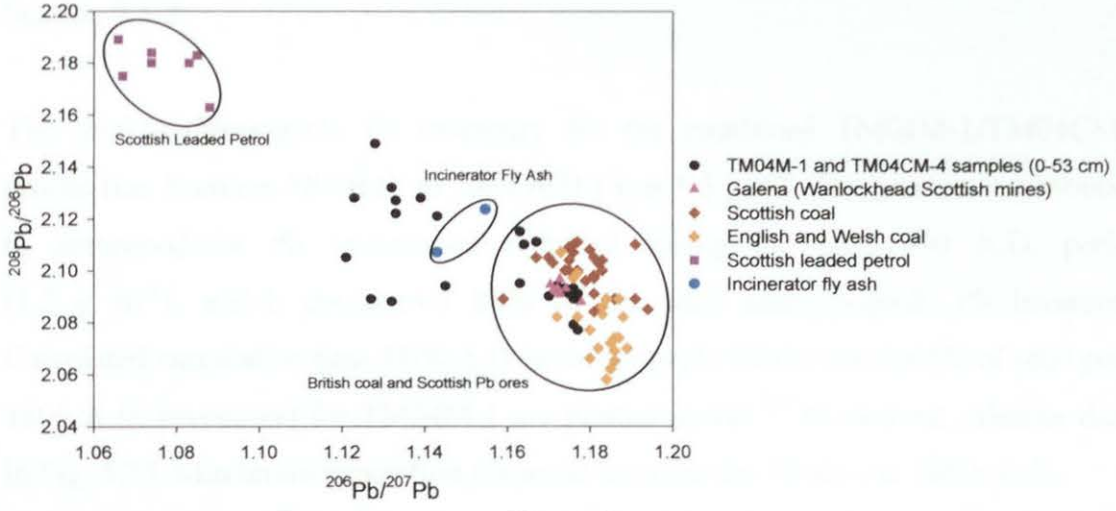

Figure 5.23: Plot of $^{208}Pb/^{206}Pb$ *versus* $^{206}Pb/^{207}Pb$ ratios for the TM04M-1 (0-47 cm) and TM04CM-4 (47-53 cm) peat samples, and for galena in Wanlockhead Scottish Pb ores (Rohl, 1996), British coal (Farmer *et al.*, 1999), leaded petrol (Farmer *et al.*, 2000) and incinerator fly ash (Monna *et al.*, 1997). Note that the single outlier point corresponding to the TM04M-1 12-14 cm section was omitted from the plot.

5.6.3.1 Historical trends in depositional fluxes and inventories of Pb

Depositional fluxes of anthropogenic Pb in TM04M-1 (A6.1 Table A12) were estimated, on the basis of measured ^{210}Pb chronologies, and plotted along with the measured $^{206}Pb/^{207}Pb$ ratios, *versus* ^{210}Pb-derived calendar dates since 1840 A.D. in Fig. 5.24.

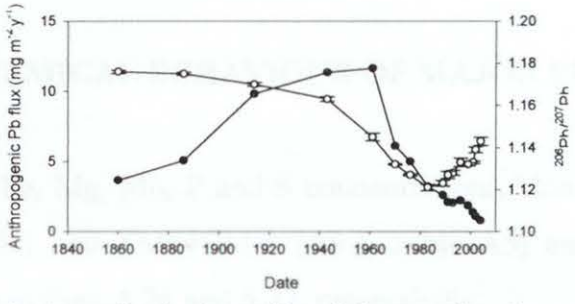

Figure 5.24: Calculated atmospheric depositional fluxes of anthropogenic Pb (mg m^{-2} y^{-1}) (closed circles) and measured $^{206}Pb/^{207}Pb$ ratios (open circles) for the TM04M-1 core *versus* ^{210}Pb-derived dates since 1840 A.D.

The maximum anthropogenic Pb flux (range 10 to 12 mg m^{-2} y^{-1}) in TM04M-1 occurred between the mid-1910s and early 1960s A.D. Note that the depositional fluxes of anthropogenic Pb and trends in $^{206}Pb/^{207}Pb$ ratios at Turclossie Moss will be

compared more closely to those found at the other sites under investigation in Section 7.5.3.

The total anthropogenic Pb inventory for the combined TM04M-1/TM04CM-4 profile (i.e. from *ca.* 380 B.C. to 2004 A.D.) was 1.5 g m^{-2}. The greatest contribution to anthropogenic Pb inventories occurred during the post-1800 A.D. period (1.2 g m^{-2}), which constituted 80% of the total anthropogenic Pb inventory. Calculated cumulative post-1800 A.D. anthropogenic Pb inventories (% of total post-1800 A.D. inventory) for TM04M-1 are plotted *versus* ^{210}Pb-derived calendar dates in Fig. 5.25. Maximum deposition occurred between the 1890s and 1960s A.D.

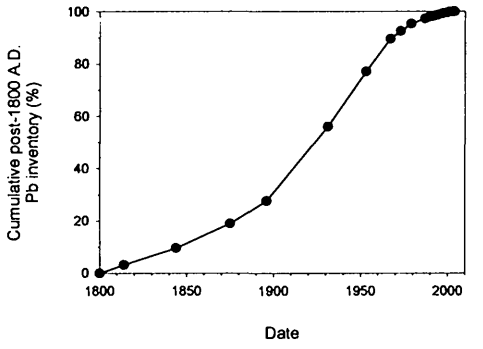

Figure 5.25: Calculated cumulative post-1800 A.D. anthropogenic Pb inventories (% of total post-1800 A.D.) for the TM04M-1 core *versus* ^{210}Pb-derived dates. Note that dates in TM04M-1 prior to *ca.* 1844 A.D. were extrapolated.

5.7 GEOCHEMICAL BEHAVIOUR OF MAJOR ELEMENTS

Profiles of total Ca, Fe, Mg, Mn, P and S concentrations, along with water and ash content, for TM04M-1 and TM04CM-4 (A6.1 Table A5) and TM04CM-2 (A6.2 Table A5) are shown in Figs. 5.26 and 5.27, respectively.

5.7.1 TM04M-1 and TM04CM-4

All six elements exhibited concentration peaks or increases in the uppermost ~ 50 cm of the cores, with the following maximum concentrations at the depths indicated:

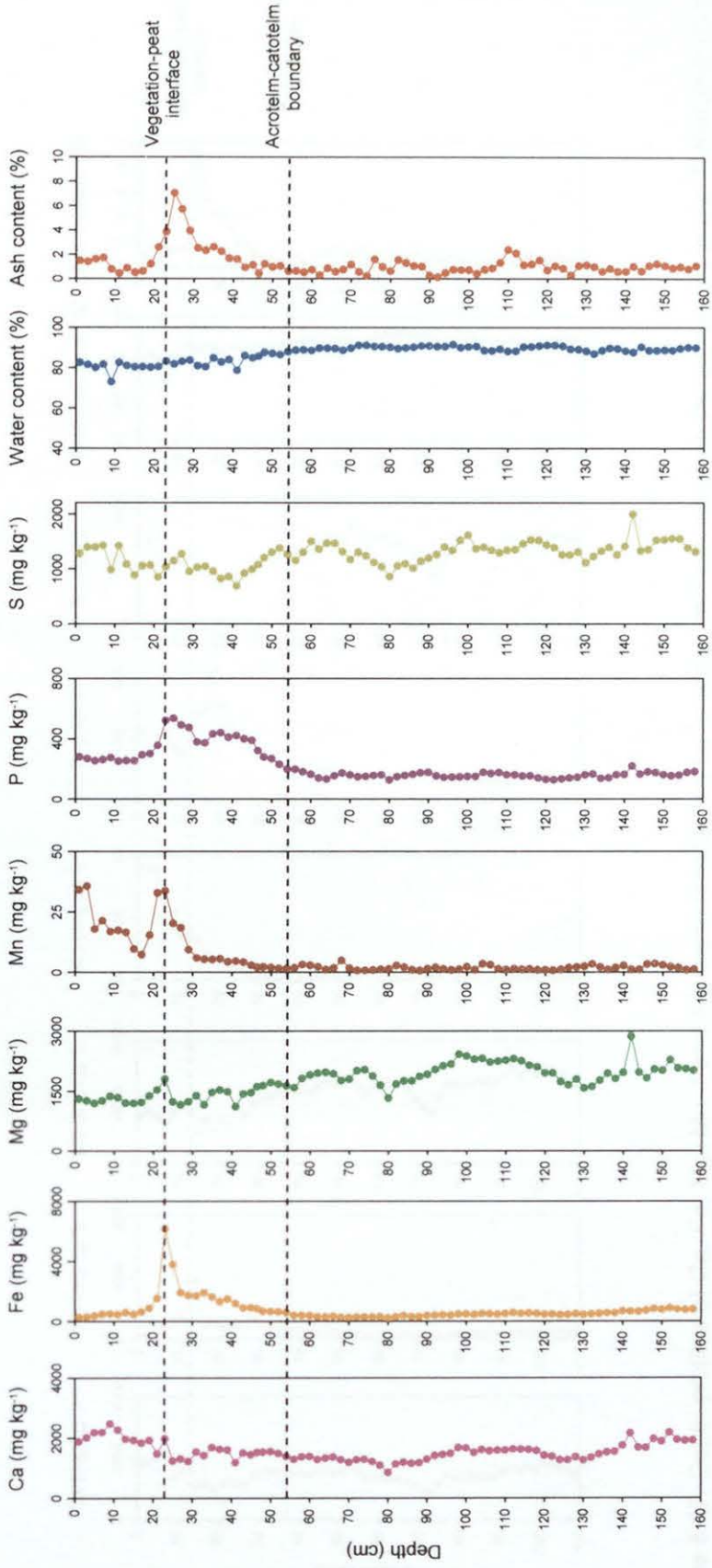

Figure 5.26: Depth profiles of Ca, Fe, Mg, Mn, Pand S concentrations (mg kg^{-1}), water and ash contents (% by weight) in the combined TM04M-1 (0-47 cm) and TM04CM-4 (47-159 cm) peat cores.

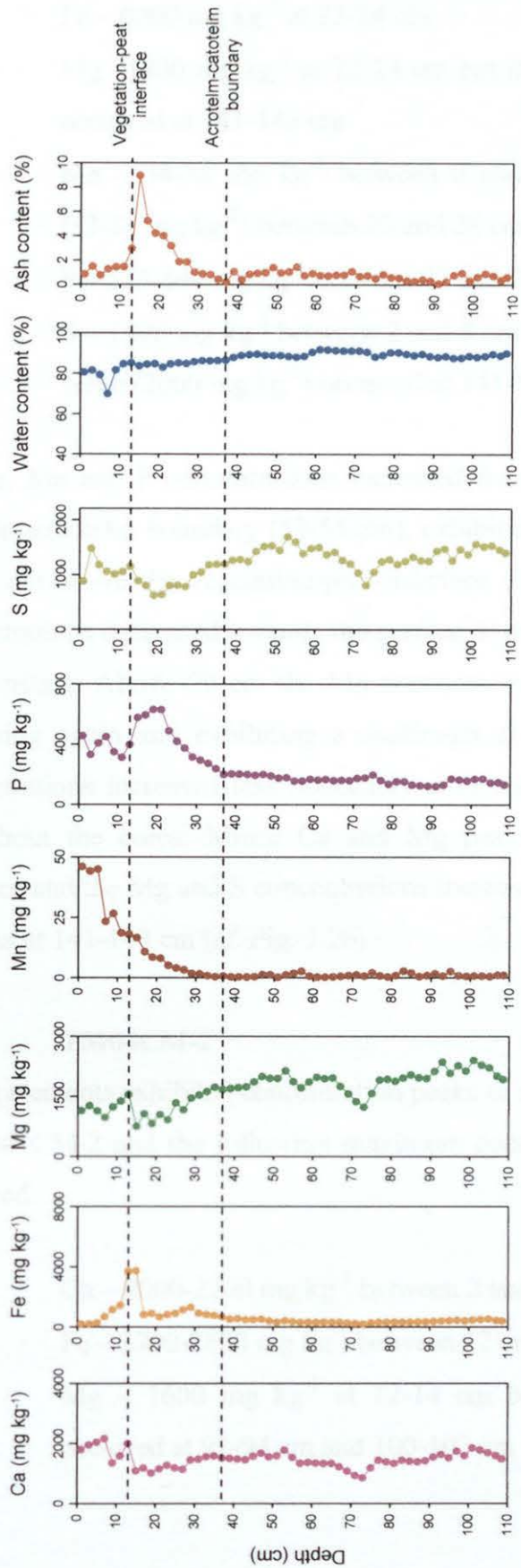

Figure 5.27: Depth profiles of Ca, Fe, Mg, Mn, Pand S concentrations (mg kg^{-1}), water and ash contents (% by weight) in the TM04CM-2 (0-109 cm) peat cores.

- Ca – 2500 mg kg^{-1} at 8-10 cm
- Fe – 6200 mg kg^{-1} at 22-24 cm
- Mg –1800 mg kg^{-1} at 22-24 cm but the maximum value (2900 mg kg^{-1}) occurred at 141-143 cm
- Mn – 34-36 mg kg^{-1} between 0 and 4 cm but there was also a peak (33-34 mg kg^{-1}) between 20 and 24 cm
- P – 520-540 mg kg^{-1} between 22 and 26 cm
- S – 1400 mg kg^{-1} between 2 and 8 cm and at 10-12 cm but the maximum value (2000 mg kg^{-1}) occurred at 141-143 cm

The Fe, Mn and P concentrations increased from low constant values beneath the acrotelm-catotelm boundary (53-55 cm), exhibiting peaks at, and also in the case of Mn, 2 cm above the vegetation-peat interface (22-24 cm), above which Fe and P concentrations decreased towards the surface, P concentrations remaining fairly high and constant. Above 20 cm the Mn concentrations decreased up to 16 cm before increasing again and exhibiting a maximum at the surface. The Ca, Mg and S concentrations increased less noticeably with concentrations remaining fairly high throughout the cores. Minor Ca and Mg peaks occurred at the vegetation-peat interface and the Mg and S concentrations increased gradually with depth, exhibiting maxima at 141-143 cm (*cf.* Fig. 5.26).

5.7.2 TM04CM-2

All six elements exhibited concentration peaks or increases in the uppermost ~ 30 cm of TM04CM-2 and the following maximum concentrations occurred, at the depths indicated:

- Ca – 2000-2200 mg kg^{-1} between 2 and 8 cm and at 12-14 cm
- Fe – 3700-3800 mg kg^{-1} between 12 and 16 cm
- Mg – 1600 mg kg^{-1} at 12-14 cm but the maximum (2400 mg kg^{-1}) occurred at 92-94 cm and 100-102 cm

- Mn – 44-46 mg kg^{-1} between 0 and 6 cm
- P – 580-630 mg kg^{-1} between 14 and 22 cm
- S – 1500 mg kg^{-1} at 2-4 cm but the maximum (1600-1700 mg kg^{-1}) occurred between 52 and 56 cm and at 100-102 cm

Trends were generally consistent with those in TM04M-1 and TM04CM-4 with Fe and P concentrations exhibiting maximum concentrations at and/or 2 cm beneath the vegetation-peat interface (12-14 cm). The Mn concentrations were at a maximum in the surface vegetation and the Ca, Mg and S concentrations were high at and above the vegetation-peat interface. The Mg and S concentrations both exhibited maxima at 100-102 cm (*cf.* Fig. 5.27).

5.7.3 Discussion

The trends for Turclossie Moss are consistent with those found in the other sites (*cf.* Sections 3.7.3 and 4.7.3). For example, there was no apparent correlation between the Ca, Fe, Mg, Mn, P and S concentration and ash content profiles (*cf.* Figs. 5.26 and 5.27) and the Ca and Mg concentration profiles indicated that contributions from sea salt inputs were minor. As found for the previous sites (*cf.* Sections 3.7.3 and 4.7.3), Ca, Fe, Mg, Mn, P and S concentration profiles are influenced by nutrient uptake and recycling. Also, Fe, Mn and P concentration profiles are influenced by redox cycling if the zones of water table fluctuation are taken to lie between ~ 20 and 53 cm in TM04M-1 and TM04CM-4, and between ~ 12 and 36 cm in TM04CM-2 and the similarity between the Fe and P concentration profiles indicates the influence of Fe on the distribution of P, although the onset of the maximum P concentrations in TM04CM-2 occurred 2 cm below the diagenetic Fe peak (*cf.* Fig. 5.27), as observed for Flanders Moss and The Red Moss of Balerno RM03CM-1 core (*cf.* Sections 3.7.3 and 4.7.3). In contrast to the previous sites, the Turclossie Moss S concentration profiles did not appear to be influenced by redox cycling, exhibiting similar trends to Ca and Mg (*cf.* Fig. 5.26 and 5.27).

5.8 GEOCHEMICAL BEHAVIOUR OF OTHER TRACE ELEMENTS

As for Pb in Section 5.6, the TM04M-1 and TM04CM-4 cores alone will be used in the interpretation of historical trends in sources of atmospheric deposition of other trace elements. Note that Hg concentrations were not determined for Turclossie Moss.

5.8.1 Sb

The TM04M-1 and TM04CM-4 Sb concentration (A6.1 Table A6) profile, along with those of Pb and Sc, is shown in Fig. 5.28.

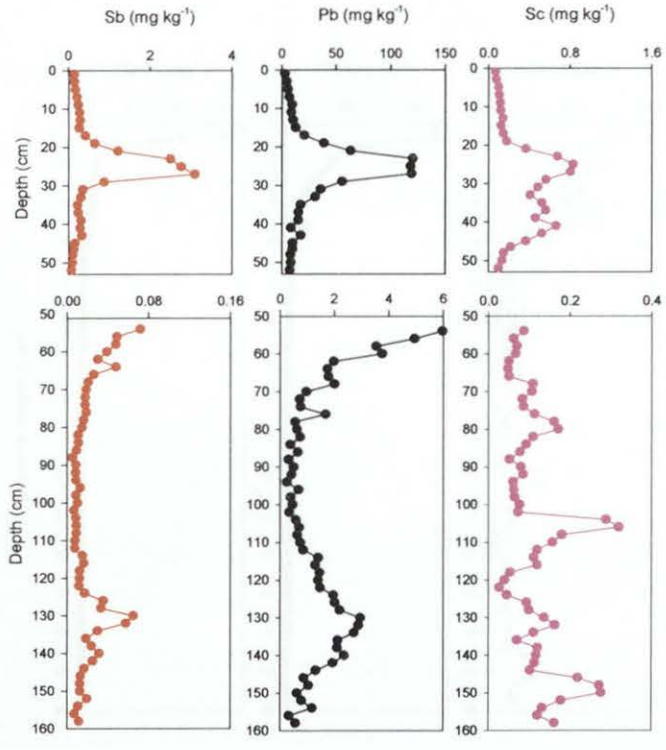

Figure 5.28: Depth profiles of Sb, Pb and Sc concentrations (mg kg^{-1}) from 0-53 cm and 53-159 cm in the combined TM04M-1 and TM04CM-4 peat cores.

0-53 cm

The Sb concentrations increased from 0.082 mg kg^{-1} at 51-53 cm to maximum values (2.5-3.1 mg kg^{-1}) between 20 and 28 cm, coincident with the Pb maxima, above which concentrations gradually decreased towards the top of the core (*cf.* Fig. 5.28).

53-159 cm

Note the changes in scale on the Sb and Pb (25-fold) and Sc (4-fold) concentrations on going from 0-53 cm to 53-159 cm. The same zones as those observed earlier for Pb concentrations (Section 5.6) were apparent for Sb: a region of minimum concentrations (mean 0.012 ± 0.004 mg kg^{-1}) from 113 to 69 cm, above which Sb increased to 0.072 mg kg^{-1} at 53-55 cm and below which from 113 to 145 cm there was a pronounced peak with a maximum concentration of 0.065 mg kg^{-1} at 129-131 cm, coincident with the Pb concentration maximum (*cf.* Fig. 5.28). There is good agreement between the Sb concentration (A6.2 Table A6) profile trends in the TM04CM-2 sections below 14 cm with those in TM04M-1 and TM04CM-4 (Fig. 5.29).

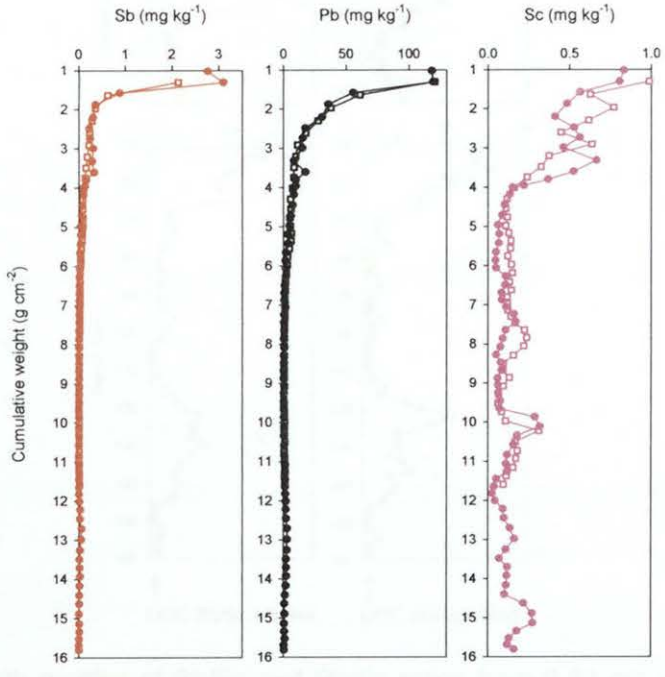

Figure 5.29: Profiles of Sb, Pb and Sc concentration (mg kg^{-1}) from 24-159 cm in the combined TM04M-1 and TM04CM-4 cores (closed circles) and from 16-107 cm in the TM04CM-2 core (open squares) *versus* cumulative weight.

5.8.1.1 Discussion

As observed for the previous sites (Sections 3.8.1 and 4.8.1), the Sb and Pb profiles show a remarkable resemblance, providing further evidence that Sb, like Pb, is also essentially immobile in ombrotrophic peat.

5.8.1.1.1 The use of Sc as an indicator of soil dust input of Sb

The profile of Sb/Sc ratios (A6.1 Table A6), along with that of Sb/Sc and Pb/Sc ratios, in TM04M-1 and TM04CM-4 is shown in Fig. 5.30. The maximum Sb/Sc ratios (mean 3.4 ± 0.4) occurred between 28 and 16 cm, similar to the maximum Pb/Sc ratios (mean 150 ± 40), which occurred between 30 and 14 cm (Section 5.5.1). The minimum mean Sb/Sc ratio (0.12 ± 0.05) occurred between 113 and 69 cm and was ~ 3-fold greater than the corresponding UCC ratio (0.044), consistent with the findings for the mean minimum Pb/Sc ratio (6.2 ± 3.0) (Section 5.5.3).

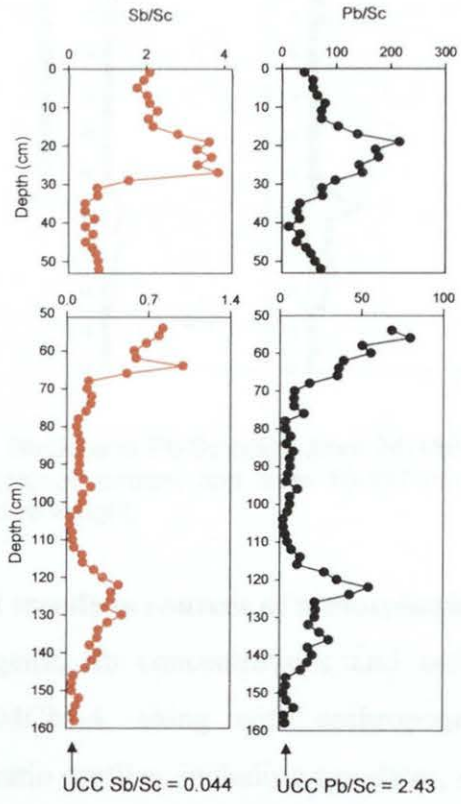

Figure 5.30: Depth profiles of Sb/Sc and Pb/Sc ratios from 0-53 cm and 53-159 cm in the combined TM04M-1 and TM04CM-4 peat cores.

There is good agreement between the Sb/Sc ratio (A6.2 Table A8) profile trends in the TM04CM-2 sections below 14 cm with those in TM04M-1 and TM04CM-4 (Fig. 5.31).

As performed for Pb (*cf.* Section 5.5.2), on the basis of the use of Sc as a conservative element, the anthropogenic Sb concentrations in the TM04M-1 and

TM04CM-4 cores were calculated (A6.1 Table A6) (*cf.* Sections 3.8.1.3.1 and 4.8.1.1.1), and these will be used to interpret historical trends in anthropogenic Sb deposition.

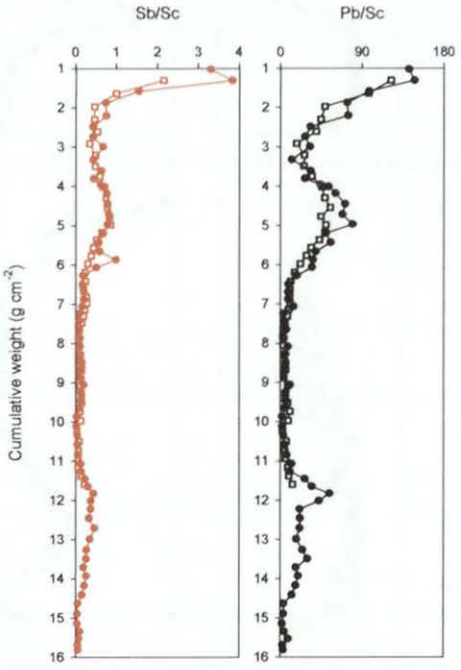

Figure 5.31: Profiles of Sb/Sc and Pb/Sc ratios from 24-159 cm in the combined TM04M-1 and TM04CM-4 cores (closed circles) and from 16-107 cm in the TM04CM-2 core (open squares) *versus* cumulative weight.

5.8.1.1.2 Historical trends in sources of atmospheric Sb deposition

Profiles of anthropogenic Sb concentrations and anthropogenic Sb/Pb ratios in TM04M-1 and TM04CM-4, along with anthropogenic Pb concentration and measured $^{206}Pb/^{207}Pb$ ratio profiles, including age-dates, are shown in Fig. 5.32.

Pre-Roman and Roman atmospheric Sb sources and deposition

The anthropogenic Sb concentrations increased from low values (mean 0.0042 ± 0.0038 mg kg^{-1}) between 159 and 145 cm in TM04CM-4, exhibiting a broad peak between 145 and 113 cm, with a maximum (0.059 mg kg^{-1}) at 129-131 cm (*ca.* 50-220 A.D.), as observed for Pb (Section 5.6.1), and can be attributed to pre-Roman and Roman metallurgical activities (*cf.* Fig. 5.32).

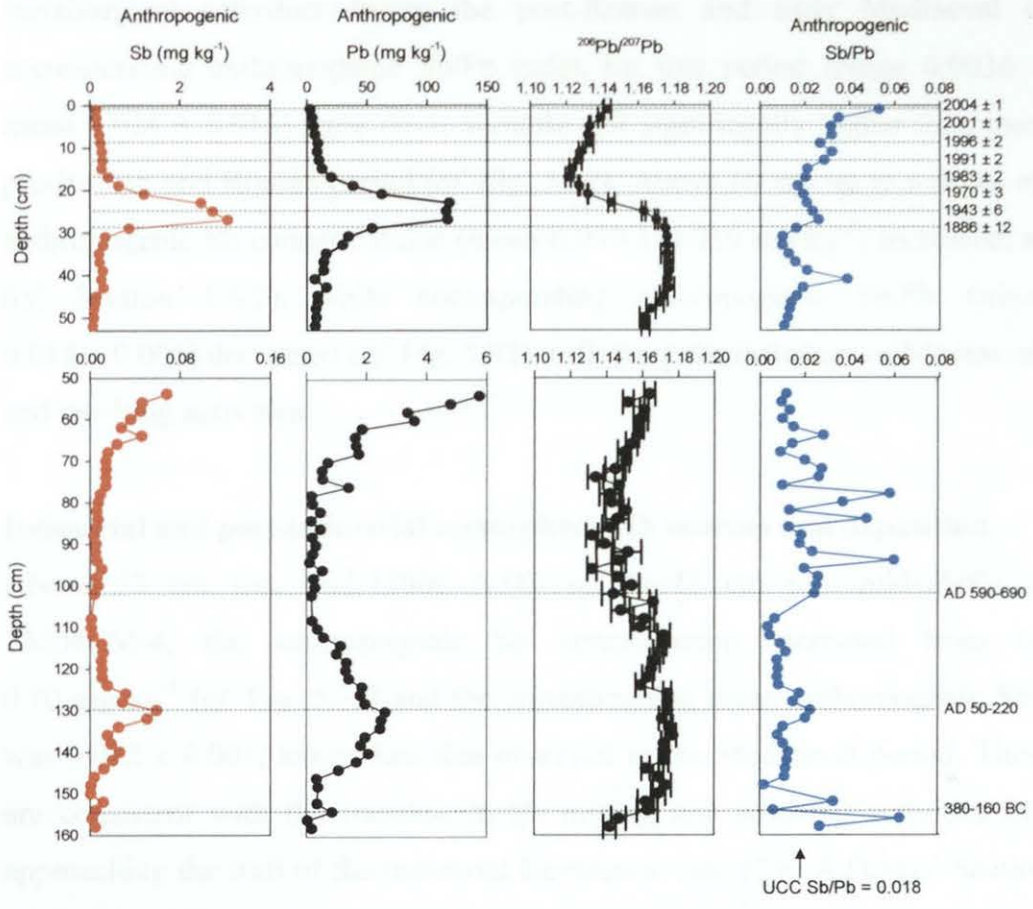

Figure 5.32: Depth profiles of anthropogenic Sb and Pb concentrations (mg kg^{-1}), measured $^{206}Pb/^{207}Pb$ and anthropogenic Sb/Pb ratios from 0-53 cm and 53-159 cm in the combined ^{210}Pb- and ^{14}C-dated TM04M-1 and TM04CM-4 peat cores.

The corresponding mean anthropogenic Sb/Pb ratio (0.012 ± 0.005) between 145 and 113 cm was lower than that of the UCC Sb/Pb ratio (0.018) but greater than the range of values (0.0033 – 0.0056) obtained for the Wanlockhead and Leadhills Scottish Pb ore samples (*cf.* Table 3.10), and perhaps provides further evidence for the atmospheric deposition of Pb (*cf.* Section 5.6.1), as well as Sb, from both Spanish and British Pb ore mining and smelting activities (*cf.* Fig. 5.32). Unfortunately, Sb and Pb concentrations, and therefore Sb/Pb ratios, were not available for Spanish Pb ores, such as those from Rio Tinto.

Post-Roman and Mediaeval atmospheric Sb sources and deposition

The minimum anthropogenic Sb concentrations (mean 0.0073 ± 0.0042 mg kg^{-1}) between 113 and 69 cm, as observed for Pb (Section 5.3.2), reflect a decline in

metallurgical activities during the post-Roman and early Mediaeval era. The corresponding anthropogenic Sb/Pb ratios for this period (range 0.0036 – 0.060; mean 0.024 ± 0.016) were more variable and significantly higher than those in the pre-Roman and Roman period (*cf.* Fig. 5.32). Above 69 cm up to a depth of 53 cm, anthropogenic Sb concentrations (mean 0.039 ± 0.016 mg kg^{-1}) increased, as for Pb (*cf.* Section 5.6.2), while corresponding anthropogenic Sb/Pb ratios (mean 0.014 ± 0.006) decreased (*cf.* Fig. 5.32), reflecting the influence of Mediaeval mining and smelting activities.

Industrial and post-industrial atmospheric Sb sources and deposition

Above 53 cm (*ca.* mid-1500s A.D.) up to 47 cm (*ca.* mid-1600s A.D.) in TM04CM-4, the anthropogenic Sb concentration increased from 0.077 to 0.10 mg kg^{-1} (*cf.* Fig. 5.32) and the corresponding mean anthropogenic Sb/Pb ratio was 0.012 ± 0.001, lower than that observed in the Mediaeval period. These trends are consistent with the increase in Pb mining and smelting activities in Britain, approaching the start of the Industrial Revolution (*ca.* 1750 A.D.) (*cf.* Section 5.6.3). Above 47 cm (*ca.* mid-1600s A.D.) up to 28 cm (*ca.* 1896 A.D.) in TM04M-1, the anthropogenic Sb concentrations continued to increase to 0.87 mg kg^{-1} and the corresponding mean anthropogenic Sb/Pb ratio (0.017 ± 0.008) increased (*cf.* Fig. 5.32). In contrast to findings at the previous sites (*cf.* Sections 3.8.1.3.2 and 4.8.1.1.2), these anthropogenic Sb/Pb ratios were considerably greater than the range of values (0.0033 – 0.0056) obtained for the Wanlockhead and Leadhills Scottish Pb ore samples (*cf.* Table 3.10, Section 3.8.1.3.2) and comparable to the range of values (0.0042 – 0.12) obtained for British and Irish coal samples (*cf.* Table 3.11, Section 3.8.1.3.2). This possibly indicates that Sb (and Pb) emissions were influenced by both coal combustion and Pb mining and smelting activities at these times, as supported by the corresponding $^{206}Pb/^{207}Pb$ ratio trends (*cf.* Section 5.6.3). Above 28 cm (*ca.* 1896 A.D.) in TM04M-1, as for Pb, anthropogenic Sb concentrations increased markedly reaching a maximum (range 2.5 - 3.1 mg kg^{-1}) between 28 and 22 cm (i.e. between *ca.* 1896 and 1967 A.D.), while the corresponding mean anthropogenic Sb/Pb ratio (0.024 ± 0.003) increased further (*cf.* Fig. 5.32),

attributable to the growing influence of coal combustion (*cf.* Table 3.11) to Sb emissions, as found for the previous sites (*cf.* Sections 3.8.1.3.2 and 4.8.1.1.2). From the late 1960s A.D. (above 22 cm) to *ca.* 1976 A.D. (18-20 cm), anthropogenic Sb concentrations and corresponding anthropogenic Sb/Pb ratios decreased, consistent with the decreasing influence of coal combustion and the increasing influence of vehicle exhaust emissions of Pb (*cf.* Section 5.6.3), as found for the previous sites (Sections 3.8.1.3.2 and 4.8.1.1.2). Between 1976 A.D. (18 cm) and 2004 A.D. (0 cm), anthropogenic Sb concentrations continued to decrease while the corresponding Sb/Pb ratios increased (from 0.020 to 0.053) (*cf.* Fig. 5.32). As found for the previous sites (Sections 3.8.1.3.2 and 4.8.1.1.2), these trends suggest a new recent source of Sb (e.g. automotive brake linings, degradation or combustion of plastics).

5.8.1.1.3 Historical trends in depositional fluxes and inventories of anthropogenic Sb

Depositional fluxes of anthropogenic Sb calculated for TM04M-1 (A6.1 Table A12) are plotted along with those of anthropogenic Pb and the anthropogenic Sb/Pb and measured $^{206}Pb/^{207}Pb$ ratios, *versus* ^{210}Pb-derived calendar dates since 1840 A.D. in Fig. 5.33. The maximum anthropogenic Sb flux (range 0.24 - 0.27 mg m^{-2} y^{-1}) occurred between the mid-1910s and early 1960s A.D., coincident with the anthropogenic Pb flux maxima. As observed for the previous sites (Sections 3.8.1.3.3 and 4.8.1.1.3), there is broad agreement between the anthropogenic Sb/Pb ratios in TM04M-1 and Sb/Pb ratios obtained independently for preserved herbarium and freshly collected *Sphagnum* moss samples of known age collected across Scotland (Fig. 5.34) (Farmer *et al.*, 2002; Halter, 2005; Halter and Farmer, *in prep.*). Note that the depositional fluxes of anthropogenic Sb, and anthropogenic Sb/Pb ratios at Turclossie Moss will be compared more closely to those found in the other Scottish peat bogs under investigation in Section 7.8.3.

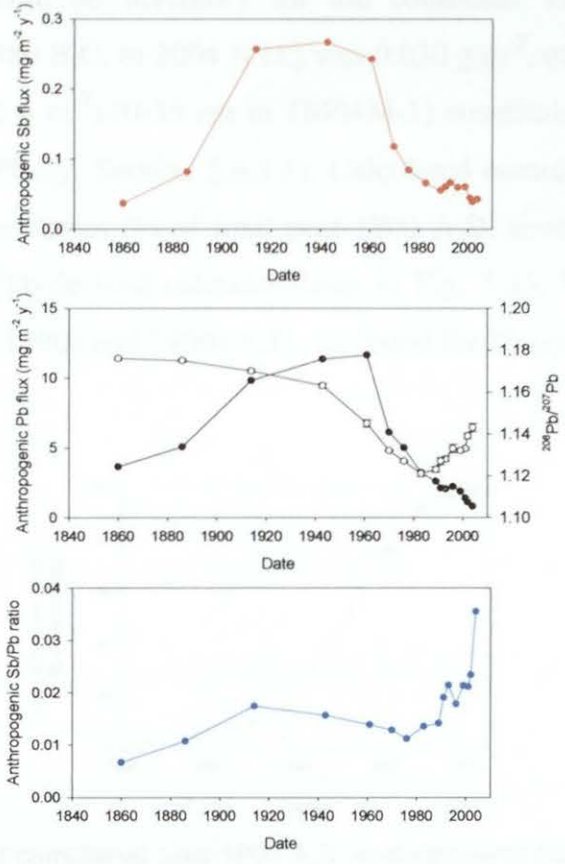

Figure 5.33: Calculated atmospheric depositional fluxes of anthropogenic Sb and Pb (mg m^{-2} y^{-1}) (closed circles), and the anthropogenic Sb/Pb and measured $^{206}Pb/^{207}Pb$ ratios (open circles) for the TM04M-1 core *versus* ^{210}Pb-derived dates since 1840 A.D.

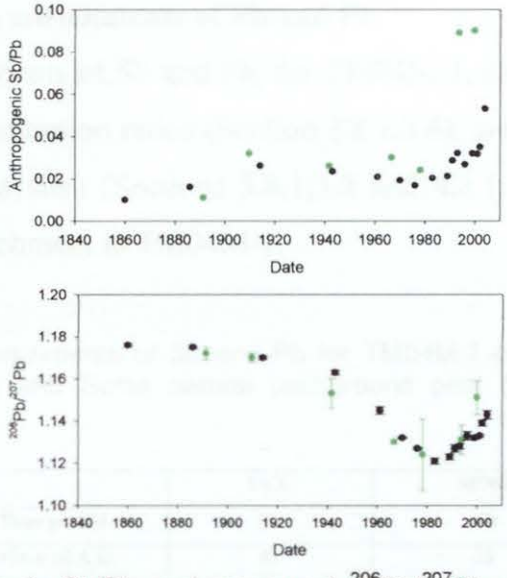

Figure 5.34: Anthropogenic Sb/Pb and measured $^{206}Pb/^{207}Pb$ ratios *versus* dates, since 1840 A.D, for herbarium moss samples (green symbols) and the TM04M-1 core.

The total anthropogenic Sb inventory for the combined TM04M-1/TM04CM-4 profile (i.e. from *ca.* 380 B.C. to 2004 A.D.) was 0.030 g m^{-2}, of which the post-1800 A.D. inventory (0.025 g m^{-2}) (0-36 cm in TM04M-1) constitutes 83%, in agreement with the finding for Pb (*cf.* Section 5.6.3.1). Calculated cumulative post-1800 A.D. anthropogenic Sb inventories (% of total post-1800 A.D. inventory) for TM04M-1 are plotted *versus* ^{210}Pb-derived calendar dates in Fig. 5.35. Maximum deposition occurred between the 1890s and 1960s A.D., as found for Pb (*cf.* Section 5.6.3.1).

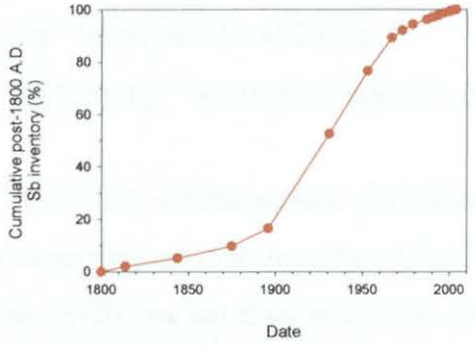

Figure 5.35: Calculated cumulative post-1800 A.D. anthropogenic Sb inventories (% of total post-1800 A.D. inventory) for the TM04M-1 core *versus* ^{210}Pb-derived dates. Note that dates in TM04M-1 prior to *ca.* 1844 A.D. were extrapolated.

5.8.1.1.4 Maximum enrichments of Sb and Pb

The maximum enrichments of Sb and Pb, for TM04M-1, calculated using UCC and SNBP elemental concentration ratios (Section 3.8.1.3.4), are shown in Table 5.7. As found for the previous sites (Sections 3.8.1.3.4 and 4.8.1.1.4), Sb and Pb exhibit similar degrees of enrichment in TM04M-1.

Table 5.7: Maximum enrichments of Sb and Pb for TM04M-1 calculated relative to upper continental crust (UCC) and Swiss natural background peat (SNBP) Sb/Sc and Pb/Sc concentration ratios.

	UCC	SPNB
Time period	**Sb**	**Sb**
1914 ± 10 A.D.	87	35
	Pb	**Pb**
1976 ± 3 A.D.	89	72

5.8.2 As, Cd, Cu, Se and Zn

Profiles for TM04M-1 and TM04CM-4 As, Cd, Cu, Se and Zn concentrations (A6.1 Table A7), along with Pb and S concentrations and ash contents, are shown in Fig. 5.36. The elements As, Cd, Cu and Se exhibited concentration peaks in the uppermost ~ 50 cm of the cores, with the following maximum concentrations at the depths indicated:

- As – 2.8 – 3.4 mg kg^{-1} between 22 and 28 cm
- Cd – 2.2 mg kg^{-1} at 22-24 cm
- Cu – 10 mg kg^{-1} between 22 and 28 cm
- Se – 0.72 – 0.84 mg kg^{-1} between 20 and 26 cm

Above these maxima, elemental concentrations decreased towards the surface, As and Cd concentrations decreasing most noticeably while Cu concentrations decreased steeply to 4.3 mg kg^{-1} at 18-20 cm but then remained constant towards the surface (*cf.* Fig. 5.36). Below these maxima, As, Cd and Cu concentrations decreased towards the bottom of the core. Below ~ 50 cm, Se concentrations decreased but remained high and constant in the anaerobic catotelm layers. The Zn concentrations were highest beneath 47 cm, with a maximum of 250 mg kg^{-1} at 55-57 cm and, like Se, remained high and constant throughout the catotelm layers (*cf.* Fig. 5.36). In general the distributions of As, Cd and Cu were similar to those of both Pb and the ash content and distributions of Se and Zn were more similar to that of S.

There is good agreement between the As, Cd, Cu, Se and Zn concentration (A6.2 Table A6) profile trends in the TM04CM-2 sections below 14 cm with those in TM04M-1 and TM04CM-4 (Fig. 5.37).

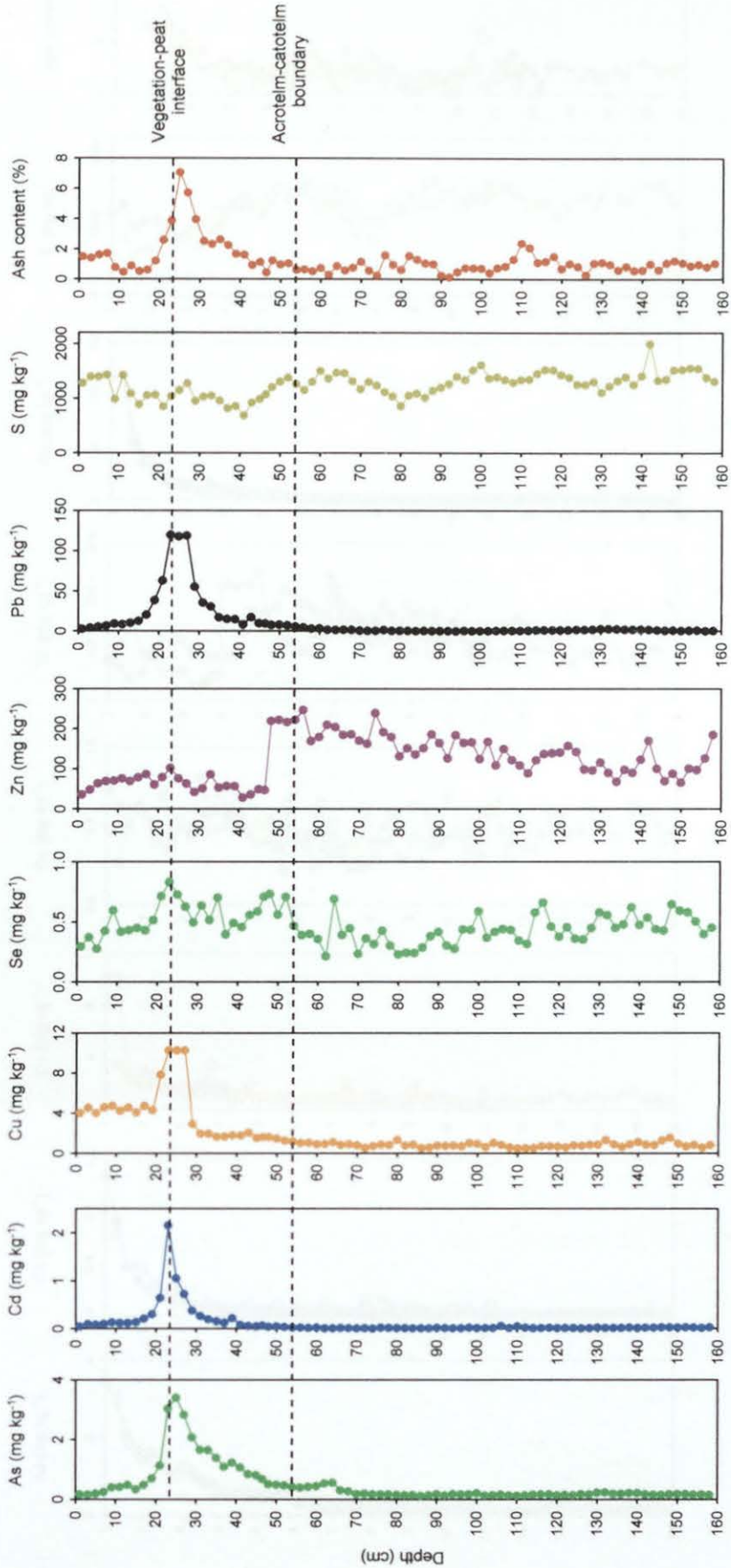

Figure 5.36: Depth profiles of As, Cd, Cu, Se, Zn, Pb and S concentrations (mg kg^{-1}) and ash contents (% by weight) in the combined TM04M-1 (0-47 cm) and TM04CM-4 (47-159 cm) peat cores.

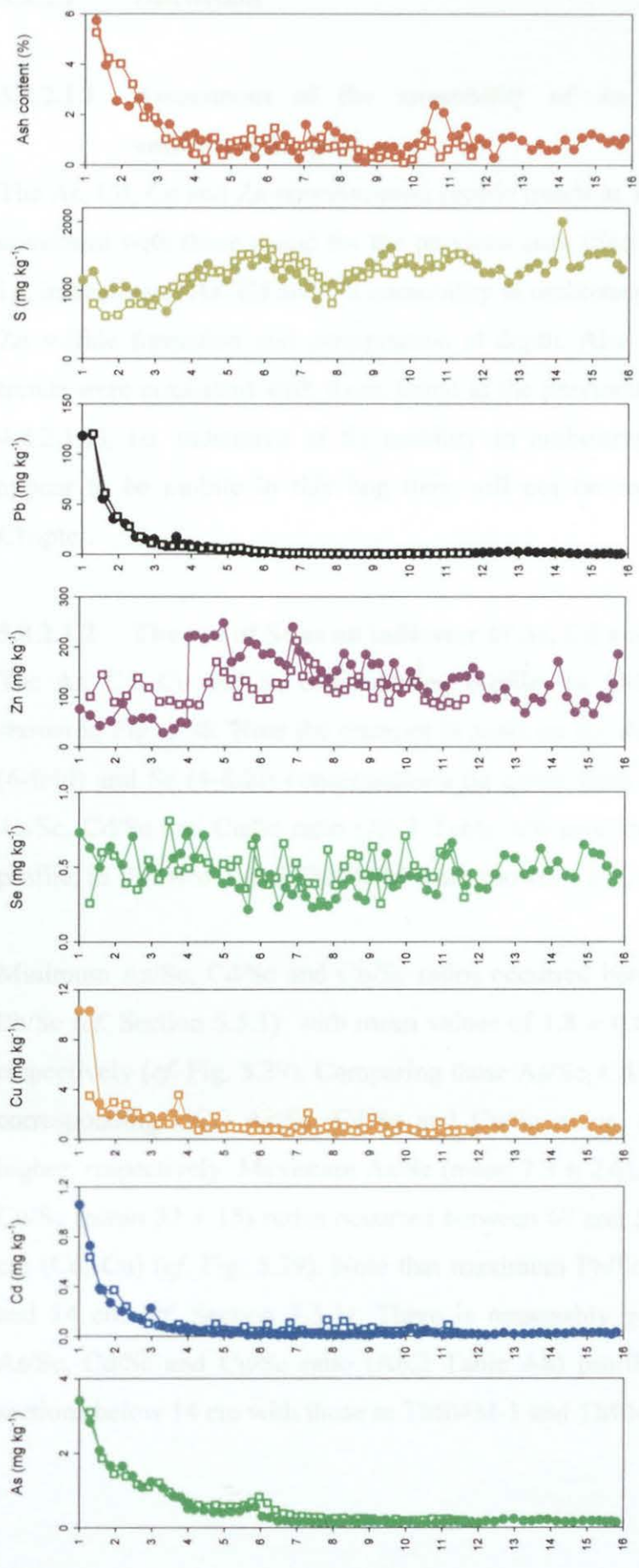

Figure 5.37: Profiles of As, Cd, Cu, Se, Zn, Pb, S concentration (mg kg^{-1}) and ash content (% by weight) from 24-159 cm in the combined TM04M-1 and TM04CM-4 cores (closed circles) and from 16-107 cm in the TM04CM-2 core (open squares) *versus* cumulative weight.

5.8.2.1 Discussion

5.8.2.1.1 Assessment of the immobility of As, Cd, Cu, Se and Zn in ombrotrophic peat

The As, Cd, Cu and Zn concentration profile trends at Turclossie Moss are generally consistent with those found for the previous sites (Sections 3.8.3.3.1 and 4.8.3.3.1), i.e. indicative of As, Cd and Cu immobility in ombrotrophic peat and the influence of Zn sulfide formation and precipitation at depth. Also the Se concentration profile trends were consistent with those found at the previous sites (Sections 3.8.2.2.1 and 4.8.2.1.2), i.e. indicative of Se mobility in ombrotrophic peat. Since Se and Zn appear to be mobile in this bog they will not be considered any further in this Chapter.

5.8.2.1.2 The use of Sc as an indicator of As, Cd and Cu soil dust input

The As, Cd, Cu and Sc concentration profiles in TM04M-1 and TM04CM-4 are shown in Fig. 5.38. Note the changes in scale on the As (10-fold), Cd (30-fold), Cu (6-fold) and Sc (4-fold) concentrations on going from 0-53 cm to 53-159 cm. The As/Sc, Cd/Sc and Cu/Sc ratio (A6.1 Table A9) profiles, along with the Pb/Sc ratio profile, in TM04M-1 and TM04CM-4 are shown in Fig. 5.39.

Minimum As/Sc, Cd/Sc and Cu/Sc ratios occurred between 113 and 69 cm, as for Pb/Sc (*cf.* Section 5.5.1), with mean values of 1.8 ± 0.8, 0.21 ± 0.08 and 8.2 ± 3.5, respectively (*cf.* Fig. 5.39). Comparing these As/Sc, Cd/Sc and Cu/Sc ratios with the corresponding UCC As/Sc, Cd/Sc and Cu/Sc ratios, they were 6, 14 and 4-fold higher, respectively. Maximum As/Sc (mean 7.3 ± 2.6), Cd/Sc (mean 1.3 ± 0.6) and Cu/Sc (mean 32 ± 15) ratios occurred between 67 and 51 cm (As) and 28 cm and 0 cm (Cd, Cu) (*cf.* Fig. 5.39). Note that maximum Pb/Sc ratios occurred between 30 and 14 cm (*cf.* Section 5.5.1). There is reasonably good agreement between the As/Sc, Cd/Sc and Cu/Sc ratio (A6.2 Table A8) profile trends in the TM04CM-2 sections below 14 cm with those in TM04M-1 and TM04CM-4 (Fig. 5.40).

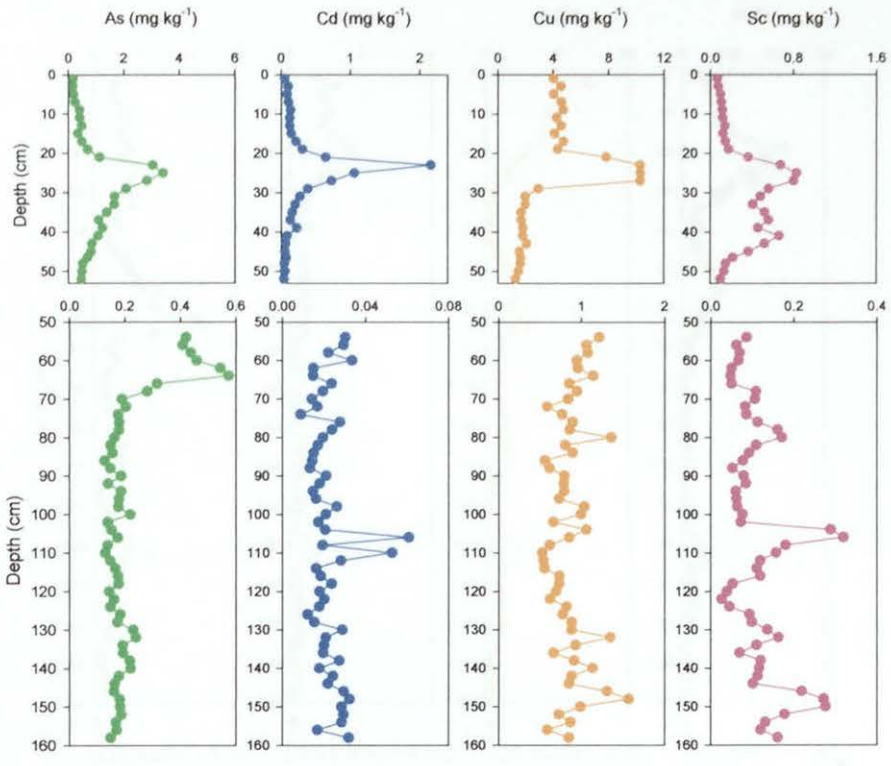

Figure 5.38: Depth profiles of As, Cd, Cu and Sc concentrations (mg kg^{-1}) from 0-53 cm and 53-159 cm in the combined TM04M-1 and TM04CM-4 peat cores.

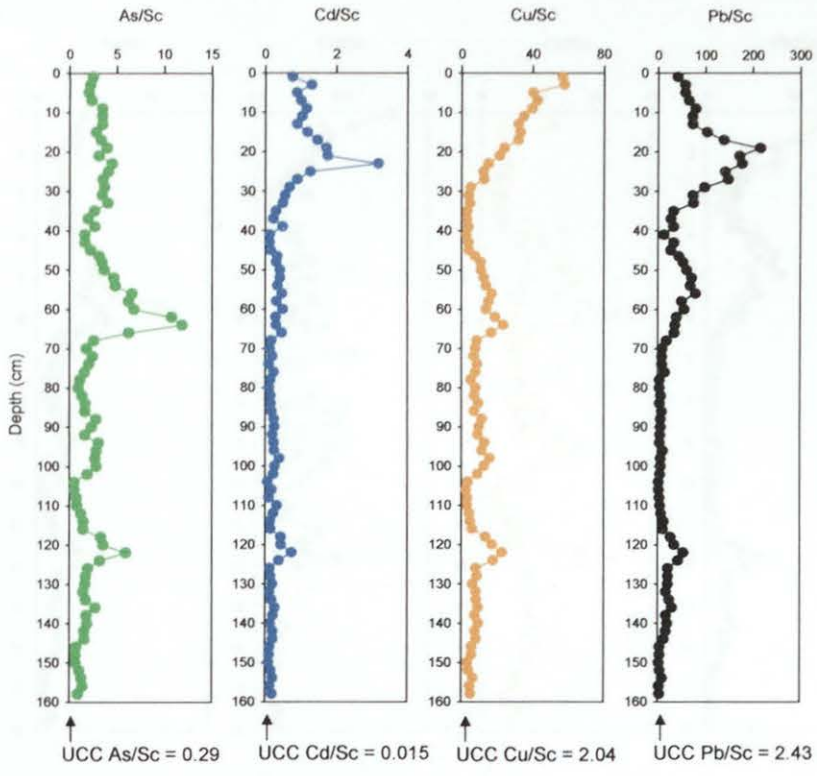

Figure 5.39: Depth profiles of As/Sc, Cd/Sc, Cu/Sc and Pb/Sc ratios in the combined TM04M-1 and TM04CM-4 (0-159 cm) peat cores.

5.8.2.1.3 Historical trends of anthropogenic As, Cd and Cu deposition

On the basis of the use of Sc as the conservative element, anthropogenic As, Cd and Cu concentrations in TM04M-1 and TM04CM-4 were calculated (A6.1 Table A10) (*cf.* Section 3.8.3.3.2) and their profiles, along with anthropogenic Pb concentrations and measured $^{206}Pb/^{207}Pb$ ratios, including age-dates, are shown in Fig. 5.41.

Pre-industrial atmospheric As, Cd and Cu sources and deposition

Between 159 and 113 cm in TM04CM-4 (*cf.* Fig. 5.41), the anthropogenic As and Cu concentrations were enhanced relative to the sections above (113 - 103 cm) with mean values of 0.15 ± 0.03 mg kg^{-1} and 0.63 ± 0.19 mg kg^{-1}, respectively. The corresponding anthropogenic Cd concentrations were not significantly enhanced (*cf.* Fig. 5.41). It seems very likely that the elevated anthropogenic As and Cu concentrations, as found for Pb (*cf.* Section 5.6.1), can be attributed to pre-Roman and Roman metallurgical activities.

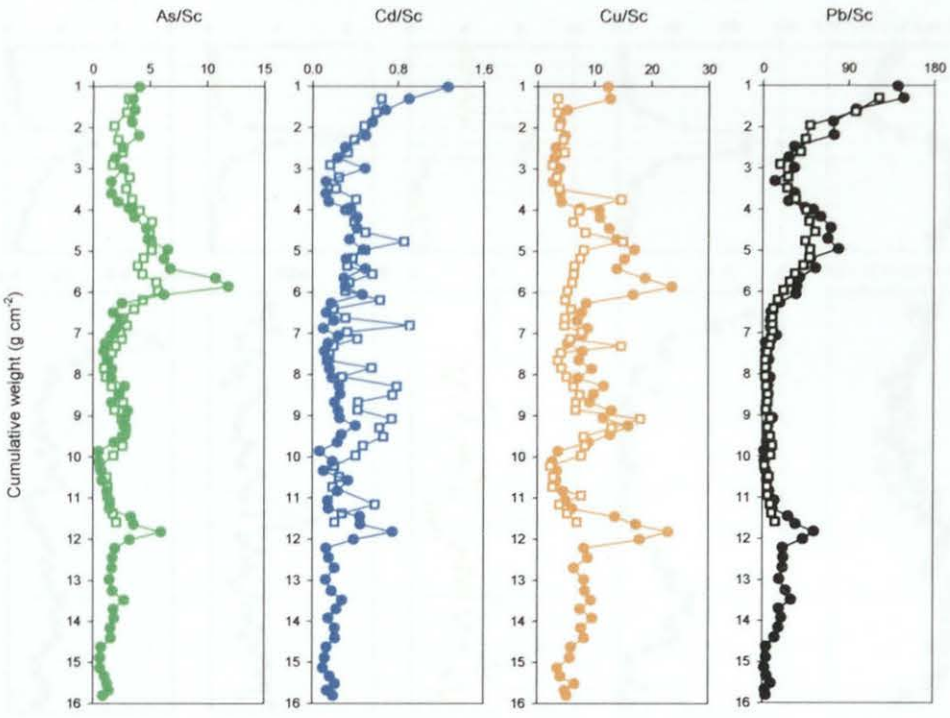

Figure 5.40: Profiles of As/Sc, Cd/Sc, Cu/Sc and Pb/Sc ratios from 24-159 cm in the combined TM04M-1 and TM04CM-4 cores (closed circles) and from 16-107 cm in the TM04CM-2 core (open squares) *versus* cumulative weight.

Between 113 and 103 cm, anthropogenic As (mean 0.087 ± 0.016 mg kg^{-1}) and Cu (mean 0.29 ± 0.11 mg kg^{-1}) concentrations were at a minimum while anthropogenic Cd concentrations exhibited peaks at 109-111 and 107-105 cm. Between 103 and 67 cm, anthropogenic As (mean 0.15 ± 0.04 mg kg^{-1}) and Cu (mean 0.64 ± 0.16 mg kg^{-1}) concentrations increased again while anthropogenic Cd concentrations (mean 0.017 ± 0.005 mg kg^{-1}) decreased (*cf.* Fig. 5.41). Above 67 cm up to a depth of 53 cm, anthropogenic As concentrations like those of Pb, increased significantly, exhibiting a peak with a maximum (0.53-0.56 mg kg^{-1}) between 65 and 61 cm. Anthropogenic Cu and Cd concentrations increased more slowly with Cu exhibiting maxima (1.0 mg kg^{-1}) at 63-65 and 55-53 cm and Cd exhibiting maxima (0.029 mg kg^{-1}) between 57 and 53 cm (*cf.* Fig. 5.41). In common with Pb (Section 5.6.2), these trends may indicate influences from metallurgical activities (e.g. mining and smelting of Pb and Cu ores) during the Mediaeval period.

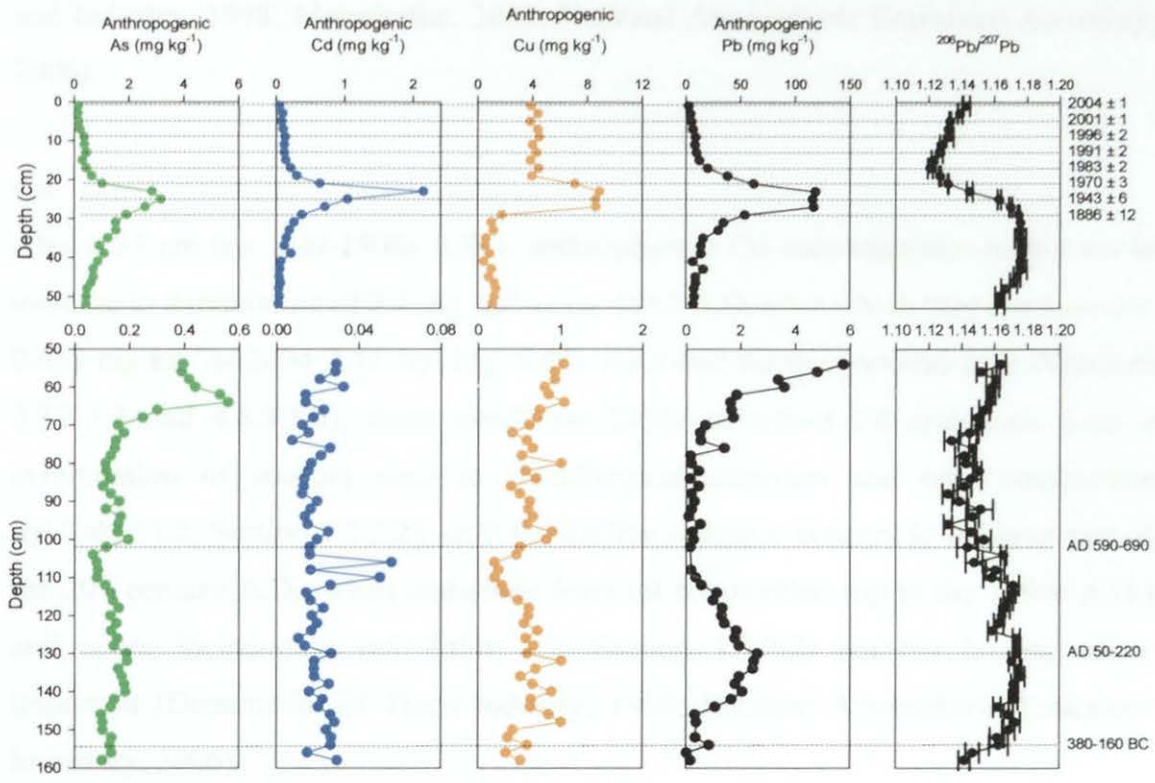

Figure 5.41: Depth profiles of anthropogenic As, Cd, Cu and Pb concentrations (mg kg^{-1}) and measured $^{206}Pb/^{207}Pb$ ratios from 0-53 cm and 53-159 cm in the combined ^{210}Pb- and ^{14}C-dated TM04M-1 and TM04CM-4 peat cores.

Industrial and post-industrial atmospheric As, Cd and Cu sources and deposition

As

Above 53 cm (*ca.* mid-1500s A.D.), anthropogenic As concentrations continued to increase to maximum values (2.6 – 3.2 mg kg^{-1}) between *ca.* 1896 and 1967 A.D., coincident with the maximum anthropogenic Pb concentrations (Section 5.6.3), after which they decreased to 0.15 – 0.16 mg kg^{-1} between *ca.* 2001 and 2004 A.D. (*cf.* Fig. 5.41). As found for the previous sites (Sections 3.8.3.3.3 and 4.8.3.3.3), these trends are consistent with As emissions from coal combustion and possibly metallurgical activities, such as Pb and Cu-Ni production (*cf.* Table 1.2, Section 1.3.2.2), until the decline in heavy industry in the later part of the 20th century A.D., when emissions from oil combustion (up to the 1990s A.D.) and waste incineration (*cf.* Table 1.2, Section 1.3.2.2) perhaps became more important (Department of Trade

and Industry, 1998; Matschullat, 2000; National Atmospheric Emissions Inventory, 2006).

Cd

Above 53 cm (*ca.* mid-1500s A.D.), anthropogenic Cd concentrations continued to increase to a maximum of 2.2 mg kg^{-1} at *ca.* 1961 A.D. after which they decreased to 0.053 mg kg^{-1} at 2004 A.D. (*cf.* Fig. 5.41). As found for the previous sites (Sections 3.8.3.3.3 and 4.8.3.3.3), these trends are likely to reflect Cd emissions from a combination of sources such as metallurgical activities and coal combustion (*cf.* Table 1.2, Section 1.3.2.2), until the decline in heavy industry in the later part of the 20th century A.D., when emissions from oil combustion (up to the 1990s A.D.) and waste incineration (*cf.* Table 1.2, Section 1.3.2.2) perhaps became more important (Department of Trade Industry, 1998; National Atmospheric Emissions Inventory, 2006).

Cu

Above 53 cm (*ca.* mid-1500s A.D.), anthropogenic Cu concentrations continued to increase to maximum values (8.6 – 8.9 mg kg^{-1}) between *ca.* 1896 and 1967 A.D., coincident with the maximum anthropogenic Pb concentrations, after which they decreased then remained fairly constant (mean 4.2 ± 0.3 mg kg^{-1}) between 1973 and 2004 A.D. (*cf.* Fig. 5.41). As found for the previous sites (Sections 3.8.3.3.3 and 4.8.3.3.3), these trends are likely to reflect Cu emissions from a combination of sources, e.g. Cu-Ni, Zn-Cd and non-ferrous metal production and coal combustion (*cf.* Table 1.2, Section 1.3.2.2), until the decline in heavy industry in the later part of the 20th century A.D., when emissions from oil combustion (up to the 1990s A.D.) and waste incineration (*cf.* Table 1.2, Section 1.3.2.2) perhaps became more important (Department of Trade and Industry, 1998; National Atmospheric Emissions Inventory, 2006). Note that, as found at the previous sites (*cf.* Sections 3.8.3.3.3 and 4.8.3.3.3), anthropogenic Cu concentrations remained relatively high, compared with As and Cd, after the late 1980s A.D. (*cf.* Fig. 5.41), perhaps providing further evidence for comparatively new recent sources of Cu e.g. automobile exhaust

and non-exhaust emissions, due to the use of Cu as an antioxidant in motor oil and its presence in new brake linings and tyres (Cadle *et al.*, 1999; Sternbeck *et al.*, 2002; Chemical Research Communications, 2003; Boulter, 2004).

5.8.2.1.4 Historical trends in depositional fluxes and inventories of anthropogenic As, Cd and Cu

Depositional fluxes were calculated for anthropogenic As, Cd and Cu in TM04M-1 (A6.1 Table A12) and plotted with those of Pb along with the measured $^{206}Pb/^{207}Pb$ ratios, *versus* ^{210}Pb-derived calendar dates since 1840 A.D. in Fig. 5.42. Depositional fluxes of anthropogenic As were at a maximum (ranging from 0.22 to 0.31 mg m^{-2} y^{-1}) between the mid-1910s and early 1960s A.D., while those of anthropogenic Cd were at a maximum (0.21 mg m^{-2} y^{-1}) during the early 1960s A.D. and those of anthropogenic Cu (ranging from 0.9 to 1.2 mg m^{-2} y^{-1}) between the late 1980s and early 2000s A.D. (*cf.* Fig. 5.40).

Total anthropogenic As, Cd and Cu inventories of 0.069, 0.015 and 0.18 g m^{-2}, respectively, for the combined TM04M-1/TM04CM-4 profile (i.e. from *ca.* 380 B.C. to 2004 A.D.) were calculated. The post-1800 A.D. As, Cd and Cu inventories (0.037, 0.011 and 0.098 g m^{-2}) (corresponding to TM04M-1 peat sections 0-36 cm) constituted 54, 73 and 54% of the total anthropogenic As, Cd and Cu inventories, respectively.

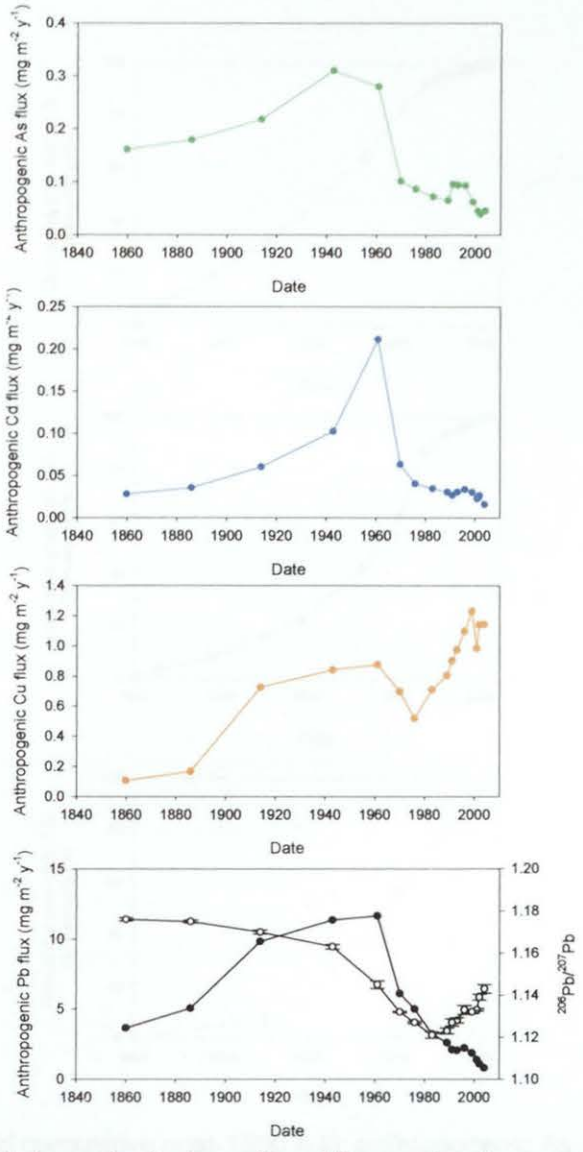

Figure 5.42: Calculated atmospheric depositional fluxes of anthropogenic As, Cd, Cu and Pb (mg m^{-2} y^{-1}) (closed circles) and the measured $^{206}Pb/^{207}Pb$ ratios (open circles) for the TM04M-1 core *versus* ^{210}Pb-derived dates since 1840 A.D.

Calculated cumulative post-1800 A.D. anthropogenic As, Cd and Cu inventories (% of total post-1800 A.D. inventory) for TM04M-1 are plotted *versus* ^{210}Pb-derived calendar dates in Fig. 5.43. Maximum As, Cd and Cu deposition occurred between the 1890s and 1960s A.D., as found for Pb (*cf.* Section 5.6.3.1).

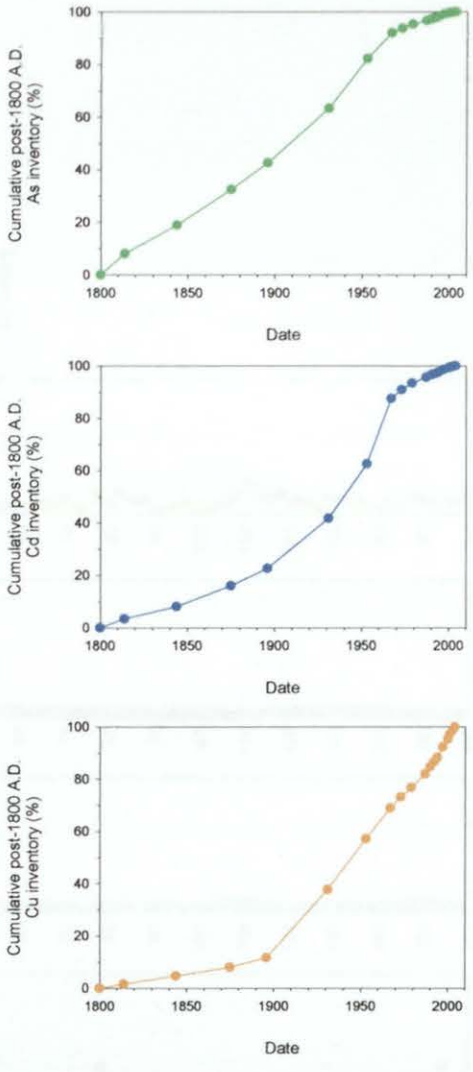

Figure 5.43: Calculated cumulative post-1800 A.D. anthropogenic As, Cd and Cu inventories (% of total post-1800 A.D. inventory) for the TM04M-1 core *versus* ^{210}Pb-derived dates. Note that dates in TM04M-1 prior to *ca.* 1844 A.D. were extrapolated.

5.8.3 Co, Cr, Ni and V

Profiles of Co, Cr, Ni and V concentrations (A6.1 Table A8) in TM04M-1 and TM04CM-4, along with Pb concentrations and ash contents, are shown in Fig. 5.44. All four elements exhibited concentration peaks in the uppermost ~ 50 cm of the cores, with the following maximum concentrations at the depths indicated:

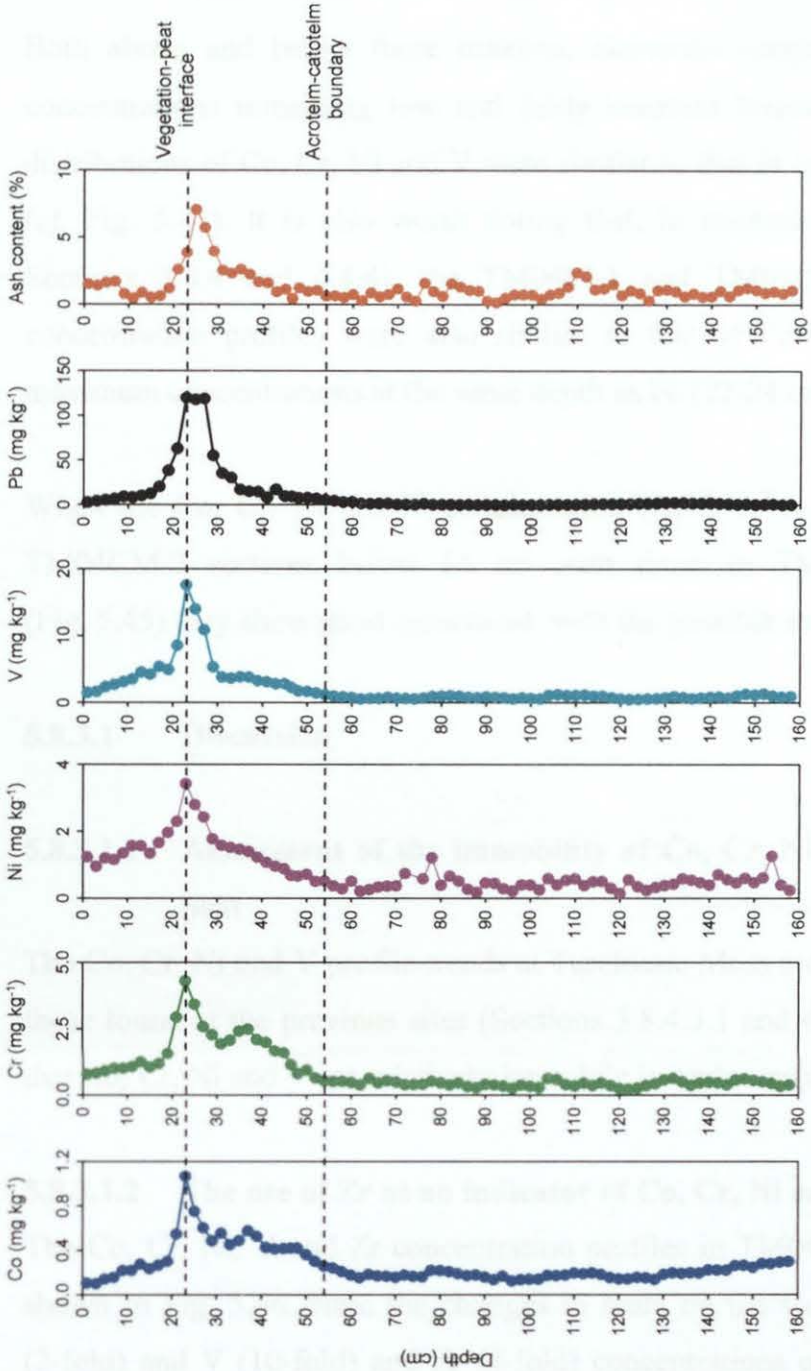

Figure 5.44: Depth profiles of Co, Cr, Ni, V and Pb concentrations (mg kg^{-1}) and ash contents (% by weight) in the combined TM04M-1 (0-47 cm) and TM04CM-4 (47-159 cm) peat cores.

- Co – 1.1 mg kg^{-1} at 22-24 cm
- Cr – 4.3 mg kg^{-1} at 22-24 cm
- Ni – 3.4 mg kg^{-1} at 22-24 cm
- V – 18 mg kg^{-1} at 22-24 cm

Both above and below these maxima, elemental concentrations decreased, with concentrations remaining low and fairly constant beneath 50 cm. In general the distributions of Co, Cr, Ni and V were similar to that of both Pb and the ash content (*cf.* Fig. 5.44). It is also worth noting that, in contrast to the previous sites (*cf.* Sections 3.8.4 and 4.8.4), the TM04M-1 and TM04CM-4 Co, Cr, Ni and V concentration profiles were also similar to that of Fe (*cf.* Fig. 5.26), exhibiting maximum concentrations at the same depth as Fe (22-24 cm).

When the Co, Cr, Ni and V concentration (A6.2 Table A7) profile trends in the TM04CM-2 sections below 14 cm with those in TM04M-1 and TM04CM-4 (Fig. 5.45) they show good agreement, with the possible exception of Co.

5.8.3.1 Discussion

5.8.3.1.1 Assessment of the immobility of Co, Cr, Ni and V in ombrotrophic peat

The Co, Cr, Ni and V profile trends at Turclossie Moss are generally consistent with those found at the previous sites (Sections 3.8.4.3.1 and 4.8.4.1.1), again indicating that Co, Cr, Ni and V are relatively immobile in ombrotrophic peat.

5.8.3.1.2 The use of Zr as an indicator of Co, Cr, Ni and V soil dust input

The Co, Cr, Ni, V and Zr concentration profiles in TM04M-1 and TM04CM-4 are shown in Fig. 5.46. Note the changes in scale on the Co (3-fold), Cr (5-fold), Ni (2-fold) and V (10-fold) and Zr (4-fold) concentrations on going from 0-53 cm to 53-159 cm in TM04M-1 and TM04CM-4.

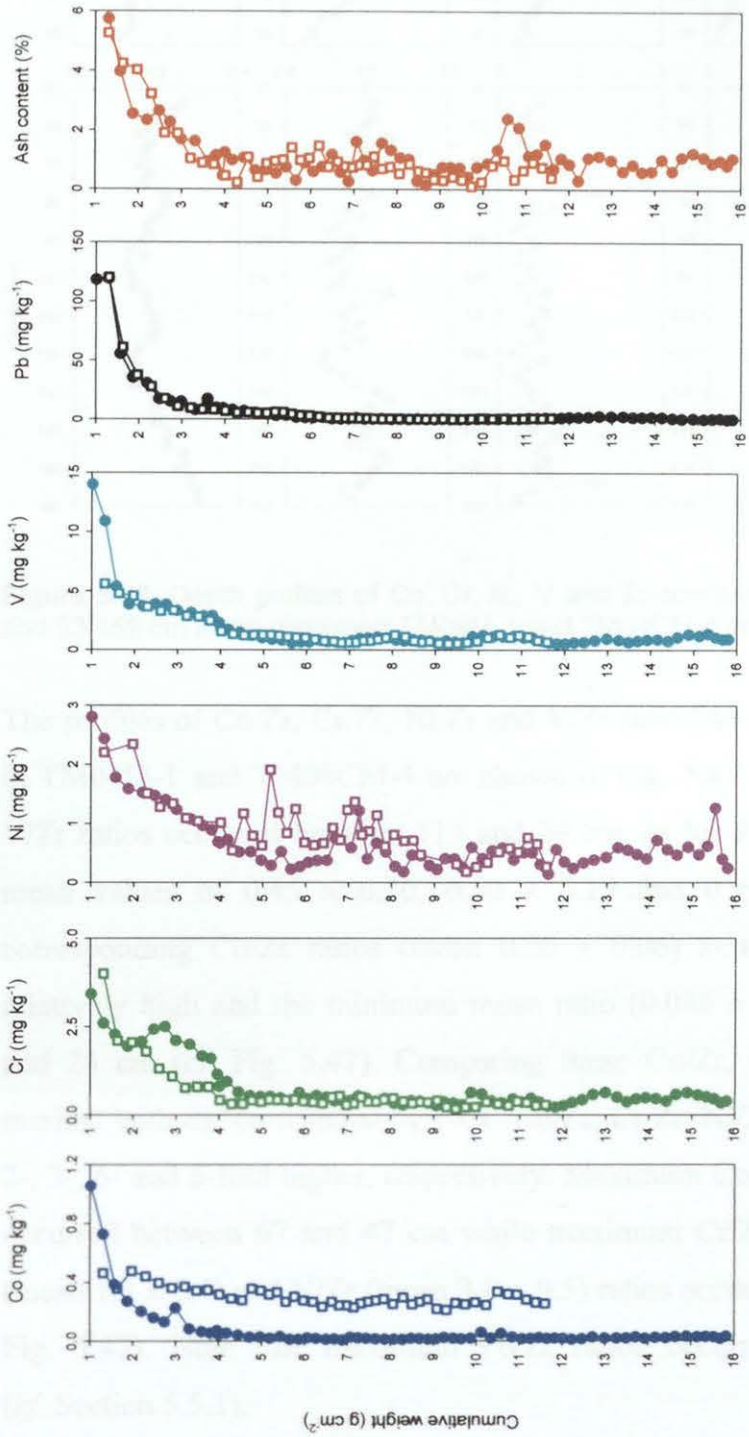

Figure 5.45: Profiles of Co, Cr, Ni, V and Pb concentration (mg kg^{-1}) and ash content (% by weight) from 24-159 cm in the combined TM04M-1 and TM04CM-4 cores (closed circles) and from 16-107 cm in the TM04CM-2 core (open squares) *versus* cumulative weight.

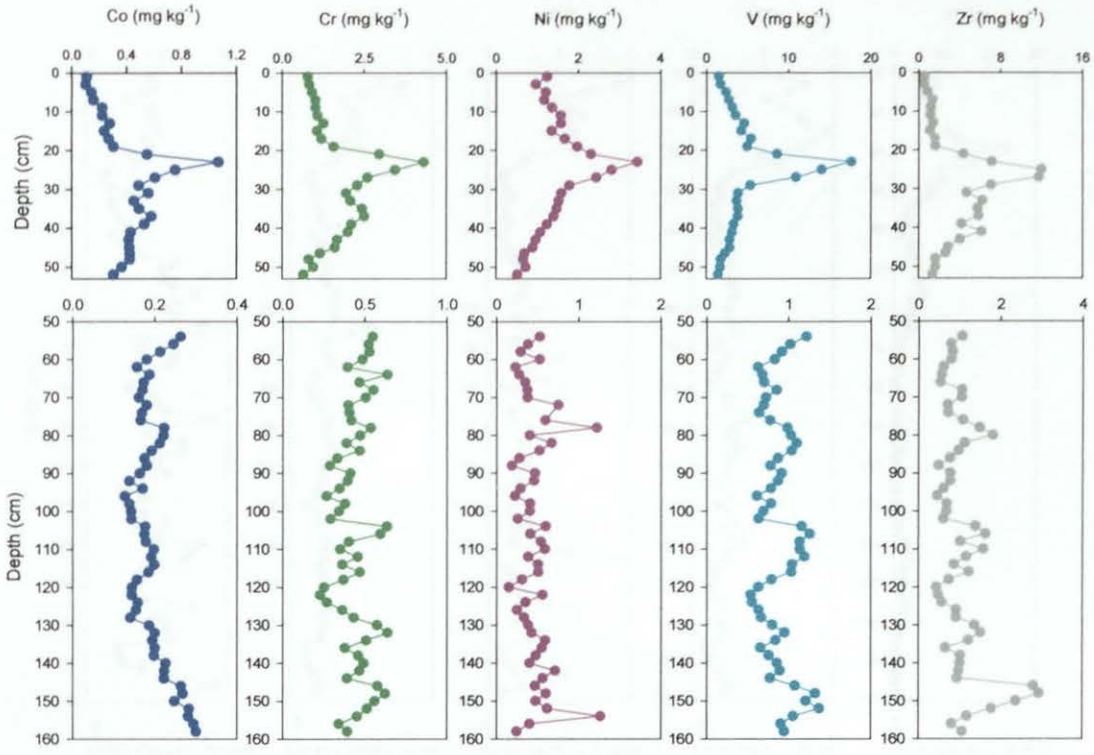

Figure 5.46: Depth profiles of Co, Cr, Ni, V and Zr concentrations (mg kg^{-1}) from 0-53 cm and 53-159 cm in the combined TM04M-1 and TM04CM-4 peat cores.

The profiles of Co/Zr, Cr/Zr, Ni/Zr and V/Zr ratio (A6.1 Table A9) and Pb/Zr ratios in TM04M-1 and TM04CM-4 are shown in Fig. 5.47. Minima in Cr/Zr, Ni/Zr and V/Zr ratios occurred between 113 and 69 cm, as for Pb/Zr (*cf.* Section 5.5.1), with mean values of 0.45 ± 0.10, 0.50 ± 0.19 and 0.99 ± 0.24, respectively. The corresponding Co/Zr ratios (mean 0.20 ± 0.06) at these depths, however, were relatively high and the minimum mean ratio (0.086 ± 0.025) occurred between 44 and 24 cm (*cf.* Fig. 5.47). Comparing these Co/Zr, Cr/Zr, Ni/Zr and V/Zr ratio minima with the corresponding UCC Co/Zr, Cr/Zr, Ni/Zr and V/Zr ratios, they were 2-, 3-, 6- and 5-fold higher, respectively. Maximum Co/Zr ratios (mean 0.26 ± 0.04) occurred between 67 and 47 cm while maximum Cr/Zr (mean 0.99 ± 0.25), Ni/Zr (mean 1.3 ± 0.4) and V/Zr (mean 3.0 ± 0.5) ratios occurred between 20 and 0 cm (*cf.* Fig. 5.47). Note that maximum Pb/Zr ratios occurred between 30 and 14 cm (*cf.* Section 5.5.1).

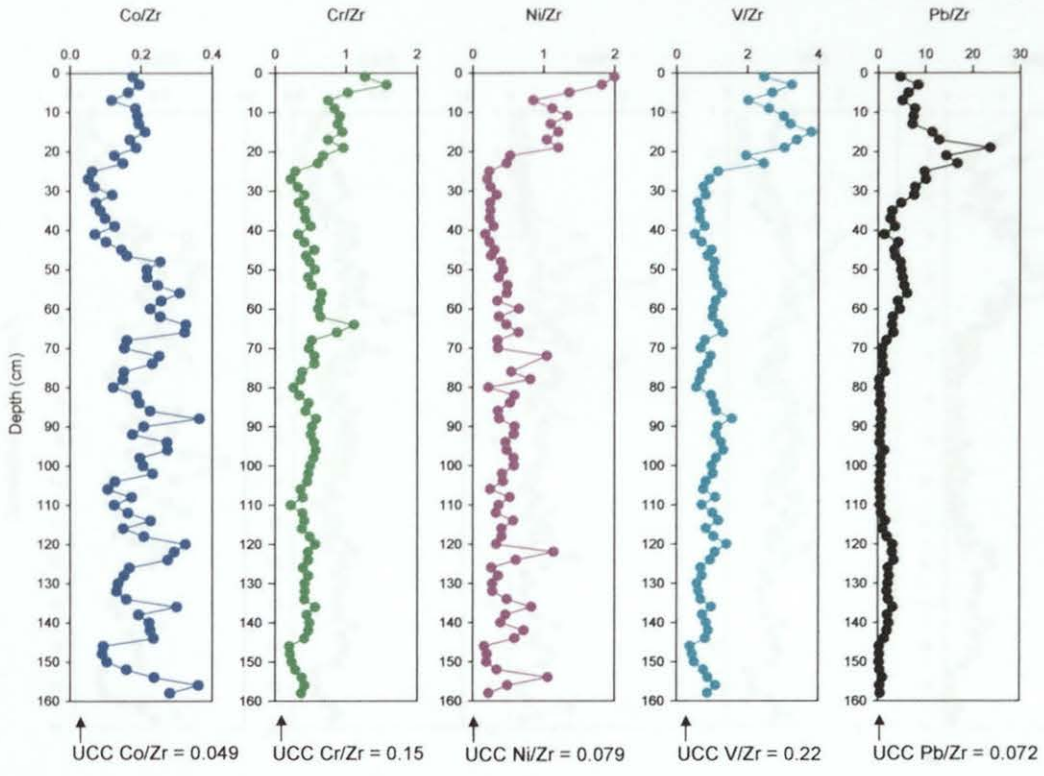

Figure 5.47: Depth profiles of Co/Zr, Cr/Zr, Ni/Zr, V/Zr and Pb/Zr ratios in the combined TM04M-1 (0-47 cm) and TM04CM-4 (47-159 cm) peat cores.

There is fairly good agreement between the Co/Zr, Cr/Zr, Ni/Zr and V/Zr ratio (A6.2 Table A8) profile trends in the TM04CM-2 sections below 14 cm with those in TM04M-1 and TM04CM-4 (Fig. 5.48).

5.8.3.1.3 Historical trends of anthropogenic Co, Cr, Ni and V deposition

On the basis of the use of Zr as the conservative element, anthropogenic Co, Cr, Ni and V concentrations in TM04M-1 and TM04CM-4 were calculated (A6.1 Table A11) (*cf.* Section 3.8.4.3.3) and their profiles, along with calculated anthropogenic Pb concentrations (A6.1 Table A11) and measured $^{206}Pb/^{207}Pb$ ratios, including age-dates are shown in Fig. 5.49.

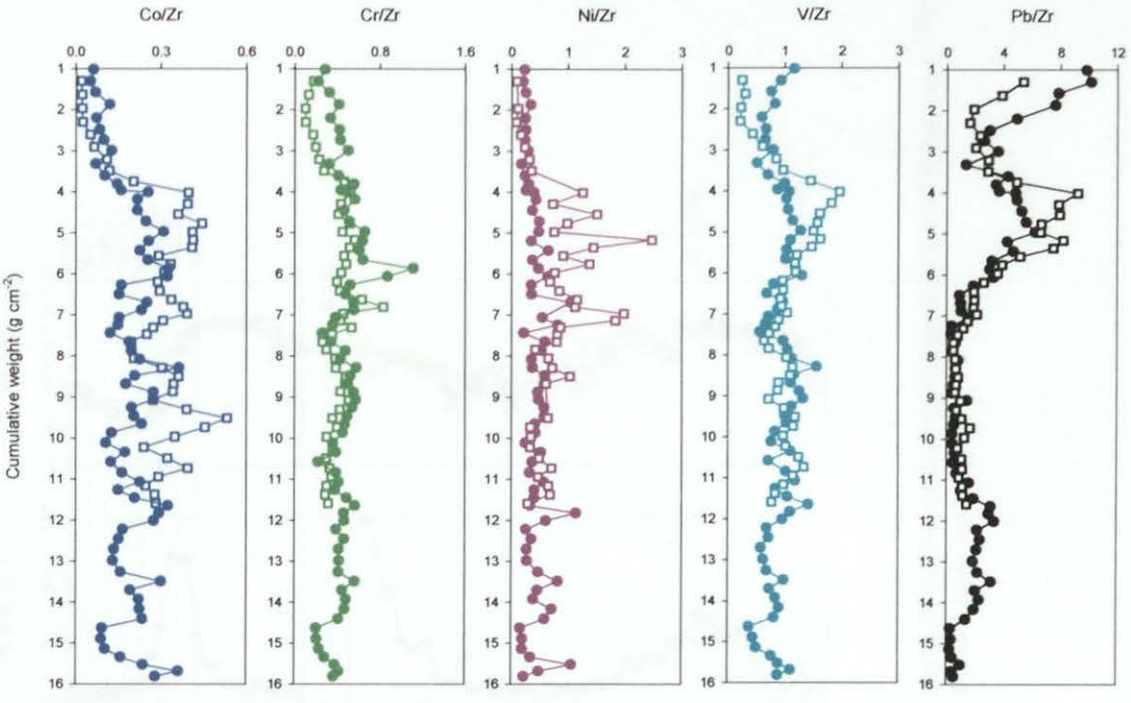

Figure 5.48: Profiles of Co/Zr, Cr/Zr, Ni/Zr, V/Zr and Pb/Zr ratios from 24-159 cm in the combined TM04M-1 and TM04CM-4 cores (closed circles) and from 16-107 cm in the TM04CM-2 core (open squares) *versus* cumulative weight.

Pre-industrial atmospheric Co, Cr, Ni and V sources and deposition

Between 159 and 151 cm in TM04CM-4, the anthropogenic Co concentrations (mean 0.23 ± 0.03 mg kg^{-1}) were enhanced relative to the sections above (151-59 cm) (mean 0.13 ± 0.02 mg kg^{-1}), above which up to 53 cm they increased again (mean 0.20 ± 0.02 mg kg^{-1}). The corresponding anthropogenic Cr concentrations were not significantly enhanced and indeed remained low and fairly constant (mean 0.28 ± 0.08 mg kg^{-1}) between 159 and 53 cm (*cf.* Fig. 5.49). The anthropogenic Ni concentrations (with the exception of peaks of ~ 1 mg kg^{-1} at 153-155 cm and 77-79 cm) also remained low and fairly constant (range 0.12 – 0.70 mg kg^{-1}) between 159 and 53 cm. The anthropogenic V concentrations exhibited a small peak (0.98 mg kg^{-1}) at 151-153 cm, and were enhanced, relative to the minima (0.55 ± 0.09 mg kg^{-1}) in sections 151 - 117 cm, between 117 and 103 cm (mean 0.86 ± 0.06 mg kg^{-1}), 85 and 81 cm (~ 0.8 mg kg^{-1}) and 55 and 53 cm (~ 1 mg kg^{-1}).

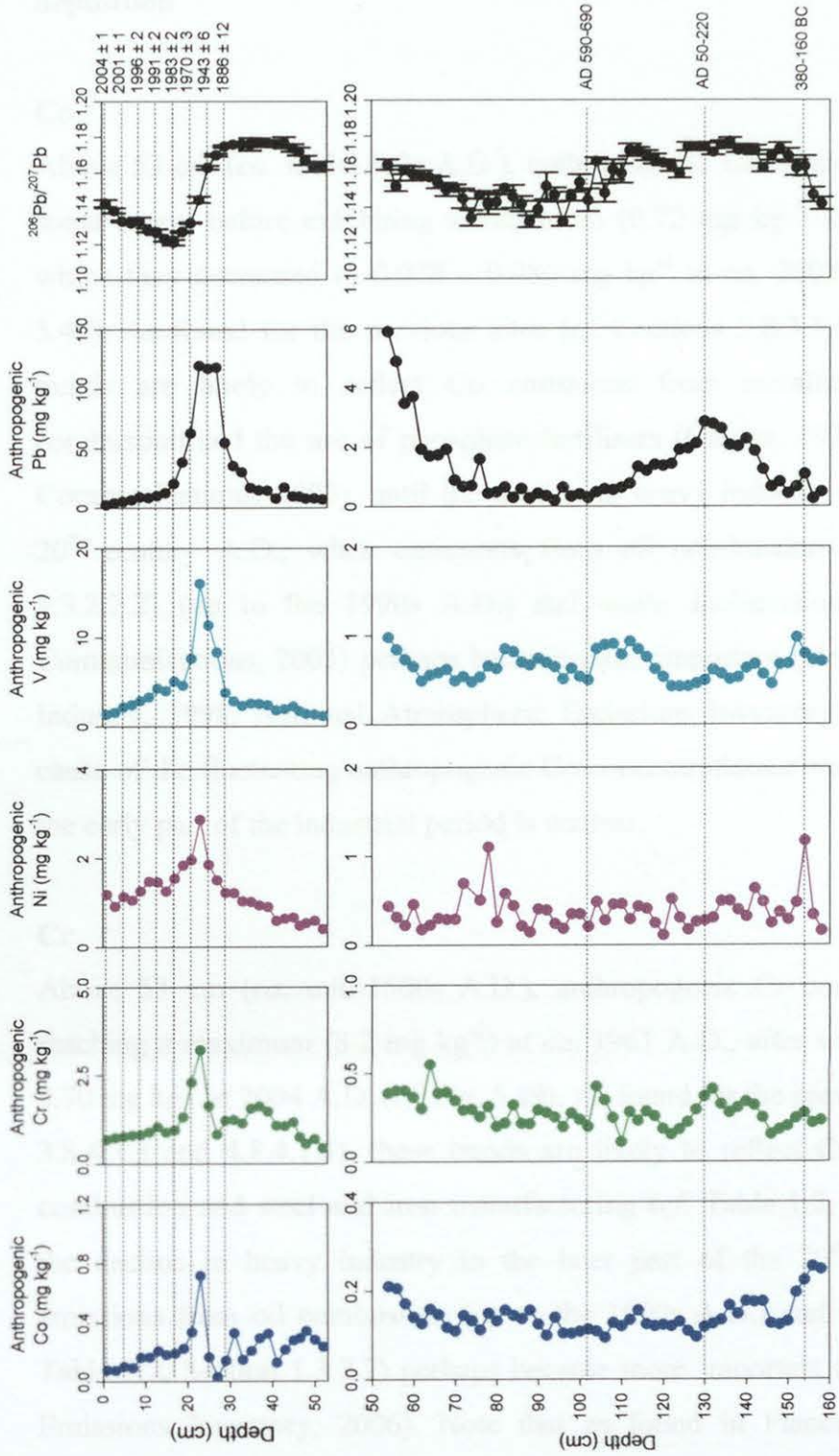

Figure 5.49: Depth profiles of anthropogenic Co, Cr, Ni, V and Pb concentrations (calculated using Zr as the conservative element) and measured $^{206}Pb/^{207}Pb$ ratios, from 0-53 cm and 53-159 cm in the combined ^{210}Pb- and ^{14}C-dated TM04M-1 and TM04CM-4 peat core.

The source of these Co, Ni and V concentration enhancements is unclear (*cf.* Fig. 5.49).

Industrial and post-industrial atmospheric Co, Cr, Ni and V sources and deposition

Co

Above 53 cm (*ca.* mid-1500s A.D.), anthropogenic Co concentrations fluctuated to some extent before exhibiting a maximum (0.72 mg kg^{-1}) at *ca.* 1961 A.D., after which they decreased to 0.078 – 0.080 mg kg^{-1} at *ca.* 2002 - 2004 A.D. (*cf.* Fig. 5.49). As found for the previous sites (*cf.* Sections 3.8.3.3.3 and 4.8.4.1.3), these trends are likely to reflect Co emissions from metallurgical activities, coal combustion and the use of phosphate fertilisers (Oehme, 1979; Chemical Research Communications, 2003), until the decline in heavy industry in the later part of the 20^{th} century A.D., when emissions from oil combustion (*cf.* Fig. 1.3, Section 1.3.2.2.2) (up to the 1990s A.D.) and waste incineration (Chemical Research Communications, 2003) perhaps became more important (Department of Trade and Industry, 1998; National Atmospheric Emissions Inventory, 2006). Note that the cause of the fluctuating anthropogenic Co concentrations observed at this site during the early part of the industrial period is unclear.

Cr

Above 53 cm (*ca.* mid-1500s A.D.), anthropogenic Cr concentrations increased, reaching a maximum (3.2 mg kg^{-1}) at *ca.* 1961 A.D., after which they decreased to 0.70 mg kg^{-1} at 2004 A.D. (*cf.* Fig. 5.49). As found for the previous sites (*cf.* Sections 3.8.4.3.3 and 4.8.4.1.3), these trends are likely to reflect Cr emissions from coal combustion and steel and iron manufacturing (*cf.* Table 1.2, Section 1.3.2.2), until the decline in heavy industry in the later part of the 20^{th} century A.D., when emissions from oil combustion (up to the 1990s A.D.) and waste incineration (*cf.* Table 1.2, Section 1.3.2.2) perhaps became more important (National Atmospheric Emissions Inventory, 2006). Note that as found in Flanders Moss (*cf.* Section

3.8.4.3.3), the anthropogenic Cr concentrations remained fairly constant after the late 1980s A.D. (*cf.* Fig. 5.49), perhaps providing further evidence for comparatively new sources of Cr emissions (e.g. automotive brake linings) (Boulter, 2004).

Ni

Above 53 cm (*ca.* mid-1500s A.D.), anthropogenic Ni concentrations increased, reaching a maximum (2.9 mg kg^{-1}) at *ca.* 1961 A.D., after which they decreased to 0.92 – 1.2 mg kg^{-1} between *ca.* 1999 and 2004 A.D. (*cf.* Fig. 5.49). As found for the previous sites (*cf.* Sections 3.8.4.3.3 and 4.8.4.1.3), these trends are likely to reflect Ni emissions from Cu-Ni production and coal combustion (*cf.* Table 1.2, Section 1.3.2.2), until the decline in heavy industry in the later part of the 20^{th} century A.D., when emissions from oil combustion (up to the 1990s A.D.) and waste incineration (*cf.* Table 1.2, Section 1.3.2.2) perhaps became more important (National Atmospheric Emissions Inventory, 2006). It is worth noting that in contrast to findings at Flanders Moss and The Red Moss of Balerno, anthropogenic Ni concentrations remained relatively high, compared with Co, Cr and V, after the late 1980s A.D., perhaps indicating emissions of Ni from comparatively new recent sources (i.e. not oil combustion or waste incineration). One such source could include the release of Ni from new automotive brake linings (Boulter, 2004).

V

Above 53 cm (*ca.* mid-1500s A.D.), anthropogenic V concentrations increased, reaching a maximum (16 mg kg^{-1}) at *ca.* 1961 A.D., after which they decreased to 1.4 – 1.6 mg kg^{-1} at *ca.* 2002 - 2004 A.D. (*cf.* Fig. 5.49). As found for the previous sites (*cf.* Sections 3.8.4.3.3 and 4.8.4.1.3), these trends are likely to reflect the pattern of V emissions from coal combustion (*cf.* Table 1.2, Section 1.3.2.2), until the decline in heavy industry in the later part of the 20^{th} century A.D., when emissions from oil combustion (up to the 1990s A.D.) perhaps became more important (Department of Trade and Industry, 1998; National Atmospheric Emissions Inventory, 2006).

5.8.3.1.4 Historical trends in depositional fluxes and inventories of anthropogenic Co, Cr, Ni and V

The anthropogenic depositional fluxes of Co, Cr, Ni and V in TM04M-1 (A6.1 Table A12) were calculated, along with the anthropogenic depositional fluxes of Pb, using Zr (*cf.* Sections 3.8.4.3.3 and 4.8.4.1.4). These fluxes, since 1840 A.D. are plotted along with the measured $^{206}Pb/^{207}Pb$ ratios, *versus* ^{210}Pb-derived calendar dates, in Fig. 5.50. The maximum depositional fluxes of anthropogenic Co, Cr, and V, 0.071, 0.32 and 1.6 mg m^{-2} y^{-1}, respectively, occurred during the early 1960s A.D., while maximum anthropogenic Ni fluxes (0.30 – 0.36 mg m^{-2} y^{-1}) occurred between the early 1990s and early 2000s A.D (*cf.* Fig. 5.50).

Total anthropogenic Co, Cr, Ni and V inventories of 0.024, 0.078, 0.083 and 0.23 g m^{-2}, respectively, were calculated for the combined TM04M-1/TM04CM-4 profile. The post-1800 A.D. Co, Cr, Ni and V inventories (0.0049, 0.030, 0.034 and 0.13 g m^{-2}) (corresponding to TM04M-1 peat sections 0-36 cm) constituted 20, 38, 41 and 57% of the total anthropogenic Co, Cr, Ni and V inventories, respectively. The low post-1800 Co, Cr and Ni inventory proportions of the total anthropogenic inventories, relative to those exhibited for the other anthropogenic elements, As, Cd, Cu, Pb, Sb and V (range 54 - 83%) at this site, could perhaps indicate that anthropogenic emissions of these three elements in recent years have not increased as markedly.

Calculated cumulative post-1800 A.D. anthropogenic Co, Cr, Ni and V inventories (% of total post-1800 A.D. inventory) for TM04M-1 are plotted *versus* ^{210}Pb-derived calendar dates in Fig. 5.51. Maximum Co, Cr, Ni and V deposition occurred between the 1950s and 2000s A.D., 1930s and 1960s A.D., 1930s and 2000s A.D. and 1890s and 1960s A.D., respectively. These trends are broadly in agreement, perhaps with the exception of Co and Ni, with that found for Pb (*cf.* Section 5.6.3.1).

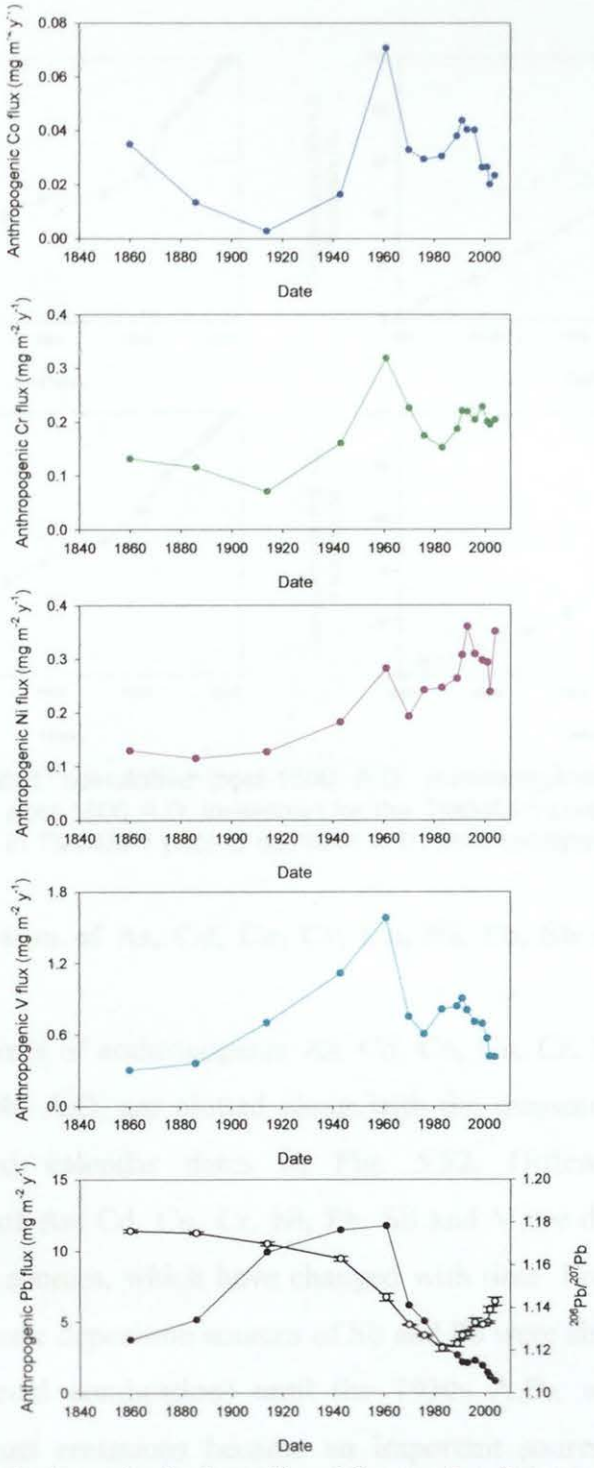

Figure 5.50: Calculated atmospheric depositional fluxes of anthropogenic Co, Cr, Ni, V and Pb (mg m^{-2} y^{-1}) (closed circles) and the measured $^{206}Pb/^{207}Pb$ ratios (open circles) for the TM04M-1 core *versus* ^{210}Pb-derived dates since 1840 A.D.

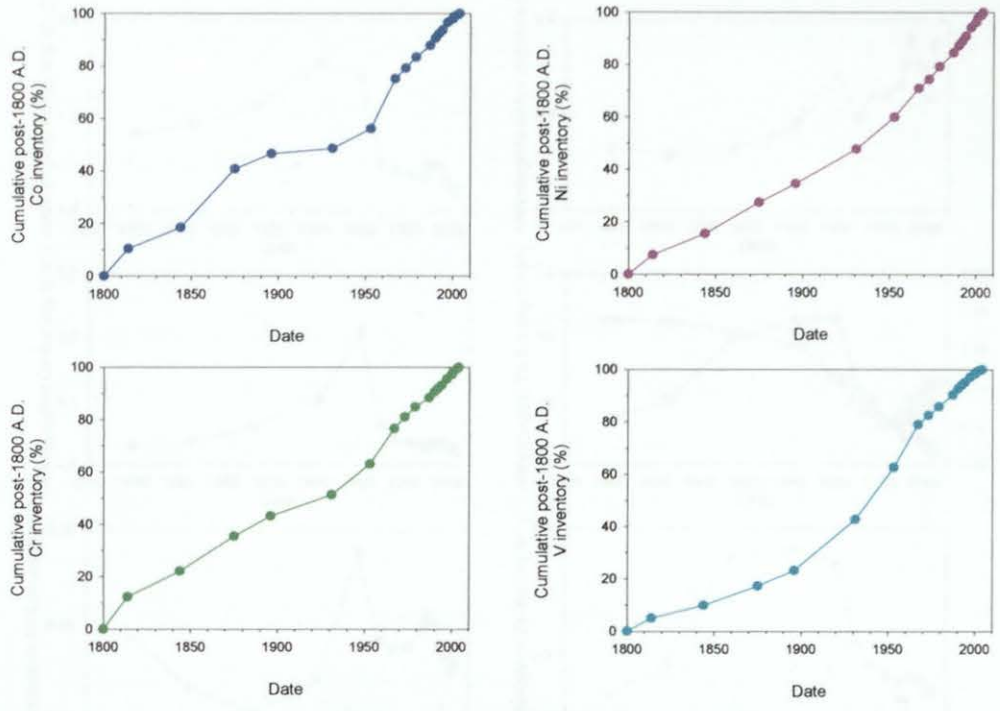

Figure 5.51: Calculated cumulative post-1800 A.D. anthropogenic Co, Cr, Ni and V inventories (% of total post-1800 A.D. inventory) for the TM04M-1 core *versus* ^{210}Pb-derived dates. Note that dates in TM04M-1 prior to *ca.* 1844 A.D. were extrapolated.

5.8.4 Comparison of As, Cd, Co, Cr, Cu, Ni, Pb, Sb and V depositional fluxes

The depositional fluxes of anthropogenic As, Cd, Co, Cu, Cr, Ni, Pb, Sb and V in TM04M-1 since 1840 A.D. are plotted along with the measured ^{206}Pb/^{207}Pb ratios *versus* ^{210}Pb-derived calendar dates in Fig. 5.52. Differences between the depositional fluxes of As, Cd, Co, Cr, Ni, Pb. Sb and V are due to differences in inputs from various sources, which have changed with time. For example, since *ca.* 1840 A.D., atmospheric deposition sources of Sb and Pb were similar (Pb ore mining and smelting and coal combustion) until the 1930s A.D., when Australian-Pb-influenced car-exhaust emissions became an important source of Pb deposition. Unfortunately, in the case of some of the elements (e.g. Co, Cr, Cu and Ni), the extent to which various different sources (e.g. metallurgical activities, coal and oil combustion, use of phosphate fertilisers, waste incineration and automotive brake linings) have influenced their atmospheric depositional flux patterns is less clear.

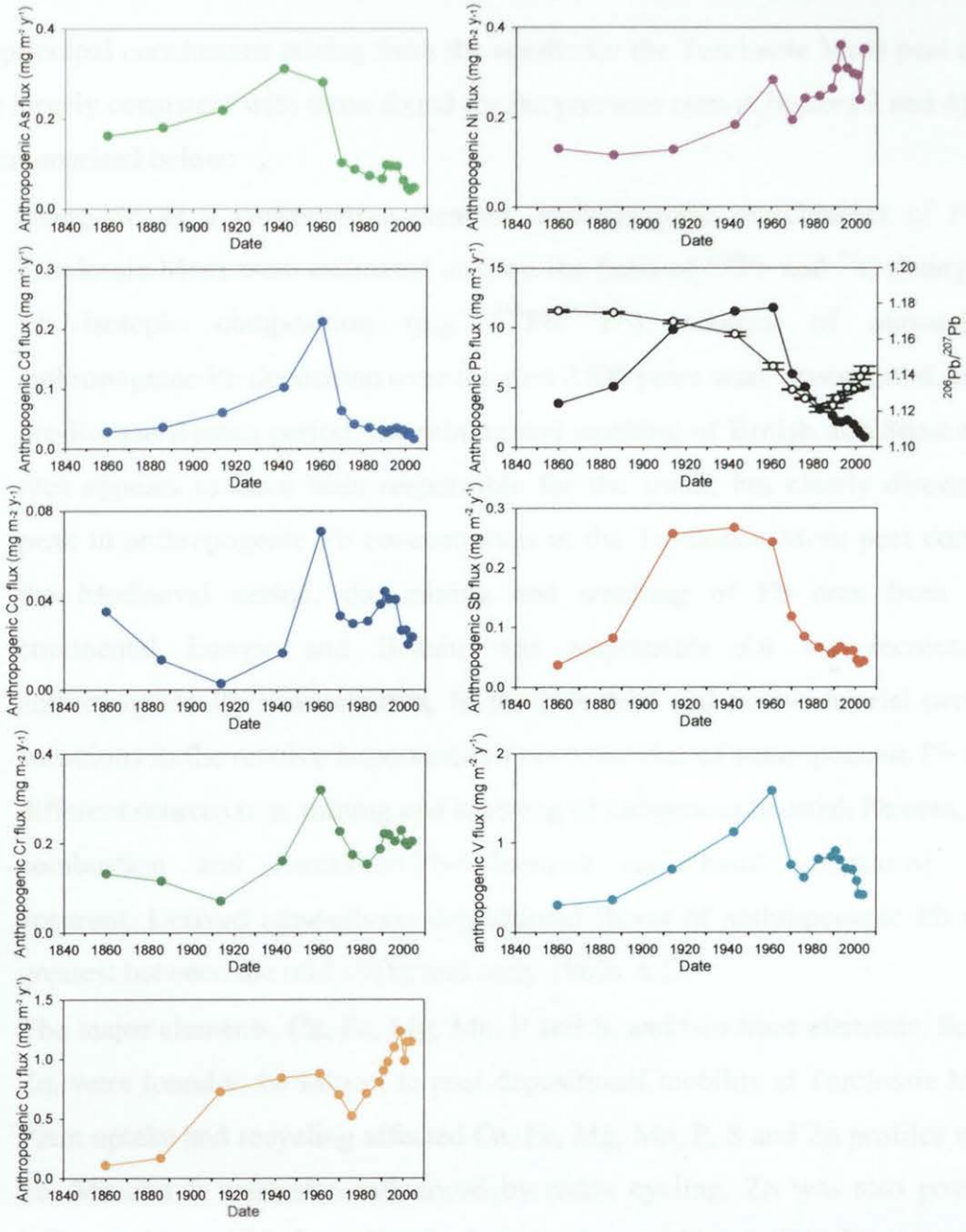

Figure 5.52: Calculated atmospheric depositional fluxes of anthropogenic As, Cd, Co, Cr, Cu, Ni, Pb, Sb and V (mg m^{-2} y^{-1}) and measured $^{206}Pb/^{207}Pb$ ratios for TM04M-1 *versus* ^{210}Pb-derived dates since 1840 A.D.

5.9 CONCLUSIONS

The principal conclusions arising from the results for the Turclossie Moss peat cores were largely consistent with those found for the previous sites (Chapters 3 and 4) and are summarised below:

- Using Sc as a conservative element, anthropogenic enrichments of Pb at Turclossie Moss were estimated and, on the basis of ^{210}Pb and ^{14}C dating and Pb isotopic composition (e.g. $^{206}Pb/^{207}Pb$), sources of atmospheric anthropogenic Pb deposition over the past 2500 years were investigated. In the pre-Roman/Roman period, the mining and smelting of British and Spanish Pb ores appears to have been responsible for the small, but clearly discernible peak in anthropogenic Pb concentration in the Turclossie Moss peat core. In the Mediaeval period, the mining and smelting of Pb ores from both continental Europe and Britain was responsible for the increase in anthropogenic Pb concentration. In the industrial and post-industrial periods, variations in the relative importance of contributions of anthropogenic Pb from different sources (e.g. mining and smelting of indigenous Scottish Pb ores, coal combustion and Australian-Pb-influenced car-exhaust emissions) were apparent. Derived atmospheric depositional fluxes of anthropogenic Pb were greatest between the mid 1910s and early 1960s A.D.
- The major elements, Ca, Fe, Mg, Mn, P and S, and two trace elements, Se and Zn, were found to be subject to post-depositional mobility at Turclossie Moss. Plant uptake and recycling affected Ca, Fe, Mg, Mn, P, S and Zn profiles while Fe, Mn and P were also influenced by redox cycling. Zn was also possibly influenced by sulfide formation in the catotelm peat layers of the bog.
- The general similarity between the Pb concentration profiles and those of the trace elements As, Cd, Co, Cr, Cu, Ni, Sb and V at Turclossie Moss suggested that these latter elements were also essentially immobile in ombrotrophic peat.
- The Sb and Pb concentration profiles at Turclossie Moss were remarkably similar. Using Sc as a conservative element, anthropogenic enrichments of Sb were estimated and on the basis of anthropogenic Sb/Pb ratios, sources of

atmospheric anthropogenic Sb deposition were investigated. During the pre-Roman/Roman and Mediaeval periods, sources of anthropogenic Sb deposition were the same as those found for Pb, and this was also the case during the Industrial period, with the exception of leaded petrol. In the post-industrial period, the influence of anthropogenic inputs of Sb from comparatively new recent sources (e.g. automotive brake linings) was apparent. Derived atmospheric depositional fluxes of anthropogenic Sb were greatest between the mid 1910s and early 1960s A.D.

- Anthropogenic As, Cd and Cu concentrations were estimated using Sc as a conservative element. In the pre-Roman/Roman period anthropogenic As and Cu concentrations were enhanced. In the Mediaeval period, the mining and smelting of Pb and Cu ores is likely to have been responsible for the anthropogenic As, Cd and Cu concentration increases. In the industrial and post-industrial periods, sources of As, Cd and Cu were attributed to a variety of sources (e.g. metallurgical activities, coal and oil combustion and waste incineration). Also, there may have been inputs of Cu from comparatively new recent anthropogenic sources (e.g. automobile exhaust and non-exhaust emissions, due to the use of Cu as an antioxidant in motor oil and its presence in new brake linings and tyres). Derived atmospheric depositional fluxes of anthropogenic As, Cd and Cu were greatest between the mid-1910s and early 1960s A.D., during the early 1960s A.D. and between the late 1980s and early 2000s A.D., respectively.
- Anthropogenic Co, Cr, Ni and V concentrations were estimated using Zr as a conservative element. In the pre-Roman/Roman and Mediaeval periods, anthropogenic Co, Ni and V concentrations were enhanced but the sources of these increases were unclear. In the industrial and post-industrial periods, sources of Co, Cr, Ni and V were attributable to a variety of sources (e.g. metallurgical activities, coal and oil combustion, use of phosphate fertilisers and waste incineration). Also, there may have been inputs of Cr and Ni from comparatively new recent anthropogenic source (e.g. automotive brake linings). Derived atmospheric depositional fluxes of anthropogenic Co, Cr and

V were greatest during the early 1960s A.D and those of Ni were greatest between the early 1990s and early 2000s A.D.

6 CARSEGOWAN MOSS

This chapter contains the results for the Carsegowan Moss peat cores, which will be treated in a similar way to the results for the peat cores from the previous sites (Chapters 3, 4 and 5).

6.1 PEAT MATRIX PROPERTIES AND EVALUATION OF TROPHIC STATUS

6.1.1 Visual observations

Visual observation depth profiles for Carsegowan Moss peat cores, CM04CM-1 and CM04M, are shown in Fig. 6.1. For CM03M, only sectional material from the upper 32 cm was used in this research project.

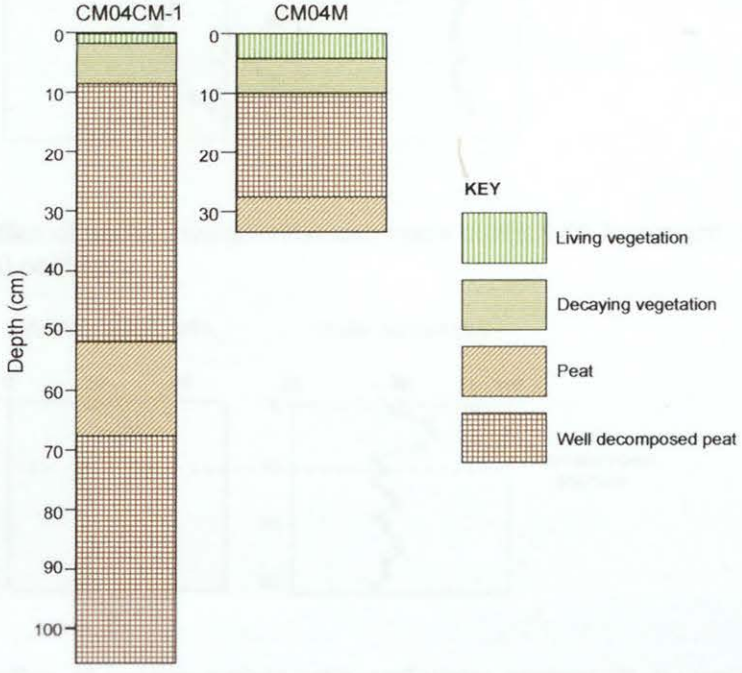

Figure 6.1: Visual observation depth profiles for CM04CM-1 and CM04M.

6.1.2 Wet/dry weight ratios and water contents

Wet and dry weights, wet/dry weight ratios, water contents and residual moisture contents for CM04CM-1 and CM04M are tabulated in Appendix A7.1 Table A1 and

A7.2 Table A1, respectively. The wet/dry weight ratio and water content profiles for CM04CM-1 and CM04M are shown in Figs. 6.2 and 6.3, respectively.

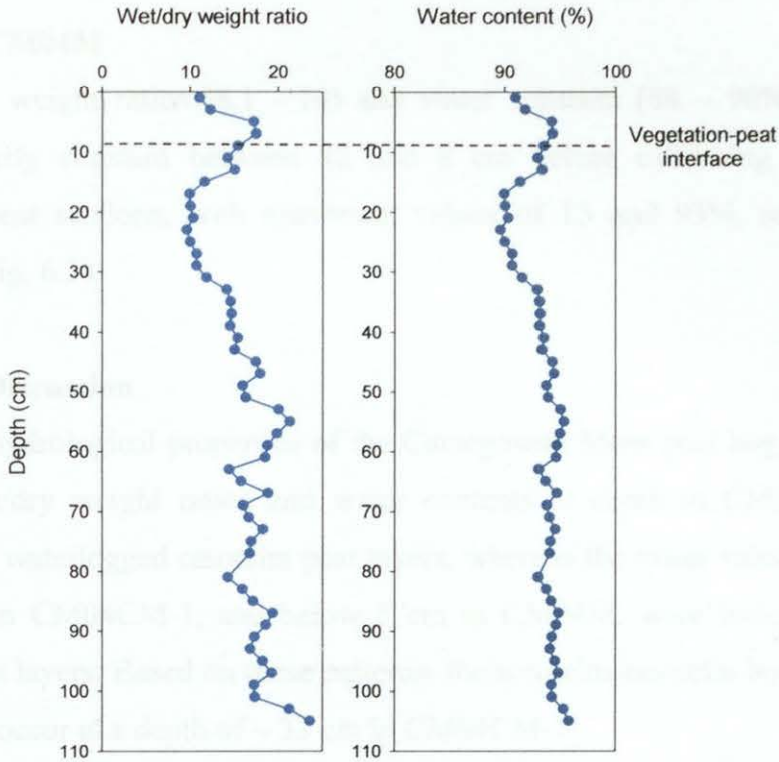

Figure 6.2: Depth profiles of wet/dry weight ratio and water content (% by weight) in the CM04CM-1 (0-106 cm) peat core.

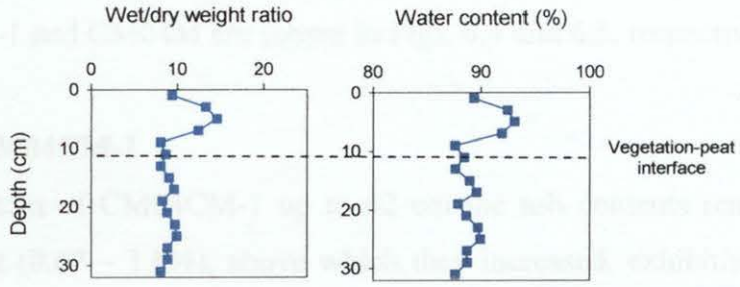

Figure 6.3: Depth profiles of wet/dry weight ratio and water content (% by weight) in the CM04M (0-32 cm) peat core.

6.1.2.1 CM04CM-1

From the bottom of CM04CM-1 up to 32 cm, wet/dry weight ratios (14 – 24) and water contents (93 – 96%) were fairly constant. Thereafter, they declined, exhibiting minimum values (~ 10 and ~ 90%, respectively) between 26 and 16 cm, before

increasing again and exhibiting broad peaks in the uppermost peat sections (*cf.* Fig. 6.2).

6.1.2.2 CM04M

The wet/dry weight ratios (8.1 - 10) and water contents (88 – 90%) in CM04M remained fairly constant between 32 and 8 cm before exhibiting peaks in the uppermost peat sections, with maximum values of 15 and 93%, respectively, at 4-6 cm (*cf.* Fig. 6.3).

6.1.2.3 Discussion

In terms of hydrological properties of the Carsegowan Moss peat bog, the high and constant wet/dry weight ratios and water contents at depth in CM04CM-1 were indicative of waterlogged catotelm peat layers, whereas the lower values between 14 and 32 cm in CM04CM-1, and below 8 cm in CM04M, were indicative of drier acrotelm peat layers. Based on these patterns, the acrotelm-catotelm boundary can be estimated to occur at a depth of ~ 33 cm in CM04CM-1.

6.1.3 Ash contents and Ca/Mg ratios

The profiles of ash contents and Ca/Mg ratios (A7.1 Table A2 and A7.2 Table A2), for CM04CM-1 and CM04M are shown in Figs. 6.4 and 6.5, respectively.

6.1.3.1 CM04CM-1

From the bottom of CM04CM-1 up to 42 cm the ash contents remained low and fairly constant (0.67 – 1.8%), above which they increased, exhibiting a broad peak between 42 and 12 cm with a maximum of 2.8% at 22-24 cm, before decreasing towards the surface. From the bottom of CM04CM-1 up to 6 cm the Ca/Mg ratios remained fairly constant (0.88 – 1.4), before peaking in the uppermost sections (maximum 3.3 at 2-4 cm) (*cf.* Fig. 6.4).

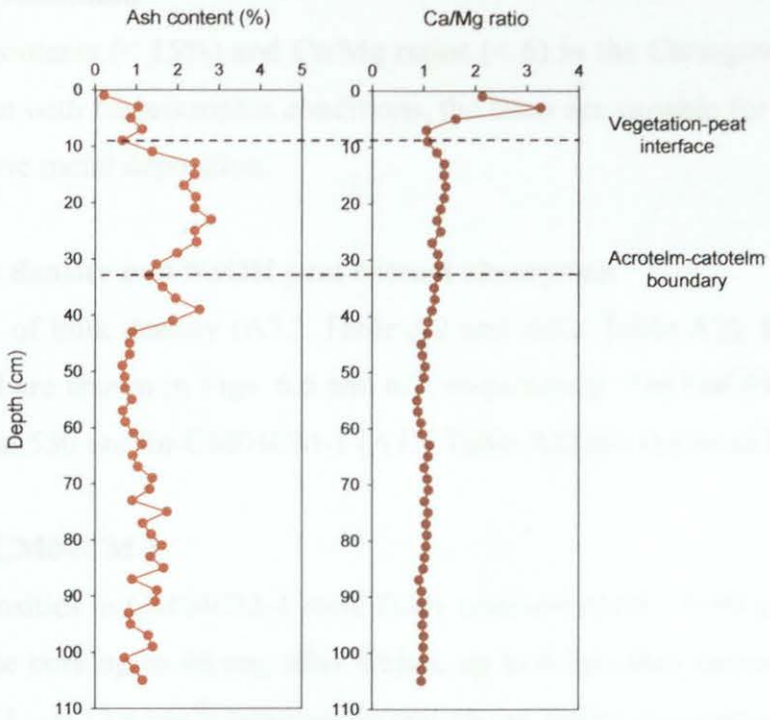

Figure 6.4: Depth profiles of ash content (% by weight) and Ca/Mg ratios in the CM04CM-1 (0-106 cm) peat core.

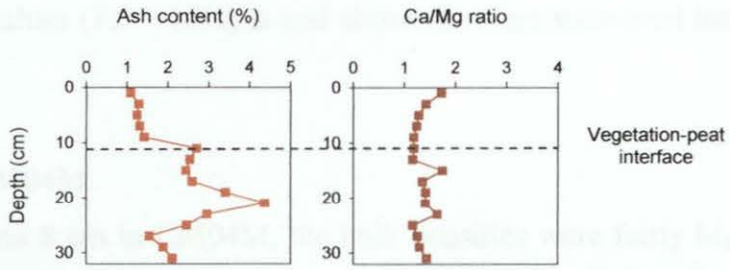

Figure 6.5: Depth profiles of ash content (% by weight) and Ca/Mg ratios in the CM04M (0-32 cm) peat core.

6.1.3.2 CM04M

A prominent peak in the CM04M ash content occurred between 26 and 10 cm, with a maximum of 4.4% at 20-22 cm. Ca/Mg ratio maxima (1.4 – 1.8) occurred between 24 and 14 cm, above and below which they were fairly constant with the exception of a gradual increase towards the surface in the uppermost 6 cm (*cf.* Fig. 6.5).

6.1.3.3 Discussion

As the ash contents (< 15%) and Ca/Mg ratios (< 6) in the Carsegowan Moss cores are consistent with ombrotrophic conditions, the latter are suitable for use as archives of atmospheric metal deposition.

6.1.4 Bulk density and NaOH peat extract absorption

The profiles of bulk density (A7.1 Table A2 and A7.2 Table A2), for CM04CM-1 and CM04M are shown in Figs. 6.6 and 6.7, respectively. The NaOH peat extract % absorptions at 550 nm for CM04CM-1 (A7.1 Table A2) are shown in Fig 6.6.

6.1.4.1 CM04CM-1

The bulk densities in CM04CM-1 were fairly constant (0.05 – 0.09 g cm^{-3}) from the bottom of the core up to 46 cm, after which, up to 4 cm, they increased, exhibiting maxima (0.11 – 0.13 g cm^{-3}) between 30 and 16 cm before decreasing to a minimum at the surface (*cf.* Fig. 6.6). The NaOH peat extract absorptions in CM04CM-1 fluctuated greatly, ranging from 17 to 45% between 106 and 10 cm before decreasing to minimum values (7.5 – 18%) at and above the vegetation-peat interface (8-10 cm) (*cf.* Fig. 6.6).

6.1.4.2 CM04M

Between 32 and 8 cm in CM04M, the bulk densities were fairly high, ranging from 0.052 - 0.11 g cm^{-3}, above which they decreased to a minimum (0.013 g cm^{-3}) at the surface (*cf.* Fig. 6.7).

6.1.4.3 Discussion

As found at the previous sites (Sections 3.1.4.3, 4.1.4.3 and 5.1.4.3), the Carsegowan Moss bulk density profiles (*cf.* Figs. 6.6 and 6.7) generally indicate a greater degree of decomposition and mass loss in the acrotelm peat layers above ~ 34 cm in CM04CM-1, relative to the underlying catotelm peat sections (*cf.* Fig. 6.6).

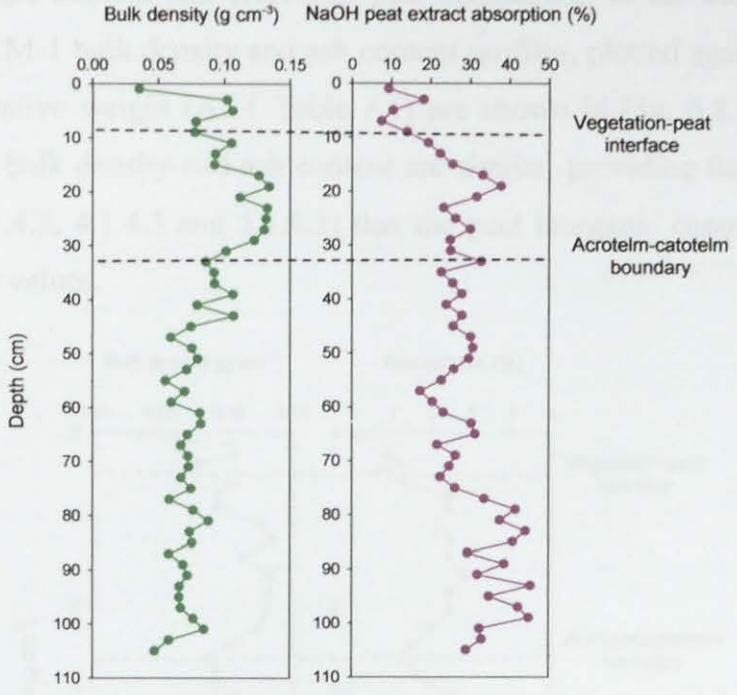

Figure 6.6: Depth profiles of bulk density (g cm^{-3}) and NaOH peat extract absorption (%) at 550 nm in the CM04CM-1 (0-106 cm) peat core.

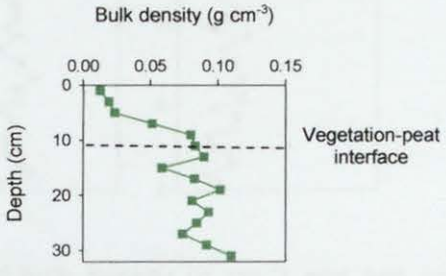

Figure 6.7: Depth profiles of bulk density (g cm^{-3}) in the CM04M (0-32 cm) peat core.

As found for the Turclossie Moss TM04CM-2 core (Section 5.1.4.3), the NaOH peat extract absorption values in CM04CM-1 were lower in the acrotelm layers (10 to 32 cm) relative to the catotelm layers between ~ 78 and 102 cm, again perhaps indicative of climate-related changes in bog surface wetness. Also as found at the previous sites, the low bulk densities and absorptions at the surface of CM04CM-1 and CM04M are attributable to the presence of decomposing and living vegetation, while the less pronounced increases in absorption values relative to bulk density values in the top ~ 34 cm sections of CM04CM-1 are attributable to contributions

from inorganic content and effects of peat compaction to the bulk density profile. The CM04CM-1 bulk density and ash content profiles, plotted against air-dried mid-point cumulative weight (A7.1 Table A1) are shown in Fig. 6.8. The near-surface increases in bulk density and ash content are similar, providing further evidence (*cf.* Sections 3.1.4.3, 4.1.4.3 and 5.1.4.3) that the peat inorganic content does influence bulk density values.

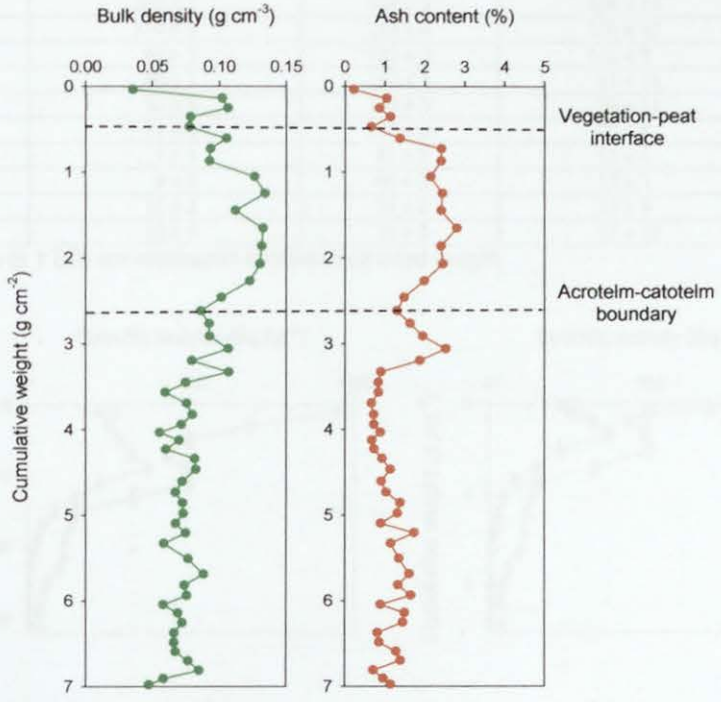

Figure 6.8: Comparison of bulk density (g cm^{-3}) and ash content (% by weight) *versus* cumulative weight (g cm^{-2}) in the CM04CM-1 peat core.

6.2 RADIONUCLIDES AND RADIOMETRIC DATING OF CARSEGOWAN MOSS PEAT CORES

6.2.1 ^{210}Pb and ^{137}Cs

^{210}Pb and ^{137}Cs were determined in the CM04M sections and, as ^{226}Ra was not detected above background in any of the CM04M peat sections, the total ^{210}Pb specific activities (Table 6.1) were taken to represent unsupported ^{210}Pb. The profiles of ^{210}Pb and ^{137}Cs specific activities are shown in Figs. 6.9 a (*vs.* depth in cm) and 6.9 b (*vs.* depth in g cm^{-2}).

Table 6.1: ^{210}Pb and ^{137}Cs specific activities (Bq kg^{-1}) and inventories (Bq m^{-2}) in the CM04M peat core.

CM04M section (cm)	Unsupported ^{210}Pb specific activity (Bq kg^{-1})	^{137}Cs specific activity (Bq kg^{-1})	Unsupported ^{210}Pb inventory (Bq m^{-2})	^{137}Cs inventory (Bq m^{-2})
0-2	311 ± 70	1345 ± 24	87 ± 20	376 ± 7
2-4	351 ± 15	950 ± 1	154 ± 7	416 ± 1
4-6	398 ± 15	689 ± 10	210 ± 8	363 ± 5
6-8	445 ± 11	598 ± 9	512 ± 13	688 ± 10
8-10	516 ± 8	671 ± 10	932 ± 14	1213 ± 18
10-12	311 ± 7	689 ± 10	574 ± 13	1272 ± 19
12-14	205 ± 7	454 ± 7	408 ± 14	903 ± 14
14-16	114 ± 9	213 ± 4	150 ± 12	279 ± 5
16-18	63 ± 5	182 ± 3	116 ± 9	336 ± 5
18-20	40 ± 7	160 ± 3	91 ± 16	364 ± 7
20-22	20 ± 6	155 ± 3	36 ± 11	280 ± 5
22-24	13 ± 4	130 ± 2	27 ± 8	270 ± 4
24-26	7 ± 3	81 ± 2	13 ± 6	154 ± 4
26-28	8 ± 2	60 ± 2	13 ± 3	98 ± 3
28-30	16 ± 2	54 ± 2	33 ± 4	111 ± 14
30-32	10 ± 5	56 ± 2	25 ± 12	139 ± 5

Specific activities (± 1 SD) are expressed relative to air-dried weight.

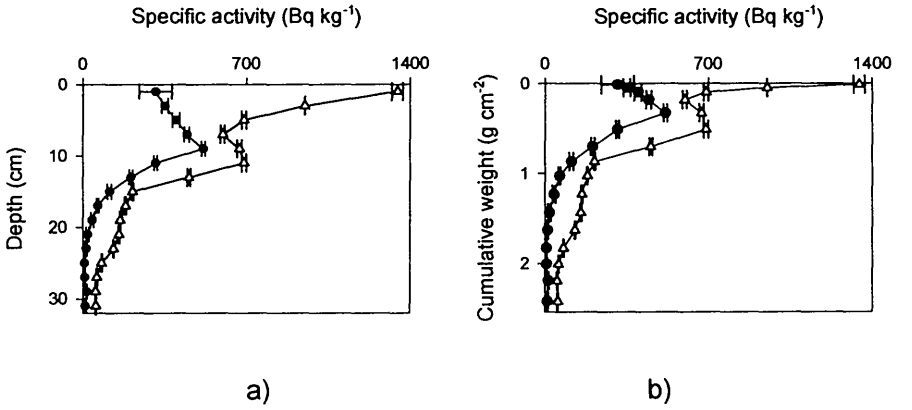

Figure 6.9: ^{210}Pb (closed circles) and ^{137}Cs (open triangles) specific activity (Bq kg^{-1}) *versus* a) depth (cm) and b) cumulative weight (g cm^{-2}) in the CM04M peat core.

6.2.2 ^{210}Pb dating of CM04M

The CRS model (Section 3.2.2) was applied to the ^{210}Pb inventories (*cf.* Table 6.1) to generate ages for the bottoms of the individual CM04M sections and, by interpolation, the mid-point dates of the sections were calculated (Table 6.2).

Table 6.2: Calculated ages and dates from the ^{210}Pb dating of the CM04M peat core.

Depth (cm)	Age (y)	Date (AD)
0	0	2004 ± 0
1		2004 ± 1
2	0.8	2003 ± 1
3		2003 ± 1
4	2.4	2002 ± 1
5		2001 ± 1
6	4.6	1999 ± 1
7		1996 ± 1
8	10.8	1993 ± 1
9		1986 ± 2
10	26.4	1977 ± 2
11		1970 ± 3
12	42.1	1962 ± 3
13		1953 ± 4
14	61.2	1943 ± 4
15		1937 ± 5
16	72.6	1931 ± 5
17		1925 ± 5
18	85.3	1919 ± 5
19		1911 ± 7
20	100.8	1903 ± 9
21		1899 ± 9
22	109.8	1894 ± 9
23		1890 ± 10
24	118.8	1885 ± 11
25		1883 ± 12
26	124.2	1880 ± 12
27		1877 ± 14
28	130.7	1873 ± 15
29		1860 ± 25
30	157.8	1846 ± 34

Dates were rounded up to the nearest whole number.

6.2.3 CM04M ^{210}Pb flux

The total unsupported ^{210}Pb inventory of CM04M was 3381 ± 46 Bq m^{-2} and the corresponding inventory-derived average ^{210}Pb flux (105 ± 1 Bq m^{-2} y^{-1}) was slightly higher than the theoretical rainfall-corrected ^{210}Pb flux (74 ± 13 Bq m^{-2} y^{-1}), which was calculated for the Carsegowan Moss area using the average annual rainfall value of 95.5 cm y^{-1} and the estimated average ^{210}Pb flux of 77 ± 14 Bq m^{-2} y^{-1} per metre of rainfall established for the UK by Smith *et al.* (1997).

6.2.4 CM04M ^{137}Cs total inventory

The total ^{137}Cs inventory in CM04M was 7.3 ± 0.0 kBq m^{-2}. This is less than that deposited in the south-west of Scotland from the atmosphere following nuclear weapons testing (~ 2 kBq m^{-2}, Peirson *et al.*, 1982), and the Chernobyl accident (10-15 kBq m^{-2}, Clark and Smith, 1988), indicating loss of ^{137}Cs from the peat bog.

6.2.5 CM04CM-1 dates

6.2.5.1 Extrapolation of ^{210}Pb CM04M dates

Dates for CM04CM-1 were obtained by extrapolation of the ^{210}Pb-derived dates obtained for the CM04M sister core. The extrapolation of these dates was aided by matching the ^{206}Pb/^{207}Pb profiles of the two cores, plotted against cumulative weight (Fig. 6.10) rather than linear depth in order to eliminate any effects from differential compaction arising from the collection of CM04CM-1 and CM04M using different techniques, i.e. Cuttle and Malcolm corer and monolith tin, respectively. Calculated and extrapolated ^{210}Pb dates and measured ^{206}Pb/^{207}Pb ratios for CM04M and the top of CM04CM-1 are shown in Table 6.3. Note that the ^{206}Pb/^{207}Pb ratio results for these cores will be discussed in Section 6.4.1.

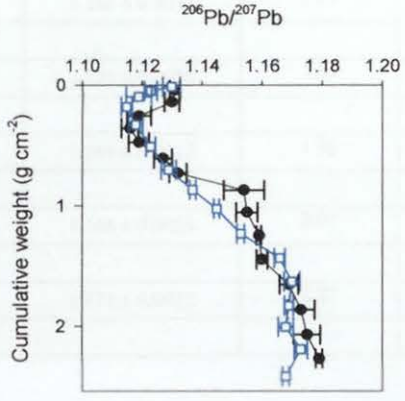

Figure 6.10: Profiles of ^{206}Pb/^{207}Pb ratio in the CM04M (0-32 cm) core (blue open squares) and from 0-30 cm in the CM04CM-1 core (black closed circles) *versus* cumulative weight.

Table 6.3: ^{210}Pb dates and corresponding $^{206}Pb/^{207}Pb$ ratios for the CM04M and CM04CM-1 peat cores.

CM04M			CM04CM-1		
Cumulative weight (g cm^{-2})	Calculated date (AD)[a]	$^{206}Pb/^{207}Pb$[a]	Cumulative weight (g cm^{-2})	Extrapolated date (AD)	$^{206}Pb/^{207}Pb$
-	2004 ± 0		-	2004 ± 0	
0.01	2004 ± 1	1.130 ± 0.0029			
0.03	2003 ± 1		0.04	2003 ± 1	1.131 ± 0.0017
0.05	2003 ± 1	1.123 ± 0.0021			
0.07	2002 ± 1				
0.10	2001 ± 1	1.119 ± 0.0042			
0.12	1999 ± 1		0.14	1998 ± 1	1.130 ± 0.0025
0.18	1996 ± 1	1.115 ± 0.0018			
0.24	1993 ± 1		0.26	1991 ± 1	1.119 ± 0.0040
0.33	1986 ± 2	1.118 ± 0.0024	0.36	1983 ± 2	1.116 ± 0.0028
0.42	1977 ± 2		0.47	1973 ± 3	1.119 ± 0.0034
0.51	1970 ± 3	1.123 ± 0.0016			
0.60	1962 ± 3		0.61	1961 ± 3	1.127 ± 0.0030
0.70	1953 ± 4	1.129 ± 0.0025	0.73	1950 ± 4	1.132 ± 0.0029
0.80	1943 ± 4				
0.87	1937 ± 5	1.137 ± 0.0010	0.87	1937 ± 5	1.154 ± 0.0067
0.93	1931 ± 5				
1.03	1925 ± 5	1.145 ± 0.0009	1.06	1923 ± 5	1.155 ± 0.0036
1.12	1919 ± 5				
1.23	1911 ± 7	1.153 ± 0.0012	1.25	1910 ± 7	1.159 ± 0.0008
1.35	1903 ± 9				
1.44	1899 ± 9	1.166 ± 0.0018	1.45	1898 ± 9	1.160 ± 0.0018
1.53	1894 ± 9				
1.63	1890 ± 10	1.170 ± 0.0026	1.65	1889 ± 10	1.169 ± 0.0031
1.74	1885 ± 11				
1.83	1883 ± 12	1.169 ± 0.0015	1.86	1882 ± 12	1.173 ± 0.0045
1.93	1880 ± 12				
2.01	1877 ± 14	1.168 ± 0.0025	2.07	1874 ± 15	1.175 ± 0.0044
2.09	1873 ± 15				
2.19	1860 ± 25	1.173 ± 0.0022	2.27	1850 ± 22	1.179 ± 0.0011
2.30	1846 ± 34				

6.2.5.2 Use of CM04CM-1 charcoal content as an independent check on extrapolated ^{210}Pb dates

It was assumed that charcoal content data could be used as an independent check on extrapolated ^{210}Pb age dates for CM04CM-1, due to a major explosion that occurred at the Carsegowan Moss explosives factory in 1945 A.D. (*cf.* Section 2.1.5) (Sawden,

2003). Note that a minor explosion also occurred in 1941 A.D. (Sawden, 2003). The profile of charcoal content (% by weight) of sections from the upper 38 cm of CM04CM-1 (A7.1 Table A2) is shown in Fig. 6.11.

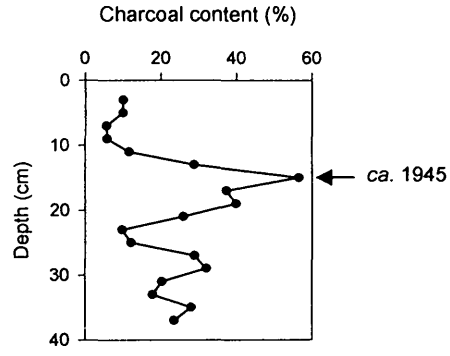

Figure 6.11: Depth profile of charcoal content (% by weight) from 0-38 cm in the CM04CM-1 core.

The charcoal content exhibited a peak between ~ 10 and 22 cm in CM04CM-1 with a maximum of 57% at a depth of 14-16 cm (*cf.* Fig. 6.11), perhaps indicative of 1945 A.D. In comparison, the extrapolated ^{210}Pb date for the 14-16 cm section was 1937 ± 5 A.D. (*cf.* Table 6.3), therefore providing additional confidence in the accuracy of the extrapolated CM04CM-1 ^{210}Pb dates.

6.2.6 Peat accumulation rates

6.2.6.1 CRS model

Peat accumulation rates (in terms of mg cm^{-2} y^{-1} and cm y^{-1}) for each CM04M section, calculated using the CRS model, are shown in Table 6.4. The actual average accumulation rates over the depth interval 0-30 cm were 15 ± 3 mg cm^{-2} y^{-1} and 0.19 ± 0.04 cm y^{-1}.

6.2.6.2 CIC model

The CIC model could not be used to calculate peat accumulation rates for CM04M, since plotting ln ^{210}Pb *versus* cumulative weight (Fig. 6.12 a) and depth (Fig. 6.12 b), respectively, resulted in a non-linear distribution of points, a consequence of the large amount of living and decaying vegetation at the top of the core (*cf.* Fig. 6.1).

Table 6.4: Sectional peat accumulation rates for the CM04M peat core determined using the CRS model.

Section (cm)	Number of years	Accumulation rate (mg cm^{-2} y^{-1})	Accumulation rate (cm y^{-1})
0-2	0.8	35	2.5
2-4	1.6	27	1.3
4-6	2.2	24	0.91
6-8	6.2	19	0.32
8-10	16	11	0.13
10-12	16	12	0.13
12-14	19	10	0.11
14-16	11	12	0.18
16-18	13	14	0.15
18-20	16	14	0.13
20-22	9.0	20	0.22
22-24	9.0	23	0.22
24-26	5.4	35	0.37
26-28	6.5	25	0.31
28-30	27	7.6	0.074

Accumulation rates are expressed in terms of air-dried peat weight.

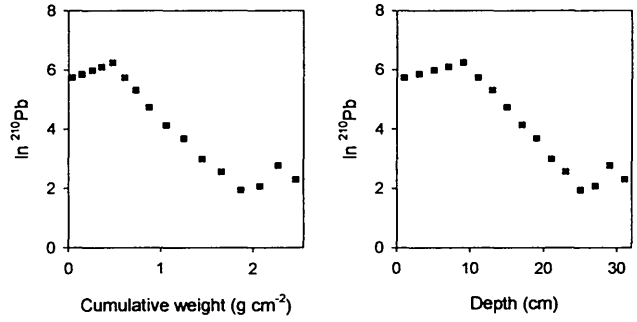

Figure 6.12: Profiles of ln [^{210}Pb (Bq kg^{-1})] *versus* a) cumulative weight and b) depth for the CM04M peat core.

6.2.6.3 Discussion

As found for Turclossie Moss (*cf.* Section 5.2.6.2), the CM04M peat accumulation rates could be derived using the CRS but not the CIC ^{210}Pb model, again demonstrating why the CRS model is preferred (*cf.* Section 1.9.1.2).

6.2.7 ^{14}C

^{14}C AMS age dates determined for selected deep peat sections of the CM04CM-1 core are shown in Table 6.5.

Table 6.5: ^{14}C age dates of selected CM04CM-1 peat samples.

CM04CM-1 section (cm)	Fraction dated	$\delta^{13}C$ (‰)	Date (^{14}C years B.P.)	Date (calendar years A.D./B.C.)	Laboratory code
40-42	Humic acid (HA1)	-27.1	750 ± 35	1215 – 1300 A.D.	GU-12938
70-72	Humic acid (HA1)	-26.6	1115 ± 35	860 – 1020 A.D.	GU-12939
76-78	Humic acid (HA1)	-27.6	1255 ± 35	680 – 890 A.D.	GU-12940
76-78	Humin	-27.3	1220 ± 35	680 – 900 A.D.	GU-12941
84-86	Humic acid (HA1)	-27.5	1385 ± 35	590 – 720 A.D.	GU-12942

Note that ^{14}C age date ranges of 231 – 530 A.D., 164 B.C. – 69 A.D. and 351 B.C. – 1 A.D. were determined for depths of 120-128 cm, 164-172 cm and 200-208 cm, respectively, in a separate peat core collected from Carsegowan Moss (Dumayne-Peaty, 1999).

6.3 CONSERVATIVE ELEMENTS

Profiles of total Al, Sc, Ti, Y and Zr concentrations for CM04CM-1 (A7.1 Table A3) and total Al and Ti concentrations for CM04M (A7.2 Table A3) are shown, along with ash contents, in Figs. 6.13 and 6.14, respectively.

6.3.1 CM04CM-1

All five elements exhibited increases between 10 and 44 cm and 70 and 86 cm in the CM04CM-1 core, with the following maximum values at the depths indicated:

- Al – 2600 - 2800 mg kg^{-1} between 14 and 24 cm
- Sc – 0.97 mg kg^{-1} at 14-16 cm and 36-38 cm and 1.1 mg kg^{-1} 76-78 cm
- Ti – 180 - 230 mg kg^{-1} between 14 and 40 cm and 180 - 280 mg kg^{-1} between 74 and 82 cm
- Y – 1.3 mg kg^{-1} at 14-16 cm
- Zr – 5.4 - 10 mg kg^{-1} between 12 and 36 cm, 6.4 mg kg^{-1} at 38-40 cm and 5.6 mg kg^{-1} at 76-78 cm
- Ash content – 2.1 - 2.8% between 12 and 28 cm and 2.5% at 38-40 cm

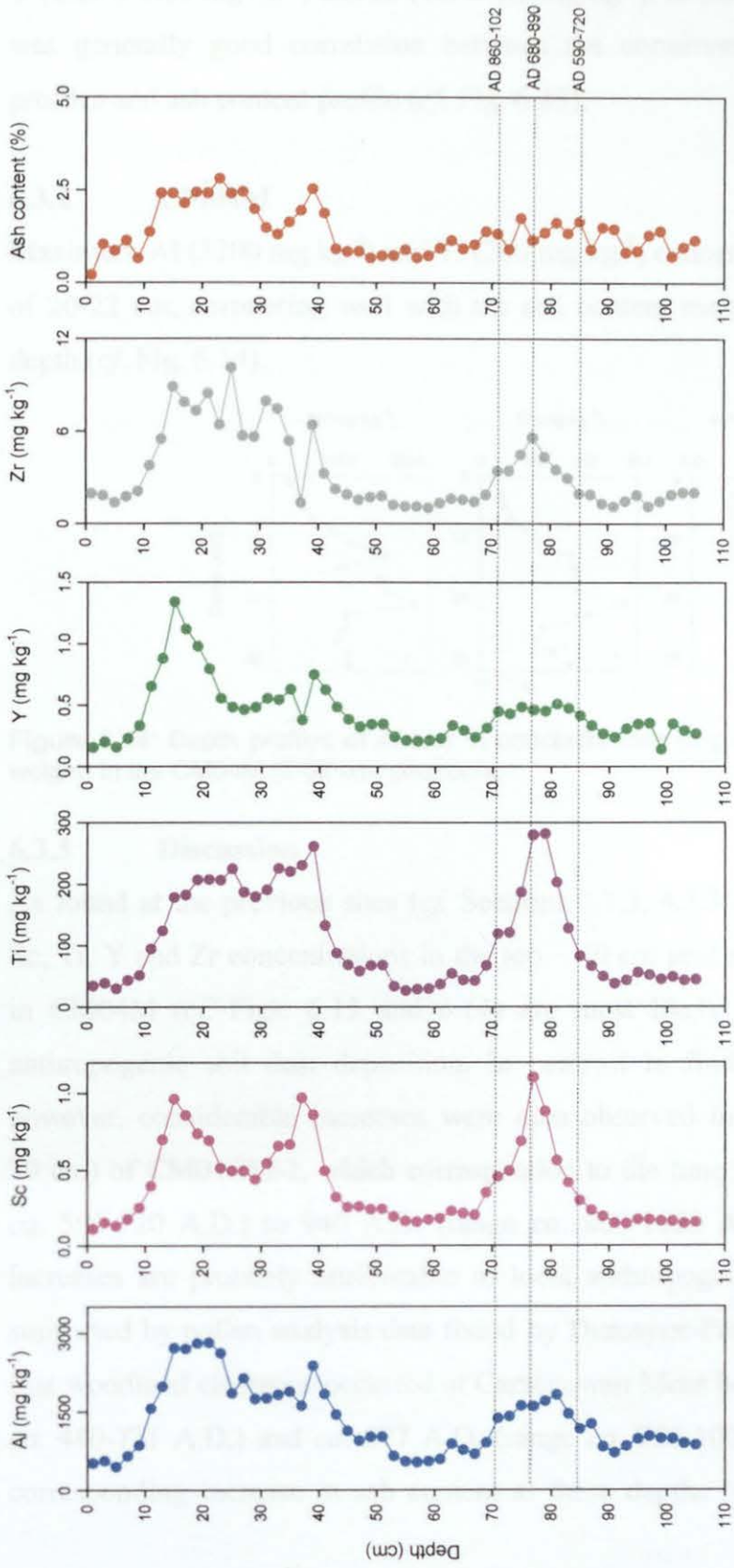

Figure 6.13: Depth profiles of Al, Sc, Ti, Y and Zr concentrations (mg kg^{-1}) and ash contents (% by weight) in the ^{14}C-dated CM04CM-1 (0-106 cm) peat core.

The following mean minimum concentrations occurred between 52 and 68 cm: Al (650 ± 120 mg kg^{-1}), Sc (0.19 ± 0.02 mg kg^{-1}), Ti (38 ± 9 mg kg^{-1}), Y (0.25 ± 0.05 mg kg^{-1}) and Zr (1.3 ± 0.2 mg kg^{-1}). In the top 40 cm of the core there was generally good correlation between the conservative element concentration profiles and ash content profile (*cf.* Fig. 6.13).

6.3.2 CM04M

Maximum Al (3200 mg kg^{-1}) and Ti (280 mg kg^{-1}) concentrations occurred at a depth of 20-22 cm, correlating well with the ash content maximum of 4.4% at the same depth (*cf.* Fig. 6.14).

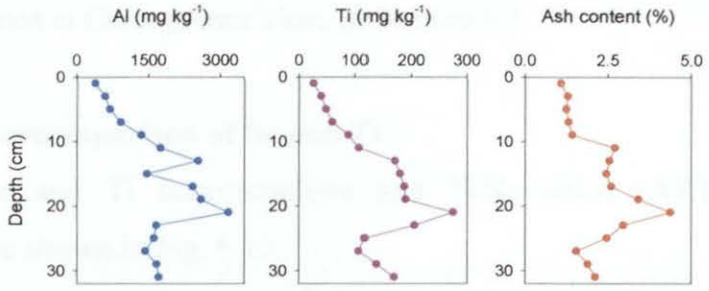

Figure 6.14: Depth profiles of Al and Ti concentrations (mg kg^{-1}) and ash contents (% by weight) in the CM04M (0-32 cm) peat core.

6.3.3 Discussion

As found at the previous sites (*cf.* Sections 3.3.3, 4.3.3 and 5.3.3), increases in Al, Sc, Ti, Y and Zr concentrations in the top ~ 40 cm peat sections of CM04CM-1 and in CM04M (*cf.* Figs. 6.13 and 6.14) are most likely caused by the increase in anthropogenic soil dust deposition. In contrast to findings at the previous sites, however, considerable increases were also observed in the lower sections (86 to 70 cm) of CM04CM-1, which corresponded to the time period *ca.* 655 A.D. (range *ca.* 590-720 A.D.) to 940 A.D. (range *ca.* 860-1020 A.D.) (*cf.* Fig. 6.13). These increases are probably attributable to local anthropogenic soil dust deposition, as supported by pollen analysis data found by Dumayne-Peaty (1999), which indicated that woodland clearance occurred at Carsegowan Moss between *ca.* 580 A.D. (range *ca.* 440-721 A.D.) and *ca.* 877 A.D. (range *ca.* 750-1005 A.D.). The absence of a corresponding increase in ash content at these depths (*cf.* Fig. 6.13) is surprising,

however, it is worth noting that their errors, based on the standard deviation of the mean value for two separate determinations, were large ($\leq 45\%$).

In contrast to similarities observed between the profiles of the pairs of elements Sc and Y, and Ti and Zr at Flanders Moss and The Red Moss of Balerno, and the pair of elements Al and Y, and the group of elements Sc, Ti and Zr, at Turclossie Moss, no specific relationship between pairs or groups of elements were apparent in the CM04CM-1 core profiles since profiles of all five conservative elements (Al, Sc, Ti, Y and Zr) appeared to exhibit similar features (*cf.* Fig. 6.13). As for the previous sites (Sections 3.5, 4.5 and 5.5), Al will not be used to correct Pb concentrations for soil dust contributions at Carsegowan Moss in Section 6.5.

6.3.3.1 Intercomparison of Sc and Ti

Profiles of Sc and Ti concentrations and Ti/Sc ratios (A7.1 Table A3) for CM04CM-1 are shown in Fig. 6.15.

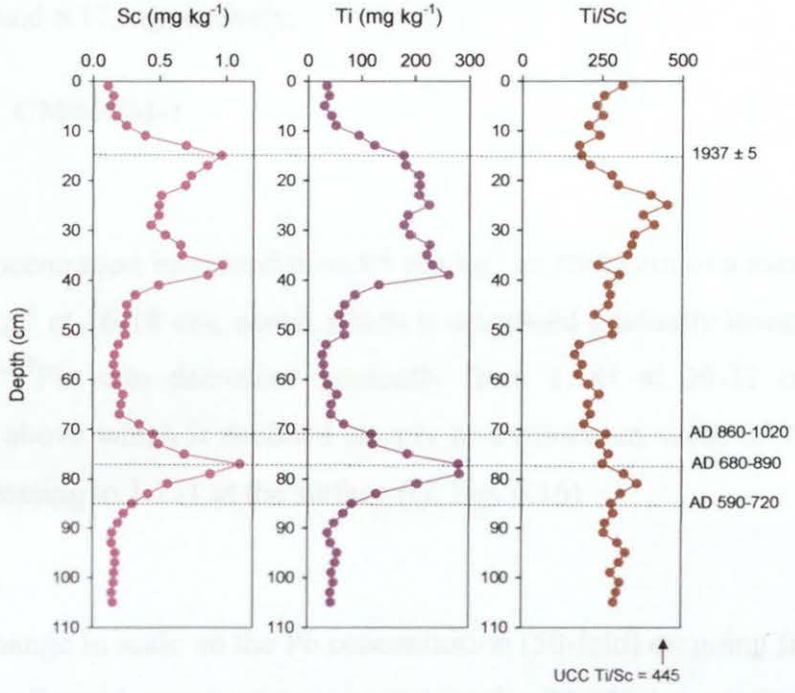

Figure 6.15: Depth profiles of Sc and Ti concentrations (mg kg^{-1}) and Ti/Sc ratios in the ^{210}Pb and ^{14}C-dated CM04CM-1 (0-106 cm) peat core.

Slight differences between the Sc and Ti concentration profiles are apparent, as indicated by the Ti/Sc ratio profile. In contrast to findings at the previous sites (*cf.* Sections 3.3.3.1, 4.3.3.1 and 5.3.3.1), the mean Ti/Sc ratio (260 ± 50) in the lower sections (40-106 cm) of the CM04CM-1 core was lower than the UCC Ti/Sc ratio (445), with a mean Ti/Sc ratio of 290 ± 40 between 70 and 86 cm, depths at which local soil dust inputs attributable to woodland clearance are likely (*cf.* Section 6.3.3). Also, in the uppermost 40 cm sections of the core, with the exception of the mean Ti/Sc ratio (380 ± 40) between 22 and 36 cm, the Ti/Sc ratios remained low (180 - 310), again, possibly attributable to local soil dust sources or direct non-soil-dust-related anthropogenic sources (e.g. coal combustion), as suggested for Flanders Moss and The Red Moss of Balerno (*cf.* Section 3.3.3.1 and 4.3.3.1).

6.4 Pb AND Pb ISOTOPIC RATIOS

Profiles of Pb concentrations and measured $^{206}Pb/^{207}Pb$, $^{208}Pb/^{206}Pb$ and $^{208}Pb/^{207}Pb$ isotopic ratios for CM04CM-1 (Table 6.6) and RM03CM-1 (Table 6.7) are shown in Figs. 6.16 and 6.17, respectively.

6.4.1 CM04CM-1

0-32 cm

The Pb concentration increased from 25 mg kg^{-1} at 30-32 cm to a maximum value of 1000 mg kg^{-1} at 16-18 cm, above which it decreased gradually towards the surface. The $^{206}Pb/^{207}Pb$ ratio decreased gradually from 1.181 at 30-32 cm to 1.154 at 14-16 cm, above which it declined steeply to a minimum value of 1.116 at 6-8 cm before increasing to 1.131 at the surface (*cf.* Fig. 6.16).

32-106 cm

Note the change in scale on the Pb concentration (50-fold) on going from 0-32 cm to 32-106 cm. Several zones were apparent in the 32-106 cm sections: a region of minimum concentrations (mean 1.0 ± 0.3 mg kg^{-1}) from 106 to 80 cm, above which, up to 52 cm they increased slightly (mean 2.7 ± 1.1 mg kg^{-1}) and then markedly (mean 16 ± 3 mg kg^{-1}) between 52 and 32 cm.

Table 6.6: Total Pb concentrations (mg kg^{-1}) and Pb isotopic ratios in the CM04CM-1 peat core.

Section (cm)	Pb (mg kg^{-1})	$^{206}Pb/^{207}Pb$	$^{208}Pb/^{206}Pb$	$^{208}Pb/^{207}Pb$
0-2	8.7 ± 1.8*	1.131 ± 0.0017	2.125 ± 0.0042	2.403 ± 0.0053
2-4	8.8 ± 0.5*	1.130 ± 0.0025	2.133 ± 0.0014	2.410 ± 0.0059
4-6	15 ± 0*	1.119 ± 0.0040	2.136 ± 0.0028	2.390 ± 0.0104
6-8	48 ± 7*	1.116 ± 0.0028	2.137 ± 0.0047	2.385 ± 0.0112
8-10	119 ± 10*	1.119 ± 0.0034	2.131 ± 0.0033	2.386 ± 0.1050
10-12	200 ± 9*	1.127 ± 0.0030	2.124 ± 0.0059	2.393 ± 0.0118
12-14	221 ± 13*	1.132 ± 0.0029	2.117 ± 0.0036	2.398 ± 0.0096
14-16	337 ± 7*	1.154 ± 0.0067	2.106 ± 0.0103	2.431 ± 0.0120
16-18	1001 ± 1*	1.155 ± 0.0036	2.114 ± 0.0046	2.442 ± 0.0125
18-20	672 ± 9*	1.159 ± 0.0008	2.109 ± 0.0008	2.444 ± 0.0011
20-22	214 ± 14*	1.160 ± 0.0018	2.093 ± 0.0033	2.428 ± 0.0062
22-24	103 ± 4*	1.169 ± 0.0031	2.088 ± 0.0041	2.442 ± 0.0102
24-26	65 ± 3*	1.173 ± 0.0045	2.096 ± 0.0024	2.460 ± 0.0112
26-28	49 ± 4*	1.175 ± 0.0044	2.096 ± 0.0026	2.464 ± 0.0111
28-30	33 ± 2*	1.179 ± 0.0011	2.090 ± 0.0024	2.464 ± 0.0048
30-32	25 ± 1*	1.181 ± 0.0006	2.092 ± 0.0024	2.470 ± 0.0018
32-34	19 ± 8*	1.166 ± 0.0034	2.092 ± 0.0019	2.439 ± 0.0087
34-36	16 ± 3*	1.167 ± 0.0028	2.089 ± 0.0022	2.439 ± 0.0074
36-38	18*	1.172 ± 0.0035	2.093 ± 0.0028	2.452 ± 0.0098
38-40	18 ± 2*	1.175 ± 0.0051	2.088 ± 0.0021	2.453 ± 0.0124
40-42	21 ± 3*	1.175 ± 0.0029	2.086 ± 0.0040	2.450 ± 0.0099
42-44	20 ± 2*	1.175 ± 0.0055	2.087 ± 0.0038	2.453 ± 0.0156
44-46	15 ± 0*	1.171 ± 0.0033	2.087 ± 0.0044	2.443 ± 0.0116
46-48	13 ± 2*	1.168 ± 0.0042	2.093 ± 0.0045	2.444 ± 0.0136
48-50	10 ± 2*	1.171 ± 0.0030	2.088 ± 0.0030	2.445 ± 0.0092
50-52	14 ± 6*	1.171 ± 0.0050	2.083 ± 0.0039	2.440 ± 0.0146
52-54	5.0 ± 0.1	1.172 ± 0.0013	2.093 ± 0.0015	2.453 ± 0.0030
54-56	3.6 ± 0.0	1.167 ± 0.0011	2.102 ± 0.0027	2.453 ± 0.0012
56-58	3.1 ± 0.0	1.166 ± 0.0017	2.102 ± 0.0072	2.451 ± 0.0106
58-60	4.0 ± 0.1	1.162 ± 0.0013	2.105 ± 0.0023	2.446 ± 0.0016
60-62	2.98 ± 0.06	1.166 ± 0.0019	2.099 ± 0.0019	2.448 ± 0.0047
62-64	3.0 ± 0.1	1.166 ± 0.0010	2.101 ± 0.0034	2.449 ± 0.0047
64-66	2.46 ± 0.02	1.163 ± 0.0010	2.104 ± 0.0045	2.446 ± 0.0040
66-68	1.25 ± 0.01	1.161 ± 0.0028	2.105 ± 0.0035	2.445 ± 0.0081
68-70	1.36 ± 0.02	1.164 ± 0.0027	2.103 ± 0.0027	2.448 ± 0.0070
70-72	1.55 ± 0.01	1.168 ± 0.0012	2.098 ± 0.0045	2.450 ± 0.0057
72-74	1.80 ± 0.02	1.166 ± 0.0015	2.101 ± 0.0024	2.450 ± 0.0039
74-76	1.87 ± 0.05	1.172 ± 0.0012	2.096 ± 0.0012	2.456 ± 0.0012
76-78	2.46 ± 0.05	1.173 ± 0.0012	2.095 ± 0.0027	2.457 ± 0.0023
78-80	3.2 ± 0.1	1.168 ± 0.0015	2.101 ± 0.0025	2.455 ± 0.0032
80-82	1.45 ± 0.01	1.173 ± 0.0019	2.094 ± 0.0027	2.457 ± 0.0038
82-84	1.42 ± 0.02	1.160 ± 0.0027	2.103 ± 0.0026	2.441 ± 0.0037
84-86	0.78 ± 0.01	1.160 ± 0.0036	2.101 ± 0.0044	2.437 ± 0.0050
86-88	0.90 ± 0.02	1.161 ± 0.0026	2.097 ± 0.0060	2.434 ± 0.0042

*Total Pb concentrations determined by ICP-OES where standard deviations were calculated as the standard deviation of the mean value for two separate sample analyses. ICP-MS Pb concentration and Pb isotopic ratio standard deviations were calculated as the standard deviation from the mean value for five consecutive determinations of the ratio/concentration of a sample solution.

Table 6.6 (continued): Total Pb concentrations (mg kg^{-1}) and Pb isotopic ratios in the CM04CM-1 peat core.

Section (cm)	Pb (mg kg^{-1})	$^{206}Pb/^{207}Pb$	$^{208}Pb/^{206}Pb$	$^{208}Pb/^{207}Pb$
88-90	0.90 ± 0.01	1.147 ± 0.0017	2.100 ± 0.0038	2.409 ± 0.0040
90-92	0.62 ± 0.01	1.150 ± 0.0021	2.100 ± 0.0038	2.415 ± 0.0031
92-94	0.69 ± 0.02	1.156 ± 0.0026	2.101 ± 0.0046	2.428 ± 0.0044
94-96	0.68 ± 0.01	1.154 ± 0.0062	2.091 ± 0.0122	2.414 ± 0.0123
96-98	1.03 ± 0.01	1.153 ± 0.0064	2.093 ± 0.0149	2.414 ± 0.0275
98-100	0.85 ± 0.00	1.157 ± 0.0021	2.102 ± 0.0069	2.432 ± 0.0047
100-102	0.81 ± 0.01	1.146 ± 0.0015	2.102 ± 0.0025	2.409 ± 0.0025
102-104	1.30 ± 0.01	1.152 ± 0.0046	2.090 ± 0.0093	2.408 ± 0.0113
104-106	1.62 ± 0.02	1.137 ± 0.0012	2.116 ± 0.0023	2.406 ± 0.0007

Table 6.7: Total Pb concentrations (mg kg^{-1}) and Pb isotopic ratios in the CM04M peat core.

Section (cm)	Pb (mg/kg)	$^{206}Pb/^{207}Pb$	$^{208}Pb/^{206}Pb$	$^{208}Pb/^{207}Pb$
0-2	18	1.130 ± 0.0029	2.126 ± 0.0028	2.402 ± 0.0063
2-4	23	1.123 ± 0.0021	2.134 ± 0.0014	2.397 ± 0.0039
4-6	30	1.119 ± 0.0042	2.140 ± 0.0027	2.394 ± 0.0091
6-8	50	1.115 ± 0.0018	2.137 ± 0.0028	2.382 ± 0.0057
8-10	93	1.118 ± 0.0024	2.153 ± 0.0016	2.407 ± 0.0050
10-12	131	1.123 ± 0.0016	2.144 ± 0.0005	2.406 ± 0.0032
12-14	186	1.129 ± 0.0025	2.141 ± 0.0031	2.417 ± 0.0024
14-16	217	1.137 ± 0.0010	2.133 ± 0.0024	2.425 ± 0.0017
16-18	205	1.145 ± 0.0009	2.121 ± 0.0012	2.428 ± 0.0009
18-20	225	1.153 ± 0.0012	2.115 ± 0.0015	2.439 ± 0.0019
20-22	189	1.166 ± 0.0018	2.106 ± 0.0024	2.457 ± 0.0025
22-24	118	1.170 ± 0.0026	2.102 ± 0.0021	2.459 ± 0.0043
24-26	80	1.169 ± 0.0015	2.102 ± 0.0016	2.457 ± 0.0031
26-28	61	1.168 ± 0.0025	2.092 ± 0.0027	2.444 ± 0.0056
28-30	49	1.173 ± 0.0022	2.098 ± 0.0018	2.460 ± 0.0048
30-32	34	1.168 ± 0.0011	2.101 ± 0.0022	2.455 ± 0.0025

Total Pb concentrations were determined by ICP-OES. Pb isotopic ratio standard deviations were calculated as the standard deviation from the mean value for five consecutive determinations of the ratio of a sample solution.

The mean $^{206}Pb/^{207}Pb$ ratios between 106 and 80 cm, 80 and 52 cm and 52 and 32 cm were 1.154 ± 0.009, 1.167 ± 0.004 and 1.171 ± 0.003, respectively (*cf.* Fig. 6.16).

6.4.2 CM04M

The Pb concentration increased from 34 mg kg^{-1} at 30-32 cm to maximum values (range 190 - 230 mg kg^{-1}) between 12 and 22 cm, above which it decreased to 18 mg kg^{-1} at the surface. The $^{206}Pb/^{207}Pb$ ratio remained fairly constant (mean 1.169 ± 0.002) from 32 to 20 cm, followed by a decrease to 1.115 at 6-8 cm, and a subsequent increase to 1.130 at the surface (*cf.* Fig. 6.17).

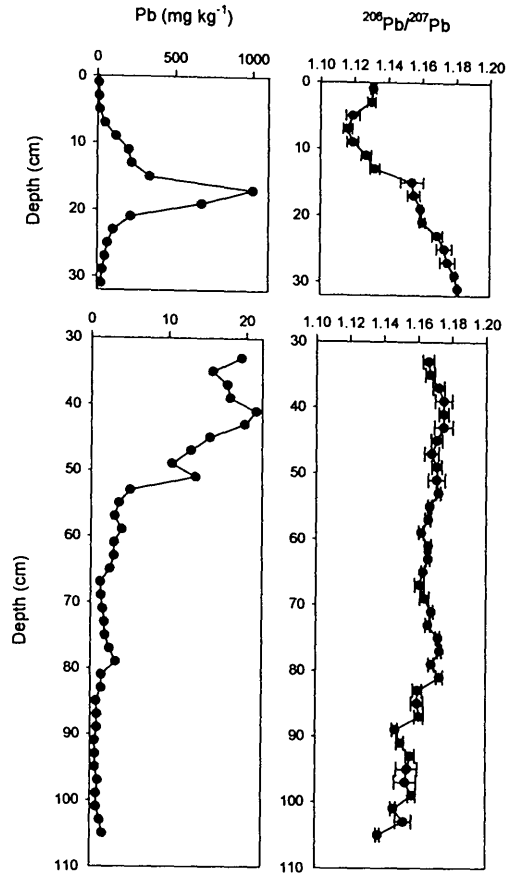

Figure 6.16: Depth profiles of Pb concentrations (mg kg^{-1}) and measured $^{206}Pb/^{207}Pb$ ratios from 0-32 cm and 32-106 cm in the CM04CM-1 peat core.

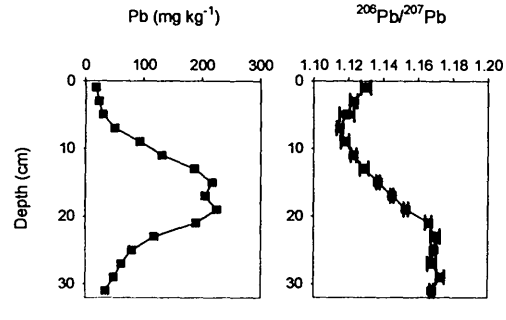

Figure 6.17: Depth profiles of Pb concentrations (mg kg^{-1}) and measured $^{206}Pb/^{207}Pb$ ratio in the CM04M (0-32 cm) peat core.

6.4.3 Discussion

As Pb is essentially immobile in ombrotrophic peat, these Pb profiles represent historical records of anthropogenic and natural atmospheric Pb deposition at

Carsegowan Moss. Comparing the Pb concentrations in the uppermost 38 cm of CM04CM-1 and in CM04M (Fig. 6.18), it is apparent that the Pb concentrations in the 14-16, 16-18 and 18-20 cm sections of CM04CM-1 are unusually high, suggesting that these sections in the core may have been unduly or unrepresentatively contaminated, perhaps as a consequence of a serendipitous event. Interestingly, Sb (which will be discussed in Section 6.8.1), was the only other metal that was similarly elevated in CM04CM-1. The other core, CM04M, represents only ~ 200 years of deposition and has concentration data for only a small selection of elements and, therefore, the CM04CM-1 core will still be used in the interpretation of historical trends in sources of atmospheric deposition of Pb (Section 6.6) and Sb (Section 6.8.1). However, since concentrations of Pb and Sb in these "contaminated" sections may not represent typical atmospheric Pb and Sb deposition, they will be excluded from interpretations of anthropogenic enrichments and historical trends.

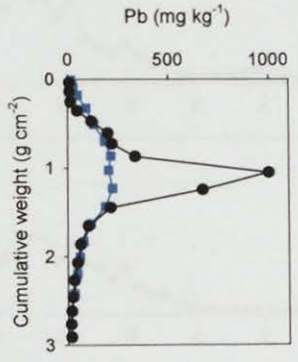

Figure 6.18: Profiles of Pb concentrations (mg kg^{-1}) from 0-38 cm in the CM04CM-1 (black closed circles) peat core and in the CM04M (0-32 cm) (blue closed squares) peat core *versus* cumulative weight.

6.5 USE OF CONSERVATIVE ELEMENTS TO ESTIMATE ANTHROPOGENIC ENRICHMENTS OF Pb

Profiles of Pb/Sc, Pb/Ti, Pb/Y and Pb/Zr ratios for CM04CM-1 (A7.1 Table A4) and Pb/Ti ratios for CM04M (A7.2 Table A4), along with Pb concentrations, are shown in Figs. 6.19 and 6.20, respectively.

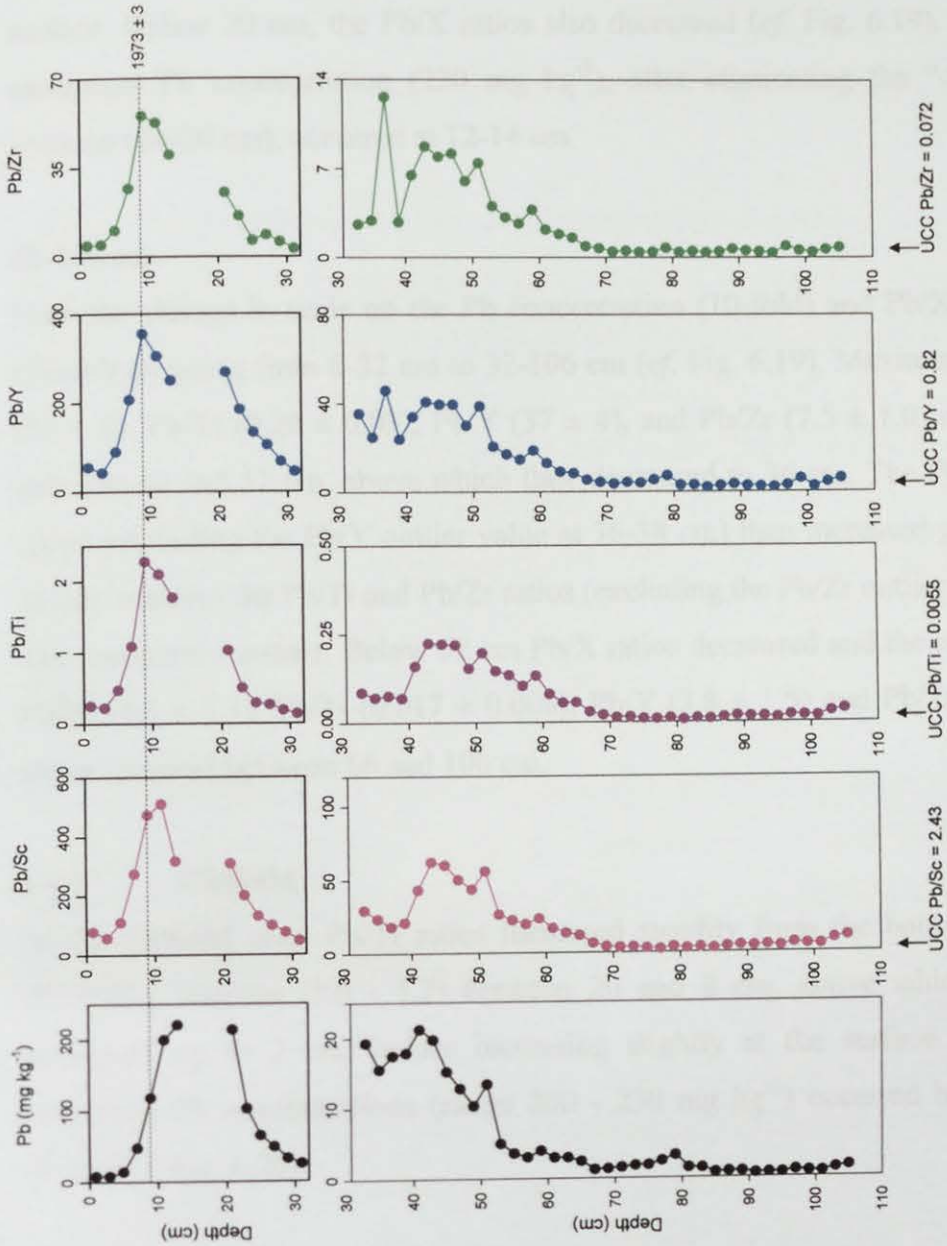

Figure 6.19: Depth profiles of Pb concentrations (mg kg^{-1}), Pb/Sc, Pb/Ti, Pb/Y and Pb/Zr ratios from 0-32 cm and 32-106 cm in the ^{210}Pb-dated CM04CM-1 peat core.

6.5.1 CM04CM-1

0-32 cm

The Pb/Sc ratios were at a maximum (510) at 10-12 cm, whereas the Pb/Ti (2.3), Pb/Y (350) and Pb/Zr (55) ratios were at a maximum at 8-10 cm. Above these maxima, Pb/X ratios decreased up to 4 cm then remained fairly constant towards the surface. Below 20 cm, the Pb/X ratios also decreased (*cf.* Fig. 6.19). Note that the maximum Pb concentration (220 mg kg^{-1}), after eliminating the "contaminated" sections (14-20 cm), occurred at 12-14 cm.

32-106 cm

Note the change in scale on the Pb concentration (10-fold) and Pb/X ratio profiles (5-fold) on going from 0-32 cm to 32-106 cm (*cf.* Fig. 6.19). Maximum mean Pb/Sc (52 ± 8), Pb/Ti (0.20 ± 0.03), Pb/Y (37 ± 4), and Pb/Zr (7.5 ± 1.0) ratios occurred between 40 and 52 cm, above which they decreased to 36 cm. The Pb/Sc and Pb/Y ratios (excluding the Pb/Y outlier value at 36-38 cm) then increased gradually up to 32 cm, whereas the Pb/Ti and Pb/Zr ratios (excluding the Pb/Zr outlier value at 36-38 cm) remained constant. Below 52 cm Pb/X ratios decreased and the minimum mean Pb/Sc (4.6 ± 2.1), Pb/Ti (0.017 ± 0.008), Pb/Y (3.8 ± 1.5) and Pb/Zr (0.56 ± 0.16) ratios occurred between 66 and 106 cm.

6.5.2 CM04M

In the CM04M core, Pb/Ti ratios increased steadily from the bottom of the core, exhibiting maxima (1.0 - 1.2) between 20 and 8 cm, above which Pb/Ti ratios decreased up to 2 cm, before increasing slightly at the surface. Note that the maximum Pb concentrations (range 200 - 230 mg kg^{-1}) occurred between 14 and 20 cm (*cf.* Fig. 6.20).

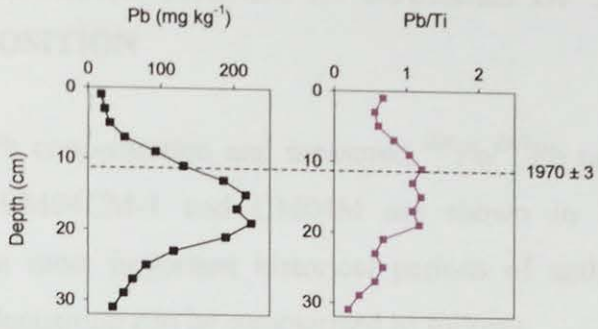

Figure 6.20: Depth profiles of Pb concentration (mg kg^{-1}) and Pb/Ti ratio in the ^{210}Pb-dated CM04M (0-32 cm) peat core.

6.5.3 Discussion and selection of conservative element

The CM04CM-1 Pb/X ratio profiles for each of the conservative elements indicated corresponding zones of anthropogenic Pb enrichment (*cf.* Fig. 6.19). The minimum Pb/X ratios (Pb/Sc (4.6 ± 2.1), Pb/Ti (0.017 ± 0.008), Pb/Y (3.8 ± 1.5) and Pb/Zr (0.56 ± 0.16)) occurred between 66 and 106 cm in CM04CM-1 and, compared with the UCC Pb/X ratios of 2.43 for Pb/Sc, 0.0055 for Pb/Ti, 0.82 for Pb/Y and 0.072 for Pb/Zr, were 2- to 8-fold higher than the UCC Pb/X ratios, as found for the previous sites (*cf.* Sections 3.5.3, 4.5.3 and 5.5.3). It is therefore unlikely that Pb concentrations are unaffected by anthropogenic Pb inputs at any depth in CM04CM-1. The maximum Pb/X ratios in CM04CM-1 and CM04M occurred ~ 2 to 4 cm above the maximum Pb concentrations (*cf.* Figs. 6.19 and 6.20), consistent with the findings for the previous sites (with the exception of the Red Moss of Balerno RM03CM-2 core (*cf.* Section 4.5)). As for the previous sites (*cf.* Sections 3.6.4, 4.5.3 and 5.5.3), the anthropogenic Pb concentrations in the CM04CM-1 core (A7.1, Table A4) were calculated on the basis of the use of Sc as a conservative element and will be used in Section 6.6 to assist interpretation of historical trends in anthropogenic Pb deposition. In the case of the CM04M core, for which Sc was not determined, Ti was used in the calculation of anthropogenic Pb concentrations (A7.2, Table A4), as performed for The Red Moss of Balerno RM03CM-1 core (*cf.* Section 4.5.3).

6.6 HISTORICAL TRENDS IN SOURCES OF ATMOSPHERIC Pb DEPOSITION

Anthropogenic Pb concentration and measured $^{206}Pb/^{207}Pb$ ratio profiles, including age dates, for CM04CM-1 and CM04M are shown in Figs. 6.21 and 6.22, respectively. The most important historical periods of anthropogenic sources of atmospheric Pb deposition can be summarised as follows:

- CM04CM-1 (106 to 32 cm) – Post-Roman and Mediaeval period
- CM04CM-1 (32 to 0 cm) and CM04M – Industrial and post-industrial period

Note that a depth of 200 cm in a separate peat core collected from Carsegowan Moss was assigned to the Roman period by pollen analysis (Barber *et al.*, 1994).

6.6.1 Post-Roman and Mediaeval atmospheric Pb sources and deposition

The minimum anthropogenic Pb concentrations (mean 0.50 ± 0.32 mg kg^{-1}) occurred between 106 and 66 cm, for which there were three age-dates (590-720 A.D., 680-890 A.D. and 860-1020 A.D.) available for the 84-86, 76-78 and 70-72 cm peat sections, respectively (*cf.* Fig. 6.21). The corresponding mean $^{206}Pb/^{207}Pb$ ratio between 106 and 66 cm was 1.159 ± 0.010, but there were two distinct zones of $^{206}Pb/^{207}Pb$ ratio values: mean 1.150 ± 0.006 from 106 to 88 cm and 1.166 ± 0.005 from 88 to 66 cm (*cf.* Fig. 6.21). These trends are likely to reflect a decline in metallurgical activities during the post-Roman and early Mediaeval era. The less radiogenic $^{206}Pb/^{207}Pb$ ratios between 106 and 88 cm, relative to those between 88 and 66 cm, could possibly reflect contributions, albeit relatively minor, from long-range atmospheric Pb deposition from post-Roman mining and smelting activities in Spain during the reign of the Visigods (after 410 A.D. to late 6^{th} century A.D.) (*cf.* Sections 3.6.2, 4.6.1 and 5.6.2). When Pb isotope ratios of the CM04CM-1 peat samples from 106 to 88 cm are plotted along with those of various British and Spanish Pb ores (Fig. 6.23), they (particularly the 104-106 cm sample) show agreement with the Pb ores from north-west Spain.

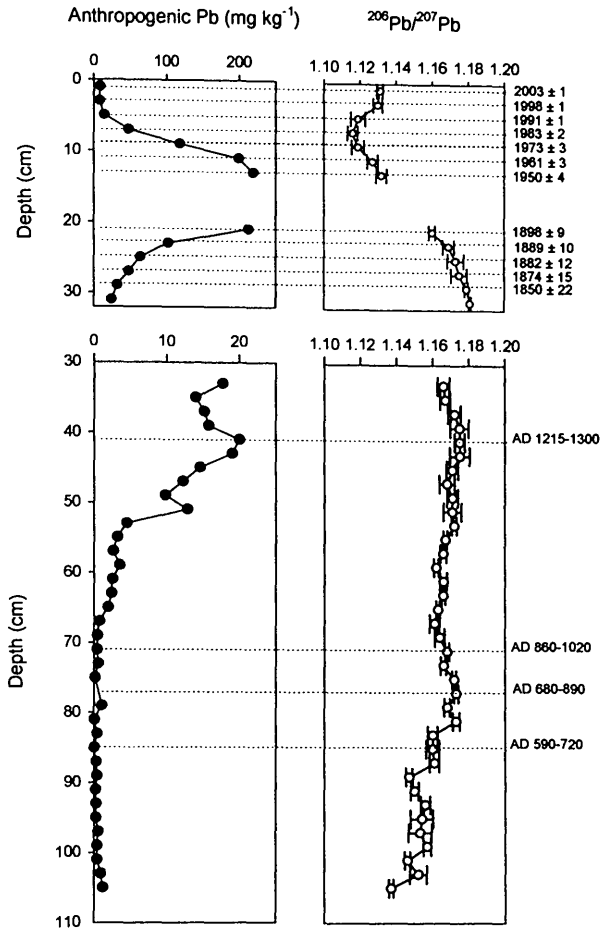

Figure 6.21: Depth profiles of anthropogenic Pb concentrations (mg kg^{-1}) and measured $^{206}Pb/^{207}Pb$ ratios from 0-32 cm and 32-106 cm in the ^{210}Pb- and ^{14}C-dated CM04CM-1 peat core.

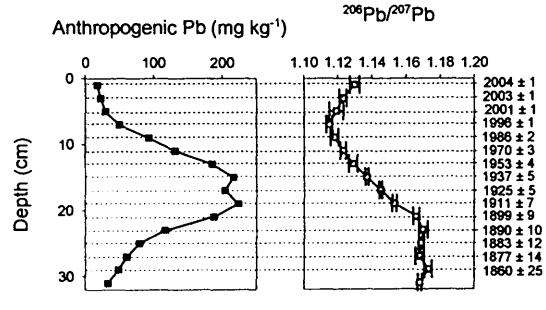

Figure 6.22: Depth profiles of anthropogenic Pb concentrations (mg kg^{-1}) (calculated using Ti as the conservative element) and measured $^{206}Pb/^{207}Pb$ ratios in the ^{210}Pb-dated CM04M (0-32 cm) peat core.

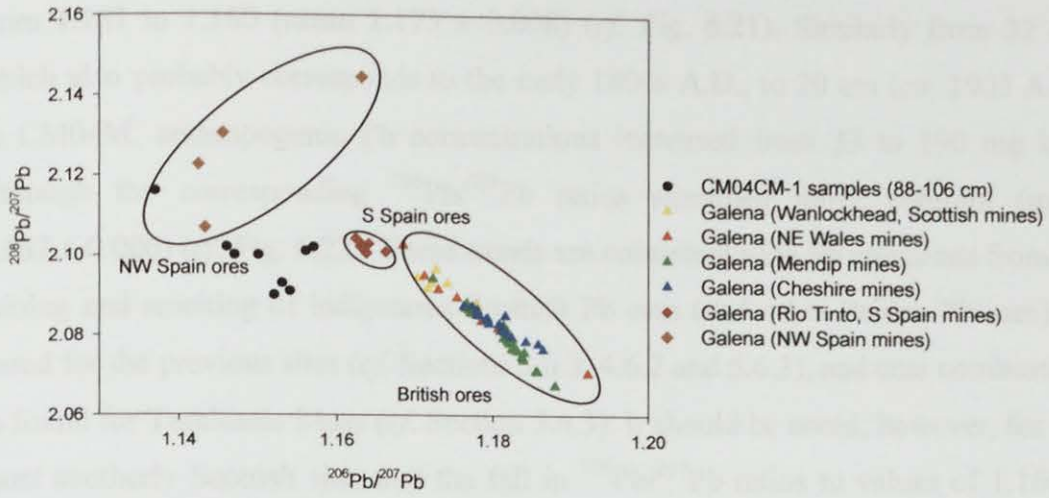

Figure 6.23: Plot of $^{208}Pb/^{206}Pb$ *versus* $^{206}Pb/^{207}Pb$ ratios for samples for the CM04CM-1 (88-106 cm) peat core and for galena in various British and Spanish Pb ores (Stos-Gale *et al.*, 1995; Rohl, 1996; Kylander *et al.*, 2005).

Above 66 cm up to a depth of 52 cm, anthropogenic Pb concentrations increased (mean 3.0 ± 0.9 mg kg^{-1}), while the corresponding $^{206}Pb/^{207}Pb$ ratios (mean 1.166 ± 0.003) were comparable to those in the underlying 88 to 66 cm sections (*cf.* Fig. 6.21), possibly reflecting the growth in Pb mining and smelting activities, especially in continental Europe, during the Mediaeval period. Between 52 and 32 cm, for which there was a single age-date of 1215-1300 A.D. available for the 40-42 cm section, the anthropogenic Pb concentrations (mean 15 ± 3 mg kg^{-1}) increased markedly, as did the corresponding $^{206}Pb/^{207}Pb$ ratios (mean 1.171 ± 0.003) (*cf.* Fig. 6.21). These trends may reflect the increasing influence of Pb emissions from mining and smelting of indigenous British Pb ores, as well as Pb ores from continental Europe.

6.6.2 Industrial and post-industrial atmospheric Pb sources and deposition

From 32 cm, a depth for which no age-date was available but, based on associated ^{210}Pb dates for the overlying regions and the ^{14}C-date (1215-1300 A.D.) for the underlying 40-42 cm section, seems likely to correspond to the early 1800s A.D., to 20 cm (*ca.* 1904 A.D.) in CM04CM-1, anthropogenic Pb concentrations increased

from 24 to 210 mg kg^{-1} and the corresponding $^{206}Pb/^{207}Pb$ ratios decreased gradually from 1.181 to 1.160 (mean 1.173 ± 0.008) (*cf.* Fig. 6.21). Similarly from 32 cm, which also probably corresponds to the early 1800s A.D., to 20 cm (*ca.* 1903 A.D.) in CM04M, anthropogenic Pb concentrations increased from 33 to 190 mg kg^{-1}, although the corresponding $^{206}Pb/^{207}Pb$ ratios remained fairly constant (mean 1.167 ± 0.006) (*cf.* Fig. 6.22). These trends are consistent with Pb emissions from the mining and smelting of indigenous Scottish Pb ores (and other British Pb ores), as found for the previous sites (*cf.* Sections 3.6.3, 4.6.2 and 5.6.3), and coal combustion, as found for Turclossie Moss (*cf.* Section 5.6.3). It should be noted, however, for this most southerly Scottish site, that the fall in $^{206}Pb/^{207}Pb$ ratios to values of 1.160 at *ca.* 1900 A.D. and 1.166 at *ca.* 1900 A.D. in CM04CM-1 and CM04M, respectively, which is well before the introduction of leaded petrol, may well indicate the early influence of the use of imported Pb ores in more southern parts of Britain. For example, it is known that Pb ores from the Australian Broken Hill mines were first imported into England in 1826 A.D. (Day and Tylecote, 1991) and that these Pb ores were smelted in Carmarthenshire (south Wales) after 1850 A.D. (Lloyd, 1939). Similar trends were recorded in archival herbage (Bacon *et al.*, 1996) and tree bark pocket and bark samples (Bellis *et al.*, 2002b; 2004) from England, thus providing further evidence that the earlier onset of the decrease in $^{206}Pb/^{207}Pb$ at Carsegowan Moss, compared with the previous sites (*ca.* 1930s/1940s A.D.) (*cf.* Sections 3.6.3, 4.6.2 and 5.6.3), may be related to the influence from the south.

At 12-14 cm (*ca.* 1950 A.D.) in CM04CM-1, anthropogenic Pb concentrations increased to 220 mg kg^{-1} and the corresponding $^{206}Pb/^{207}Pb$ ratio decreased to 1.132 (*cf.* Fig. 6.21). Similarly, between 20 cm and 14 cm (i.e. between *ca.* 1903 and 1943 A.D.) in CM04M, Pb concentrations were at a maximum (200-220 mg kg^{-1}) while corresponding $^{206}Pb/^{207}Pb$ ratios decreased from 1.153 at *ca.* 1911 A.D. to 1.137 at *ca.* 1937 A.D. (*cf.* Fig. 6.22). These trends are consistent with the general decline in the British Pb mining industry and growing influence of the use of leaded petrol from the 1930s A.D., and the intermediate $^{206}Pb/^{207}Pb$ ratio values indicate that there were significant contributions from other sources of Pb, such as coal combustion. Above

12 cm in CM04CM-1 (*ca.* 1956 A.D.) and 14 cm in CM04M (*ca.* 1943 A.D.) the anthropogenic Pb concentrations decreased, as did the corresponding $^{206}Pb/^{207}Pb$ ratios to minimum values of 1.116 at *ca.* 1983 A.D. and 1.115 at *ca.* 1996 A.D. in CM04CM-1 and CM04M, respectively (*cf.* Figs. 6.21and 6.22). As found for the previous sites (Sections 3.6.3, 4.6.2 and 5.6.3), these trends reflect the decreasing influence of coal combustion and increasing influence of car exhaust emissions of Pb. From the late-1980s/1990s to early 2000s A.D. (i.e. the top 6 cm of CM04CM-1 and CM04M, respectively), anthropogenic Pb concentrations continued to fall while the $^{206}Pb/^{207}Pb$ ratios increased to 1.131 at 2003 A.D. in CM04CM-1 and 1.130 at 2004 A.D. in CM04M (*cf.* Figs. 6.21 and 6.22), reflecting the steep fall in Pb emissions from car exhausts, consistent with findings for the previous sites (Sections 3.6.3, 4.6.2 and 5.6.3). The 3-isotope plot (Fig. 6.24) provides evidence for the multiple contributions to Pb deposition during the industrial and post-industrial era, e.g. from the sources mentioned above and incinerator fly ash. Note that, for this site, isotope ratio values for galena from different British Pb ores (not just Scottish Wanlockhead Pb ores) and the Australian Broken Hill Pb ores (Kylander *et al.*, 2005) are also plotted.

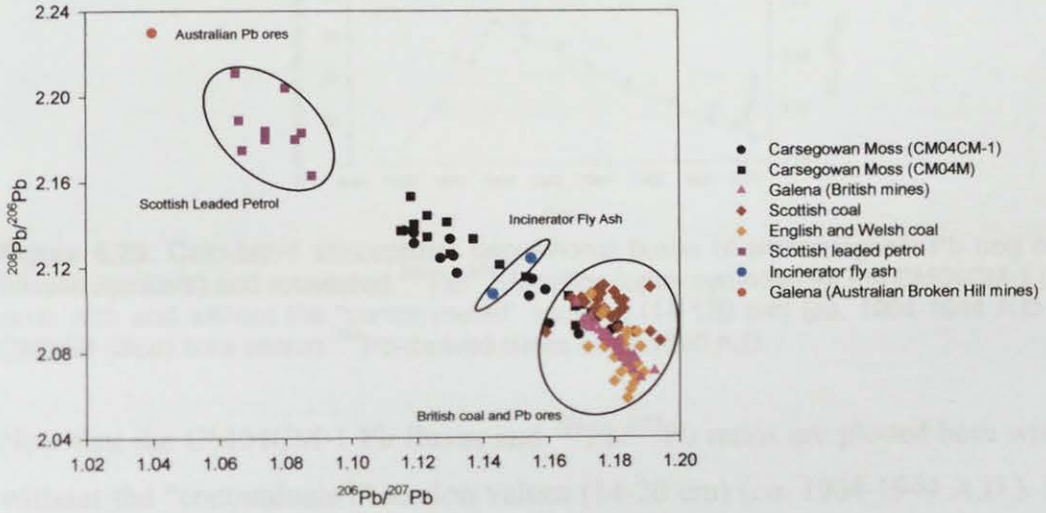

Figure 6.24: Plot of $^{208}Pb/^{206}Pb$ *versus* $^{206}Pb/^{207}Pb$ ratios for the CM04CM-1 (0-32 cm) and CM04M (0-32 cm) peat samples, and for galena in various British Pb ores (Rohl, 1996) and the Australian Broken Hill Pb ores (Kylander *et al.*, 2005), British coal (Farmer *et al.*, 1999), leaded petrol (Farmer *et al.*, 2000) and incinerator fly ash (Monna *et al.*, 1997).

6.6.2.1 Historical trends in depositional fluxes and inventories of Pb

Depositional fluxes of anthropogenic Pb in CM04CM-1 (A7.1 Table A12) and CM04M (A7.2 Table A6) peat sections were estimated, on the basis of extrapolated and measured ^{210}Pb chronologies, and are plotted (since 1840 A.D.), along with the measured ^{206}Pb/^{207}Pb ratios, *versus* ^{210}Pb-derived calendar dates in Fig. 6.25.

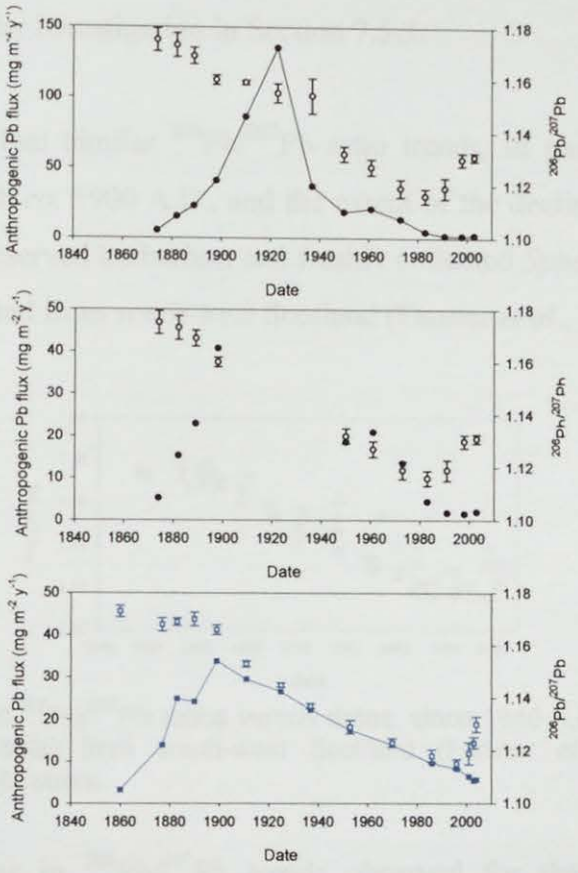

Figure 6.25: Calculated atmospheric depositional fluxes of anthropogenic Pb (mg m^{-2} y^{-1}) (closed symbols) and measured ^{206}Pb/^{207}Pb ratios (open symbols) for the CM04CM-1 (black) core, with and without the "contaminated" sections (14-120 cm) (*ca.* 1904-1944 A.D.), and CM04M (blue) core *versus* ^{210}Pb-derived dates since 1840 A.D.

Note that the CM04CM-1 Pb fluxes and ^{206}Pb/^{207}Pb ratios are plotted both with and without the "contaminated" section values (14-20 cm) (*ca.* 1904-1944 A.D.). In the plot including the "contaminated" sections, the maximum anthropogenic Pb flux was unusually high, with a value of 140 mg m^{-2} y^{-1} occurring during the early 1920s A.D., whereas, in the plot omitting the "contaminated" sections, the maximum

anthropogenic Pb flux was ~ 3-fold lower, with a value of 41 mg m^{-2} y^{-1} occurring at *ca.* 1900 A.D. (*cf.* Fig. 6.25). In CM04M, the maximum anthropogenic Pb flux of 34 mg m^{-2} y^{-1} occurred at *ca.* 1900 A.D., significantly earlier than observed at the previous sites (*cf.* Sections 3.6.3.1, 4.6.2.1 and 5.6.3.1), but in agreement with that found in the CM04CM-1 core when the "contaminated" sections were omitted (*cf.* Fig. 6.25). Note that depositional fluxes of anthropogenic Pb and trends in $^{206}Pb/^{207}Pb$ ratios at Carsegowan Moss will be compared more closely to those found at the other sites under investigation in Section 7.5.3.

It should be noted that similar $^{206}Pb/^{207}Pb$ ratio trends, in particular the onset of decline in $^{206}Pb/^{207}Pb$ *ca.* 1900 A.D., and the extent of the decline by *ca.* 1980 A.D., were observed in preserved herbarium and freshly collected *Sphagnum* moss samples of known age collected from *south-west* Scotland (Farmer *et al.*, 2002) (Fig. 6.26).

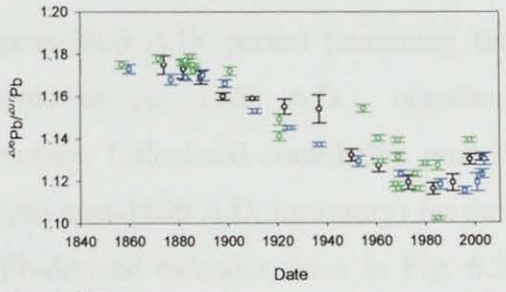

Figure 6.26: Measured $^{206}Pb/^{207}Pb$ ratios *versus* dates, since 1840 A.D, for herbarium moss samples (green symbols) from south-west Scotland (Farmer *et al.*, 2002) and the CM04CM-1 and CM04M cores.

Also, the similarities in $^{206}Pb/^{207}Pb$ trends observed for the Carsegowan Moss samples, archival herbage samples from Rothamsted, south-east England (Bacon *et al.*, 1996), and tree bark pocket and bark samples from Swinton, near Sheffield, north England (Bellis *et al.*, 2002b; 2004) are illustrated in Fig. 6.27.

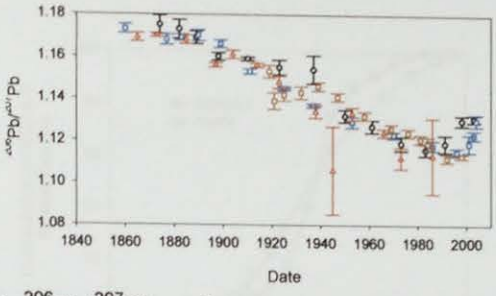

Figure 6.27: Measured $^{206}Pb/^{207}Pb$ ratios *versus* dates, since 1840 A.D, for herbage samples (red symbols) from south-east England (Bacon *et al.*, 1996), tree bark samples (brown symbols) from north England (Bellis *et al.*, 2002b; 2004) and the CM04CM-1 and CM04M cores.

The total anthropogenic Pb inventories for CM04CM-1 (i.e. from *ca.* 400 to 2004 A.D.) and CM04M (i.e. from *ca.* early 1800s to 2004 A.D.) were 5.2 g m^{-2} and 2.7 g m^{-2}, respectively. Note that the "contaminated" CM04CM-1 sections (14-20 cm) (*ca.* 1904-1944 A.D.) (*cf.* Section 6.4.3) were included in this calculation. The greatest contribution to anthropogenic Pb inventory in CM04CM-1 (5.0 g m^{-2}) occurred during the post-1800 A.D. period (assuming that a depth of 32 cm in CM04CM-1 corresponds to *ca.* 1800 A.D.), constituting 96% of the total anthropogenic Pb inventory. Calculated cumulative post-1800 A.D. anthropogenic Pb inventories (% of total post-1800 A.D. inventory) for the Carsegowan Moss cores are plotted *versus* ^{210}Pb-derived calendar dates in Fig. 6.28. Maximum deposition occurred between the 1880s and 1970s A.D., although it should be remembered that the Pb inventories between *ca.* 1904-1944 A.D. in CM04CM-1 were calculated using "contaminated" Pb concentrations and this, along with uncertainties associated with the ^{210}Pb dates extrapolated for CM04CM-1 from CM04M, can perhaps account for differences in the vertical (temporal) distribution (%) of anthropogenic Pb inventories between the two cores.

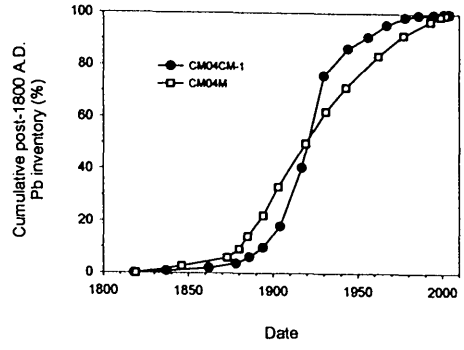

Figure 6.28: Calculated cumulative post-1800 A.D. anthropogenic Pb inventories (% of total post-1800 A.D. inventory) for the CM04CM-1 and CM04M cores *versus* ^{210}Pb-derived dates. Note that dates in CM04CM-1 and CM04M prior to *ca.* 1862 A.D. and *ca* 1846 A.D., respectively, were extrapolated.

6.7 GEOCHEMICAL BEHAVIOUR OF MAJOR ELEMENTS

Profiles of total Ca, Fe, Mg, Mn, P and S concentrations, along with water and ash content, for CM04CM-1 (A7.1 Table A5) and CM04M (A7.2 Table A5) are shown in Figs. 6.29 and 6.30, respectively.

6.7.1 CM04CM-1

All six elements exhibited concentration peaks or increases in the uppermost ~ 30 cm of the core, with the following maximum concentrations at the depths indicated:

- Ca – 2900 mg kg^{-1} between 0 and 4 cm
- Fe – 1900 mg kg^{-1} between 8 and 12 cm
- Mg – 1400 - 1600 mg kg^{-1} between 6 and 12 cm but the maximum value (1800 - 2200 mg kg^{-1}) in the core occurred between 92 and 106 cm
- Mn – 340 mg kg^{-1} at 0-2 cm
- P – 520 mg kg^{-1} at 2-4 cm but there was also a maximum (450 - 500 mg kg^{-1}) between 10 and 16 cm
- S – 1800 mg kg^{-1} at 2-4 cm and 16-18 cm but the maximum value (2100 - 2200 mg kg^{-1}) in the core occurred between 98 and 104 cm

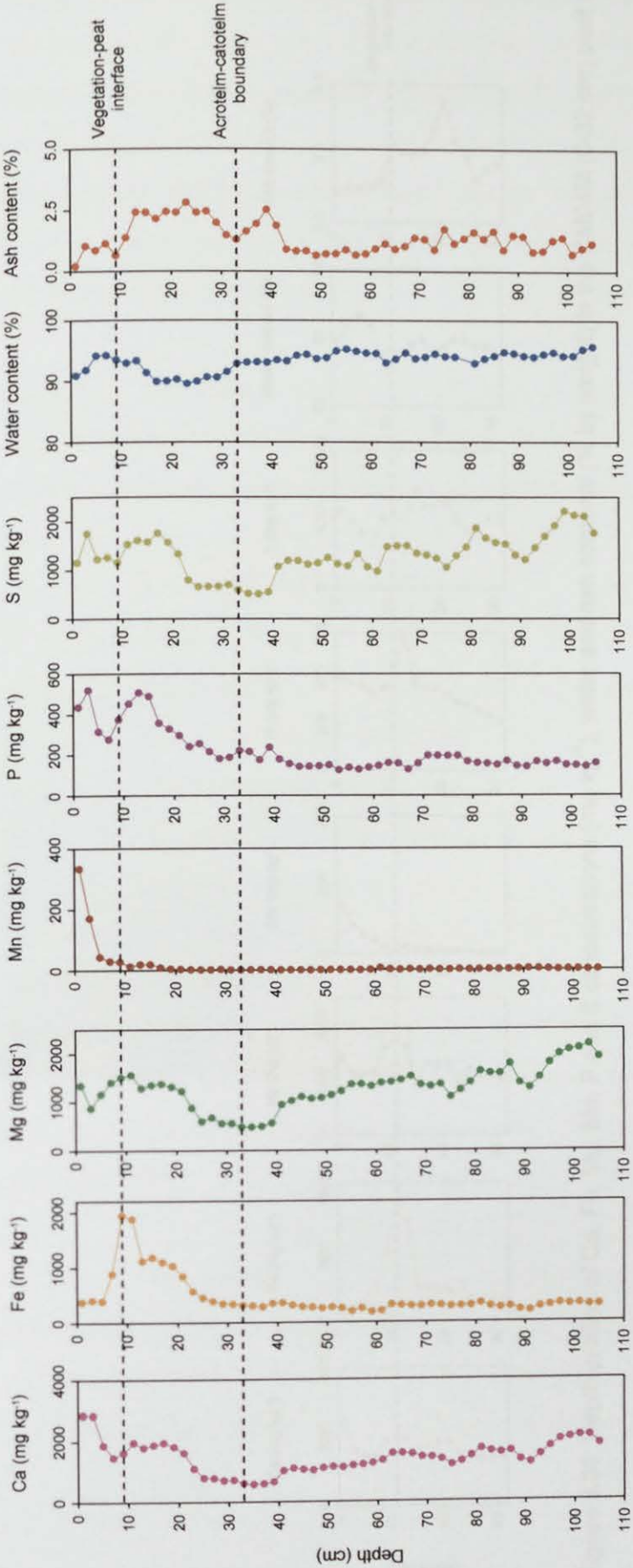

Figure 6.29: Depth profiles of Ca, Fe, Mg, Mn, P and S concentrations (mg kg^{-1}), water and ash contents (% by weight) in the CM04CM-1 (0-106 cm) peat core.

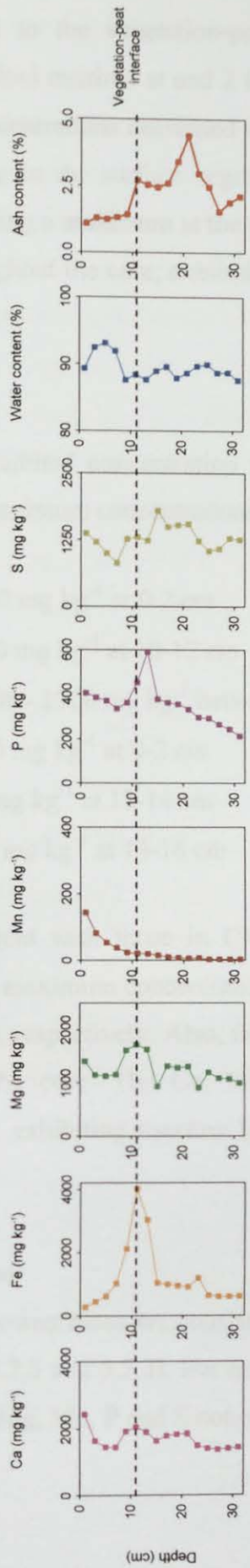

Figure 6.30: Depth profiles of Ca, Fe, Mg, Mn, P and S concentrations (mg kg^{-1}), water and ash contents (% by weight) in the CM04M (0-32 cm) peat core.

The Fe, Mn and P concentrations increased markedly from low constant values at depth. With respect to the vegetation-peat interface (8-10 cm), the Fe and P concentrations exhibited maxima at and 2 to 6 cm below it, respectively. Above the interface, the Fe concentrations decreased while the P concentrations decreased to 6 cm before increasing in the surface vegetation. The Mn concentrations increased above 18 cm, exhibiting a maximum at the surface. The Ca, Mg and S concentrations remained high throughout the core, exhibiting increases above ~ 26 cm and below ~ 40 cm (*cf.* Fig. 6.29).

6.7.2 CM04M

All six elements exhibited concentration peaks or increases throughout CM04M, with the following maximum concentrations at the depths indicated:

- Ca – 2400 mg kg^{-1} at 0-2 cm
- Fe – 4000 mg kg^{-1} at 10-12 cm
- Mg – 1600 - 1700 mg kg^{-1} between 8 and 14 cm
- Mn – 140 mg kg^{-1} at 0-2 cm
- P – 590 mg kg^{-1} at 12-14 cm
- S – 1800 mg kg^{-1} at 14-16 cm

Trends were consistent with those in CM04CM-1, i.e. Fe and P concentrations exhibited peaks with maximum concentrations at and 2 cm below the vegetation-peat interface (10-12 cm), respectively. Also, the Mn concentrations were at a maximum at the surface of the core. The Ca, Mg and S concentrations remained high throughout the core, exhibiting maxima between 22 and 8 cm and at the surface (*cf.* Fig. 6.30).

6.7.3 Discussion

The trends at Carsegowan Moss are consistent with those found at the previous sites (*cf.* Sections 3.7.3, 4.7.3 and 5.7.3). For example, there was no apparent correlation between the Ca, Fe, Mg, Mn, P and S concentration profiles and ash content profiles

(*cf.* Figs. 6.29 and 6.30). Also, the Ca and Mg concentration profiles indicated that contributions from sea salt inputs were minor. As found for the previous sites (*cf.* Sections 3.7.3, 4.7.3 and 5.7.3), Ca, Fe, Mg, Mn, P and S concentration profiles appeared to be influenced by nutrient uptake and recycling and Fe, Mn and P concentration profiles appeared to be influenced by redox cycling, if the zones of water table fluctuation are taken to lie between ~ 8 and 34 cm in CM04CM-1 and below ~ 10 cm in CM04M. Also, the similarity between the Fe and P concentration profiles perhaps indicated the influence of Fe on the distribution of P, although the diagenetic P peak maxima occurred 2 cm below the diagenetic Fe peaks (*cf.* Figs. 6.29 and 6.30), as observed for Flanders Moss, The Red Moss of Balerno RM03CM-1 core and TM04CM-2 core (*cf.* Sections 3.7.3, 4.7.3 and 5.7.3). As found at Turclossie Moss (*cf.* Section 5.7.3), the S concentration profiles did not appear to be strongly influenced by redox cycling, exhibiting similar trends to Ca and Mg (*cf.* Fig. 6.29 and 6.30).

6.8 GEOCHEMICAL BEHAVIOUR OF OTHER TRACE ELEMENTS

6.8.1 Sb

Concentrations of Sb (A7.1 Table A6) were determined only for CM04CM-1. The Sb profile, along with those of Pb and Sc, is shown in Fig. 6.31.

0-32 cm

The Sb concentration increased from 0.44 mg kg^{-1} at 30-32 cm to a maximum value of 9.9 mg kg^{-1} at 16-18 cm, above which, up to 6 cm it decreased markedly to 0.67 mg kg^{-1}, before decreasing more gradually to 0.33 mg kg^{-1} at the surface (*cf.* Fig. 6.31).

32-106 cm

Note the changes in scale on the Sb (40-fold) and Pb (10-fold) concentrations on going from 0-32 cm to 32-106 cm. Similar zones as those observed earlier for Pb concentrations (*cf.* Section 6.6) were apparent for Sb: a region of minimum

concentrations (mean 0.024 ± 0.008 mg kg^{-1}) from 106 to 82 cm, above which, up to 46 cm, they increased (mean 0.061 ± 0.021 mg kg^{-1}), before increasing markedly (mean 0.19 ± 0.03 mg kg^{-1}) between 46 and 32 cm (*cf.* Fig. 6.31).

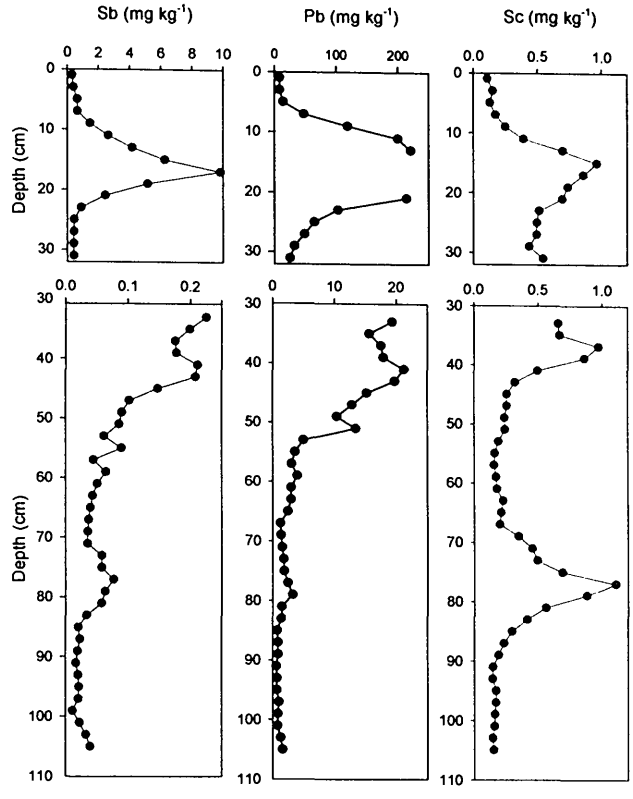

Figure 6.31: Depth profiles of Sb, Pb and Sc concentrations (mg kg^{-1}) from 0-32 cm and 32-106 cm in the CM04CM-1 peat core.

6.8.1.1 Discussion

As observed for the previous sites (*cf.* Sections 3.8.1, 4.8.1 and 5.8.1), the Sb and Pb profiles show a remarkable resemblance, providing further evidence that Sb, like Pb, is also essentially immobile in ombrotrophic peat. It is also apparent, however, that the high Sb concentrations in the 14-16, 16-18 and 18-20 cm sections, as observed for Pb (*cf.* Section 6.4.3), perhaps suggest that Sb concentrations, like Pb, have been affected by a source of contamination and they will therefore be excluded from interpretations of anthropogenic enrichments and historical trends. It is also worth noting that there is a slight increase in Pb, and more so, in Sb concentrations, at

depths of 70 to 86 cm, coincident with the increases observed in the conservative element concentrations (*cf.* Section 6.3.3).

6.8.1.1.1 The use of Sc as an indicator of soil dust input of Sb

The profile of Sb/Sc ratios (A7.1 Table A6), along with that of Pb/Sc ratios, in CM04CM-1 is shown in Fig. 6.32.

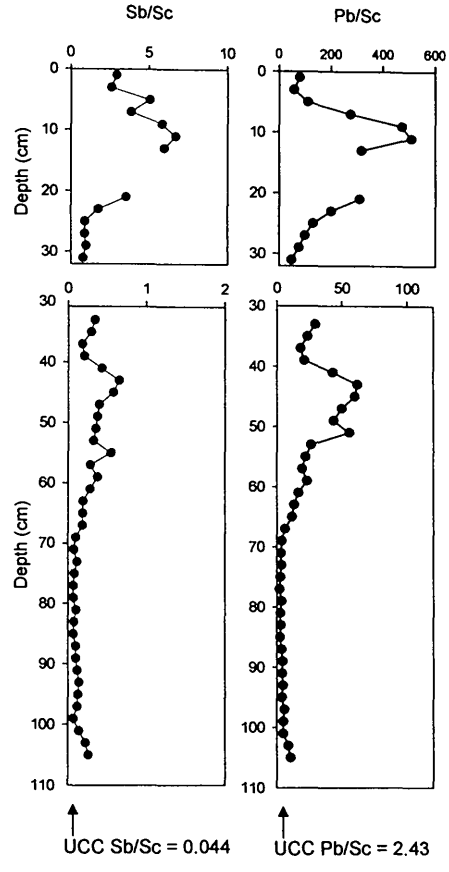

Figure 6.32: Depth profiles of Sb/Sc and Pb/Sc ratios from 0-32 cm and 32-106 cm in the CM04CM-1 peat core.

The maximum Sb/Sc ratio (6.7) occurred at 10-12 cm, the same depth as the maximum Pb/Sc ratio (510) (*cf.* Section 6.5.1). As found for Pb/Sc ratios, the minimum mean Sb/Sc ratio (0.12 ± 0.05) occurred between 66 and 106 cm, which is ~ 3-fold greater than the corresponding UCC ratio (0.044), similar to the ~ 2-fold greater mean minimum Pb/Sc ratio (*cf.* Section 6.5.3). As performed for Pb (*cf.* Section 6.5.3), on the basis of the use of Sc as a conservative element, the anthropogenic Sb concentrations in the CM04CM-1 core were calculated (A7.1,

Table A6) (*cf.* Sections 3.8.1.3.1, 4.8.1.1.1 and 5.8.1.1.1) and will be used to interpret historical trends in anthropogenic Sb deposition.

6.8.1.1.2 Historical trends in sources of atmospheric Sb deposition

Anthropogenic Sb and Pb concentration, measured $^{206}Pb/^{207}Pb$ and anthropogenic Sb/Pb ratio profiles for CM04CM-1, including age-dates, are shown in Fig. 6.33.

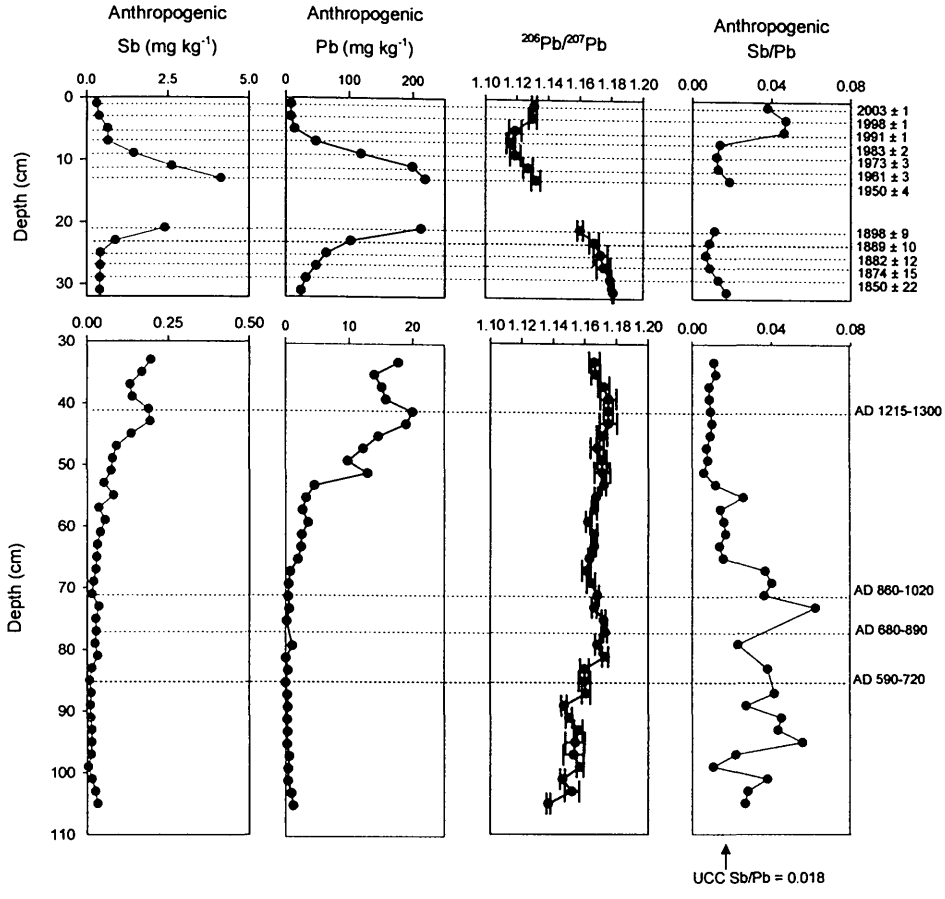

Figure 6.33: Depth profiles of anthropogenic Sb and Pb concentrations, measured $^{206}Pb/^{207}Pb$ and anthropogenic Sb/Pb ratios from 0-32 cm and 32-106 cm in the ^{210}Pb- and ^{14}C-dated CM04CM-1 peat core.

Post-Roman and Mediaeval atmospheric Sb sources and deposition

For the depth interval 106 to 66 cm, the anthropogenic Sb concentrations (mean 0.020 ± 0.009 mg kg^{-1}) were at a minimum, as observed for Pb (*cf.* Fig. 6.33), consistent with the decline in metallurgical activities during the post-Roman and early Mediaeval era (*cf.* Section 5.6.1). The corresponding mean anthropogenic Sb/Pb ratio between 106 and 66 cm was 0.036 ± 0.013 but, given that the

anthropogenic Sb and Pb concentrations were very small (≤ 0.037, ≤ 1.2 mg kg^{-1}) at these depths, the associated anthropogenic Sb/Pb ratios have quite a high uncertainty (typically ± 36%). Above 66 cm up to a depth of 52 cm, anthropogenic Sb concentrations (mean 0.049 ± 0.018 mg kg^{-1}) increased, as for Pb, while the corresponding anthropogenic Sb/Pb ratios (mean 0.016 ± 0.004) decreased (*cf.* Fig. 6.33), possibly reflecting the growth in Pb mining and smelting activities, especially in continental Europe, during the Mediaeval period (*cf.* Section 5.6.1). Between 52 and 32 cm the anthropogenic Sb concentrations (mean 0.14 ± 0.05 mg kg^{-1}) increased, although less markedly than those of Pb, and the corresponding anthropogenic Sb/Pb ratios (mean 0.0092 ± 0.0018) continued to decrease (*cf.* Fig. 6.33). The decline in anthropogenic Sb/Pb ratios to values more comparable to the range of values (0.0033 – 0.0056) obtained for the Wanlockhead and Leadhills Scottish Pb ore samples (*cf.* Table 3.10, Section 3.8.1.3.2), along with the corresponding increase in $^{206}Pb/^{207}Pb$ ratios (mean 1.171 ± 0.003) (*cf.* Section 5.6.1), perhaps provides further evidence for the increasing influence of Sb (and Pb) emissions from mining and smelting of indigenous British Pb ores, as well as Pb ores from continental Europe.

Industrial and post-industrial atmospheric Sb sources and deposition

From 32 cm (*ca.* early 1800s A.D.) to 20 cm (*ca.* 1904 A.D.) anthropogenic Sb concentrations increased from 0.42 to 2.4 mg kg^{-1}, as for Pb, but Sb increases were less marked (*cf.* Fig. 6.33). The corresponding anthropogenic Sb/Pb ratios (mean 0.011 ± 0.004) were higher than those in the underlying Mediaeval peat sections (32-52 cm) (mean 0.0092 ± 0.0018). These trends perhaps provide further evidence that Sb (and Pb) emissions were influenced by both coal combustion (*cf.* Table 3.11, Section 3.8.1.3.2) and Pb mining and smelting activities at these times (*cf.* Section 6.6.2), as found for Turclossie Moss (*cf.* Section 5.8.1.1.2). The increase in anthropogenic Sb/Pb ratios also possibly indicates influences from the smelting of Australian Broken Hill Pb ores, which have a higher Ag and therefore Sb content than British Pb ores (*cf.* Section 3.8.1.3.2) (Craddock, 1995; Mass *et al.*, 2002).

At 12-14 cm (*ca.* 1950 A.D.), anthropogenic Sb concentrations and Sb/Pb ratios increased to 4.1 mg kg^{-1} and 0.019, respectively (*cf.* Fig. 6.33). As also found for Pb in Section 6.6.2, these trends are consistent with the general decline in the British Pb mining industry and increase in coal combustion. Above 12 cm (*ca.* 1956 A.D.) up to 6 cm (*ca.* 1987 A.D.), the anthropogenic Sb concentrations, as for Pb, and corresponding anthropogenic Sb/Pb ratios decreased (mean 0.013 ± 0.001). As found at the previous sites (*cf.* Sections 3.6.3, 4.6.2 and 5.6.3) and previously for Pb (*cf.* Sections 6.6.2), these trends are consistent with the decreasing influence of coal combustion and the increasing influence of car exhaust emissions of Pb. After 1987 A.D. up to 2004 A.D., the anthropogenic Sb concentrations continued to decrease (from 0.66 to 0.32 mg kg^{-1}), but not as markedly as Pb (*cf.* Fig. 6.32), and the corresponding anthropogenic Sb/Pb ratios increased markedly (mean 0.044 ± 0.005). As found for the previous sites, (Sections 3.8.1.3.2, 4.8.1.1.2 and 5.8.1.1.2), these trends suggest a new recent source of Sb (e.g. automotive brake linings, degradation or combustion of plastics).

6.8.1.1.3 Historical trends in depositional fluxes and inventories of anthropogenic Sb

Depositional fluxes of anthropogenic Sb (A7.1 Table A12) are plotted, along with those of anthropogenic Pb and the anthropogenic Sb/Pb and measured $^{206}Pb/^{207}Pb$ ratios, since 1840 A.D., *versus* ^{210}Pb-derived calendar dates for CM04CM-1 and CM04M in Fig. 6.34. Note that the CM04CM-1 Sb fluxes and Sb/Pb ratios are plotted both with and without the "contaminated" section values (14-20 cm) (*ca.* 1904-1944 A.D.). In the plot including the "contaminated" sections, the maximum anthropogenic Sb flux was unusually high, with a value of 1.3 mg m^{-2} y^{-1} during the early 1920s A.D., whereas, in the plot omitting the "contaminated" sections, the maximum anthropogenic Sb flux was ~ 3-fold lower, as for Pb (*cf.* Section 6.6.2.1), with a value of 0.46 mg m^{-2} y^{-1} occurring at *ca.* 1900 A.D. (*cf.* Fig. 6.34).

As observed for the previous sites (Sections 3.8.1.3.3, 4.8.1.1.3 and 5.8.1.1.3), there is broad agreement between the anthropogenic Sb/Pb ratios in CM04CM-1 and

Sb/Pb ratios obtained independently for preserved herbarium and freshly collected *Sphagnum* moss samples of known age collected across Scotland (Fig. 6.35) (Farmer *et al.*, 2002; Halter, 2005; Halter and Farmer, *in prep.*). Note that the depositional fluxes of anthropogenic Sb and anthropogenic Sb/Pb ratios at Carsegowan Moss will be compared more closely to those found in the other Scottish peat bogs under investigation in Section 7.8.3.

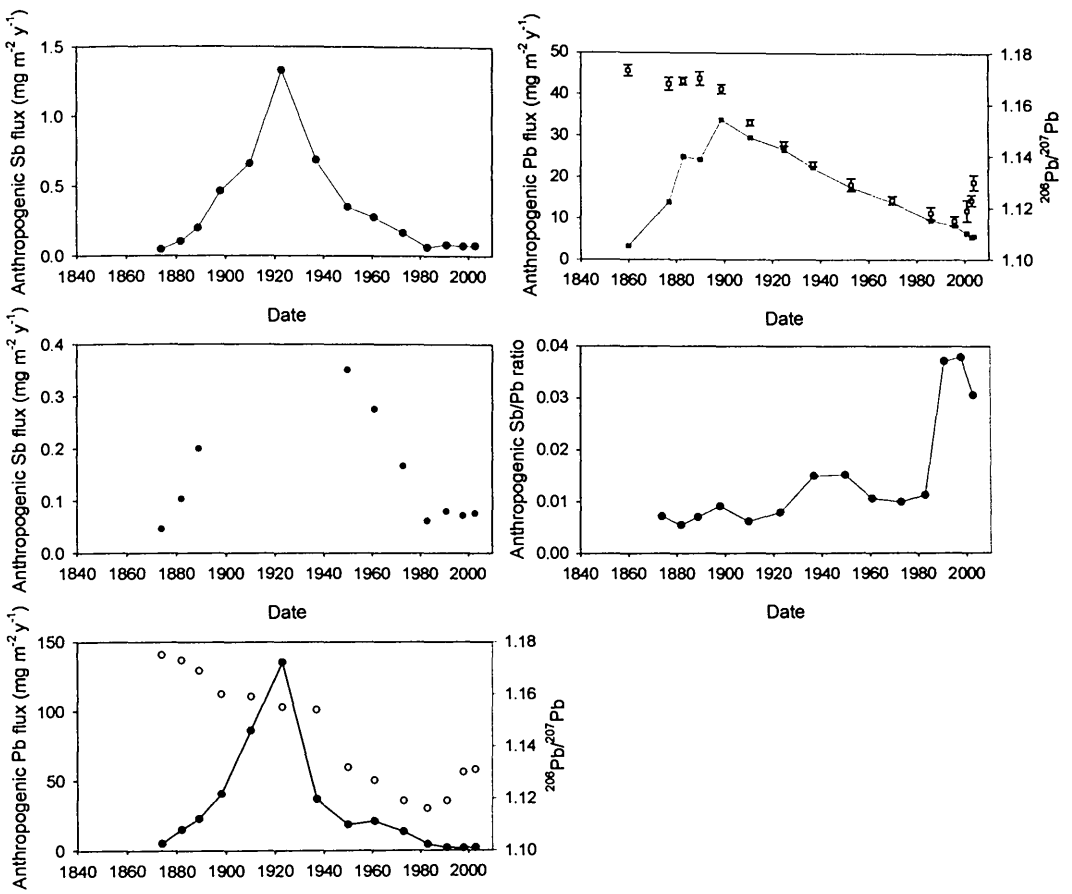

Figure 6.34: Calculated atmospheric depositional fluxes of anthropogenic Sb (red symbols) and Pb (mg m^{-2} y^{-1}), and the anthropogenic Sb/Pb (light blue symbols) and measured $^{206}Pb/^{207}Pb$ ratios (open symbols) for the CM04CM-1 and CM04M (dark blue symbols) cores *versus* ^{210}Pb-derived dates since 1840 A.D.

The total anthropogenic Sb inventory for CM04CM-1 (i.e. from *ca.* 400 to 2004 A.D.) was 0.058 g m^{-2} of which the post-1800 A.D. Sb inventory (0.056 g m^{-2}) (corresponding to peat sections 0-32 cm) constitutes 97%, in agreement with the findings for Pb (*cf.* Section 6.6.2.1). Note that as for Pb, the "contaminated" CM04CM-1 sections (14-20 cm) (*ca.* 1904-1944 A.D.) were included in this

calculation. Calculated cumulative post-1800 A.D. anthropogenic Sb inventories (% of total post-1800 A.D. inventory) for CM04CM-1 are plotted *versus* ^{210}Pb-derived calendar dates in Fig. 6.36.

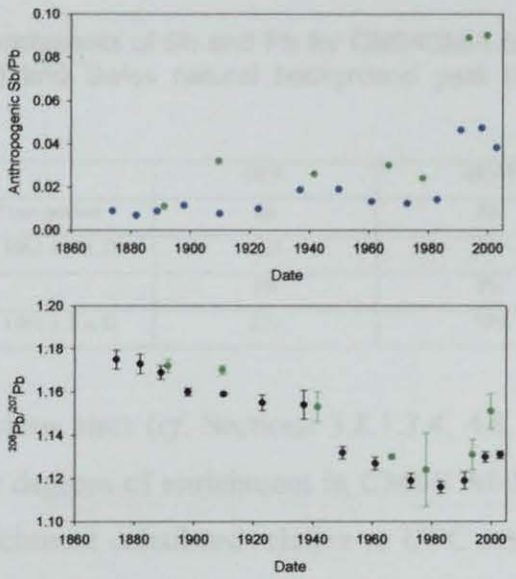

Figure 6.35: Anthropogenic Sb/Pb and measured ^{206}Pb/^{207}Pb ratios *versus* dates, since 1860 A.D, for Scottish herbarium moss samples (green symbols) and the CM04CM-1 core.

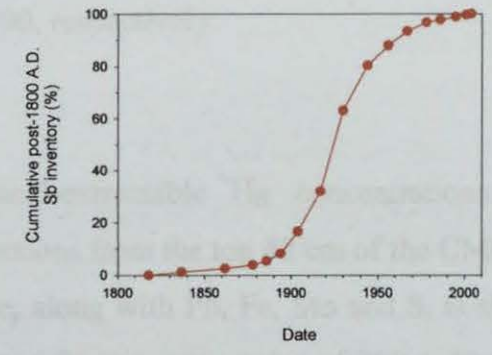

Figure 6.36: Calculated cumulative post-1800 A.D. anthropogenic Sb inventories (% of total post-1800 A.D. inventory) for the CM04CM-1 core *versus* ^{210}Pb-derived dates. Note that dates in CM04CM-1 prior to *ca.* 1862 A.D. were extrapolated.

Maximum deposition occurred between the 1890s and 1960s A.D., broadly in agreement with that found for Pb (*cf.* Section 6.6.2.1) (*cf.* Fig. 6.36), although it should be remembered that the Sb (and Pb) inventories between *ca.* 1904-1944 A.D. in CM04CM-1 were calculated using "contaminated" Sb (and Pb) concentrations.

6.8.1.1.4 Maximum enrichments of Sb and Pb

The maximum enrichments of Sb and Pb for the CM04CM-1 core, not including the "contaminated sections", calculated using UCC and SNBP elemental concentration ratios (Section 3.8.1.3.4), are shown in Table 6.8.

Table 6.8: Maximum enrichments of Sb and Pb for CM04CM-1 calculated relative to upper continental crust (UCC) and Swiss natural background peat (SNBP) Sb/Sc and Pb/Sc concentration ratios.

	UCC	SPNB
Time period	**Sb**	**Sb**
ca. 1961 ± 3 A.D.	150	61
	Pb	**Pb**
ca. 1961 ± 3 A.D.	210	170

As found for the previous sites (*cf.* Sections 3.8.1.3.4, 4.8.1.1.4 and 5.8.1.1.4), Sb and Pb exhibit similar degrees of enrichment in CM04CM-1. It is worth noting that the degrees of Sb enrichment calculated relative to UCC and SPNB Sb/Sc ratios, in the "contaminated" sections (14 to 20 cm) (between *ca.* 1944 and 1904 A.D.), ranged from 150 - 260 and 59 – 100, respectively. Similarly, the degrees of Pb enrichment calculated relative to UCC and SPNB Pb/Sc ratios in these sections, ranged from 140 - 480 and 120 - 390, respectively.

6.8.2 Hg

The HNO_3/H_2SO_4 acid-extractable Hg concentrations (A7.1 Table A7) were determined only in sections from the top 48 cm of the CM04CM-1 core (MacDonald, 2005). The Hg profile, along with Pb, Fe, Mn and S, is shown in Fig. 6.37. The Hg concentrations increased from a mean value of 200 ± 40 μg kg^{-1} between 48 and 24 cm to a maximum (550 - 600 μg kg^{-1}) between 18 and 12 cm, above which they declined to a minimum (150 μg kg^{-1}) at 6-8 cm before exhibiting a minor peak between 6 and 0 cm, with a maximum concentration (300 μg kg^{-1}) at 2-4 cm (*cf.* Fig. 6.37).

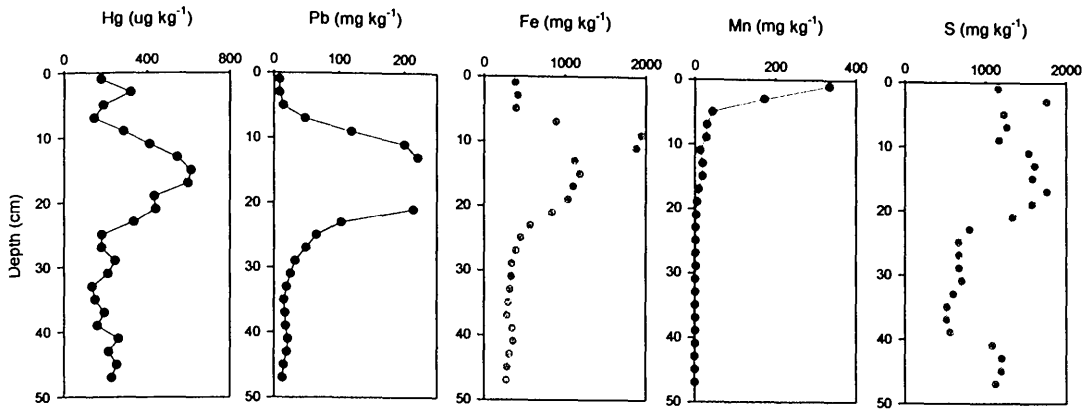

Figure 6.37: Depth profiles of Hg (μg kg^{-1}) and Pb, Fe, Mn and S concentrations (mg kg^{-1}) from 0-48 cm in the CM04CM-1 peat core.

6.8.2.1 Discussion

6.8.2.1.1 Assessment of the immobility of Hg in ombrotrophic peat

The Hg concentrations, as for Pb, were elevated in the top ~ 24 cm sections of CM04CM-1 (*cf.* Fig. 6.37). Note that Hg concentrations in the 14-16, 16-18 and 18-20 cm sections did not appear to be affected by the source of contamination observed for Pb and Sb (*cf.* Sections 6.4.3 and 6.8.1.1). The general similarity between the Hg and Pb concentration profiles perhaps provides further evidence for the immobility of Hg, at least in recent ombrotrophic peat layers, as found for Flanders Moss and The Red Moss of Balerno (Sections 3.8.2.2 and 4.8.2.1.1). Comparing the Hg concentration profile with those of Fe and Mn (*cf.* Fig. 6.37), the distribution of Hg is clearly different, with the maximum Hg concentrations occurring below those of Fe and Mn, as found for Flanders Moss and The Red Moss of Balerno (*cf.* Sections 3.8.2.2.1 and 4.8.2.1.1), providing further evidence that the Hg profile is not affected by Hg adsorption to Fe and Mn oxides and hydroxides. The Hg and S concentration profiles generally exhibited similarities in the acrotelm layers (uppermost 32 cm), however, in contrast to findings for Flanders Moss and The Red Moss of Balerno (*cf.* Sections 3.8.2.2.1 and 4.8.2.1.1), they were not particularly similar in the lower catotelm layers (32-106 cm) (*cf.* Fig. 6.37), and therefore did not indicate control of Hg as HgS precipitates.

6.8.2.1.2 Normalisation of Hg to Se and NaOH peat extract absorption (Abs)

The CM04CM-1 profiles for Hg and Se concentrations (A7.1 Table A7), NaOH peat extract absorptions and Hg/Se and Hg/Abs ratios (A7.1 Table A7) are shown in Fig. 6.38. When the CM04CM-1 Hg and Se concentration profiles are compared, it is apparent, as found for The Red Moss of Balerno (Section 4.8.2.1.2), that they show some similarities, particularly in the top ~ 22 cm.

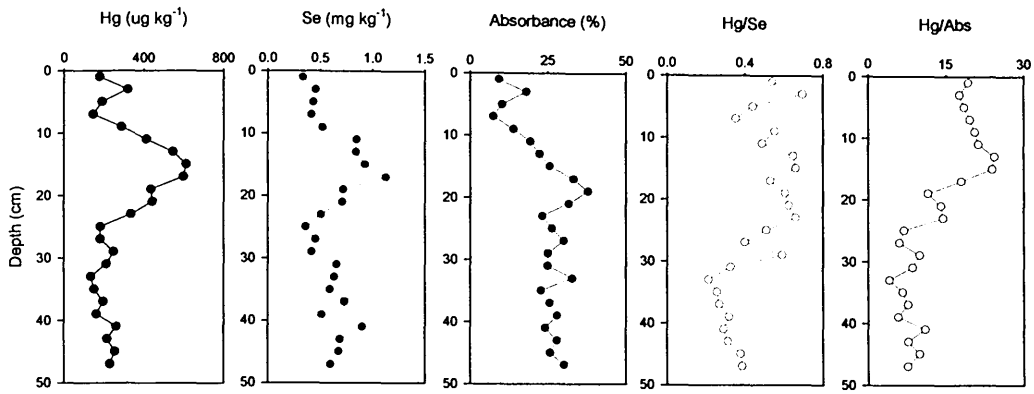

Figure 6.38: Depth profiles of Hg (μg kg^{-1}) and Se (mg kg^{-1}) concentrations, NaOH peat extract absorptions (%), Hg/Se and Hg/Abs ratios from 0-48 cm in the CM04CM-1 peat core.

The Hg/Se ratios increased from a mean value of 0.31 ± 0.06 between 48 and 30 cm to a mean value of 0.55 ± 0.10 between 30 and 0 cm (*cf.* Fig. 6.38). As mentioned in Sections 3.8.2.2.1 and 4.8.2.1.2, the similarity in anthropogenic sources (e.g. coal combustion) of Hg and Se is a potential problem when Se is used to normalise Hg concentrations and may account for the similarities observed between the Hg and Se (and S) profiles in CM04CM-1 (*cf.* Figs. 6.37 and 6.38). Note that the complete CM04CM-1 Se concentration profile from 0-106 cm will be investigated in Section 6.8.3. When the Hg concentration and NaOH peat extract absorption profiles in CM04CM-1 (*cf.* Fig. 6.38) are compared it is apparent that changes in Hg concentrations do not relate to the changes in peat decomposition, as found for Flanders Moss and The Red Moss of Balerno (*cf.* Sections 3.8.2.2.1 and 4.8.2.1.2). However, it is worth noting that coincident increases in Hg concentration and NaOH extract absorption were apparent in the CM04CM-1 surface vegetation (i.e. top 8 cm sections). Also, in contrast to the small changes in absorption within the profile, the changes in the Hg/Abs ratio profile (*cf.* Fig. 6.38) are far greater, as found for The

Red Moss of Balerno, indicating that organic matter decomposition cannot explain the magnitude of the variation in Hg concentrations with depth in the profile.

6.8.2.1.3 Historical trends in sources of atmospheric Hg deposition

The Hg and Pb concentration and $^{206}Pb/^{207}Pb$ ratio profiles for CM04CM-1, including ^{210}Pb age-dates, are shown in Fig. 6.39.

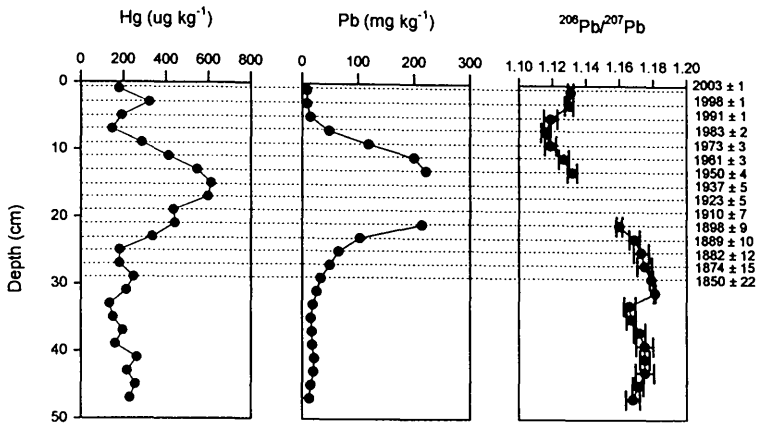

Figure 6.39: Depth profiles of Hg (μg kg^{-1}) and Pb (mg kg^{-1}) concentrations and measured $^{206}Pb/^{207}Pb$ ratios in the ^{210}Pb-dated CM04CM-1 peat core, from 0-48 cm.

From 48 cm in CM04CM-1, a depth for which no age-date was available but, based on the ^{14}C-dates 860-1020 A.D. in the underlying 70-72 cm section and 1215-1300 A.D. in the overlying 40-42 cm section, seems likely to correspond to the late 1000s A.D., to 24 cm (*ca.* 1886 A.D.), Hg concentrations were fairly constant (200 ± 40 μg kg^{-1}). Above 24 cm (*ca.* 1886 A.D.) the Hg concentrations increased to reach maximum values (550 - 600 μg kg^{-1}) between 18 and 12 cm (i.e. between *ca.* 1917 and 1956 A.D.) (*cf.* Fig. 6.39). These trends are most likely to be attributable to Hg emissions from coal combustion, as found for Flanders Moss and The Red Moss of Balerno (*cf.* Sections 3.8.2.2.2 and 4.8.2.1.3). After 1956 A.D., the Hg concentrations decreased to a minimum (150 μg kg^{-1}) at *ca.* 1991 A.D., reflecting a decrease in coal combustion emissions. However, between *ca.* 1991 A.D. and 2004 A.D., the Hg concentrations increased again, reaching a concentration of 300 μg kg^{-1} at 2003 A.D. (*cf.* Fig. 6.39). The Pb concentrations did not exhibit a similar increase, possibly reflecting Hg emissions from a relatively recent source that

does not contribute to Pb emissions (i.e. not waste incineration), although such a source is not known. It is worth noting that the recent Hg concentration increases in CM04CM-1 occur above the vegetation-peat interface (8-10 cm) (*cf.* 6.39), and, therefore, another explanation for the surface Hg concentration increases could be either differences in organic matter decomposition, at least in the growing and decomposing vegetation, as reflected in the NaOH peat extract absorption profile (*cf.* Fig. 6.38), or perhaps the efficiency of different species of vegetation in scavenging Hg (Barraclough *et al.*, 2002b).

6.8.2.1.4 Historical trends in depositional fluxes and inventories of Hg

Depositional fluxes of Hg (A7.1 Table A12) and anthropogenic Pb since 1840 A.D. are plotted, along with the measured $^{206}Pb/^{207}Pb$ ratios, *versus* ^{210}Pb-derived calendar dates for CM04CM-1 and CM04M in Fig. 6.40.

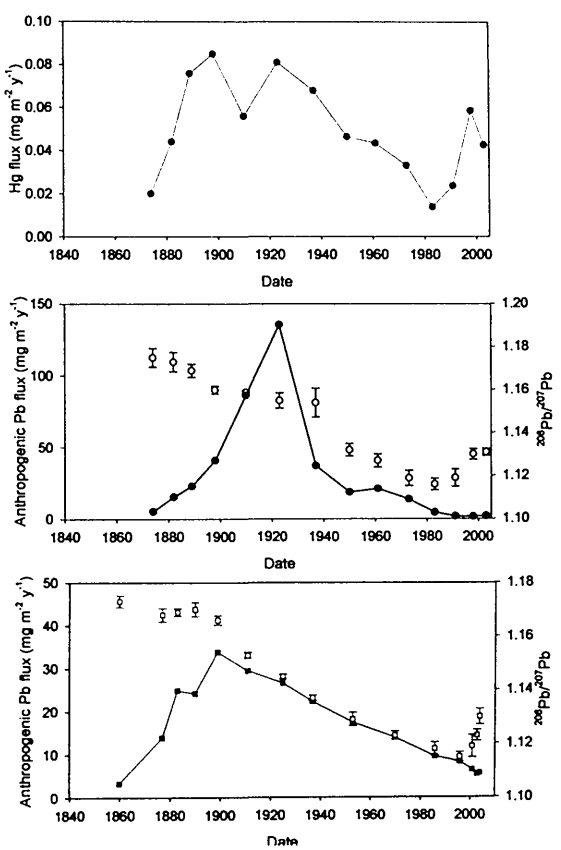

Figure 6.40: Calculated atmospheric depositional fluxes of Hg (light blue symbols) and anthropogenic Pb (mg m^{-2} y^{-1}) and measured $^{206}Pb/^{207}Pb$ ratios (open symbols) for the CM04CM-1 and CM04M (dark blue symbols) cores *versus* ^{210}Pb-derived dates since 1840 A.D.

Maximum Hg fluxes (~ 0.056 - 0.085 mg m^{-2} y^{-1}) occurred between the late 1880s and late 1930 A.D., after which Hg fluxes declined to 0.014 mg m^{-2} y^{-1} at 1983 A.D, before increasing again to 0.059 and 0.043 mg m^{-2} y^{-1} in 1998 and 2003 A.D., respectively (*cf.* Fig. 6.40). This 1998 A.D. flux is greater than the modelled Hg wet deposition value of ~ 0.013 mg m^{-2} y^{-1}, recorded in south-west Scotland during 1998 A.D. (Lee *et al.*, 2002). It is worth noting that there are considerable errors (mean 0.0090 ± 0.012 mg m^{-2} y^{-1}, range 0.00012 - 0.045 mg m^{-2} y^{-1}) associated with the Hg fluxes when errors on the Hg concentrations (A7.1 Table A7) are taken into account. Also, it should be remembered that there are significant uncertainties associated with the number of years for each CM04CM-1 peat section and, therefore, additional errors on the calculated fluxes.

The Hg inventory from 0 to 48 cm in the CM04CM-1 core was 11 mg m^{-2}, and the post-1800 A.D. Hg inventory (corresponding to peat sections 0-32 cm) was 8.7 mg m^{-2}. Calculated cumulative post-1800 A.D. Hg inventories (% of total post-1800 A.D. inventory) for CM04CM-1 are plotted *versus* ^{210}Pb-derived calendar dates in Fig. 6.41. Maximum deposition occurred between the 1880s and 1970s A.D., as found for Pb (*cf.* Section 6.6.2.1).

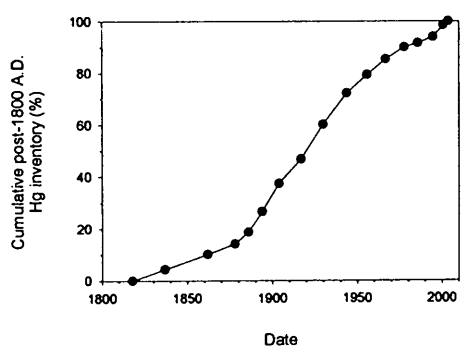

Figure 6.41: Calculated cumulative post-1800 A.D. Hg inventories (% of total post-1800 A.D. inventory) for the CM04CM-1 core *versus* ^{210}Pb-derived dates. Note that dates in CM04CM-1 prior to *ca.* 1862 A.D. were extrapolated.

6.8.3 As, Cd, Cu, Se and Zn

Although concentrations of As, Cd and Se were determined only for the CM04CM-1 core, concentrations of Cu and Zn were determined for both the CM04CM-1 and CM04M cores. Profiles of As, Cd, Cu, Se and Zn concentration (A7.1 Table A8), along with Pb and S concentration and ash content in CM04CM-1, are shown in Fig. 6.42. Profiles of Cu and Zn concentration (A7.2 Table A3) along with Pb and S concentration and ash content in CM04M, are shown in Fig. 6.43.

6.8.3.1 CM04CM-1

All five elements exhibited concentration peaks in the uppermost ~ 30 cm of the core, with the following maximum concentrations at the depths indicated:

- As – 9.7 mg kg^{-1} at 18-20 cm
- Cd – 2.3 mg kg^{-1} at 10-12 cm
- Cu – 24 mg kg^{-1} at 16-18 cm
- Se – 1.1 mg kg^{-1} at 16-18 cm
- Zn – 420 mg kg^{-1} at 0-2 cm but there was a peak (360 mg kg^{-1}) at 8-10 cm

Above these maxima, elemental concentrations decreased towards the surface, with the exception of Cu and Zn, which decreased up to 4 and 2 cm, respectively, before increasing again towards the surface (*cf.* Fig. 6.42). Below these maxima, elemental concentrations decreased towards the bottom of the core, with the exception of Se and Zn, which decreased down to ~ 30 cm before increasing again, remaining high and fairly constant in the anaerobic catotelm layers. Also, As and Cu exhibited minor peaks (4.5 and ~ 4 mg kg^{-1}, respectively) at 30-32 cm and between 76 and 80 cm, respectively, but, in general, the distributions of As, Cd and Cu were similar to those of Pb (excluding the "contaminated" Pb concentrations). The distributions of Se and Zn were generally more similar to that of S (*cf.* Fig. 6.42). Note that none of these elements appeared to be affected from 14 to 20 cm by the source of contamination experienced by Pb and Sb (*cf.* Sections 6.4.3 and 6.8.1.1).

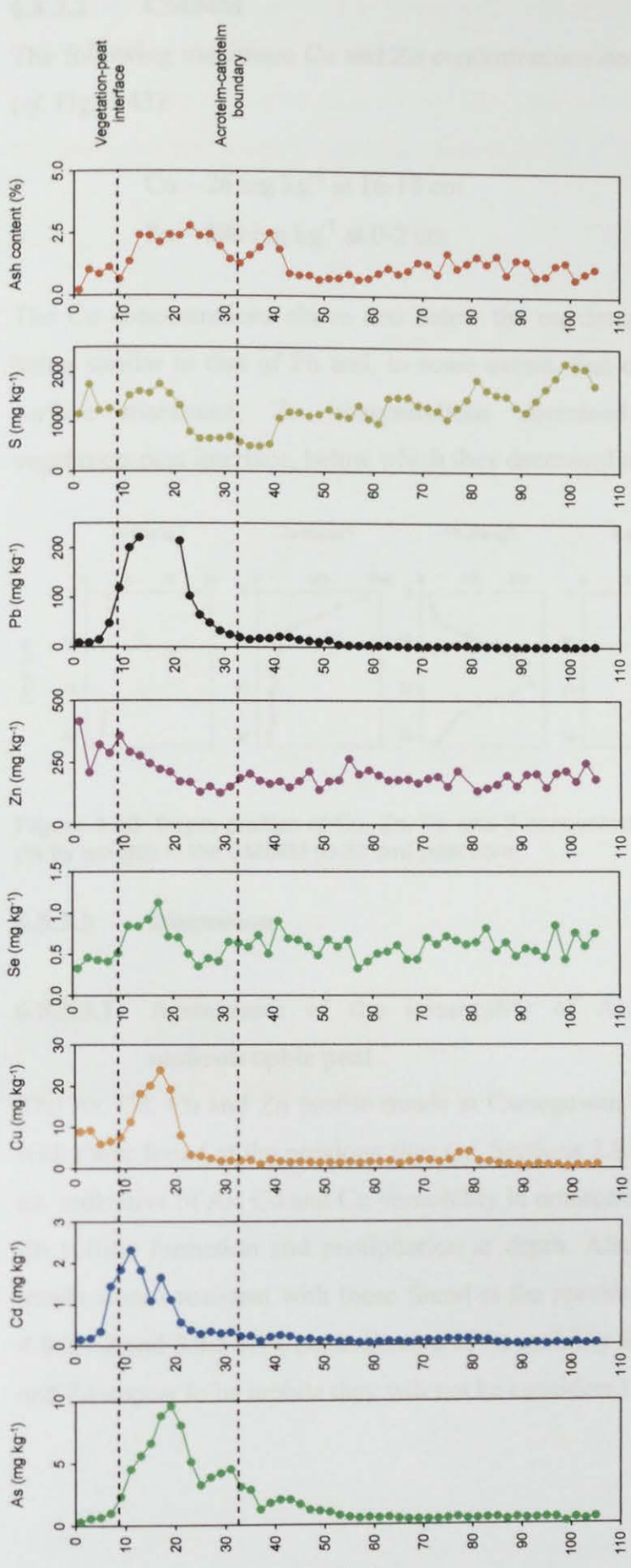

Figure 6.42: Depth profiles of As, Cd, Cu, Se, Zn, Pb and S concentrations (mg kg^{-1}) and ash contents (% by weight) in the CM04CM-1 (0-106 cm) peat core.

6.8.3.2 CM04M

The following maximum Cu and Zn concentrations occurred at the depths indicated (*cf.* Fig. 6.43):

- Cu – 26 mg kg^{-1} at 16-18 cm
- Zn – 880 mg kg^{-1} at 0-2 cm

The Cu concentrations above and below the maximum decreased, the distribution being similar to that of Pb and, to some extent, that of the ash content. Below the surface maximum, Zn concentrations decreased markedly down to the vegetation-peat interface, below which they decreased more gradually (*cf.* Fig. 6.43).

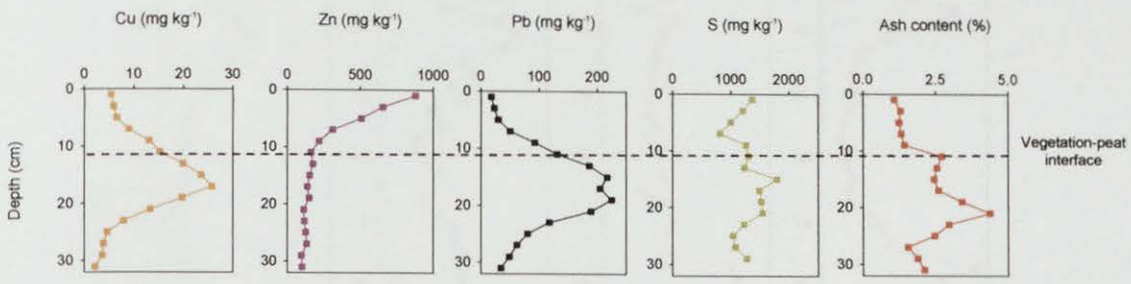

Figure 6.43: Depth profiles of Cu, Zn, Pb and S concentrations (mg kg^{-1}) and ash contents (% by weight) in the CM04M (0-32 cm) peat core.

6.8.3.3 Discussion

6.8.3.3.1 Assessment of the immobility of As, Cd, Cu, Se and Zn in ombrotrophic peat

The As, Cd, Cu and Zn profile trends at Carsegowan Moss are generally consistent with those found at the previous sites (*cf.* Sections 3.8.3.3.1, 4.8.3.3.1 and 5.8.3.3.1), i.e. indicative of As, Cd and Cu immobility in ombrotrophic peat and the influence of Zn sulfide formation and precipitation at depth. Also the Se concentration profile trends were consistent with those found at the previous sites (*cf.* Sections 3.8.2.2.1, 4.8.2.1.2 and 5.8.3.3.1), i.e. indicative of Se mobility in ombrotrophic peat. Since Se and Zn appear to be mobile they will not be considered any further in this Chapter.

6.8.3.3.2 The use of Sc and Ti as an indicator of As, Cd and Cu soil dust input

The As, Cd, Cu and Sc concentration profiles in CM04CM-1 are shown in Fig. 6.44, and, since Sc concentrations were not determined in CM04M, Cu and Ti concentration profiles in CM04M are shown in Fig. 6.45.

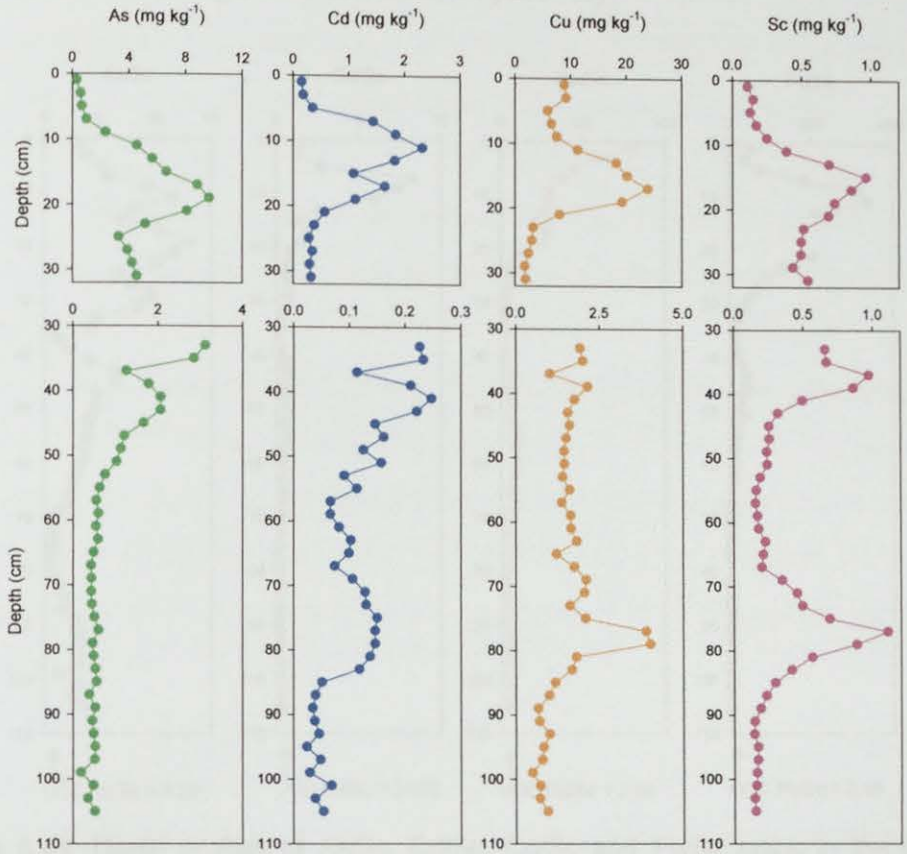

Figure 6.44: Depth profiles of As, Cd, Cu and Sc concentrations (mg kg^{-1}) from 0-32 cm and 32-106 cm in the CM04CM-1 peat core.

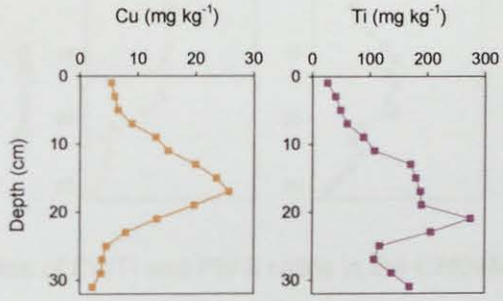

Figure 6.45: Depth profiles of Cu and Ti concentrations (mg kg^{-1}) in the CM04M (0-32 cm) peat core.

Note the change in scale on the As (3-fold), Cd (10-fold) and Cu (6-fold) concentrations on going from 0-32 cm to 32-106 cm in CM04CM-1. The As/Sc, Cd/Sc and Cu/Sc ratios in CM04CM-1 (A7.1 Table A9) and Cu/Ti ratios in CM04M (A7.2 Table A4) were calculated and their profiles, along with Pb/Sc and Pb/Ti ratios, are shown in Figs. 6.46 and 6.47, respectively.

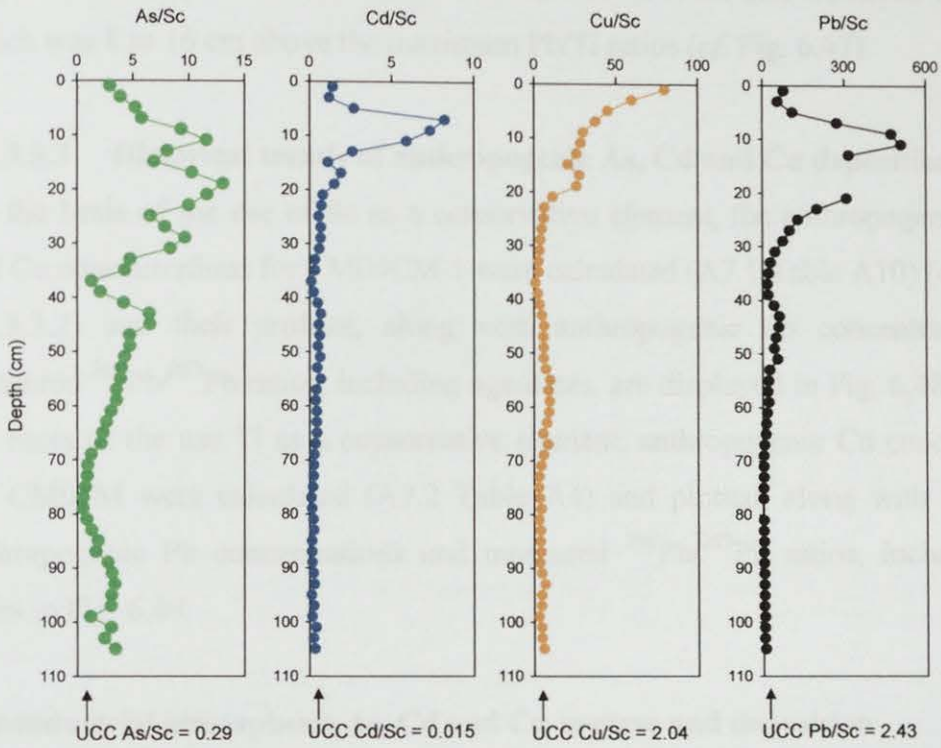

Figure 6.46: Depth profiles of As/Sc, Cd/Sc, Cu/Sc and Pb/Sc ratios in the CM04CM-1 (0-106 cm) peat core.

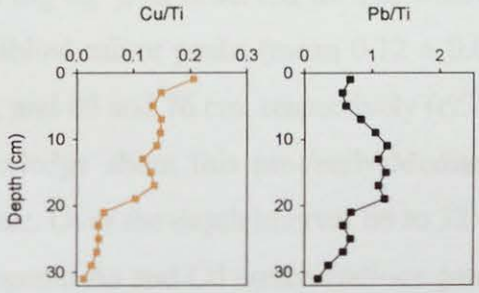

Figure 6.47: Depth profiles of Cu/Ti and Pb/Ti ratios in the CM04M (0-32 cm) peat core.

As for Pb/Sc ratios (*cf.* Section 6.5.1), the As/Sc, Cd/Sc and Cu/Sc ratios were at a minimum between 66 and 106 cm, with mean values of 1.9 ± 1.0, 0.25 ± 0.08 and 4.7 ± 1.4, respectively (*cf.* Fig. 6.46). Also, when comparing these As/Sc, Cd/Sc and

Cu/Sc ratios with the corresponding UCC As/Sc, Cd/Sc and Cu/Sc ratios, they were 7, 17 and 2-fold higher, respectively. Maximum As/Sc, Cd/Sc and Cu/Sc ratios in CM04CM-1 occurred at depths of 18-20 cm, 6-8 cm and 0-2 cm, respectively (*cf.* Fig. 6.46), which were different from the depth of the peak Pb/Sc ratio (10-12 cm) (*cf.* Section 6.5.1) (not taking the Pb/Sc ratios in the "contaminated" sections (14-20 cm) into account). The maximum Cu/Ti ratio in CM04M also occurred at 0-2 cm, which was 8 to 16 cm above the maximum Pb/Ti ratios (*cf.* Fig. 6.47).

6.8.3.3.3 Historical trends of anthropogenic As, Cd and Cu deposition

On the basis of the use of Sc as a conservative element, the anthropogenic As, Cd and Cu concentrations for CM04CM-1 were calculated (A7.1 Table A10) (*cf.* Section 3.8.3.3.2) and their profiles, along with anthropogenic Pb concentrations and measured $^{206}Pb/^{207}Pb$ ratios, including age-dates, are displayed in Fig. 6.48. Also, on the basis of the use Ti as a conservative element, anthropogenic Cu concentrations for CM04M were calculated (A7.2 Table A4) and plotted, along with calculated anthropogenic Pb concentrations and measured $^{206}Pb/^{207}Pb$ ratios, including age-dates in Fig. 6.49.

Pre-industrial atmospheric As, Cd and Cu sources and deposition

Over the depth interval 106 to 66 cm, the anthropogenic As concentrations were at a minimum (0.36 ± 0.10 mg kg^{-1}), as observed for Pb, whereas anthropogenic Cd and Cu concentrations exhibited minor peaks (mean 0.12 ± 0.01 and 1.9 ± 0.4 mg kg^{-1}) between 84 and 68 cm, and 80 and 76 cm, respectively (*cf.* Fig. 6.48). Due to the lack of archaeological knowledge about this pre-/early-Mediaeval period, the origin of these increases is unclear. Over the depth interval 66 to 32 cm (ignoring the decrease at 36-38 cm), anthropogenic As and Cd concentrations generally increased, reaching maximum values of 2.9 and 0.24 mg kg^{-1} at 32-34 cm and 40-42 cm, respectively, while the anthropogenic Cu concentrations decreased (mean 0.96 ± 0.28 mg kg^{-1}) (*cf.* Fig. 6.48).

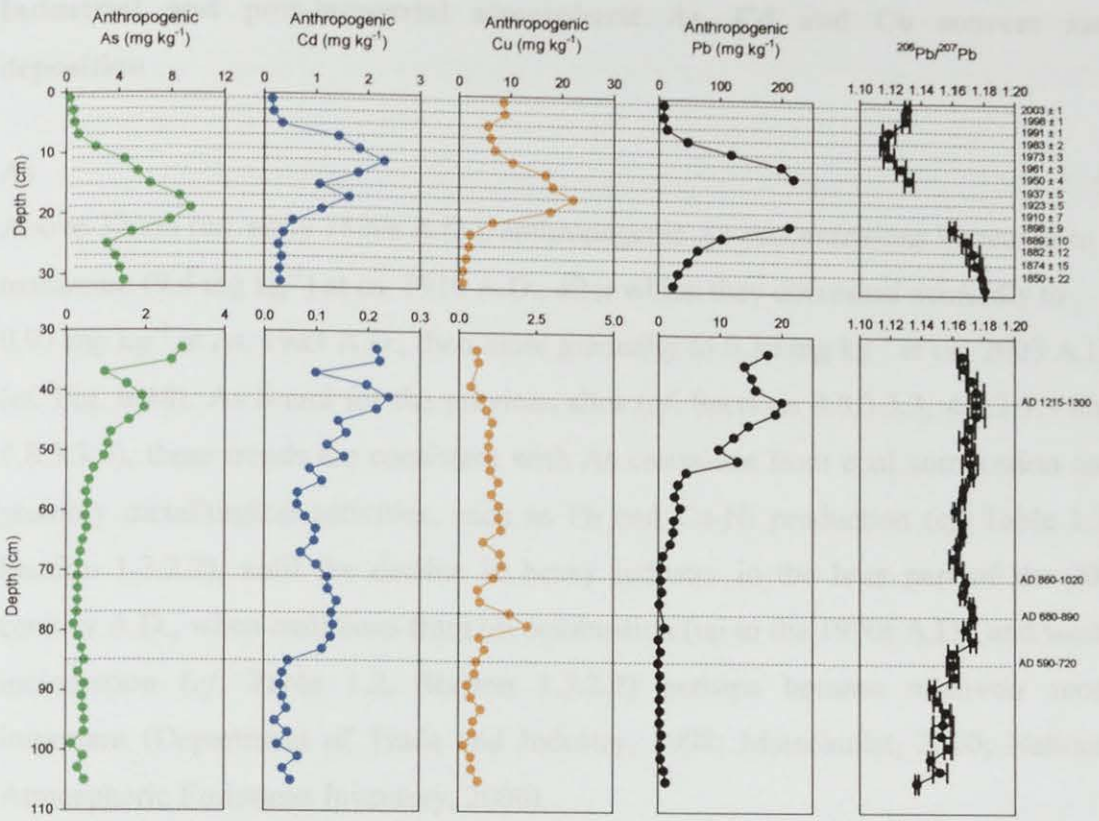

Figure 6.48: Depth profiles of anthropogenic As, Cd, Cu and Pb concentrations and measured $^{206}Pb/^{207}Pb$ ratios from 0-32 cm and 32-106 cm in the ^{210}Pb- and ^{14}C-dated CM04CM-1 peat core.

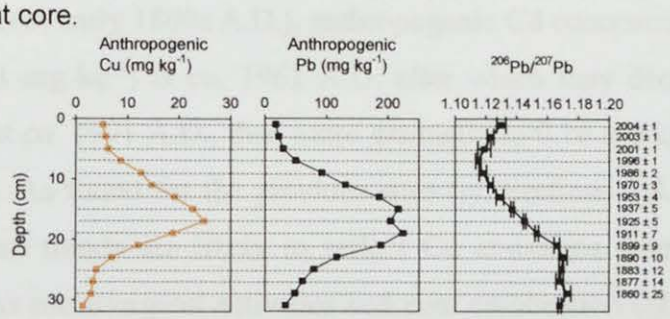

Figure 6.49: Depth profiles of anthropogenic Cu and Pb concentrations (calculated using Ti as the conservative element) and measured $^{206}Pb/^{207}Pb$ ratios in the ^{210}Pb-dated CM04M (0-32 cm) peat core.

It seems likely that the increases in anthropogenic As and Cd concentrations reflect emissions from the mining and smelting of Pb and Cu ores during the Mediaeval period. The anthropogenic Cu concentration profile, however, was dissimilar to that of Pb, exhibiting no increase during the Mediaeval period.

Industrial and post-industrial atmospheric As, Cd and Cu sources and deposition

As

Above 32 cm (*ca.* early 1800s A.D.), anthropogenic As concentrations increased to a maximum (9.4 mg kg^{-1}) at *ca.* 1910 A.D., after which they decreased markedly to 0.97 mg kg^{-1} at *ca.* 1983 A.D., then more gradually to 0.30 mg kg^{-1} at *ca.* 2003 A.D. (*cf.* Fig. 6.48). As found for the previous sites (*cf.* Sections 3.8.3.3.3, 4.8.3.3.3 and 5.8.3.3.3), these trends are consistent with As emissions from coal combustion and possibly metallurgical activities, such as Pb and Cu-Ni production (*cf.* Table 1.2, Section 1.3.2.2), until the decline in heavy industry in the later part of the 20th century A.D., when emissions from oil combustion (up to the 1990s A.D.) and waste incineration (*cf.* Table 1.2, Section 1.3.2.2) perhaps became relatively more important (Department of Trade and Industry, 1998; Matschullat, 2000; National Atmospheric Emissions Inventory, 2006).

Cd

Above 32 cm (*ca.* early 1800s A.D.), anthropogenic Cd concentrations increased to a maximum (2.3 mg kg^{-1}) at *ca.* 1961 A.D. after which they decreased markedly to 0.35 mg kg^{-1} at *ca.* 1991 A.D., then more gradually to 0.16 mg kg^{-1} at *ca.* 2003 A.D. (*cf.* Fig. 6.48). As found for the previous sites (*cf.* Sections 3.8.3.3.3, 4.8.3.3.3 and 5.8.3.3.3), these trends are likely to reflect Cd emissions from a combination of sources such as metallurgical activities and coal combustion (*cf.* Table 1.2, Section 1.3.2.2), until the decline in heavy industry in the later part of the 20th century A.D., when emissions from oil combustion (up to the 1990s A.D.) and waste incineration (*cf.* Table 1.2, Section 1.3.2.2) perhaps became more important (Department of Trade and Industry, 1998; National Atmospheric Emissions Inventory, 2006).

Cu

Above 32 cm (*ca.* early 1800s A.D.), anthropogenic Cu concentrations increased to a maximum (22 mg kg^{-1}) at *ca.* 1923 A.D., after which they decreased markedly to

5.7 mg kg^{-1} at *ca.* 1991 A.D., then increased to ~ 9 mg kg^{-1} between *ca.* 1998 and 2003 A.D. (*cf.* Fig. 6.48). Similarly, above 32 cm (*ca.* early 1800 A.D.) in CM04M, anthropogenic Cu concentrations increased to a maximum (25 mg kg^{-1}) at *ca.* 1925 A.D., after which they decreased markedly to 6.4 mg kg^{-1} at *ca.* 2001 A.D., then remained fairly constant towards the surface (*cf.* Fig. 6.49). As found for the previous sites (*cf.* Sections 3.8.3.3.3, 4.8.3.3.3 and 5.8.3.3.3), these trends are likely to reflect Cu emissions from a combination of sources, e.g. Cu-Ni, Zn-Cd and non-ferrous metal production and coal combustion (*cf.* Table 1.2, Section 1.3.2.2), until the decline in heavy industry in the later part of the 20th century A.D., when emissions from oil combustion (up to the 1990s A.D.) and waste incineration (*cf.* Table 1.2, Section 1.3.2.2) perhaps became more important (Department of Trade and Industry, 1998; National Atmospheric Emissions Inventory, 2006). Note that, as found at the previous sites (*cf.* Sections 3.8.3.3.3, 4.8.3.3.3 and 5.8.3.3.3), anthropogenic Cu concentrations remained relatively high, compared with As and Cd, in recent years (*cf.* Figs. 6.48 and 6.49), perhaps providing further evidence for comparatively new recent sources of Cu e.g. automobile exhaust and non-exhaust emissions, due to the use of Cu as an antioxidant in motor oil and its presence in new brake linings and tyres (Cadle *et al.*, 1999; Sternbeck *et al.*, 2002; Chemical Research Communications, 2003; Boulter, 2004).

6.8.3.3.4 Historical trends in depositional fluxes and inventories of anthropogenic As, Cd and Cu

Anthropogenic depositional fluxes were calculated for As, Cd and Cu in CM04CM-1 (A7.1 Table A12) and for Cu in CM04M (A7.2 Table A6). Anthropogenic As, Cd and Cu fluxes, since 1840 A.D., are plotted along with the anthropogenic Pb fluxes and measured $^{206}Pb/^{207}Pb$ ratios, *versus* ^{210}Pb-derived calendar dates, for CM04CM-1 and CM04M in Fig. 6.50. Depositional fluxes of anthropogenic As, Cd and Cu were at a maximum (1.5, 0.24 and 3.0 mg m^{-2} y^{-1}) at *ca.* 1900 A.D., during the early 1960s A.D. and early 1920s A.D., respectively (*cf.* Fig. 6.47). Depositional fluxes of anthropogenic Cu in CM04M were at a maximum (3.2 mg m^{-2} y^{-1}) at 1925 A.D. (*cf.* Fig. 6.50).

Total anthropogenic As, Cd and Cu inventories of 0.14, 0.024 and 0.22 g m^{-2}, respectively, were calculated for CM04CM-1, with a corresponding Cu inventory of 0.25 g m^{-2} for CM04M. For CM04CM-1, the post-1800 A.D. As, Cd and Cu inventories (0.11, 0.019 and 0.19 g m^{-2}) (corresponding to peat sections 0-32 cm) constituted 79, 79 and 86% of the total anthropogenic As, Cd and Cu inventories.

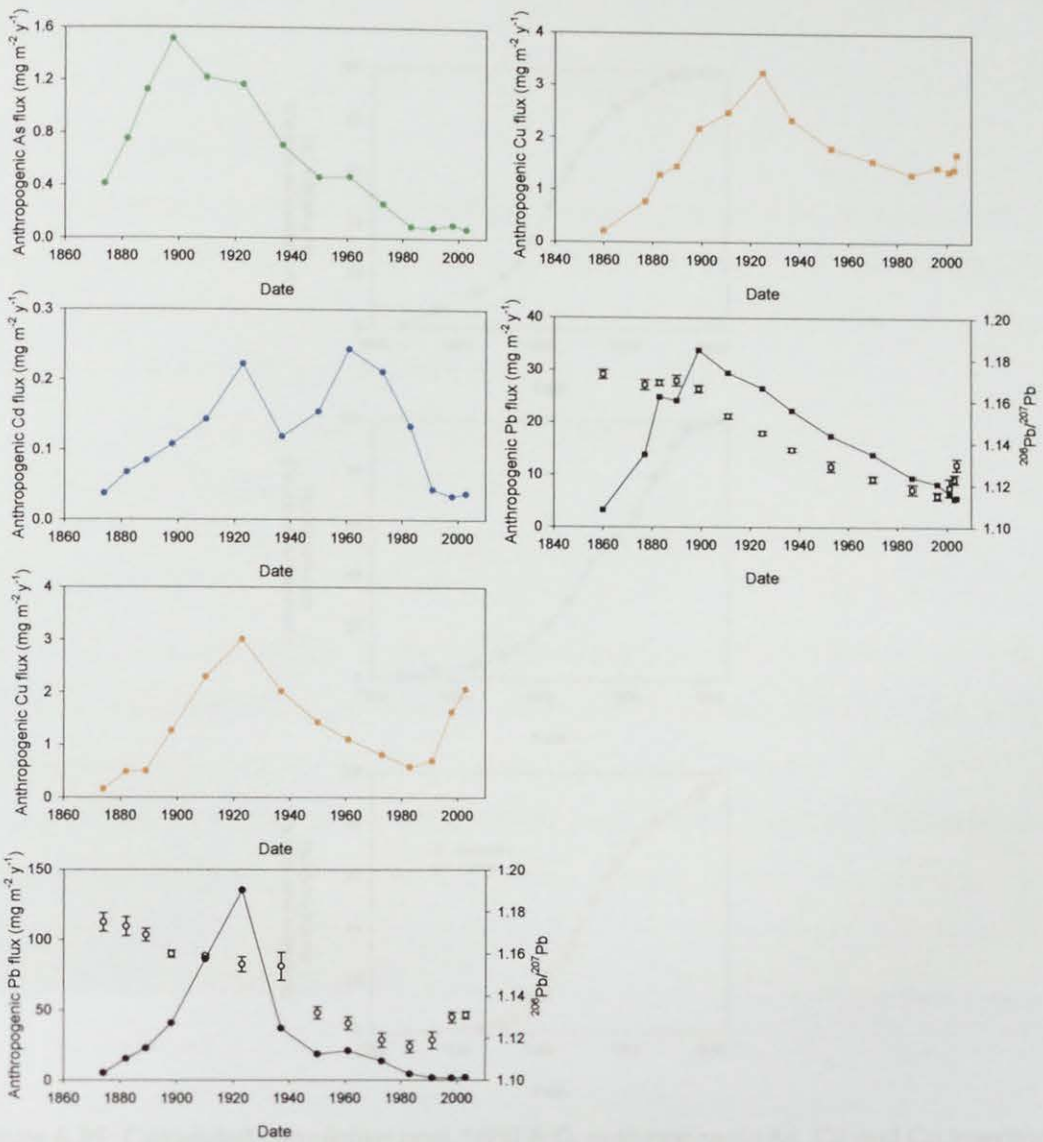

Figure 6.50: Calculated atmospheric depositional fluxes of anthropogenic As, Cd, Cu and Pb (mg m^{-2} y^{-1}) (closed symbols) and the measured $^{206}Pb/^{207}Pb$ ratios (open symbols) for the CM04CM-1 (circles) and CM04M (squares) cores *versus* ^{210}Pb-derived dates since 1840 A.D.

Calculated cumulative post-1800 A.D. anthropogenic As, Cd and Cu inventories (% of total post-1800 A.D. inventory) for CM04CM-1, with corresponding values for Cu

in CM04M, are plotted *versus* ^{210}Pb-derived calendar dates in Fig. 6.51. Maximum As, Cd and Cu deposition occurred between the 1880s and 1950s A.D., 1890s and 1970s A.D., and 1880s and 1980s A.D., respectively, broadly in agreement with that found for Pb (*cf.* Section 6.6.2.1) (*cf.* Fig. 6.51). There was good agreement between Cu deposition trends in the two cores.

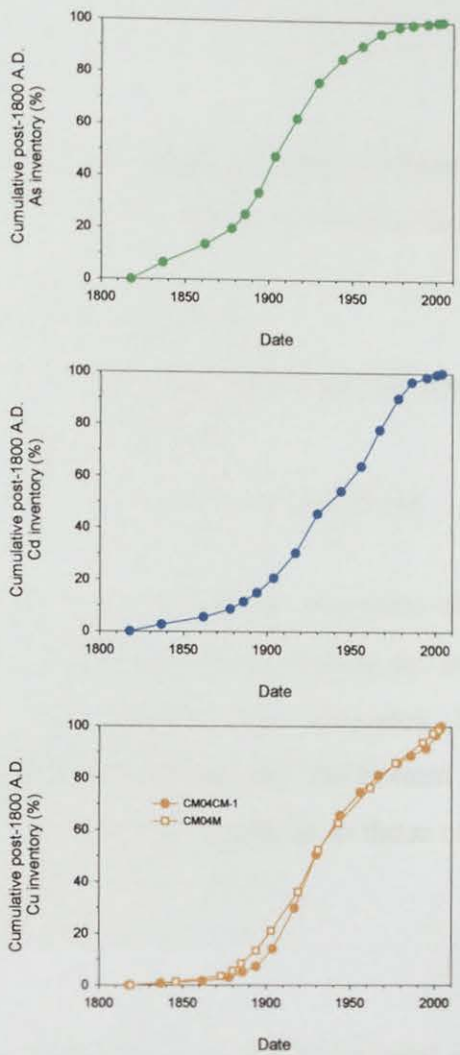

Figure 6.51: Calculated cumulative post-1800 A.D. anthropogenic As, Cd and Cu inventories (% of total post-1800 A.D. inventory) for the CM04CM-1 core and cumulative post-1800 A.D. anthropogenic Cu inventories (% of total post-1800 A.D. inventory) for the CM04M core *versus* ^{210}Pb-derived dates. Note that dates in CM04CM-1 and CM04M prior to *ca.* 1862 A.D. and *ca* 1846 A.D., respectively, were extrapolated.

6.8.4 Co, Cr, Ni and V

Although concentrations of Co, Cr and Ni were determined only for the CM04CM-1 core, concentrations of V were determined for both the CM04CM-1 and CM04M cores. Profiles of Co, Cr, Ni and V concentrations (A7.1 Table A8), along with Pb concentrations and ash contents, are shown in Fig. 6.52. Profiles for CM04M V concentrations (A7.2 Table A3), along with Pb and ash contents, are shown in Fig. 6.53.

6.8.4.1 CM04CM-1

All four elements exhibited concentration peaks or increases in the uppermost ~ 30 cm of the core, with the following maximum concentrations at the depths indicated:

- Co – 3.9 mg kg^{-1} at 14-16 cm
- Cr – 8.0 – 8.5 mg kg^{-1} between 12 and 16 cm
- Ni – 5.4 mg kg^{-1} at 10-12 cm
- V – 18 - 19 mg kg^{-1} between 12 and 16 cm

Elemental concentrations, with the possible exception of Co, decreased towards the top of the core and, in the peat sections underlying the concentration peaks, with the exception of V which exhibited clear increases between 70 and 90 cm, concentrations generally decreased towards the bottom of the core. In general the distributions of Co, Cr, Ni and V were similar to those of Pb and the ash content (*cf.* Fig. 6.52).

6.8.4.2 CM04M

The maximum V concentration (14 mg kg^{-1}) occurred at 12-14 cm in the CM04M core (*cf.* Fig. 6.53), at the upper edge of the broad Pb maximum from 12 to 22 cm.

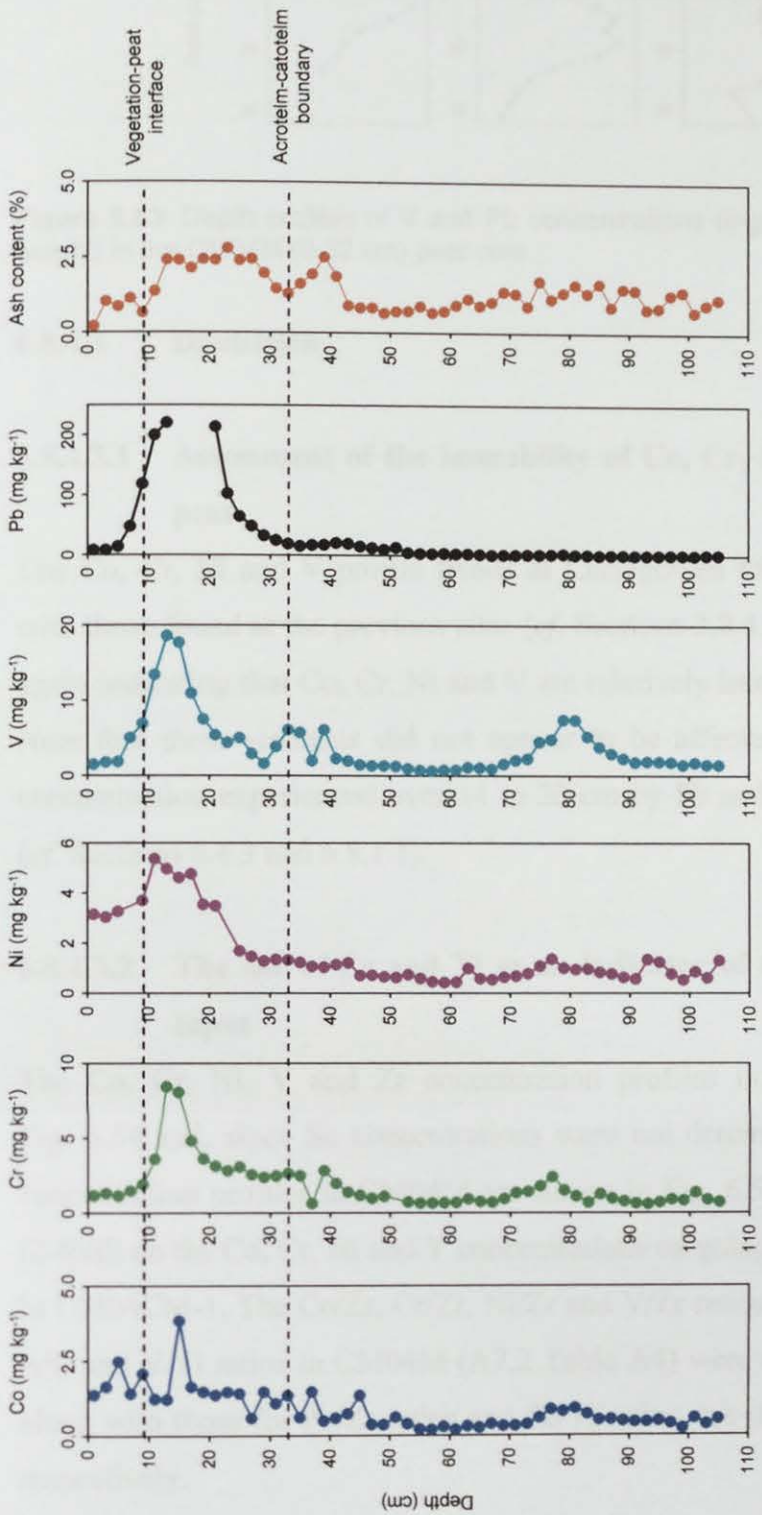

Figure 6.52: Depth profiles of Co, Cr, Ni, V and Pb concentrations (mg kg^{-1}) and ash contents (% by weight) in the CM04CM-1 (0-106 cm) peat core.

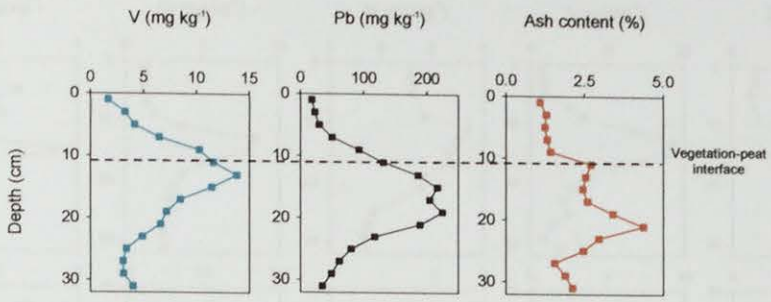

Figure 6.53: Depth profiles of V and Pb concentrations (mg kg^{-1}) and ash contents (% by weight) in the CM04M (0-32 cm) peat core.

6.8.4.3 Discussion

6.8.4.3.1 Assessment of the immobility of Co, Cr, Ni and V in ombrotrophic peat

The Co, Cr, Ni and V profile trends at Carsegowan Moss are generally consistent with those found at the previous sites (*cf.* Sections 3.8.4.3.1, 4.8.4.1.1 and 5.8.3.1.1), again indicating that Co, Cr, Ni and V are relatively immobile in ombrotrophic peat. Note that these elements did not appear to be affected by the specific source of contamination experienced over 14 to 20 cm by Pb and Sb in the CM04CM-1 core (*cf.* Sections 6.4.3 and 6.8.1.1).

6.8.4.3.2 The use of Zr and Ti as an indicator of Co, Cr, Ni and V soil dust input

The Co, Cr, Ni, V and Zr concentration profiles in CM04CM-1 are shown in Fig. 6.54 and, since Sc concentrations were not determined in CM04M, V and Ti concentration profiles in CM04M are shown in Fig. 6.55. Note the changes in scale (2-fold) on the Co, Cr, Ni and V concentrations on going from 0-32 cm to 32-106 cm in CM04CM-1. The Co/Zr, Cr/Zr, Ni/Zr and V/Zr ratios in CM04CM-1 (A7.1 Table A9) and V/Ti ratios in CM04M (A7.2 Table A4) were calculated and their profiles, along with those for Pb/Zr ratios and Pb/Ti ratios, are shown in Figs. 6.56 and 6.57, respectively.

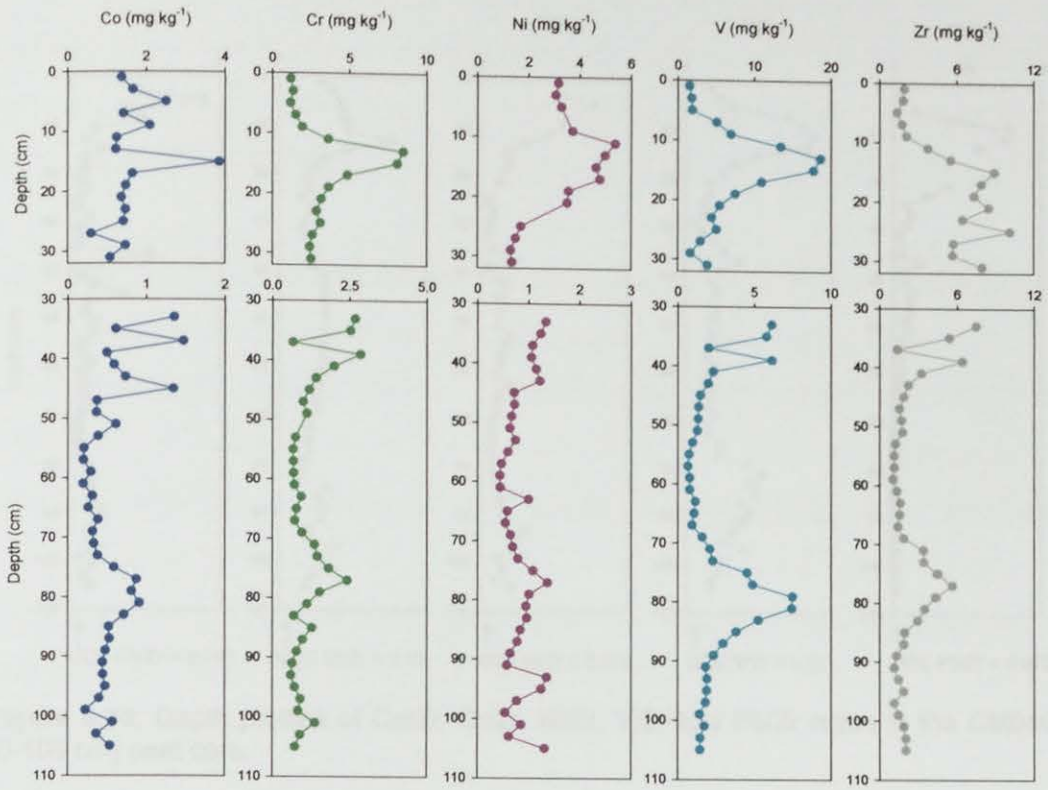

Figure 6.54: Depth profiles of Co, Cr, Ni, V and Zr concentrations (mg kg^{-1}) from 0-32 cm and 32-106 cm in the CM04CM-1 peat core.

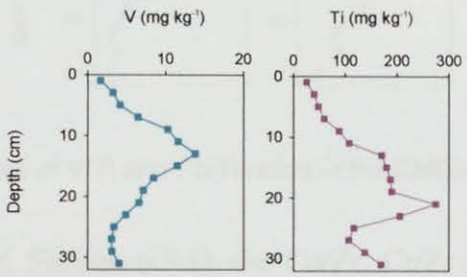

Figure 6.55: Depth profiles of V and Ti concentrations (mg kg^{-1}) in the CM04M (0-32 cm) peat core.

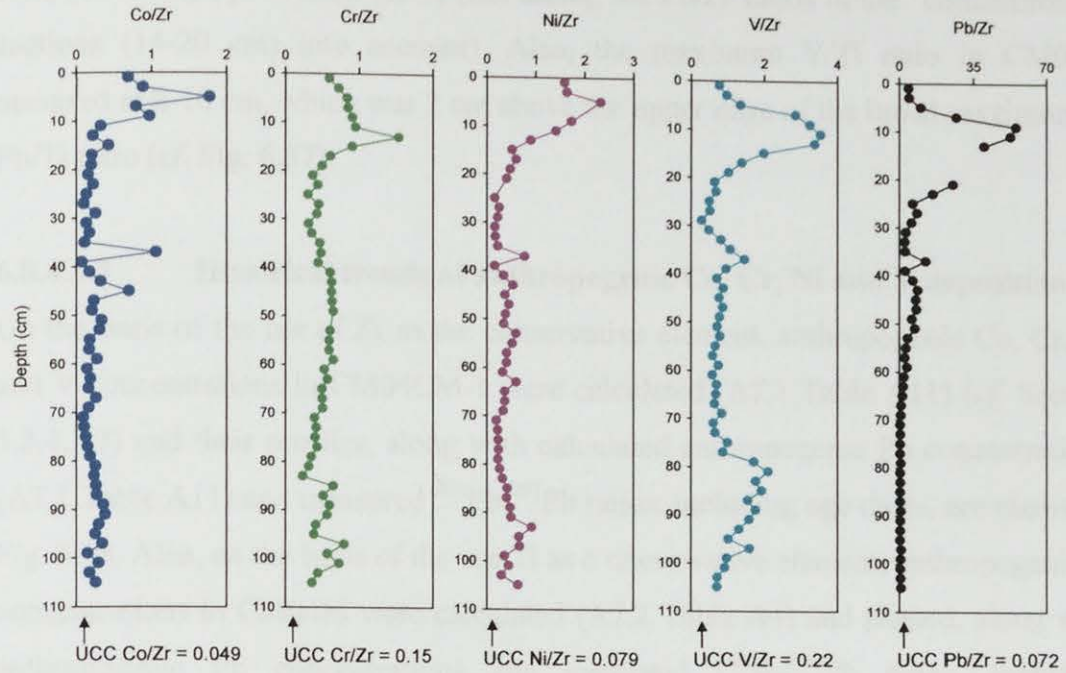

Figure 6.56: Depth profiles of Co/Zr, Cr/Zr, Ni/Zr, V/Zr and Pb/Zr ratios in the CM04CM-1 (0-106 cm) peat core.

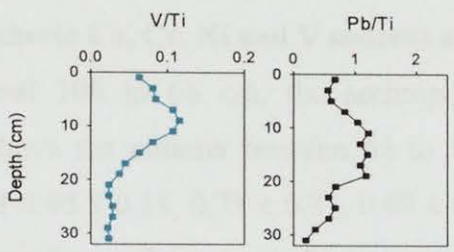

Figure 6.57: Depth profiles of V/Ti and Pb/Ti ratios in the CM04M (0-32 cm) peat core.

As for Pb/Zr ratios (*cf.* Section 6.5.1), the Co/Zr, Cr/Zr and Ni/Zr ratios were at a minimum between 66 and 106 cm, with mean values of 0.24 ± 0.08, 0.48 ± 0.14 and 0.42 ± 0.19, respectively. The corresponding V/Zr ratios at these depths exhibited a broad peak between 74 and 102 cm, with a maximum value of 2.1 at 80-82 cm. The minimum mean V/Zr ratio (0.72 ± 0.09) occurred between 74 and 40 cm (*cf.* Fig. 6.56). The Co/Zr, Cr/Zr, Ni/Zr and V/Zr ratio minima were 3- to 5-fold higher than the corresponding UCC Co/Zr, Cr/Zr, Ni/Zr and V/Zr ratios. Maximum Co/Zr, Cr/Zr, Ni/Zr and V/Zr ratios at depths of 4-6 cm, 12-14 cm, 4-6 cm and 10-12 cm, respectively (*cf.* Fig. 6.56), which were different from the depth of the peak Pb/Zr

ratio (8-10 cm) (*cf.* Section 6.5.1) (not taking the Pb/Zr ratios in the "contaminated" sections (14-20 cm) into account). Also, the maximum V/Ti ratio in CM04M occurred at 8-10 cm, which was 2 cm above the upper edge of the broad maximum in Pb/Ti ratio (*cf.* Fig. 6.57).

6.8.4.3.3 Historical trends of anthropogenic Co, Cr, Ni and V deposition

On the basis of the use of Zr as the conservative element, anthropogenic Co, Cr, Ni and V concentrations in CM04CM-1 were calculated (A7.1 Table A11) (*cf.* Section 3.8.4.3.3) and their profiles, along with calculated anthropogenic Pb concentrations (A7.1 Table A11) and measured $^{206}Pb/^{207}Pb$ ratios, including age-dates, are shown in Fig. 6.58. Also, on the basis of the use Ti as a conservative element, anthropogenic V concentrations in CM04M were calculated (A7.2 Table A4) and plotted, along with anthropogenic Pb concentrations and measured $^{206}Pb/^{207}Pb$ ratios, including age-dates, in Fig. 6.59.

Pre-industrial atmospheric Co, Cr, Ni and V sources and deposition

Over the depth interval 106 to 66 cm, the anthropogenic Co, Cr, Ni and V concentrations were above the minima between 66 to 52 cm (*cf.* Fig. 6.58), with mean concentrations of 0.40 ± 0.15, 0.73 ± 0.31, 0.69 ± 0.25 and 2.4 ± 1.8 mg kg^{-1}. In contrast, the corresponding anthropogenic Pb concentrations at these depths were at a minimum (*cf.* Fig. 6.58). The V concentrations, in contrast to those of the other elements, were clearly enhanced between 90 and 74 cm (mean 4.1 ± 1.7 mg kg^{-1}) (*cf.* Fig. 6.58). Interestingly, this V enhancement appears to be less when the anthropogenic V concentrations are calculated using the conservative elements Sc and Ti instead of Zr (Fig. 6.60). Although minor peaks between 78 and 90 cm, with maxima of ~ 3 and 4 mg kg^{-1}, when using Sc and Ti, respectively, are apparent.

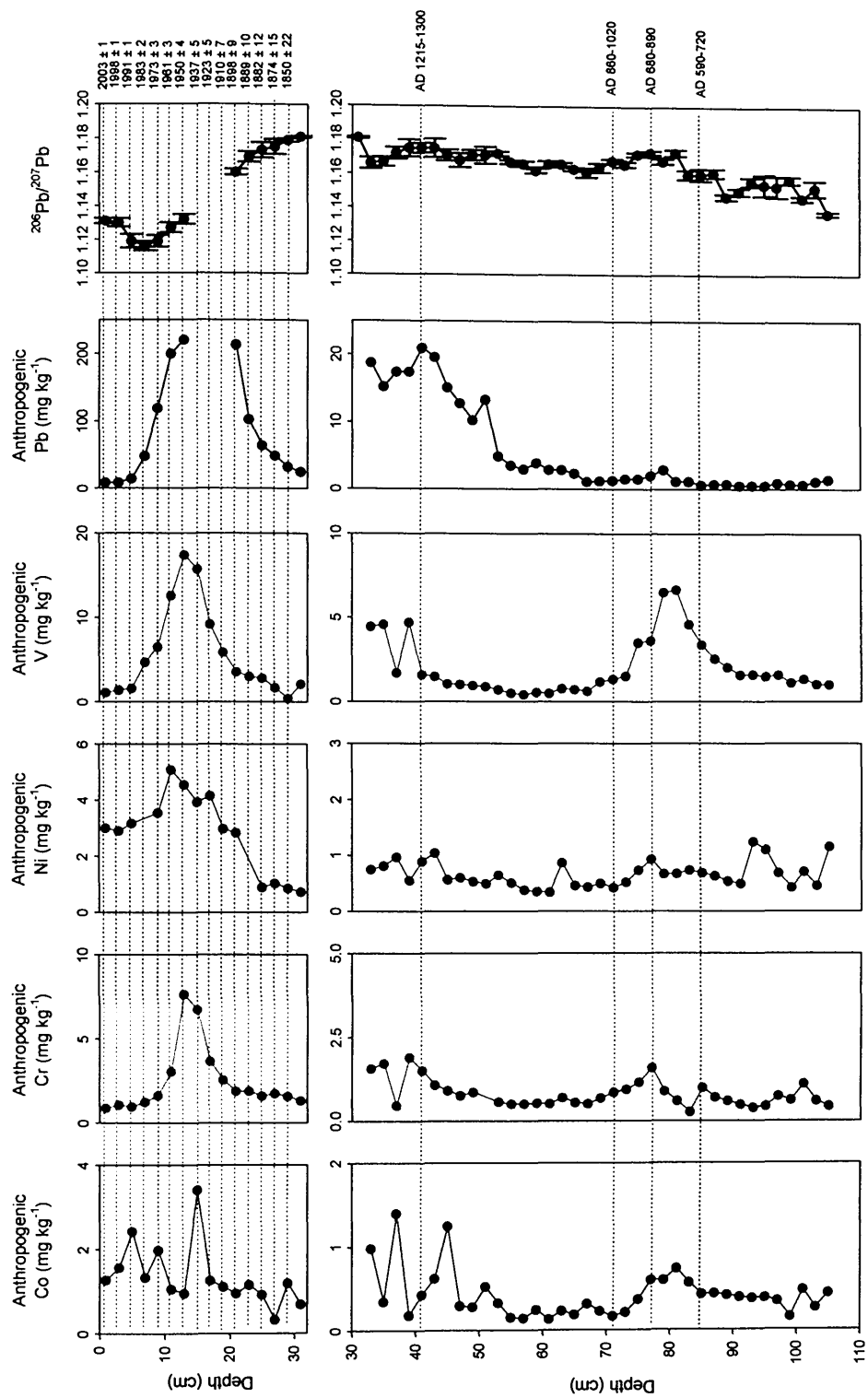

Figure 6.58: Depth profiles of anthropogenic Co, Cr, Ni, V and Pb concentrations (calculated using Zr as the conservative element) and measured $^{206}Pb/^{207}Pb$ ratios, from 0-32 cm and 32-106 cm in the ^{210}Pb- and ^{14}C-dated CM04CM-1 peat core.

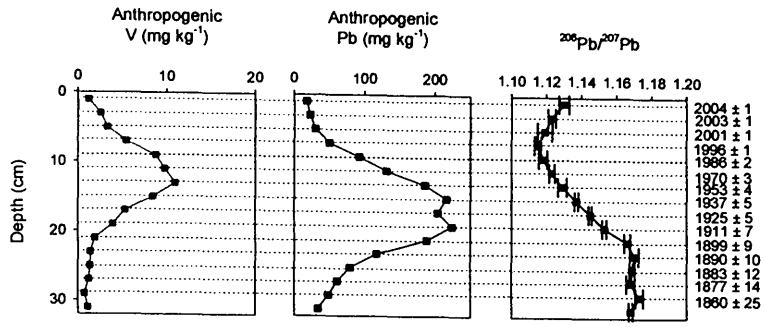

Figure 6.59: Depth profiles of anthropogenic V and Pb concentrations (calculated using Ti as the conservative element) and measured $^{206}Pb/^{207}Pb$ ratios in the ^{210}Pb-dated CM04M (0-32 cm) peat core.

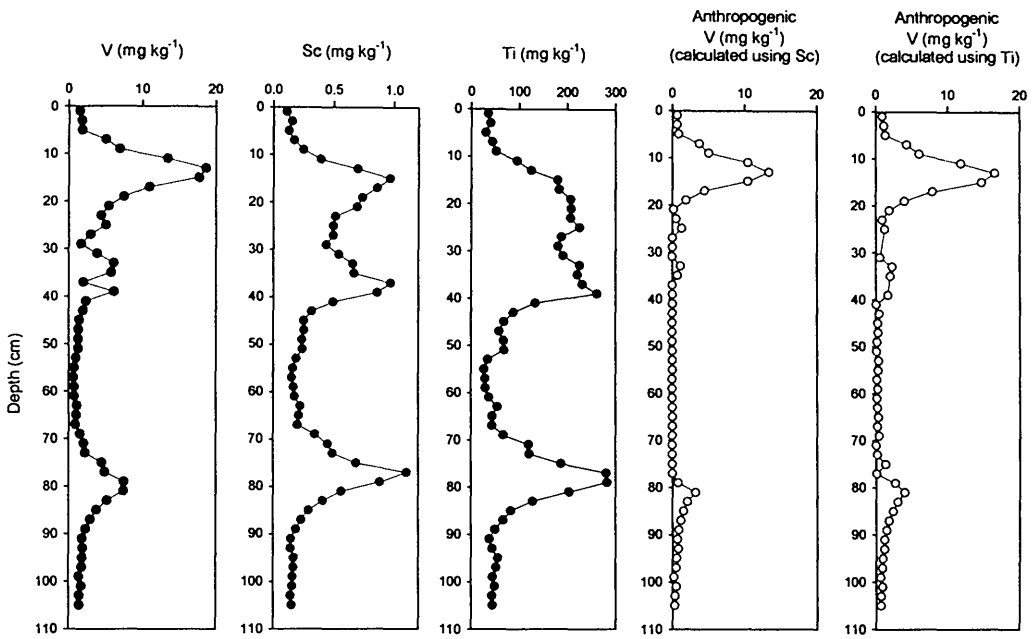

Figure 6.60: Depth profiles of V, Sc, Ti and anthropogenic V concentrations (calculated using Sc and Ti) (mg kg^{-1}) in the CM04CM-1 (0-106 cm) peat core.

Zoller *et al.* (1974) proposed that V was a lithogenic element like Sc, Ti and Zr, and one possible explanation for the V enhancements observed at depth in the CM04CM-1 core is local soil dust inputs attributable to woodland clearance at Carsegowan Moss during post-Roman/early Mediaeval times (*cf.* Section 6.3.3), where the soil dust is relatively more enriched in V than Sc, Ti and, in particular, Zr. Over the depth interval 66 to 52 cm, anthropogenic Co, Cr, Ni and V concentrations were at a minimum with mean concentrations of 0.20 ± 0.07, 0.56 ± 0.07, 0.51 ±

0.19 and 0.60 ± 0.14 mg kg^{-1}, respectively. Over the depth interval 52 to 32 cm (omitting the Co, Cr and V values at 36-38 cm), anthropogenic Co, Cr, Ni and V concentrations generally increased (*cf.* Fig. 6.58), with mean concentrations of 0.55 ± 0.36, 1.3 ± 0.4 0.72 ± 0.20 and 2.3 ± 1.7 mg kg^{-1}, respectively. Enhanced Pb concentrations during these periods reflect emissions from Mediaeval mining and smelting activities (*cf.* Sections 5.6.1), but these activities are not considered to be a significant source of these other elements (*cf.* Table 1.2, Section 1.3.2.2) (Nriagu and Pacyna, 1988) and, therefore, the cause of their slightly enhanced concentrations is unclear.

Industrial and post-industrial atmospheric Co, Cr, Ni and V sources and deposition

Co

The anthropogenic Co concentrations fluctuated greatly but in general, above 32 cm (*ca.* early 1800s A.D.), they increased to a maximum (3.4 mg kg^{-1}) at *ca.* 1937 A.D. (*cf.* Fig. 6.58), after which they decreased markedly to 0.96 mg kg^{-1} at *ca.* 1950 A.D. They then increased gradually to 2.4 mg kg^{-1} at *ca.* 1991 A.D. before decreasing again to 1.3 mg kg^{-1} at 2003 A.D. Note that the cause of the fluctuating anthropogenic Co concentrations, as observed at Turclossie Moss (*cf.* Section 5.8.3.1.3), during these industrial/post-industrial periods is unclear but, in general, as found for the previous sites (*cf.* Sections 3.8.4.3.3, 4.8.4.1.3 and 5.8.3.1.3), these trends are likely to reflect Co emissions from metallurgical activities, coal combustion and the use of phosphate fertilisers (Oehme, 1979; Chemical Research Communications, 2003), until the decline in heavy industry in the later part of the 20th century A.D., when emissions from oil combustion (*cf.* Fig. 1.3, Section 1.3.2.2.2) (up to the 1990s A.D.) and waste incineration (Chemical Research Communications, 2003) perhaps became more important (Department of Trade and Industry, 1998; National Atmospheric Emissions Inventory, 2006).

Cr

Above 32 cm (*ca.* early 1800s A.D.), anthropogenic Cr concentrations increased to a maximum (7.7 mg kg^{-1}) at *ca.* 1950 A.D., after which they decreased markedly to 1.6 mg kg^{-1} at *ca.* 1973 A.D., then more gradually to 0.90 mg kg^{-1} at *ca.* 2003 A.D. (*cf.* Fig. 6.58). As found for the previous sites (*cf.* Sections 3.8.4.3.3, 4.8.4.1.3 and 5.8.3.1.3), these trends are likely to reflect Cr emissions from coal combustion and steel and iron manufacturing (*cf.* Table 1.2, Section 1.3.2.2), until the decline in heavy industry in the later part of the 20th century A.D., when emissions from oil combustion (up to the 1990s A.D.) and waste incineration (*cf.* Table 1.2, Section 1.3.2.2) perhaps became more important (Department of Trade and Industry, 1998; National Atmospheric Emissions Inventory, 2006). Note that as found for Flanders Moss and Turclossie Moss (*cf.* Sections 3.8.4.3.3 and 5.8.3.1.3), the anthropogenic Cr concentrations remained fairly constant after the late 1980s A.D. (*cf.* Fig. 6.58), perhaps providing further evidence for comparatively new sources of Cr emissions (e.g. automotive brake linings) (Boulter, 2004).

Ni

Above 32 cm (*ca.* early 1800s A.D.), anthropogenic Ni concentrations increased to a maximum (5.1 mg kg^{-1}) at *ca.* 1961 A.D., after which they decreased markedly to 3.6 mg kg^{-1} at *ca.* 1973 A.D., then more gradually to 3.0 mg kg^{-1} at *ca.* 2003 A.D. (*cf.* Fig. 6.58). As found for the previous sites (*cf.* Sections 3.8.4.3.3, 4.8.4.1.3 and 5.8.3.1.3), these trends are likely to reflect Ni emissions from Cu-Ni production and coal combustion (*cf.* Table 1.2, Section 1.3.2.2), until the decline in heavy industry in the later part of the 20th century A.D., when emissions from oil combustion (up to the 1990s A.D.) and waste incineration (*cf.* Table 1.2, Section 1.3.2.2) perhaps became more important (Department of Trade and Industry, 1998; National Atmospheric Emissions Inventory, 2006). It is worth noting that, as found for Turclossie Moss (*cf.* Section 5.8.3.1.3), anthropogenic Ni concentrations remained relatively high, compared with Co, Cr and V, after the late 1980s A.D., perhaps providing further evidence for comparatively new sources of Ni emissions (e.g. automotive brake linings) (Boulter, 2004).

V

Above 32 cm (*ca.* early 1800s A.D.), anthropogenic V concentrations increased to a maximum (17 mg kg^{-1}) at *ca.* 1950 A.D., after which they decreased markedly to 1.6 mg kg^{-1} at *ca.* 1991 A.D., then more gradually to 1.1 mg kg^{-1} at *ca.* 2003 A.D. (*cf.* Fig. 6.58). Similarly, above 32 cm (*ca.* early 1800 A.D.) in CM04M, anthropogenic V concentrations increased to a maximum (11 mg kg^{-1}) at *ca.* 1953 A.D., after which they decreased gradually to 1.2 mg kg^{-1} at *ca.* 2003 A.D. (*cf.* Fig. 6.59). As found for the previous sites (*cf.* Sections 3.8.4.3.3, 4.8.4.1.3 and 5.8.3.1.3), these trends are likely to reflect V emissions from coal combustion (*cf.* Table 1.2, Section 1.3.2.2), until the decline in heavy industry in the later part of the 20th century A.D., when emissions from oil combustion (up to the 1990s A.D.) perhaps became relatively more important (Department of Trade and Industry, 1998; National Atmospheric Emissions Inventory, 2006).

6.8.4.3.4 Historical trends in depositional fluxes and inventories of anthropogenic Co, Cr, Ni and V

The anthropogenic depositional fluxes of Co, Cr, Ni and V in CM04CM-1 (A7.1 Table A12) and for V in CM04M (A7.2 Table A6) were calculated, along with the anthropogenic depositional fluxes of Pb, using Zr (*cf.* Section 3.8.4.3.3). These fluxes, since 1840 A.D. are plotted along with the measured $^{206}Pb/^{207}Pb$ ratios, *versus* ^{210}Pb-derived calendar dates, for CM04CM-1 and CM04M in Fig. 6.61. Maximum depositional fluxes of anthropogenic Co, Cr and V (0.38, 0.75 and 1.7 mg m^{-2} y^{-1}, respectively), occurred during the late 1930s A.D., while that of Ni (0.71 mg m^{-2} y^{-1}) occurred during the early 2000s A.D. Depositional fluxes of anthropogenic V in CM04M (*cf.* Fig. 6.61) were at a maximum (1.0 mg m^{-2} y^{-1}) between the early 1950s and early 1970s A.D. The differences between V flux trends observed in CM04CM-1 and CM04M (*cf.* Fig. 6.61) could perhaps be attributable to depositional variability at the peat bog surface (Bindler *et al.*, 2004).

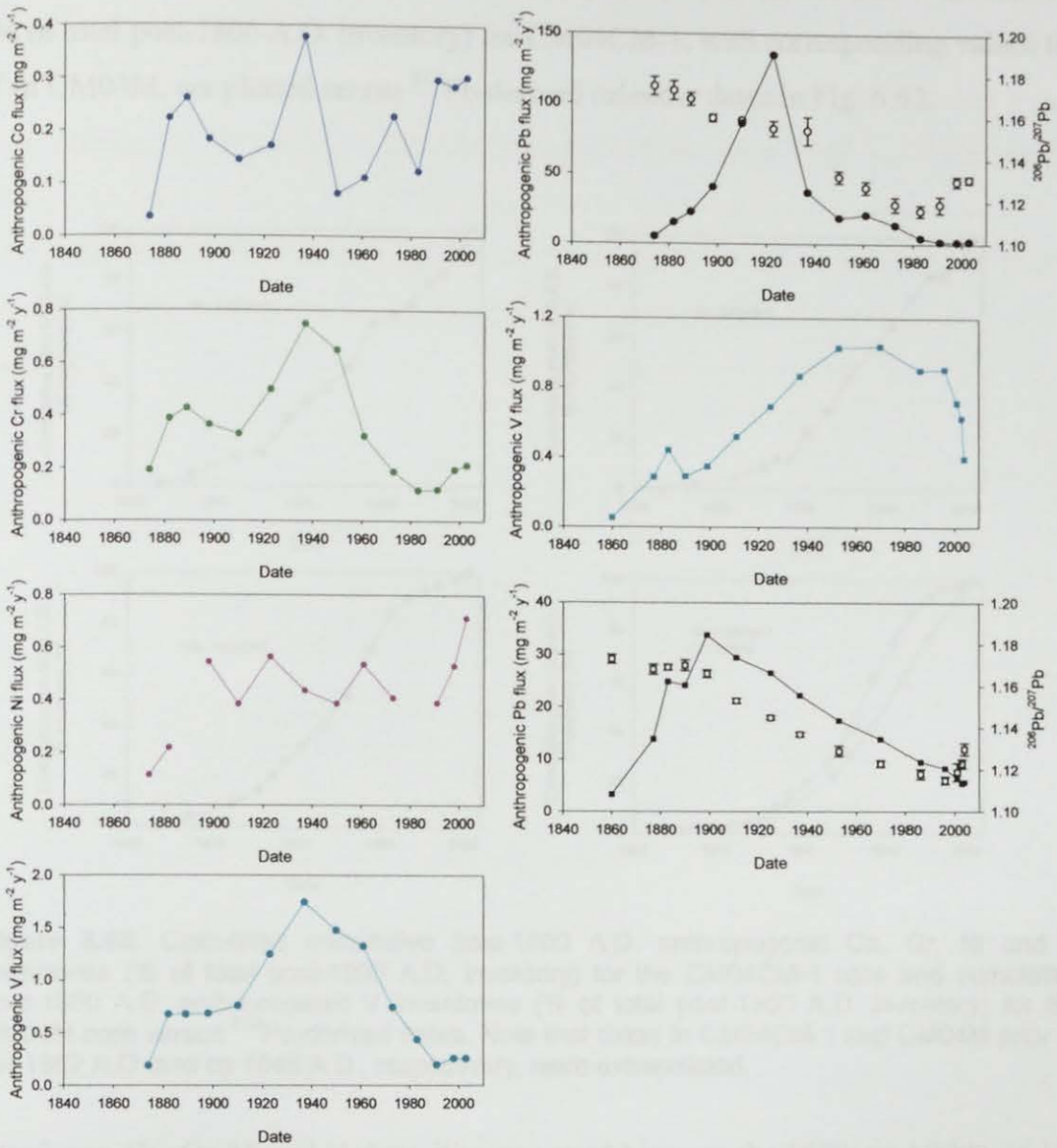

Figure 6.61: Calculated atmospheric depositional fluxes of anthropogenic Co, Cr, Ni, V and Pb (mg m^{-2} y^{-1}) (closed symbols) and the measured $^{206}Pb/^{207}Pb$ ratios (open symbols) for the CM04CM-1 (circles) and CM04M (squares) cores *versus* ^{210}Pb-derived dates since 1840 A.D.

Total anthropogenic Co, Cr, Ni and V inventories of 0.047, 0.090, 0.080 and 0.21 g m^{-2}, respectively, were calculated for CM04CM-1, with a corresponding V inventory of 0.099 g m^{-2} for CM04M (remembering that CM04M only dates back to *ca* 1800 A.D.). The post-1800 A.D. Co, Cr, Ni and V inventories (0.030, 0.056, 0.054 and 0.12 g m^{-2}) (corresponding to peat sections 0-32 cm) constituted 64, 62, 68 and 57% of the total anthropogenic Co, Cr, Ni and V inventories, respectively.

Calculated cumulative post-1800 A.D. anthropogenic Co, Cr, Ni and V inventories (% of total post-1800 A.D. inventory) for CM04CM-1, with corresponding values for V in CM04M, are plotted *versus* ^{210}Pb-derived calendar dates in Fig. 6.62.

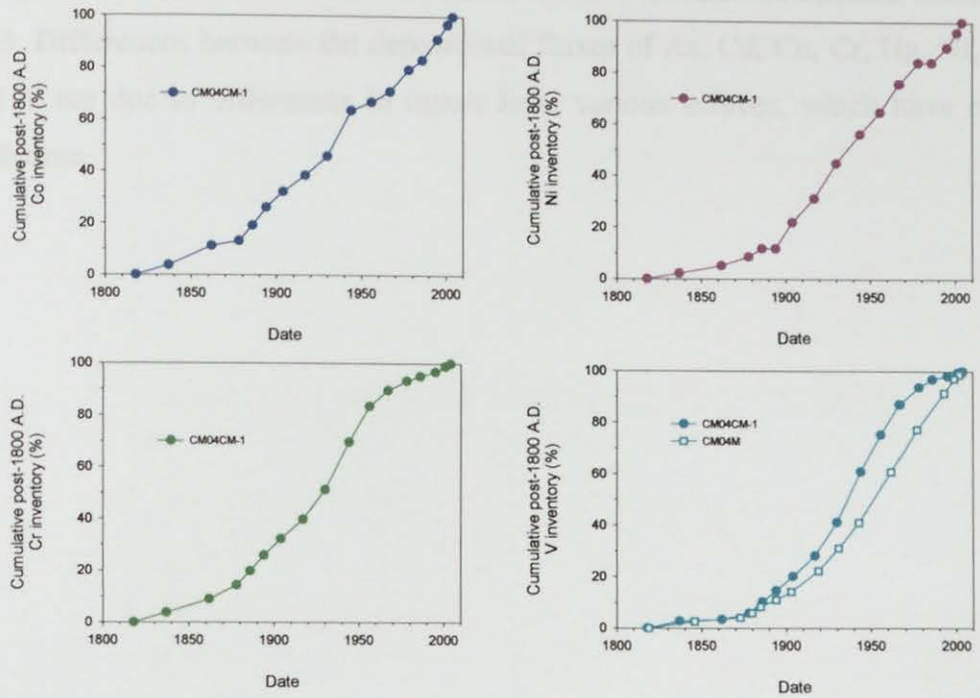

Figure 6.62: Calculated cumulative post-1800 A.D. anthropogenic Co, Cr, Ni and V inventories (% of total post-1800 A.D. inventory) for the CM04CM-1 core and cumulative post-1800 A.D. anthropogenic V inventories (% of total post-1800 A.D. inventory) for the CM04M core *versus* ^{210}Pb-derived dates. Note that dates in CM04CM-1 and CM04M prior to *ca.* 1862 A.D. and *ca* 1846 A.D., respectively, were extrapolated.

Maximum Co, Cr, Ni and V deposition occurred between the 1880s and 2000s A.D., 1880s and 1960s A.D., 1890s and 1960s A.D. and 1890s and 1980s A.D., respectively, broadly in agreement, perhaps with the exception of V, with that found for Pb (*cf.* Section 6.6.2.1). Uncertainties associated with the ^{210}Pb dates extrapolated for CM04CM-1 from CM04M, can perhaps account for differences in the vertical (temporal) distribution (%) of anthropogenic V inventories between the two cores.

6.8.5 Comparison of As, Cd, Co, Cr, Cu, Hg, Ni, Pb, Sb and V depositional fluxes

The depositional fluxes of anthropogenic As, Cd, Co, Cu, Cr, Ni, Pb, Sb and V and depositional Hg fluxes for CM04CM-1 and CM04M since 1840 A.D. are plotted along with the measured $^{206}Pb/^{207}Pb$ ratios *versus* ^{210}Pb-derived calendar dates in Fig. 6.63. Differences between the depositional fluxes of As, Cd, Co, Cr, Hg, Ni, Pb. Sb and V are due to differences in inputs from various sources, which have changed with time.

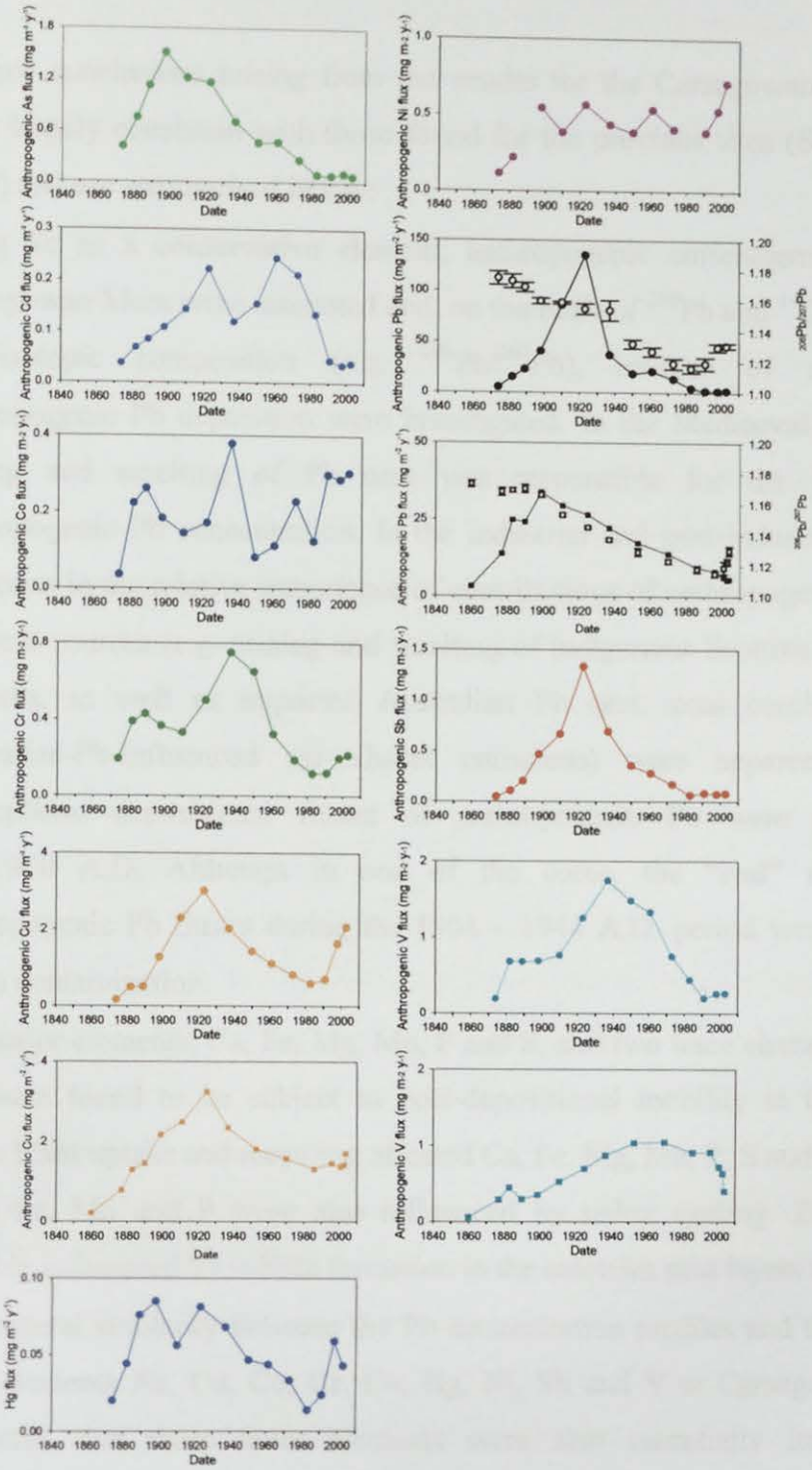

Figure 6.63: Calculated atmospheric depositional fluxes of anthropogenic As, Cd, Co, Cr, Cu, Ni, Pb, Sb and V (mg m^{-2} y^{-1}), depositional fluxes of Hg (mg m^{-2} y^{-1}) and measured $^{206}Pb/^{207}Pb$ ratios for the CM04CM-1 (circles) and CM04M (squares) cores *versus* ^{210}Pb-derived dates since 1840 A.D.

6.9 CONCLUSIONS

The principal conclusions arising from the results for the Carsegowan Moss peat cores were largely consistent with those found for the previous sites (Sections 3.9, 4.9 and 5.9) and are summarised below:

- Using Sc as a conservative element, anthropogenic enrichments of Pb at Carsegowan Moss were estimated and, on the basis of ^{210}Pb and ^{14}C dating and Pb isotopic composition (e.g. $^{206}Pb/^{207}Pb$), sources of atmospheric anthropogenic Pb deposition were investigated. In the Mediaeval period, the mining and smelting of Pb ores was responsible for the increase in anthropogenic Pb concentration. In the industrial and post-industrial periods, variations in the relative importance of contributions of anthropogenic Pb from different sources (e.g. mining and smelting of indigenous Scottish and British Pb ores, as well as imported Australian Pb ores, coal combustion and Australian-Pb-influenced car-exhaust emissions) were apparent. Derived atmospheric depositional fluxes of anthropogenic Pb were greatest at *ca.* 1900 A.D. Although in one of the cores, the "real" depositional anthropogenic Pb fluxes during the 1904 – 1944 A.D. period were unknown due to contamination.
- The major elements, Ca, Fe, Mg, Mn, P and S, and two trace elements, Se and Zn, were found to be subject to post-depositional mobility at Carsegowan Moss. Plant uptake and recycling affected Ca, Fe, Mg, Mn, P, S and Zn profiles while Fe, Mn and P were also influenced by redox cycling. Zn was also possibly influenced by sulfide formation in the catotelm peat layers of the bog.
- The general similarity between the Pb concentration profiles and those of the trace elements As, Cd, Co, Cr, Cu, Hg, Ni, Sb and V at Carsegowan Moss suggested that these latter elements were also essentially immobile in ombrotrophic peat.
- The Sb and Pb concentration profiles at Carsegowan Moss were remarkably similar. Using Sc as a conservative element, anthropogenic enrichments of Sb were estimated and, on the basis of anthropogenic Sb/Pb ratios, sources of

atmospheric anthropogenic Sb deposition were investigated. During the Mediaeval period, sources of anthropogenic Sb deposition were the same as those found for Pb, and this was also the case during the Industrial period, with the exception of leaded petrol. In the post-industrial period, the influence of anthropogenic inputs of Sb from comparatively new recent sources (e.g. automotive brake linings) was apparent. Derived atmospheric depositional fluxes of anthropogenic Sb appeared to be greatest at *ca.* 1900 A.D., but the "real" depositional anthropogenic Sb fluxes during the 1904 – 1944 A.D. period were unknown due to contamination.

- In the industrial and post-industrial periods, coal combustion and waste incineration, respectively, are likely to have been the most important sources of Hg. However, Hg concentration increases in the surface vegetation layers of the bog may have been attributable to either a new recent source or perhaps differences in organic matter decomposition and/or the differential Hg scavenging efficiency of different species of vegetation. Derived atmospheric depositional fluxes of Hg were greatest in the industrial era, peaking between the late 1880s and late 1930s A.D.
- Anthropogenic As, Cd and Cu concentrations were estimated using Sc as a conservative element. In the Mediaeval period, the mining and smelting of Pb and Cu ores is likely to have been responsible for the increase in anthropogenic As and Cd concentrations. In the industrial and post-industrial periods, sources of As, Cd and Cu were attributed to a variety of sources (e.g. metallurgical activities, coal and oil combustion and waste incineration). Also, there may have been inputs of Cu from comparatively new recent anthropogenic sources (e.g. automobile exhaust and non-exhaust emissions, due to the use of Cu as an antioxidant in motor oil and its presence in new brake linings and tyres). Derived atmospheric depositional fluxes of anthropogenic As, Cd and Cu were greatest at *ca.* 1900 A.D., during the early 1960s A.D. and early 1920s A.D., respectively.
- Anthropogenic Co, Cr, Ni and V concentrations were estimated using Zr as a conservative element. In the Mediaeval period, anthropogenic Co, Cr, Ni and V

concentrations generally increased but the sources of these increases were unclear. In the industrial and post-industrial periods, sources of Co, Cr, Ni and V were attributable to a variety of sources (e.g. metallurgical activities, coal and oil combustion, use of phosphate fertilisers and waste incineration). Also, there may have been inputs of Cr and Ni from comparatively new recent anthropogenic sources (e.g. automotive brake linings). Derived atmospheric depositional fluxes of anthropogenic Co and Cr were greatest during the late 1930s A.D., while those of Ni were greatest during the early 2000s A.D and those of V were greatest between the late 1930s and early 1970s A.D.

- Differences between the timings of the maximum anthropogenic V fluxes, but not the anthropogenic Cu and Pb fluxes, were apparent for the two cores collected from Carsegowan Moss.

7 SITE COMPARISON

This chapter will compare the results found at each of the four Scottish peat bog sites. Findings regarding peat matrix properties, radionuclides, conservative elements and the geochemical behaviour of the elements investigated will be summarised. The histories of atmospheric As, Cd, Co, Cr, Cu, Hg, Ni, Pb, Sb and V deposition at each site will be compared and geographical variations within Scotland will be investigated and, where possible, compared with trends found in other parts of Europe.

7.1 INTRODUCTORY OVERVIEW

It is worth remembering that geographically the sites fall into two categories (*cf.* Fig. 2.1, Section 2.1.1): Flanders Moss (FM) and The Red Moss of Balerno (RM) are much closer to the industrial and heavily populated central belt of Scotland than the more remote rural sites Turclossie Moss (TM) in north-east Scotland and Carsegowan Moss (CM) in south-west Scotland. Also, the average annual rainfall at the four sites varies in the order FM > CM > TM > RM (Table 7.1) (*cf.* Sections 2.1.2.4, 2.1.3.4, 2.1.4.4 and 2.1.5.4), generally reflecting a west to east decrease, in line with the prevailing wind direction in the UK from south-west to north-east.

Table 7.1: Average annual rainfall data for each peat bog site.

Site	Annual Rainfall (cm y^{-1})
Flanders Moss	150
Carsegowan Moss	96
Turclossie Moss	82
The Red Moss of Balerno	63

7.2 PEAT MATRIX PROPERTIES

7.2.1 Visual observations

The vegetation-peat interface positions were different in each of the cores collected (*cf.* Sections 3.1.1, 4.1.1, 5.1.1 and 6.1.1), ranging from depths of ~ 4 to 24 cm,

remembering that, as a result of the removal of some vegetation prior to the collection of the FM01CM-1 core (*cf.* Sections 2.2.2.1 and 3.1.1), living vegetation was absent from the surface of this core.

7.2.2 Wet/dry weight ratios and water contents

The acrotelm-catotelm boundary positions were also different in each of the cores collected (*cf.* Sections 3.1.2, 4.1.2, 5.1.2 and 6.1.2), ranging from depths of ~ 22 to 54 cm. Similar wet/dry weight ratio and water content profile trends were observed in each of the bogs, but, in general, lower values were observed at RM and TM peat cores, reflecting the unique hydrological properties found at each bog as a result of the annual and/or seasonal rainfall patterns, as well as differences in the water-holding capacities of different types of vegetation (e.g. RM cores were collected from *Pleurozium schreberi* moss hummocks whereas cores from the other sites were collected from *Sphagnum* moss hummocks).

7.2.3 Ash contents and Ca/Mg ratios

The ash content and Ca/Mg ratio values in all of the cores collected (*cf.* Sections 3.1.3, 4.1.3, 5.1.3 and 6.1.3) were consistent with ombrotrophic conditions, i.e. < 15% and 6, respectively (Hulme *et al.*, 1991; Shotyk, 1996a; Berner and Berner, 1997; Weiss *et al.*, 1998). Near-surface increases in ash contents and Ca/Mg ratios were observed at each of the sites, attributable to increased anthropogenic and natural dust inputs and to nutrient cycling, there being a preferential uptake of Ca over Mg by plants (Shotyk, 1996a; Weiss *et al.*, 1997). In general, for RM and CM cores, ash contents were lower and exhibited broader near-surface peaks, even after eliminating effects from peat compaction (*cf.* Sections 3.1.4.3, 4.1.4.3, 5.1.4.3 and 6.1.4.3). These trends are possibly indicative of temporal differences in atmospheric dust inputs, however, as mentioned in Section 1.5.2, variations in ash contents from bog to bog and within bogs may in part reflect the ash content of individual plant species (Shotyk, 1996a).

7.2.4 Bulk density and NaOH peat extract absorption

Bulk density and NaOH peat extract absorption profiles for cores from each of the sites generally indicated a greater degree of decomposition and mass loss in the acrotelm peat layers, relative to the underlying catotelm peat layers (*cf.* Sections 3.1.4, 4.1.4, 5.1.4 and 6.1.4). The TM04CM-2 core and CM04CM-1 core absorption profiles were the only exception to this trend, with lower absorption values in the acrotelm peats relative to the catotelm peats. Low bulk densities and absorption values were exhibited at the surface of each of the cores due to the presence of decomposing and growing vegetation. Also, at each of the sites, the absorption profiles were found to show less pronounced near-surface increases than the bulk density profiles, which are influenced by inorganic content of anthropogenic origin.

7.3 RADIONUCLIDES

The unsupported ^{210}Pb and ^{137}Cs inventories, ^{210}Pb fluxes and peat accumulation rates for the dated peat cores from each site are summarised in Table 7.2 (*cf.* Sections 3.2, 4.2, 5.2 and 6.2).

7.3.1 Comparison of ^{210}Pb inventories and fluxes at each site

Total unsupported ^{210}Pb inventories and inventory-derived average ^{210}Pb fluxes determined at the four sites were found to vary in the order CM > RM > TM > FM (*cf.* Table 7.2). In contrast, the calculated theoretical ^{210}Pb fluxes, based on the annual rainfall (*cf.* Table 7.1), vary in the order FM > CM > TM > RM (*cf.* Table 7.2). It should be noted that RM, TM and CM inventory-derived average ^{210}Pb fluxes were higher than their corresponding theoretical rainfall-corrected ^{210}Pb fluxes, and the disagreement between the actual and theoretical ^{210}Pb flux trends can perhaps be attributed to local, as well as regional, differences in the composition and/or quantity of bulk precipitation (*cf.* Sections 4.2.3, 5.2.3 and 6.2.3). It is also worth noting that ^{210}Pb focussing or micro-topographic effects could also be important.

Table 7.2: Calculated unsupported ^{210}Pb and ^{137}Cs inventories, ^{210}Pb fluxes and peat accumulation rates for the dated peat cores from each site.

Site	Unsupported ^{210}Pb inventory (Bq m^{-2})	Unsupported ^{210}Pb flux (Bq m^{-2} y^{-1})	Theoretical unsupported ^{210}Pb flux (Bq m^{-2} y^{-1})	^{137}Cs inventory (kBq m^{-2})	Average accumulation rate (CRS model) (mg cm^{-2} y^{-1})	Average accumulation rate (CRS model) (cm y^{-1})
Flanders Moss FM04-1-M	2535 ± 53	79 ± 2	102 ± 18	5.9 ± 0.4	15 ± 1	0.16 ± 0.02
The Red Moss of Balerno RM03CM-1	2952 ± 136	92 ± 4	48 ± 9	1.5 ± 0.1	17 ± 5	0.16 ± 0.05
Turclossie Moss TM04M-1	2620 ± 51	81 ± 2	63 ± 11	1.5 ± 0.0	13 ± 2	0.20 ± 0.03
Carsegowan Moss CM04M	3381 ± 46	105 ± 1	74 ± 13	7.3 ± 0.0	15 ± 3	0.19 ± 0.04

7.3.2 Comparison of ^{137}Cs inventories at each site

Total inventories of ^{137}Cs determined at the four sites were found to vary in the order CM > FM > RM and TM (*cf.* Table 7.2). It should be noted that total ^{137}Cs inventories were generally lower than their corresponding estimated totals based on measurements of nuclear fallout and Chernobyl deposition (Peirson *et al.*, 1982; Clark and Smith, 1988), indicating loss of ^{137}Cs from the peat bogs.

7.3.3 Comparison of peat accumulation rates at each site

The CRS-derived accumulation rates at the four sites were very similar, ranging from 13 - 17 mg cm^{-2} y^{-1} and 0.16 – 0.20 cm y^{-1} (*cf.* Table 7.2).

7.4 CONSERVATIVE ELEMENTS

The conservative element (Al, Sc, Ti, Y and Zr) concentration profiles, as for ash content profiles, exhibited increases in the near-surface sections of cores from each of the sites (*cf.* Sections 3.3.3, 4.3.3, 5.3.3 and 6.3.3), again attributable to increases in soil dust deposition from anthropogenic activities. Interestingly, considerable increases were also observed at depth in the CM04CM-1 core (*cf.* Section 6.3.3),

probably attributable to local anthropogenic soil dust deposition as a result of woodland clearance during post-Roman/early Mediaeval times, as supported by pollen analysis data (Dumayne-Peaty, 1999).

In the FM and RM cores, the concentration profiles for the pairs of elements Sc and Y, and Ti and Zr, exhibited similar features. In contrast, the pair of elements Al and Y, and group of elements Sc, Ti and Zr, exhibited similar features in the TM cores, while no specific relationships between pairs or groups of elements were apparent in the CM cores. The conservative element Al was not used to correct measured element concentrations for soil dust contributions because of its possible mobility under acidic conditions in ombrotrophic peat.

7.4.1 Intercomparison of Sc and Ti

Slight differences in trend between the Sc and Ti concentration profiles, as indicated by Ti/Sc ratio profiles, were apparent in the cores from each of the sites (*cf.* Sections 3.3.3.1, 4.3.3.1, 5.3.3.1 and 6.3.3.1). Throughout the combined TM04M-1/TM04CM-4 core and at depth in the FM and RM cores Ti/Sc ratios were in close agreement with the UCC Ti/Sc ratio, suggesting that natural soil dust contributions are the most important sources of these metals at these depths. In contrast, the Ti/Sc ratio values at depth in the CM04CM-1 core were lower than the UCC Ti/Sc ratio perhaps reflecting the influence of local soil dust inputs arising from woodland clearance. In the near-surface sections of the FM, RM and CM cores, general decreases in the Ti/Sc ratios occurred, which could reflect different soil dust sources or possibly direct non-soil-dust-related anthropogenic sources (e.g. coal combustion).

7.5 COMPARISON OF HISTORICAL TRENDS IN ATMOSPHERIC Pb DEPOSITION

7.5.1 Pre-Roman and Roman atmospheric Pb deposition

Pre-Roman and Roman Pb concentration peaks were found in the FM01CM-1 (between *ca.* 210-40 B.C. and 20-220 A.D., peaking at *ca.* 210-40 B.C.) and

TM04M-1/TM04CM-4 (peaking at *ca.* 50-220 A.D.) cores (*cf.* Sections 3.6.1 and 5.6.1). The concentration increases were greater for the more southerly FM site than the remote northern TM site. Studies of long term peat records from Sweden (Bränvall *et al.*, 1997; Klaminder *et al.*, 2003), England (West *et al.* (1997); Le Roux *et al.*, 2004), Switzerland (Weiss *et al.*, 1997; Shotyk *et al.*, 1998) and Spain (Martinez-Cortizas *et al.*, 1997, 2002b) have also identified Roman Pb peaks, generally more pronounced in Spain than more northerly Europe (Bindler, 2006).

During the periods embracing the FM and TM pre-Roman and Roman Pb peaks, corresponding mean $^{206}Pb/^{207}Pb$ ratios of 1.175 ± 0.003 and 1.170 ± 0.005, respectively, were found and three-isotope plots of Pb indicated that the mining and smelting of British Pb ores appeared to be the predominant source of Pb contamination at FM, as found for Lindow Bog in north-west England (Le Roux *et al.*, 2004), whereas Pb contamination at TM seemed to reflect the mining and smelting of both British and Spanish Pb ores. Interestingly, Shotyk *et al.* (1998) attributed enrichments of Pb during the Roman period in a Swiss peat core from EGR to ancient Pb mining and long-range transport of aerosols from Spain. Rosman *et al.* (1997) also invoked this source to explain Pb enrichments at the same time in Greenland ice.

7.5.2 Post-Roman and Mediaeval atmospheric Pb deposition

The Pb concentrations were at their lowest in cores from each of the sites during the post-Roman/early Mediaeval period (*cf.* Sections 3.6.2, 4.6.1, 5.6.2 and 6.6.1), reflecting the decline in metallurgical activities after the fall of the Roman Empire (*ca.* 410 A.D.). Also, the corresponding $^{206}Pb/^{207}Pb$ ratios during these periods were significantly less radiogenic relative to those found during the pre-Roman/Roman periods in the FM and TM cores, with mean values ranging from ~ 1.148 to 1.164. Interestingly, from *ca.* 410 A.D. to the late 6th century A.D. at each of the sites, three-isotope plots of Pb indicated that there may have been contributions, albeit minor, from long range atmospheric Pb deposition from post-Roman mining and smelting activities in Spain during the reign of the Visigods. Martinez-Cortizas *et al.*

(1997) attributed Pb enrichments in a peat core from north-west Spain to these same sources.

Increases in the Pb concentration were exhibited in cores from each of the sites during the Mediaeval period (generally between *ca.* 9th and 15th centuries A.D.) (*cf.* Sections 3.6.2, 4.6.1, 5.6.2 and 6.6.1). The magnitude of the concentration increases at the four sites decreased in the order CM > FM, RM > TM, perhaps reflecting the closer proximity of the most southerly site, CM, to English Mediaeval Pb mining and smelting sources or differences in the histories of colonisation and exploitation in each of the Scottish regions. Other studies of long term peat records from Sweden (Bränvall *et al.*, 1997; Klaminder *et al.*, 2003), England (Le Roux *et al.*, 2004), Switzerland (Shotyk *et al.*, 1998) and Spain (Martinez-Cortizas *et al.*, 1997, 2002b) have also identified Mediaeval increases, although as for the Roman peaks, it is worth noting that these records have also indicated that the specific timing and intensity of changes vary regionally, e.g. the Mediaeval increase is strongest in central Europe and less visible in Spain (Bindler, 2006).

During the period of Mediaeval Pb concentration increases, the corresponding $^{206}Pb/^{207}Pb$ ratios at each of the four Scottish sites increased, with mean values ranging from ~ 1.157 to 1.176, and it is interesting to note that Klaminder *et al.* (2003) found $^{206}Pb/^{207}Pb$ values of ~1.155-1.170 in peat sections dated at *ca.* 1500 A.D. from Dumme Mosse and Traneröd Mosse in southern Sweden.

7.5.3 Industrial and Post-industrial atmospheric Pb deposition

Marked increases in Pb concentrations were found in cores from each of the sites during the Industrial period (between *ca.* 1750 and 1970 A.D.) (*cf.* Sections 3.6.3, 4.6.2, 5.6.3 and 6.6.2). Depositional fluxes of anthropogenic Pb since the mid-19th century A.D. for cores from each of the sites are plotted, along with the measured $^{206}Pb/^{207}Pb$ ratios, *versus* ^{210}Pb-derived calendar dates in Fig. 7.1.

To summarise, maximum anthropogenic Pb fluxes occurred as follows: ~ 21 mg m^{-2} y^{-1} from the mid-1920s to the mid-1950s A.D. at FM (*cf.* Section 3.6.3.1), ~ 29 to 38 mg m^{-2} y^{-1} between the late 1910s and late 1960s A.D. at RM (*cf.* Section 4.6.2.1), ~ 10 to 12 mg m^{-2} y^{-1} between the mid-1910s and early 1960s A.D. at TM (*cf.* Section 5.6.3.1) and ~ 34 to 41 mg m^{-2} y^{-1} at *ca.* 1900 A.D. at CM (i.e. excluding the CM04CM-1 fluxes between *ca.* 1904-1944 A.D., which were 'contaminated' (*cf.* Section 6.6.2.1)) (*cf.* Fig. 7.1).

The timings of the maximum anthropogenic Pb fluxes at each of the sites, with the exception of the significantly earlier increases at CM, were in close agreement. The fluxes decreased in the order CM > RM > FM > TM, perhaps reflecting the closer proximity of CM to major Pb pollution sources in England and the closer proximity of the RM and FM sites to industrial/transportation sources of Pb pollution in the heavily populated central belt of Scotland. The apparently greater Pb fluxes at RM in eastern Scotland compared with FM in western Scotland is surprising but it is worth remembering (*cf.* Section 3.6.3.1) that maximum Pb depositional fluxes ranging from 20-60 mg m^{-2} y^{-1} have previously been observed for FM (Farmer *et al.*, 1997; Farmer *et al.*, 2006). This highlights the significant variations in apparent depositional fluxes that can be found from the analysis of different cores from the same bog, sometimes arising as a consequence of topographical and plant compositional features that affect the efficiency of particle trapping and retention (Norton *et al.*, 1997; Bindler *et al.*, 2004).

Comparing the $^{206}Pb/^{207}Pb$ ratio trends at each of the sites, the ratios remained fairly constant (~ 1.170) from the mid-19th century A.D. (*cf.* Fig. 7.1) until the onset of the decline *ca.* 1920 - 1930 A.D. at FM, RM and TM. At CM, this decline began earlier (*ca.* late 19th century A.D), perhaps due to the influence of the earlier use of imported Pb ores in more southern parts of Britain (*cf.* Section 6.6.2). During the post-industrial period (after *ca.* 1970 A.D.), a feature common to each of the four sites was the decline in $^{206}Pb/^{207}Pb$ ratios to minimum values (~ 1.11 – 1.13) during the 1980s and 1990s A.D., followed by an increase (to ~ 1.13 – 1.15) in recent years.

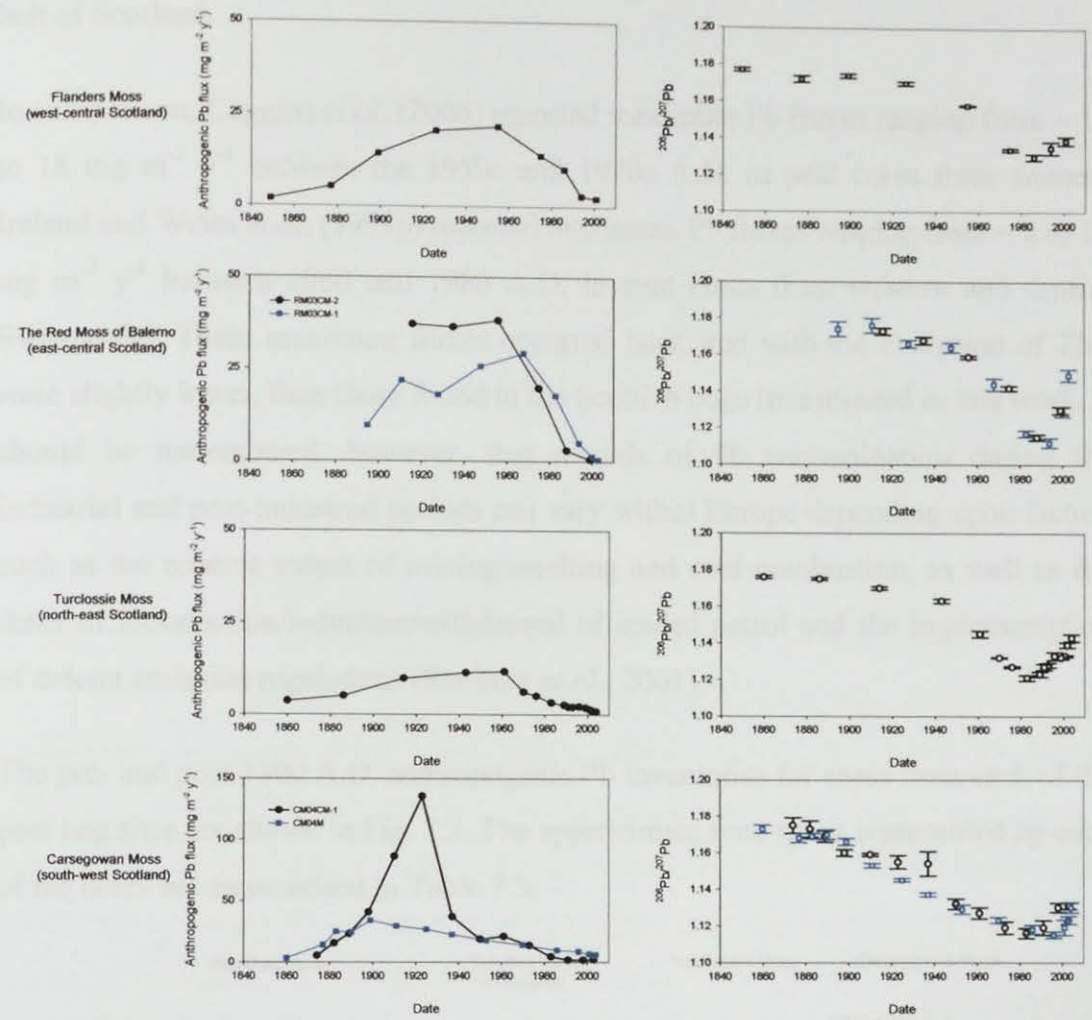

Figure 7.1: Calculated atmospheric depositional fluxes of anthropogenic Pb (mg m^{-2} y^{-1}) and measured $^{206}Pb/^{207}Pb$ ratios for cores from each peat bog site *versus* ^{210}Pb-derived dates since 1840 A.D.

In general, similar key features in the trends in the $^{206}Pb/^{207}Pb$ ratios provide evidence that each of the sites were influenced by similar sources of Pb pollution during the industrial and post-industrial periods (*cf.* Sections 3.6.3, 4.6.2, 5.6.3 and 6.6.2).

Interestingly, MacKenzie *et al.* (1997) also found a higher maximum Pb flux (~ 37 mg m^{-2} y^{-1}) in a peat core from FM relative to that (~ 5.0 mg m^{-2} y^{-1}) found in a core from a remote site at North Uist (north-west Scotland). Also, MacKenzie *et al.* (1998b) reported a depositional Pb flux peak of ~ 50 mg m^{-2} y^{-1} at *ca.* 1940 A.D. in a peat core from South Drumboy Hill, approximately 18 km south-west of Glasgow, in

fairly good agreement with those found at FM and RM, also situated in the central belt of Scotland.

In comparison, Coggins *et al.* (2006) reported maximum Pb fluxes ranging from ~ 15 to 18 mg m^{-2} y^{-1} between the 1950s and 1970s A.D. in peat cores from western Ireland and Weiss *et al.* (1999b) reported maximum Pb fluxes ranging from ~ 9 to 16 mg m^{-2} y^{-1} between 1960 and 1980 A.D. in peat cores from western and central Switzerland. These maximum fluxes occurred later, and with the exception of TM, were slightly lower, than those found in the Scottish bogs investigated in this work. It should be remembered, however, that records of Pb contamination during the industrial and post-industrial periods can vary within Europe depending upon factors such as the relative extent of mining/smelting and coal combustion, as well as the dates of introduction/reduction/withdrawal of leaded petrol and the implementation of stricter emission regulations (Renberg *et al.*, 2001).

The pre- and post-1800 A.D. anthropogenic Pb inventories for cores from each of the peat bog sites are shown in Fig. 7.2. The approximate time spans represented by each of the cores are summarised in Table 7.3.

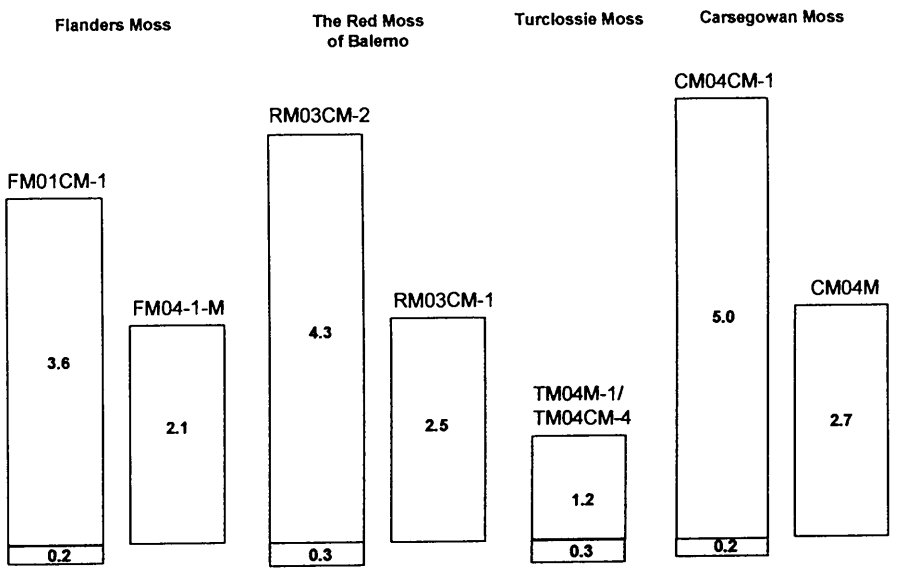

Figure 7.2: Calculated pre- (shaded) and post- (clear) 1800 A.D. anthropogenic Pb inventories (g m^{-2}) for cores from each site.

Table 7.3: Approximate time spans represented by cores from each site.

Site	Core	Approximate time span
Flanders Moss	FM01CM-1	*ca.* 500 B.C. to mid-1980s A.D.
	FM04-1-M	*ca.* late 1700s to 2004 A.D.
The Red Moss of Balerno	RM03CM-2	*ca.* 600 to 2003 A.D.
	RM03CM-1	*ca.* late 1700s to 2003 A.D.
Turclossie Moss	TM04M-1 /TM04CM-4	*ca.* 380 B.C. to 2004 A.D.
Carsegowan Moss	CM04CM-1	*ca.* 400 to 2004 A.D.
	CM04M	*ca.* early 1800s to 2004 A.D.

At FM, RM and CM, Pb deposition during the industrial and post-industrial periods was > 90% of the total, compared with ~ 80% at TM. The post-1800 A.D. inventories decreased in the order CM > RM > FM > TM, as found for the anthropogenic Pb fluxes (*cf.* Fig. 7.2). In similar fashion to the geographical variation in peat core inventories of Pb for the industrial/post-industrial period, Eades *et al.* (2002) found higher Pb inventories for sediments from Loch Lomond (west-central Scotland) relative to Loch Ness (north Scotland).

Calculated cumulative post-1800 A.D. anthropogenic Pb inventories (% of total post-1800 A.D. inventory) for cores from each of the sites (*cf.* Sections 3.6.3.1, 4.6.2.1, 5.6.3.1 and 6.6.2.1) are plotted *versus* ^{210}Pb-derived calendar dates in Fig. 7.3. In general, at each of the sites the maximum post-1800 A.D. anthropogenic Pb deposition occurred between the 1880s and 1970s A.D.

7.5.4 Conclusions

In conclusion, during the pre-Roman and Roman periods, the FM and TM sites were influenced by similar Pb pollution sources, although the more southerly FM site may have been more strongly influenced by local British sources than the TM site, where

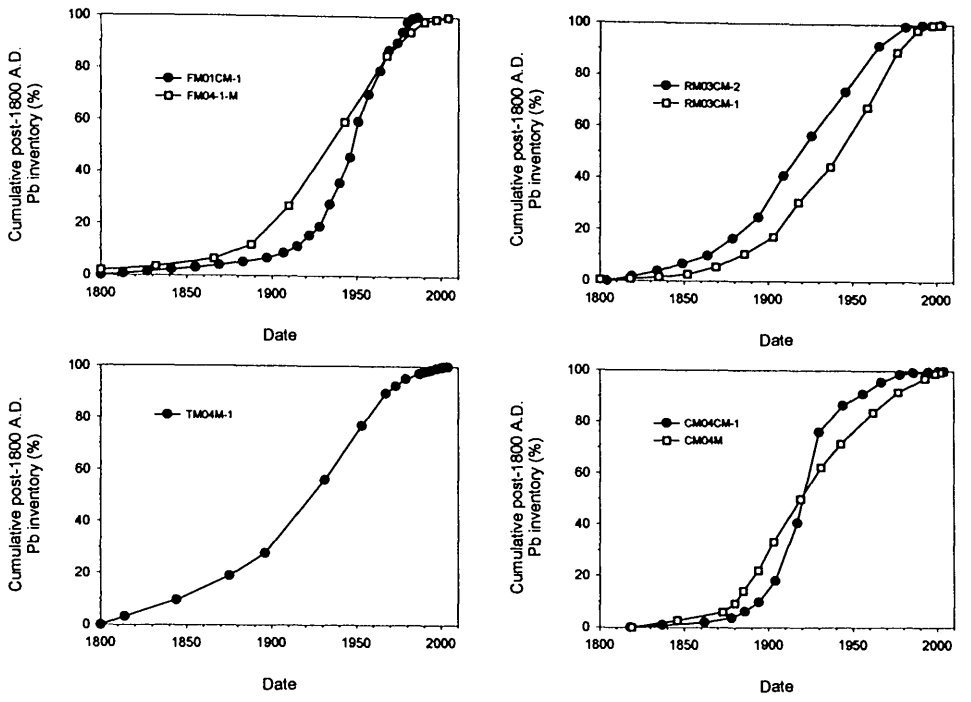

Figure 7.3: Calculated cumulative post-1800 A.D. anthropogenic Pb inventories (% of total post-1800 A.D. inventory) for cores from each peat bog site *versus* ^{210}Pb-derived dates.

the relative influence of long range atmospheric deposition from elsewhere in Europe may have been stronger. All four sites exhibited increases in Pb contamination during the Mediaeval period, with the intensity of contamination decreasing from the south to the north of Scotland. During the industrial and post-industrial periods, all four sites, with the exception of CM during the late 19th and early 20th centuries A.D., were influenced by similar Pb pollution sources, and again, levels of Pb contamination were highest in the south (CM) and lowest in the north (TM) of Scotland. Note that similar south to north Pb pollution gradients have been found in Swedish lake sediments (Renberg *et al.*, 2001) and Swedish and Norwegian peat bogs (Hvatum *et al.*, 1987; Jensen, 1997). It is important to note, however, that sources of atmospheric pollution to these Scandinavian countries predominantly come from mainland Europe.

7.6 GEOCHEMICAL BEHAVIOUR OF MAJOR ELEMENTS

The concentration profiles of Ca, Fe, Mg, Mn, P and S in the cores from each site were dissimilar to the ash content profiles, reflecting the redistribution of these elements in ombrotrophic peat bogs via well known mechanisms, i.e. nutrient uptake and cycling (Ca, Fe, Mg, Mn, P and S) and redox cycling (Fe, Mn, P and, perhaps to some extent, S, as indicated for FM and RM). Note that the S concentration profiles in the TM and CM cores did not appear to be strongly influenced by redox cycling, exhibiting similar trends to Ca and Mg.

7.7 GEOCHEMICAL BEHAVIOUR OF Se AND Zn

7.7.1 Se

At each of the sites investigated, the Se concentration profiles suggested that Se was mobile in ombrotrophic peat (*cf.* Sections 3.8.2.2.1, 4.8.2.1.2, 5.8.2.1.1 and 6.8.3.3.1). For example, the FM Hg and Se concentration profiles, despite having similar anthropogenic sources, were dissimilar, although in the uppermost sections of the RM03CM-2 and CM04CM-1 cores, the Hg and Se concentration profiles were more alike.

7.7.2 Zn

At each of the sites investigated, the Zn concentration profiles suggested that Zn was mobile in ombrotrophic peat (*cf.* Sections 3.8.3.3.1, 4.8.3.3.1, 5.8.2.1.1 and 6.8.3.3.1). The Zn concentration profiles in the uppermost sections of the cores were consistent with the effects of plant uptake and recycling, whereas similarities between the Zn and S concentration profiles at depth in the catotelm peat layers of the cores possibly indicated the influence of Zn sulfide formation and precipitation.

7.8 COMPARISON OF HISTORICAL TRENDS IN ATMOSPHERIC Sb DEPOSITION

The similarity between the Pb and Sb concentration profiles at each of the sites suggested that Sb was also essentially immobile in ombrotrophic peat.

7.8.1 Pre-Roman and Roman atmospheric Sb deposition

As for Pb, pre-Roman and Roman Sb concentration peaks were found in the FM01CM-1 and TM04M-1/TM04CM-4 cores (*cf.* Sections 3.8.1.3.2 and 5.8.1.1.2), with slightly greater Sb concentration increases for FM than TM. Shotyk *et al.* (1996, 2004) also reported Sb enrichments dating back to Roman times in a peat core from Switzerland. During the periods embracing FM and TM pre-Roman and Roman Sb (and Pb) peaks, the corresponding mean anthropogenic Sb/Pb ratio was 0.012 at both sites, perhaps providing some evidence that the mining/smelting of Pb ores was the predominant source of Sb (and Pb) contamination at these sites (*cf.* Sections 3.8.1.3.2 and 5.8.1.1.2).

7.8.2 Post-Roman and Mediaeval atmospheric Sb deposition

As for Pb, the Sb concentrations were at their lowest in cores from each of the sites during the post-Roman/early Mediaeval period but increased during the Mediaeval period (*cf.* Sections 3.8.1.3.2, 4.8.1.1.2, 5.8.1.1.2 and 6.8.1.1.2). Interestingly, the magnitude of the concentration increases at the four sites decreased in the order CM > FM > TM > RM, which was slightly different from that observed for Pb (CM > FM, RM > TM), perhaps indicating differences in Pb and Sb sources (e.g. continental European Pb ores generally having higher Sb contents than British ores), as well as differences in the proximity of the sites to regional and local sources of Sb and Pb contamination.

7.8.3 Industrial and Post-industrial atmospheric Sb deposition

As for Pb, marked increases in Sb concentrations were found in cores from each of the sites during the Industrial period (*cf.* Sections 3.8.1.3.2, 4.8.1.1.2, 5.8.1.1.2 and 6.8.1.1.2). Depositional fluxes of anthropogenic Sb and Pb since the mid-19th century A.D. for cores from each of the sites are plotted, along with the measured anthropogenic Sb/Pb and $^{206}Pb/^{207}Pb$ ratios, *versus* ^{210}Pb-derived calendar dates in Fig. 7.4.

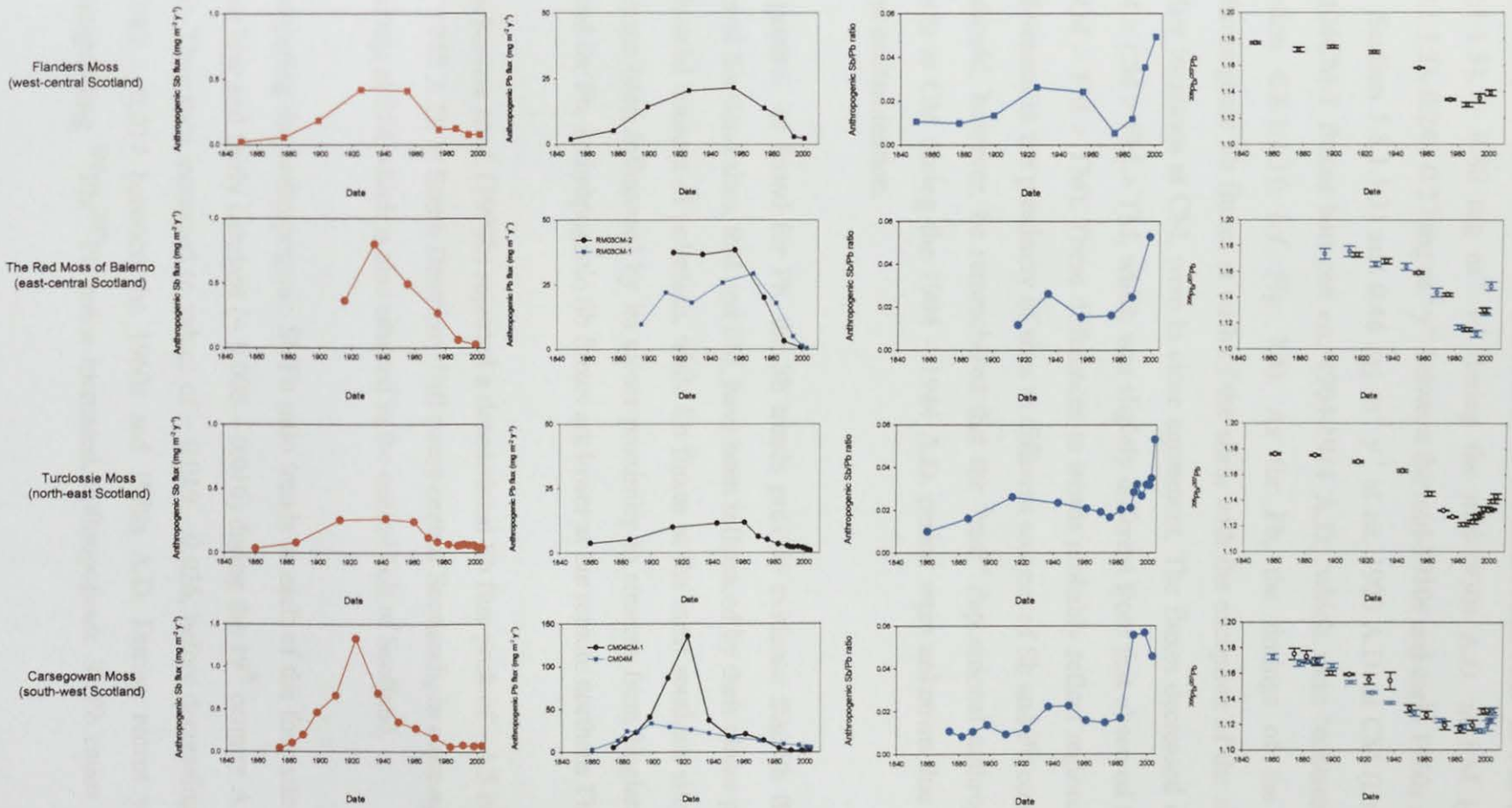

Figure 7.4: Calculated atmospheric depositional fluxes of anthropogenic Sb and Pb (mg m^{-2} y^{-1}) and measured anthropogenic Sb/Pb and $^{206}Pb/^{207}Pb$ ratios for cores from each peat bog site *versus* ^{210}Pb-derived dates since 1840 A.D.

To summarise, maximum anthropogenic Sb fluxes occurred as follows: ~ 0.42 mg m^{-2} y^{-1} from the mid-1920s to the mid-1950s A.D. at FM (*cf.* Section 3.8.1.1.3), ~ 0.80 mg m^{-2} y^{-1} during the mid-1930s A.D. at RM (*cf.* Section 4.8.1.1.3), 0.24 - 0.27 mg m^{-2} y^{-1} between the mid-1910s and early 1960s A.D. at TM (*cf.* Section 5.8.1.1.3) and 0.46 mg m^{-2} y^{-1} at *ca.* 1900 A.D. at CM (i.e. excluding CM04CM-1 fluxes between *ca.* 1904-1944 A.D., which were 'contaminated' (*cf.* Section 6.8.1.1.3)) (*cf.* Fig. 7.4). As for Pb, the timings of the maximum anthropogenic Sb fluxes at each of the sites, with the exception of the significantly earlier increases at CM, were in close agreement. The fluxes decreased in the order RM > CM > FM > TM, which was slightly different from that observed for Pb (CM > RM > FM > TM). These differences in trends probably reflect regional and local differences in the proximity of sites to different sources of Sb and Pb contamination. It should, however, be remembered that the "real" depositional anthropogenic Sb fluxes at CM during the 1904 – 1944 A.D. period were unknown due to possible local contamination.

In general, as found for Pb, the Sb trends provide evidence that Sb fluxes at the central Scotland sites, RM and FM, have been influenced by their closer proximity to industrial sources of pollution, while Sb fluxes at the most southern site, CM, have perhaps been influenced by its closer proximity to sources from England. Also, as found for Pb, anthropogenic Sb fluxes are lower at the remote northern TM site.

MacKenzie *et al.* (1998b) reported a depositional Sb flux peak of ~ 1.5 mg m^{-2} y^{-1} at *ca.* 1940 A.D. at South Drumboy Hill (west-central Scotland), in close agreement to findings at RM which is also situated in the central belt of Scotland.

Comparing the anthropogenic Sb/Pb ratio trends at each of the four sites, the ratios were low and fairly constant (~ 0.006 – 0.016) during the 19th century A.D. (*cf.* Fig. 7.4). They then increased to values of ~ 0.019 – 0.026, before decreasing again to ~ 0.0082 – 0.017 between the 1960s and 1980s A.D. During recent years, when corresponding $^{206}Pb/^{207}Pb$ ratios increased, anthropogenic Sb/Pb ratios (~ 0.034 –

0.053) also increased at each of the sites. In general, similar key features in the trends in the anthropogenic Sb/Pb ratios provide evidence that each of the sites was influenced by similar sources of Sb (and Pb) pollution during the industrial and post-industrial periods (*cf.* Sections 3.8.1.3.2, 4.8.1.1.2, 5.8.1.1.2 and 6.8.1.1.2).

The pre- and post-1800 A.D. anthropogenic Sb inventories for cores from each of the peat bog sites are shown in Fig. 7.5.

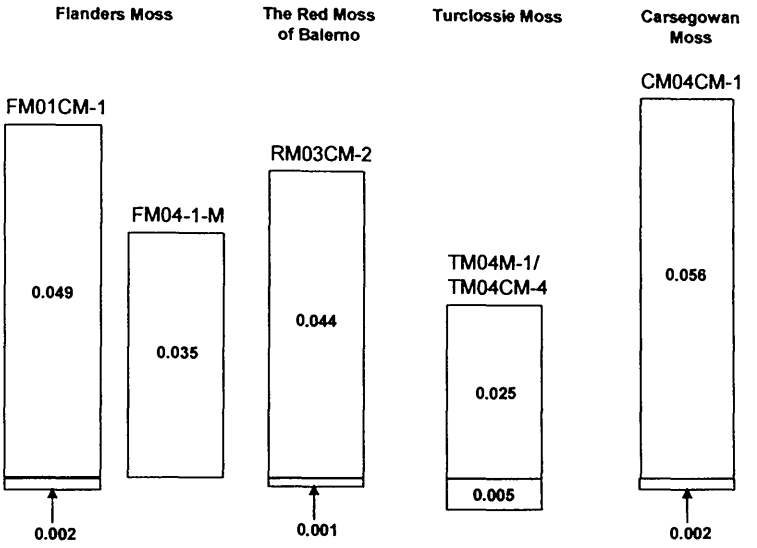

Figure 7.5: Calculated pre- (shaded) and post- (clear) 1800 A.D. anthropogenic Sb inventories (g m^{-2}) for cores from each site.

At FM, RM and CM, Sb deposition during the industrial and post-industrial periods was > 90% of the total, compared with ~ 80% at TM. The post-1800 A.D. inventories decreased in the order CM > FM > RM > TM. Calculated cumulative poat-1800 A.D. anthropogenic Sb inventories (% of total post-1800 A.D. inventory) for cores from each of the sites (*cf.* Sections 3.8.1.1.3, 4.8.1.1.3, 5.8.1.1.3 and 6.8.1.1.3) are plotted *versus* ^{210}Pb-derived calendar dates in Fig. 7.6. In general, at each of the sites the maximum post-1800 A.D. anthropogenic Sb deposition occurred between the 1890s and 1970s A.D.

The maximum enrichments of Sb and Pb for each of the sites calculated using UCC and SNBP elemental concentration ratios are shown in Table 7.4.

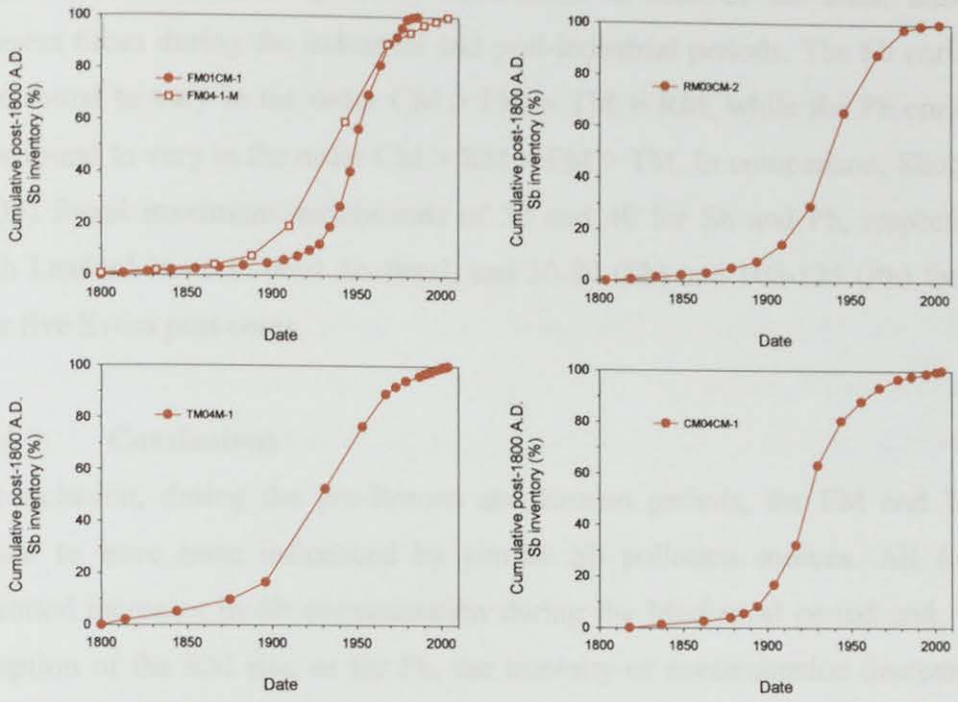

Figure 7.6: Calculated cumulative post-1800 A.D. anthropogenic Sb inventories (% of total post-1800 A.D. inventory) for cores from each peat bog site *versus* ^{210}Pb-derived dates.

Table 7.4: Maximum enrichments of Sb and Pb in each of the sites calculated relative to upper continental crust (UCC) and Swiss natural background peat (SNBP) Sb/Sc and Pb/Sc concentration ratios.

	Maximum Sb Enrichment Factor			Maximum Pb Enrichment Factor		
Site	**UCC**	**SPNB**	**Time period**	**UCC**	**SPNB**	**Time period**
Flanders Moss						
FM01CM-1	110	47	*ca.* 1960 ± 9 A.D.	120	99	*ca.* 1980s A.D.
FM04-1-M	58	24	*ca.* 1926 ± 6 A.D.	76	61	*ca.* 1986 ± 2 A.D.
The Red Moss of Balerno RM03CM-2	67	28	*ca.* 1999 ± 2 A.D.	139	112	*ca.* 1800 A.D.
Turclossie Moss TM04M-1	87	35	*ca.* 1914 ± 10 A.D.	89	72	*ca.* 1976 ± 3 A.D.
Carsegowan Moss CM04CM-1	150	61	*ca.* 1961 ± 3 A.D.	210	170	*ca.* 1961 ± 3 A.D.

Note that Pb enrichment factors of 82 and 67 were calculated relative to UCC and SNBP Pb/Sc ratios, respectively, at *ca.* 1916 A.D. in RM03CM-2 (*cf.* Section 4.8.1.1.4).

In general, Sb (UCC: 58 – 150; SPNB: 24 - 61) and Pb (UCC: 76 – 210; SPNB: 61 - 170) exhibited similar degrees of enrichment at each of the sites, although at different times during the industrial and post-industrial periods. The Sb enrichments were found to vary in the order CM > FM > TM > RM, while the Pb enrichments were found to vary in the order CM > RM > FM > TM. In comparison, Shotyk *et al.* (2004) found maximum enrichments of 30 and 40 for Sb and Pb, respectively, at Loch Laxford in north-west Scotland, and 30-80 (Sb) and 100-125 (Pb) for four of their five Swiss peat cores.

7.8.4 Conclusions

In conclusion, during the pre-Roman and Roman periods, the FM and TM sites appear to have been influenced by similar Sb pollution sources. All four sites exhibited increases in Sb contamination during the Mediaeval period and, with the exception of the RM site, as for Pb, the intensity of contamination decreased from the south to the north of Scotland. During the Industrial and Post-industrial periods, all four sites were influenced by similar Sb pollution sources and levels of Sb contamination were generally highest in south (CM) and central (FM and RM) Scotland and lowest in north (TM) Scotland. Note that similar south to north Sb pollution gradients have been found in Swedish and Norwegian peat bogs (Hvatum *et al.*, 1987).

7.9 COMPARISON OF HISTORICAL TRENDS IN ATMOSPHERIC Hg DEPOSITION

Note that Hg concentrations were not determined for the TM site. The Hg concentration profiles in the older catotelm peats of the FM and RM cores indicated that the vertical distribution of Hg was possibly influenced by sulfide formation (*cf.* Sections 3.8.2.2.1 and 4.8.2.1.1). The similarity between the Pb and Hg concentration profiles in the uppermost sections of the FM, RM and CM cores, however, suggested that Hg was also essentially immobile in ombrotrophic peat (*cf.*

Sections 3.8.2.2.1 and 4.8.2.1.1. and 6.8.2.1.1). Note that Hg concentrations were determined in the FM01CM-1 sister core, FM01CM-2 (Shimwell, 2002).

7.9.1 Industrial and Post-industrial atmospheric Hg deposition

As for Pb, marked increases in Hg concentrations were found in cores from FM, RM and CM during the Industrial period (*cf.* Sections 3.8.2.2.2, 4.8.2.1.3 and 6.8.2.1.3). Depositional fluxes of Hg and anthropogenic Pb since the mid-19th century A.D. for cores from FM, RM and CM are plotted, along with the measured $^{206}Pb/^{207}Pb$ ratios, *versus* ^{210}Pb-derived calendar dates in Fig. 7.7. To summarise, a maximum Hg flux of ~ 0.19 mg m^{-2} y^{-1} occurred at *ca.* 1950 A.D. at FM (note that a corresponding maximum Pb flux of ~ 58 mg m^{-2} y^{-1} was also found at *ca.* 1950 A.D. in the FM01CM-2 core) (*cf.* Section 3.8.2.2.3). A maximum Hg flux of ~ 0.085 mg m^{-2} y^{-1} occurred during the mid-1930s A.D. at RM (*cf.* Section 4.8.2.1.4) and of ~ 0.056 - 0.085 mg m^{-2} y^{-1} *ca.* between the late 1880s and late 1930s A.D. at CM (*cf.* Section 6.8.2.1.4) (*cf.* Fig. 7.7). The timings of the maximum Hg fluxes varied from site to site, with earlier increases at CM, as observed for Pb and Sb. The magnitude of the fluxes decreased in the order FM > RM, CM, perhaps indicating local geographical factors related to the proximity of major Hg pollution sources such as coal combustion. Note that, when taking the FM01CM-2 core Pb fluxes into account, the Pb fluxes decreased in the order FM > CM > RM. In general, English sources of Pb pollution (e.g. the smelting of imported Pb ores) did not appear to influence Hg so strongly as Pb at CM.

The Hg fluxes found for these Scottish bogs were considerably higher than the maximum Hg flux (~ 0.018 mg m^{-2} y^{-1}) between the 1950s and 1970s A.D. based on lake sediment studies at Lochnagar (north-east Scotland) (Yang *et al.*, 2002). They were, however, in better agreement with those (0.06 - 0.07 mg m^{-2} y^{-1}) derived from peat cores from western Ireland for the 1950s - 1970s A.D. (Coggins *et al.*, 2006). Also, a similar maximum Hg flux of ~ 0.11 mg m^{-2} y^{-1} occurred at *ca.* 1910 A.D. at EGR peat bog in Switzerland (Roos-Barraclough *et al.*, 2002a).

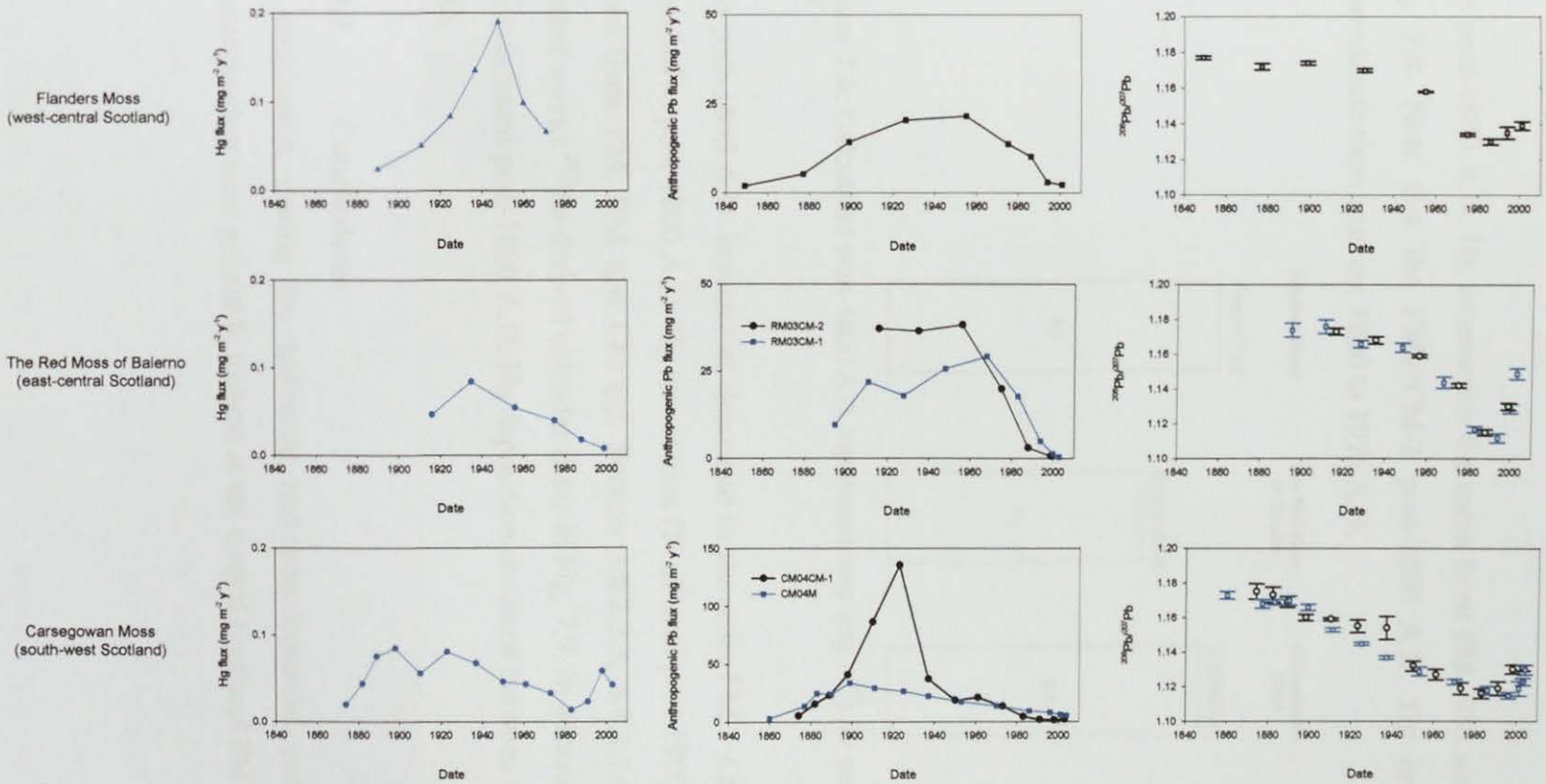

Figure 7.7: Calculated atmospheric depositional fluxes of Hg and anthropogenic Pb (mg m^{-2} y^{-1}) and measured $^{206}Pb/^{207}Pb$ ratios for cores from Flanders Moss, The Red Moss of Balerno and Carsegowan Moss *versus* ^{210}Pb-derived dates since 1840 A.D. Note that the Hg and anthropogenic Pb fluxes, and measured $^{206}Pb/^{207}Pb$ ratios for Flanders Moss are those found for FM01CM-2 (triangles), the FM01CM-1 sister core, and FM04-1-M (squares).

Interestingly, the maximum Hg flux at FM was in closest agreement with the maximum Hg fluxes of 0.16 and 0.18 mg m^{-2} y^{-1} (dated at *ca.* 1953 A.D.), derived from peat cores from Greenland and Denmark, respectively (Shotyk *et al.*, 2003).

The post-1800 A.D. Hg inventories for cores from FM, RM and CM are shown in Fig. 7.8. Note that the FM01CM-2 post-1800 A.D. Hg inventory covers the approximate time span *ca.* 1800 to 1976 A.D.

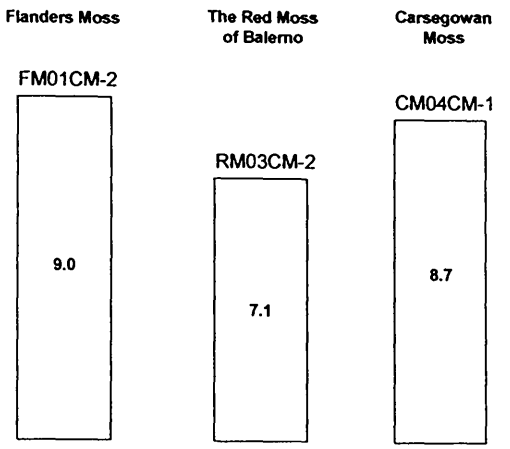

Figure 7.8: Calculated post-1800 A.D. Hg inventories (mg m^{-2}) for cores from FM, RM and CM.

The post-1800 A.D. inventories decreased in the order FM > CM > RM. Calculated cumulative post-1800 A.D. Hg inventories (% of total post-1800 A.D. inventory) for cores from FM, RM and CM (*cf.* Section 3.8.2.2.3, 4.8.2.1.4 and 6.8.2.1.4) are plotted *versus* ^{210}Pb-derived calendar dates in Fig. 7.9. In general, at these three sites the maximum post-1800 A.D. Hg deposition occurred between the 1880s and 1970s A.D.

7.9.2 Conclusions

In conclusion, during the industrial and post-industrial periods, levels of Hg contamination were generally highest at the central Scotland FM site.

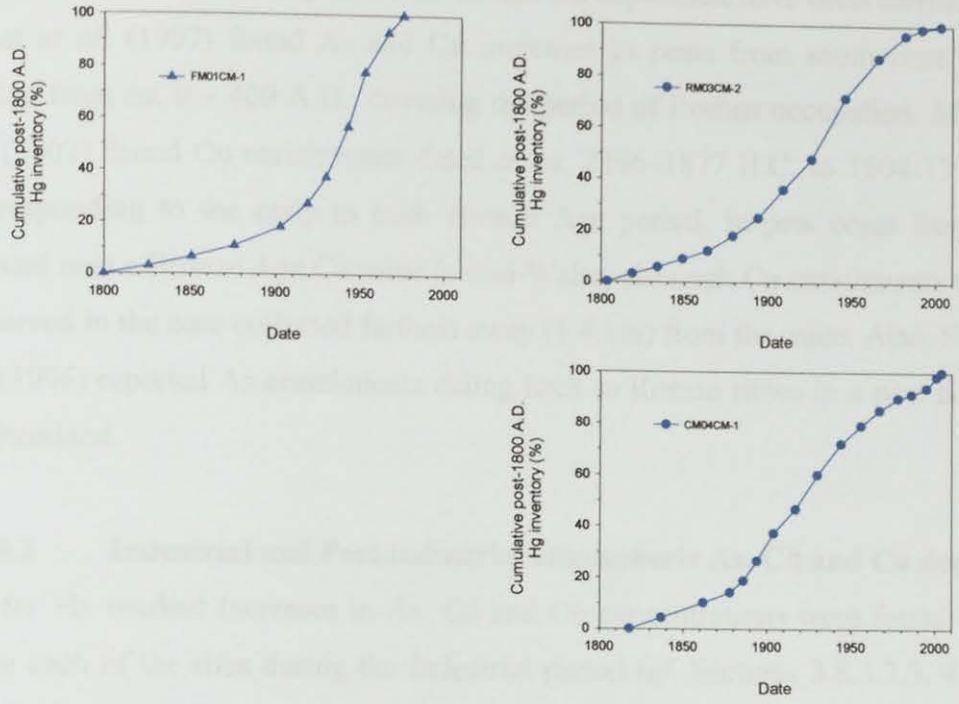

Figure 7.9: Calculated cumulative post-1800 A.D. Hg inventories (% of total post-1800 A.D. inventory) for cores from each peat bog site *versus* ^{210}Pb-derived dates.

7.10 COMPARISON OF HISTORICAL TRENDS IN ATMOSPHERIC As, Cd AND Cu DEPOSITION

The similarity between the Pb concentration profiles and those of the trace elements As, Cd and Cu at each of the sites suggested that these elements were also essentially immobile in ombrotrophic peat.

7.10.1 Pre-industrial atmospheric As, Cd and Cu deposition

During the pre-Roman and Roman period, increases in As and Cu concentrations were observed at TM but not FM. During the Mediaeval period, however, increases in As concentrations were observed at each of the sites, with Cd increases at TM and CM and Cu increases at TM (*cf.* Sections 3.8.3.3.3, 4.8.3.3.3, 5.8.2.1.3 and 6.8.3.3.3). The magnitude of the As concentration increases at the four sites decreased in the order CM > FM > TM > RM, as found for Sb. These variable trends in As, Cd and Cu deposition may reflect regional and local differences in the

proximity of the sites to sources of As, Cd and Cu at these times. Few long term studies of historical atmospheric As, Cd and Cu deposition have been carried out but West *et al.* (1997) found As and Cu increases in peats from south-west England dating from *ca.* 0 – 400 A.D., covering the period of Roman occupation. Mighall *et al.* (2002) found Cu enrichments dated at *ca.* 2396–1877 B.C. to 1604-1396 B.C., corresponding to the early to mid- Bronze Age period, in peat cores from a bog located near a Bronze Age Cu mine in mid-Wales, although Cu enrichments were not observed in the core collected furthest away (1.4 km) from the mine. Also, Shotyk *et al.* (1996) reported As enrichments dating back to Roman times in a peat core from Switzerland.

7.10.2 Industrial and Post-industrial atmospheric As, Cd and Cu deposition

As for Pb, marked increases in As, Cd and Cu concentrations were found in cores from each of the sites during the Industrial period (*cf.* Sections 3.8.3.3.3, 4.8.3.3.3, 5.8.2.1.3 and 6.8.3.3.3).

As

Depositional fluxes of anthropogenic As and Pb since the mid-19th century A.D. for cores from each of the sites are plotted, along with the measured $^{206}Pb/^{207}Pb$ ratios, *versus* ^{210}Pb-derived calendar dates in Fig. 7.10. To summarise, a maximum anthropogenic As flux of ~ 0.48 mg m^{-2} y^{-1} occurred during the mid-1920s A.D. at FM (*cf.* Section 3.8.3.3.4), of ~ 0.40 to 0.52 mg m^{-2} y^{-1} between the late 1910s and mid-1950s A.D. at RM (*cf.* Section 4.8.3.3.4), of ~ 0.22 to 0.31 mg m^{-2} y^{-1} between the *ca.* mid-1910s and early 1960s A.D. at TM (*cf.* Section 5.8.2.1.4) and of ~ 1.5 mg m^{-2} y^{-1} at *ca.* 1900 A.D. at CM (*cf.* Section 6.8.3.3.4) (*cf.* Fig. 7.10).

As for Pb, the timings of the maximum anthropogenic As fluxes at each of the sites, with the exception of the significantly earlier increases at CM, were in close agreement.

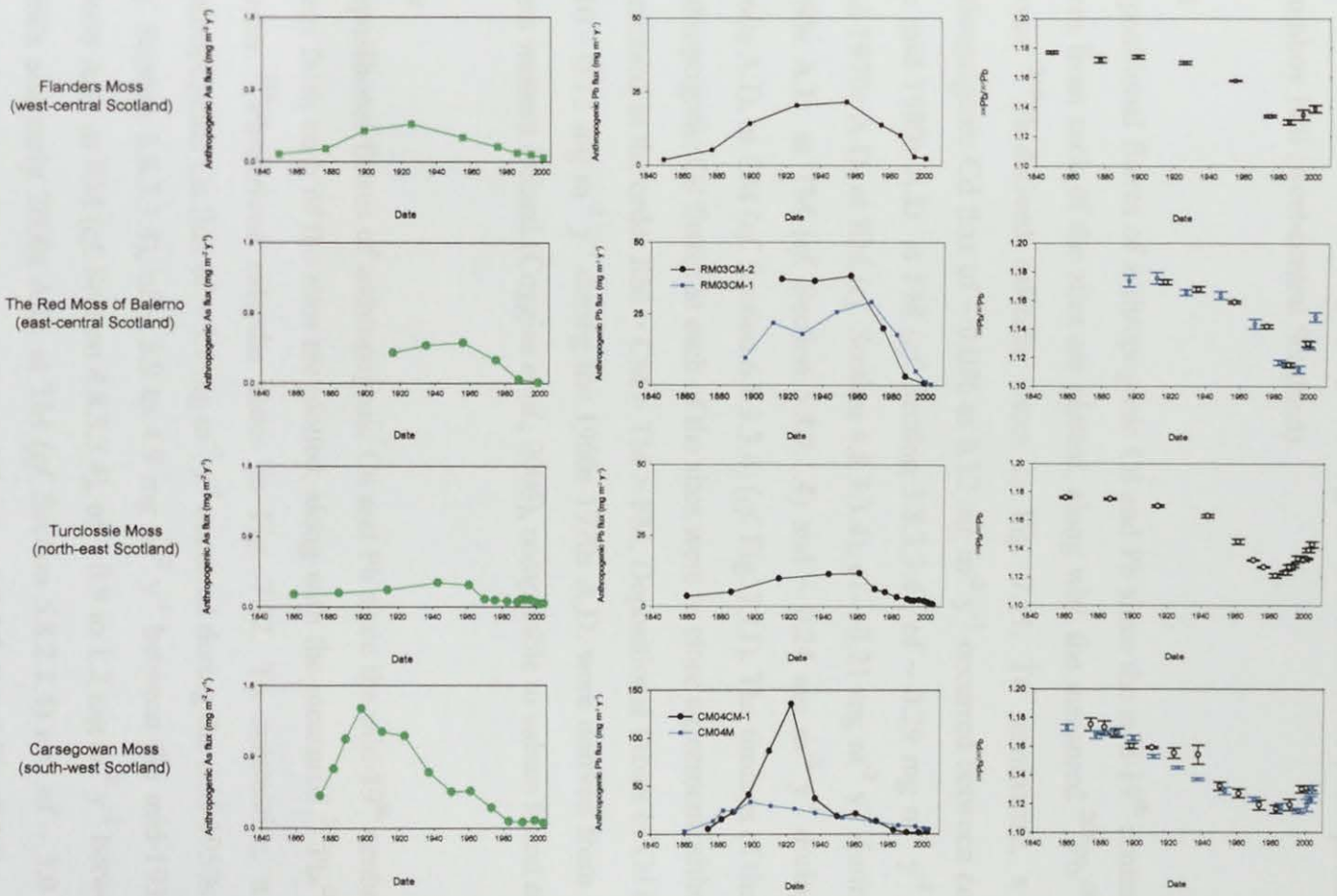

Figure 7.10: Calculated atmospheric depositional fluxes of anthropogenic As and Pb (mg m^{-2} y^{-1}) and measured $^{206}Pb/^{207}Pb$ ratios for cores from each peat bog site *versus* ^{210}Pb-derived dates since 1840 A.D.

The fluxes decreased in the order CM > RM > FM > TM, which was the same as that observed for Pb. It is worth noting that in FM01CM-2 (the FM01CM-1 sister core), maximum As fluxes in the range 1.7 to 1.8 mg m^{-2} y^{-1} were found during the 1930s-1950s A.D. (Yafa, 2004; Farmer *et al.*, 2006). Also, MacKenzie *et al.* (1998b) found a peak As flux of ~ 4 mg m^{-2} y^{-1} during the *ca.* 1940-1950 A.D. period at South Drumboy Hill (west-central Scotland).

Cd

Depositional fluxes of anthropogenic Cd and Pb since the mid-19th century A.D. for cores from each of the sites are plotted, along with the measured $^{206}Pb/^{207}Pb$ ratios, *versus* ^{210}Pb-derived calendar dates in Fig. 7.11. To summarise, a maximum anthropogenic Cd flux of ~ 0.076 to 0.12 mg m^{-2} y^{-1} occurred between *ca.* 1900 and the mid-1980s A.D. at FM (*cf.* Section 3.8.3.3.4), of ~ 0.29 mg m^{-2} y^{-1} during the mid-1970s A.D. at RM (*cf.* Section 4.8.3.3.4), of ~ 0.21 mg m^{-2} y^{-1} during the early 1960s A.D. at TM (*cf.* Section 5.8.2.1.4) and ~ 0.24 mg m^{-2} y^{-1} during the early 1960s A.D. at CM (*cf.* Section 6.8.3.3.4) (*cf.* Fig. 7.11). The timings of the maximum anthropogenic Cd fluxes at each of the sites were in close agreement, although fluxes decreased in the order RM > CM > TM > FM. Depositional fluxes of Cd in the range 0.10 - 0.12 mg m^{-2} y^{-1} during the 1960s-1970s A.D. were derived from a peat core from western Ireland (Coggins *et al.*, 2006), comparable to values found at FM.

Cu

Depositional fluxes of anthropogenic Cu and Pb since the mid-19th century A.D. for cores from each of the sites are plotted, along with the measured $^{206}Pb/^{207}Pb$ ratios, *versus* ^{210}Pb-derived calendar dates in Fig. 7.12. To summarise, a maximum anthropogenic Cu flux of ~ 3.1 mg m^{-2} y^{-1} occurred during the mid-1950s A.D at FM (*cf.* Section 3.8.3.3.4), of ~ 3.9 to 4.9 mg m^{-2} y^{-1} between the mid-1930s and late 1960s A.D. at RM (*cf.* Section 4.8.3.3.4), of ~ 0.9 to 1.2 mg m^{-2} y^{-1} between the late 1980s and early 2000s A.D. at TM (*cf.* Section 5.8.2.1.4) and of ~ 3.0 mg m^{-2} y^{-1} during the early 1920s A.D. at CM (*cf.* Section 6.8.3.3.4) (*cf.* Fig. 7.12).

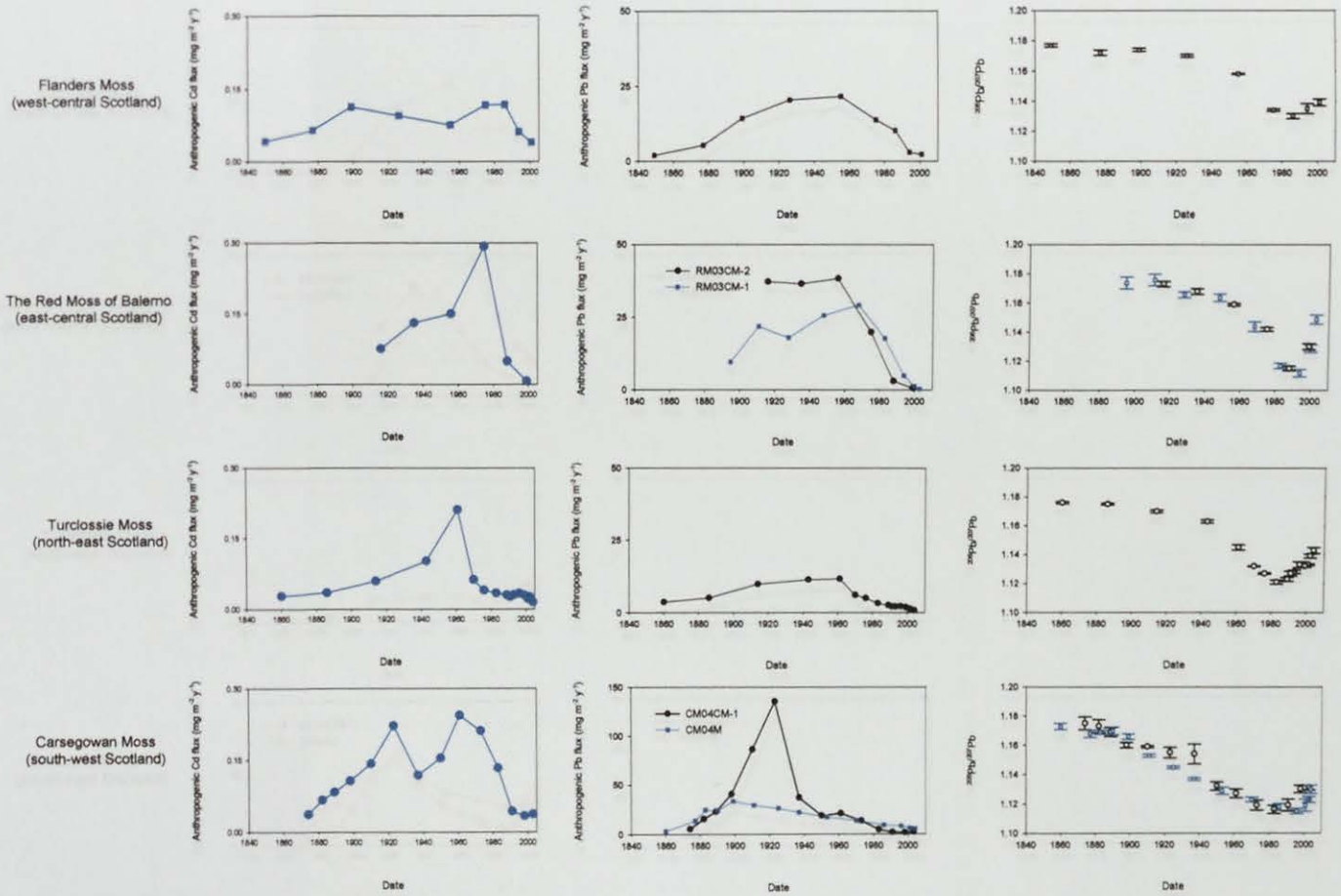

Figure 7.11: Calculated atmospheric depositional fluxes of anthropogenic Cd and Pb (mg m^{-2} y^{-1}) and measured $^{206}Pb/^{207}Pb$ ratios for cores from each peat bog site *versus* ^{210}Pb-derived dates since 1840 A.D.

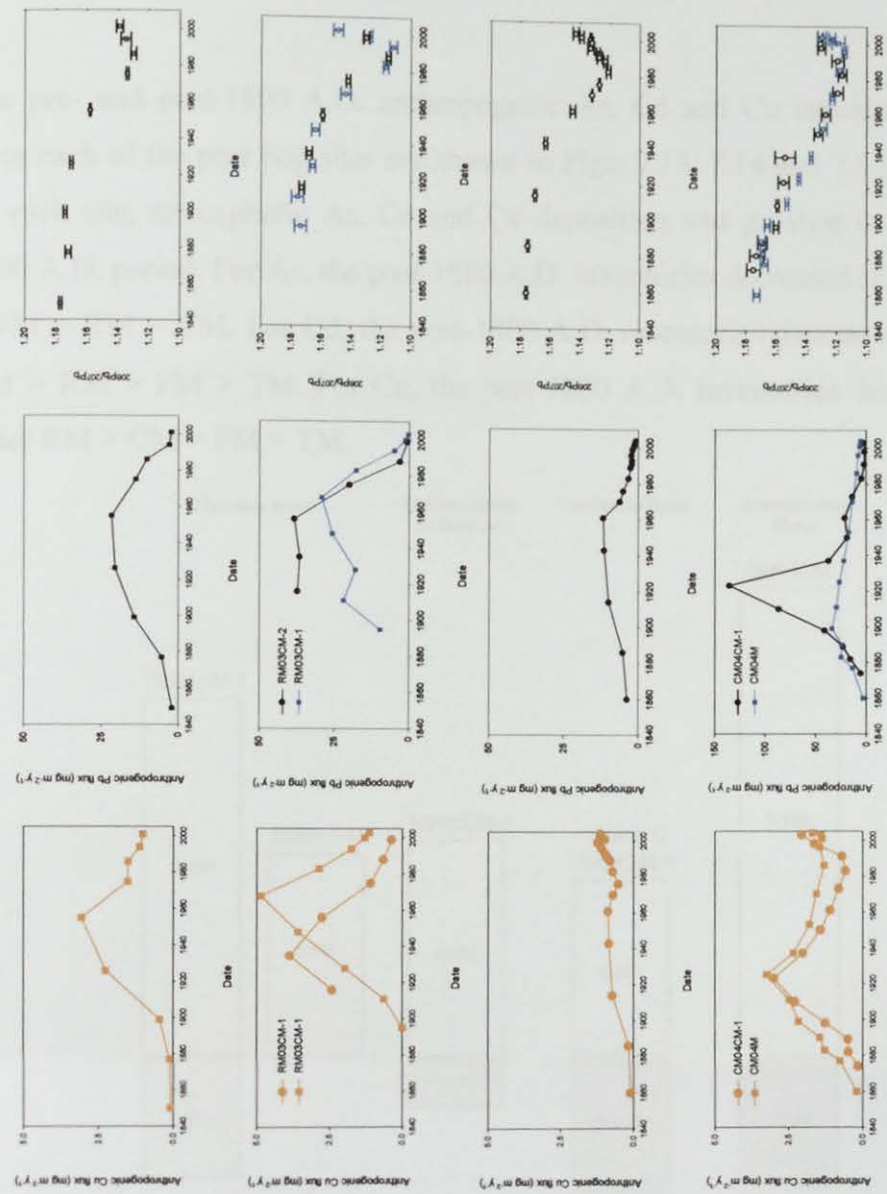

Figure 7.12: Calculated atmospheric depositional fluxes of anthropogenic Cu and Pb (mg m^{-2} y^{-1}) and measured $^{206}Pb/^{207}Pb$ ratios for cores from each peat bog site *versus* ^{210}Pb-derived dates since 1840 A.D.

The timings of the maximum anthropogenic Cu fluxes varied from site to site and, in contrast to Pb, the magnitude of fluxes decreased in the order RM > FM > CM > TM. MacKenzie *et al.* (1998b) found a peak Cu flux of ~ 2.8 mg m^{-2} y^{-1} during the *ca.* 1940-1950 A.D. period at South Drumboy Hill (west-central Scotland), in close agreement with the record at FM.

The pre- and post-1800 A.D. anthropogenic As, Cd and Cu inventories for cores from each of the peat bog sites are shown in Figs. 7.13, 7.14 and 7.15, respectively. At each site, atmospheric As, Cd and Cu deposition was greatest during the post-1800 A.D. period. For As, the post-1800 A.D. inventories decreased in the order CM > FM > RM > TM. For Cd, the post-1800 A.D. inventories decreased in the order CM > RM > FM > TM. For Cu, the post-1800 A.D. inventories decreased in the order RM > CM > FM > TM.

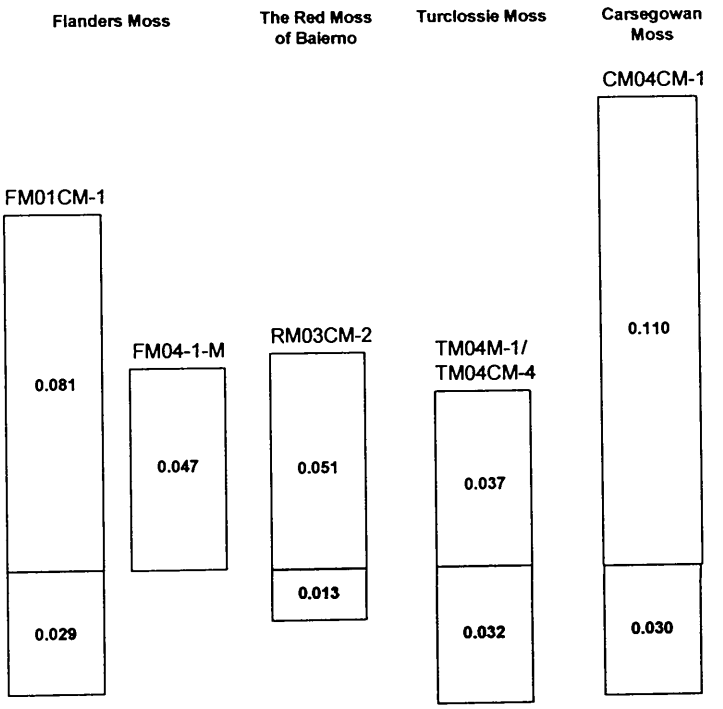

Figure 7.13: Calculated pre- (shaded) and post- (clear) 1800 A.D. anthropogenic As inventories (g m^{-2}) for cores from each site.

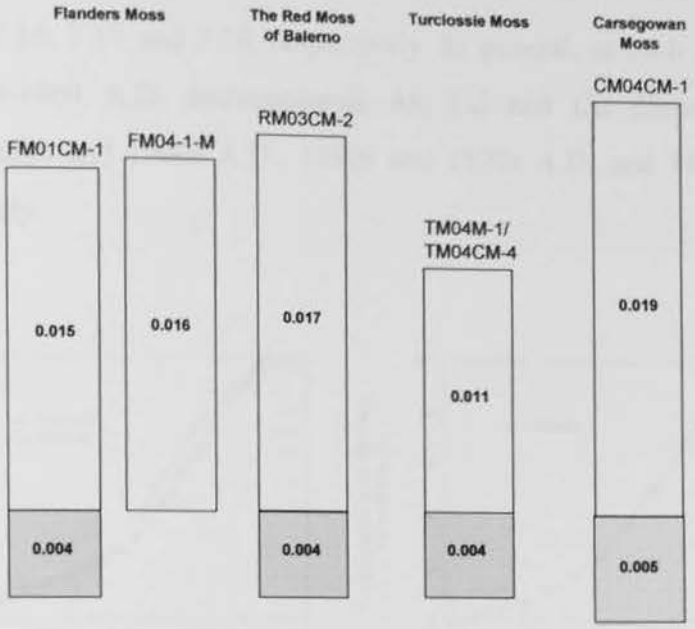

Figure 7.14: Calculated pre- (shaded) and post- (clear) 1800 A.D. anthropogenic Cd inventories (g m^{-2}) for cores from each site.

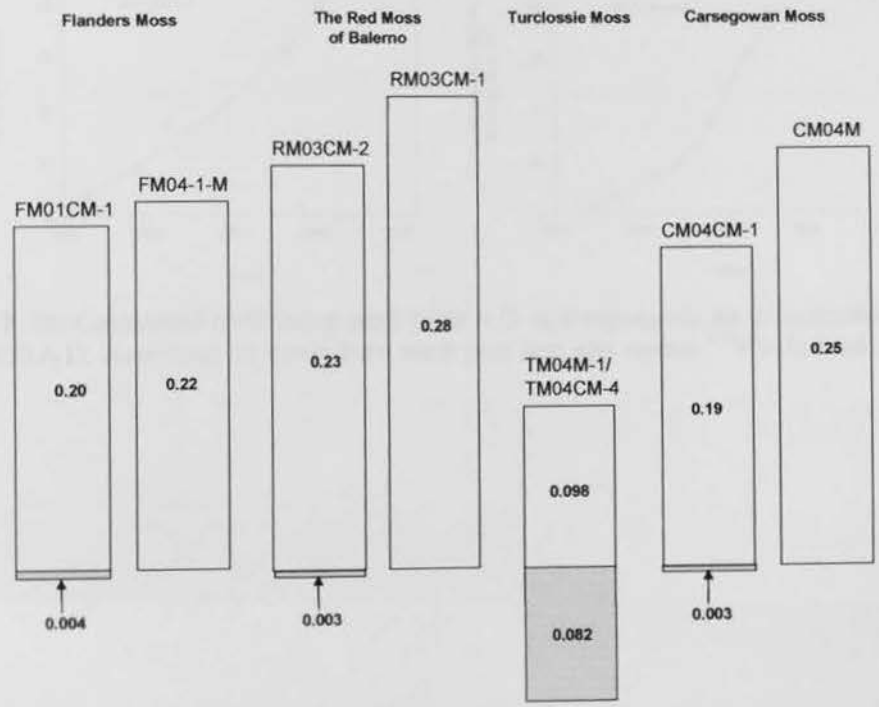

Figure 7.15: Calculated pre- (shaded) and post- (clear) 1800 A.D. anthropogenic Cu inventories (g m^{-2}) for cores from each site.

Calculated cumulative post-1800 A.D. anthropogenic As, Cd and Cu inventories (% of total post-1800 A.D. inventory) for cores from each of the sites (*cf.* Sections 3.8.3.3.4, 4.8.3.3.4, 5.8.2.1.4 and 6.8.3.3.4) are plotted *versus* ^{210}Pb-derived calendar

dates in Figs. 7.16, 7.17 and 7.18, respectively. In general, at each of the sites the maximum post-1800 A.D. anthropogenic As, Cd and Cu deposition occurred between the 1880s and 1960s A.D., 1890s and 1970s A.D. and 1880s and 1980s A.D., respectively.

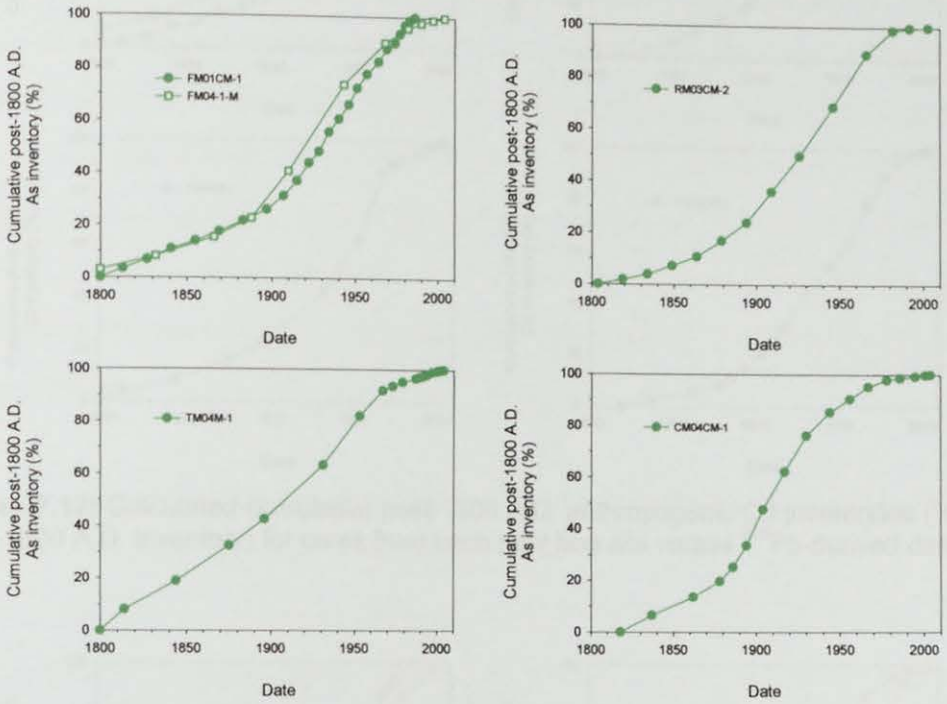

Figure 7.16: Calculated cumulative post-1800 A.D. anthropogenic As inventories (% of total post-1800 A.D. inventory) for cores from each peat bog site *versus* ^{210}Pb-derived dates.

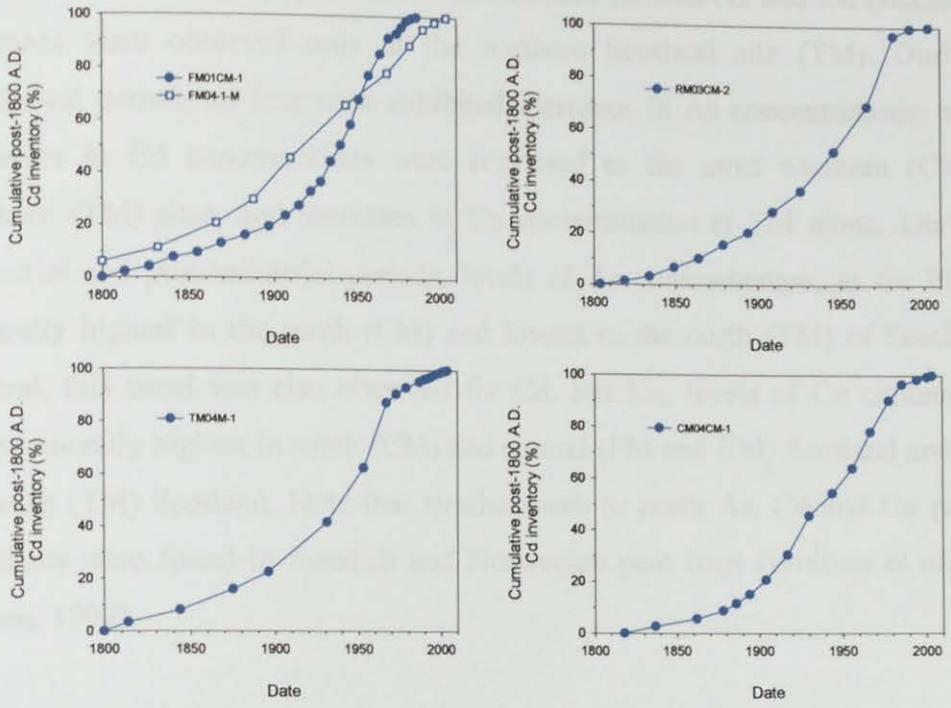

Figure 7.17: Calculated cumulative post-1800 A.D. anthropogenic Cd inventories (% of total post-1800 A.D. inventory) for cores from each peat bog site *versus* ^{210}Pb-derived dates.

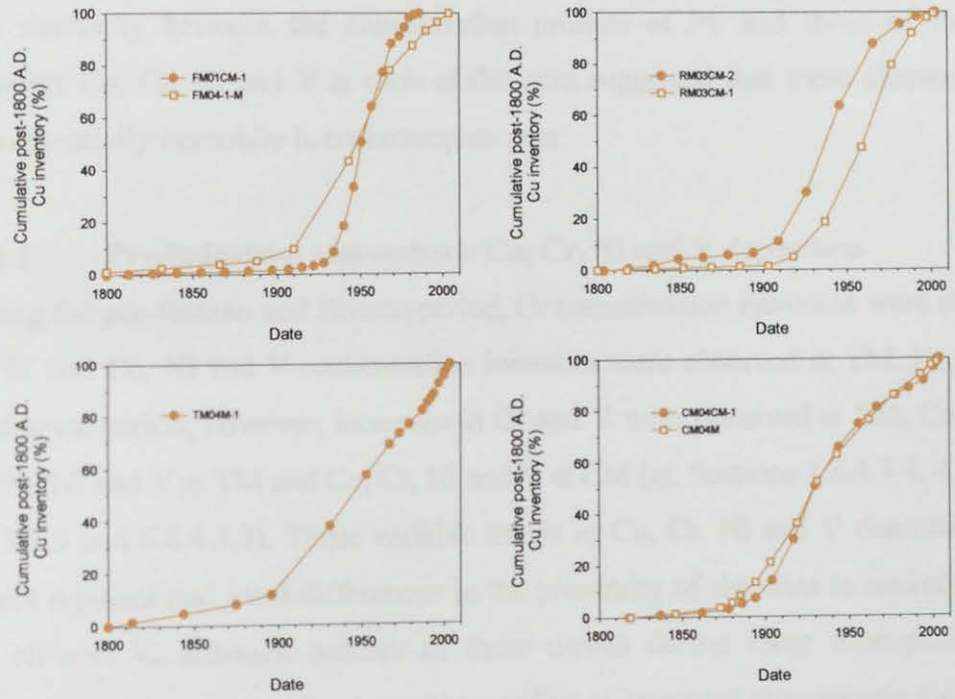

Figure 7.18: Calculated cumulative post-1800 A.D. anthropogenic Cu inventories (% of total post-1800 A.D. inventory) for cores from each peat bog site *versus* ^{210}Pb-derived dates.

7.10.3 Conclusions

In conclusion, during the pre-Roman and Roman periods As and Cu concentration increases were observed only at the northern Scotland site (TM). During the Mediaeval period, all four sites exhibited increases in As concentrations, whereas increases in Cd concentrations were restricted to the most southern (CM) and northern (TM) sites, and increases in Cu contamination at TM alone. During the industrial and post-industrial periods, levels of As contamination, as for Pb, were generally highest in the south (CM) and lowest in the north (TM) of Scotland. In general, this trend was also observed for Cd. For Cu, levels of Cu contamination were generally highest in south (CM) and central (FM and RM) Scotland and lowest in north (TM) Scotland. Note that similar south to north As, Cd and Cu pollution gradients were found in Swedish and Norwegian peat bogs (Hvatum *et al.*, 1987; Jensen, 1997).

7.11 COMPARISON OF HISTORICAL TRENDS IN ATMOSPHERIC Co, Cr, Ni AND V DEPOSITION

The similarity between the concentration profiles of Pb and those of the trace elements Co, Cr, Ni and V at each of the sites suggested that these elements were also essentially immobile in ombrotrophic peat.

7.11.1 Pre-industrial atmospheric Co, Cr, Ni and V deposition

During the pre-Roman and Roman period, Cr concentration increases were observed at FM and Co, Ni and V concentration increases were observed at TM. During the Mediaeval period, however, increases in Cr and V were observed at FM, Co and Cr at RM, Ni and V at TM and Co, Cr, Ni and V at CM (*cf.* Sections 3.8.4.3.4, 4.8.4.1.3, 5.8.3.1.3 and 6.8.4.3.3). These variable trends in Co, Cr, Ni and V deposition may reflect regional and local differences in the proximity of the sites to sources of Co, Cr, Ni and V, although sources of these metals during these time periods are uncertain. Unfortunately, few long term studies of historical atmospheric Co, Cr, Ni and V deposition have been carried out but pre-Roman/Roman and Mediaeval Cr, Ni

and V enhancements were not found in Swiss peat cores from EGR in Switzerland (Krachler *et al.*, 2003a).

7.11.2 Industrial and Post-industrial atmospheric Co, Cr, Ni and V deposition

As for Pb, marked increases in Co, Cr, Ni and V concentrations were found in cores from each of the sites during the Industrial period (*cf.* Sections 3.8.4.3.4, 4.8.4.1.3, 5.8.3.1.3 and 6.8.4.3.3). Krachler *et al.* (2003a) found Cr, Ni and V enrichments during the Industrial period in peat cores from EGR in Switzerland.

Co

Depositional fluxes of anthropogenic Co and Pb since the mid-19th century A.D. for cores from each of the sites are plotted, along with the measured $^{206}Pb/^{207}Pb$ ratios, *versus* ^{210}Pb-derived calendar dates in Fig. 7.19. To summarise, maximum anthropogenic Co fluxes of ~ 0.16 to 0.17 mg m^{-2} y^{-1} occurred between the mid-1950s and mid-1980s A.D. at FM (*cf.* Section 3.8.4.3.5), of ~ 0.43 mg m^{-2} y^{-1} during the mid-1950s A.D. at RM (*cf.* Section 4.8.4.1.4), ~ 0.071 mg m^{-2} y^{-1} during the early 1960s A.D. at TM (*cf.* Section 5.8.3.1.4) and ~ 0.38 mg m^{-2} y^{-1} during the late 1930s A.D. at CM (*cf.* Section 6.8.4.3.4) (*cf.* Fig. 7.19). The timings of the maximum anthropogenic Co fluxes at each of the sites, with the exception of the earlier increases at CM, were generally in close agreement. The fluxes decreased in the order RM > CM > FM > TM. MacKenzie *et al.* (1998b) found a minor increase in Co fluxes to values of ~ 3 to 4 mg m^{-2} y^{-1} during the *ca.* 1940-1950 A.D. period at South Drumboy Hill (west-central Scotland), but these values are significantly higher than those found at the sites investigated here.

Cr

Depositional fluxes of anthropogenic Cr and Pb since the mid-19th century A.D. for cores from each of the sites are plotted, along with the measured $^{206}Pb/^{207}Pb$ ratios, *versus* ^{210}Pb-derived calendar dates in Fig. 7.20. To summarise, a maximum anthropogenic Cr flux of ~ 1.2 mg m^{-2} y^{-1} occurred during the mid-1950s A.D. at FM

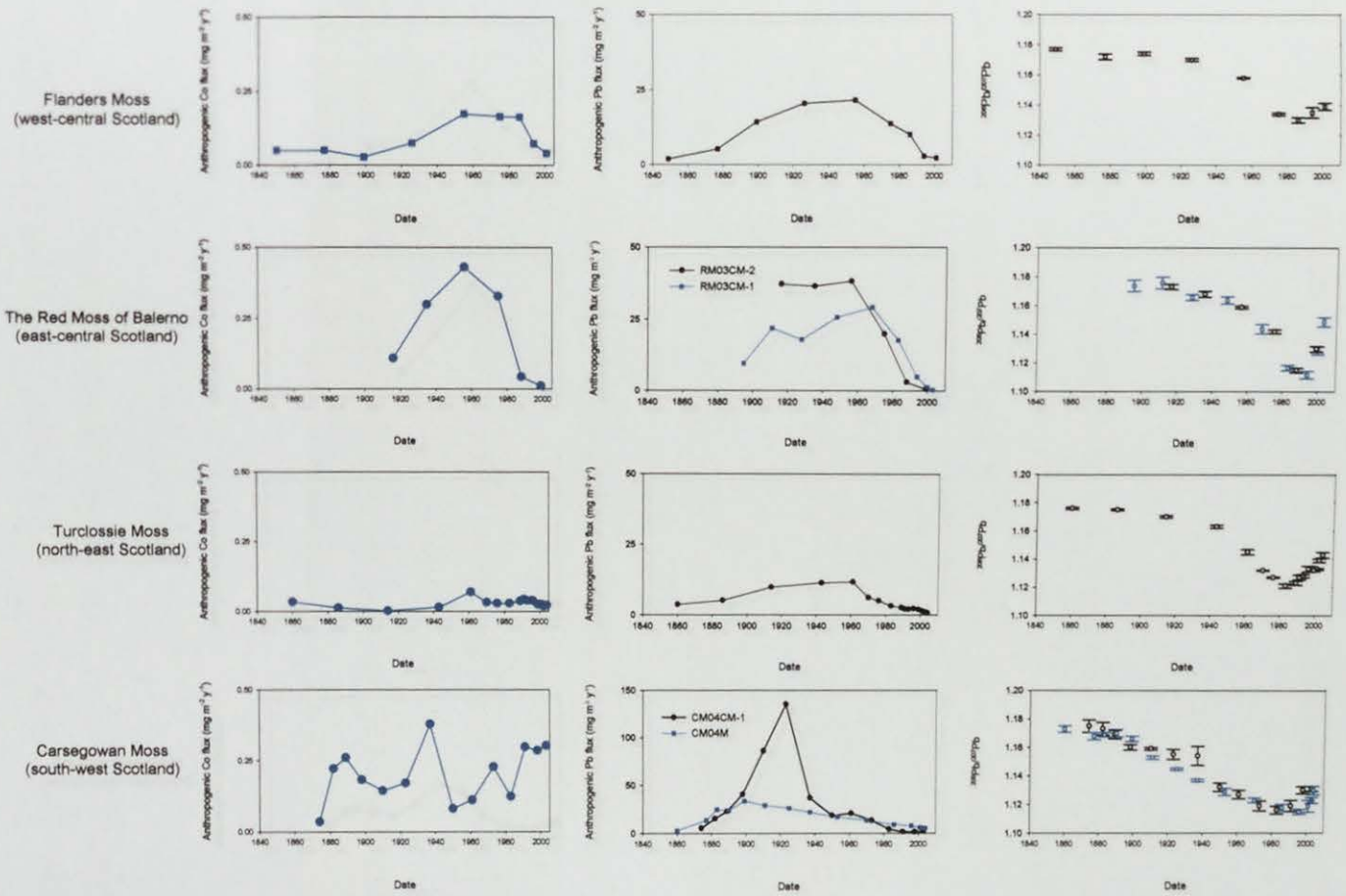

Figure 7.19: Calculated atmospheric depositional fluxes of anthropogenic Co and Pb (mg m^{-2} y^{-1}) and measured $^{206}Pb/^{207}Pb$ ratios for cores from each peat bog site *versus* ^{210}Pb-derived dates since 1840 A.D.

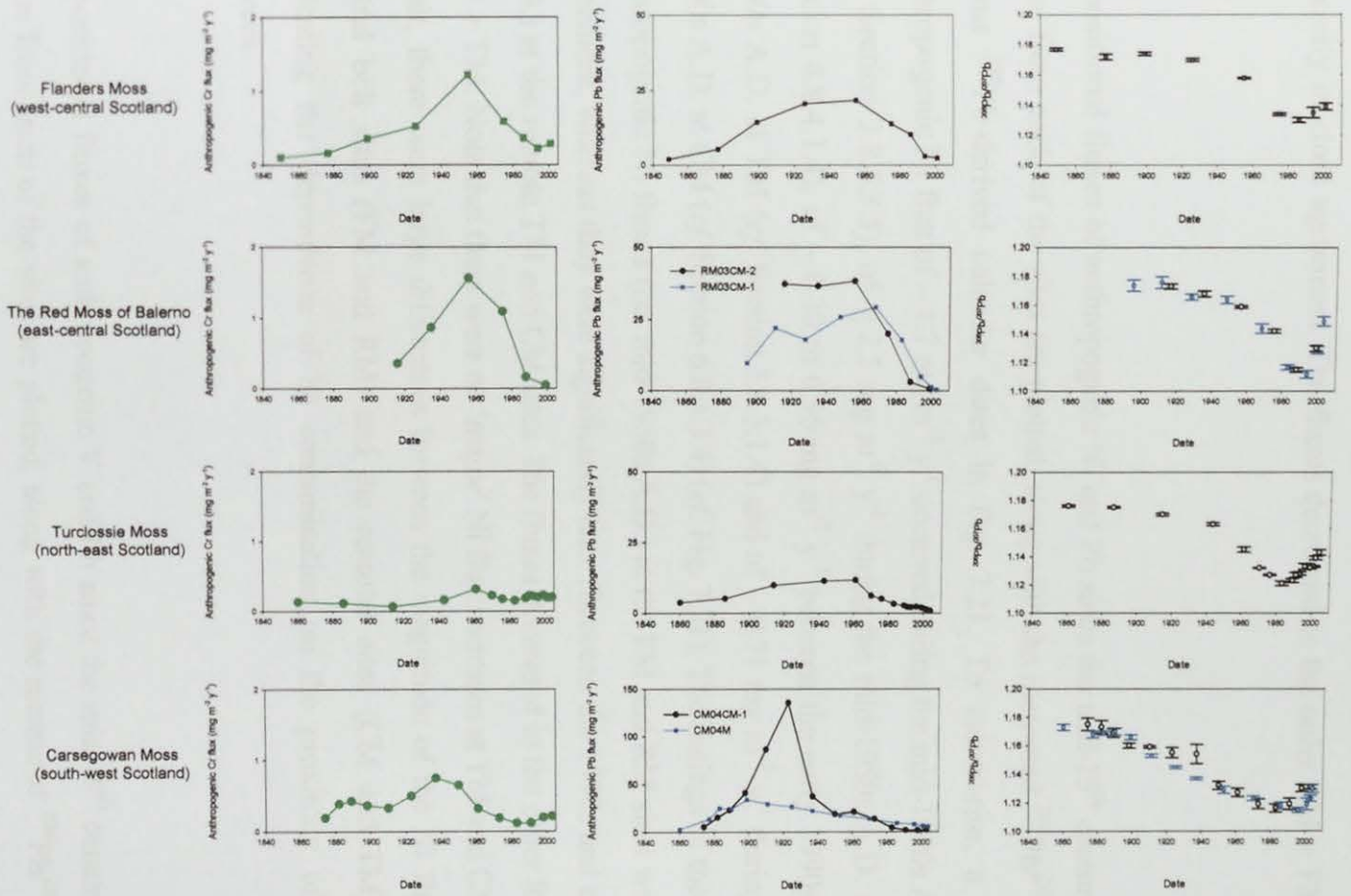

Figure 7.20: Calculated atmospheric depositional fluxes of anthropogenic Cr and Pb (mg m^{-2} y^{-1}) and measured $^{206}Pb/^{207}Pb$ ratios for cores from each peat bog site *versus* ^{210}Pb-derived dates since 1840 A.D.

(*cf.* Section 3.8.4.3.5), of ~ 1.6 mg m^{-2} y^{-1} during the mid-1950s A.D. at RM (*cf.* Section 4.8.4.1.4), of ~ 0.32 mg m^{-2} y^{-1} during the early 1960s A.D. at TM (*cf.* Section 5.8.3.1.4) and of ~ 0.75 mg m^{-2} y^{-1} during the late 1930s A.D. at CM (*cf.* Section 6.8.4.3.4) (*cf.* Fig. 7.20). The timings of the maximum anthropogenic Cr fluxes at each of the sites, with the exception of the earlier increases at CM, were generally in close agreement. The fluxes decreased in the order RM > FM > CM > TM.

Ni

Depositional fluxes of anthropogenic Ni and Pb since the mid-19th century A.D. for cores from each of the sites are plotted, along with the measured $^{206}Pb/^{207}Pb$ ratios, *versus* ^{210}Pb-derived calendar dates in Fig. 7.21. To summarise, a maximum anthropogenic Ni flux of ~ 1.7 mg m^{-2} y^{-1} occurred during the mid-1950s A.D. at FM (*cf.* Section 3.8.4.3.5), of ~ 2.5 mg m^{-2} y^{-1} during the mid-1950s A.D. at RM (*cf.* Section 4.8.4.1.4), of ~ 0.30 to 0.36 mg m^{-2} y^{-1} between the early 1990s and early 2000s A.D. at TM (*cf.* Section 5.8.3.1.4) and of ~ 0.71 mg m^{-2} y^{-1} during the early 2000s A.D. at CM (*cf.* Section 6.8.4.3.4) (*cf.* Fig. 7.21). The timings of the maximum anthropogenic Ni fluxes (*ca.* mid-1950s A.D.) at the FM and RM sites were in good agreement, whereas they were significantly later (between the 1990s and early 2000s A.D.) at the remote TM and CM sites. The fluxes decreased in the order RM > FM > CM > TM. Note that there were no 'major' Ni flux increases at TM and CM and, as a result, there were large differences between the magnitude of the Ni fluxes at the central belt sites (FM and RM) and the remoter sites (CM and TM), possibly indicating the dependence of Ni contamination on the proximity of industrial sources.

V

Depositional fluxes of anthropogenic V and Pb since the mid-19th century A.D. for cores from each of the sites are plotted, along with the measured $^{206}Pb/^{207}Pb$ ratios, *versus* ^{210}Pb-derived calendar dates in Fig. 7.22. To summarise, a maximum anthropogenic V flux of ~ 2.0 mg m^{-2} y^{-1} occurred during the mid-1950s A.D. at FM

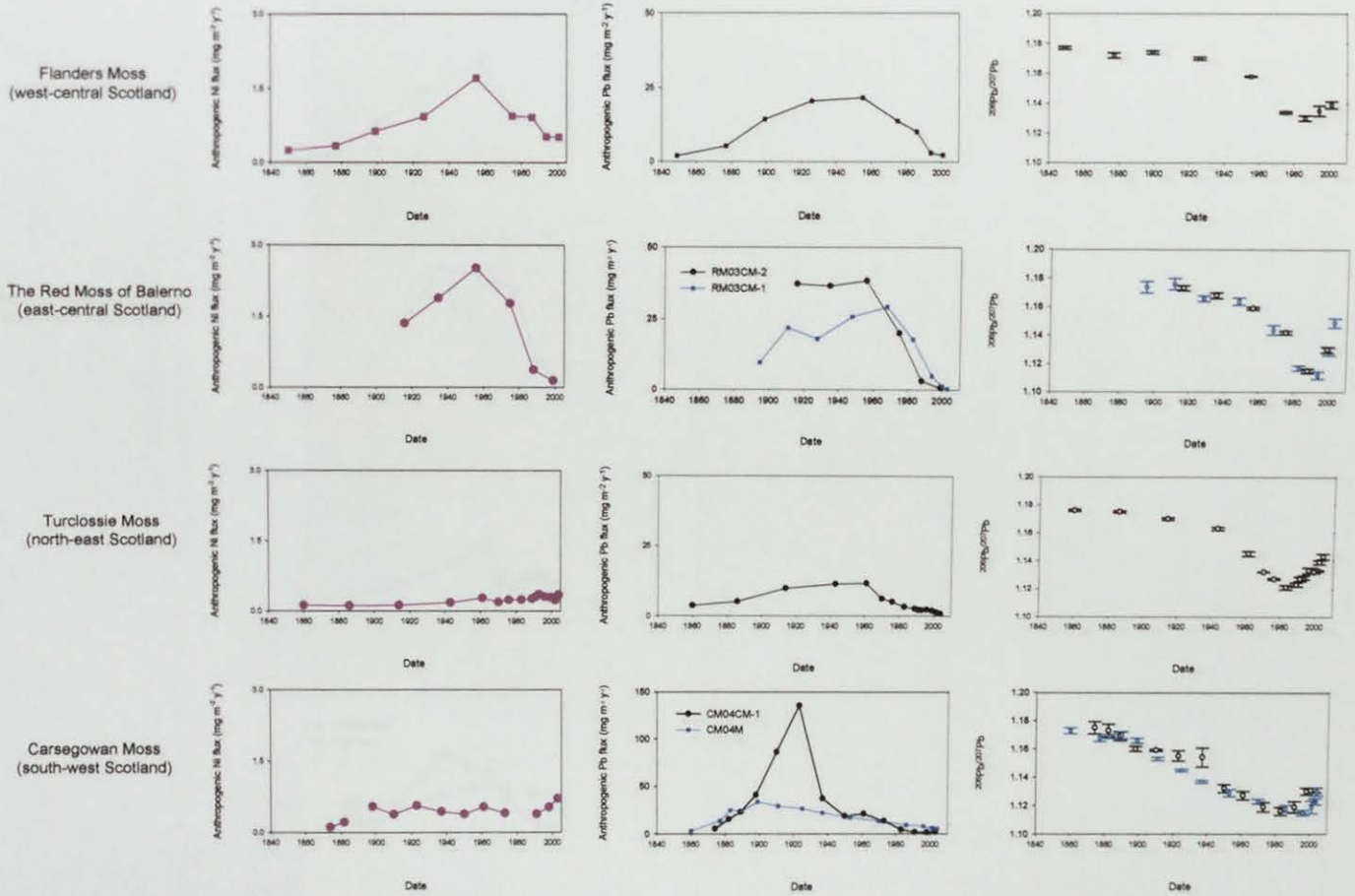

Figure 7.21: Calculated atmospheric depositional fluxes of anthropogenic Ni and Pb (mg m^{-2} y^{-1}) and measured $^{206}Pb/^{207}Pb$ ratios for cores from each peat bog site *versus* ^{210}Pb-derived dates since 1840 A.D.

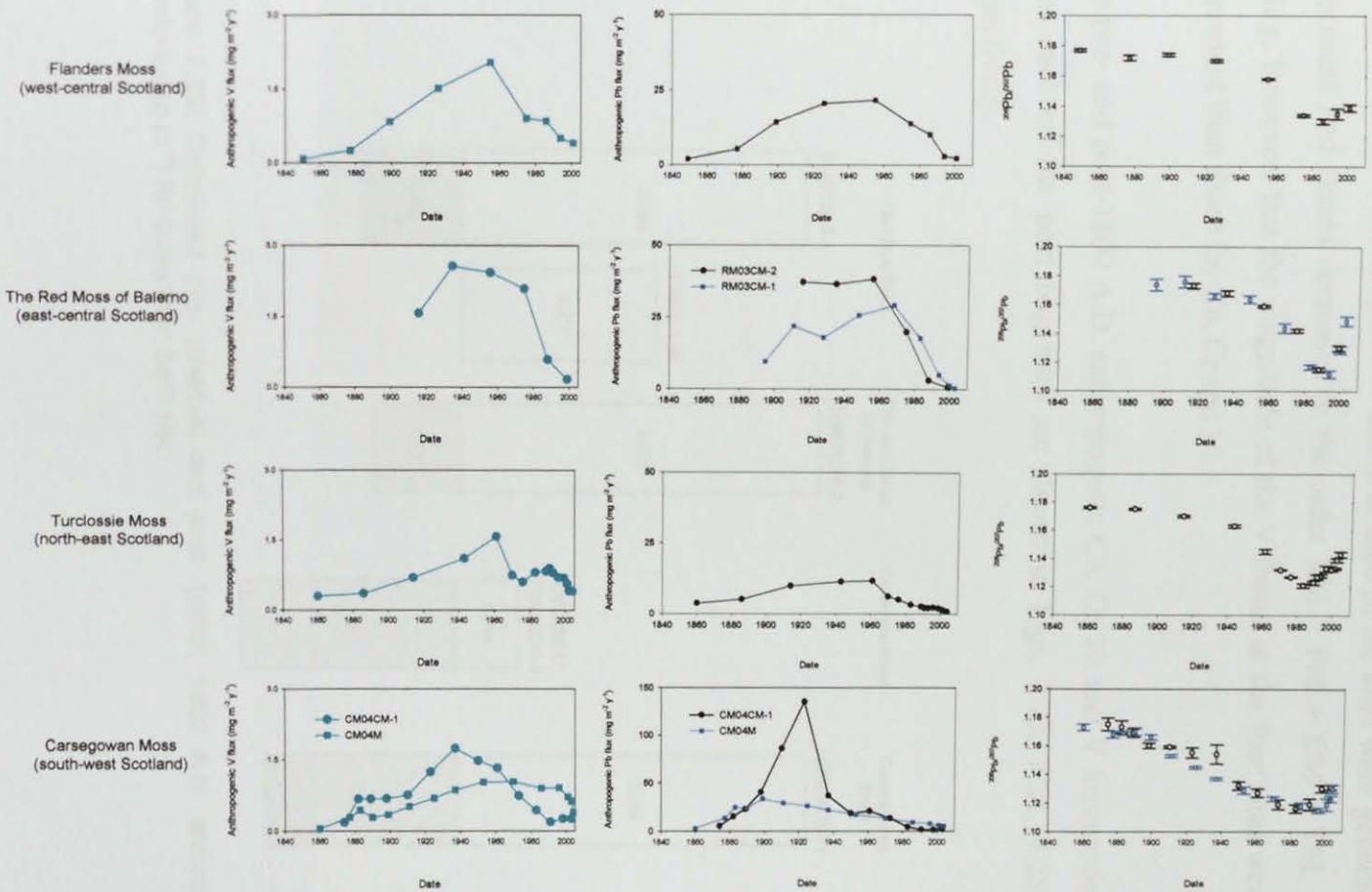

Figure 7.22: Calculated atmospheric depositional fluxes of anthropogenic V and Pb (mg m^{-2} y^{-1}) and measured $^{206}Pb/^{207}Pb$ ratios for cores from each peat bog site *versus* ^{210}Pb-derived dates since 1840 A.D.

(*cf.* Section 3.8.4.3.5), of ~ 2.1 to 2.6 mg m^{-2} y^{-1} between the mid-1930s and mid-1970s A.D at RM (*cf.* Section 4.8.4.1.4), of ~ 1.6 mg m^{-2} y^{-1} during the early 1960s A.D. at TM (*cf.* Section 5.8.3.1.4) and of ~ 1.0 to 1.7 mg m^{-2} y^{-1} between the late 1930s and early 1970s A.D. at CM (*cf.* Section 6.8.4.3.4) (*cf.* Fig. 7.22). The timings of the maximum anthropogenic V fluxes at each of the sites were generally in close agreement and fluxes decreased in the order RM > FM > CM > TM. It is worth noting, however, that the magnitude of the V fluxes at the four sites were in closer agreement than those for Co, Cr and Ni.

The pre- and post-1800 A.D. anthropogenic Co, Cr, Ni and V inventories for cores from each of the peat bog sites are shown in Figs. 7.23, 7.24, 7.25 and 7.26, respectively.

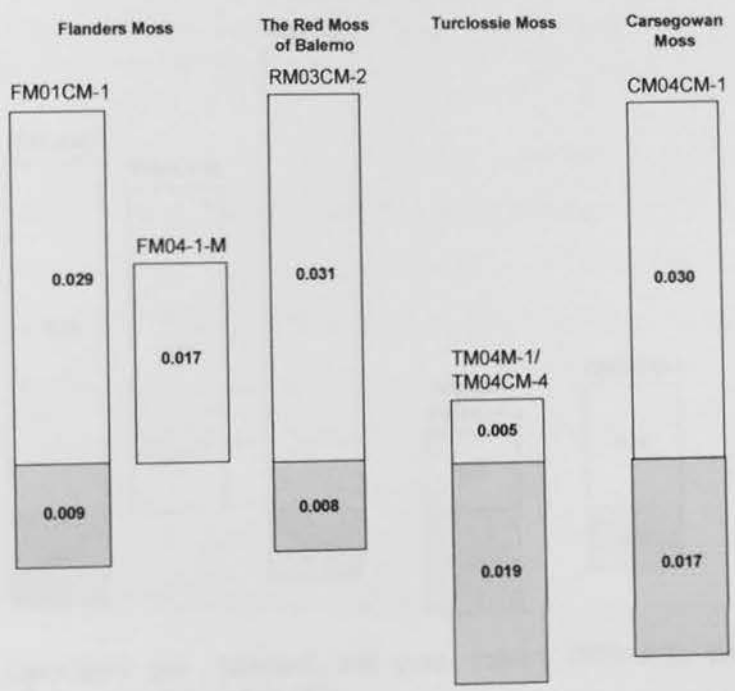

Figure 7.23: Calculated pre- (shaded) and post- (clear) 1800 A.D. anthropogenic Co inventories (g m^{-2}) for cores from each site.

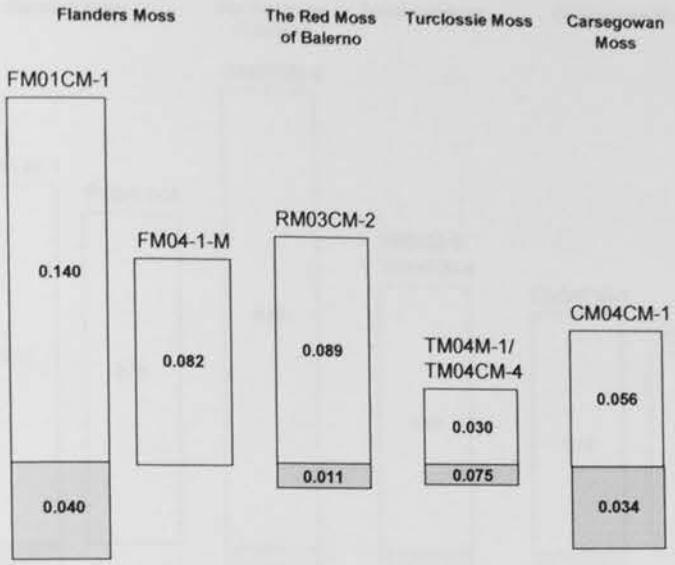

Figure 7.24: Calculated pre- (shaded) and post- (clear) 1800 A.D. anthropogenic Cr inventories (g m^{-2}) for cores from each site.

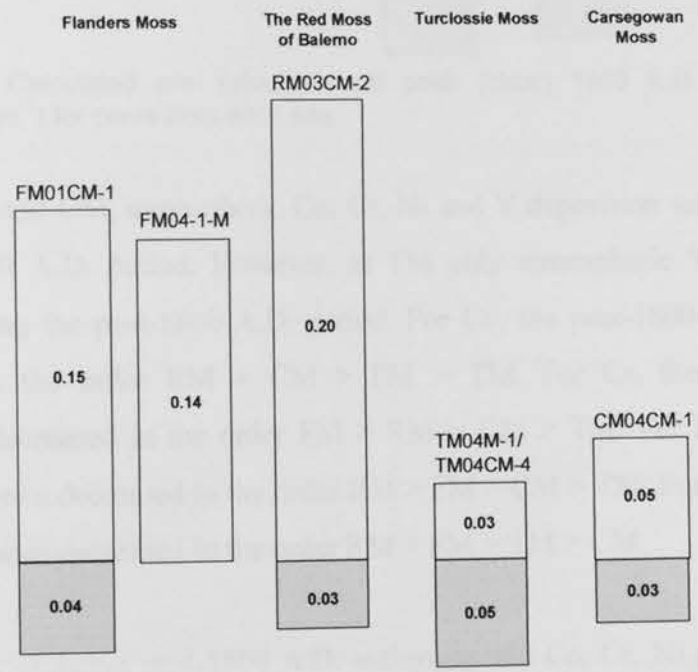

Figure 7.25: Calculated pre- (shaded) and post- (clear) 1800 A.D. anthropogenic Ni inventories (g m^{-2}) for cores from each site.

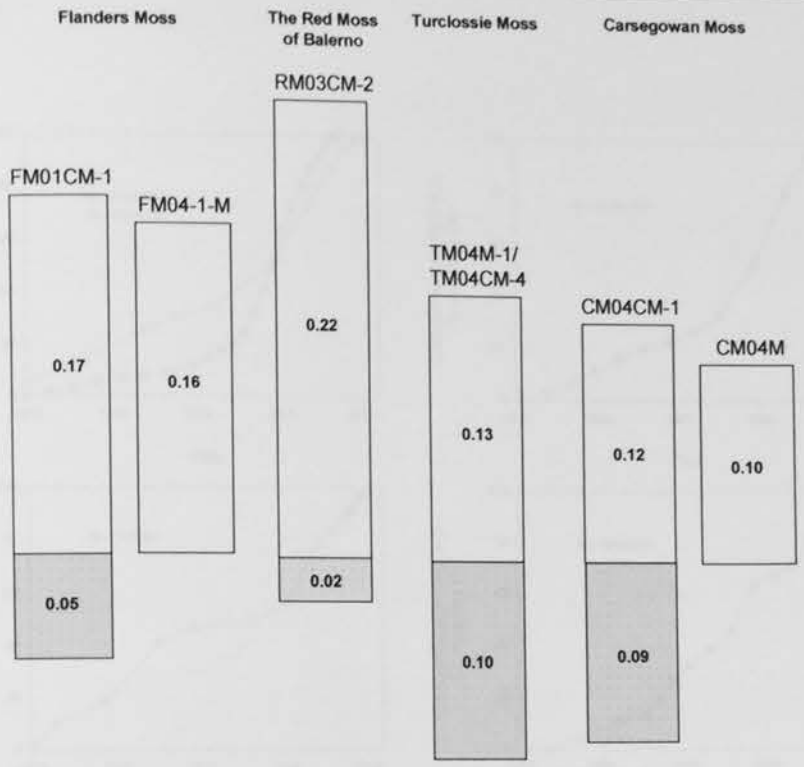

Figure 7.26: Calculated pre- (shaded) and post- (clear) 1800 A.D. anthropogenic V inventories (g m^{-2}) for cores from each site.

At FM, RM and CM, atmospheric Co, Cr, Ni and V deposition was greatest during the post-1800 A.D. period. However, at TM only atmospheric V deposition was greatest during the post-1800 A.D. period. For Co, the post-1800 A.D. inventories decreased in the order RM > CM > FM > TM. For Cr, the post-1800 A.D. inventories decreased in the order FM > RM > CM > TM. For Ni, the post-1800 A.D. inventories decreased in the order RM > FM > CM > TM. For V, the post-1800 A.D. inventories decreased in the order RM > FM > TM > CM.

Calculated cumulative post-1800 A.D. anthropogenic Co, Cr, Ni and V inventories (% of total post-1800 A.D. inventory) for cores from each of the sites (*cf.* Sections 3.8.4.3.5, 4.8.4.1.4, 5.8.3.1.4 and 6.8.4.3.4) are plotted *versus* ^{210}Pb-derived calendar dates in Figs. 7.27, 7.28, 7.29 and 7.30, respectively.

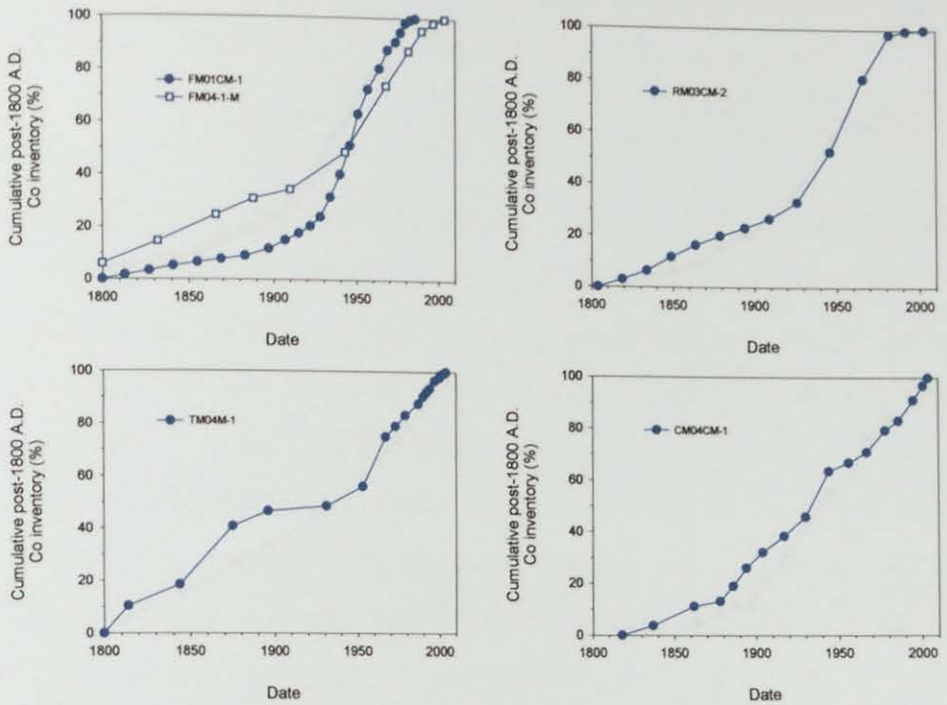

Figure 7.27: Calculated cumulative post-1800 A.D. anthropogenic Co inventories (% of total post-1800 A.D. inventory) for cores from each peat bog site *versus* ^{210}Pb-derived dates.

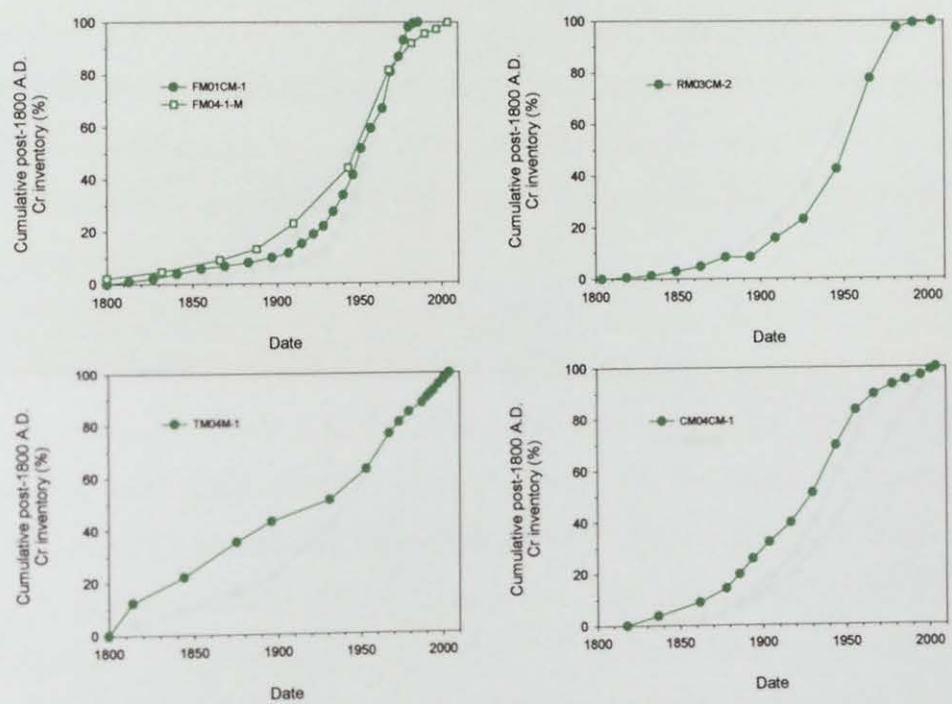

Figure 7.28: Calculated cumulative post-1800 A.D. anthropogenic Cr inventories (% of total post-1800 A.D. inventory) for cores from each peat bog site *versus* ^{210}Pb-derived dates.

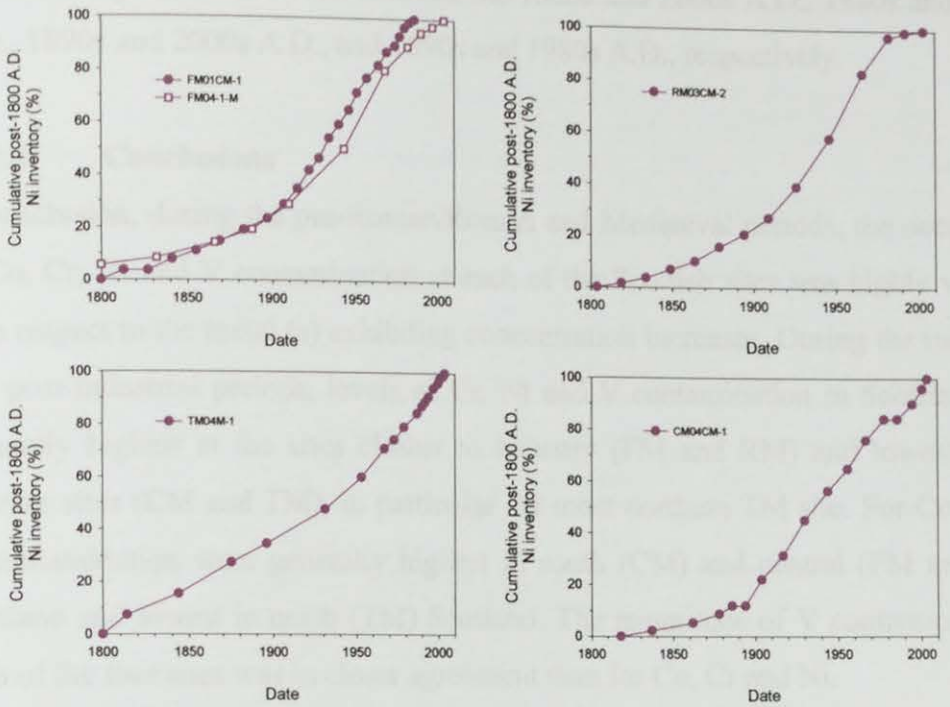

Figure 7.29: Calculated cumulative post-1800 A.D. anthropogenic Ni inventories (% of total post-1800 A.D. inventory) for cores from each peat bog site *versus* ^{210}Pb-derived dates.

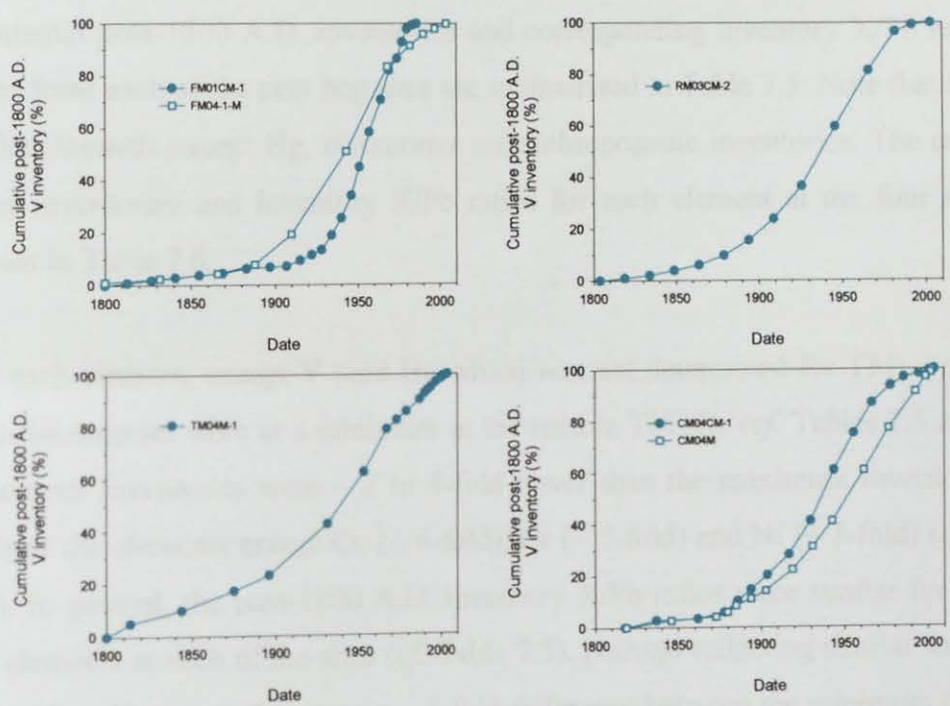

Figure 7.30: Calculated cumulative post-1800 A.D. anthropogenic V inventories (% of total post-1800 A.D. inventory) for cores from each peat bog site *versus* ^{210}Pb-derived dates.

In general, at each of the sites the maximum post-1800 A.D. anthropogenic Co, Cr, Ni and V deposition occurred between the 1880s and 2000s A.D., 1880s and 1970s A.D., 1890s and 2000s A.D., and 1890s and 1980s A.D., respectively.

7.11.3 Conclusions

In conclusion, during the pre-Roman/Roman and Mediaeval periods, the occurrence of Co, Cr, Ni and V contamination at each of the Scottish sites was highly variable with respect to the metal (s) exhibiting concentration increases. During the industrial and post-industrial periods, levels of Cr, Ni and V contamination in Scotland were generally highest at the sites closest to industry (FM and RM) and lowest at the remoter sites (CM and TM), in particular the most northern TM site. For Co, levels of contamination were generally highest in south (CM) and central (FM and RM) Scotland and lowest in north (TM) Scotland. The magnitude of V contamination at each of the four sites was in closer agreement than for Co, Cr and Ni.

7.12 SUMMARY OF ELEMENTAL POST-1800 A.D. INVENTORIES

Elemental post-1800 A.D. inventories and corresponding inventory X/Pb ratios for cores from each of the peat bog sites are summarised in Table 7.5. Note that for each of the elements except Hg, inventories are anthropogenic inventories. The ranges of these inventories and inventory X/Pb ratios for each element at the four sites are shown in Table 7.6.

For each element, except V (and Hg which was not determined for TM), post-1800 A.D. inventories were at a minimum at the remote TM site (*cf.* Tables 7.5 and 7.6). Minimum inventories were ~ 2 to 4-fold lower than the maximum inventories for each of the elements except Co (~ 6-fold), Cr (~ 5-fold) and Ni (~ 7-fold) (*cf.* Table 7.6). In general, the post-1800 A.D. inventory X/Pb ratios were similar for each of the elements at each of the sites (*cf.* Table 7.5), perhaps reflecting similar sources of deposition. However, there was a ~ 7-fold difference between the minimum (0.010 at CM) and maximum (0.066 at FM) inventory Ni/Pb ratios, and ~ 5-fold difference

between the minimum (0.024 at CM) and maximum (0.107 at TM) inventory V/Pb ratios, which could be attributable to different sources of anthropogenic Ni and V at these sites.

Table 7.5: Summary of post-1800 A.D. anthropogenic As, Cd, Co, Cr, Cu, Ni, Pb, Sb and V inventories (g m^{-2}), post-1800 A.D. Hg inventories (g m^{-2}) and corresponding inventory X/Pb ratios for cores from each peat bog site.

	Flanders Moss				The Red Moss of Balerno			
	FM01CM-1		FM04M-1		RM03CM-2		RM03CM-1	
Element	Post-1800 A.D. inventory (g m^{-2})	Inventory X/Pb ratio	Post-1800 A.D. inventory (g m^{-2})	Inventory X/Pb ratio	Post-1800 A.D. inventory (g m^{-2})	Inventory X/Pb ratio	Post-1800 A.D. inventory (g m^{-2})	Inventory X/Pb ratio
As	0.081	0.023	0.047	0.022	0.051	0.012		
Cd	0.015	0.0042	0.016	0.0076	0.017	0.0040		
Co	0.029	0.0081	0.017	0.0081	0.031	0.0073		
Cr	0.140	0.039	0.082	0.039	0.089	0.021		
Cu	0.20	0.056	0.22	0.104	0.23	0.054	0.28	0.114
Hg	-	-	-	-	0.0071	0.0017		
Ni	0.15	0.042	0.14	0.066	0.20	0.047		
Pb	3.59	-	2.11	-	4.26	-	2.45	-
Sb	0.049	0.014	0.035	0.017	0.044	0.010		
V	0.17	0.047	0.16	0.076	0.22	0.052		

Note that the FM01CM-2 post-1800 A.D. Hg and Pb (Yafa, 2004) inventories were 0.0090 and 2.4 g m^{-2}, respectively, and the corresponding inventory Hg/Pb ratio was 0.0038.

Table 7.5 (continued): Summary of post-1800 A.D. anthropogenic As, Cd, Co, Cr, Cu, Ni, Pb, Sb and V inventories (g m^{-2}), post-1800 A.D. Hg inventories (g m^{-2}) and corresponding inventory X/Pb ratios for cores from each peat bog site.

	Turclossie Moss		Carsegowan Moss			
	TM04M-1		CM04CM-1		CM04M	
Element	Post-1800 A.D. inventory (g m^{-2})	Inventory X/Pb ratio	Post-1800 A.D. inventory (g m^{-2})	Inventory X/Pb ratio	Post-1800 A.D. inventory (g m^{-2})	Inventory X/Pb ratio
As	0.037	0.030	0.110	0.022		
Cd	0.011	0.0090	0.019	0.0038		
Co	0.005	0.0041	0.030	0.0060		
Cr	0.030	0.025	0.056	0.011		
Cu	0.098	0.080	0.19	0.038	0.25	0.091
Hg	-	-	0.0087	0.0018		
Ni	0.03	0.025	0.05	0.010		
Pb	1.22	-	4.97	-	2.74	-
Sb	0.025	0.020	0.056	0.011		
V	0.13	0.107	0.12	0.024	0.10	0.036

Table 7.6: Ranges of elemental post-1800 A.D. inventories (g m^{-2}) and inventory X/Pb ratios at the four peat bog sites.

Element	Post-1800 A.D. inventory range (g m^{-2})	Inventory X/Pb ratio range
As	0.037 – 0.110	0.012 – 0.030
Cd	0.011 – 0.019	0.0038 – 0.0090
Co	0.005 – 0.031	0.0041 – 0.0081
Cr	0.030 – 0.140	0.011 – 0.039
Cu	0.098 – 0.28	0.038 – 0.114
Hg	0.0038 – 0.0090	0.0017 – 0.0038-
Ni	0.03 – 0.20	0.010 – 0.066
Pb	1.22 – 4.97	-
Sb	0.025 – 0.056	0.010 – 0.020
V	0.10 – 0.22	0.024 – 0.107

Note that these values are taken from Table 7.5.

7.13 CONCLUSIONS

The principal conclusions arising from the comparison of results for the peat bog sites were as follows:

- In general, at each of the sites studied there was good agreement between findings for the peat matrix properties, conservative elements and the geochemical behaviour of the elements investigated. Also, each site indicated ^{137}Cs mobility in peat bogs.
- Clear indications of Pb and Sb contamination were found during the pre-Roman and Roman periods at FM and TM, the only sites for which cores dating back to these times were collected. Clear indications of Pb, Sb and As contamination were found during the Mediaeval period at each of the four sites.
- In general, at each of the sites, atmospheric As, Cr, Hg, Pb and Sb deposition was greatest during the industrial period (between the late 1880s and late 1960s A.D.) and atmospheric Cd, Co, Cu, Ni and V deposition was greatest during the industrial and post-industrial periods (between *ca.* 1900 and the early 2000s A.D.), although increases in As, Co, Cr, Hg, Pb and Sb deposition were earliest (during the late 19th and early 20th century A.D.) at CM.

- During the industrial and post-industrial periods, levels of As, Pb and Cd contamination were generally highest in the south (CM) and lowest in the north (TM) of Scotland.
- During the industrial and post-industrial periods, levels of Cu, Co and Sb contamination were generally highest in south (CM) and central (FM and RM) Scotland and lowest in the north (TM) of Scotland.
- During the industrial and post-industrial periods, levels of Cr, Ni and V contamination were generally highest in the sites closest to industry (FM and RM) and lowest in the remoter sites (CM and TM), being lowest in the most northern TM site.
- Levels of Hg contamination during the industrial and post-industrial periods were found to be higher in the FM site relative to the RM and CM sites.
- Overall, the existence of a south to north As, Cd, Co, Cr, Cu, Ni, Pb, Sb and V pollution gradient in Scotland (inventories being higher in the south relative to the north) was evident, as found, at least for As, Cd, Cu, Pb and Sb, in other parts of Europe.

8 CONCLUSIONS

8.1 Summary of conclusions of thesis

The main findings of this thesis were as follows:

- Profiles of Pb concentration and isotopic composition obtained in cores from four Scottish ombrotrophic peat bogs (Chapters 3, 4, 5 and 6) reinforced the view that Pb is essentially immobile in such deposits. Using Sc, Ti and Zr as conservative elements, anthropogenic enrichments of Pb at the four peat bogs were estimated and, on the basis of ^{210}Pb and ^{14}C dating and Pb isotopic composition (e.g. $^{206}Pb/^{207}Pb$), sources of atmospheric anthropogenic Pb deposition across Scotland, since the pre-Roman/Roman period, were investigated (Chapters 3, 4, 5 and 6). Clear indications of Pb contamination during the pre-Roman/Roman and Mediaeval periods were attributed to the mining and smelting of Pb ores (from Britain and elsewhere in Europe). During the industrial and post-industrial periods, variations in the relative importance of contributions of anthropogenic Pb from different sources were apparent. From *ca.* the early 17th century A.D. at FM (Chapter 3), RM (Chapter 4) and TM (Chapter 5), the mining and smelting of indigenous Scottish Pb ores, until the early 20th century A.D., were found to be the most important sources of anthropogenic Pb deposition. In contrast, at CM (Chapter 6), influences from the use of both British Pb ores and imported Australian Pb ores (in more southern parts of Britain) since the late 19th century A.D. were evident. At each of the sites, the increasing importance of Australian-Pb-influenced car-exhaust emissions from the 1930s to late 1990s A.D., along with significant contributions from coal combustion (until the late 1960s A.D.) was evident.
- Profiles of Ca, Fe, Mg, Mn, P, S, Se and Zn concentrations in cores from the four peat bogs (Chapters 3, 4, 5 and 6) suggested that these eight elements were mobile in ombrotrophic peat.
- Profiles of As, Cd, Co, Cr, Cu, Hg (at least during the industrial and post-industrial periods), Ni, Sb and V concentrations in cores from the four

peat bogs (Chapters 3, 4, 5 and 6) suggested that these nine elements, like Pb, were essentially immobile in ombrotrophic peat.

- Profiles of Sb and Pb concentrations in cores from the four peat bogs (Chapters 3, 4, 5 and 6) were remarkably similar. Records of atmospheric anthropogenic Sb deposition across Scotland since the pre-Roman/Roman period were investigated (Chapters 3, 4, 5 and 6) and, in general, major trends in the concentration profiles of anthropogenic Sb and Pb suggested common sources of these two elements. Perturbations in the anthropogenic Sb/Pb ratios since *ca.* 1800 A.D., however, were attributed to temporal variations in the relative importance of atmospheric emissions from different sources such as Pb ore mining/smelting, coal combustion and, in recent decades, automobile-related use of compounds of Pb (in leaded petrol) and of Sb (in brake linings).
- Records of atmospheric Hg deposition across Scotland since the onset of the industrial period were investigated (Chapters 3, 4, and 6) and, in general, during the industrial and post-industrial periods, coal combustion and waste incineration, respectively, were likely to be the most important sources of Hg.
- Records of atmospheric anthropogenic As, Cd, Co, Cr, Cu, Ni and V deposition across Scotland since the pre-Roman/Roman period were investigated (Chapters 3, 4, 5 and 6). Clear indications of As contamination during the Mediaeval period were probably attributable to the mining and smelting of Pb and Cu ores. During the industrial and post-industrial periods, sources of As, Cd, Co, Cr, Cu, Ni and V were attributable to a variety of sources (e.g. metallurgical activities, coal and oil combustion, use of phosphate fertilisers and waste incineration). Also, in recent years, atmospheric Cu emissions from automobile-related use of compounds of Cu (in motor oil, brake linings and tyres) may have been important.
- Inter-site and inter-elemental comparison of records of atmospheric metal deposition across Scotland indicated that, in general, atmospheric As, Cr, Hg, Pb and Sb deposition was greatest during the industrial period (between the late 1880s and late 1960s A.D.) and atmospheric Cd, Co, Cu, Ni and V deposition was greatest during the industrial and post-industrial periods (between *ca.* 1900

and the early 2000s A.D.), although increases in As, Co, Cr, Hg, Pb and Sb deposition were earliest (during the late 19th and early 20th century A.D.) at the most southerly site (CM) (Chapter 7).

- Inter-site and inter-elemental comparison of records of atmospheric metal deposition across Scotland also indicated that during the industrial and post-industrial periods, levels of As, Pb and Cd contamination were generally highest in the south of Scotland, Cu, Co and Sb in south and central Scotland, and Cr, Ni and V in central Scotland (Chapter 7). Overall, the existence of a south to north As, Cd, Co, Cr, Cu, Ni, Pb, Sb and V pollution gradient in Scotland was evident.

8.2 Recommendations for further work

The following are suggested as areas for further research:

1. Further assessment of the influence of within-bog spatial variability on elemental distributions, concentrations and inventories in peat bog profiles via the collection of multiple peat cores from a peat bog site.
2. Use of other dating techniques (e.g. pollen and tephra analysis), in addition to radiometric dating techniques (e.g. ^{210}Pb and ^{14}C), in order to provide a greater degree of confidence in established chronologies for interpreting historical records of atmospheric metal deposition.
3. Investigation of the validity of using UCC M/X ratios to estimate variations in the extent of anthropogenic and natural sources of metals in peat bog profiles with time via their comparison with M/X ratios measured in "background" pre-anthropogenic peat samples.
4. Investigation of pre-anthropogenic atmospheric metal deposition records and characterisation of the Pb isotopic composition of pre-pollution Pb aerosol (e.g. soil dust) in Scotland via the collection of longer peat cores (> ~ 2 metres).
5. Further work is required to confirm whether there are interesting spatial changes in atmospheric metal deposition across Scotland.

9 BIBLIOGRAPHY

Aaby. B., 1986, Palaeoecological studies of mires, in Berglund B.E. (editor) *Handbook of Holocene Palaeoecology and Palaeohydrology*, Wiley, Chichester.

Aaby B. and Jacobsen J., 1979, Changes in biotic conditions and metal deposition in the last millennium as reflected in ombrotrophic peat in Draved Mose, Denmark, *Dansmark Geologiske Undersogelse*, 5-43.

Åberg G., Abrahamsen G., Steinnes E. and Hjelmseth H., 2004, Utilization of bark pockets as time capsules of atmospheric-lead pollution in Norway, *Atmospheric Environment*, **38**, 6231-6237.

Appleby P.G. and Oldfield F., 1978, The calculation of lead-210 dates assuming a constant rate of supply of unsupported ^{210}Pb to the sediment, *Catena*, **5**, 1-8.

Appleby P.G., Shotyk W. and Fankhauser A., 1997, Lead-210 age dating of the 3 peat cores in the Jura Mountains, Switzerland, *Water, Air and Soil Pollution*, **100**, 223-231.

Bacon J. R., Jones K. C., McGrath S. P. and Johnston A. E., 1996, Isotopic character of Pb deposited from the atmosphere at a grassland site in the UK since 1860, *Environmental Science & Technology*, **30**, 2511-2518.

Baes C.F. and McLaughlin S.B., 1984, Trace elements in tree rings, evidence of recent and historical air pollution, *Science*, **224**, 494-497.

Baes C.F. and Mesmer R.E., 1976, *The Hydrolysis of Cations*, John Wiley and Sons, New York.

Barbante C., Shotyk W., Biester H., Cheburkin A., Emons H., Farmer J.G., Hoffman E., Martinez-Cortizas A., Matschullat J., Norton S., Schweyer J. and Steinnes E., 2000, A peat reference material for trace element analyses, in *Proceedings from the 11th International Conference for Heavy metals in the Environment*, (ed. J. O. Nriagu), University of Michigan, School of Public Health, Ann Arbour, MI USA (CD-ROM) Contribution No. 1106.

Barber K.E., Dumayne L. and Stoneman R., 1994, Climatic Change and Human Impact during the Late Holocene in Northern Britain, in Chambers F.M. (editor) *Climate Change and Human Impact on the Landscape: Studies in Palaeoecology and Environmental Archaeology*, Chapman and Hall, London.

Bellis D.J., McLeod C.W. and Satake K., 2001, The potential of elemental and isotopic analysis of tree bark for discriminating sources of airborne Pb contamination in the UK, *Journal of Environmental Monitoring*, **3**, 194-197.

Bellis D.J., Satake K., Noda M. and McLeod C.W., 2002a, Evaluation of the historical records of lead pollution in the annual growth rings and bark pockets of a

250-year-old Quercus Crispua in Nikko, Japan, *The Science of the Total Environment*, **295**, 91-100.

Bellis D.J., McLeod C.W. and Satake K., 2002b, Pb and $^{206}Pb/^{207}Pb$ isotopic analysis of a tree bark pocket near Sheffield, UK recording historical change in airbourne pollution during the 20th century, *The Science of the Total Environment*, **289**, 169-176.

Bellis D.J., Satake K. and McLeod C.W., 2004, A comparison of lead isotope ratios in the bark pockets and annual rings of two beech trees collected in Derbyshire and south Yorkshire, UK, *Science of the Total Environment*, **321**, 105-113.

Benoit J.M., Fitzgerald W. and Damman A.W.H., 1998, The biogeochemistry of an ombrotrophic bog: Evaluation of use as an archive of atmospheric mercury deposition, *Environmental Research*, **78**, 118-133.

Berner E.K. and Berner R.A., 1997, *Global Environment: Water, Air and Geochemical Cycles*, Prentice Hall, New Jersey.

Biester H., Martinez-Cortizas A., Birkenstock S. and Kilian R., 2003, Effect of peat decomposition and mass loss on historic mercury records in peat bogs from Patagonia, *Environmental Science & Technology*, **37**, 32-39.

Bindler R., 2003, Estimating the natural background atmospheric deposition rate of mercury utilizing ombrotrophic bogs in southern Sweden, *Environmental Science & Technology*, **37**, 40-46.

Bindler R., Renberg I., Klaminder J. and Emteryd O., 2004a, Tree rings as Pb pollution archives? A comparison of $^{206}Pb/^{207}Pb$ isotope ratios in pine and other environmental media, *Science of the Total Environment*, **319**, 173-183.

Bindler R., Klarqvist M., Klaminder J. and Förster J., 2004b, Does within-bog spatial variability of mercury and lead constrain reconstructions of absolute deposition rates from single peat records? The example of Store Mosse, Sweden, *Global Biogeochemical Cycles*, **18**, GB3020.

Bindler R., 2006, Mired in the past – looking to the future: Geochemistry of peat and the analysis of past environmental changes, *Global and Planetary Change*, **53**, 209-221.

Blackford J.J. and Chambers F.M., 1993, Determining the degree of peat decomposition for peat-based palaeoclimatic studies, *International Peat Journal*, **5**, 7-24.

Blackford J.J., 2000, Palaeoclimatic records from peat bogs, *Trends in Ecology and Evolution*, **15**, 193-198.

Bonn B.A. and Fish W., 1993, Measurement of electrostatic and site specific associations of alkali metal cations with humic acid, *Journal of Soil Science*, **44**, 335-345.

Bottrell S., Coulson J., Spence M., Roworth P., Novák M. and Forbes L., 2004, Impacts of pollutant loading, climate variability and site management on the surface water quality of a lowland raised bog, Thorne Moors, E.England, UK, *Applied Geochemistry*, **19**, 413-422.

Boulter P.G., 2004, *A Review of Emission Factors and Models for Road Vehicle Non-exhaust Particulate Matter*, published project report PPR065, TRL limited, Wokingham.

Boutron C.F. and Patterson C.C., 1986, Lead concentration changes in Antarctic ice during the Wisconsin/Holocene transition, *Nature*, **323**, 222-225.

Boutron C.F., Görlach U., Candelone J-P, Bolshov M.A., and Delmas R.J., 1991, Decrease in anthropogenic lead, cadmium and zinc in Greenland snows since the late 1960s, *Nature*, **353**, 153-156.

Boutron C.F., Candelone J-P and Hong S., 1994, Past and recent changes in the large-scale tropospheric cycles of lead and other heavy metals as documented in Antarctic and Greenland snow and ice, *Geochimica et Cosmochimica Acta,* **58**, 3217-3225.

Bowen H.J.M., 1979, *Environmental Chemistry of the Elements*, Academic Press, New York.

Boyle R.W. and Jonasson I.R., 1984, The geochemistry of Sb and its use as an indicator element in geochemical prospecting, *Journal of Geochemical Exploration*, **20**, 223-302.

Brady N.C. and Weil R.R., 1999, *The Nature and Properties of Soil*, Prentice Hall, New Jersey.

Bragg O.M. and Tallis J.H., 2001, The sensitivity of peat-covered upland landscapes, *Catena*, **42**, 345-360.

Bragg O.M., 2002, Hydrology of peat forming wetlands in Scotland, *The Science of the Total Environment*, **294**, 111-129.

Brännvall M.L., Bindler R., Emteryd O., Nilsson M. and Renberg I., 1997, Stable isotope and concentration records of atmospheric Pb pollution in peat and lake sediments in Sweden, *Water, Air and Soil Pollution*, **100**, 243-252.

Brimblecombe P., 1996, *Air Composition and Chemistry*, Cambridge University Press, Cambridge.

Brooks S. and Stoneman R.E., 1997, *Conserving Bogs: The Management Handbook*, The Stationery Office, Edinburgh.

Cadle S.H., Mulawa P.A., Hunsanger E.C., Nelson K., Ragazzi R.A., Barrett R., Gallagher G.L., Lawson D.R., Knapp K.T. and Snow R., 1999, Composition of light-duty motor vehicle exhaust particulate matter in the Denver, Colorado area, *Environmental Science & Technology*, **33**, 2328-2339.

Caseldine C.J., Baker A., Charman D.J. and Hendon D., 2000, A comparative study of optical properties of NaOH peat extracts: implications for humification studies, *The Holocene*, **8**, 97-103.

Chemical Research Communications, 2003, http://toxprof.crcpress.com

Chow T.J., Synder C.B. and Earl J.L., 1975, *Isotope Ratios of Lead as Pollutant Source Indicators*, UN, FAO and IAEA Symposium, IAEA-SM-191/4, Vienna.

Clark M.J. and Smith F.B., 1988, Wet and dry deposition of Chernobyl releases, *Nature*, **332**, 245-249.

Cloy J.M., Farmer J.G., Graham M.C., MacKenzie A.B. and Cook. G.T., 2005, A comparison of antimony and lead profiles over the past 2500 years in Flanders Moss ombrotrophic peat bog, Scotland, *Journal of Environmental Monitoring*, **7**, 1137-1147.

Clymo R.S., 1963, Ion exchange in Sphagnum and its relation to bog ecology, *Annals of Botany*, **27**, 309-324.

Clymo R.S., 1987, Interactions of *Sphagnum* with water and air, in *Effects of Atmospheric Pollutants in Forests, Wetlands and Agricultural Ecosystems*, Springer-Verlag, New York.

Clymo R.S. and MacKay D., 1987, Upwash and downwash of pollen and spores in the unsaturated surface-layer of *Sphagnum*-dominated peat, *New Phytologist*, **105**, 175-183.

Clymo R.S., Oldfield F., Appleby P.G., Pearson G.W., Ratnesar P. and Richardson N., 1990, The record of atmospheric deposition on a rainwater-dependent peatland, *Philosophical Transactions of the Royal Society of London*, **B327**, 331-338.

Cocozza C., D'Orazio V., Miano T.M. and Shotyk W., 2003, Characterization of solid and aqueous phases of a peat bog profile using molecular fluorescence spectroscopy, ESR and FT-IR, and comparison with physical properties, *Organic Geochemistry*, **34**, 49-60.

Coggins A.M., Jennings S.G. and Ebinghaus R., 2006, Accumulation rates of the heavy metals lead, mercury and cadmium in ombrotrophic peatlands in the west of Ireland, *Atmospheric Environment*, **40**, 260-278.

Cook G. T., Dugmore A. J. and Shore J. S., 1998, The influence of pre-treatment on humic acid yield and ^{14}C age of carex peat, *Radiocarbon*, **40**, 21-27.

Cuttle S.P. and Malcolm D.C., 1979, A corer for taking undisturbed peat samples, *Plant and Soil*, **51**, 297-300.

Damman A.W.H., 1978, Distribution and movement of elements in ombrotrophic peat bogs, *OIKOS*, **30**, 480-495.

Damman A.W.H., 1986, Hydrology, development and biogeochemistry of ombrogenous peat bogs with special reference to nutrient relocation in a western Newfoundland bog, *Canadian Journal of Botany*, **64**, 384-394.

Daniels R.E., 1978, Floristic analyses of British mires and mire communities, *Journal of Ecology*, **66**, 773-802.

Davies C. and Turner J., 1979, Pollen diagrams from Northumberland, *New Phytologist*, **82**, 783-804.

Day J. and Tylecote R.F., 1991, *The Industrial Revolution in Metals*, Institute of Metals, London.

Department for Environment, Food and Rural Affairs, 2002, *Digest of Environmental Statistics,*
http://www.defra.gov.uk/environment/statistics/des/index.htm.

Department of Trade and Industry, 1998, *The Energy Report*, Volume 2, The Stationery Office, London.

Drever J.I., 1982, *The Geochemistry of Natural Waters, Surface and Groundwater Environments*, Prentice Hall Limited, New Jersey.

Duarte L.M., 1996, *Jornadas sobre Mineria y Technologia en la Edad Media Penninsular*, Fundación Hullera Vasco-Leonesa, 67-90.

Duce R.A., Hoffman G. L. and Zoller W. H., 1975, Atmospheric trace metals at remote northern and southern hemisphere sites: Pollution or natural? *Science*, **18**, 59-61.

Dugmore, A. J., Cook, G. T., Shore, J. S., Newton, A. J., Edwards, K. J. and Larsen, G., 1995, Radiocarbon dating tephra layers in Britain and Iceland, *Radiocarbon*, **37**, 379-388.

Dugmore A.J., Newton A.J., Edwards K.J., Larsen G., Blackford J.J. and Cook G.T., 1996, Long-distance marker horizons from small-scale eruptions of Hekla, Iceland, *Journal of Quaternary Science*, **11**, 511-516.

Dumayne-Peaty L., 1999, Continuity or discontinuity? Vegetation change in the Hadrianic-Antonine frontier zone of northern Britain at the end of the Roman occupation, *Journal of Biogeography*, **26**, 643-665.

Eades L.J., Farmer J.G., MacKenzie A.B., Kirika A. and Bailey-Watts A.E., 2002, Stable Pb isotopic characterisation of the historical record of environmental Pb contamination in dated freshwater lake sediment cores from northern and central Scotland, *The Science of the Total Environment*, **292**, 55-67.

Espi E., Boutron C.F., Hong S., Pourchet M., Ferrari C., Shotyk W. and Charlet L., 1997, Changing concentrations of Cu, Zn, Cd and Pb in a high altitude peat bog from Bolivia during the past three centuries, *Water, Air and Soil Pollution*, **100**, 289-296.

Farmer J.G. and Lovell M.A., 1986, Natural enrichment of arsenic in Loch Lomond sediments, *Geochimica et Cosmochimica Acta*, **50**, 2059-2067.

Farmer J.G., 1991, The perturbations of historical pollution records in aquatic sediments, *Environmental Geochemistry and Health*, **13**, 76-83.

Farmer J.G., Eades L.J., MacKenzie A.B., Kirika A. and Bailey-Watts T.E., 1996, Stable Pb isotope record of Pb pollution in Loch Lomond sediments since 1630 A.D., *Environmental Science & Technology*, **30**, 3080-3083.

Farmer J.G., MacKenzie A.B., Eades L.J., Kirika A. and Bailey-Watts A.E., 1997a, Influences on the extent and records of heavy metal pollution in sediment cores from Loch Tay in a mineralised area of Scotland, *Journal of Geochemical Exploration*, **58**, 195-202.

Farmer J.G., MacKenzie A.B., Sugden C.L., Edgar P.J. and Eades L.J., 1997b, A comparison of the historical Pb pollution records in peat and freshwater sediments from central Scotland, *Water Air and Soil pollution*, **100**, 253-270.

Farmer J.G., Eades L.J. and Graham M.C., 1999, The Pb content and isotopic composition of British coals and their implications for past and present releases of Pb to the UK environment, *Environmental Geochemistry and Health*, **21**, 257-272.

Farmer J.G., Eades L.G., Graham M.C. and Bacon J.R., 2000, The changing nature of the $^{206}Pb/^{207}Pb$ isotopic ratio of Pb in rainwater, atmospheric particulates, pine needles and leaded petrol in Scotland, 1982-1998, *Journal of Environmental Monitoring*, **2**, 49-57.

Farmer J.G., Eades L.J., Atkins H. and Chamberlain D.F., 2002, Historical trends in the lead isotopic composition of archival *Sphagnum* mosses from Scotland (1838-2000), *Environmental Science & Technology*, **36**, 152-157.

Farmer J.G., Graham M.C., Bacon J.R., Dunn S.M., Vinogradoff S.I. and MacKenzie A.B., 2005, Isotopic characterisation of the historical lead deposition record at

Glensaugh, an organic-rich, upland catchment in rural N.E. Scotland, *Science of the Total Environment*, **346**, 121-137.

Farmer J.G., Graham M.C., Yafa C., Cloy J.M., Freeman A.J. and MacKenzie A.B., 2006, Use of $^{206}Pb/^{207}Pb$ ratios to investigate the surface integrity of peat cores used to study the recent depositional history and geochemical behaviour of inorganic elements in peat bogs, *Global and Planetary Change*, **53**, 240-248.

Faure G., 1986, *Principles of Isotope Geology*, John Wiley and Sons, New York.

Faure G., 1991, *Principles and Applications of Inorganic Geochemistry*, MacMillan, New York.

Faure G., 1998, *Principles and Applications of Geochemistry*, Prentice Hall Inc., New Jersey.

Fraser G.K., 1943, *Peat Deposits of Scotland, Part 1, General Account*, London, Department of Scientific and Industrial research, Geological Survey of Great Britain: Scotland, Wartime pamphlet No 36.

Fraser G.K., 1948, *Peat deposits of Scotland, Part 2, Peat Mosses of Aberdeenshire, Banffshire and Morayshire*, London, Department of Scientific and Industrial research, Geological Survey of Great Britain: Scotland, Wartime pamphlet No 36.

Gao K., Pearce J., Jones J. and Taylor C., 1999, Interaction between peat humic acid and aqueous metal ions, *Environmental Geochemistry and Health*, **21**, 13-26.

Givelet N., Roos-Barraclough F. and Shotyk W., 2003, Predominant anthropogenic sources and rates of atmospheric mercury accumulation in southern Ontario recorded by peat cores from three bogs: comparison with natural "background" values (past 8000 years), *Journal of Environmental Monitoring*, **5**, 935-949.

Givelet N., Le Roux G., Cheburkin A., Chen B., Frank J., Goodsite .E., Kempter H., Krachler M., Noernberg T., Rausch N., Rheinberger S., Roos-Barraclough F., Sapkota A., Scholz C. and Shotyk W., 2004, Suggested protocol for collecting, handling and preparing peat cores and peat samples for mineralogical and isotopic analyses, *Journal of Environmental Monitoring*, **6**, 481-492.

Goodsite M.E., Rom W., Heinemeier J., Lange T., Ooi S., Appleby P.G., Shotyk W., van der Knaap W.O., Lohse C. and Hansen T.S., 2001, High-Resolution AMS ^{14}C dating of post-bomb peat archives of atmospheric pollutants, *Radiocarbon*, **43**, 495-515.

Görres M. and Frenzel B., 1997, Ash and metal concentrations in peat bogs as indicators of anthropogenic activity, *Water, Air and Soil Pollution*, **100**, 355-365.

Greenwood N.N. and Earnshaw A., 1997, *Chemistry of the Elements*, Butterworth-Heinemann, Oxford.

Grousset F.E., Quétel C.R., Thomas B., Buat-Ménard P., Donard O.F.X. and Bucher A., 1994, Transient Pb isotopic signatures in the Western European atmosphere, *Environmental Science & Technology*, **28**, 1605-1608.

Halter M., 2005, *Investigation of the Validity of using Enrichment Factors in Research on Peat Bogs as Archives of Atmospheric Metal Deposition*, Diploma thesis, Department Umweltwissenschaften der ETH Zürich at the University of Edinburgh.

Harrison J.G., 2002, *Flanders Moss Historical Background, A report for Scottish Natural Heritage.*

Hansom J.D. and Evans D.J.A., 2000, The Carse of Stirling, (Scottish Landform Example No.23), *Scottish Geographical Journal*, **116**, 71-78.

Helmer E.H., Urban N.R. and Eisenteich S.J., 1990, Aluminium geochemistry in peatland waters, *Biogeochemistry*, **9**, 247-276.

Hill M.O., 1992, *Sphagnum: A field Guide*, Joint Nature Conservation Committee, Petersborough.

Hulme P.D., Clayton P. and Griffiths P., 1991, *Characterisation of Scottish Peat as Fuel in: Scottish Peat Resources and their Energy Potential*, Department of Energy, Harwell.

Hvatum O.Ø., Bølviken B. and Steinnes E., 1987, Regional differences and temporal trends in heavy metal deposition from the atmosphere studied by analyses of ombrotrophic peat, in Lindberg S.E. and Hutchinson T.C. (editors), *Proceedings from the International Conference on Heavy Metals in the Environment*, CEP Publishers, Edinburgh.

Ingram H.A.P., 1978, Soil layers in mires: function and terminology, *Journal of Soil Science*, **29**, 224-227.

Irving M. and Williams R.J.P., 1948, Order of stability of metal complexes, *Nature*, **162**, 767-747.

Jahns H.M., 1980, *Ferns, Mosses and Lichens of Britain*, Collins, London.

Jensen A., 1997, Historical deposition rates of Cd, Cu, Pb and Zn in Norway and Sweden estimated by ^{210}Pb dating and measurement of trace elements in cores of peat bogs, *Water, Air and Soil Pollution*, **95**, 205-220.

Johnson L.C. and Damman A.W.H., 1991, Species-controlled sphagnum decay on a south Swedish raised bog, *OIKOS*, **61**, 234-242.

Johnston E. and Soulsby C., 2000, Peatland conservation in Buchan, North-east Scotland: The historic context and contemporary issues, *Scottish Geographical Journal*, **116**, 283-298.

Jones J.M. and Hao J., 1993, Ombrotrophic peat as a medium for historical monitoring of heavy metal pollution, *Environmental Geochemistry and Health*, **15**, 67-74.

Jowsey P.C., 1965, An improved peat sampler, *New Phytologist*, **65**, 245-248.

Keleman J.C. and Ingram H.A.P., 1999, The use of large bottomless lysimeters in the determination of water balances for a raised mire, *Hydrological Processes*, **13**, 101-111.

Kellner E., 2003, *Wetlands – Different types, their Properties and Functions*, Department of Earth Sciences/Hydrology, Uppsala University, Technical Report TR-04-08, SKB.

Kempter H., Görres M. and Frenzel B., 1997, Ti and Pb concentrations in rainwater fed bogs in Europe as indicators of past anthropogenic activities, *Water, Air and Soil Pollution*, **100**, 367-377.

Kempter H. and Frenzel B., 2000, The Impact of early mining and smelting on the local tropospheric aerosols detected in ombrotrophic peat bogs in The Harz, Germany, *Water, Air and Soil Pollution*, **121**, 93-103.

Klaminder J., Renberg I. and Bindler R., 2003, Isotopic trends and background fluxes of atmospheric lead in northern Europe: Analyses of three ombrotrophic bogs from south Sweden, *Global Biogeochemical Cycles*, **17**, art. no. 1019.

Krachler M., Mohl C., Emons H. and Shotyk W., 2003a, Atmospheric deposition of V, Cr and Ni since the late glacial: Effects of climatic cycles, human impacts and comparison with crustal abundances, *Environmental Science & Technology*, **37**, 2658-2667.

Krachler M., Mohl C., Emons H. and Shotyk W., 2003b, Two thousand years of atmospheric rare earth element deposition as revealed by an ombrotrophic peat bog profile, Jura Mountains, Switzerland, *Journal of Environmental Monitoring*, **5**, 1, 111-121.

Krosshaven M., Steinnes E. and Varskog P., 1992, Binding of Cd, Cu, Pb and Zn in soil organic matter with different vegetational background, *Water, Air and Soil Pollution*, **71**, 185-193.

Kylander M.E., Weiss D.E., Martinez-Cortizás A., Spiro B., Garcia-Sanchez R. and Coles B.J., 2005, Refining the pre-industrial atmospheric Pb-isotope evolution curve in Europe using an 8000 year old peat core from north-west Spain, *Earth and Planetary Science Letters*, **240**, 467-485.

Langdon P.G. and Barber K. E., 2004, Snapshots in time: precise correlations of peat-based proxy climate records in Scotland using mid-Holocene tephras, *The Holocene*, **14**, 21-33.

Langmuir D., 1997, *Aqueous Environmental Geochemistry*, Prentice Hall, New Jersey.

Lee J.A. and Tallis J.H., 1973, Regional and historical aspects of Pb pollution in Britain, *Nature*, **245**, 216-218.

Le Roux G., Weiss D., Grattan J., Givelet N., Krachler M., Cheburkin A., Rausch N., Kober B. and Shotyk W., 2004, Identifying the sources and timing of ancient and medieval atmospheric lead pollution in England using a peat profile from Lindow bog, Manchester, *Journal of Environmental Monitoring*, **6**, 502-510.

Lindsay R., 1995, *Bogs; the Ecology, Classification and Conservation of Ombrotrophic Mires*, Scottish Natural Heritage, Edinburgh.

Livett E.A., Lee J.A. and Tallis J.H., 1979, Lead, zinc, and copper analyses of British blanket peats, *Journal of Ecology*, **67**, 865-891.

Livett E.A., 1988, Geochemical monitoring of atmospheric heavy metal pollution: Theory and application, *Advances in Ecological Research*, **18**, 65-157.

Livingstone D.A., 1963, *Chemical Composition of Rivers and Lakes*, 6th edition, U.S. Geological Survey Professional Paper, 440-G.

Lloyd J.E., 1939, *A History of Carmarthenshire*, Vol. 2, London Carmarthenshire Society, Cardiff.

Logan E.M., Pulford I.D., Cook G.T. and MacKenzie A.B., 1997, Complexation of Cu^{2+} and Pb^{2+} by peat and humic acid, *European Journal of Soil Science*, **48**, 685-696.

MacDonald D., 2005, *Mercury in Carsegowan Moss, an Ombrotrophic Peat Bog in South-West Scotland*, Environmental Chemistry BSc Honours thesis, University of Edinburgh.

MacKenzie A.B., Farmer J.G. and Sugden C.L., 1997, Isotopic evidence of the relative retention and mobility of Pb and radiocaesium in Scottish ombrotrophic peats, *The Science of the Total Environment*, **203**, 115-127.

MacKenzie A.B., Logan E.M., Cook G.T. and Pulford L.D., 1998a, Distributions, inventories and isotopic composition of Pb in ^{210}Pb-dated peat cores from contrasting biogeochemical environments: Implications for Pb mobility, *The Science of the Total Environment*, **223**, 25-35.

MacKenzie A.B., Logan E.M., Cook G.T. and Pulford I.D., 1998b, A historical record of atmospheric depositional fluxes of contaminants in west-central Scotland derived from an ombrotrophic peat core, *The Science of the Total Environment*, **222**, 157-166.

Madsen P., 1981, Peat bog records of atmospheric mercury deposition, *Nature*, **293**, 127-129.

Malmer N., 1958, Notes on the relation between the chemical composition of mire plants and peat, *Botaniska Notiser*, **111**, 274-288.

Martinez-Cortizas A., Pontevedra-Pombal X., Novoa Munoz J.C. and Garcia-Rodeja E., 1997, 4000 years of atmospheric Pb, Cd and Zn deposition recorded by the ombrotrophic peat bog of Penido vello (north-west Spain), *Water, Air and Soil Pollution*, **100**, 387-403.

Martinez-Cortizas A., Pontevedra-Pombal X., Novoa Munoz J.C., Garcia-Rodeja E. and Shotyk W., 1999, Hg in a Spanish peat bog: Archives of climate change and atmospheric deposition, *Science*, **284**, 939-942.

Martinez-Cortizas A., Garcia-Rodeja E. and Weiss D., 2002a, Peat bog archives of atmospheric metal deposition, *The Science of the Total Environment*, **292**, 1-5.

Martinez-Cortizas A., Garcia-Rodeja E., Pontevedra-Pombal X., Weiss D., Cheburkin A.K. and Novoa Munoz J.C., 2002b, Atmospheric Pb deposition in Spain during the last 4600 years recorded by two ombrotrophic peat bogs and implications for the use of peat as archive, *The Science of the Total Environment*, **292**, 33-44.

Mason R.P., Fitzgerald W.F. and Morel F.M.M., 1994, The biogeochemical cycling of elemental mercury: Anthropogenic influences, *Geochimica et Cosmochimica Acta*, **58**, 3191-3198.

Matschullat J., 2000, Arsenic in the geosphere – a review, *The Science of the Total Environment*, **249**, 297-312.

Matsumoto A. and Hinkley T.K., 2001, Trace metal suites in 75,000 years of Antarctic ice are consistent with emissions from quiescent degassing of volcanoes worldwide, *Earth and Planetary Science Letters*, **186**, 33-43.

Matthews E. and Fung I., 1987, Methane emissions from natural wetlands: global distribution, area and environmental characteristics of sources, *Global Biogeochemical Cycles*, **1**, 61-86.

McNichol A.P., Jull A.J.T. and Burr G.S., 2001, Converting AMS data to radiocarbon values: considerations and conventions, *Radiocarbon*, **43**, 313-320.

Mighall T.M., Abrahams P.W., Grattan J.P., Hayes D., Timberlake S. and Forsyth S., 2002, Geochemical evidence for atmospheric pollution derived from prehistoric Cu

mining at Copa Hill, Cwmystwyth, mid-Wales UK, *The Science of the Total Environment*, **292**, 69-80.

Miller J.N. and Miller J.C., 2000, *Statistics and Chemometrics for Analytical Chemistry*, 4th Ed., Prentice Hall, Harlow.

Milnes A.R. and Fitzpatrick R.W., 1989, Ti and Zr minerals, in Dixon J.B. and Weed S.B. (editors), *Minerals in Soil Environments*, Soil Science Society of America.

Monitoring and Assessment Research Centre, 1985, *Historical Monitoring*, Report 31, Chelsea College, University of London.

Monna F., Lancelot J., Croudace I.W., Cundy A.B. and Lewis J.T., 1997, Pb isotopic composition of airbourne particulate material from France and the southern United Kingdom: implications for Pb pollution sources in urban areas, *Environmental Science & Technology*, **31**, 2277-2286.

Monna F., Petit C., Guillaumet J.P., Jouffroy-Bapicot I., Blanchot C., Dominik J., Losno R., Richard H., Lévêque J. and Chateau C., 2004, History and environmental impact of mining activity in Celtic Aeduan territory recorded in a Peat Bog, *Environmental Science & Technology*, **38**, 665-673.

Moorbath S., 1962, Lead isotope abundance studies on mineral occurrences in the British Isles, and their geological significance, *Philosophical Transactions of the Royal Society of London*, Ser A, **254**, 295-360.

Murozomi M., Chow T.J. and Patterson L.C., 1969, Chemical concentrations of pollutant Pb aerosols, terrestrial and sea salts in Greenland and Antarctic snow strata, *Geochimica et Cosmochimica Acta*, **33**, 1247-1294.

National Atmospheric Emissions Inventory, 2006, http://www.naei.org.uk/pollutantdetail.php.

Nesbitt H.W. and Markovics G., 1997, Weathering of granodioritic crust, long-term storage of elements in weathering profiles, and peterogenesis of siliclastic sediments, *Geochimica et Cosmochimica Acta*, **61**, 1653-1670.

Norton S.A. and Kahl J.S., 1986, A comparison of lake sediments and ombrotrophic peat deposits as long term monitors of atmospheric pollution, *American Society of Testing and Materials, Proceedings of Monitoring of Aquatic Ecosystems*, STP#940, 40-57.

Norton S.A. and Kahl J.S., 1987, *Geochemical Analysis of Sediment Cores, Wind River Mountains, Wyoming*, final report to the U.S. forest service.

Norton S.A., Dillon P.J., Evans R.D., Mierle G. and Kahl J.S., 1990, *The History of Atmospheric Deposition of Cd, Hg and Pb in North America: Evidence from Lake and Peat Bog Sediments*, in Acidic Precipitation, volume 3, *Sources Deposition and*

Canopy interactions, Advances in Environmental Science, Springer-Verlag, New York.

Norton S.A., Evans G.C. and Kahl J.S., 1997, Comparison of Hg and Pb fluxes to hummocks and hollows of ombrotrophic big heath bog and to nearby Sargent Mountain pond, Maine USA, *Water, Air and Soil Pollution*, **100**, 271-286.

Novák M., Adamova M. and Milićić J., 2003, Sulfur metabolism in polluted sphagnum peat bogs: A combined ^{34}S-^{35}S-^{210}Pb study, *Water, Air and Soil Pollution*, **3**, 181-200.

Nriagu J.O., 1978, *The Biogeochemistry of Lead in the Environment, Part A, Ecological Cycles*, 1A, Elsevier, North-Holland Biomedical Press.

Nriagu J.O., 1983, *Lead and lead Poisoning in Antiquity*, John Wiley and Sons, New York.

Nriagu J.O. and Pacyna J.M., 1988, Quantitative assessment of worldwide contamination of air, water and soils by trace metals, *Nature*, **333**, 134-139.

Nriagu J.O., 1990, The rise and fall of leaded gasoline, *The Science of the Total Environment*, **92**, 13-28.

Nriagu J.O., 1996, History of global metal pollution, *Science*, **272**, 223-224.

Nriagu J.O., 1998, Tales told in lead, *Science*, **281**, 1622-1623.

Oehme F.W., 1979, *Toxicity of heavy metals in the environment*, part 2, Dekker, New York.

Oldfield F., Appleby P.G., Cambray R.S., Eakins J.D., Barber K.E., Battarbee R.W., Pearson G.R. and Williams J.M., 1979, ^{210}Pb, ^{137}Cs and ^{239}Pu profiles in ombrotropic peat, *OIKOS*, **33**, 40-45.

Olmez I. and Gordon G.E., 1985, Rare Earths: Atmospheric Signatures for Oil-fired Power Plants and Refineries, *Science*, **229**, 966-969.

Ordnance Survey, 2005 <www.streetmap.co.uk>

Overbeck F., 1947, Studien zur Hochmoorentwichlung im Niedersachsen und die Bestimmung der Hummifizierung bei stratigraphisch-pollenanalytischen Mooruntersuchungen, *Planta*, **35**, 1-56.

Pakarinen P. and Tolonen K., 1976, Regional survey of heavy metals in peat mosses, *Ambio*, **5**, 38-40.

Pakarinen P., 1978, Element content of *Sphagnum*: variations and its sources, *Bryophytorium Bibliotheca*, **13**, 751-762.

Paquette K. and Helz G., 1995, Solubility of cinnabar (Red HgS) and implications for mercury speciation in sulfidic waters, *Water, Air and Soil Pollution*, **80**, 1053-1056.

Patrick G.J. and Farmer J.G., 2006, A stable lead isotopic investigation of the use of sycamore tree rings as a historical biomonitor of environmental lead contamination, *Science of the Total Environment*, **362**, 278-291.

Patterson C.C., 1972, Silver stocks and losses in ancient and Medieval times. *The Economic History Review*, **25**, 205-235.

Pearson R.G., 1963, Hard and soft acids and bases, *Journal of the American Chemical Society*, **85**, 3533-3539.

Peirson D.H., Cawse P.A., Salmon L. and Cambray R.S., 1973, Trace elements in the atmospheric environment, *Nature*, **241**, 252-256.

Peirson D.H., Cambray R.S., Cawse P.A., Eakins J.D. and Pattenden N.J., 1982, Environmental radioactivity in Cumbria, *Nature*, **300**, 27-31.

Pilcher J.R., Hall V.A. and McCormac F.F., 1996, An outline tephrachronology for the north of Ireland, *Journal of Quaternary Science*, **11**, 485-494.

Puché O. and Bosch J., 1996, Act. I. *Jornadas sobre Mineria y Technologia en la Edad Media Penninsular*, Fundación Hullera Vasco-Leonesa, 198-216.

Rahn K.A., 1976, *The Chemical Composition of the Atmospheric Aerosol*. Technical Report of the Graduate School of Oceanography, University of Rhode Island, Kingston, R.I. USA.

Rausch N., Nieminen T., Ukonmaanaho L., Le Roux G., Krachler M., Cheburkin A.K., Bonani G. and Shotyk W., 2005a, Comparison of atmospheric deposition of Cu, Ni, Co, Zn and Cd recorded by Finnish peat cores with monitoring data and emission records, *Environmental Science & Technology*, **39**, 5989-5998.

Rausch N., Ukonmaanaho L., Nieminen T.M., Krachler M. and Shotyk. W., 2005b, Porewater evidence of metal (Cu, Ni, Co, Zn, Cd) mobilization in an acidic ombrotrophic bog impacted by a smelter, Harjavalta, Finland and comparison with reference sites, *Environmental Science & Technology*, **39**, 8207-8213.

Reimann C. and de Caritat P., 2000, Intrinsic flaws of element enrichment factors (EFs) in environmental geochemistry, *Environmental Science & Technology*, **34**, 5084-5091.

Reimann C. and de Caritat P., 2005, Distinguishing between natural and anthropogenic sources for elements in the environment: regional geochemical surveys versus enrichment factors, *Science of the Total Environment*, **337**, 91-107.

Renberg I., Persson M.W. and Emteryd O., 1994, Pre-industrial atmospheric lead contamination detected in Swedish lake sediments, *Nature*, **368**, 323-326.

Renberg I., Bindler R. and Brännvall M.L., 2001, Using the historical atmospheric lead-deposition record as a chronological marker in sediment deposits in Europe, *The Holocene*, **11**, 511-516.

Renberg I., Bränvall M.L., Bindler R. and Emteryd O., 2002, Stable Pb isotopes and lake sediments – a useful combination for the study of atmospheric Pb pollution history, *The Science of the Total Environment.*, **292**, 45-54.

Richardson D.H.S., 1981, *The Biology of Mosses*, Blackwell Scientific Publications, Oxford.

Ritchie G. and Ritchie A., 1991, *Scotland Archaeology and Early History*, Edinburgh University Press, Edinburgh.

Rohl B.M., 1996, Lead isotope data from the isotrace laboratory, Oxford: *Archaeometry* data base 2, Galena from Britain and Ireland, *Archaeometry*, **38**, 165-180.

Roos-Barraclough F., Martinez-Cortizas A., Garcia-Rodeja Gayoso E. and Shotyk W., 2002a, A 14500 year record of the accumulation of atmospheric Hg in peat: volcanic signals, anthropogenic influences and a correlation to Bromine accumulation, *Earth Planetary Science Letters*, **202**, 435-451.

Roos-Barraclough F., Givelet N., Martinez-Cortizas A., Goodsite M.E., Biester H. and Shotyk W., 2002b, An analytical protocol for the determination of total Hg concentrations in solid peat samples, *The Science of the Total Environment*, **292**, 129-139.

Roos-Barraclough F. and Shotyk W., 2003, Milennial-scale records of atmospheric mercury deposition obtained from ombrotrophic and minerotrophic peatlands in the Swiss Jura Mountains, *Environmental Science & Technology*, **37**, 235-244.

Roos-Barraclough F., Givelet N., Cheburkin A.K., Shotyk W. and Norton S.A., 2006, Use of Br and Se in peat to reconstruct the natural and anthropogenic fluxes of atmospheric Hg: a 1000-year record from Caribou bog, Maine, *Environmental Science & Technology*, **40**, 3188-3194.

Rosman K.J.R., Chisholm W., Hong S., Candelone J-P and Boutron C. F., 1997, Lead from Carthaginian and roman Spanish mines isotopically identified in Greenland ice dated from 600 B.C. to 300 A.D., *Environmental Science & Technology*, **31**, 3413-3416.

Roulet M. and Lucotte M., 1995, Geochemistry of mercury in pristine and flooded ferralitic soils of tropical rain forest in French Guiana, South America, *Water, Air and Soil Pollution*, **80**, 1079-1088.

Rühling Å. and Tyler G., 1973, Heavy metals deposition in Scandanavia, *Water, Air and Soil Pollution*, **2**, 445-455.

Rühling Å. and Tyler G., 1984, Recent changes in the deposition of heavy metals in northern Europe, *Water, Air and Soil Pollution*, **22**, 173-180.

Sanderson K., 2004, *Digging up evidence of metal pollution*, Chemistry World, Royal Society of Chemistry, London, October issue, volume 1, 44-47.

Satake K., Tanaka A. and Kimura K., 1996, Accumulation of lead in tree trunk bark pockets as pollution time capsules, *The Science of the Total Environment*, **181**, 25-30.

Sawden D., 2003, *Carsegowan Moss Explosives Factory 1940-1945*, The Studio, Newton Stewart.

Schnitzer M. and Hansen E.M., 1970, Organo-metallic interactions in soils: 8. An evaluation of methods for the determination of stability constants of metal-fulvic acid complexes, *Soil Science*, **109**, 333-340.

Schroeder W.H., 1987, The roles of the atmosphere in influencing the pathways and fate of heavy metals in the environment – an overview, in Lindberg S.E. and Hutchinson T.C. (editors), *Proceedings from the International Conference on Heavy Metals in the Environment*, CEP Publishers, Edinburgh.

Schroeder W.H. and Munthe J., 1998, Atmospheric mercury – an overview, *Atmospheric Environment*, **32**, 809-822.

Schütz L. and Rahn K.A., 1982, Trace-element concentrations in erodible soils, *Atmospheric Environment*, **16**, 171-176.

Schütz L., 1989, Atmospheric mineral dust – properties and source markers, NATO ASI, Serial C, *Mathematical and Physical Science*, **282**, 359-383.

Schwikowski M., Barbante C., Doering T., Gaeggeler H.W., Boutron C., Schotterer U., Tobler L., Van de Velde K., Ferrari C., Cozzi G., Rosman K. and Cescon P., 2004, Post-17th-century changes in high-altitude alpine snow and ice, *Environmental Science & Technology*, **38**, 957-964.

Scottish Natural Heritage, 2005, <http://www.snh.org.uk/Peatlands>.

Scottish Wildlife Trust, 2005, <http://www.jncc.gov.uk./protectedsites/sacselection>.

Scottish Wildlife Trust, 2001, Red Moss site management plan, Edinburgh.

Settle D.M. and Patterson C.C., 1980, Lead in Albacore: Guide to lead pollution in Americans, *Science*, **207**, 1167-1176.

Shaw D.M., Reilly G.A., Muysson J.R., Pattenden G.E. and Campbell F.E., 1967, The chemical composition of the Canadian Precambrian shield, *Canadian Journal of Earth Science*, **4**, 829-854.

Shaw D.M., Dostal J. and Keays R.R., 1976, Additional estimates of continental surface Precambrian shield composition in Canada, *Geochimica et Cosmochimica Acta*, **40**, 73-84.

Shepherd R., 1993, *Ancient Mining*, Elsevier Science Publishers Ltd, London.

Sheppard J.C. and Funk W.H., 1975, Trees as environmental sensors monitoring long-term heavy metal contamination of Spokane River, Idaho, *Environmental Science & Technology*, **9**, 638-642.

Shimwell J., 2002, *The Determination and Interpretation of the Mercury Concentration Profile in a Scottish Ombrotrophic Peat Bog,* Environmental Chemistry BSc Honours thesis, University of Edinburgh.

Shotyk W., 1988, Review of the inorganic geochemistry of peats and peatland waters, *Earth-Science Reviews*, **25**, 95-176.

Shotyk W., 1996a, Peat bog archives of atmospheric metal deposition: geochemical evaluation of peat profiles, natural variations in metal concentrations and metal enrichment factors, *Environmental Reviews*, **4**, 149-183.

Shotyk W., 1996b, Natural and anthropogenic enrichments of As, Cu, Pb, Sb and Zn in rain-water dominated versus ground-water dominated peat bog profiles, Jura Mountains, Switzerland, *Water, Air and Soil Pollution*, **90**, 375-405.

Shotyk W., Cheburkin A.K., Appleby P.G., Fankhauser A. and Kramers J.D., 1996, Two thousand years of atmospheric arsenic, antimony and lead deposition recorded in an ombrotrophic peat bog profile, Jura Mountains, Switzerland, *Earth and Planetary Science Letters*, **145**, E1-E7.

Shotyk W., 1997, Atmospheric deposition and mass balance of major and trace elements in two oceanic peat bog profiles, northern Scotland and Shetland Islands, *Chemical Geology*, **138**, 55-72.

Shotyk W., Cheburkin A.K., Appleby P.G., Fankhauser A. and Kramers J.D., 1997, Pb in three peat bog profiles, Jura Mountains, Switzerland: Enrichment factors, isotopic composition and chronology of atmospheric deposition, *Water, Air and Soil Pollution*, **100**, 297-309.

Shotyk W., Weiss D., Appleby P.G., Cheburkin A.K., Frei R., Gloor M., Kramers J.D., Reese S. and van der Knaap W.O., 1998, History of atmospheric Pb deposition since 12,370 ^{14}C years BP from a peat bog, Jura Mountains, Switzerland, *Science*, **281**, 1635-1639.

Shotyk W., Weiss D., Kramers J.D., Frei R., Cheburkin A.K., Gloor M. and Reese S., 2001, Geochemistry of the peat bog at Etang de la Guére, Jura Mt, Switzerland and its record of atmospheric Pb and lithogenic trace metals (Sc, Ti, Y, Zr, REE) since 12,370 ^{14}C yr BP, *Geochimica et Cosmochimica Acta.*, **65**, 2337-2360.

Shotyk W., Krachler M., Martinez-Cortizas A., Cheburkin A.K. and Emons H., 2002, A peat bog record of natural, pre-anthropogenic enrichments of trace elements in atmospheric aerosols since 12,370 ^{14}C yr BP and their variation with Holocene climate change, *Earth and Planetary Science Letters,* **199**, 21-37.

Shotyk W., Goodsite M.E., Roos-Barraclough F., Frei R., Heinemeier J., Asmund G., Lohse C. and Hansen T.S., 2003, Anthropogenic contributions to atmospheric Hg, Pb and As accumulation recorded by peat cores from southern Greenland and Denmark dated using the ^{14}C "bomb pulse curve", *Geochimica et Cosmochimica Acta*, **67**, 3991-4011.

Shotyk W., Krachler M. and Chen B., 2004, Antimony in recent ombrotrophic peat from Switzerland and Scotland: comparison with natural background values (5,320 to 8,020 ^{14}C yr BP) and implications for the global atmospheric Sb cycle, *Global Biogeochemical Cycles*, **18**, GB1016, 1-13.

Sparks D.L., 1995, *Environmental Soil Chemistry*, Academic Press Limited, London.

Steinmann P. and Shotyk W., 1997, Geochemistry, mineralogy, and geochemical mass balance on major elements in two peat bog profiles (Jura Mountains, Switzerland), *Chemical Geology*, **138**, 25-53.

Steinmann P. and Shotyk W., 1996, Chemical composition, pH, and redox state of sulfur and iron in complete vertical porewater profiles from two Sphagnum peat bogs, Jura Mountains, Switzerland, *Geochimica et Cosmochimica Acta*, **61**, 1146-1163.

Steinnes E., 1977, *Atmospheric Deposition of Trace Elements in Norway Studied by Means of Moss Analysis*, Institute for Atomic Energy, Kjeller, Norway, Report KR-154.

Steinnes E., 1995, A critical evaluation of the use of naturally growing moss to monitor the deposition of atmospheric metals, *The Science of the Total Environment*, **160**, 243-249.

Steinnes E., 1997, Trace element profiles in ombrogenous peat cores from Norway: Evidence of long range atmospheric transport, *Water, Air and Soil Pollution*, **100**, 405-413.

Sternbeck J., Sjodin A. and Andreasson K., 2002, Metal emissions from road traffic and the influence of resuspension-results from two tunnel studies, *Atmospheric Environment*, **36**, 4735-4744.

Stevenson F.J., 1994, *Humus Chemistry: Genesis, Composition and Reactions*, John Wiley and Sons, New York.

Stos-gale Z., Gale N.H., Houghton J. and Speakman R., 1995, Lead isotope data from the isotrace laboratory, Oxford: *Archaeometry* data base I, ores from the western Mediterranean, *Archaeometry*, **37**, 407-415.

Stuiver M. and Braziunas T.F., 1989, Atmospheric ^{14}C and century-scale oscillations, *Nature*, **338**, 405-408.

Sugden C.L., Farmer J.G. and MacKenzie A.B., 1993, Isotopic ratios of lead in contemporary environmental material from Scotland, *Environmental Geochemistry and Health*, **15**, 59-66.

Taylor R.E., 1987, *Radiocarbon Dating: an Archaeological Perspective*, John Wiley, New York.

Thermo Electron, 2004, US EPA SW-846 Method 6020A using the X series ICP-MS, Application note: AN_E0619 <http://www.thermo.com/elemental>.

Turetsky M.R., Manning S.W. and Wieder R.K., 2004, Dating recent peat deposits, *Wetlands*, **24**, 2, 324-356.

Tylecote R. F., 1976, *A History of Metallurgy*, Metals Society, London.

Tylecote R.F., 1986, *The Prehistory of Metallurgy in the British Isles*, The Institute of metals, London.

Urban N.R., Eisenreich S.J., Grigal D.F. and Schurr K.T., 1990, Mobility and diagenesis of Pb and ^{210}Pb in peat, *Geochemica et Cosmochimica Acta*, **54**, 3329-3346.

Ure A.M. and Shand C.A., 1974, The determination of mercury in soils and related materials by cold-vapour atomic absorption spectrometry, *Analytica Chimica Acta*, **72**, 63-77.

Vile M.A., Kelman Wieder R. and Novák M., 1999, Mobility of Pb in *Sphagnum*-derived peat, *Biogeochemistry*, **45**, 35-52.

von Post L. and Granlund E., 1925, Sodra Sverigs tortillgangar (in Swedish), *Sveriges Geologiska Undersökning*, Årsbok, **19**.

Wardenaar E.C.P., 1986, A new hand tool for cutting peat profiles, *Canadian Journal of Botany*, **65**, 1772-1773.

Wardenaar E.C.P., 1987, A new hand tool for cutting soil monoliths, *Canadian Journal of Soil Science*, **67**, 405-407.

Wedepohl K.H., 1995, The composition of the continental crust, *Geochimica et Cosmochimica Acta*, **59**, 1217-1232.

Weiss D., Shotyk W., Cheburkin A.K., Gloor M. and Reese S., 1997, Atmospheric Pb deposition from 21,400 to c.a. 2000 yrs BP in a peat bog profile, Jura Mountains, Switzerland, *Water, Air and Soil Pollution*, **100**, 311-324.

Weiss D., Cheburkin A.K., Shotyk W. and Gloor M., 1998, Determination of lead in the ash fraction of plants and peats using the Energy-dispersive Miniprobe Multielement Analyser (EMMA), *Analyst*, **123**, 2097-2102.

Weiss D., Shotyk W., Kramers J.D. and Gloor M., 1999a, *Sphagnum* mosses as archives of recent and past atmospheric Pb deposition in Switzerland, *Atmospheric Environment*, **33**, 3751-3763.

Weiss D., Shotyk W., Appleby P.G., Kramers J.D. and Cheburkin A.K., 1999b, Atmospheric lead deposition since the Industrial Revolution recorded by five Swiss peat profiles: Enrichment factors, fluxes, isotopic composition, and sources, *Environmental Science & Technology*, **33**, 1340-1352.

Weiss D., Shotyk W. and Kempf O., 1999c, Archives of atmospheric lead pollution, *Naturwissenschaften*, **86**, 262-275.

Weiss D., Shotyk W., Rieley J., Page S., Gloor M., Reese S. and Martinez-Cortizas A., 2002a, The geochemistry of major and selected trace elements in a forested peat bog, Kalimantan, SE Asia, and its implications for past atmospheric dust deposition, *Geochimica et Cosmochimica Acta*, **66**, 2307-2323.

Weiss D., Shotyk W., Boyle E.A., Kramers J.D., Appleby P.G. and Cheburkin A.K., 2002b, Comparative study of the temporal evolution of atmospheric Pb deposition in Scotland and eastern Canada using blanket peat bogs, *The Science of the Total Environment*, **292**, 7-18.

Wheeler D., 1999, <http://www.weather.org.uk/climate/scotclim.html>.

West S., Charman D.J., Grattan J.P. and Cheburkin A.K., 1997, Heavy Metals in Holocence Peats from South West England: Detecting Mining Impacts and Atmospheric Pollution, *Water, Air and Soil Pollution*, **100**, 343-353.

Winkler M.G., 1985, Charcoal analysis for paleoenvironmental interpretation: a chemical assay, *Quaternary Research*, **23**, 313-326.

Witting R., 1993, General Aspects of Biomonitoring Heavy Metals by Plants, in *Indicators for heavy metals in the terrestrial environment*, Weinheim, New York.

Yafa C., Farmer J.G., Graham M.C., Bacon J.R., Barbante C., Cairns W.R.L., Bindler R., Renberg I., Cheburkin A., Emons H., Handley M.J., Norton S.A., Krachler M., Shotyk W., Li X.D., Martinez-Cortizas A., Pulford I.D., MacIver V.,

Schweyer J., Steinnes E., Sjøbakk T.E., Weiss D., Dolgopolova A. and Kylander M., 2004, Development of an ombrotrophic peat bog (low ash) reference material for the determination of elemental concentrations, *Journal of Environmental Monitoring*, **6**, 493-501.

Yafa C., 2004, *The Accurate Analysis and Environmental Geochemistry of Inorganic Elements in Peat Bogs*, PhD Thesis, University of Edinburgh.

Yafa C. and Farmer J.G., 2006, A comparative study of acid-extractable and total digestion methods for the determination of inorganic elements in peat material by inductively coupled plasma-optical emission spectrometry, *Analytica Chimica Acta*, **557**, 296-303.

Zechmeister H.G., Hohenwallner D., Riss A. and Hanus-Illnar A., 2003, Variations in heavy metal concentrations in the moss species *Abietinella abietina* (Hedw.) Fleisch, according to sampling time, within site variability and increase in biomass, *The Science of the Total Environment*, **301**, 55-65.

Zoller, W.H., Gladney, E.S. and Duce, R.A., 1974, Atmospheric concentrations and sources of trace metals at the South Pole, *Science*, **183**, 198-200.

PAPER

A comparison of antimony and lead profiles over the past 2500 years in Flanders Moss ombrotrophic peat bog, Scotland†

JEM
www.rsc.org/jem

Joanna M. Cloy,[a] John G. Farmer,*[a] Margaret C. Graham,[a] Angus B. MacKenzie[b] and Gordon T. Cook[b]

[a] School of GeoSciences, The University of Edinburgh, West Mains Road, Edinburgh, UK EH9 3JJ. E-mail: J.G.Farmer@ed.ac.uk; Fax: +44 131 6504757; Tel: +44 131 6504757
[b] Scottish Universities Environmental Research Centre, East Kilbride, UK G75 0QF

Received 1st August 2005, Accepted 12th October 2005
First published as an Advance Article on the web 8th November 2005

Two cores collected in 2001 and 2004 from Flanders Moss ombrotrophic peat bog in central Scotland were dated (^{14}C, ^{210}Pb) and analysed (ICP-OES, ICP-MS) to derive and compare the historical atmospheric deposition records of Sb and Pb over the past 2500 years. After correction, *via* Sc, for contributions from soil dust, depositional fluxes of Sb and Pb peaked from *ca.* 1920–1960 A.D., with >95% of the anthropogenic inventories deposited post-1800 A.D. Over the past two centuries, trends in Sb and Pb deposition have been broadly similar, with fluctuations in the anthropogenic Sb/Pb ratio reflecting temporal variations in the relative input from emission sources such as the mining and smelting of Pb ores (in which Sb is commonly present, as at Leadhills/Wanlockhead in southern Scotland), combustion of coal (for which the Sb/Pb ratio is approximately an order of magnitude greater than in Pb ores) and exhaust emissions (Pb from leaded petrol) and abrasion products from the brake linings (Sb from heat-resistant Sb compounds) of automobiles. The influence of leaded petrol has been most noticeable in recent decades, firstly through the resultant minima in Sb/Pb and $^{206}Pb/^{207}Pb$ ratios (the latter arising from the use of less radiogenic Australian Pb in alkylPb additives) and then, during its phasing out and the adoption of unleaded petrol, complete by 2000 A.D., the subsequent increase in both Sb/Pb and $^{206}Pb/^{207}Pb$ ratios. The extent of the 20th century maximum anthropogenic enrichment of Sb and Pb, relative to the natural Sc-normalised levels of the Upper Continental Crust, was similar at ~50- to 100-fold. Prior to 1800 A.D., the influence of metallurgical activities on Sb and Pb concentrations in the peat cores during both the Mediaeval and Roman/pre-Roman periods was discernible, small Sb and Pb peaks during the latter appearing attributable, on the basis of Pb isotopic composition, to the mining/smelting of Pb ores indigenous to Britain.

John Farmer, in whose group Joanna Cloy is a PhD research student, was born in the UK in 1947. He received his PhD in Radionuclide and Stable Isotope Geochemistry from the University of Glasgow, UK, in 1972. After two post-doctoral years at Woods Hole Oceanographic Institution, USA, he returned to Glasgow as a Research Fellow in Forensic Medicine/Environmental Health, with interests in the environmental geochemistry and human health effects of potentially harmful elements. A move to the University of Edinburgh, UK, as Lecturer (1987), Senior Lecturer (1990) and Reader (1997) in Environmental Chemistry and then Professor (2004) of Environmental Geochemistry, facilitated major ongoing research efforts on the speciation and behaviour of lead, arsenic, chromium, manganese, antimony and uranium in the environment. A recurring theme is the study of environmental change via the analysis of dated freshwater lake and coastal marine sediments, peat bogs, archival moss, tree rings and human teeth.

Introduction

In recent years ombrotrophic peat bogs have been used to study the changing rates and sources of atmospheric metal deposition as they receive all their nutrient, pollutant and water inputs solely by dry and wet deposition from the atmosphere. Cores from such bogs have proved especially useful as archives of atmospheric Pb deposition as Pb is essentially immobile in ombrotrophic peat.[1–3] Considerable research has been carried out using ombrotrophic peat bogs as well as other archives to characterize historical trends in the extent and sources of environmental Pb pollution,[3–18] including previous work on the Flanders Moss site under investigation in the study reported here.[1,19,20] In contrast, there have been only a few studies of Sb in ombrotrophic peat bogs,[21–24] although similarities with the distribution of Pb, even back to Roman times,[21,24] have suggested that Sb too is essentially immobile in ombrotrophic peat. In a recent study[24] of Swiss peat extending back to 12 370 ^{14}C y BP, the lowest "background" values of Sb occurred in peat dating from 8030 to 5320 ^{14}C y BP. A comparison with those in recent peat samples suggested

† This work was presented at the First International Workshop on Antimony in the Environment, Heidelberg, Germany, 16th to 19th May 2005.

DOI: 10.1039/b510987f

Table 1 Mean Pb, Sb and Sc concentrations in six certified reference materials

Material	Measured Pb concentration/ mg kg^{-1} (±1 SD)	Certified Pb concentration/ mg kg^{-1}	Measured Sb concentration/ mg kg^{-1} (±1 SD)	Certified Sb concentration/ mg kg^{-1}	Measured Sc concentration/ mg kg^{-1} (±1 SD)	Certified Sc concentration/ mg kg^{-1}
Ombrotrophic Peat (NIMT/UOE/FM001)	173 ± 11 (n = 67)	174 ± 8	2.30 ± 0.33 (n = 59)	—	0.82 ± 0.15 (n = 59)	—
Canadian Peat (1878 P)	70.9 ± 4.7 (n = 10)	78.8 ± 2.9	0.33 ± 0.07 (n = 11)	0.34 ± 0.05[b]	0.83 ± 0.04 (n = 11)	1.04[a]
Bush Branches and Leaves (DC73349)	44 ± 3 (n = 14)	47 ± 3	0.100 ± 0.009 (n = 13)	0.095 ± 0.014	0.30 ± 0.02 (n = 11)	0.32 ± 0.04
Peach Leaves (GBW 08501)	0.99 ± 0.10 (n = 10)	0.99 ± 0.08	—	—	—	—
Coal (BCR CRM No. 40)	23.0 ± 2.0 (n = 5)	24.2 ± 1.7	4.24 ± 0.19 (n = 5)	—	5.56 ± 0.36 (n = 5)	6.25 ± 0.52[a]
Coal (NBS SRM 1635)	2.0 ± 0.2 (n = 5)	1.9 ± 0.2	0.14 ± 0.01 (n = 5)	0.14[a]	0.65 ± 0.06 (n = 5)	0.63[a]

[a] Information only values. [b] Information only value for Sb,[35] but additional information only value of 0.305 ± 0.018 mg kg^{-1} was determined by Q-ICP-MS.[36]

UK), equipped with a cross-flow nebuliser and autosampler. For single sectional samples from 04-1-M, ICP-OES measurements were carried out once, using a Perkin Elmer Optima 5300 DV instrument (Perkin Elmer, Beaconsfield, UK) equipped with a gem-cone cross-flow nebuliser and AS 93 plus autosampler. ICP-MS measurements of concentration were carried out once on single sectional samples from both cores using a PlasmaQuad (PQ) 3 instrument (Thermo Electron, Winsford, UK), equipped with a Meinhard nebuliser, nickel sampler and skimmer cones, Gilson autosampler and a Gilson Minipuls 3 peristaltic pump (Anachem, Luton, UK). Calibration solutions were prepared daily by adequate dilution of the relevant standard solutions containing 10 mg l^{-1} of the element of interest. Overall analytical precision (±1 RSD) for Pb determination in duplicate samples by ICP-OES was ±5%, while analytical precision for ICP-MS determination of Sb, Pb and Sc in single samples was ≤±8%.

For the determination of Pb isotopic ratios by ICP-MS, a solution of the National Institute of Standards and Technology (NIST) common Pb isotopic reference standard SRM 981 (^{206}Pb/^{207}Pb = 1.093, ^{208}Pb/^{206}Pb = 2.168, ^{208}Pb/^{207}Pb = 2.370) was used for calibration and mass bias correction.[27] Analytical precision on these ratios was typically <±0.3%.

In addition to the above, a sample of galena (PbS) from Wanlockhead lead mines, southern Scotland, was also analysed for Sb, Pb and ^{206}Pb/^{207}Pb following HNO_3–HF hot plate digestion of ~0.1 g sub-samples. Sb concentrations were also determined in a selection of British coal samples (n = 19) that had previously been analysed for both Pb concentration and isotopic composition.[34]

To ensure the quality of analytical procedures and data, six different reference materials were analysed along with the samples: Ombrotrophic Peat (NIMT/UOE/FM001),[32] Canadian Peat (1878 P),[35] Bush Branches and Leaves (DC73349), Peach Leaves (GBW 08501), Coal (BCR CRM No. 4) and Coal (NBS SRM 1635). Good agreement between measured and certified values was obtained (Table 1). The isotope ratios ^{206}Pb/^{207}Pb, ^{208}Pb/^{206}Pb and ^{208}Pb/^{207}Pb determined in the ombrotrophic peat reference material as 1.176 ± 0.002, 2.091 ± 0.004 and 2.460 ± 0.006, respectively, (n = 58, ±1 SD) were in good agreement with corresponding "information only" values of 1.176 ± 0.001, 2.092 ± 0.002 and 2.461 ± 0.003.[32]

Age dating

^{210}Pb. Analyses for ^{210}Pb, ^{226}Ra and ^{137}Cs were performed by gamma spectrometry using low-background, planar High Purity Ge gamma photon detectors, with a Canberra detector being used for a sister core 01CM-2, collected at the same time as 01CM-1, and an EG&G Ortec detector for core 04-1-M. Sample weights varied depending upon the quantity of material available for analysis. For core 01CM-2, sample weights in the range 1 to 2 g of dried, ground material were used. The samples were accurately weighed into polycarbonate containers, which were then sealed and stored for a minimum of three weeks before analysis in order to allow ^{222}Rn to come to radioactive equilibrium with ^{226}Ra. The sample containers were positioned in a holder, which ensured reproducible geometry, on the end face of the detector for analysis. For core 04-1-M, sample weights of 10, 15 or 20 g were used and, in this case, samples were compressed into discs, using a 12 tonne hydraulic press, to give uniform counting geometries. The discs were then sealed in polycarbonate containers for analysis, as above. Detection efficiencies were determined for each counting geometry using standards prepared by spiking appropriate weights of peat, which had non-detectable activities of the nuclides of interest, with known activities of ^{210}Pb, ^{226}Ra and ^{137}Cs using certified standard solutions (Amersham plc). The standards were then prepared in the same geometry as the samples.

The constant rate of supply (CRS) model[37] was applied to ^{210}Pb inventories (total 2.53 ± 0.05 kBq m^{-2}) calculated from the unsupported ^{210}Pb data (Fig. 2) to generate age dates for sections in 04-1-M. In the case of the 01CM-1 core, ^{210}Pb dates were obtained by extrapolation, aided by matching of ^{206}Pb/^{207}Pb profiles, from data from the sister core, 01CM-2, collected on the same date.[20]

^{14}C. Humic acid fractions from seven peat sections (38–40, 48–50, 56–57, 76–77, 85–86, 91–93 and 94–96 cm) from core 01CM-1 were obtained using a standard acid–base–acid pretreatment procedure[38] and radiocarbon dated by accelerator mass spectrometry (AMS). The humic acid samples were firstly combusted at 850 °C in sealed quartz tubes containing copper oxide as the oxidant and a small quantity of silver foil to remove halides. The CO_2 was then purified by cryogenic pumping and a 2 ml sub-sample converted to graphite by Fe/Zn reduction and analysed for ^{14}C at the SUERC AMS facility (NEC 5 MV terminal voltage instrument) operated at 4.5 MV and with carbon in the 4+ charge state. A further sub-sample of the CO_2 was used for δ^{13}C analysis using a VG Sira 10 isotope ratio mass spectrometer. The δ^{13}C values were used to correct the measured ^{14}C/^{13}C ratios for isotopic fractionation prior to radiocarbon age determinations. The radiocarbon ages were subsequently calibrated to calendar age ranges using the Oxford Radiocarbon Accelerator Unit calibration program (OxCal 3).

that the natural levels of Sb in the atmospheric environment have previously been overestimated by a factor of ten and that the global atmospheric Sb cycle may have been affected to at least the same extent as that of Pb. In view of the comparable toxicity of Sb to that of Pb, Shotyk *et al.*[24,25] have suggested that the potential threat of environmental Sb to human health may have been overlooked.

As Sb is a chalcophilic trace element and is found in practically all sulfide minerals (including galena and other Pb minerals) and coals,[24,25] it might be expected that anthropogenic Sb deposition from the atmosphere has closely followed that of the Pb emanating from mining/smelting and coal combustion emissions in the past. During the second half of the 20th century, however, there were significant emissions of Pb to the atmosphere from vehicle exhausts as a consequence of the use of anti-knock alkylPb additives in petrol. As a result of reductions in the maximum permitted concentration of lead in petrol and the introduction of unleaded petrol in 1986, however, such emissions in the UK declined from a maximum of *ca.* 8500 tonnes Pb in 1973 essentially to zero at the time of the outright ban in 2000.[26] During the 20th century and the early years of the 21st century, such changes in Pb source have been reflected in variations in the isotopic composition (*e.g.* $^{206}Pb/^{207}Pb$) of atmospheric[27,28] and deposited[3–20] Pb. Meanwhile, especially in recent years, the uses (and potential releases) of Sb compounds have expanded to include Sb_2S_3 as a lubricant in automobile brake linings and Sb_2O_3 as a fire retardant in plastics *etc.*[25]

The aim of this study was therefore to investigate the extent and nature of past and present relationships between Sb and Pb emissions to the environment by comparing trends in new age-dated profiles of Sb and Pb concentrations and Pb isotopic composition in cores from Flanders Moss ombrotrophic peat bog in central Scotland.

Materials and methods

Sampling site

Two peat cores were collected from the southwest dome of Flanders Moss ombrotrophic peat bog, which lies 16 km to the west of Stirling in central Scotland (Fig. 1). The largest remaining lowland ombrotrophic peat bog in Britain with 548 ha of active bog, Flanders Moss was formed on top of Carse clay deposits after the Menteith glacier melted over 11 000 years ago. Vegetation is currently dominated by *Sphagnum* mosses, lichens, heather, fens and grasses with some scattered birch.[29,30]

Sample collection

A 106 cm long peat core (01CM-1) of cross-sectional dimensions 5 cm × 5 cm was collected in September 2001 using a Cuttle and Malcolm corer,[31] which was pushed vertically into the bog after ~7 cm of grassy vegetation was first removed with a knife to enable penetration of the corer. A 33 cm long monolith peat core (04-1-M) of cross-sectional dimensions 20 cm × 10 cm, was collected in October 2004 using a monolith tin, which was inserted into the vertical face of a freshly dug pit. Cores 01CM-1 and 04-1-M were cut into 1 cm and 3 cm sections, respectively, in the field using a serrated stainless steel knife and sections were packed into polyethylene bags and transported to the laboratory.

Sample preparation

The wet peat sections were weighed, air-dried at 30 °C for ~30 days on drying trays, re-weighed and then ground using a mortar and pestle. The remaining moisture content of each air-dried peat section was determined on sub-samples by oven-drying at 105 °C and the residual ash content was estimated by weighing air-dried sub-samples (subsequently corrected for moisture content) before and after ashing at 450 °C for 4 hours. Sub-samples (~0.25 g) of air-dried peat (subsequently corrected for moisture content) were digested using a modified US EPA Method 3052 Protocol microwave-assisted $HF–HNO_3$ digestion method.[32,33] Digests were evaporated to 1 ml on a hotplate and then made up to 25 ml with 2% (v/v) HNO_3. All reagents used in sample preparation were of the highest analytical quality available, *i.e.* Aristar HNO_3 (69%) and HF (48%) and high purity water (18.2 MΩ cm) from a Milli-Ro water system (Millipore, Watford, UK).

Sample analysis

With the exception of the highest Pb concentrations (01CM-1, 0–33 cm; 04-1-M, 0–33 cm), which were measured using ICP-OES, Sb, Pb and Sc concentrations were determined in the prepared 2% v/v HNO_3 solutions using ICP-MS. ICP-OES measurements of concentration were carried out once on duplicate sectional samples from 01CM-1 using a Thermo Jarrell Ash IRIS instrument (Thermo Electron, Cambridge,

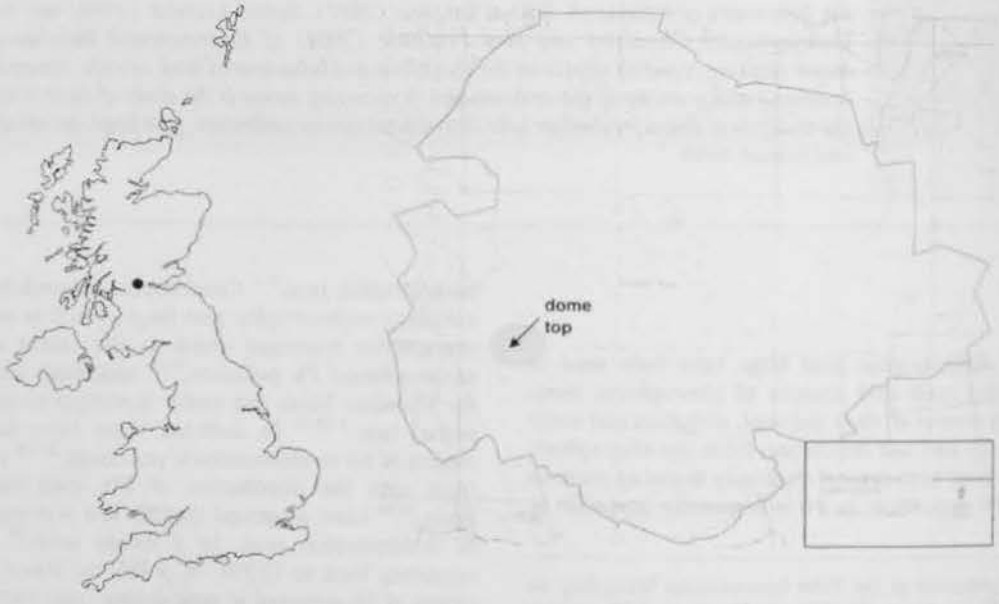

Fig. 1 Location and map of Flanders Moss, showing the sampling site on the southwest dome.

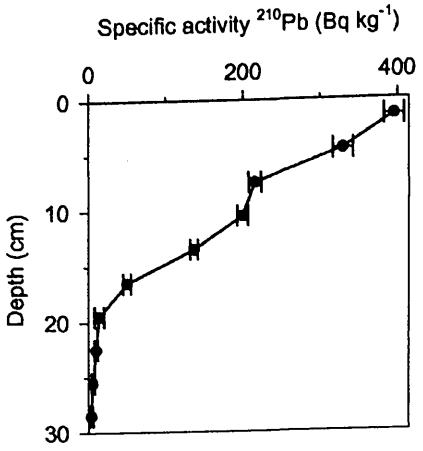

Fig. 2 ^{210}Pb specific activity profile in Flanders Moss core 04-1-M.

Results

01CM-1

0–33 cm (Fig. 3). Sb and Pb concentrations (Fig. 3) increased from 0.10 and 4.4 mg kg^{-1} at 32–33 cm to maximum values of 4.2 mg kg^{-1} and 264 mg kg^{-1}, respectively, at a depth of 8.5 cm, which was dated at 1948 ± 10 A.D. Above these peaks, concentrations of Sb and Pb decreased gradually towards the top of the core, which in this case did not equate to the surface of the bog and 2001 A.D. because of the loss of some material during core collection.[20] The ^{206}Pb/^{207}Pb ratios remained constant at a mean value of 1.173 ± 0.002 from 33 cm to 12 cm (1928 ± 11 A.D.), above which they declined steeply to a constant value of ~1.134 from 3.5 cm (1976 ± 7 A.D.) upwards. The Sc concentrations, averaging 0.21 ± 0.01 mg kg^{-1} from 33 to 30 cm, increased less markedly than those of Sb and Pb but did exhibit a distinct concentration peak of 1.76 mg kg^{-1} at 9–10 cm, *i.e.* 1 cm below the Sb and Pb maxima, with a smaller peak of 1.27 mg kg^{-1} at 4–5 cm.

33–106 cm (Fig. 3). The concentrations of Sb and Pb were much lower than those in the uppermost 0–33 cm of the core, never exceeding 0.10 and 4.6 mg kg^{-1}, respectively. Several distinct zones were apparent for Sb: a region of minimum concentrations (mean 0.016 ± 0.004 mg kg^{-1}) from 86 cm to 53 cm, corresponding to 20–220 A.D. to *ca.* 430–640 A.D., above which Sb increased steadily to 0.10 mg kg^{-1} by 33 cm and below which from 86 cm to 96 cm there was a pronounced peak with a maximum concentration of 0.072 mg kg^{-1} at 92–93 cm, corresponding to *ca.* 210–40 B.C. Distinct zones were also apparent for Pb: a region of minimum concentrations (mean 1.05 ± 0.16 mg kg^{-1}) from 71 to 53 cm, above which Pb increased to 2.5 ± 0.3 mg kg^{-1} by 40 cm (660–830 A.D.) to 33 cm and below which from 71 to 102 cm there was a pronounced peak with a maximum concentration of 4.63 mg kg^{-1} at 90–91 cm. The ^{206}Pb/^{207}Pb ratio in the zone of minimum Pb concentration (53–71 cm) averaged 1.164 ± 0.006, with corresponding means of 1.168 ± 0.004 in the zone above (33–53 cm) and 1.176 ± 0.003 over the zone (71–102 cm) containing the Pb peak below. Sc concentrations averaged 0.16 ± 0.08 mg kg^{-1} from 33 to 106 cm, never exceeding 0.45 mg kg^{-1}, but with some minor peaks at 68–70 cm and 84–88 cm and a zone of

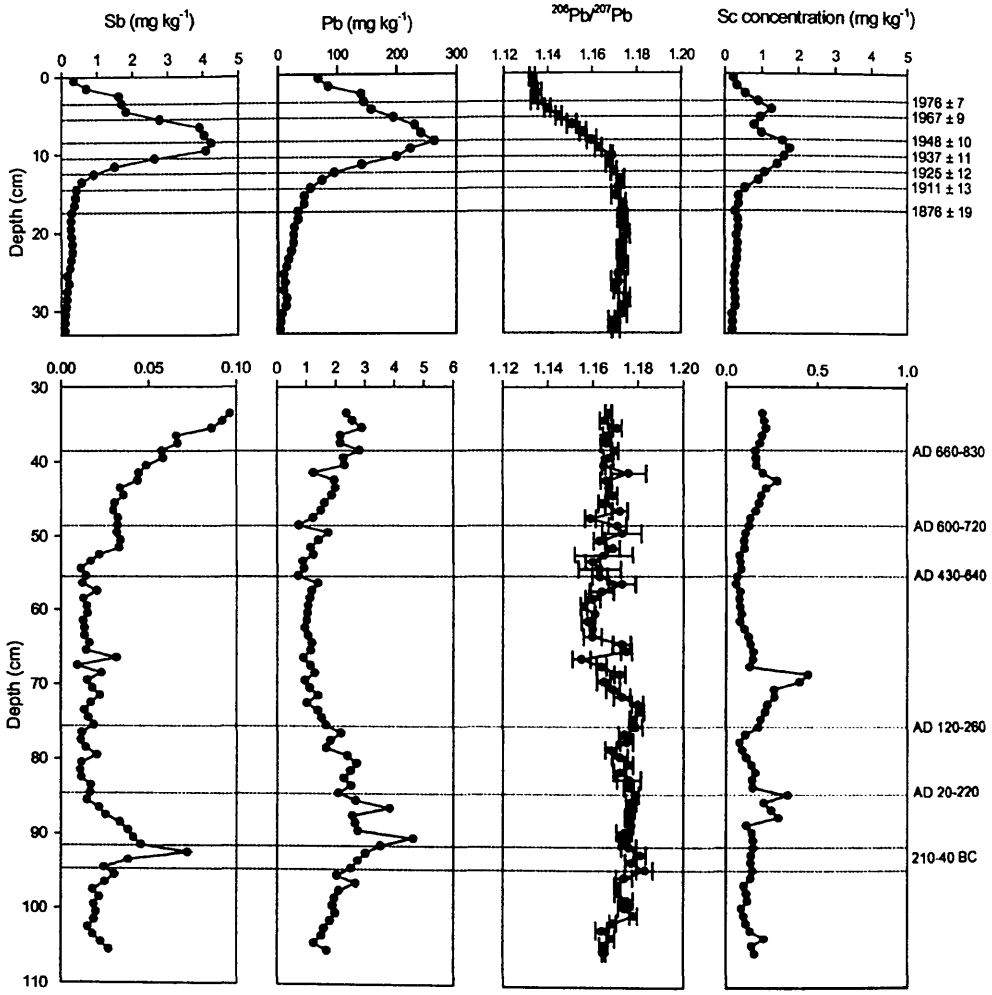

Fig. 3 Profiles of Sb, Pb and Sc concentrations and ^{206}Pb/^{207}Pb ratio from 0–33 cm and 33–106 cm in the ^{210}Pb- and ^{14}C-dated Flanders Moss core 01CM-1.

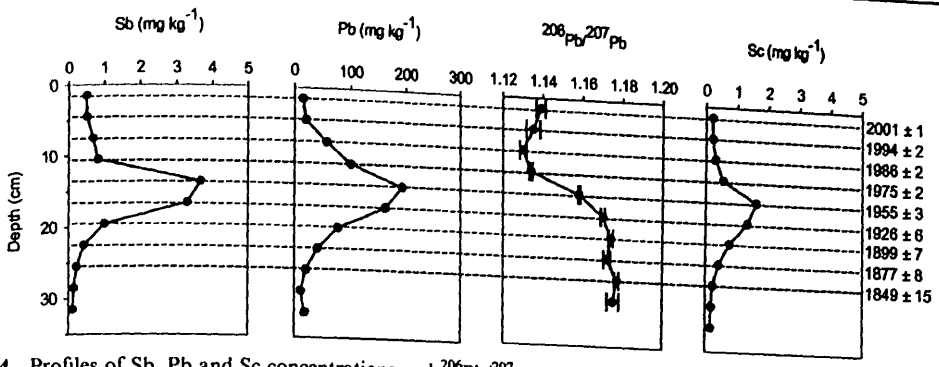

Fig. 4 Profiles of Sb, Pb and Sc concentrations and $^{206}Pb/^{207}Pb$ ratio in the ^{210}Pb-dated Flanders Moss core 04-1-M.

minimum concentration (mean 0.07 ± 0.01 mg kg^{-1}) from 52 to 62 cm.

04-1-M (Fig. 4)

Sb and Pb concentrations increased from 0.12 and 18 mg kg^{-1} at 30–33 cm to maximum values of 3.7 mg kg^{-1} and 193 mg kg^{-1}, respectively, at 12–15 cm, which was dated at 1943–1968 A.D., the section mid-point of 13.5 cm corresponding to 1955 ± 3 A.D. Above these peaks, concentrations of Sb and Pb decreased towards the top of the core to concentrations of 0.50 mg kg^{-1} and 15 mg kg^{-1} in the 0–3 cm section, which was dated at 1997–2004 A.D. The $^{206}Pb/^{207}Pb$ ratios remained constant at a mean value of 1.175 ± 0.002 from 30 to 18 cm (1910 ± 8 A.D.) and then declined to 1.170 ± 0.001 at 15–18 cm, which was dated at 1910–1943 A.D., the section mid-point of 16.5 cm corresponding to 1926 ± 6 A.D. Above 15 cm, the $^{206}Pb/^{207}Pb$ ratio declined to a minimum of 1.130 ± 0.002 at 6–9 cm (1982–1990 A.D., with mid-point of 7.5 cm at 1986 ± 2 A.D.) before increasing to 1.139 ± 0.002 at 0–3 cm (1997–2004 A.D.). This reversal in the $^{206}Pb/^{207}Pb$ ratio was absent from the top of the 01CM-1 core because of the loss of some surface material during core collection.[20] The Sc concentrations, averaging 0.20 ± 0.03 mg kg^{-1} from 33 to 24 cm, increased less markedly than those of Sb and Pb, as also seen in the 01CM-1 core, reaching a maximum of 1.6 mg kg^{-1} at 12–15 cm, above which values declined to 0.21 mg kg^{-1} in the surface 0–3 cm section.

Coal and Pb ore

In 19 samples of British coal that had been previously analysed for Pb and $^{206}Pb/^{207}Pb$,[34] Sb concentrations ranged from 0.07 to 4.6 mg kg^{-1} (mean 0.75 ± 1.02 mg kg^{-1}, median 0.49 mg kg^{-1}), with a mean Sb/Pb ratio of 0.036 ± 0.032 (median 0.027). For all the British coals (n = 60) previously investigated, the mean $^{206}Pb/^{207}Pb$ ratio was 1.182 ± 0.009 (Scottish, 1.181 ± 0.006, n = 30), with average Pb concentrations of 23.9 mg kg^{-1} and 11.0 mg kg^{-1} for coals from Scotland and England & Wales, respectively.[34] In the Pb ore sample from Wanlockhead, the Sb/Pb ratio was 0.0056 ± 0.0004, approximately one order of magnitude lower than in coal. The measured $^{206}Pb/^{207}Pb$ ratio in the Pb ore was 1.172 ± 0.003, in agreement with the value of 1.170 ± 0.003 found for Leadhills/Wanlockhead Pb ore.[39–41]

Discussion

The use of Sc as an indicator of soil dust input of Sb and Pb

Conservative lithogenic elements such as Al, Ti, Sc and Zr have at times been taken to indicate variations in the atmospheric deposition of soil dust to peat bogs.[23,42] In contrast to the other conservative elements, Sc is especially favoured as it exhibits no preference for specific mineral phases and thus tends to be uniformly distributed throughout the environment. The aim is to enable distinction between anthropogenic inputs (for example from mining, smelting, coal burning and vehicle emissions) of heavy metals (*e.g.* Sb, Pb) and natural, sometimes climate-related, inputs *via* wind-entrained soil dust.[23,42] There can of course also be human-related impacts upon soil dust input, for example arising from the clearance of land for agricultural purposes. Although there can sometimes be specific-element-related problems with this approach,[43] the use of metal/Sc concentration ratios, such as Sb/Sc and Pb/Sc here, in peat profiles can be of assistance in estimating the extent of Sb and Pb contributions from sources that are unrelated to direct anthropogenic inputs to the observed variations in the Sb and Pb concentration profiles. The lowest Sb/Sc and Pb/Sc ratios in the 01CM-1 core occurred over the depth region 67–75 cm, with mean values of 0.066 ± 0.016 and 5.3 ± 2.5, respectively, close to the corresponding ratios of 0.044 and 2.43 for the Earth's Upper Continental Crust (UCC).[44] It is most unlikely, however, that Sb and Pb concentrations are unaffected by anthropogenic inputs of these metals at any depth over the *ca.* 2500 years represented by 01CM-1. In Switzerland, Shotyk *et al.*[24] found the lowest Sb (0.008 ± 0.003 mg kg^{-1}) and Pb (0.23 ± 0.04 mg kg^{-1}) concentrations (a factor of 2–5 lower than those in the zones of minimum Sb and Pb concentrations in Flanders Moss 01CM-1) in peats dating from 5320 to 8020 ^{14}C y BP, with corresponding Sb/Sc, Pb/Sc and Sb/Pb ratios of 0.105, 3.0 and 0.035 ± 0.014, respectively. For the UCC, the corresponding Sb/Sc, Pb/Sc and Sb/Pb ratios of 0.044, 2.43 and 0.018 demonstrate the variability that can occur in such ratios of natural elemental concentrations.

Pre-Roman and Roman atmospheric Sb and Pb sources and deposition

In 01CM-1, it seems very likely that the elevated Sb/Sc (mean 0.29 ± 0.05) and Pb/Sc (mean 19.8 ± 6.1) ratios (Fig. 5) associated with the elevated Sb and Pb concentrations (Fig. 3) from 96–86 cm, dated at 210–40 B.C. to 20–220 A.D., can be attributed to pre-Roman and Roman metallurgical activities. The Roman Pb mining industry is well documented[45,46] but, as the Romans did not occupy Britain until 43 A.D., these elevations in metal concentrations from 210 B.C. predate the Roman occupation by two centuries, suggesting the existence of a pre-Roman Pb extraction industry in the UK.[17,47] Indeed, despite lower Sb and Pb concentrations over the earlier 96–102 cm depth interval, the corresponding Sb/Sc and Pb/Sc ratios were also enhanced at 0.19 ± 0.05 and 20.5 ± 4.1. In the UK, evidence has been found for the addition of Pb in varying amounts to mixtures of Cu and Sn during the late Bronze Age (*ca.* 900–500 B.C.) as a new technique to make bronze that flowed more freely during the casting process[48] and the mines of Alderley Edge in Cheshire, west-central England, are believed to have been worked mainly for Cu from the early Bronze Age (*ca.* 2000 B.C.) and possibly Pb by the late Bronze Age.[45,46] Iron working was also introduced *ca.* 500 B.C. and was well established before the arrival of the Romans.[48]

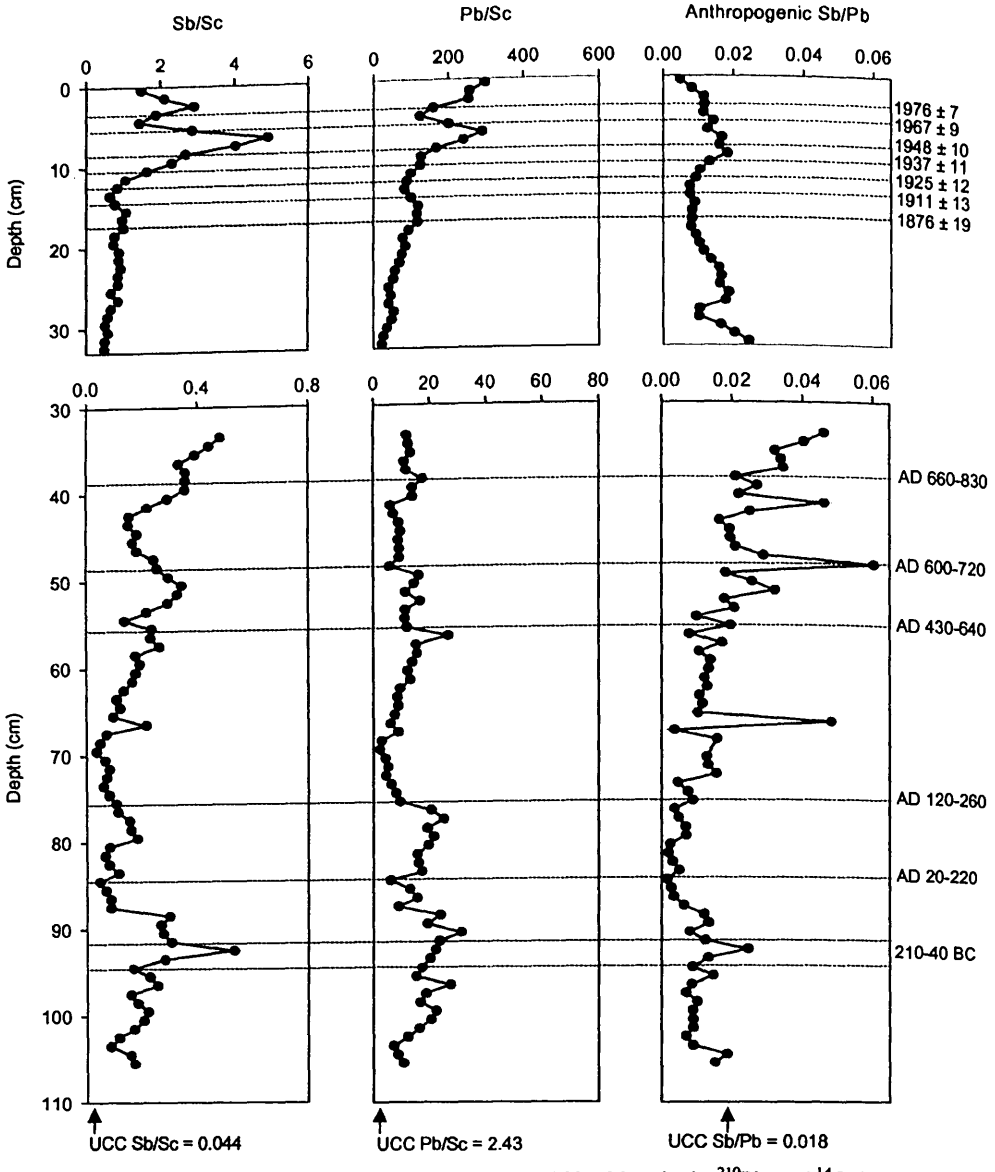

Fig. 5 Profiles of Sb/Sc, Pb/Sc and anthropogenic Sb/Pb ratios from 0–33 cm and 33–106 cm in the ^{210}Pb- and ^{14}C-dated Flanders Moss core 01CM-1.

Copper and Fe metallurgy are also sources of Sb and Pb to the environment given the association of Sb and Pb with sulfide minerals.[25] Later, the Mendip Pb mines in southwest England were worked by 49 A.D.,[45,46] only 6 years after the Roman conquest, further suggesting the prior existence of a local mining industry before the arrival of the Romans. The Pb deposits of northeast Wales were worked by the late 1st century A.D. as were those of Derbyshire, central England, by 117–138 A.D.[45,46] In Swiss peat cores from Etang de la Gruère, Shotyk *et al.*[24,25] have found enrichments of Sb in association with those of Pb at *ca.* 2000 ^{14}C y BP and have attributed the latter to ancient Pb mining and long-range transport of aerosols from the Iberian Peninsula during the period of greatest Roman mining.[6]

When Pb isotope ratios of the 01CM-01 peat samples for the 210–40 B.C. to 20–220 A.D. period are plotted along with those of various Pb ores (Fig. 6), they are in much better agreement with those of British origin than with those from the major Spanish mines of Rio Tinto and Murcia,[49] which were widely exploited during the Iron Age and Roman times (*ca.* 200 B.C.–400 A.D.).[45] This supports the finding by Le Roux *et al.*,[17] based on research on Lindow Bog in NW England, that Pb contamination in Britain during this period resulted primarily from the mining and smelting of British ores.

From 86 to 76 cm, *i.e.* corresponding to 20–220 A.D. to 120–260 A.D., Pb concentrations (Fig. 3) and Pb/Sc ratios (mean 17.4 ± 5.2) (Fig. 5) were still elevated, but those of Sb and Sb/Sc (mean 0.11 ± 0.04) much less so. The mean ^{206}Pb/^{207}Pb ratio of 1.175 ± 0.003, however, was very similar to those for 86–96 cm (1.177 ± 0.003) and 96–102 cm (1.173 ± 0.003) and indeed for 71–102 cm (1.176 ± 0.003). While it is possible to estimate the soil dust Pb contribution (mean of 0.38 ± 0.15 mg kg^{-1} over 71–102 cm), and by difference the anthropogenic Pb contribution, to the total Pb concentration *via* the use of the Pb/Sc ratios in peat and the UCC, it is not possible to do likewise for the ^{206}Pb/^{207}Pb ratio of the specifically anthropogenic Pb, as the Pb isotopic composition of the soil dust Pb is unknown.

Over the various depth intervals from 71 to 102 cm, the mean measured Sb/Pb ratios were 0.013 ± 0.003 (71–76 cm), 0.006 ± 0.002 (76–86 cm), 0.013 ± 0.005 (86–96 cm) and 0.010 ± 0.001 (96–102 cm), with an overall average (71–102 cm) of 0.010 ± 0.004. The soil dust contribution of Sb can be estimated in similar fashion to that of Pb, enabling calculation of the anthropogenic contribution to both Sb and Pb. The corresponding calculated mean anthropogenic Sb/Pb ratios were 0.010 ± 0.004 (71–76 cm), 0.004 ± 0.002 (76–86 cm), 0.012 ± 0.006 (86–96 cm) and 0.009 ± 0.001 (96–102 cm), with an overall average of 0.008 ± 0.005. This is similar to the value of 0.0056 ± 0.0004 obtained for the Sb/Pb ratio in the Pb ore sample from Wanlockhead, southern Scotland, and in general is in line with the <0.8% Sb content in the galena (PbS) of Pb ores.[25]

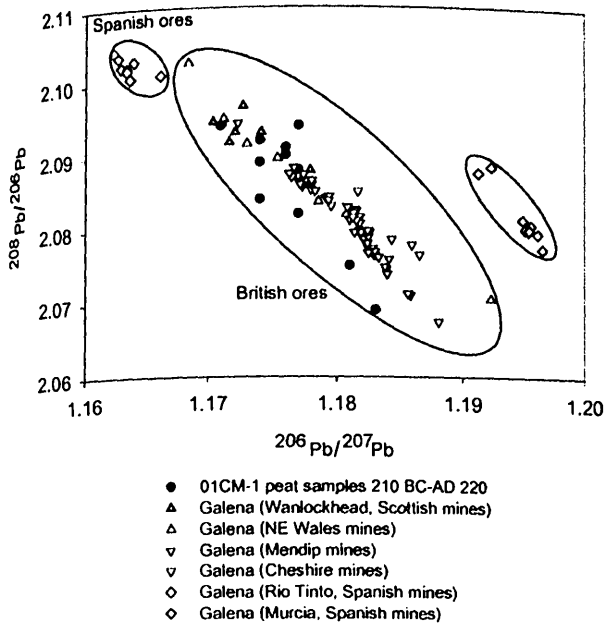

Fig. 6 Plot of $^{208}Pb/^{206}Pb$ *versus* $^{206}Pb/^{207}Pb$ ratios for samples from 210 B.C. to 220 A.D. in Flanders Moss core 01CM-1 and for galena in various British and Spanish Pb ores.

Post-Roman and Mediaeval atmospheric Sb and Pb sources and deposition

Sb and Pb concentrations (Fig. 3) and the corresponding Sb/Sc (0.15 ± 0.07; 53–71 cm) and Pb/Sc (10.5 ± 5.6; 53–71 cm) ratios, with a calculated mean anthropogenic Sb/Pb ratio of 0.013 ± 0.004 (excluding the single outlier peak of 0.048 at 66–67 cm), were at their lowest towards the end of (*ca.* 410 A.D.) and after the Roman occupation of Britain until *ca.* 650 A.D. (Fig. 5). Thereafter, to 33 cm, Sb concentrations rose more rapidly than those of Pb (Fig. 3), reflected in a mean Sb/Sc ratio of 0.29 ± 0.009 compared with a value of 11.5 ± 3.4 for Pb/Sc from 53 to 33 cm (Fig. 5). The corresponding mean anthropogenic Sb/Pb ratio was also higher, averaging 0.028 ± 0.009 (excluding the single outlier peak of 0.061 at 48–49 cm). The mean $^{206}Pb/^{207}Pb$ ratio for the period was 1.168 ± 0.004, compared with a value of 1.164 ± 0.006 from 53 to 71 cm. It is interesting to speculate that these less radiogenic values could reflect deposition of Pb from Rio Tinto, at least to the early Middle Ages (*cf.* 840 A.D. in Monna *et al.*,[50] corresponding to ~38 cm in 01CM-1), although such low values of $^{206}Pb/^{207}Pb$ were not observed in Lindow Bog, NW England. The higher anthropogenic Sb/Pb ratios, which indeed averaged 0.032 ± 0.008 from 41 to 33 cm, could reflect influences from continental Europe perhaps due to the developing Ag industry associated with the well known Mediaeval German Ag mining district in the Harz, which brought about the revival of mining in Europe by the 11th century.[51] A modified method of cupellation involving the melting of Cu ores with Pb to recover Ag was introduced in the mid-15th century and by *ca.* 1500 A.D. both this and the Pb mining and smelting industry were prominent in Europe.[45,46] It is interesting to note that Klaminder *et al.*[13] found $^{206}Pb/^{207}Pb$ minima of ~1.155–1.17 in peat sections dated at *ca.* 1500 A.D. from Dumme Mosse and Tranerod Mosse in southern Sweden, close to the height of Mediaeval metal production in Europe.[51]

Industrial and post-industrial atmospheric Sb and Pb sources and deposition

Above 33 cm in 01CM-1, a depth for which no age-date is available, both Sb and Pb concentrations (Fig. 3) and the corresponding Sb/Sc (0.67 ± 0.15; 33-23 cm) and Pb/Sc (42 ± 12) ratios increased to a depth of 23 cm (Fig. 5). The corresponding anthropogenic Sb/Pb ratio was lower than from 53 to 33 cm, however, averaging 0.017 ± 0.004, while the $^{206}Pb/^{207}Pb$ ratio was fairly constant at 1.173 ± 0.002. It seems significant that the indigenous Scottish Pb mining industry developed during the 17th century[52] at Leadhills and Wanlockhead as emissions from there would have had the effect of increasing atmospheric Sb and Pb concentrations, while lowering the anthropogenic Sb/Pb ratio from its former higher value in Mediaeval times. Furthermore, the $^{206}Pb/^{207}Pb$ ratio of Pb ore from Leadhills and Wanlockhead is 1.170 ± 0.003,[39–41] similar to the value of 1.173 ± 0.002 observed from 33 to 23 cm in 01CM-1 at Flanders Moss.

The depth of 23 cm in 01CM-1, based on a match of $^{206}Pb/^{207}Pb$ values and associated ^{210}Pb dates in the overlying upper regions of 01CM-1 and 04-1-M, probably corresponds to *ca.* 1800 A.D. The ^{210}Pb date of 1876 ± 19 A.D. for 17.5 cm in 01CM-1 is in agreement with that of 1877 ± 8 A.D. for 22.5 cm in 04-1-M, for which the earliest ^{210}Pb date is 1832 ± 19 A.D. at 27 cm. It seems likely that a depth of 33 cm in 04-1-M corresponds to the late 1700s A.D.

From 23 cm (*ca.* 1800 A.D.) to 12 cm (1928 ± 11 A.D.) in 01CM-1, both Sb and Pb concentrations and the corresponding mean Sb/Sc (0.87 ± 0.13) and Pb/Sc (93 ± 18) ratios continued to increase (Fig. 3 and 5). The mean anthropogenic Sb/Pb ratio of 0.009 ± 0.002, however, was lower than formerly but the mean $^{206}Pb/^{207}Pb$ ratio remained the same at 1.173 ± 0.002. Similarly, from 33 cm (late 1700s A.D.) to 18 cm (1910 ± 8 A.D.) in 04-1-M, Sb and Pb concentrations increased (Fig. 4) while the corresponding mean Sb/Sc (0.98 ± 0.24) and Pb/Sc (89 ± 16) ratios, mean anthropogenic Sb/Pb ratio of 0.011 ± 0.003 (Fig. 7) and mean $^{206}Pb/^{207}Pb$ ratio of 1.175 ± 0.002 (Fig. 4) were similar to those in 01CM-1. While these trends are consistent with increasing input of both Sb and Pb, the lower anthropogenic Sb/Pb ratio is indicative of relatively greater inputs of Pb, including, as further suggested by the specific value of the observed $^{206}Pb/^{207}Pb$ ratio, contributions from indigenous Pb ore sources (*e.g.* at Leadhills and Wanlockhead), which have lower Sb/Pb (0.0056) and $^{206}Pb/^{207}Pb$ (1.170) ratios than those of coal (0.0036; 1.181). The mining and smelting of indigenous Pb ores, however, which for Leadhills and Wanlockhead was greatest from 1850 to 1920 until closure in the 1930s,[52] went into general decline in the UK after the 19th century.[53,54]

Over the time periods 1928 ± 11 A.D. to 1969 ± 8 A.D. in 01CM-1 (12 to 5 cm) and 1910 ± 8 A.D. to 1968 ± 2 A.D. in 04-1-M (18 to 12 cm), the main features for the two cores were similar: maximum concentrations in Sb and Pb (at 1948 ± 10; 1955 ± 3 A.D.), maximum Sb/Sc ratios (4.89; 2.54), elevated Pb/Sc ratios (reaching 288; 125), increased mean anthropogenic Sb/Pb ratios (0.014 ± 0.003; 0.020 ± 0.001), and decreasing $^{206}Pb/^{207}Pb$ ratios (to 1.145 at 1967 ± 9 A.D.; 1.158 for 1943 ± 4 to 1968 ± 2 A.D.) (Fig. 3, 4, 5, 7). The increasing influence of imported Australian Pb ($^{206}Pb/^{207}Pb$ ratio = 1.04), used along with Pb from other sources in the manufacture of alkylPb additives for petrol from the 1930s and then emitted to the atmosphere as inorganic Pb compounds in vehicle exhaust emissions, can be seen in the decline in $^{206}Pb/^{207}Pb$ ratios. The intermediate values observed for $^{206}Pb/^{207}Pb$ ratios, however, indicate that there were significant contributions from other sources of Pb, such as coal combustion. Farmer *et al.*[9,34] have previously demonstrated how varying emission contributions from coal combustion ($^{206}Pb/^{207}Pb$ = 1.181) and the mining, smelting and subsequent use of indigenous (1.170) and Australian (1.04) Pb could give rise to the observed trends in atmospheric $^{206}Pb/^{207}Pb$ during the 20th century. Consumption of coal in the UK peaked in *ca.* 1950–1960 A.D. and was always greater than 150 Mt y^{-1} from *ca.* 1900 to 1970 A.D.[34] For 1930 in Scotland,[34] the calculated estimated contributions to anthropogenic Pb in the atmosphere from Scottish coal

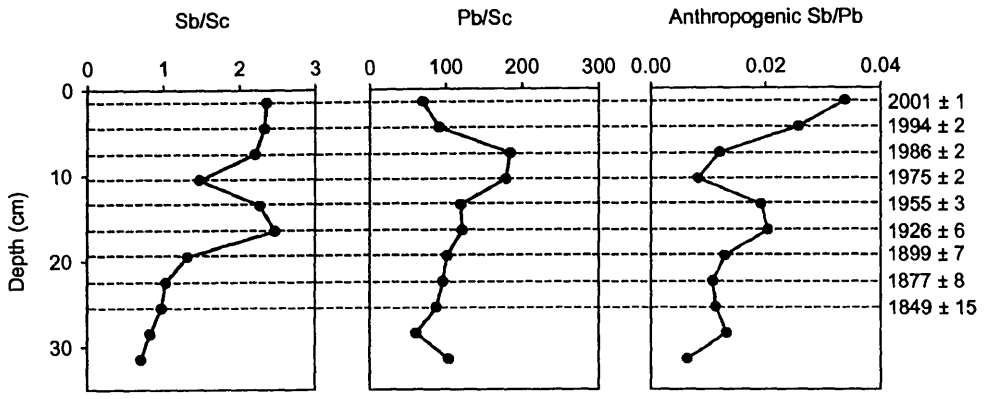

Fig. 7 Profiles of Sb/Sc, Pb/Sc and anthropogenic Sb/Pb ratios in the ^{210}Pb-dated Flanders Moss core 04-1-M.

(46%), Pb smelting in Scotland (35%) and sources in the rest of the UK (19%, with a directly measured $^{206}Pb/^{207}Pb$ ratio[55] of 1.145) gave rise to a calculated $^{206}Pb/^{207}Pb$ ratio of 1.170, the same as that observed in both Flanders Moss peat cores here (Fig. 3 and 4). Using these percentage contributions and the measured Sb/Pb values for coal (0.036) and the indigenous Pb ore (0.0056), along with an estimated value for the rest of the UK of 0.026 (based on a 2 : 1 ratio for coal : smelter Pb emissions, *cf.* Table 4 in Farmer *et al.*[34]), yields an estimated anthropogenic Sb/Pb ratio of 0.023, which is close to the maximum values of 0.018 and 0.020 observed in 01CM-1 and 04-1-M, respectively. This is further confirmation of the influence of coal combustion on Sb emissions during the first 70 years of the 20th century.

From the late 1960s to the early 1980s A.D. (*i.e.* from 5 to 3 cm and 12 to 9 cm in 01CM-1 and 04-1-M, respectively), both Sb and Pb concentrations and the corresponding Sb/Sc (1.67 ± 0.32; 1.15) and Pb/Sc (142 ± 25) ratios, with the exception of Pb/Sc (179) for 04-1-M, decreased (Fig. 3, 4, 5, 7). The corresponding mean anthropogenic Sb/Pb ratios also decreased (to 0.012 ± 0.001; 0.008) quite markedly (Fig. 5 and 7), as did the $^{206}Pb/^{207}Pb$ ratios (to 1.134) (Fig. 3 and 4), indicative of the decreasing influence of coal combustion and the increasing influence of vehicle exhaust emissions of Pb.

From 1982 to 1990 A.D. (*i.e.* 9 to 6 cm) in 04-1-M, Sb and Pb concentrations continued to fall (Fig. 4) while the Sb/Sc ratio increased to 2.23 and the Pb/Sc ratio, at 184, was similar to the previous value of 179 (Fig. 7). The anthropogenic Sb/Pb ratio of 0.012 (Fig. 7), however, was higher, while the $^{206}Pb/^{207}Pb$ ratio attained its minimum value of 1.130 (Fig. 4). This evidence suggests a new source of Sb during the period of maximum influence of petrol Pb on the $^{206}Pb/^{207}Pb$ ratio. Although UK Pb emissions from car exhausts are known to have fallen, in response to reductions in the maximum permitted concentration of Pb in petrol, from *ca.* 8500 t y^{-1} in the early 1970s A.D. to *ca.* 7000 t y^{-1} by the early 1980s A.D., the final reduction to 0.15 g l^{-1} and the introduction of unleaded petrol produced a sharp fall to *ca.* 2900 t in 1986 A.D. and *ca.* 2200 t by 1990 A.D.[26] In 01CM-1, dates for the three sections from 0-3 cm were not available due to the loss of material from the top of this core and a sister Cuttle and Malcolm core collected in 2001.[20] Nevertheless, the results for 01CM-1 were in broad agreement with those of 01-4-M, *viz.* decreasing Sb and Pb concentrations, increasing Sb/Sc (2.18 ± 0.71) and Pb/Sc (269 ± 25), an anthropogenic Sb/Pb ratio of 0.008 ± 0.003 and a minimum mean $^{206}Pb/^{207}Pb$ value of 1.134 ± 0.001 (Fig. 3 and 5).

The suggestion of new recent sources of Sb while inputs of Pb have been declining is strengthened by the data for the top 6 cm (1990–2004 A.D.) of 01-4-M (Fig. 4 and 7): (i) Sb concentrations and Sb/Sc ratios (2.35 ± 0.04) levelling out while Pb concentrations and Pb/Sc ratios (81 ± 14) decline, (ii) a significant increase in the corresponding mean anthropogenic Sb/Pb ratio to 0.030 ± 0.006, and (iii) an increase in the $^{206}Pb/^{207}Pb$ ratio to 1.139 ± 0.002. Thus while Pb emissions from car exhausts fell steeply, for example to 800 t by 1997 A.D.,[26] as the use of unleaded petrol became increasingly predominant and then complete with the ban on leaded petrol from 2000 A.D., the input of Sb from comparatively new recent sources (*i.e.* not coal combustion, which has been declining) has probably contributed to the increase in the Sb/Pb ratio. Such recent sources could include the release of Sb from automotive brake linings, where it has been used instead of asbestos to improve heat resistance, and from the degradation or combustion of a variety of other products, including plastics, to which it is added (in the form of Sb_2O_3) as a flame retardant.[25]

Historical trends in depositional fluxes and inventories of Sb and Pb

The calculated inferred atmospheric depositional fluxes of anthropogenic Sb and Pb since the mid-19th century are plotted, along with the anthropogenic Sb/Pb ratios and the measured $^{206}Pb/^{207}Pb$ ratios, *versus* ^{210}Pb-derived calendar dates for 04-1-M in Fig. 8. The maxima of ~0.42 and ~21 mg m^{-2} y^{-1} for the anthropogenic Sb and Pb fluxes from the mid-1920s to the mid-1950s are evident. The influence of contributions from coal combustion emissions explains both the enhancement in the associated anthropogenic Sb/Pb ratio over the late 19th century to ~0.20 at that time and, to a certain extent, the limitation of the post-19th century decline in $^{206}Pb/^{207}Pb$ that stemmed from the introduction and use of Australian Pb in alkylPb additives in petrol. MacKenzie *et al.*[7] have reported peaks in depositional fluxes of Sb and Pb at *ca.* 1940 A.D. in a peat core from South Drumboy Hill, approximately 18 km southwest of Glasgow although, interestingly, the magnitudes of the maximum fluxes there were greater, at ~1.5 mg m^{-2} y^{-1} and ~50 mg m^{-2} y^{-1}, respectively. This could reflect geographical factors related to the proximity to industry *etc.*, but it should also be borne in mind, however, that significant variations in apparent depositional fluxes can be found in the analysis of cores from even the same bog as a consequence of topographical and plant compositional features that affect the efficiency of particle trapping and retention.[4,16] Indeed, we have previously observed a range of calculated maximum Pb depositional fluxes from 20–60 mg m^{-2} y^{-1} for Flanders Moss.[19,20] Further to the northwest in Scotland, at the remote rural Loch Laxford peat bog, Shotyk *et al.*[24,25] found that maximum, albeit much lower, anthropogenic Sb and Pb concentrations of 0.8 mg kg^{-1} and 27 mg kg^{-1}, respectively, occurred during the same time period at *ca.* 1930 A.D.

After 1960 A.D., the rapid decline in coal combustion emissions at the same time as the increase in vehicle exhaust emissions is reflected in not only the fall in the $^{206}Pb/^{207}Pb$ ratio

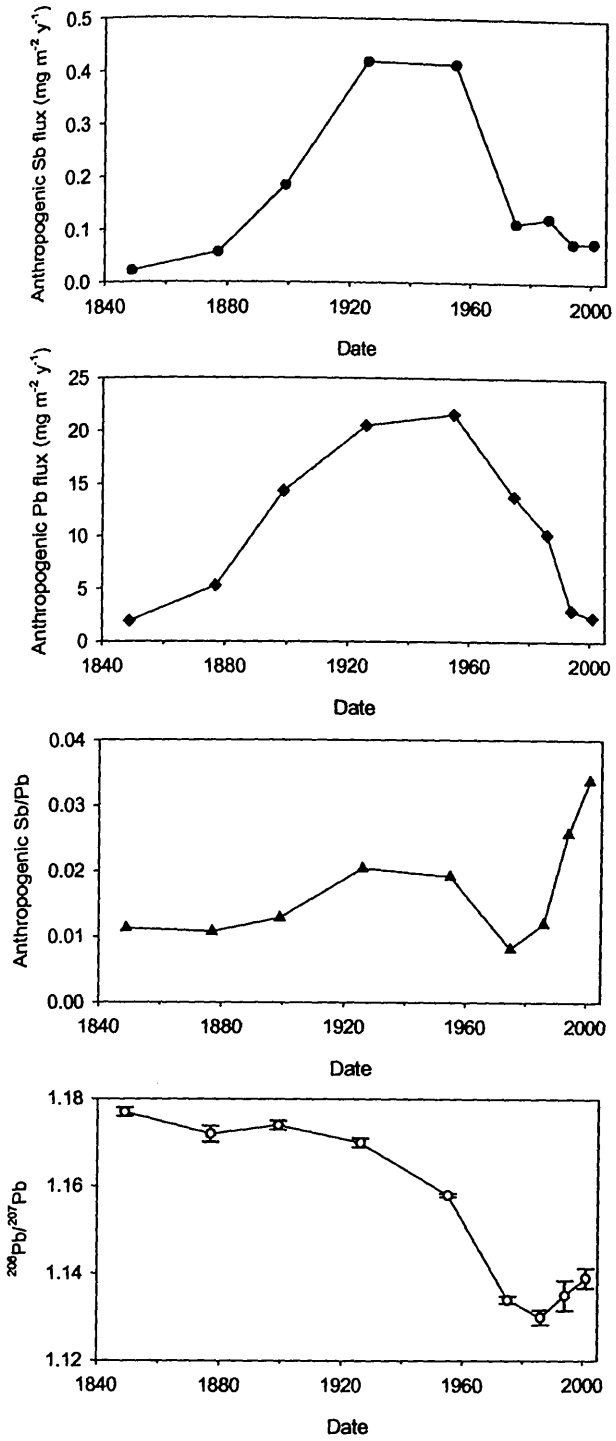

Fig. 8 Calculated atmospheric depositional fluxes of anthropogenic Sb and Pb, and the anthropogenic Sb/Pb and measured $^{206}Pb/^{207}Pb$ ratios for the Flanders Moss core 04-1-M *versus* ^{210}Pb-derived dates since 1840 A.D.

but also in the steeper decline in anthropogenic Sb fluxes (to ~0.1 mg m^{-2} y^{-1}) relative to those of Pb, with a concomitant decline in the corresponding Sb/Pb ratio to its minimum value of 0.008 in the mid-1970s A.D. (Fig. 8). Thereafter, the Sb fluxes stayed relatively constant while those of Pb, due to the phasing out of leaded petrol, continued to fall. The $^{206}Pb/^{207}Pb$ ratio, after reaching a minimum in the mid-1980s A.D., increased to the present because of the increasing relative importance of other sources of Pb (*e.g.* waste incineration) relative to petrol. The increase in the anthropogenic Sb/Pb ratio, however, probably began slightly earlier, in the mid-1970s A.D., increasing to 0.034 by the early 2000s A.D.

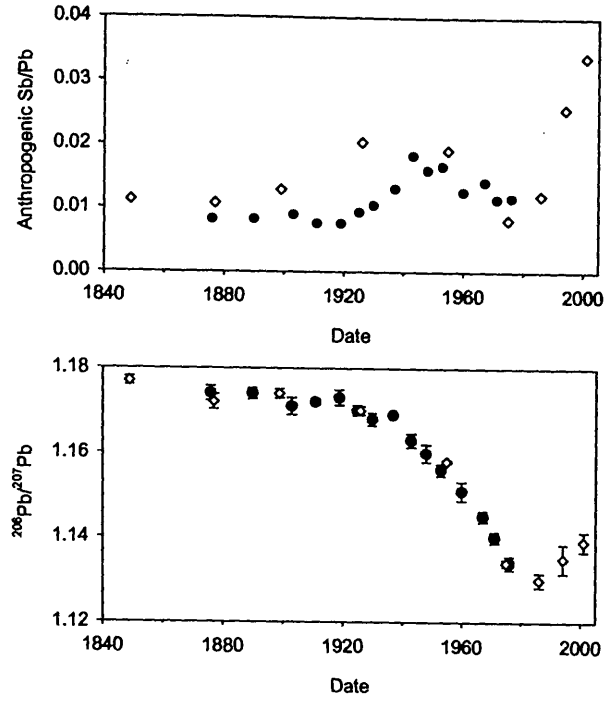

Fig. 9 Anthropogenic Sb/Pb and measured $^{206}Pb/^{207}Pb$ ratios *versus* ^{210}Pb-derived dates since 1840 for Flanders Moss cores 04-1-M (open symbols) and 01CM-1 (shaded symbols).

The corresponding values of anthropogenic Sb/Pb ratios and measured $^{206}Pb/^{207}Pb$ ratios for core 01CM-1 (^{210}Pb-dated by extrapolation from sister core 01CM-2, but only up to the 1970s A.D.) are generally in good agreement with those for 04-1-M (Fig. 9). Likewise there is broad agreement with values obtained independently for preserved herbarium and freshly collected *Sphagnum* moss samples of known age collected across Scotland.[9,56] The mean anthropogenic Sb/Pb ratios for the moss samples over various time periods from the mid-19th century were 0.010 ± 0.005 for 1855–1904 A.D. (n = 9), 0.028 ± 0.013 for 1909–1969 A.D. (n = 16), 0.028 ± 0.019 for 1970–1988 A.D. (n = 10) and 0.107 ± 0.065 for 1991–2000 A.D. (n = 11),[56] *i.e.* there was a near 3-fold increase from the lower values of the second half of the 19th century for most of the 20th century and then, in the final decade of the 20th century, a 10-fold increase, somewhat greater than that observed in the peat cores. Interestingly, a freshly collected *Sphagnum* moss sample at Wanlockhead in 2000 A.D. had an anthropogenic Sb/Pb ratio of 0.0023, in accord with the much lower Sb/Pb ratios observed in former Pb mining/smelting areas.

The total anthropogenic Sb and Pb inventories for core 04-1-M (*i.e.* from the late 1700s to 2004 A.D.) were 0.035 g m^{-2} and 2.10 g m^{-2}, respectively, of which 3.1% and 1.7% were deposited post-1990 A.D., 7.5% and 13.2% from 1968 to 1990 A.D., 70.2% and 58.3% from 1910 to 1968 A.D., and 19.2% and 26.7% pre-1910 A.D. For the 01CM-1 core, the total anthropogenic Sb and Pb inventories (*i.e.* from *ca.* 500 B.C. to *ca.* mid-1980s, given that the very top of the core was lost during collection) were 0.051 g m^{-2} and 3.77 g m^{-2}, respectively, of which 0.0485 g m^{-2} and 3.59 g m^{-2} were deposited post-1800 A.D. Of the post-1800 inventories of anthropogenic Sb and Pb, 10.4% and 12.9% were deposited from 1969 A.D. to the mid-1980s, 83.6% and 78.4% from 1907 to 1969 A.D., and 6.0% and 8.7% pre-1907 A.D. Compared with the data for 04-1-M, the higher percentages for the *ca.* 1910–1970 A.D. period in 01CM-1 may partially be attributable to the loss of surface material from the latter and the inclusion of late 1700s data for the former. It should be remembered, however, that the ^{210}Pb dating for 01CM-1 is

extrapolated from that of a sister core 01CM-2 and this, with its associated uncertainty, may contribute to some differences in the vertical (temporal) distribution (%) of anthropogenic elemental inventories between the two cores.

For 01CM-1, the pre-1800 A.D. inventories of 0.0023 g Sb m^{-2} and 0.17 g Pb m^{-2} constitute just 4.6% of the total anthropogenic Sb and Pb inventories for the core. For the period embracing the Sb peak (86–96 cm) corresponding to 210/40 B.C. to 20/220 A.D. in pre-Roman/Roman times, the anthropogenic Sb and Pb inventories were 0.000 22 g m^{-2} and 0.019 g m^{-2}, respectively. If the mid-points of the ^{14}C-derived dates are taken (*i.e.* 125 B.C. to 120 A.D.), the corresponding average depositional fluxes over this period would be 0.9 μg Sb m^{-2} y^{-1} and 0.078 mg Pb m^{-2} y^{-1}. These correspond to only ~0.2% and ~0.4% of the maximum fluxes of anthropogenic Sb and Pb during the 20th century but are ~2.6 and ~7.8 times those estimated by Shotyk *et al.*[24] to be the natural background rate of deposition of Sb and Pb for Switzerland. Over the entirety of the Pb peak in the 01CM-1 core at that time (*i.e.* 71–102 cm), the anthropogenic Sb and Pb inventories were 0.000 29 g m^{-2} and 0.045 g m^{-2}.

The extent of maximum enrichment of Sb and Pb relative to "natural background" can be calculated, using measured Sb/Sc and Pb/Sc ratios and corresponding values for the Upper Continental Crust, *via* the following expressions:

$$\text{Sb EF} = ([\text{Sb}]/[\text{Sc}])_{MAX}/([\text{Sb}]/[\text{Sc}])_{UCC} \text{ and}$$

$$\text{Pb EF} = ([\text{Pb}]/[\text{Sc}])_{MAX}/([\text{Pb}]/[\text{Sc}])_{UCC}$$

For 04-1-M and 01CM-01, the maximum enrichments of Sb are 58 (1926 ± 6 A.D.) and 111 (1960 ± 9 A.D.), while those of Pb are 76 (1986 ± 2 A.D.) and 123 (1980s A.D.), respectively. If, instead of using Upper Continental Crust Sb/Sc and Pb/Sc ratios, those of Shotyk *et al.*[24] for Swiss natural background peat, *i.e.* [Sb]/[Sc] = 0.105 and [Pb]/[Sc] = 3.0, are used, the corresponding values for maximum enrichments of Sb are 24 and 47 and of Pb are 61 and 99, respectively. Notwithstanding the uncertainties inherent in calculating enrichments in this manner,[43] it thus appears that Sb and Pb exhibit similar degrees of enrichment. Shotyk *et al.*[24] found maximum enrichments of 30 and 40 for Sb and Pb, respectively, at Loch Laxford in northwest Scotland, and 30–80 (Sb) and 100–125 (Pb) for four of their five Swiss peat cores.

Conclusions

The general agreement in the major trends in the concentration profiles of Sb and Pb over the past 2500 years in dated cores from Flanders Moss ombrotrophic peat bog suggests common sources of these two elements and supports the view that Sb, like Pb, is immobile in peat. The derived atmospheric deposition fluxes of anthropogenic Sb and Pb were greatest in the industrial era, peaking during 1920–1960 A.D. Perturbations in the anthropogenic Sb/Pb ratio since 1800 are attributable to temporal variations in the relative importance of atmospheric emissions from different sources such as Pb ore mining and smelting, coal combustion and, in recent decades, automobile-related use of compounds of Pb (in leaded petrol) and of Sb (in brake linings). In the Roman/pre-Roman period, some two millennia ago, the mining and smelting of British Pb ores appears to have been responsible for the small, but clearly discernible, peaks in Sb and Pb concentration in the Flanders Moss peat core. Overall, the 50- to 100-fold maximum enhancement of both Sb and Pb in the atmosphere during the 20th century, when compared with ancient natural levels, suggests that the toxicological threat from Sb may well have been underestimated in the past and warrants further study, especially in the light of continuing input of Sb from newer sources such as waste incineration of plastics.

Acknowledgements

We gratefully acknowledge permission from Scottish Natural Heritage to collect peat cores from Flanders Moss, and the assistance of L. J. Eades, M. Halter and C. Yafa at the University of Edinburgh in various aspects of field work, sample preparation and elemental/isotopic analysis. We also acknowledge the SUERC AMS staff for their assistance in making the ^{14}C measurements and C. Donnelly for gamma spectrometric analysis. J.M.C. thanks the Natural Environment Research Council for funding her PhD studentship.

References

1 A. B. MacKenzie, J. G. Farmer and C. L. Sugden, *Sci. Total Environ.*, 1997, **203**, 115.
2 M. A. Vile, R. K. Wieder and M. Novak, *Biogeochemistry*, 1999, **45**, 35.
3 W. Shotyk, M. E. Goodsite, F. Roos-Barraclough, N. Givelet, G. Le Roux, D. Weiss, A. K. Cheburkin, K. Knudsen, J. Heinemeier, W. O. van der Knaap, S. A. Norton and C. Lohse, *Geochim. Cosmochim. Acta*, 2005, **69**, 1.
4 S. A. Norton, G. C. Evans and J. S. Kahl, *Water, Air, Soil Pollut.*, 1997, **100**, 271.
5 W. Shotyk, A. K. Cheburkin, P. G. Appleby, A. Fankhauser and J. D. Kramers, *Water, Air, Soil Pollut.*, 1997, **100**, 297.
6 W. Shotyk, D. Weiss, P. G. Appleby, A. K. Cheburkin, R. Frei, M. Gloor, J. D. Kramers, S. Reese and W. O. van der Knaap, *Science*, 1998, **281**, 1635.
7 A. B. MacKenzie, E. M. Logan, G. T. Cook and I. D. Pulford, *Sci. Total Environ.*, 1998, **223**, 25.
8 D. Weiss, W. Shotyk, P. G. Appleby, J. D. Kramers and A. K. Cheburkin, *Environ. Sci. Technol.*, 1999, **33**, 1340.
9 J. G. Farmer, L. J. Eades, H. Atkins and D. F. Chamberlain, *Environ. Sci. Technol.*, 2002, **36**, 152.
10 D. Weiss, W. Shotyk, E. A. Boyle, J. D. Kramers, P. G. Appleby and A. K. Cheburkin, *Sci. Total Environ.*, 2002, **292**, 7.
11 A. Martinez-Cortizas, E. García-Rodeja, X. Pontevedra Pombal, J. C. Nóvoa Muñoz, D. Weiss and A. Cheburkin, *Sci. Total Environ.*, 2002, **292**, 33.
12 L. J. Eades, J. G. Farmer, A. B. MacKenzie, A. Kirika and A. E. Bailey-Watts, *Sci. Total Environ.*, 2002, **292**, 55.
13 J. Klaminder, I. Renberg and R. Bindler, *Global Biogeochem. Cycles*, 2003, **17**, art. no. 1019.
14 M. Novák, S. Emmanuel, M. A. Vile, Y. Erel, A. Véron, T. Pačes, R. Wieder, M. Vaněček, M. Štěpánova, E. Břízová and J. Hovorka, *Environ. Sci. Technol.*, 2003, **37**, 437.
15 W. Shotyk, M. E. Goodsite, F. Roos-Barraclough, R. Frei, J. Heinemeier, G. Asmund, C. Lohse and T. S. Hansen, *Geochim. Cosmochim. Acta*, 2003, **67**, 3991.
16 R. Bindler, M. Klarqvist, J. Klaminder and J. Forster, *Global Biogeochem. Cycles*, 2004, **18**, art. no. GB3020.
17 G. Le Roux, D. Weiss, J. Grattan, N. Givelet, M. Krachler, A. Cheburkin, N. Rausch, B. Kober and W. Shotyk, *J. Environ. Monit.*, 2004, **6**, 502.
18 J. G. Farmer, M. C. Graham, J. R. Bacon, S. M. Dunn, S. I. Vinogradoff and A. B. MacKenzie, *Sci. Total Environ.*, 2005, **346**, 121.
19 J. G. Farmer, A. B. MacKenzie, C.L. Sugden, P. J. Edgar and L. J. Eades, *Water, Air, Soil Pollut.*, 1997, **100**, 253.
20 J. G. Farmer, M. C. Graham, C. Yafa, J. M. Cloy, A. J. Freeman and A. B. MacKenzie, *Global Planet. Change*, in press.
21 W. Shotyk, A. K. Cheburkin, P. G. Appleby, A. Fankhauser and J. D. Kramers, *Earth Planet. Sci. Lett.*, 1996, **145**, E1.
22 A. B. MacKenzie, E. M. Logan, G. T. Cook and I. D. Pulford, *Sci. Total Environ.*, 1998, **222**, 157.
23 W. Shotyk, M. Krachler, A. Martinez-Cortizas, A. K. Cheburkin and H. Emons, *Earth Planet. Sci. Lett.*, 2002, **199**, 21.
24 W. Shotyk, M. Krachler and B. Chen, *Global Biogeochem. Cycles*, 2004, **18**, art. no. GB1016.
25 W. Shotyk, M. Krachler and B. Chen, in *Biogeochemistry, Availability, and Transport of Metals in the Environment, Metal Ions in Biological Systems*, ed. A. Sigel, H. Sigel and R. K. O. Sigel, M. Dekker, New York, 2005, vol. 44, pp. 177–203.
26 *Digest of Environmental Statistics*, Department for Environment, Food and Rural Affairs (DEFRA), 2002, http://www.defra.gov.uk/environment/statistics/des/index.htm.
27 J. G. Farmer, L. J. Eades, M. C. Graham and J. R. Bacon, *J. Environ. Monit.*, 2000, **2**, 49.

28 S. I. Vinogradoff, M. C. Graham, G. J. P. Thornton, S. M. Dunn, J. R. Bacon and J. G. Farmer, *J. Environ. Monit.*, 2005, 7, 431.
29 R. Lindsay, *Bogs: The Ecology, Classification and Conservation of Ombrotrophic Mires*, Scottish Natural Heritage, Edinburgh, 1995.
30 S. Brooks and R. E. Stoneman, *Conserving Bogs: The Management Handbook*, The Stationery Office, Edinburgh, 1997.
31 S. P. Cuttle and D. C. Malcolm, *Plant Soil*, 1979, **51**, 297.
32 C. Yafa, J. G. Farmer, M. C. Graham, J. R. Bacon, C. Barbante, W. R. L. Cairns, R. Bindler, I. Renberg, A. Cheburkin, H. Emons, M. J. Handley, S. A. Norton, M. Krachler, W. Shotyk, X. D. Li, A. Martinez-Cortizas, I. D. Pulford, V. MacIver, J. Schweyer, E. Steinnes, T. E. Sjøbakk, D. Weiss, A. Dolgopolova and M. Kylander, *J. Environ. Monit.*, 2004, **6**, 493.
33 C. Yafa and J. G. Farmer, *Anal. Chim. Acta*, in press.
34 J. G. Farmer, L. J. Eades and M. C. Graham, *Environ. Geochem. Health*, 1999, **21**, 257.
35 C. Barbante, W. Shotyk, H. Biester, A. Cheburkin, H. Emons, J. G. Farmer, E. Hoffman, A. Martinez-Cortizas, J. Matschullat, S. Norton, J. Schweyer and E. Steinnes, in *Proceedings of the 11th International Conference on Heavy Metals in the Environment*, ed. J. O. Nriagu, Ann Arbor, MI, USA, 2000, Contribution No. 1106 (CD-ROM).
36 M. Krachler, H. Emons, C. Barbante, G. Cozzi, P. Cescon and W. Shotyk, *Anal. Chim. Acta*, 2002, **458**, 387.
37 P. G. Appleby, W. Shotyk and A. Fankhauser, *Water, Air, Soil Pollut.*, 1997, **100**, 223.
38 G. T. Cook, A. J. Dugmore and J. S. Shore, *Radiocarbon*, 1998, **40**, 21.
39 S. Moorbath, *Philos. Trans. R. Soc. London, Ser. A*, 1962, **254**, 295.
40 C. L. Sugden, J. G. Farmer and A. B. MacKenzie, *Environ. Geochem. Health*, 1993, **15**, 59.
41 M. Rohl, *Archaeometry*, 1996, **38**, 165.
42 W. Shotyk, D. Weiss, J. D. Kramers, R. Frei, A. K. Cheburkin, M. Gloor and S. Reese, *Geochim. Cosmochim. Acta*, 2001, **65**, 2337.
43 C. Reimann and P. de Caritat, *Environ. Sci. Technol.*, 2000, **34**, 5084.
44 K. H. Wedepohl, *Geochim. Cosmochim. Acta*, 1995, **59**, 1217.
45 R. F. Tylecote, *A History of Metallurgy*, Metals Society, London, 1976.
46 R. F. Tylecote, *The Prehistory of Metallurgy in the British Isles*, The Institute of Metals, London, 1986.
47 J. O. Nriagu, *Lead and Lead Poisoning in Antiquity*, John Wiley and Sons, New York, 1983.
48 G. Ritchie and A. Ritchie, *Scotland Archaeology and Early History*, Edinburgh University Press, Edinburgh, 1991.
49 Z. Stos-Gale, N. H. Gale, J. Houghton and R. Speakman, *Archaeometry*, 1995, **37**, 407.
50 F. Monna, C. Petit, J.-P. Guillaumet, J. Jouffroy-Bapicot, C. Blanchot, J. Dominik, R. Losno, H. Richard, J. Lévêque and C. Chateau, *Environ. Sci. Technol.*, 2004, **38**, 665.
51 M.-L. Bränvall, R. Bindler, I. Renberg, O. Emteryd, J. Bartnicki and K. Billström, *Environ. Sci. Technol.*, 1999, **33**, 4391.
52 G. V. Wilson, *Special Reports on the Mineral Resources of Great Britain*, Memoirs of the Geological Survey, Scotland, 1921, Vol. XVII.
53 W. Y. Elliott, E. S. May, J. W. F. Rowe, A. Skelton and D. H. Wallace, *International Control in the Non-Ferrous Metals*, McMillan, New York, 1937.
54 J. Day and R. F. Tylecote, *The Industrial Revolution in Metals*, The Institute of Metals, London, 1991.
55 J. R. Bacon, K. C. Jones, S. P. McGrath and A. E. Johnston, *Environ. Sci. Technol.*, 1996, **30**, 2511.
56 M. Halter and J. G. Farmer, in preparation.

Available online at www.sciencedirect.com
ScienceDirect
Global and Planetary Change 53 (2006) 240–248
GLOBAL AND PLANETARY CHANGE
www.elsevier.com/locate/gloplacha

Use of $^{206}Pb/^{207}Pb$ ratios to investigate the surface integrity of peat cores used to study the recent depositional history and geochemical behaviour of inorganic elements in peat bogs

J.G. Farmer [a,*], M.C. Graham [a], C. Yafa [a], J.M. Cloy [a], A.J. Freeman [a], A.B. MacKenzie [b]

[a] School of GeoSciences, Joseph Black Building, University of Edinburgh, King's Buildings, West Mains Road, Edinburgh EH9 3JJ, Scotland, UK
[b] Scottish Universities Environmental Research Centre, East Kilbride G75 0QF, Scotland, UK

Received 1 April 2005; accepted 23 March 2006
Available online 23 June 2006

Abstract

The well characterised temporal trend in the $^{206}Pb/^{207}Pb$ atom ratio of atmospheric lead deposition in Scotland during the 20th century was used to investigate the surface integrity of several cores collected by different methods from Flanders Moss ombrotrophic peat bog, central Scotland, during 1996–2001. Based on $^{206}Pb/^{207}Pb$ profile comparisons, in conjunction with identified ^{210}Pb radionuclide inventory deficits for two of the cores, it was deduced that 25±7 yrs worth of material was missing from the more seriously affected core. After allowing for an appropriate vertical offset based on $^{206}Pb/^{207}Pb$ profile matching, the subsequent matching of profiles of titanium, lead, sulfur, arsenic, iron, phosphorus and manganese in three cores for which total concentration data were available was excellent. Without such offset correction, erroneous conclusions could have been drawn concerning the recent historical record of anthropogenic lead and arsenic deposition, the position of the redox boundary, which controls geochemical cycling and enrichment of iron, and the nutrient recycling status of manganese and phosphorus in the near-surface vegetation. Topographic, vegetative and coring (both device and operator) influences may have been responsible, thus endorsing the use of reliable, multiple core sampling and the use of lead isotope ratio profiles, supplemented by appropriate radionuclide data, in both assessing and ensuring the surface integrity of peat cores.

Keywords: peat; elements; deposition; geochemistry; stable lead isotopes: ^{210}Pb inventories

1. Introduction

Dated ombrotrophic peat core profiles are increasingly being used to investigate the history of metal deposition from the atmosphere since the end of the last Ice Age (Shotyk et al., 1998; Martinez-Cortizas et al., 1999; Shotyk et al., 2002; Krachler et al., 2003; Shotyk and Krachler, 2004). Both anthropogenic (ancient, pre-industrial, industrial, recent/post-industrial) and climate-related natural (pre-anthropogenic) factors have influenced the deposition records. Anthropogenic factors have included land use changes (such as agriculture), metal mining and smelting, fossil fuel combustion and other industrial and traffic-related emissions.

* Corresponding author. Tel./fax: +44 131 650 4757.
E-mail address: J.G.Farmer@ed.ac.uk (J.G. Farmer).

0921-8181/$ - see front matter © 2006 Elsevier B.V. All rights reserved.
doi:10.1016/j.gloplacha.2006.03.006

One of the most intensively studied metals in this context has been lead. In addition, considerable use has been made of variations in the isotopic composition of lead, which has four naturally occurring stable isotopes (primordial ^{204}Pb and radiogenic ^{206}Pb, ^{207}Pb and ^{208}Pb), to distinguish between different sources, e.g. lead ores, coal (Farmer et al., 1999), and to assess their relative contributions to the environmental burden of lead resulting from various sources/pathways of anthropogenic emission. This has probably been most successful in Europe, where the introduction and use of Australian lead of characteristic $^{206}Pb/^{207}Pb$ ratio (1.04) during the late 19th and 20th centuries, especially in the manufacture of anti-knock alkyllead additives for petrol, resulted in emissions that produced a noticeable reduction in atmospheric $^{206}Pb/^{207}Pb$ ratios from the values prevalent during the industrial revolution of the 19th century (Farmer et al., 1997; MacKenzie et al., 1997; Shotyk et al., 1997, 1998; Dunlap et al., 1999; Weiss et al., 1999; Klaminder et al., 2003; Novák et al., 2003; Shotyk et al., 2003; Le Roux et al., 2004; Shotyk et al., 2005). Thus, in Scotland, the $^{206}Pb/^{207}Pb$ ratio, which had a value of ~1.17 for atmospherically deposited lead in the 19th century had decreased by the mid-1980s to ~1.07 in urban atmospheric particulate material (Farmer et al., 2000) and to ~1.12 in surface deposits in rural peat bogs (Farmer et al., 1997; Weiss et al., 2002), *Sphagnum* mosses (Farmer et al., 2002) and freshwater lake sediments (Farmer et al., 1996; Eades et al., 2002). Thereafter, as a consequence of the withdrawal of leaded petrol over much of Europe, the atmospheric $^{206}Pb/^{207}Pb$ ratio increased to values as high as 1.15–1.16 by the early 2000s (Farmer et al., 2005; Vinogradoff et al., 2005). The historical record of $^{206}Pb/^{207}Pb$ in Scottish herbarium mosses for the period 1838–2000 (Farmer et al., 2002) clearly illustrates these trends (Fig. 1).

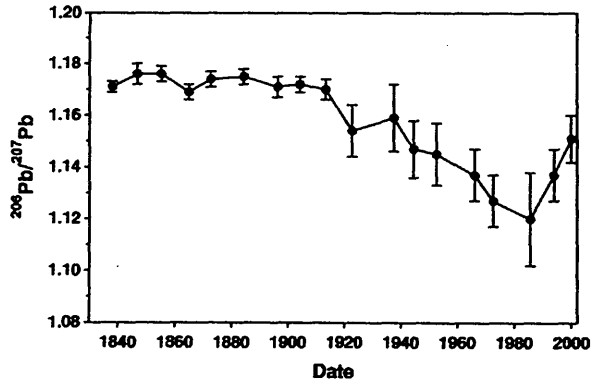

Fig. 1. $^{206}Pb/^{207}Pb$ trends in archival Scottish *Sphagnum* mosses 1838–2000 (Farmer et al., 2002).

In this paper, however, we report on another application of $^{206}Pb/^{207}Pb$ ratios, which makes use of the aforementioned records, to investigate the surface integrity of several peat cores collected by different methods from Flanders Moss ombrotrophic peat bog, central Scotland, during 1996–2001. This is important, not only because of the possibility of the loss of surface material, arising from past cutting of peat for fuel (cf. Lindow Bog in Le Roux et al., 2004) or unreliable peat core collection, but also because of the natural variability that may occur in topography (hummocks and hollows) and species of moss (with different sorption characteristics) across peat bog surfaces. Furthermore, Bindler et al. (2004) have recently drawn attention to the dangers of drawing erroneous conclusions, for example on the degree of current and past environmental metal contamination, based on metal concentrations for a single peat core that may not itself be truly representative or, for whatever reason, is incomplete. These are circumstances where the $^{206}Pb/^{207}Pb$ isotopic ratio method can be especially useful.

2. Site description and methods

Flanders Moss, with 548 ha of active raised bog, equivalent to 13.7% of the total area of those left in Britain, is an ombrotrophic peat bog situated 16 km to the west of Stirling in central Scotland (Fig. 2) and has been the subject of previous investigations (Farmer et al., 1997; MacKenzie et al., 1997). Cores were collected at various times between 1996 and 2001 (Table 1) from the south-west dome of the bog (Fig. 2) using a monolith tin (M: 50 cm × 15 cm × 7 cm), which was inserted into the vertical face of a freshly dug pit, and a Cuttle and Malcolm (1979) corer (CM: 1 m × 5 cm × 5 cm) pushed vertically into the bog. In 2001, some 5–10 cm of grassy vegetation was first cut with a knife to enable penetration of the CM corer in the collection of 01CM-1 and 01CM-2 cores. The M and CM cores, ranging from 43 to 106 cm in length, were sliced on-site into sections of thicknesses indicated in Table 1 and then taken to the laboratory for processing. After drying, aliquots of the sections from the different cores, as specifically indicated in Table 1, were analysed for ^{210}Pb by gamma spectrometry (Canberra low-background, planar high purity Ge gamma photon detector), total elemental concentrations (e.g. titanium, lead, arsenic, sulfur, iron, phosphorus, manganese) by ICP–OES (TJA IRIS) and lead isotopic composition (e.g. $^{206}Pb/^{207}Pb$) by ICP–MS (VG PQ3), using physical/chemical preparation and analytical methods described elsewhere (MacKenzie et al., 1997; Farmer et al., 2000, 2002; Yafa et al., 2004; Farmer et al., 2005). The

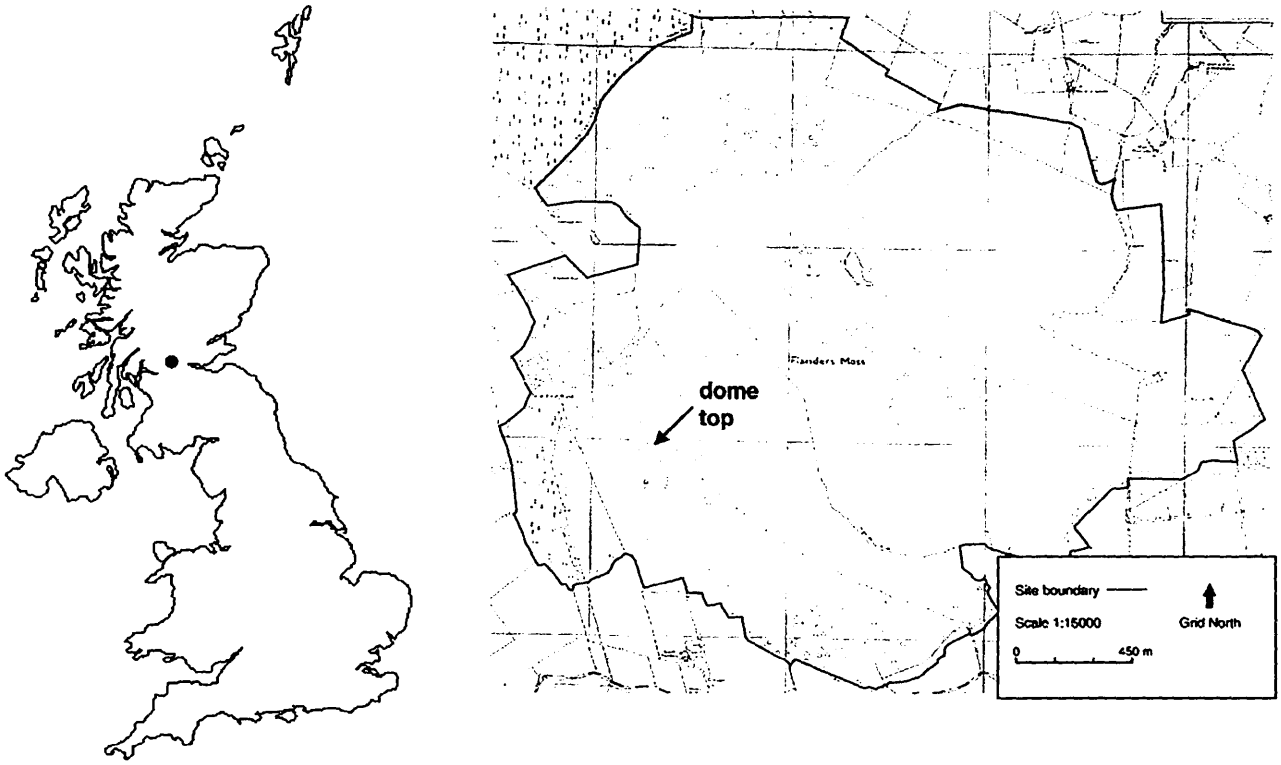

Fig. 2. Map of Flanders Moss ombrotrophic peat bog, central Scotland, showing the south-west dome sampling area.

average precision for elemental determination in duplicate peat samples by ICP–OES following microwave-assisted HF/HNO_3 dissolution was typically ±4–10% (RSD). The average precision on $^{206}Pb/^{207}Pb$ measurements by ICP–MS was typically ±0.1–0.2%. Accuracy of elemental and isotopic data was confirmed by analysis of the certified ombrotrophic peat reference material NIMT/UOE/FM/001 (Yafa et al., 2004).

3. Results and discussion

Selected profiles of the ash (450 °C) and water contents, lead, titanium, arsenic, sulfur, iron, phosphorus and manganese concentrations and $^{206}Pb/^{207}Pb$ ratios for depths ranging from 0 to 50 cm in cores 96M, 99M, 01CM-1 and 01CM-2 are presented in Figs. 3–8, as discussed below. The ^{210}Pb inventories for cores 96M, 99CM and 01CM-2 were 4.64±0.48, 1.98±0.12 and 1.73±0.12 kBq m^{-2}, respectively.

At first glance, the 01CM-2 profiles of lead concentration and $^{206}Pb/^{207}Pb$, which both decline towards the surface (Fig. 3), appear to be reasonably consistent with expected trends, although there is an absence of the reversal in $^{206}Pb/^{207}Pb$ decline that has been observed in recent Scottish moss samples (Fig. 1). Intriguingly, however, when the constant rate of supply model (Appleby et al., 1997) is applied to the ^{210}Pb data for the core, the calculated date of 1962 for the

Table 1
Collection and analytical details for Flanders Moss peat cores 1996–2001

Details/Designations	96M	99M	99CM	01CM-1	01CM-2
Collection date	10/1996	07/1999	07/1999	09/2001	09/2001
Monolith tin (M)	Yes	Yes	–	–	–
Cuttle and Malcolm (1979) (CM)	–	–	Yes	Yes	Yes
Length (cm)	59	43	100	106	96
Section thicknesses (cm)	0.5, 1	1	2	1	2
^{210}Pb	Yes	–	Yes	–	Yes
Elements – total concentrations	–	Yes	–	Yes	Yes
$^{206}Pb/^{207}Pb$	Yes	Yes	–	Yes	Yes

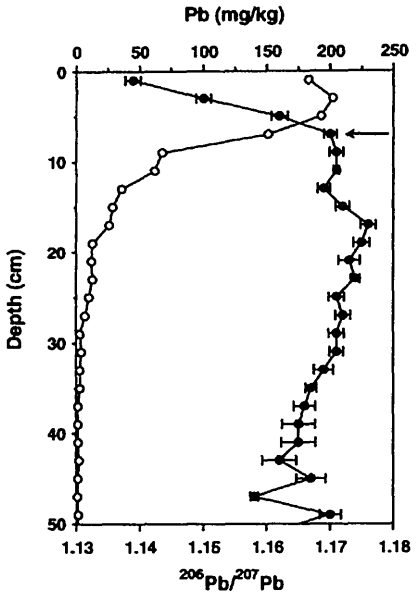

Fig. 3. Lead (O) and $^{206}Pb/^{207}Pb$ (●) profiles in Flanders Moss peat core 01CM-2. Indicated by an arrow, the major point of inflexion in the $^{206}Pb/^{207}Pb$ profile at 7 cm is dated by ^{210}Pb as A.D. 1962 if the surface is taken as corresponding to 2001.

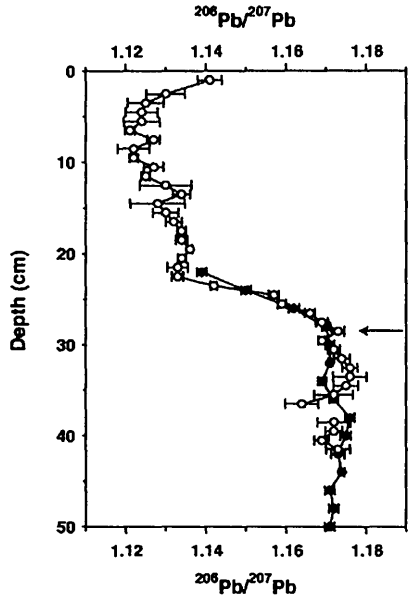

Fig. 5. $^{206}Pb/^{207}Pb$ profiles for the Flanders Moss peat cores 99M (O) and 01CM-2 (●), plotted with a 21-cm offset between the cores. The arrow indicates the major point of inflexion in the $^{206}Pb/^{207}Pb$ profiles.

onset of the major Australian-lead-influenced shift in $^{206}Pb/^{207}Pb$ (Fig. 3) is much too recent (Fig. 1). Furthermore, the inventory-derived average ^{210}Pb flux of 53.5±3.7 Bq m^{-2} yr^{-1} for 01CM-2, comparable to the 61±4 Bq m^{-2} yr^{-1} for 99CM, is much lower than the 144±15 Bq m^{-2} yr^{-1} for 96M. It is also lower than

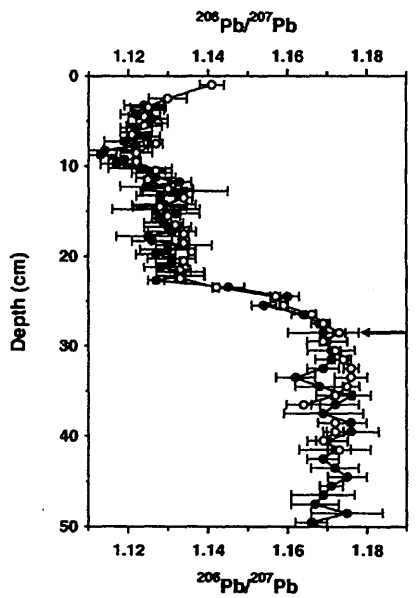

Fig. 4. $^{206}Pb/^{207}Pb$ profiles for the Flanders Moss peat cores 96M (●) and 99M (O), plotted with a 3-cm offset between the cores. The arrow indicates the major point of inflexion in the $^{206}Pb/^{207}Pb$ profiles.

the theoretical rainfall-corrected value of 102± 18 Bq m^{-2} yr^{-1} expected for this latitude in the UK (Smith et al., 1997) and the values of 110 and 113 Bq m^{-2} yr^{-1} obtained for a 1990 Flanders Moss core (Farmer et al., 1997; MacKenzie et al., 1997) and a 1991 sediment core from nearby Loch Lomond (Eades et al., 2002), respectively. As the mean value (n=4) of 117±18 Bq m^{-2} yr^{-1} for the average ^{210}Pb flux corresponds to an inventory of 3.78±0.59 kBq m^{-2} at Flanders Moss, the CRS model suggests that there is at least 25±7 yrs of material missing (for whatever reason) from the top of the 01CM-2 core and a similar amount from the top of the 99CM core.

This suggestion is strengthened when the $^{206}Pb/^{207}Pb$ profile of 96M is compared with that for 99M, the monolith core collected 3 yrs later. There is a very good match between the monolith profiles when plotted with a 3-cm offset (Fig. 4) to account for the difference in the date of collection and the presence of vegetation accumulating at ~1 cm yr^{-1} in the upper sections. There is agreement in a steep major shift in $^{206}Pb/^{207}Pb$ from ~1.17 to ~1.13 over a 4- to 5-cm depth interval lying between 20 and 30 cm, a minimum of 1.11–1.12 just above 10 cm, and thereafter an increase towards the surface, exemplified by the value of ~1.14 for the top section of 99M. Then, when the $^{206}Pb/^{207}Pb$ profile of 99M is overlain with that of 01CM-2, the best match, using the steep gradient of $^{206}Pb/^{207}Pb$ change from 1.17 to 1.13, occurs when they are plotted with a 21-cm

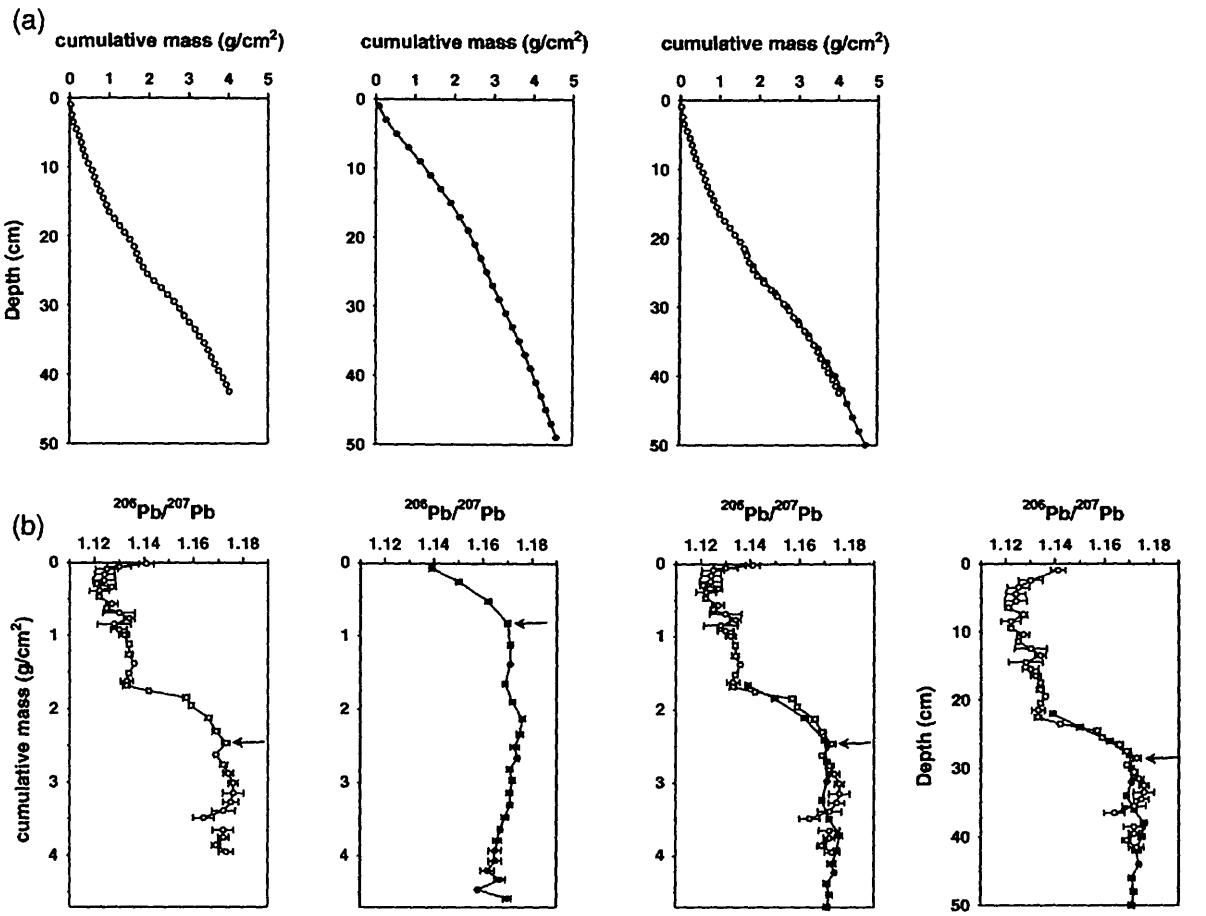

Fig. 6. (a) Profiles of cumulative mass per unit area plotted against linear depth for Flanders Moss peat cores 99M (O) and 01CM-2 (●) before and after a 21-cm offset between the cores. (b) Profiles of $^{206}Pb/^{207}Pb$ plotted against cumulative mass per unit area for Flanders Moss peat cores 99M (O) and 01CM-2 (●) before and after a 1.60 g cm^{-2} offset between the cores. The $^{206}Pb/^{207}Pb$ profiles plotted against linear depth, with a 21-cm offset between the cores, are shown for comparison. The arrows indicate the major point of inflexion in the $^{206}Pb/^{207}Pb$ profiles.

offset (Fig. 5). The suggestion that the top of the 01CM-2 core corresponds to ca. 1976, or even ca. 1969, is much strengthened by this comparison of lead isotopic ratios. The aforementioned removal of some surface grassy vegetation prior to collection of the 01CM-2 core probably accounts for most of the required 21-cm offset.

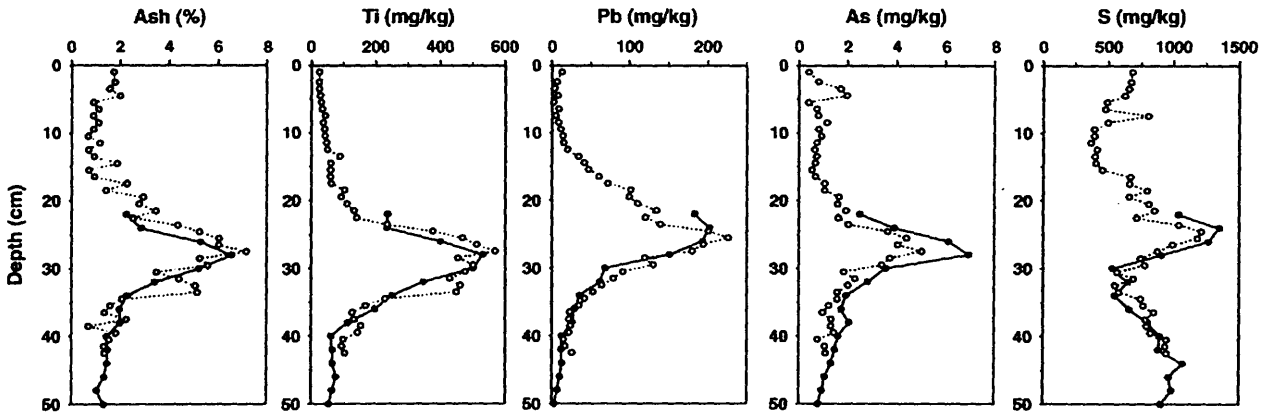

Fig. 7. Ash, titanium, lead, arsenic and sulfur concentration profiles in Flanders Moss peat cores 99M (O) and 01CM-2 (●), plotted with a 21-cm offset between the cores.

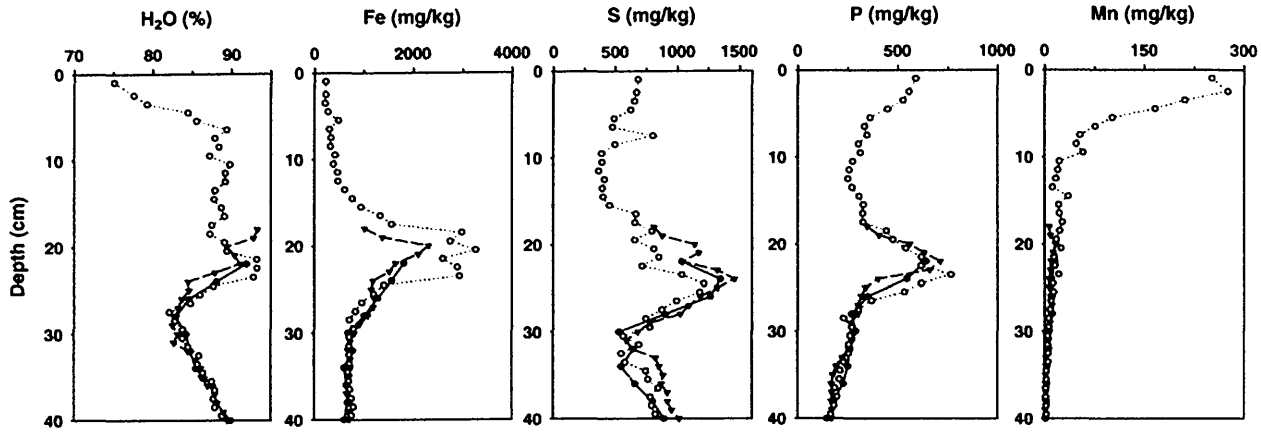

Fig. 8. Water, iron, sulfur, phosphorus and manganese concentration profiles in Flanders Moss peat cores 99M (O), 01CM-1 (▼) and 01CM-2 (●), plotted with 17.5-cm and 21-cm offsets between 99M and the 01CM-1 and 01CM-2 cores, respectively.

Indeed, when the cumulative mass per unit area (g cm^{-2}) is plotted for 01CM-2 and compared with that for 99M (Fig. 6), the clear disparity is removed when allowance is made for the offset of 21 cm, corresponding to 1.60 g cm^{-2} from 0 to 21 cm in 99M (Table 2). Similarly, when the $^{206}Pb/^{207}Pb$ ratio is plotted against cumulative mass for both 99M and 01CM-2 (Fig. 6), the clear initial disparity is removed when allowance is made for an offset of 1.60 g cm^{-2}. Thus it is the loss of material prior to core collection, rather than compaction of vegetation during collection, by the Cuttle and Malcolm corer that is the likely major cause of the offset between the 99M and 01CM-2 profiles. Furthermore, the plots, with appropriate offsets, of $^{206}Pb/^{207}Pb$ versus cumulative mass (g cm^{-2}) and linear depth (cm) for 99M and 01CM-2 are in excellent agreement with respect to the key features, such as the point of inflection and the steep ensuing gradient, of the $^{206}Pb/^{207}Pb$ profile (Fig. 6). Therefore, on this occasion, there is no advantage in using cumulative mass (g cm^{-2}) rather than linear depth (cm) for the depth axis.

Table 2
Comparison of elemental inventories in Flanders Moss cores 99M and 01CM-2

Element/ Core	99M 0–21 cm (g m^{-2})	99M 21–43 cm (g m^{-2})	01CM-2 0–22 cm (g m^{-2})	Ratio 99M (21–43 cm)/01CM-2 (0–22 cm)
Ti	0.98	8.33	7.66	1.09
Pb	0.74	2.41	2.38	1.01
As	0.017	0.060	0.081	0.75
S	9.27	20.43	22.16	0.92
Fe	19.78	24.47	23.90	1.02
P	6.03	7.54	7.61	0.99
Mn	0.89	0.17	0.19	0.90
Dry mass (g cm^{-2})	1.60	2.46	2.59	0.95

When the ash, titanium, lead, arsenic and sulfur concentrations for 99M and 01CM-2 are likewise plotted with a 21-cm offset, there is remarkably good agreement between the cores in the depth profiles for each element, especially with respect to the magnitude and position of the peaks (Fig. 7). Similarly, the inventories for titanium, lead, arsenic and sulfur from 21 to 43 cm in 99M are in good agreement with those from 0 to 22 cm in 01CM-2, the significant inventories present from 0 to 22 cm in 99M being absent from 01CM-2 (Table 2). The subtleties of the inter-element differences in the position of the maximum concentration are discussed below for titanium, lead and arsenic, but it is worth noting the potential for erroneous interpretation in terms of atmospheric deposition/ geochemical behaviour that could result if the top of 01CM-2 were taken to correspond to 2001.

This is perhaps even better illustrated when the profiles of water content, iron, sulfur, phosphorus and manganese concentrations for both 99M and 01CM-2 and an additional core, 01CM-1, are plotted with offsets of 21 cm and 17.5 cm relative to 99M for 01CM-2 and 01CM-1, respectively (Fig. 8). If based solely on the CM cores, a considerable portion of the profiles for the nutrient elements, manganese, phosphorus and sulfur, which are recycled by living vegetation, would have been missed. This would have been particularly significant for manganese, which reaches concentrations approaching 300 mg kg^{-1} in the upper sections of 99M (Fig. 8). The inventories of manganese, in particular, and of iron and phosphorus from 0 to 21 cm in 99M are significant (Table 2). In addition, the position of the diagenetically enriched peak for iron, a redox-active

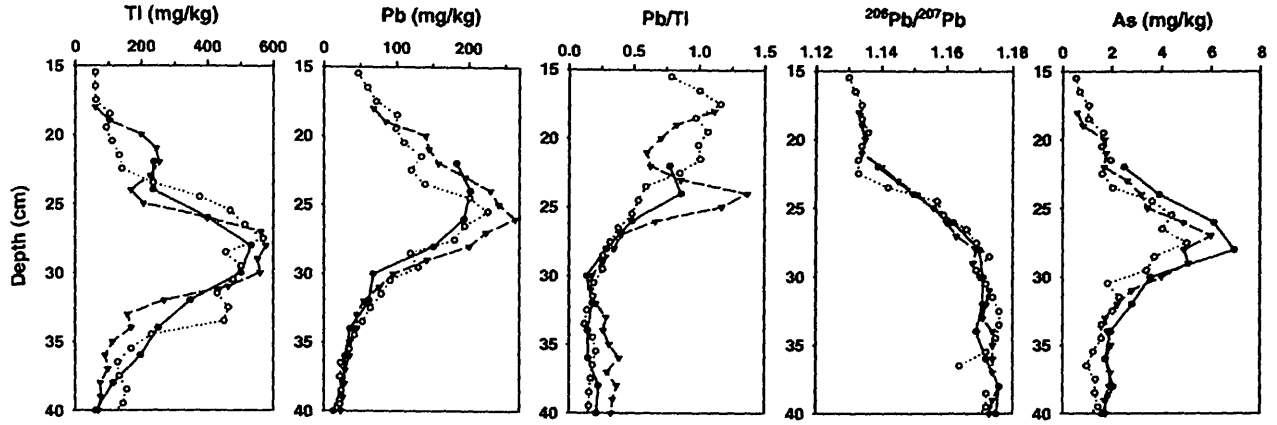

Fig. 9. Profiles of titanium concentration, lead concentration, lead/titanium ratio, $^{206}Pb/^{207}Pb$ ratio and arsenic concentration over the depth range 15–40 cm in Flanders Moss peat cores 99M (○), 01CM-1 (▼) and 01CM-2 (●), plotted with 17.5-cm and 21-cm offsets between 99M and the 01CM-1 and 01CM-2 cores, respectively.

mobile element in the bog, would have been missed by 01CM-2, although to a lesser extent by 01CM-1, for which the elemental profiles are offset by 3.5 cm relative to 01CM-2.

Fig. 9 focuses on the concentration profiles of titanium, lead and arsenic and on the profiles of lead/titanium and $^{206}Pb/^{207}Pb$ ratios over the 15–40 cm depth region at Flanders Moss, again allowing for offsets of 21 cm and 17.5 cm between 99M and the two CM cores, 01CM-2 and 01CM-1, respectively. The titanium, lead and arsenic concentrations peak at about 26–31 cm, 24–28 cm and 25–29 cm, respectively. The major decrease in the $^{206}Pb/^{207}Pb$ ratio occurs from 28 cm upwards to 22 cm, and the lead/titanium ratio, while a bit more variable for the three cores, increases from about 30 cm and is most enhanced over the 15–26 cm region. With titanium often taken as an indicator of soil dust input (Martinez-Cortizas et al., 2002; Shotyk et al., 2002; Weiss et al., 2002), the changes in lead/titanium and $^{206}Pb/^{207}Pb$ relative to the changes in the lead and arsenic concentrations probably reflect the increasing input of lead from car-exhaust emissions relative to that from coal combustion. This is reflected in the plot of lead and arsenic fluxes derived from the ^{210}Pb dating of 01CM-2 and assuming that the top of the core corresponds to 1976, i.e. with 25 yrs of material missing from the top (Fig. 10). The arsenic flux rises with the lead flux to peak at ca. 1950, but declines more steeply thereafter as coal combustion declines (Farmer et al., 1999) and also becomes a less important source as manifested in the declining $^{206}Pb/^{207}Pb$ trend. MacKenzie et al. (1998a,b), in work on another ombrotrophic bog (South Drumboy Hill) in west-central Scotland, found that fluxes of lead and arsenic peaked ca. 1940. At Flanders Moss, the onset of the major shift in $^{206}Pb/^{207}Pb$ (Fig. 10) also suggests that the estimated date (1937) could be at least 10 yrs too recent, but it should be noted that there is in any case an uncertainty of ±11 yrs associated with the date, arising from both uncertainty on the extent of loss of surface material and counting statistics.

The implications of the differences between the types of cores (M, CM) are potentially more serious for time-related studies of the recent phenomena (i.e. nutrient

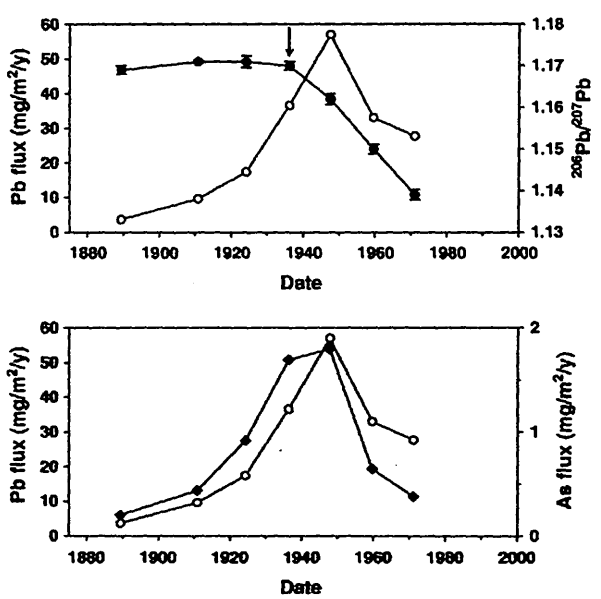

Fig. 10. Temporal trends in the $^{206}Pb/^{207}Pb$ ratio and fluxes of lead and arsenic of atmospheric deposition at Flanders Moss, as derived from the data for the ^{210}Pb-dated peat core 01CM-2 and allowing for 25 years' worth of material missing from the top of the core. The arrow indicates the major point of inflexion in the $^{206}Pb/^{207}Pb$ profile.

cycling, industrial and post-industrial era metal contamination) discussed above than for such studies of much earlier phenomena (e.g. lead mining/smelting during the period of the Roman Empire). In theory, there are several possible causes of the observed differences between the cores. These could have included: (1) differences in the topography of the bog, which could have led to hummock/hollow effects on trapping of deposition (Urban et al., 1990) at the sites chosen for collection of the cores by the different coring mechanisms (M, CM); (2) differences in the surface vegetation of the bog, which could have led to differential trapping and retention of lead, for example, and different retention of vegetation during sampling at the sites where the corers were inserted; (3) different effects induced by the operating mechanism of the corers, e.g. compression of vegetation by the CM corers; (4) operator-induced effects, e.g. leading to loss of surface material before or during coring.

We believe that, while all four may have been implicated in this particular study, the last was probably by far the most important, for the reasons stated earlier. But the implications of the work are far wider and, as a result of this study, we would make the following recommendations:

(1) use of $^{206}Pb/^{207}Pb$ to investigate surface integrity of collected cores, which could be usefully supplemented by the use of radionuclides (e.g. bomb ^{14}C, ^{210}Pb, ^{241}Am, ^{7}Be) (Oldfield et al., 1995; Goodsite et al., 2002; Turetsky et al., 2004);
(2) establishment of reliable protocols for collecting, handling and preparing peat cores and peat samples for physical, chemical, mineralogical and isotopic analyses (Givelet et al., 2004; Yafa et al., 2004);
(3) multiple coring to take account of spatial variability on the surface of peat bogs (Bindler et al., 2004);
(4) consideration of all surface and near-surface factors and processes that may influence trapping and retention of chemical entities deposited from the atmosphere to peat bogs (Damman, 1978; Clymo et al., 1990; Urban et al., 1990; Norton et al., 1997).

4. Conclusions

The use of $^{206}Pb/^{207}Pb$ ratios, against a backdrop of knowledge about the recent historical trends in atmospheric lead, has proved effective in checking the surface integrity of cores collected from ombrotrophic peat bogs and correcting for the loss or absence of material from the top of cores.

Acknowledgements

We thank Scottish Natural Heritage for permission to sample on Flanders Moss, D.G. Lumsdon (1999), G.J. Patrick (2001) and R.P. Thomas (2001) for assistance with field work, A. Pott, K. Lorimer and C. Newey for laboratory preparation of core material (1996, 1999), L. J. Eades for analytical expertise, and the Thai Government (CY), NERC (JMC) and EPSRC (AJF) for studentship funding.

References

Appleby, P.G., Shotyk, W., Fankhauser, A., 1997. Lead-210 age dating of three peat cores in the Jura Mountains Switzerland. Water Air Soil Pollut. 100, 223–231.

Bindler, R., Klarqvist, M., Klaminder, J., Forster, J., 2004. Does within-bog variability of mercury and lead constrain reconstruction of absolute deposition rates from single peat records? The example of Store Mosse, Sweden. Glob. Biogeochem. Cycles 18 (art. no. GB3020).

Clymo, R.S., Oldfield, F., Appleby, P.G., Pearson, G.W., Ratnesar, P., Richardson, N., 1990. The record of atmospheric deposition on a rainwater-dependent peatland. Philos. Trans. R. Soc. Lond., B 327, 331–338.

Cuttle, S.P., Malcolm, D.C., 1979. A corer for taking undisturbed soil samples. Plant Soil 51, 297–300.

Damman, A.W.H., 1978. Distribution and movement of elements in ombrotrophic peat bogs. Oikos 30, 480–495.

Dunlap, C.E., Steinnes, E., Flegal, A.R., 1999. A synthesis of lead isotopes in two millennia of European air. Earth Planet. Sci. Lett. 167, 81–88.

Eades, L.J., Farmer, J.G., MacKenzie, A.B., Kirika, A., Bailey-Watts, A.E., 2002. Stable lead isotopic characterisation of the historical record of environmental lead contamination in dated freshwater lake sediment cores from northern and central Scotland. Sci. Total Environ. 292, 55–67.

Farmer, J.G., Eades, L.J., MacKenzie, A.B., Kirika, A., Bailey-Watts, A.E., 1996. Stable lead isotope record of lead pollution in Loch Lomond sediments since 1630 A.D. Environ. Sci. Technol. 30, 3080–3083.

Farmer, J.G., MacKenzie, A.B., Sugden, C.L., Edgar, P.J., Eades, L.J., 1997. A comparison of the historical lead pollution records in freshwater lake sediments and peat cores from central Scotland. Water Air Soil Pollut. 100, 253–270.

Farmer, J.G., Eades, L.J., Graham, M.C., 1999. The lead content and isotopic composition of British coals and their implications for past and present releases of lead to the U.K. environment. Environ. Geochem. Health 21, 257–272.

Farmer, J.G., Eades, L.J., Graham, M.C., Bacon, J.R., 2000. The changing nature of the $^{206}Pb/^{207}Pb$ isotopic ratio of lead in rainwater, atmospheric particulates, pine needles and leaded petrol in Scotland 1982–1998. J. Environ. Monit. 2, 49–57.

Farmer, J.G., Eades, L.J., Atkins, H., Chamberlain, D.F., 2002. Historical trends in the lead isotopic composition of archival

Sphagnum mosses from Scotland (1838–2000). Environ. Sci. Technol. 36, 152–157.

Farmer, J.G., Graham, M.C., Bacon, J.R., Dunn, S.M., Vinogradoff, S.I., MacKenzie, A.B., 2005. Isotopic characterization of the historical lead deposition at Glensaugh, an organic-rich, upland catchment in rural N.E. Scotland. Sci. Total Environ. 346, 121–137.

Givelet, N., Le Roux, G., Cheburkin, A., Chen, B., Frank, J., Goodsite, M.E., Kempter, H., Krachler, M., Noernberg, T., Rausch, N., Rheinberger, S., Roos-Barraclough, F., Sapkota, A., Scholz, C., Shotyk, W., 2004. Suggested protocol for collecting, handling and preparing peat cores and peat samples for physical, chemical, mineralogical and isotopic analyses. J. Environ. Monit. 6, 481–492.

Goodsite, M.E., Heinemeier, J., Rom, W., Lange, T., Ooi, S., Appleby, P.G., Shotyk, W., van der Knaap, W.O., Lohse, C., Hansen, T.S., 2002. High resolution AMS ^{14}C dating of post-bomb peat archives of atmospheric pollutants. Radiocarbon 43, 495–515.

Klaminder, J., Renberg, I., Bindler, R., 2003. Isotopic trends and background fluxes of atmospheric lead in northern Europe: analyses of three ombrotrophic bogs from south Sweden. Glob. Biogeochem. Cycles 17 (art. no. 1019).

Krachler, M., Mohl, C., Emons, H., Shotyk, W., 2003. Atmospheric deposition of V, Cr, and Ni since the Late Glacial: effects of climatic cycles, human impacts, and comparison with crustal abundances. Environ. Sci. Technol. 37, 2658–2667.

Le Roux, G., Weiss, D., Grattan, J., Givelet, N., Krachler, M., Cheburkin, A., Rausch, N., Kober, B., Shotyk, W., 2004. Identifying the sources and timing of ancient and medieval atmospheric lead pollution in England using a peat profile from Lindow Bog, Manchester. J. Environ. Monit. 6, 502–510.

MacKenzie, A.B., Farmer, J.G., Sugden, C.L., 1997. Isotopic evidence of the relative retention and mobility of lead and radiocaesium in Scottish ombrotrophic peats. Sci. Total Environ. 203, 115–127.

MacKenzie, A.B., Logan, E.M., Cook, G.T., Pulford, I.D., 1998a. A historical record of atmospheric depositional fluxes of contaminants in west-central Scotland derived from an ombrotrophic peat core. Sci. Total Environ. 222, 157–166.

MacKenzie, A.B., Logan, E.M., Cook, G.T., Pulford, I.D., 1998b. Distributions, inventories and isotopic composition of lead in ^{210}Pb-dated peat cores from contrasting biogeochemical environments: implications for lead mobility. Sci. Total Environ. 223, 25–35.

Martinez-Cortizas, A., Pontevedra-Pombral, X., Garcia-Rodeja, E., Nóvoa-Muñoz, J.C., Shotyk, W., 1999. Mercury in a Spanish peat bog: archive of climate change and atmospheric metal deposition. Science 282, 939–942.

Martinez-Cortizas, A., Garcia-Rodeja, E., Pontevedra Pombal, X., Nóvoa Muñoz, J.C., Weiss, D., Cheburkin, A., 2002. Atmospheric Pb deposition in Spain during the past 4600 years recorded by two ombrotrophic peat bogs and implications for the use of peat as an archive. Sci. Total Environ. 292, 33–44.

Norton, S.A., Evans, G.C., Kahl, J.S., 1997. Comparison of Hg and Pb fluxes to hummocks and hollows of ombrotrophic Big Heath Bog and to nearby Sargent Mt. Pond. Water Air Soil Pollut. 100, 271–286.

Novák, M., Emmanuel, S., Vile, M.A., Erel, Y., Véron, A., Pačes, T., Wieder, R., Vaněček, M., Štěpánova, M., Břízová, E., Hovorka, J., 2003. Origin of lead in eight Central European peat bogs determined from isotope ratios, strengths, and operation times of regional pollution sources. Environ. Sci. Technol. 37, 437–445.

Oldfield, F., Richardson, N., Appleby, P.G., 1995. Radiometric dating (^{210}Pb, ^{137}Cs, ^{241}Am) of recent ombrotrophic peat accumulation and evidence for changes in mass balance. Holocene 5, 141–148.

Shotyk, W., Krachler, M., 2004. Atmospheric deposition of silver and thallium since 12370 ^{14}C years BP recorded by a Swiss peat bog profile, and comparison with lead and cadmium. J. Environ. Monit. 6, 427–433.

Shotyk, W., Cheburkin, A.K., Appleby, P.G., Fankhauser, A., Kramers, J.D., 1997. Lead in three peat bog profiles, Jura Mountains, Switzerland: enrichment factors, isotopic composition, and chronology of atmospheric deposition. Water Air Soil Pollut. 100, 289–296.

Shotyk, W., Weiss, D., Appleby, P.G., Cheburkin, A.K., Frei, R., Gloor, M., Kramers, J.D., Reese, S., Van Der Knaap, W.O., 1998. History of atmospheric lead deposition since 12,370 ^{14}C yr BP from a peat bog, Jura Mountains, Switzerland. Science 281, 1635–1640.

Shotyk, W., Krachler, M., Martinez-Cortizas, A., Cheburkin, A.K., Emons, H., 2002. A peat bog record of natural pre-anthropogenic enrichments of trace elements in atmospheric aerosols since 12370 ^{14}C yr BP, and their variations with Holocene climatic change. Earth Planet. Sci.Lett. 199, 21–37.

Shotyk, W., Goodsite, M.E., Roos-Barraclough, F., Frei, R., Heinemeier, J., Asmund, G., Lohse, C., Hansen, T.S., 2003. Anthropogenic contributions to atmospheric Hg, Pb and As accumulation recorded by peat cores from southern Greenland and Denmark dated using the ^{14}C "bomb pulse curve". Geochim. Cosmochim. Acta 67, 3991–4011.

Shotyk, W., Goodsite, M.E., Roos-Barraclough, F., Givelet, N., Le Roux, G., Weiss, D., Cheburkin, A.K., Knudsen, K., Heinemeier, J., van Der Knaap, W.O., Norton, S.A., Lohse, C., 2005. Accumulation rates and predominant atmospheric sources of natural and anthropogenic Hg and Pb on the Faroe Islands. Geochim. Cosmochim. Acta 69, 1–17.

Smith, J.T., Appleby, P.G., Hilton, J., Richardson, N., 1997. Inventories and fluxes of ^{210}Pb, ^{137}Cs and ^{241}Am determined from the soils of three small catchments in Cumbria, UK. J. Environ. Radioact. 37, 127–142.

Turetsky, M.R., Manning, S.W., Wieder, R.K., 2004. Dating recent peat deposits. Wetlands 24, 324–356.

Urban, N.R., Eisenreich, S.J., Grigal, D.F., Schurr, K.T., 1990. Mobility and diagenesis of Pb and ^{210}Pb in peat. Geochim. Cosmochim. Acta 54, 3329–3346.

Vinogradoff, S.I., Graham, M.C., Thornton, G.J.P., Dunn, S.M., Bacon, J.R., Farmer, J.G., 2005. Investigation of the concentration and isotopic composition of inputs and outputs of Pb in waters at an upland catchment in NE Scotland. J. Environ. Monit. 7, 431–444.

Weiss, D., Shotyk, W., Appleby, P.G., Kramers, J.D., Cheburkin, A.K., 1999. Atmospheric Pb deposition since the Industrial Revolution recorded by five Swiss peat profiles: enrichment factors, fluxes, isotopic composition, and sources. Environ. Sci. Technol. 33, 1340–1352.

Weiss, D., Shotyk, W., Boyle, E.A., Kramers, J.D., Appleby, P.G., Cheburkin, A.K., 2002. Comparative study of the temporal evolution of atmospheric lead deposition in Scotland and eastern Canada using blanket peat bogs. Sci. Total Environ. 292, 7–18.

Yafa, C., Farmer, J.G., Graham, M.C., Bacon, J.R., Barbante, C., Cairns, W.R.L., Bindler, R., Renberg, I., Cheburkin, A., Emons, H., Handley, M.J., Norton, S.A., Krachler, M., Shotyk, W., Li, X.D., Martinez-Cortizas, A., Pulford, I.D., MacIver, V., Schweyer, J., Steinnes, E., Sjøbakk, T.E., Weiss, D., Dolgopolova, A., Kylander, M., 2004. Development of an ombrotrophic peat bog (low ash) reference material for the determination of elemental concentrations. J. Environ. Monit. 6, 493–501.